HIGHWAY RESEARCH BOARD

Bulletin 342

Stress Distribution in Earth Masses

1962

National Academy of Sciences—
National Research Council

publication 1025

HIGHWAY RESEARCH BOARD

Officers and Members of the Executive Committee

1962

OFFICERS

R. R. BARTELSMEYER, *Chairman* C. D. CURTISS, *First Vice Chairman*

WILBUR S. SMITH, *Second Vice Chairman*

FRED BURGGRAF, *Director* WILLIAM N. CAREY, JR., *Assistant Director*

Executive Committee

REX M. WHITTON, *Federal Highway Administrator, Bureau of Public Roads* (ex officio)

A. E. JOHNSON, *Executive Secretary, American Association of State Highway Officials* (ex officio)

LOUIS JORDAN, *Executive Secretary, Division of Engineering and Industrial Research, National Research Council* (ex officio)

PYKE JOHNSON, *Retired* (ex officio, Past Chairman 1960)

W. A. BUGGE, *Director of Highways, Washington Department of Highways* (ex officio, Past Chairman 1961)

R. R. BARTELSMEYER, *Chief Highway Engineer, Illinois Division of Highways*

E. W. BAUMAN, *Director, National Slag Association, Washington, D. C.*

DONALD S. BERRY, *Professor of Civil Engineering, Northwestern University*

MASON A. BUTCHER, *County Manager, Montgomery County, Md.*

J. DOUGLAS CARROLL, JR., *Director, Chicago Area Transportation Study*

C. D. CURTISS, *Special Assistant to the Executive Vice President, American Road Builders' Association*

HARMER E. DAVIS, *Director, Institute of Transportation and Traffic Engineering, University of California*

DUKE W. DUNBAR, *Attorney General of Colorado*

MICHAEL FERENCE, JR., *Executive Director, Scientific Laboratory, Ford Motor Company*

D. C. GREER, *State Highway Engineer, Texas State Highway Department*

JOHN T. HOWARD, *Head, Department of City and Regional Planning, Massachusetts Institute of Technology*

BURTON W. MARSH, *Director, Traffic Engineering and Safety Department, American Automobile Association*

OSCAR T. MARZKE, *Vice President, Fundamental Research, U. S. Steel Corporation*

J. B. MCMORRAN, *Superintendent of Public Works, New York State Department of Public Works*

CLIFFORD F. RASSWEILER, *Vice President for Research and Development, Johns-Manville Corporation*

GLENN C. RICHARDS, *Commissioner, Detroit Department of Public Works*

C. H. SCHOLER, *Applied Mechanics Department, Kansas State University*

WILBUR S. SMITH, *Wilbur Smith and Associates, New Haven, Conn.*

K. B. WOODS, *Head, School of Civil Engineering, and Director, Joint Highway Research Project, Purdue University*

Editorial Staff

FRED BURGGRAF
2101 Constitution Avenue

HERBERT P. ORLAND
Washington 25, D. C.

Stress Distribution in Earth Masses

1962

HIGHWAY RESEARCH BOARD
Bulletin 342

Stress Distribution in Earth Masses

1962

Presented at the
41st ANNUAL MEETING
January 8-12, 1962

National Academy of Sciences—
National Research Council
Washington, D. C.
1962

Department of Soils, Geology and Foundations

Miles S. Kersten, Chairman
Professor of Civil Engineering
University of Minnesota, Minneapolis

COMMITTEE ON STRESS DISTRIBUTION IN EARTH MASSES

H. Bolton Seed, Chairman
Department of Civil Engineering
University of California, Berkeley

Richard G. Ahlvin, Chief Engineer, Special Projects Section, Waterways Experiment Station, Vicksburg, Mississippi
E.S. Barber, Consulting Engineer, Soil Mechanics and Foundations, Arlington, Va.
B.E. Colley, Portland Cement Association, Chicago, Illinois
Melvin T. Davisson, University of Illinois, Urbana
Lawrence A. DuBose, Testing Service Corporation, Lombard, Illinois
Austin H. Emery, Associate Soils Engineer, Bureau of Soil Mechanics, New York State Department of Public Works, Albany
Jacob Feld, Consulting Engineer, New York, N.Y.
Hamilton Gray, Chairman, Department of Civil Engineering, Ohio State University, Columbus
Milton E. Harr, Assistant Professor, School of Civil Engineering, Purdue University, Lafayette, Indiana
R.G. Hennes, Department of Civil Engineering, University of Washington, Seattle
W.S. Housel, University of Michigan, Ann Arbor
F.N. Hveem, Materials and Research Engineer, California Division of Highways, Sacramento
T.F. McMahon, Department of Civil Engineering, University of Kansas, Lawrence
Robert L. McNeill, Supervisor, Soil Dynamics, Shock Tube Laboratory, University Station, Albuquerque, New Mexico
Neil E. Mason, Columbus Testing Laboratory, Columbus, Ohio
J.O. Osterberg, Civil Engineering Department, Northwestern University, Evanston, Illinois
F.E. Richart, Civil Engineering Department, University of Florida, Gainesville
Robert L. Schiffman, Associate Professor of Soil Mechanics, Renssalear Polytechnic Institute, Troy, N.Y.
Werner E. Schmid, Assistant Professor, Department of Civil Engineering, Princeton University, Princeton, New Jersey
F.H. Scrivner, Pavement Research Engineer, Texas Transportation Institute, A & M College of Texas, College Station

Contents

TABULATED VALUES FOR DETERMINING THE COMPLETE PATTERN OF STRESSES, STRAINS, AND DEFLECTIONS BENEATH A UNIFORM CIRCULAR LOAD ON A HOMOGENEOUS HALF SPACE

R. G. Ahlvin and H. H. Ulery 1

DISTRIBUTION OF STRESSES ON AN UNYIELDING SURFACE BENEATH A PNEUMATIC TIRE

D. R. Freitag and A. J. Green 14

STRESSES IN YIELDING SOILS UNDER MOVING WHEELS AND TRACKS

D. R. Freitag and S. J. Knight 24

USE OF STRESS LOCI FOR DETERMINATION OF EFFECTIVE STRESS PARAMETERS

R. Yong and E. Vey 38

Discussion: Charles C. Ladd 49

Closure: R. Yong and E. Vey 51

A RHEOLOGICAL ANALYSIS OF SHEAR AND CONSOLIDATION OF SATURATED CLAYS

Adel S. Saada 52

Discussion: Robert L. Schiffman 76

Closure: Adel S. Saada 84

VERTICAL STRESSES IN SUBGRADES BENEATH STATICALLY LOADED FLEXIBLE PAVEMENTS

George F. Sowers and Aleksandar B. Vesic 90

Discussion: Robert L. Schiffman 120

Closure: George F. Sowers and Aleksandar B. Vesic 121

LATERAL STABILITY OF RIGID POLES SUBJECTED TO A GROUND-LINE THRUST

Robert L. Kondner and Gordon E. Green 124

THREE-DIMENSIONAL CONSOLIDATION

J. A. deWet 152

TABLES OF STRESSES IN THREE-LAYER ELASTIC SYSTEMS

A. Jones 176

STRESS AND STRAIN FACTORS FOR THREE-LAYER ELASTIC SYSTEMS

K. R. Peattie 215

Tabulated Values for Determining the Complete Pattern of Stresses, Strains, and Deflections Beneath a Uniform Circular Load on a Homogeneous Half Space

R. G. AHLVIN and H. H. ULERY, respectively, Chief and Engineer, Special Projects Section, Flexible Pavement Branch, Soils Division, U. S. Army Engineer Waterways Experiment Station, Vicksburg

Results of extensive computations are presented in a manner that permits simple determination of the complete pattern of stress, strain, and deflection at points beneath a uniform circular load on an elastic, homogeneous, isotropic, half space. Tabulations are presented of eight factors for a dense network of points in terms of depth below the load and radial distance from the load axis. Simple formulas are presented using these factors and Poisson's ratio by which any coordinate stress, strain, or deflection may be determined for any value of Poisson's ratio.

•THIS PAPER presents results of computations of stress, strain, and deflection at points beneath a uniform circular load on an elastic, homogeneous, isotropic half space. These results are being reported in the hope that they will provide a useful reference to anyone concerned with the distribution of stress and strain induced by tire or footing loads that may be treated as uniformly distributed circular loads. Computations of this type are not new (1, 2, 3); but the results presented are somewhat more extensive, provide a denser network of values, give greater accuracy, and treat Poisson's ratio more directly than previously published information. The method of presentation is also somewhat different in that tabulations have been made of each of eight functions which can be combined through simple equations to give any coordinate stress, strain, or deflection for any value of Poisson's ratio.

The computations reported were made in connection with an investigation of pressures and deflections in homogeneous soil masses. This was part of a larger study of the action of loads on flexible pavements conducted at the U. S. Army Engineer Waterways Experiment Station. Theoretical values of stress, strain, and deflection were developed for comparison with equivalent values measured in field test sections (7, 8, 9). These theoretical values were computed using equations developed by Love (5) and other methods (8 and 9).

In the computations, certain functions were obtained that repeat themselves and are independent of Poisson's ratio. These are the functions that are tabulated and presented which combine in simple formulas to give stress, strain, or deflection for any value of Poisson's ratio. Tables 1 through 8 give the data in terms of depth below the loaded area and offset distance from the center of the loaded area, of the eight functions needed to determine any desired stress, strain, or deflection. The tables give values for depths in radii of 0, 0.5, 1, 1.5, 2, 2.5, 3, 4, 5, 6, 7, 8, and 9 for offset distances from the load axis in radii of 0, 1, 2, 3, 4, 5, 6, 7, 8, 10, 12, and 14. In addition, values are presented for depths in radii of 0.1, 0.2, 0.3, 0.4, 0.5, 0.6, 0.7, 0.8, 0.9, 1, 1.2, 1.5, 2, 2.5, 3, and 4 at offset distances in radii of 0.2, 0.4, 0.6, 0.8, 1.2, and 1.5. A few values are included for depths of 10 radii and a few for fractional radii depths at other offset distances. The values included represent those needed for comparison with equivalent values measured in test sections as mentioned previously.

It might appear strange that, with the modern computing equipment now available, tabular results of the type reported are not already commonly available.

Table 1

Function "A"

Depth (Z) in Radii	Offset (ρ) in Radii																	
	0	0.2	0 4	0.6	0 8	1	1.2	1.5	2	3	4	5	6	7	8	10	12	14
0	1 0	1.0	1 0	1 0	1.0	5	0	0	0	0	0	0	0	0	0	0	0	0
0.1	90050	.89748	88679	86126	.78797	.43015	09645	02787	00856	.00211	00084	00042						
0.2	80388	79824	77884	73483	63014	.38269	15433	05251	01680	.00419	.00167	00083	00048	00030	00020			
0.3	.71265	.70518	.68316	.62690	52081	34375	.17964	.07199	02440	.00622	.00250							
0.4	62861	62015	59241	.53767	.44329	31048	18709	.08593	03118									
0.5	.55279	54403	51622	46448	38390	28156	18556	.09499	.03701	01013	00407	.00209	00118	00071	00053	00025	.00014	00009
0.6	48550	47691	45078	40427	33676	25588	17952	.10010										
0.7	42654	.41874	.39491	35428	29833	21727	17124	.10228	04558									
0 8	37531	36832	34729	31243	.26581	21297	16206	.10236										
0 9	33104	32492	30669	27707	23832	19488	15253	.10094										
1	29289	28763	27005	24697	.21468	17868	14329	09849	05185	01742	00761	00393	00226	00143	00097	00050	.00029	00018
1.2	23178	22795	21662	19890	.17626	15101	12570	.09192	05260	.01935	.00871	00459	00269	00171	00115			
1.5	16795	16552	15877	14804	.13436	.11892	10296	08048	.05116	02142	01013	00548	.00325	.00210	00141	00073	00043	00027
2	10557	.10453	10140	09647	09011	08269	07471	06275	04496	.02221	.01160	00659	00399	00264	00180	.00094	00056	00036
2.5	07152	07098	06947	06698	.06373	05974	.05555	.04880	03787	.02143	.01221	00732	.00463	.00308	00214	00115	.00068	00043
3	05132	05101	.05022	.04886	.04707	.04487	.04241	.03839	03150	.01980	.01220	00770	.00505	00346	00242	00132	00079	00051
4	.02986	.02976	.02907	.02802	.02832	02749	02651	.02490	02193	01592	.01109	00768	00536	00384	.00282	00160	00099	00065
5	01942	01938				.01835			01573	.01249	.00949	00708	00527	.00394	00298	00179	00113	00075
6	01361					01307			01168	.00983	.00795	00628	00492	00384	00299	00188	00124	00084
7	01005					00976			00894	00784	.00661	00548	00445	00360	00291	00193	00130	00091
8	.00772					00755			.00703	.00635	00554	00472	00398	00332	00276	00189	00134	00094
9	00612					00600			00566	00520	.00466	00409	00353	00301	00256	00184	00133	00096
10								00477	00465	00438	00397	00352	00326	00273	00241			

Table 2

Function "B"

Depth (Z) in Radii	Offset (ρ) in Radii																	
	0	0 2	0 4	0 6	0 8	1	1 2	1.5	2	3	4	5	6	7	8	10	12	14
0	0	0	0	0	0	0	0	0	0	0	0	0	0	0	0	0	0	0
0.1	09852	10140	11138	13424	18796	05388	-.07899	- 02672	- 00845	- 00210	- 00084	- 00042						
0.2	18857	19306	20772	23524	25983	08513	- 07759	- 04448	- 01593	- 00412	-.00166	- 00083	- 00024	- 00015	- 00010			
0.3	26362	26787	.28018	29483	27257	10757	- 04316	-.04999	- 02166	- 00599	-.00245							
0.4	32016	32259	32748	32273	26925	12404	- 00766	- 04535	- 02522									
0.5	35777	35752	.35323	33106	26236	13591	.02165	-.03455	- 02651	-.00991	- 00388	- 00199	- 00116	- 00073	- 00049	- 00025	- 00014	- 00009
0.6	37831	37531	.36308	32822	25411	14440	04457	-.02101										
0.7	38487	37962	36072	31929	24638	.14986	06209	-.00702	- 02329									
0.8	.38091	37408	.35133	30699	.23779	.15292	.07530	.00614										
0.9	36962	36275	.33734	29299	22891	.15404	.08507	01795										
1	35355	.34553	.32075	27819	.21978	15355	09210	02814	- 01005	- 01115	- 00608	- 00344	- 00210	-.00135	- 00092	- 00048	- 00028	- 00018
1.2	.31485	30730	28481	24836	.20113	14915	10002	04378	00023	- 00995	-.00632	- 00378	- 00236	- 00156	- 00107			
1.5	25602	25025	23338	20694	17368	13732	10193	05745	01385	- 00669	-.00600	- 00401	- 00265	- 00181	- 00126	- 00068	- 00040	- 00026
2	17889	18144	16644	15198	13375	11331	09254	.06371	02836	00028	-.00410	- 00371	- 00278	- 00202	- 00148	- 00084	- 00050	- 00033
2.5	12807	12633	12126	11327	.10298	09130	07869	06022	03429	00661	- 00130	-.00271	- 00250	- 00201	- 00156	- 00094	- 00059	- 00039
3	09487	09394	09099	08635	08033	07325	06551	05354	.03511	01112	.00157	- 00134	- 00192	- 00179	- 00151	- 00099	- 00065	- 00046
4	05707	05666	.05562	05383	05145	04773	04532	.03995	03066	01515	00595	00155	- 00029	- 00094	- 00109	- 00094	- 00068	- 00050
5	03772	03760				03384			02474	01522	00810	00371	00132	00013	- 00043	- 00070	- 00061	- 00049
6	02666					02468			01968	01380	00867	00496	00254	00110	00028	- 00037	- 00047	- 00045
7	01980					01868			01577	01204	.00842	00547	.00332	00185	00093	- 00002	- 00029	- 00037
8	01526					01459			01279	01034	00779	00554	00372	00236	.00141	00035	- 00008	- 00025
9	01212					.01170			.01054	00888	00705	00533	.00386	00265	00178	00066	00012	- 00012
10								00924	00879	00764	.00631	00501	.00382	00281	00199			

Table 3

Function "C"

Depth (Z) in Radii	Offset (ρ) in Radii																	
	0	0.2	0.4	0 6	0.8	1	1.2	1.5	2	3	4	5	6	7	8	10	12	14
0	0	0	0	0	0	0	0	0	0	0	0	0	0	0	0	0	0	0
0.1	-.04926	-.05142	-.05903	-.07708	-.12108	.02247	.12007	.04475	.01536	.00403	.00164	.00082						
0.2	-.09429	-.09755	-.10872	-.12977	- 14552	.02419	.14896	.07892	.02951	.00796	.00325	00164	.00094	00059	.00039			
0.3	-.13181	-.13484	-.14415	-.15023	-.12990	.01988	.13394	.09816	.04148	.01169	.00483							
0.4	-.16008	-.16188	-.16519	-.15985	- 11168	.01292	.11014	.10422	.05067									
0.5	-.17889	-.17835	-.17497	-.15625	-.09833	.00483	.08730	.10125	.05690	.01824	.00778	00399	.00231	.00146	.00098	.00050	.00029	.00018
0.6	-.18915	-.18664	-.17336	-.14934	-.08967	-.00304	.06731	.09313										
0.7	-.19244	-.18831	-.17393	-.14147	-.08409	-.01061	.05028	.08253	.06129									
0.8	- 19046	-.18481	-.16784	-.13393	- 08066	-.01744	.03582	.07114										
0.9	-.18481	-.17841	-.16024	-.12664	-.07828	-.02337	.02359	.05993										
1	-.17678	-.17050	-.15188	-.11995	- 07634	-.02843	.01331	.04939	.05429	.02726	.01333	.00726	00433	.00278	00188	.00098	00057	.00036
1.2	-.15742	-.15117	-.13467	-.10763	-.07289	-.03575	-.00245	.03107	.04552	.02791	.01467	.00824	.00501	.00324	.00221			
1.5	-.12801	-.12277	-.11101	-.09145	-.06711	-.04124	-.01702	.01088	03154	.02652	.01570	.00933	00585	00386	00266	.00141	00083	00039
2	- 08944	-.08491	-.07976	-.06925	-.05560	-.04144	-.02687	-.00782	01267	.02070	.01527	.01013	.00321	00462	00327	.00179	00107	00069
2.5	-.06403	-.06068	-.05839	-.05259	-.04522	-.03605	-.02800	-.01536	.00103	.01384	.01314	00987	.00707	.00506	.00369	00209	00128	00083
3	- 04744	-.04560	-.04339	-.04089	-.03642	-.03130	- 02587	-.01748	-.00528	.00792	.01030	.00888	.00689	.00520	.00392	.00232	.00145	.00096
4	-.02854	-.02737	-.02562	- 02585	-.02421	- 02112	-.01964	-.01586	-.00956	.00038	.00492	00602	.00561	.00476	00389	00254	.00168	00115
5	- 01886	- 01810				-.01568			-.00939	- 00293	-.00128	.00329	.00391	00380	00341	00250	00177	00127
6	-.01333					-.01118			-.00819	-.00405	-.00079	00129	00234	.00272	00272	00227	00173	.00130
7	-.00990					-.00902			-.00678	-.00417	-.00180	- 00004	.00113	.00174	00200	00193	00161	00128
8	-.00763					-.00699			- 00552	-.00393	-.00225	-.00077	.00029	.00096	.00134	.00157	.00143	.00120
9	-.00607					-.00423			-.00452	-.00353	-.00235	-.00118	- 00027	.00037	00082	00124	00122	00110
10								-.00381	-.00373	-.00314	-.00233	-.00137	-.00063	.00030	.00040			

Table 4

Function "D"

Depth (Z) in Radii	Offset (ρ) in Radii																	
	0	0.2	0.4	0.6	0.8	1	1.2	1.5	2	3	4	5	6	7	8	10	12	14
0	0	0	0	0	0	0	0	0	0	0	0	0	0	0	0	0	0	0
0.1	.04926	.04998	.05235	.05716	.06687	.07635	.04108	.01803	.00691	.00193	.00080	.00041						
0.2	.09429	09552	.09900	10546	.11431	.10932	.07139	.03444	.01359	.00384	.00159	.00081	.00047	.00029	00020			
0.3	13181	.13305	.14051	.14062	.14267	.12745	.09078	.04817	01982	.00927	.00238							
0.4	.16008	.16070	.16229	.16288	.15756	.13696	.10248	.05887	.02545									
0.5	17889	.17917	.17826	.17481	16403	.14074	.10894	.06670	.03039	00921	.00390	.00200	00116	.00073	.00049	00025	00015	00009
0.6	.18915	.18867	18573	.17887	.16489	14137	11186	.07212										
0.7	19244	.19132	.18679	17782	.16229	13926	11237	.07551	.03801									
0.8	.19046	.18927	18348	.17306	.15714	13548	11115	.07728										
0.9	.18481	.18349	17709	16635	.15063	.13067	10866	.07788										
1	17678	.17503	.16886	.15824	14344	12513	.10540	.07753	.04456	.01611	.00725	00382	.00224	.00142	00096	.00050	00029	00018
1.2	.15742	.15618	15014	14073	12823	11340	09757	.07484	.04575	.01796	.00835	.00446	.00264	00169	00114			
1.5	12801	12754	.12237	11549	.10657	09608	08491	.06833	.04539	.01983	.00970	.00532	.00320	00205	.00140	00073	.00043	00027
2	08944	.09080	.08668	08273	.07814	.07187	06566	.05589	.04103	02098	.01117	.00643	.00398	.00260	.00179	00095	00056	.00036
2.5	.06403	.06565	06284	.06068	05777	.05525	.05069	.04486	.03532	02045	.01183	00717	00457	.00306	.00213	.00115	00068	.00044
3	.04744	.04834	.04760	.04548	.04391	.04195	.03963	.03606	.02983	.01904	.01187	.00755	.00497	00341	.00242	00133	.00080	00052
4	.02854	.02928	.02996	.02798	.02724	.02661	.02568	.02408	.02110	.01552	.01087	00757	00533	.00382	00280	.00160	00100	.00065
5	01886	.01950				.01816			.01535	.01230	.00939	.00700	.00523	.00392	00299	00180	.00114	.00077
6	.01333					.01351			.01149	.00976	.00788	.00625	.00488	00381	.00301	.00190	00124	.00086
7	.00990					.00966			00899	.00787	.00662	.00542	00445	00360	00292	.00192	00130	.00092
8	00763					.00759			.00727	.00641	.00554	00477	.00402	.00332	.00275	.00192	00131	.00096
9	.00607					00746			.00601	.00533	.00470	.00415	.00358	00303	00260	.00187	.00133	00099
10								.00542	00506	.00450	.00398	.00364	.00319	00278	00239			

Table 5

Function "E"

Depth (Z) in Radii	Offset (ρ) in Radii																	
	0	0 2	0 4	0 6	0.8	1	1.2	1.5	2	3	4	5	6	7	8	10	12	14
0	5	5	.5	.5	.5	5	34722	.22222	12500	05556	03125	02000	.01389	01020	.00781	.00500	.00347	00255
0.1	45025	449494	.44698	.44173	.43008	.39198	30445	20399	.11806	.05362	.03045	.01959						
0.2	40194	400434	.39591	.38660	36798	32802	26598	.18633	.11121	.05170	.02965	.01919	01342	.00991	00762			
0.3	35633	.35428	.33809	33674	.31578	28003	.23311	.16967	.10450	.04979	.02886							
0.4	.31431	31214	.30541	.29298	27243	24200	.20526	.15428	.09801									
0.5	.27639	.27407	.26732	.25511	.23639	21119	18168	14028	09180	04608	.02727	.01800	01272	.00946	00734	00475	.00332	.00246
0.6	.24275	.24247	.23411	.22289	.20634	.18520	.16155	.12759										
0.7	.21327	.21112	.20535	.19525	.18093	16356	.14421	.11620	.08027									
0.8	.18765	.18550	.18049	17190	.15977	.14523	.12928	.10602										
0.9	.16552	.16337	.15921	.15179	.14168	.12954	.11634	.09686										
1	.14645	.14483	.14610	.13472	.12618	.11611	.10510	.08865	.06552	.03736	.02352	.01602	.01157	.00874	.00683	00450	.00318	.00237
1.2	.11589	.11435	.11201	.10741	.10140	.09431	.08657	.07476	.05728	.03425	.02208	.01527	.01113	00847	.00664			
1.5	.08398	.08356	.08159	.07885	.07517	.07088	.06611	.05871	.04703	.03003	.02008	01419	.01049	00806	.00636	.00425	.00304	.00228
2	.05279	05105	.05146	.05034	.04850	.04675	.04442	.04078	.03454	.02410	.01706	.01248	.00943	.00738	00590	.00401	.00290	00219
2.5	.03576	.03426	.03489	.03435	.03360	.03211	.03150	.02953	02599	.01945	.01447	.01096	.00850	00674	.00546	00378	.00276	00210
3	.02566	.02519	.02470	.02491	.02444	.02389	.02330	.02216	.02007	.01585	.01230	.00962	.00763	.00617	00505	.00355	00263	00201
4	.01493	01452	.01495	.01526	.01446	.01418	.01395	.01356	.01281	.01084	.00900	00742	.00612	00511	00431	00313	00237	.00185
5	.00971	00927				.00929			.00873	.00774	.00673	.00579	.00495	00425	.00364	.00275	.00213	.00168
6	.00680					.00632			.00629	00574	.00517	00457	.00404	00354	00309	00241	00192	00154
7	.00503					.00493			.00466	.00438	.00404	.00370	.00330	.00296	.00264	.00213	.00172	00140
8	.00386					.00377			.00354	.00344	.00325	.00297	.00273	.00250	.00228	.00185	00155	.00127
9	.00306					.00227			00275	00273	.00264	.00246	.00229	.00212	.00194	.00163	00139	00116
10								00210	.00220	.00225	00221	.00203	.00200	.00181	.00171			

Table 6

Function "F"

Depth (Z) in Radii	Offset (ρ) in Radii																	
	0	0 2	0 4	0 6	0 8	1	1 2	1.5	2	3	4	5	6	7	8	10	12	14
0	5	.5	5	5	5	0	-.34722	-.22222	-.12500	-.05556	-.03125	-.02000	- 01389	- 01020	- 00781	- 00500	-.00347	- 00255
0.1	45025	.44794	43981	41954	.35789	03817	-.20800	-.17612	-.10950	-.05151	- 02961	- 01917						
0 2	40194	39781	38294	34823	26215	05466	- 11165	-.13381	- 09441	- 04750	-.02798	-.01835	-.01295	-.00961	- 00742			
0.3	.35633	.35094	34508	29016	20503	06372	- 05346	- 09768	- 08010	-.04356	-.02636							
0.4	31431	30801	.28681	.24469	.17086	.06848	-.01818	-.06835	- 06684									
0.5	.27639	.26997	24890	20937	.14752	07037	00388	- 04529	-.05479	- 03595	-.02320	-.01590	-.01154	- 00875	- 00681	-.00450	-.00318	-.00237
0.6	24275	.23444	21667	18138	13042	07068	01797	- 02749										
0.7	21327	.20762	.18956	.15903	11740	.06963	.02704	-.01392	-.03469									
0.8	18765	.18287	16679	14053	10604	06774	03277	- 00365										
0.9	16552	16158	14747	.12528	.09664	.06533	.03619	00408										
1	.14645	.14280	12395	11225	.08850	.06256	03819	.00984	- 01367	-.01994	-.01591	-.01209	-.00931	-.00731	- 00587	-.00400	- 00289	-.00219
1.2	11589	.11360	10460	09449	07486	05670	03913	.01716	- 00452	- 01491	-.01337	- 01068	- 00844	-.00676	- 00550			
1.5	08398	08196	.07719	.06918	.05919	04804	03686	.02177	.00413	- 00879	-.00995	- 00870	-.00723	- 00596	- 00495	-.00353	- 00261	- 00201
2	05279	05348	04994	04614	04162	03593	03029	02197	.01043	-.00189	-.00546	- 00589	-.00544	- 00474	-.00410	-.00307	- 00233	-.00183
2.5	03576	.03673	.03459	03263	.03014	02762	02406	01927	01188	00198	-.00226	- 00364	-.00386	- 00366	- 00332	- 00263	- 00208	- 00166
3	02566	.02586	02255	02395	02263	02097	.01911	01623	.01144	.00396	-.00010	- 00192	-.00258	- 00271	- 00263	- 00223	- 00183	- 00150
4	01493	.01536	.01412	01259	01386	.01331	.01256	.01134	.00912	.00508	.00209	.00026	- 00076	- 00127	-.00148	- 00153	-.00137	-.00120
5	.00971	01011				00905			00700	.00475	00277	00129	.00031	-.00030	- 00066	- 00096	- 00099	- 00093
6	00680					00675			00538	00409	.00278	.00170	00088	00030	- 00010	- 00053	-.00066	-.00070
7	00503					00483			00428	00346	.00258	00178	00114	.00064	00027	-.00020	- 00041	- 00049
8	00386					00380			.00350	.00291	.00229	.00174	.00125	00082	.00048	.00003	-.00020	-.00033
9	00306					00374			00291	00247	.00203	.00163	00124	00089	00062	00020	- 00005	- 00019
10								00267	00246	.00213	.00176	00149	.00126	00092	00070			

Table 7

Function "G"

Depth (Z) in Radii	Offset (ρ) in Radii																	
	0	0.2	0.4	0.6	0.8	1	1.2	1.5	2	3	4	5	6	7	8	10	12	14
0	0	0	0	0	0	.31831	0	0	0	0	0	0	0	0	0	0	0	0
0.1	0	.00315	.00802	.01951	.06682	.31405	.05555	.00865	.00159	.00023	.00007	.00003						
0.2	0	.01163	.02877	.06441	.16214	.30474	.13592	.03060	.00614	.00091	.00026	.00010	.00005	00003	.00002			
0.3	0	.02301	.05475	.11072	.21465	.29228	.18216	05747	.01302	00201	.00059							
0.4	0	.03460	.07883	.14477	23442	.27779	.20195	.08233	.02138									
0.5	0	.04429	.09618	.16426	.23652	.26216	.20731	.10185	03033	.00528	.00158	00063	.00030	00016	00009	.00004	00002	00001
0.6	0	.04966	.10729	17192	.22949	.24574	.20496	.11541										
0.7	0	.05484	.11256	.17126	.21772	.22924	19840	.12373	04718									
0.8	0	.05590	.11225	.16534	.20381	.21295	.18953	.12855										
0.9	0	.05496	.10856	.15628	.18904	.19712	.17945	.28881										
1	0	.05266	.10274	.14566	.17419	.18198	.16884	.12745	06434	.01646	.00555	.00233	.00113	.00062	00036	.00015	.00007	.00004
1.2	0	.04585	.08831	.12323	.14615	.15408	14755	.12038	.06967	.02077	.00743	.00320	.00159	.00087	00051			
1.5	0	.03483	.06688	.09293	.11071	.11904	.11830	.10477	.07075	.02599	.01021	.00460	.00233	00130	00078	.00033	00016	.00009
2	0	.02102	.04069	.05721	.06948	.07738	.08067	.07804	.06275	.03062	.01409	.00692	00369	.00212	00129	00055	00027	.00015
2.5	0	.01293	.02534	.03611	.04484	.05119	.05509	.05668	.05117	.03099	.01650	.00886	.00499	.00296	.00185	.00082	.00041	.00023
3	0	.00840	.01638	.02376	.02994	.03485	.03843	.04124	.04039	.02886	.01745	.01022	.00610	.00376	.00241	.00110	.00057	00032
4	0	.00382	.00772	.01149	.01480	.01764	.02004	.02271	.02475	.02215	.01639	.01118	.00745	.00499	00340	00167	.00090	00052
5	0	.00214				.00992		.01343	.01551	.01601	.01364	.01105	.00782	.00560	.00404	.00216	.00122	00073
6	0					.00602		.00845	.01014	01148	.01082	00917	00733	.00567	.00432	.00243	.00150	00092
7	0					.00396			00687	.00830	.00842	00770	.00656	00539	00432	.00272	.00171	.00110
8	0					.00270			.00481	.00612	.00656	.00631	.00568	00492	00413	00278	00185	.00124
9	0					.00177			00347	.00459	.00513	.00515	.00485	00438	.00381	00274	00192	00133
10	0							.00199	.00258	.00351	.00407	.00420	00411	.00382	00346			

Table 8

Function "H"

Depth (Z) in Radii	Offset (ρ) in Radii																
	0	0.2	0.4	0.6	0 8	1	1.2	1.5	2	3	4	5	6	7	8	10	12	14
0	2 0	1 97987	1.91751	1.80575	1.62553	1.27319	.93676	.71185	51671	.33815	.25200	20045	.16626	14315	12576	.09918	08346	07023
0.1	1 80998	1.79018	1.72886	1.61961	1 44711	1.18107	.92670	.70888	51627	.33794	.25184	20081						
0.2	1.63961	1.62068	1.56242	1 46001	1 30614	1 09996	.90098	70074	51382	.33726	.25162	.20072	16688	14288	12512			
0.3	1.48806	1.47044	1 40979	1 32442	1 19210	1.02740	.86726	.68823	.50966	33638	.25124							
0.4	1.35407	1.33802	1.28963	1.20822	1.09555	.96202	.83042	.67238	.50412									
0.5	1.23607	1.22176	1.17894	1.10830	1.01312	.90298	79308	65429	.49728	.33293	.24996	.19982	.16668	.14273	.12493	09996	08295	.07123
0.6	1 13238	1.11998	1.08350	1.02154	94120	.84917	.75653	.63469										
0.7	1 04131	1.03037	.99794	91049	.87742	.80030	72143	.61442	.48061									
0.8	.96125	.95175	.92386	87928	.82136	.75571	.68809	.59398										
0.9	.89072	.88251	.85856	.82616	.77950	.71495	.65677	.57361										
1	.82843	.85005	.80465	.76809	.72587	.67769	62701	.55364	.45122	.31877	.24386	.19673	16516	.14182	.12394	09952	08292	07104
1.2	.72410	.71882	70370	67937	.64814	.61187	.57329	51552	43013	.31162	.24070	.19520	.16369	14099	12350			
1.5	.60555	60233	.57246	.57633	.55559	.53138	50496	46379	39872	.29945	.23495	.19053	.16199	14058	12281	09876	08270	07064
2	47214	.47022	.44512	.45656	.44502	.43202	41702	39242	35054	.27740	.22418	.18618	15846	13762	12124	09792	08196	07026
2 5	.38518	.38403	.38098	.37608	36940	36155	35243	.33698	30913	.25550	.21208	17898	15395	13463	11928	09700	08115	06980
3	32457	.32403	.32184	31887	.31464	30969	30381	.29364	27453	23487	.19977	17154	14919	13119	.11694	09558	.08061	06897
4	24620	24588	24820	.25128	24168	23932	23668	23164	22188	19908	.17640	15596	13864	12396	.11172	09300	.07864	06848
5	.19805	.19785				.19455			18450	17080	.15575	14130	12785	11615	10585	08915	07675	06695
6	16554					.16326			.15750	14868	13842	12792	11778	10836	.09990	08562	.07452	06522
7	14217					14077			.13699	.13097	.12404	11620	10843	.10101	09387	08197	07210	06377
8	12448					12352			12112	.11680	.11176	.10600	09976	.09400	08848	.07800	06928	06200
9	.11079					.10989			10854	.10548	.10161	.09702	.09234	08784	08298	07407	06678	05976
10								.09900	09820	.09510	.09290	08980	08300	08180	07710			

The computations, however, involve elliptic functions and were made through use of values tabulated by Legendre in 1826 (4). Direct determination of elliptic functions as part of a computer program is sufficiently complex and time consuming that extensive results of the type being presented herein have not been programmed, computed, and reported.

The simple relations which combine the tabulated functions and Poisson's ratio to give stresses, strains, or deflections are

Bulk stress

$$\theta = 2p(1+\nu)A = \sigma_z + \sigma_\rho + \sigma_\theta = e\frac{E_m}{1-2\nu} \tag{1}$$

Vertical stress

$$\sigma_z = p\left[A + B\right] \tag{2}$$

Radial horizontal stress

$$\sigma_\rho = p\left[2\nu A + C + (1-2\nu)F\right] \tag{3}$$

Tangential horizontal stress

$$\sigma_\theta = p\left[2\nu A - D + (1-2\nu)E\right] \tag{4}$$

Vertical-radial shear stress

$$\tau_{\rho z} = \tau_{z\rho} = pG \tag{5}$$

Bulk strain

$$e = p\frac{2(1+\nu)}{E_m}(1-2\nu)A = \epsilon_z + \epsilon_\rho + \epsilon_\theta = \theta\frac{1-2\nu}{E_m} \tag{6}$$

Vertical strain

$$\epsilon_z = p\frac{1+\nu}{E_m}\left[(1-2\nu)A + B\right] \tag{7}$$

Radial horizontal strain

$$\epsilon_\rho = p\frac{1+\nu}{E_m}\left[(1-2\nu)F + C\right] \tag{8}$$

Tangential horizontal strain

$$\epsilon_\theta = p\frac{1+\nu}{E_m}\left[(1-2\nu)E - D\right] \tag{9}$$

Vertical-radial shear strain

$$\gamma_{\rho z} = \gamma_{z\rho} = p\frac{2(1+\nu)}{E_m}G = \frac{2(1+\nu)}{E_m}\tau_{\rho z} \tag{10}$$

Vertical deflection

$$\omega_z = p\frac{1+\nu}{E_m}r\left[zA + (1-\nu)H\right] \tag{11}$$

Radial horizontal deflection

$$\omega_\rho = p\frac{1+\nu}{E_m}(-\rho r)\left[(1-2\nu)E - D\right] = -\rho r\epsilon_\theta \tag{12}$$

Tangential horizontal deflection

$$\omega_\theta = 0 \tag{13}$$

Symbols and sign conventions follow Timoshenko (6). Figure 1 may give a clearer concept of most of the symbols.

A, B, C ... H = functions, whose values are given in Tables 1 through 8;
z, ρ, θ = coordinate distances in radii, cylindrical coordinates—positive to the right, outward, and downward;
σ = normal stress—positive for compression;
σ_z, σ_ρ, σ_θ = letter subscript indicates axis parallel to which the line of action of the stress lies;
Θ = sum of three mutually perpendicular normal stresses at a point;
τ = shear stress—positive in positive quadrant and negative in mixed quadrant;
$\tau_{\rho z}$ = letter subscripts for shear stresses indicate (a) direction perpendicular to plane on which stress acts, and (b) the direction in which it acts;
γ = shearing strain;
$\gamma_{\rho z}$ = subscripts for shearing strain have same meanings as those for shear stress;
ϵ = strain—positive for compression;
ϵ_z, ϵ_ρ, ϵ_θ = subscripts for strain have same meanings as those for normal stress;
e = sum of three mutually perpendicular strains at a point;
ω = deflection—positive downward and outward;
ω_z, ω_ρ, ω_θ = subscripts for deflection have same meanings as those for normal stress;
ν = Poisson's ratio;
E_m = modulus of elasticity in compression—always positive;
p = surface contact pressure; and
r = radius of circular loaded area.

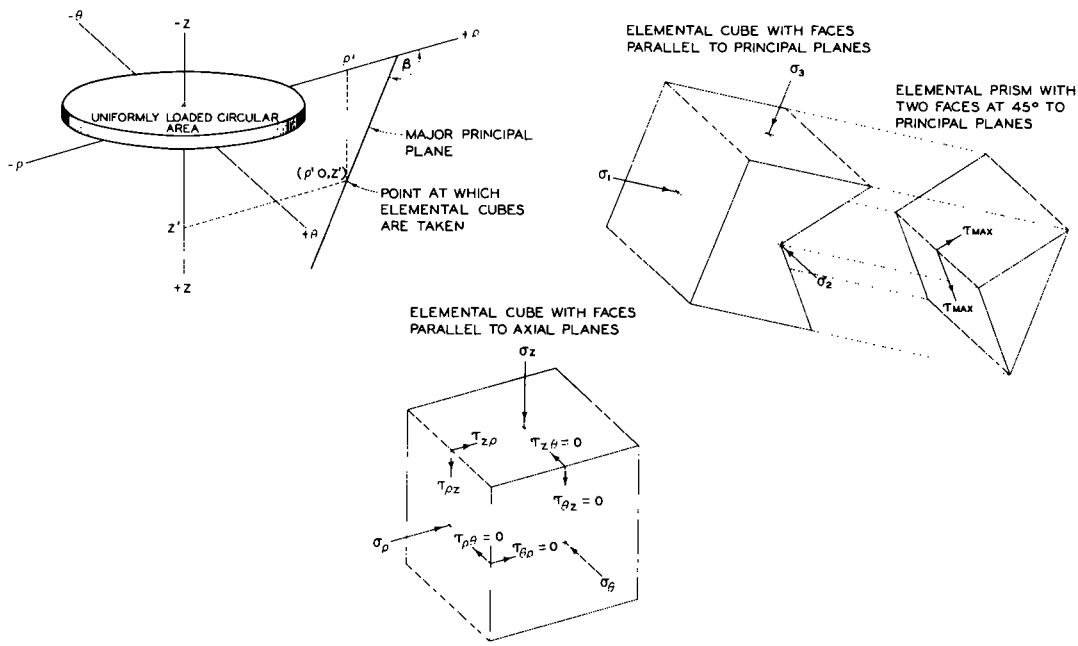

Figure 1. Stress directions.

From the symmetry of the circular load, it can readily be seen that there is no shear on vertical planes through the load axis. It follows that these must be principal planes; therefore, the tangential-horizontal stress, σ_ρ, must be a principal stress (the same is true for strain). The remaining two principal stresses may be obtained from the following expression:

$$\sigma_{1,\,2,\,3} = \frac{(\sigma_z + \sigma_\rho) \pm \sqrt{(\sigma_z - \sigma_\rho)^2 + (2\tau_{\rho z})^2}}{2}$$

in which $\sigma_{1,\,2,\,3}$ are principal stresses. Maximum shear stress, τ_{max}, may be obtained from the expression:

$$\tau_{max} = \frac{\sigma_1 - \sigma_3}{2}$$

These expressions can be found elsewhere (6, 7, or in almost any textbook on mechanics). They are included here for ready reference.

As an example of the use of the functions and equations presented, assume that vertical stress, strain, and deflection values are desired at a depth of 3.0 radii and offset of 6.0 radii for a Poisson's ratio of 0.3, modulus of elasticity of 10,000 psi, and surface contact pressure of 100 psi for a circular loaded area of 10-in. radius. Vertical stress, σ_z, will be determined from Eq. 2. Taking the value of function A from Table 1, for 3 radii depth and 6 radii offset, to be 0.00505 and for B from Table 2 to be -0.00192 and substituting it in Eq. 2,

$$\sigma_z = 100\,(0.00505 - 0.00192) = 0.313 \text{ psi}$$

Vertical strain, ϵ_z, is determined from Eq. 7. Inasmuch as functions A and B again apply, the preceding values again are used. Substituting them in Eq. 7,

$$\epsilon_z = 100\,\frac{1 + 0.3}{10,000}\,\Big[(1 - 0.6)0.00505 - 0.00192\Big] = 13 \times 10^{-7} \text{ in./in.}$$

Vertical deflection, ω_z, is determined from Eq. 11. Function A again applies, but function H must be obtained for 3 radii depth and 6 radii offset in Table 8. The value is 0.14919. Substituting in Equation 11,

$$\omega_z = 100\,\frac{1 + 0.3}{10,000}\;10\Big[(3)0.00505 + (1 - 0.3)\,0.14919\Big] = 0.015545 \text{ in.}$$

In summary, this paper presents tabular values for eight functions that can be combined in simple equations to give values of coordinate normal or shear stress or strain or of coordinate deflections for any desired value of Poisson's ratio for a uniformly distributed, circular load on an elastic, homogeneous, isotropic half space. Values are presented to five decimal place accuracy for each radius of offset from the load axis up to 14 and for each radius of depth up to 9. Values for fractional radii offset and depth are given to depths up to 4 radii for points beneath and just out from under the load. The paper is being presented for use as a reference to the computational results included rather than for the more usual purpose of reporting recent research findings.

REFERENCES

1. Barber, E. S., "Application of Triaxial Compression Test Results to the Calculation of Flexible Pavement Thickness." HRB Proc., 26: 26-39 (1946).
2. Fergus, S. M., and Miner, W. E., "Distributed Loads on Elastic Foundations: The Uniform Circular Load." HRB Proc., 34:582-597 (1955).
3. Foster, C. R., and Ahlvin, R. G., "Stresses and Deflections Induced by a Uniform Circular Load." HRB Proc., 33:467-470 (1954).
4. Legendre, A. M., "Traite des Fonctions Elliptiques." Vol. II, Paris (1826). (Available at John Crerar Library, Chicago, Ill.)

5. Love, A. E. H., "The Stress Produced in a Semi-Infinite Body by Pressure on Part of the Boundary." Philosoph. Trans., Royal Society, Series, A, Vol. 228 (1929).

6. Timoshenko, S., "Theory of Elasticity." McGraw-Hill (1934).

7. U. S. Army Engineer Waterways Experiment Station, "Investigations of Pressures and Deflections for Flexible Pavements. Report 1, Homogeneous Clayey-Silt Test Section." Tech. Memo. 3-323, Vicksburg, Miss. (March 1951).

8. U. S. Army Engineer Waterways Experiment Station, "Investigations of Pressures and Deflections for Flexible Pavements. Report 3, Theoretical Stresses Induced by Uniform Circular Loads." Tech. Memo. 3-323, Vicksburg, Miss. (Sept. 1953).

9. U. S. Army Engineer Waterways Experiment Station, "Investigations of Pressures and Deflections for Flexible Pavements. Report 4, Homogeneous Sand Test Section." Tech. Memo. 3-323, Vicksburg, Miss. (Dec. 1954).

Distribution of Stresses on an Unyielding Surface Beneath a Pneumatic Tire

D. R. FREITAG and A. J. GREEN, Respectively, Chief and Engineer, Mobility Section, Army Mobility Research Center, U. S. Army Engineer Waterways Experiment Station, CE, Vicksburg, Miss.

Small diaphragm-type pressure-sensitive cells were set flush with the surface of a rigid steel plate to measure vertical pressures beneath pneumatic tires. Measurements were made while the tire was stationary and while it was moving at about 2 mph. Tests were made with several sizes of smooth-tread tires to evaluate the effect of load, inflation pressure, and type of tire construction on the magnitude and distribution of pressures at the tire-surface interface. The data show that under many conditions the distribution of pressures over the contact area was far from uniform.

•THE ASSIGNED MISSION of the Army Mobility Research Center, U. S. Army Engineer Waterways Experiment Station, Vicksburg, Miss., is to conduct research that will lead to an increased capability of the Army to travel off the road.

Before any marked improvement in the mobility of military vehicles can be effected, a basic understanding of how soft, yielding soils support and provide traction to wheeled and tracked vehicles must be developed. One phase of the research being conducted at the AMRC to acquire this knowledge is concerned with the distribution of stresses induced by a pneumatic tire in the medium on which it operates. It includes the measurement of stresses at the interface between the tire and the surface that supports it and at locations within a yielding mass of soil.

This paper describes results obtained from that portion of the research dealing with the interface stresses beneath a pneumatic tire on an unyielding surface.

TEST APPARATUS

Pressure Cells

Commercially available pressure-sensitive cells of the deflecting-diaphragm type, manufactured by Consolidated Electrodynamic Corporation, were used to measure the stresses. These cells were ½ in. in diameter and were fitted into holes in a rigid steel plate. The surfaces of the cells were aligned with the plane of the upper surface of the plate. These cells, particularly when inserted in the plate, are insensitive to lateral forces and, it is believed, give accurate measurements of the vertical stresses caused by the imposed tire loads at the surface. Bonse and Kühn have done similar work (1); however, they measured horizontal as well as vertical forces.

Tires

The tires used in this program were selected from among those being used in other phases of the mobility research programs to provide a range of sizes, shapes, and constructional details. All were tested without tread. These tires are shown in Figure 1 and a brief description of each is given in Table 1.

TABLE 1

TEST TIRES

Size	No. of Plies	Original Tire Tread Pattern	Construction	Section Height[1] (in.)
11.00-20	12	Military, nondirectional cross-country	Conventional	9.03
9.00-14	8	Molded smooth without tread	Conventional	5.48
9.00-14	2	Molded smooth without tread	Conventional	6.05
6.00-16	4	High-speed highway	Conventional	4.91
6.00-16	4	Agricultural lug	Radial ply	5.20
16.00-15	2	Molded smooth without tread	Bag-type tire	5.28

[1] Section height is vertical distance from highest point on rim to a plane tangent to crown as unloaded tire.

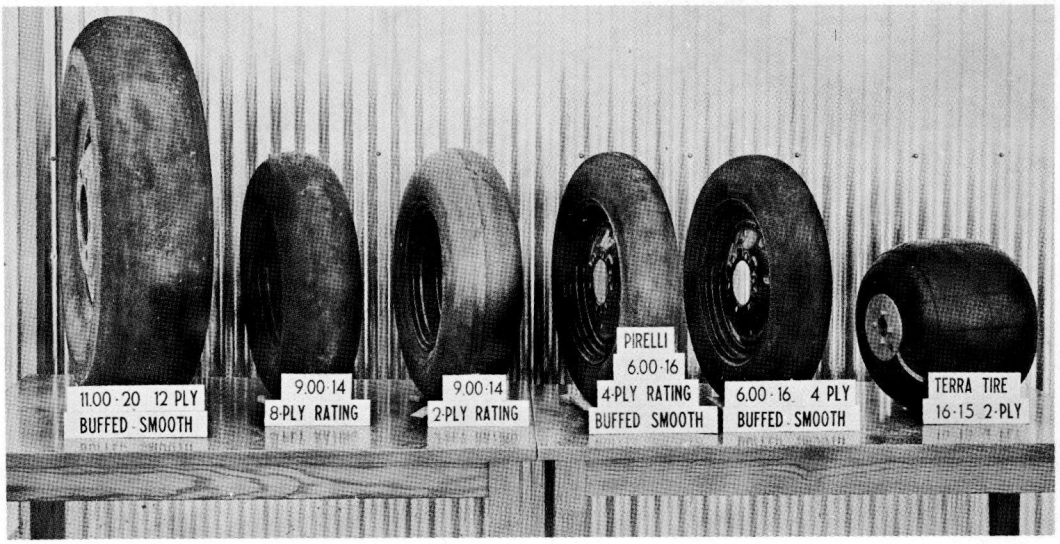

Figure 1. Tires used in program.

TEST PROCEDURES

The test tire was mounted in a single-wheel mobility test carriage, as shown in Figure 2, and towed slowly (about 1 ft per sec) over the steel plate containing from 2 to 10 cells inset side by side. The relative position of the tire with respect to each of the cells was carefully measured and recorded, as was the total width of tire actually in contact with the surface. The response of each cell to the tire load was recorded continuously on an oscillograph. A typical cell registration is shown in Figure 3.

After the wheel had rolled over the cells, it was lifted off the surface, shifted laterally a predetermined distance, and rolled over the cells again to obtain stress measurements at a different line on the face of the tire. When only two cells were employed, many such shifts were made. In all tests replicate measurements were made. These included stress measurements under the same point on the tire by means of more than one pressure cell.

During the repeated passes of the test tires, it was found that the data scatter was decreased and reproducibility enhanced by causing the same cross-section of the tire to contact the same cells on every pass. Apparently slight differences in smoothness

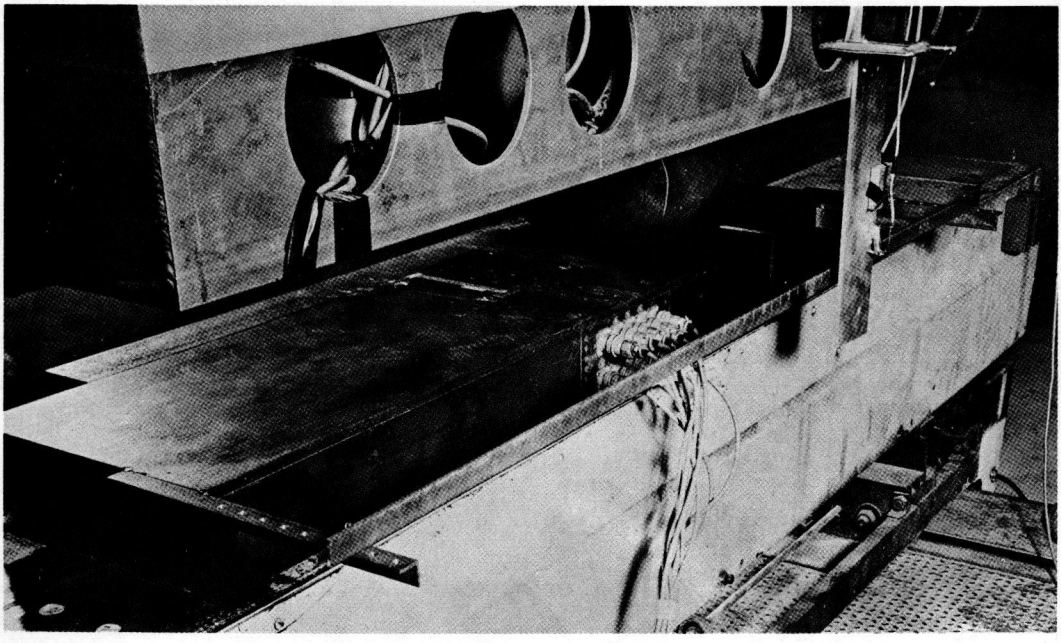

Figure 2. Arrangement for measuring contact pressure on a hard surface with 9.00-14 smooth tire in place.

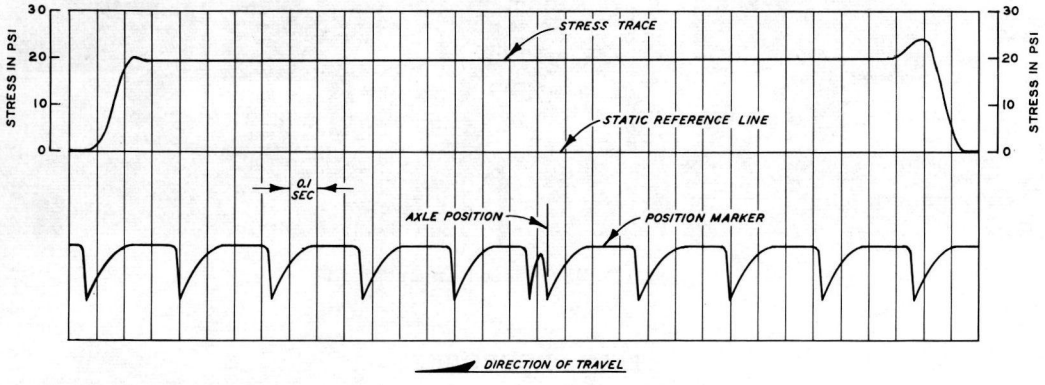

Figure 3. Typical recording, 9.00-14, 2-PR smooth tire, 890-lb load, 25 percent deflection.

of the tire surface can cause differences in the registration of the cell. These difficulties were especially pronounced in the case of the 6.00-16 radial-ply tire. This tire originally had a heavy lug tread. Buffing left the outside surface of the tire fairly smooth, but a variable wall thickness was evidenced by a rippled interior surface.

RESULTS OF TESTS

Method of Presenting Data

The raw data from the test runs consist of a series of pressure cell registrations, each representing the variation in pressure induced over the length of the tire contact area at a particular distance from the centerline of the tire path. These registrations

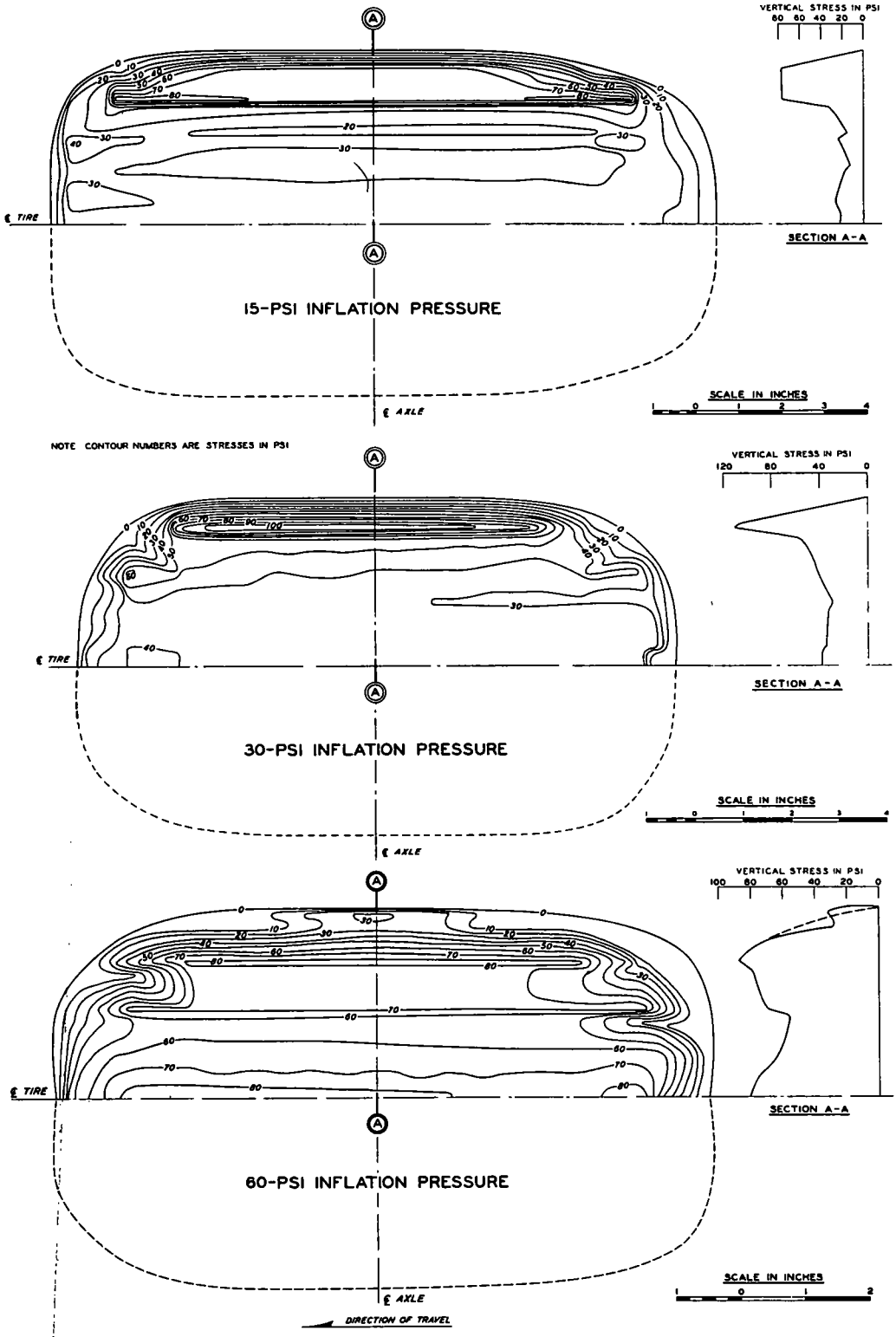

Figure 4. Distribution of vertical stresses under 11.00-20, 12-PR smooth tire, 3,000-lb load, at three inflation pressures.

are readily converted to stresses by means of the cell calibrations and, as such, represent longitudinal sections of the total stress pattern. From the longitudinal sections and the recorded distance that each cell was offset from the path centerline, lateral sections of the stress pattern are drawn. Finally, if desired, a plan of the dynamic tire-contact patch can be drawn and on it a map of equal stress lines constructed.

Effect of Inflation Pressure on Interface Stresses

The effect of tire inflation pressure on the distribution of vertical interface stresses is illustrated by the stress maps shown in Figure 4. These maps were developed from data obtained in tests with the 11.00-20, 12-PR tire carrying a 3,000-lb load.

It can be seen that the interface stresses are not uniformly distributed, particularly at the lower inflation pressures. A ridge of high pressure, which probably results from the transmission of the load through the relatively stiff tire sidewalls, is found to exist at each side of the contact patch. There is a tendency, also, for an area of relatively high stress to exist at the leading and trailing edges of the contact area.

A summary of the stress data shown in Figure 4 is given in Table 2.

These data reveal that the average contact pressure was greater than the inflation pressure for 15- and 30-psi inflation and less for 60-psi inflation. The stress recorded in the central portion of the contact area appears to bear a fairly consistent relation to the inflation pressure. On the other hand, the maximum stress recorded is relatively constant and independent of inflation pressure. The exception to this generalization, the localized high stresses recorded at 30-psi inflation pressure, could have been due to tire irregularities. In all instances the magnitude of the maximum stress is much greater than might be expected on the basis of the inflation pressures. The load computed from these stresses ranges from 1.2 to 13.9 percent higher than the measured load. Similar work is reported by Vanden Berg and Gill of the National Tillage Machinery Laboratory, U.S. Dept. of Agriculture (2).

Effect of Tire Load on Interface Stress

Figure 5 shows lateral and longitudinal sections of the stress patterns developed by the 11.00-20, 12-PR tire at each of three tire loads, 1,500, 3,000, and 4,500 lb. Wheel loads computed from these stress measurements were 1,641, 3,154, and 4,693 lb, respectively. The inflation pressure was maintained constant at 30 psi in all of these tests. The lateral section delineates the stresses beneath the axle centerline, and the longitudinal section shows those at the centerline of the tire path (see Fig. 5). These sections are simpler to construct and view than are the stress maps, and indicate the stresses almost as well.

TABLE 2

SUMMARY OF STRESS DATA

Tire	Inflation Pressure (psi)	Tire Deflection[1] (%)	Stress at Center Point (psi)	Ratio of Inflation Pressure to Center Point Stresses[2]	Average Contact Pressure (3,000 Lb/ Contact Area)(psi)	Maximum Stress Measured (psi)	Measured Wheel Load (lb)	Computed Wheel Load[3] (lb)	Ratio of Maximum Stress to Center Point Stresses
11.00-20, 12-PR	15	30.4	21	0.72	26.5	89	3,000	3,418	4.26
	30	19.4	39	0.77	37.0	111	3,000	3,154	2.84
	60	12.5	80	0.75	52.3	88	3,000	3,035	1.10

[1]Tire deflection is defined as difference between unloaded and loaded tire section heights (as measured from rim to hard surface) divided by the unloaded tire section height, all multiplied by 100

[2]Stress recorded in central portion of contact area

[3]Load computed from measured stresses

The pattern of distribution of stress across the lateral sections is different from each test load. The variation does not seem to follow a consistent trend with the change in load, however. This suggests that at least some of the stress variation may be due to tire surface irregularities. The data for the 3,000-lb, 30-psi load are the same as described previously, and there was some doubt of the accuracy of the maximum stress registration in that comparison also.

Although a rather broad generalization must be made, the data appear to suggest that the maximum stresses, which are recorded at the edges of the contact area, are chiefly a function of the load. The stresses at the interior of the contact area, with some notable exceptions, could be said to be independent of load and, therefore, probably determined principally by the inflation pressure. The average contact pressures for the 1,500-, 3,000-, and 4,500-lb loads are 35.1, 37.0, and 38.8 psi, respectively, increasing approximately in proportion to the wheel load.

Effect of Number of Plies in Tire Carcass on Interface Stresses

The two 9.00-14 tires used in the tests described in this section were constructed in the same mold using the same type of material. They are intended to be identical, insofar as possible, in all respects except in the number of cord layers used in their construction. To date, stresses under these tires have been measured only for one tire load and at relatively few inflation pressures, but the effect of the sidewall stiffness on the stresses is very evident in the data obtained.

Stress maps and lateral sections under the axle center line are shown for the two tires in Figure 6; both tires carried the same load. The inflation pressures were

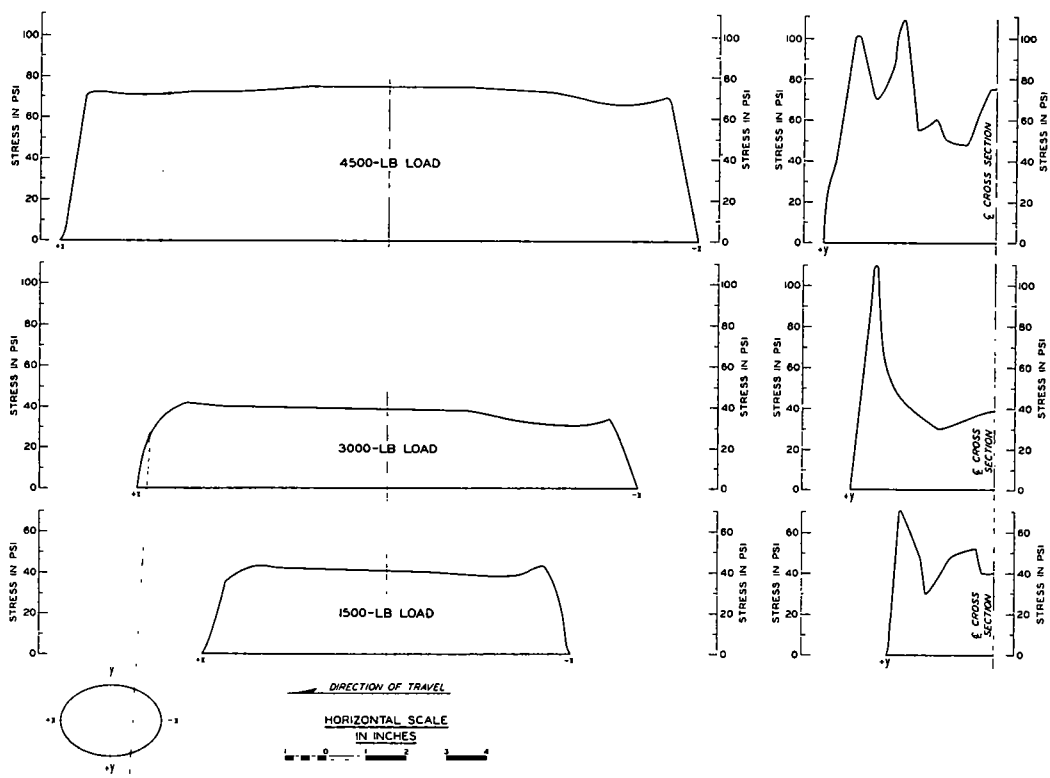

Figure 5. Vertical stresses along principal axes of contact ellipse, 11.00-20, 12-PR smooth tire, 30-psi inflation pressure.

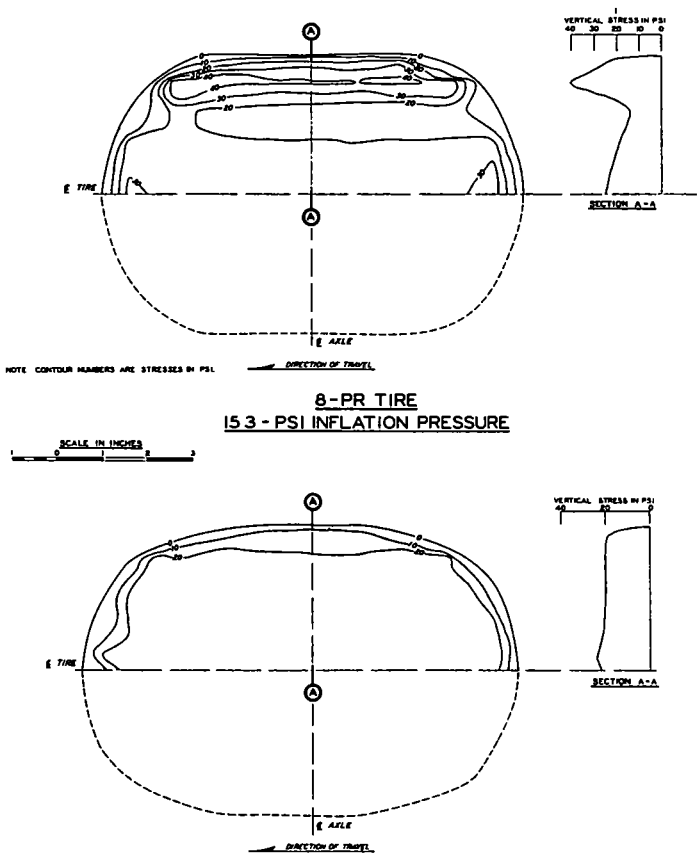

Figure 6. Distribution of vertical stresses under two 9.00-14 tires of different ply ratings, 890-lb load, 25 percent deflection.

TABLE 3

DISTRIBUTION OF VERTICAL STRESSES UNDER TWO 9 00-14 TIRES OF DIFFERENT PLY RATINGS

Tire	Inflation Pressure (psi)	Tire Deflection (%)	Stress at Center Point (psi)	Ratio of Inflation Pressure to Center Point Stresses	Average Contact Pressure (890 Lb/ Contact Area) (psi)	Maximum Stress Measured (psi)	Measured Wheel Load (lb)	Computed Wheel Load (lb)	Ratio of Maximum Stress to Center Point Stresses
9.00-14, 8-PR	15 3	25	25	0.75	16.9	49	890	1,082	2.40
9 00-14, 2-PR	17.6	25	22	0.90	16.3	26	890	977	1.32

adjusted to allow the same percentage deflection and, as a consequence, to obtain about the same average contact pressure—16.3 psi for the 2-PR tire, 16.9 psi for the 8-PR tire.

Table 3 gives a summary of the data in Figure 6.

For these conditions it is apparent that the stiffer tire distributes its load less evenly than the more flexible tire. The stress pattern under the 9.00-14, 8-PR tire is similar in most respects to the patterns found for the 11.00-20, 12-PR tire; i.e., there are zones of high pressure near the sides and near the leading and trailing edges, the maximum stresses are much higher than the inflation pressure, and the ratio of the inflation pressure to the measured interior pressure is about 0.75.

The average pressure under the 9.00-14, 2-PR tire is very close to the inflation pressure. The maximum stresses are comparatively low and not markedly greater than the inflation pressure. The ratio of inflation pressure to the measured stresses in the interior of the contact area for this 2-PR tire is about 0.90.

Effect of Type of Construction on Interface Stresses

Stress measurements were made beneath tires representing three rather dissimilar types of construction. Unfortunately, the sizes and shapes of the tires also were different, and a quantitative comparison of construction effects on stress magnitudes is therefore very difficult. These tires were (a) a conventionally constructed tire in which the plies cross at approximately a 45° angle, (b) a radial ply or belted tire in which one set of cords radiates from the tire axis and the other crosses at about 90°, being wrapped around the tire periphery, and (c) a bag-type tire in which the construction process is designed to create a tire with a roughly rectangular cross-section instead of the usual circular cross-section.

Longitudinal and lateral sections of the stress pattern measured under each of these tires are shown in Figure 7. A 6.00-16, 4-PR tire was the only size of radial-ply tire available for the tests. Therefore, to provide the closest possible comparison, data for a conventionally constructed tire were collected using a standard 6.00-16, 4-PR passenger-car tire buffed smooth. The bag-type tire used is the largest tire of this type that could be fitted readily into the test apparatus. All the tests were run with the same tire loading, and tire deflection was controlled rather than the inflation pressure.

Stresses along the lateral and longitudinal axles beneath the standard 6.00-16, 4-PR tire are shown in Figure 7a. The ratio of the average measured interior stresses to the inflation pressure is 0.84 at 35 percent deflection and 0.78 at 15 percent deflection. A ridge of higher stresses exists near the edge of the contact area when the tire is deflected by 35 percent. The ratio of the stresses along this ridge to the average measured interior stress is 1.67. Table 4 contains data related to the standard 6.00-16, 4-PR tire and the radial-ply 6.00-16, 4-PR tire.

TABLE 4

COMPARISON OF TWO 4-PR TIRES

Tire	Inflation Pressure (psi)	Tire Deflection (%)	Stress at Center Point (psi)	Ratio of Inflation Pressure to Center Point Stresses	Average Contact Pressure (890 Lb/ Contact Area) (psi)	Maximum Stress Measured (psi)	Measured Wheel Load (lb)	Computed Wheel Load (lb)	Ratio of Maximum Stress to Center Point Stresses
Standard 6.00-16, 4-PR	42.6	15	60	0.85	42.4	63	890	924	1.25
	12.5	35	18	0.78	15.1	46	890	993	2.86
Radial-ply 6.00-16, 4-PR	46.6	15	75	0.78	49.8	79	890	897	1.37
	15.0	35	23	0.75	20.9	37	890	946	1.85

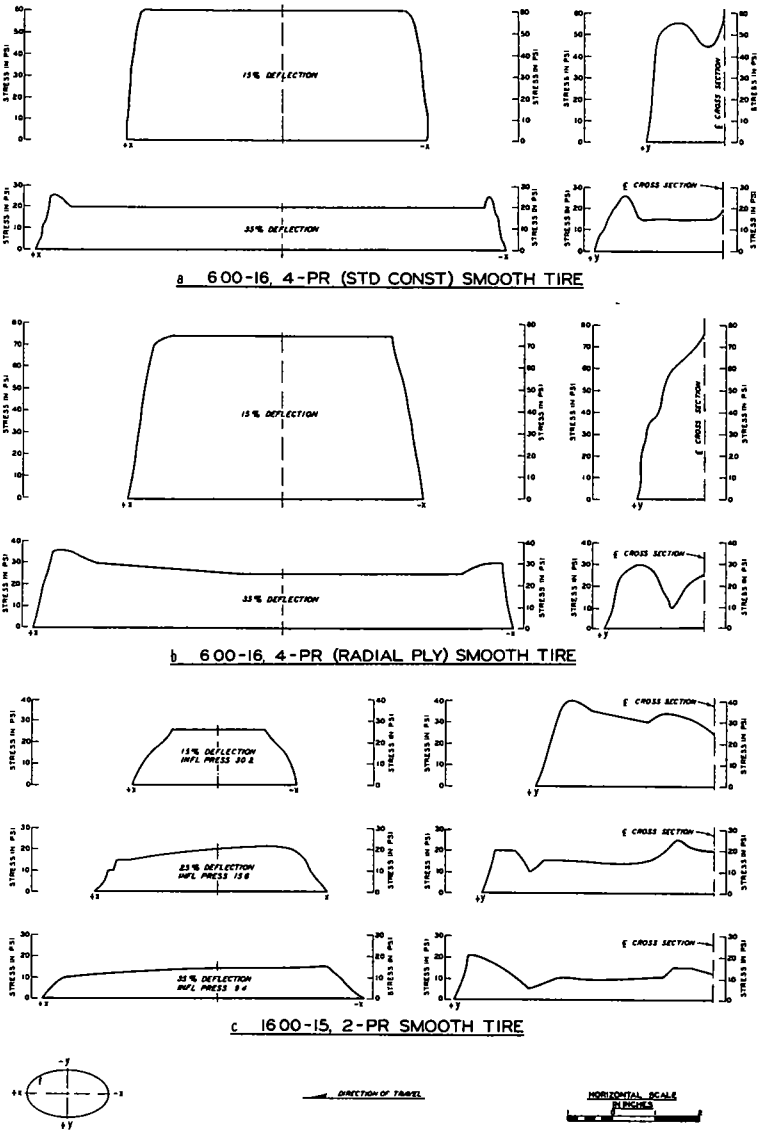

Figure 7. Vertical stresses along principal axes of contact ellipse of three tires of dissimilar construction under 890-lb load.

TABLE 5

VERTICAL STRESSES ALONG PRINCIPAL AXIS OF CONTACT ELLIPSE OF 2-PR TIRE

Tire	Inflation Pressure (psi)	Tire Deflection (%)	Stress at Center Point (psi)	Ratio of Inflation Pressure to Center Point Stresses	Average Contact Pressure (890 Lb/ Contact Area) (psi)	Maximum Stress Measured (psi)	Measured Wheel Load (lb)	Computed Wheel Load (lb)	Ratio of Maximum Stress to Center Point Stresses
Terra	30 2	15	28	0.90	27.5	42	890	894	1.25
16 00-15,	15 6	25	18	0.89	16.2	31	890	860	1.77
2-PR	9.4	35	13	0.90	11 0	30	890	906	2.87

In testing the radial-ply 6.00-16, 4-PR tire, it was necessary to obtain four to five replicate readings at each lateral position and average these readings to minimize the effects of surface roughness or nonuniformities in carcass stiffness. (Molding of agricultural lugs left impressions on the interior of this tire.)

Data representing the radial-ply 6.00-16, 4-PR tire are shown in Figure 7b. The measured stresses at 15 percent deflection follow a unique pattern; i.e., pressures along the lateral section increase continuously from the edge to the center of the tire. When the radial-ply tire is deflected 35 percent, the effect of the relatively stiff tire sidewalls is indicated by a ridge of higher pressures along the side of the contact patch.

Comparing the two tires, it can be seen that for a specific load and percentage deflection, the contact patch beneath the radial-ply, 6.00-16, 4-PR tire is somewhat narrower than the one beneath the standard 6.00-16, 4-PR tire; accordingly, the average contact pressures are higher for the radial-ply tire. Measured stresses at any specific point beneath the radial-ply tire are higher than those measured at comparable locations beneath the standard 6.00-16 tire.

The differences in the stresses measured beneath these two tires can be attributed primarily to the type of tire construction; however, they appear to be influenced to a slight degree by the differences in the tire inflation pressures (see Table 4).

The stress sections for the bag-type tire (Fig. 7c) are somewhat irregular even though these tires were molded without tread. However, the manufacture of such tires is difficult and mold marks, seams, and unevenness of the tire contours were visually evident in the finished tires. The rather pronounced stress rise visible near the tire path centerline on the lateral sections of the stress pattern is believed to be due to such a molding irregularity.

It can be seen that there is still a tendency for the maximum stress to occur beneath the tire sidewalls. For the two lowest inflation pressures, the maximums are about equal. At all inflation pressures the ratio of the inflation pressure to an average measured stress in the interior of the contact area is of the order of 0.90. Table 5 gives data related to the plot in Figure 7c.

SUMMARY

Although the interface stress measurements reported cannot always be adequately explained in terms of load, inflation pressure, tire type, etc., the data obtained suggest some general trends.

For a specific tire at a constant inflation pressure, the magnitude of the load is reflected by the magnitude of the maximum stresses occurring at the interface on an unyielding surface. The general trend of these data is for the maximum stresses to be associated with the relative stiffness of the tire sidewalls. Considering all the factors involved, the ratio of the maximum stress to the average center point stresses is largest for the stiffer tires at relatively low inflation pressure. This supports a popular theory that when a tire is underinflated, its sidewalls support a proportionally large share of the wheel load, causing wear near the edge of the contact patch and gradual deterioration of the tire's sidewalls.

The wheel load computed from the stresses measured usually exceeded the actual measurement, indicating that possibly an overregistration of stresses had occurred due to testing techniques. The inflation pressure seems to have primary control over the magnitude of the stresses in the center part of the contact path. Of secondary importance in determination of these stresses is the relative stiffness of the tire carcass. The average measured interior stresses are consistently greater than the inflation pressures. The ratio of the inflation pressure to these stresses ranges from 0.72 for the stiffest tires to 0.90 for the most flexible tires tested.

REFERENCES

1. Bonse, R. P. H., and Kühn, S. H., "Dynamic Forces Exerted by Moving Vehicles on a Road Surface." HRB Bull. 233, 9-28 (1959).
2. Vanden Berg, G. E., and Gill, W. R., "Pressure Distribution Between a Smooth Tire and Soil." 52nd Annual Meeting, Amer. Soc. Agric. Engrs., New York (June 1959).

Stresses in Yielding Soils Under Moving Wheels And Tracks

D. R. FREITAG and S. J. KNIGHT, respectively, Chief, Mobility Section, and Chief, Army Mobility Research Center, Soils Division, U. S. Army Engineer Waterways Experiment Station, Vicksburg, Miss.

As part of the study of cross-country vehicular movement conducted by the U. S. Army Engineer Waterways Experiment Station, research has been initiated to determine the nature of the interaction between a vehicle's traction elements and a yielding soil. In one phase of this work, pressure-sensitive cells have been embedded in soft soils to measure stress intensities induced by vehicles moving on the surface of that mass. The work is complicated by problems of soil homogeneity, instrument reliability, and data interpretation, and by soil flow that results in displacement of the cells. Measurements have been made in soil beneath a pneumatic tire, a rigid wheel, and two types of crawler tracks. Results, although chiefly qualitative, provide some insight into the manner in which vehicle stresses are transmitted to soft soils.

•THE KEYNOTE of present-day military planning is mobility—the quick, precise movement of forces on the ground and in the air. However, the mobility envisioned by military strategists is not of convoys moving along roads and aircraft operating from permanent airfields, but rather of vehicles moving freely over the landscape without dependence on previously constructed facilities. If this concept is to be realized, the Army must acquire the most agile, mobile, and versatile overland vehicles that can be devised.

Commercial interests have had very little motivation to develop vehicles with a high degree of cross-country mobility. Usually, it has been more practical and economical to build and improve roads than to improve vehicles. Recently, however, mineral and oil exploration in northern tundra and muskeg regions, in tropical forests, and in desert sands has stimulated an interest in vehicles capable of operating in the most forbidding regions of the world.

Present-day vehicles have been designed by rule of thumb, by instinct, or from fragmentary theoretical concepts. A complete, rigorous statement of the fundamental principles that govern vehicular overland movement has not yet been formulated. Research studies that eventually will provide the basis for this formulation are being conducted by the Army Mobility Research Center (AMRC), a facility of the U. S. Army Engineer Waterways Experiment Station (WES). One phase of these studies involves the measurement of the stresses induced within a yielding soil mass by the passage of a vehicle.

To date, the stress measurement program has been chiefly exploratory. Wheels and tracks of various types have been used to apply loads mainly on soft clay soils, and stresses have been measured with three different kinds of pressure-sensitive cells. Many problems of measurement and analysis have arisen; some of these seem to have been circumvented, whereas others remain annoyingly present. This paper describes the equipment and techniques employed in this study, some of the difficulties encountered, and the results obtained thus far.

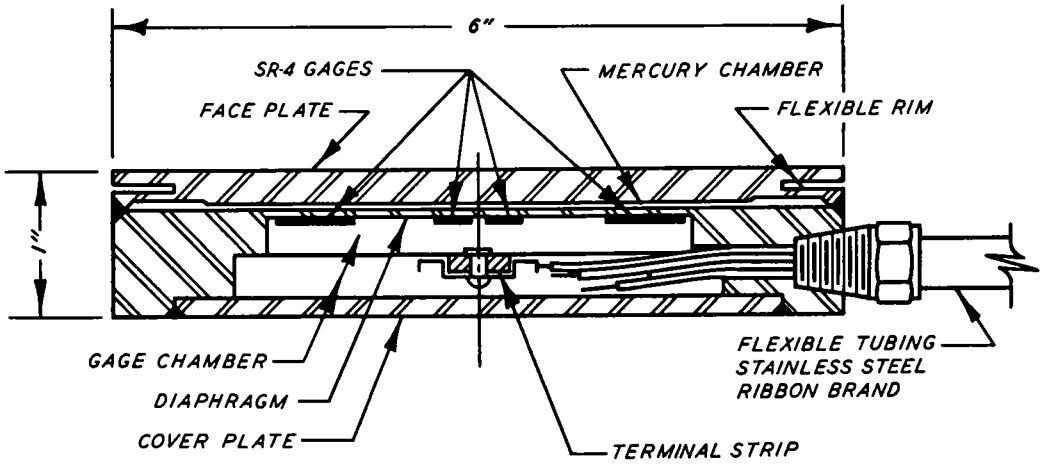

Figure 1. Schematic drawing, WES earth pressure cell.

PRESSURE CELLS

Types of Cells

The WES earth pressure cell (Fig. 1) is 6 in. in diameter and is fabricated from stainless steel. Basic components are a mercury-filled fluid chamber with diaphragm, and a full Wheatstone bridge circuit consisting of four SR-4 strain gages hermetically sealed within the cell. Pressure applied to the face plate of the cell is transmitted through the mercury in the fluid chamber to an internal flexible diaphragm and produces deflection of the diaphragm proportional to the load. The four SR-4 strain gages are mounted on the diaphragm and are actuated by its deflection. The full Wheatstone bridge circuit practically eliminates the effects of temperature and of resistance variations in the lead wires. The strain-gage readings are calibrated by applying known loads to the face plate of the cell. Generally, a 60-μ in. movement of the SR-4 strain gage corresponds to about a 1-psi load on the face plate of the cell. The cells are instrumented so that strain measurements are converted to stress and recorded directly in pounds per square inch on a direct-writing oscillograph. The cells used are rated at 50-psi capacity but can withstand somewhat larger pressures without damage.

The WES fluid pressure cell (Fig. 2) is a single-diaphragm type in which the diaphragm is directly exposed to the soil and deflects in proportion to the applied pressure. Four strain gages (Baldwin SR-4) are cemented to the interior side of the diaphragm so that two gages are in tension when the other two are in compression. The four gages are joined to a four-arm Wheatstone bridge circuit. Pressure applied to the cell results in a resistance change in the gages which is linearly proportional to the pressure. The resulting signal is amplified and recorded on suitable equipment. The location of the gages on the same diaphragm and within the same housing produces good temperature compensation. The cells are hermetically sealed to prevent moisture from entering and causing cell deterioration.

The CEC, type 4-312, pressure cell (Fig. 3) used in this study is a small, single-diaphragm, fluid pressure cell, hermetically sealed (absolute), manufactured by the Consolidated Electrodynamics Corporation of Pasadena, Calif. In this study the small ½-in. diameter cell was mounted in a 3-in. diameter cell mount to provide greater positional stability. Applied pressure deflects the diaphragm of the cell a small amount (0.0008 in. maximum deflection) causing a star spring arm to move outward, which, in turn, causes the strain-sensitive wires to be distorted. The distortion (strain) of the wires causes a change in resistance which is translated by the amplifying and recording equipment into a record proportional to the distortion. Inactive strain-gage arms are

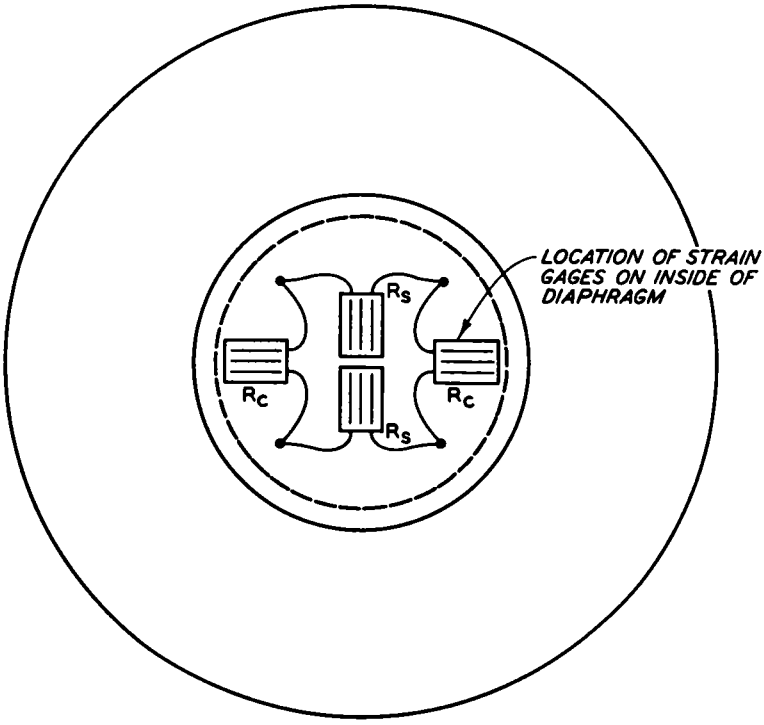

TOP VIEW

NOTE:

DIAPHRAGM THICKNESS VARIES WITH PRESSURE RANGE. DIAPHRAGM AND HOUSING MACHINED FROM SOLID STOCK AND THICKNESS OF DIAPHRAGM CLOSELY CONTROLLED.

DIAPHRAGM WITH HOUSING HEAT-TREATED AFTER MACHINING.

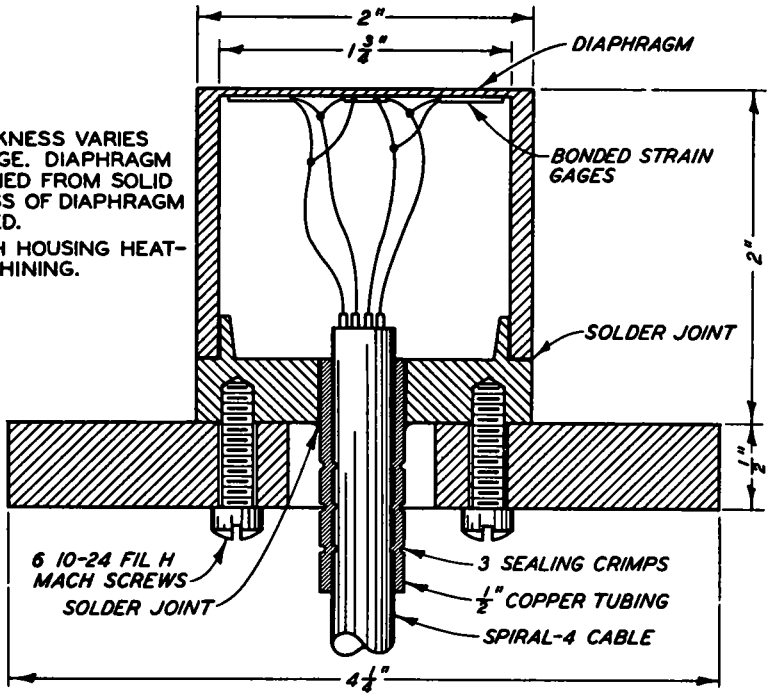

SECTIONAL ELEVATION

Figure 2. WES fluid pressure cell.

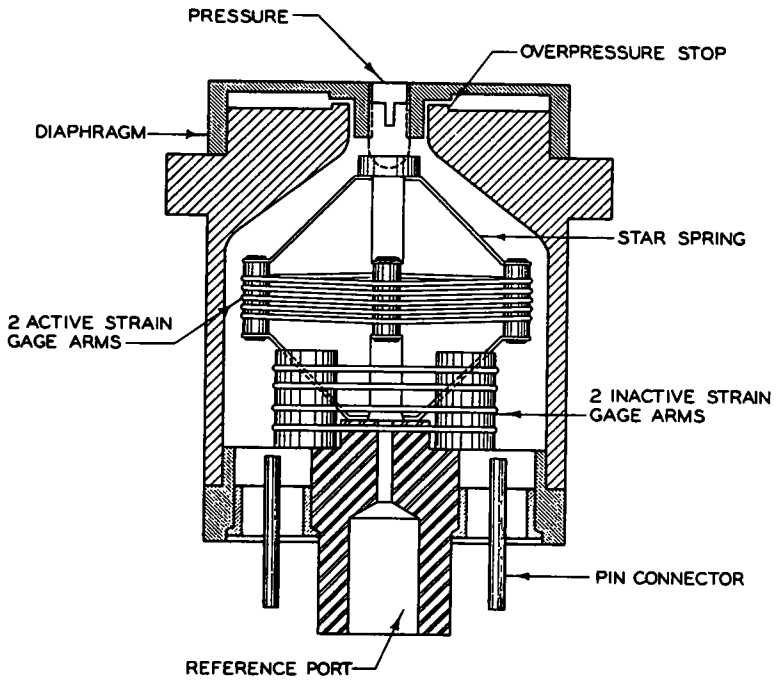

NOTE ALL CELLS USED IN TRAFFICABILITY STUDIES ARE OF THE ABSOLUTE PRESSURE TYPE — THE REFERENCE PORT BEING HERMETICALLY SEALED.

Figure 3. Sectional view of CEC pressure cell.

mounted within the cell housing to compensate for temperature changes. The resistance arms are unbonded strain-gage windings connected internally in a four-arm Wheatstone bridge (full bridge) circuit with two active arms.

Calibration of Pressure Cells

The pressure cells used in these tests were calibrated in a reinforced steel tank in which the air pressure is built up in controlled amounts. In the calibration procedure, the pressure measured by the cells is indicated on a direct-writing oscillograph or Baldwin SR-4 strain indicator, and compared with the pressure read on the laboratory test gage. Where a recorder is used, the gain of the amplifiers is adjusted so that the maximum range of the recording paper is equivalent to the maximum applied air pressure in the tank. This gain and resulting recorder indication can be reproduced in the field by means of calibrating resistors built into the amplifiers. When an SR-4 indicator is used in the field, the pressure is calculated from the readings taken by the operator, using the calibration factor obtained in the laboratory test.

With both the CEC and WES fluid pressure cells, the air pressure is applied directly to the cell diaphragm in the calibration tank. However, in most cases the WES earth pressure cells are calibrated in what is called a "double-diaphragm" test chamber. In this procedure the air pressure is applied to the earth pressure cell through two diaphragms, one on each side of the cell. This method applies the force, developed by the air pressure on the diaphragm, evenly across the two faces of the cell, thus closely simulating soil action on a cell installed underground.

TEST CONDITIONS

Soil Preparation

Tests were conducted on soils carefully placed in test pits. These pits were about 4 ft deep, approximately 50 ft long, and wide enough to insure that the loaded area was at a distance at least twice its width from the edge of the pit. Most of the data have been obtained from tests conducted on a high-plasticity clay soil, but some are from tests on a low-plasticity clay and a clean sand. In all cases the test soil was built up uniformly in lifts. Water content was controlled to achieve the desired properties in the clay, and density was controlled in the air-dried sand.

Cell Installation

After the test area was constructed, pressure cells were installed at various depths along the centerline of the intended vehicle path and at prescribed offsets. The minimum horizontal spacing between cells was 1 ft. To install a cell at a given spot in the test area, a 7-in. diameter hole was dug to the desired depth. The cell was then placed (aligned horizontally or vertically) in the hole at a specified depth, after which the soil was replaced and compacted manually.

The position and movement of the cells were determined by making the following measurements before and after a test: (a) the north-south position (i.e., the station number) of the center of the cell; (b) the east-west horizontal offset distance from the centerline of the intended vehicle path to the center of the cell; and (c) the elevation of the center of the face of the cell, and of points (usually four) on the edge of horizontally placed cells.

Test Loads

Loads were applied to the test soils by a variety of moving wheels and tracks. In the early phases an actual vehicle was driven along a preselected path over the test area. These tests included runs with the M29C weasel, the D4 and D7 engineer tractors, and an M135 2 ½-ton truck with 11.00-20 tires. Later a load cart guided by a rail system was used to operate a single rigid wheel or a single pneumatic-tired wheel.

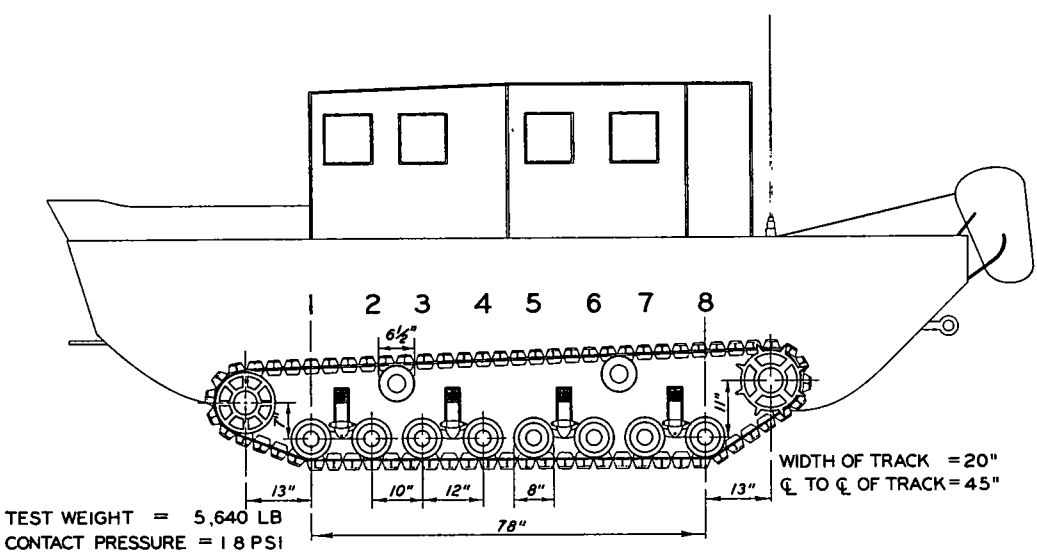

Figure 4. Schematic diagram M29C weasel.

The M29C weasel (see diagram, Fig. 4) weighed approximately 5,640 lb, with operator. The weight of the weasel is transferred to its tracks through four transverse springs attached to the underside of the chassis. A yoke at each end of each spring carries a pair of 8-in. diameter bogies. The two bogies of each pair are 12 in. apart (center to center), and pairs of bogies are 22 in. apart. The distance from the hub of the drive sprocket (at the rear) to the idler wheel is 104 in. On firm soil, a 78-in. length of the 20-in. wide tracks is in contact with the ground. The nominal contact pressure for the weasel is 1.8 psi.

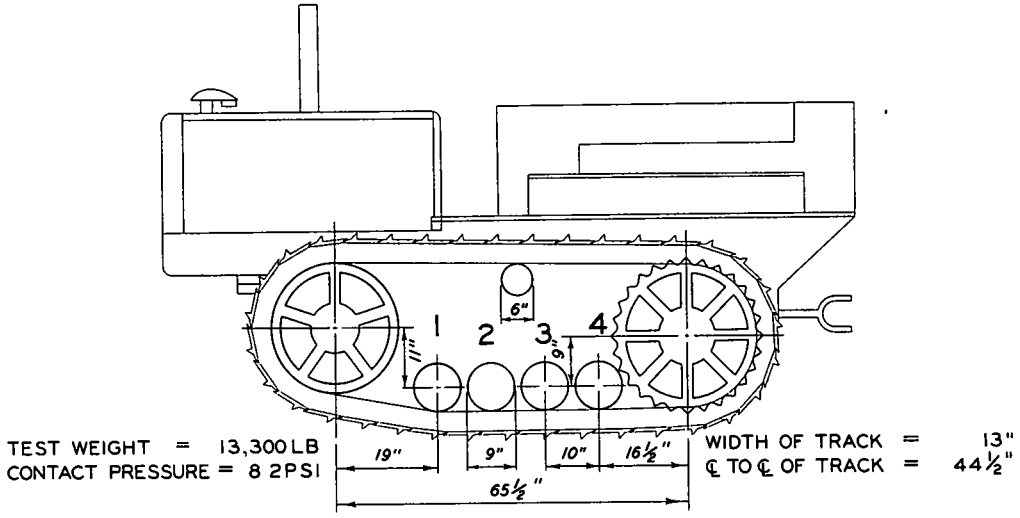

Figure 5. Schematic diagram D4 tractor.

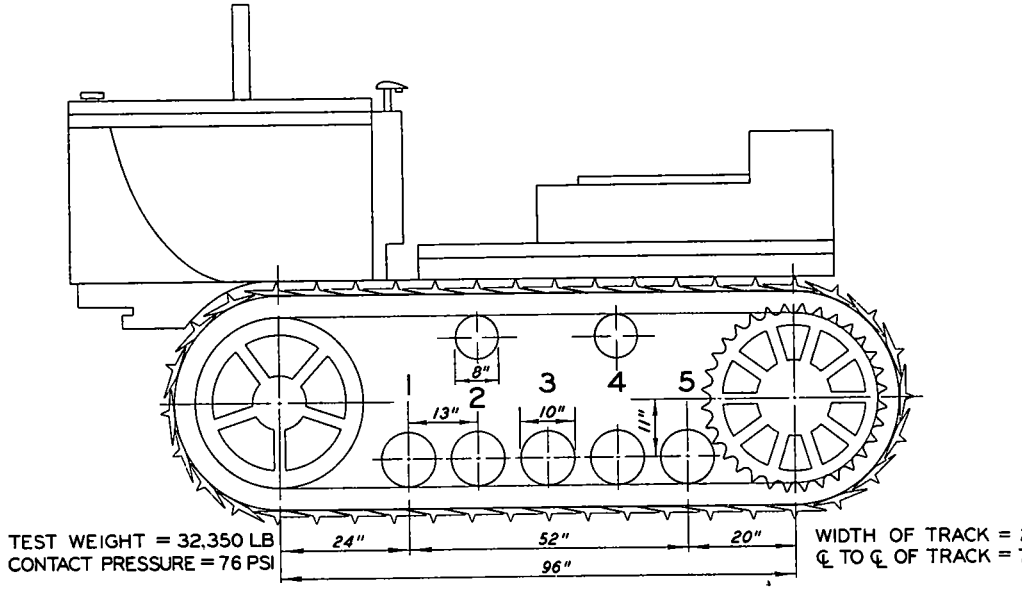

Figure 6. Schematic diagram D7 tractor.

The D4 engineer tractor weighs 14,800 lb (with blade). This weight is distributed to the soil through tracks 13 in. wide and 64 in. long, resulting in a nominal contact pressure of 8.9 psi. The girder-type track system consists of a large drive sprocket (at the rear), a large idler wheel, and four 9-in. diameter unsprung track rollers on 10-in. centers. Each track pad is 7 in. long, with a grouser 1 ½ in. high. Figure 5 shows the D4 tractor without the blade.

The D7 tractor weighs 32,400 lb, and each track is 22 in. wide by 96 in. long. Its nominal contact pressure (with blade) is 7.7 psi. The track system is generally similar to that of the D4. There are five 10-in. diameter track rollers spaced on 13-in.

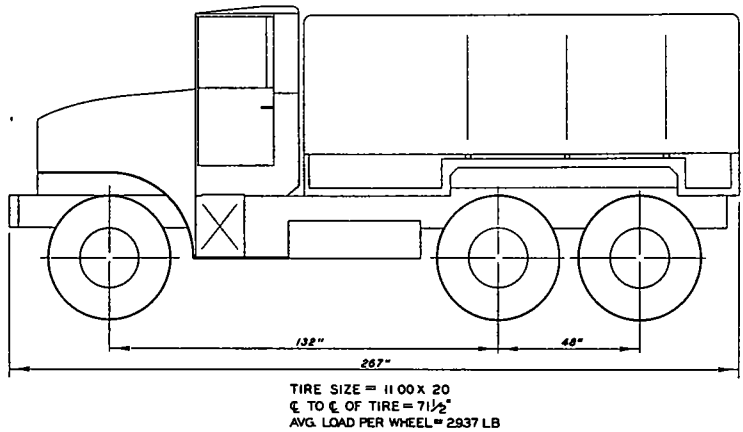

Figure 7. Schematic diagram M135 2½-ton truck.

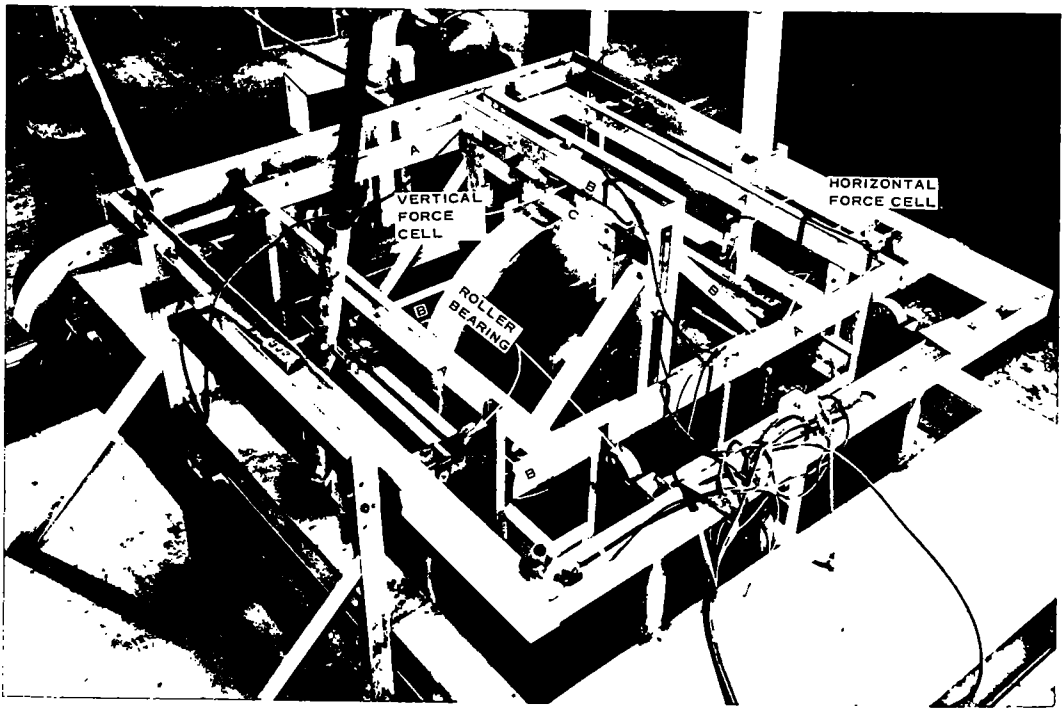

Figure 8. Load cart.

centers. Each track pad is 8 in. long, and the grouser height is 2 in. A schematic drawing of the D7, without the blade, is shown in Figure 6.

The M135, 2 ½-ton, 6x6 cargo truck has single-tandem wheels equipped with 11.00-20, 12-ply rating tires with nondirectional cross-country treads. A schematic diagram of this vehicle is shown in Figure 7. The truck was loaded with 5,000 lb of steel distributed uniformly over the truck bed. The gross weight of the vehicle was 17,600 lb. The front, front tandem, and rear tandem axles weighed 5,900, 5,600, and 6,100 lb, respectively. For the tests the tires were inflated to 15 and 60 psi. At 15-psi inflation pressure the average contact pressure over the area of the total tire contact patch was 30.4 psi; and at 60-psi inflation pressure the average contact pressure was 52.3 psi.

The load cart used in these tests was designed to permit testing a single wheel isolated from the influence of a vehicular suspension system (Fig. 8). The mechanical arrangements of the cart are such that the wheel is free to move vertically (and to roll down the test section) and yet the horizontal and vertical forces on the wheel can be separated and measured. The cart has been used with a rigid wheel 48 in. in diameter and 6 in. wide, and with a buffed-smooth 11.00-20 tire at several load and inflation pressures on a variety of soil surfaces.

SOURCES OF EXPERIMENTAL ERROR

The difficulties of measuring stresses within a soil mass are well known. Even under the simplest and best-controlled static test conditions results are often erratic and not fully explainable. Chief among the factors that can influence results and over which the maximum possible control must be exercised are the soil conditions, the alignment and position of the vehicle, and the position and orientation of the cells.

Soil Conditions

Considerable importance was attached to achieving and maintaining the most uniform soil conditions possible. In particular, great care was taken in replacing soil excavated to insert the pressure cells. Voids or hard lumps at the soil-cell interface are likely to affect the registration of the cell. Similarly, if the soil replaced around the cell is significantly firmer, softer, or compacts differently than the adjacent soil, false registrations of stress could result.

Whenever possible, the excavated soil was maintained at its original water content and packed carefully by hand back into the hole and around the cell. The procedure was found to be much easier if the electrical connections entered the cell from the side rather than from the bottom. Also, it is believed that the most uniform and consistent results were obtained when the soil was quite soft. If the soil was stiff, some difficulty was experienced in filling the larger voids and in achieving a state of compaction comparable to that of the surrounding soil.

During the course of the test program, it was noted that the stress registrations obtained on the first few repetitive passes tended to be more erratic than for subsequent passes. This effect was believed to be due, at least in part, to the compaction of the replaced soil and the "seating" of the cell within the soil mass. It was observed also that the cell often indicated a residual stress even after the load had passed. This phenomenon has been noted and reported in conjunction with other tests (1). In evaluation of the stresses induced by the passage of the vehicle, the residual stress was considered the zero state for each pass and only the stress increment was employed in the analysis.

Vehicle Alignment and Position

The position of the load relative to the pressure cells must be known if an analysis of the stresses is to be made. In all tests the position of the load elements at any time along the length of the test lane was determined electronically.

Tracked vehicles were guided down the test lane by the driver, who was aided only by markers indicating the intended location of the track path. Control of lateral position or alignment in this manner was not particularly precise and some variations in

stress registrations are believed to have resulted, particularly when a vehicle's track did not penetrate into the soil.

In tests with the trucks, a channel was used to guide the wheels of the nontest side of the vehicle. This was helpful but not completely satisfactory, because the degree of control varied with tire inflation pressure and depth of rutting. The most recent approach has been to separate the test wheel from the vehicle and place it in the load test cart, described earlier, with flanged wheels rolling on rails. This h s provided a positive control of wheelpath.

Cell Position and Orientation

The pressure cells were precisely positioned during installation. However, as the soil yielded under the loads, the embedded pressure cells moved with it. Cell displacements of as much as 5 in. have been recorded. Depending on the original position of the cell relative to the load, the cells could move in any direction, tilt, twist, or combine all these movements. In general, the cell movements corresponded to hypothesized soil-flow patterns. Cells directly beneath the load path tended to move downward and along the traffic path in a direction opposite to the direction of travel. Cells some distance outside the path of the load element often moved upward. If the vertically placed cells tilted, they tended to tilt away from the centerline of the traffic path. Some movements such as cell twisting are not so readily explained, however.

Cell movement introduces an element of doubt in the validity and applicability of the stress registrations. Except in a few instances, it is not known if the cells moved gradually over the duration of the test or if the movements were rather abrupt. However, even if position corrections could be made for each cell registration, there is no assurance that the moving cell measures a true stress.

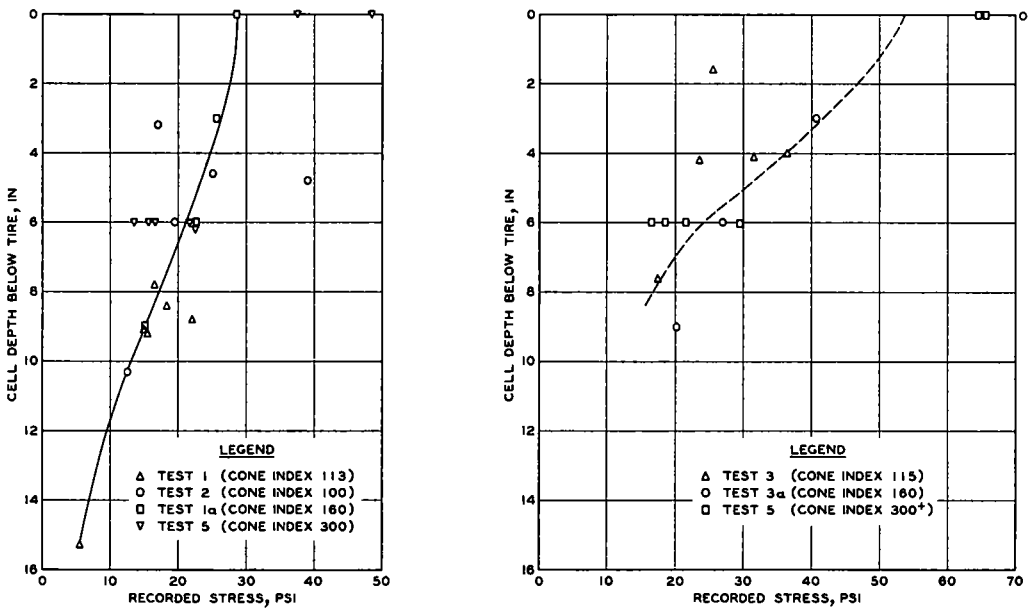

Figure 9. Maximum vertical stress under 11.00-20, 12-PR tire, M135 2½-ton truck; average wheel load, 2,933 lb.

RESULTS OF TESTS

Typical Test Data

In Figure 9 the maximum stresses recorded at various cell depths beneath the center of an 11.00-20, 12-PR pneumatic tire have been plotted. The plotted points in Figure 9a represent data obtained when the tire was inflated to 15-psi pressure; in Figure 9b, the data are from 60-psi inflation pressure tests. It can be seen that inflation pressure has little apparent effect on stress levels below about 6 in. At lesser depths, the high stresses are associated with the high inflation pressure.

Also, at the 6-in. depth the strength of the test soil had little influence on the stress level. Test 5 was conducted in a very firm soil that might be expected to be capable of spreading the load more effectively than a softer soil. This does not appear to have been the case, although it is possible that the observed values are due merely to an effect on the registration of the cells.

The amount of scatter displayed in these plots illustrates the problems involved in the analysis of the data. In Figure 9a, for example, the three data points above the 6-in. depth representing test 2 results are quite divergent. However, inasmuch as this section was relatively soft, these shallow-depth cells experienced considerable movement. The cell of this group that registered about 17-psi stress moved 1.4 in. downward, 3.5 in. laterally, and 1.0 in. along the traffic path while tilting sideways 19½ degrees. The cell registering about 25.0 psi moved downward 1.9 in., laterally 1.3 in., longitudinally 1.8 in., and tilted 23 ½ degrees. The cell registering about 39 psi moved downward 2.8 in., laterally 0.5 in., and longitudinally 1.3 in.; its tilt was less than 6 degrees.

Effect of Vehicle Type

The several vehicles used in the test program can be grouped into three broad classes: (a) vehicles with unsprung wheels rolling on a relatively rigid track; i.e., the D4 and D7 engineer tractors; (b) vehicles with spring-suspended wheels rolling on a relatively flexible track; i.e., the M29C; and (c) vehicles with wheels but no track. The great difference in size and weight of the vehicles representing each of the classes as well as differences in the soil conditions tested precludes any logical comparison of the actual magnitudes of the stresses recorded. However, the patterns of stress induced by each of the vehicle types can be studied readily, and these are found to be of some significance.

In Figure 10 the stresses recorded under the wheeled vehicle are shown. Well-defined maximum stresses are associated with the passage of each wheel. The stress

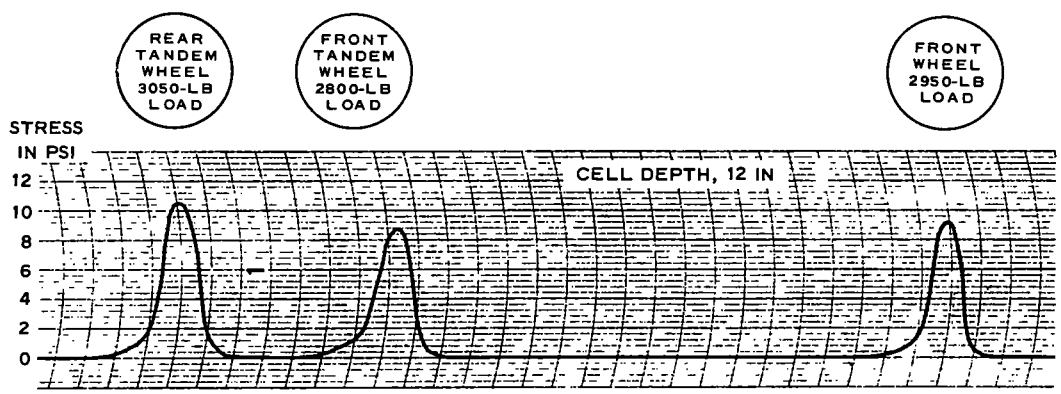

Figure 10. Stresses in fine-grained soil, M135 2½-ton truck, 15-psi tire inflation pressure.

varies smoothly and in proportion to load imposed by each wheel. The stresses recorded under the vehicle with a flexible track are shown in Figure 11. It is seen that the track has transferred some of the stress from the soil immediately under the wheel to the region between the wheels. Nevertheless, a definite maximum occurs in the stress trace in association with each wheel of the vehicle. The maximums differ in magnitude but this can be shown to be due to differences in the load on each of the wheels.

Finally, the stress under a rigid-track vehicle appears as in Figure 12. The trace is not smooth. The fluctuations apparently are not caused primarily by stress intensities under each wheel but seem to occur in a random fashion. The rigid track tends to distribute the loads carried by the wheels, but in doing so pays a penalty in terms of vibrations and shock loadings. The stresses under the rear of the vehicle are very low. This is believed due to the bulldozer blade that makes the tractor rather nose-heavy.

Thus, from these data it can be concluded that a rigid-track distributes the load much more uniformly than the more flexible track, and that the greatest stress intensities are found under the wheels when there is no track at all. This observation agrees well with the known soil-strength requirements for the three vehicle types (2). The engineer tractors are able to operate on soft clay soils that cause difficulty to flexible-track vehicles and are impassable to wheeled vehicles.

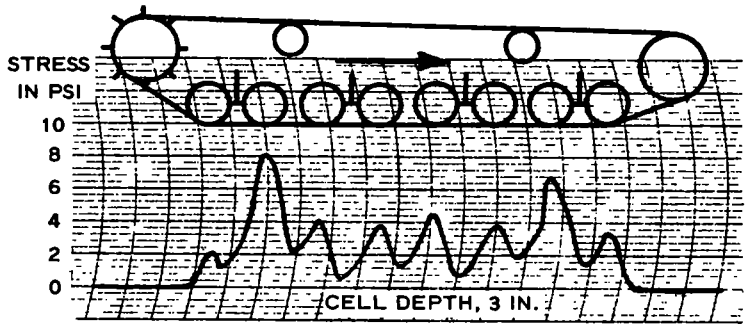

Figure 11. Stresses in fine-grained soil, M29C Weasel, 1.8-psi contact pressure.

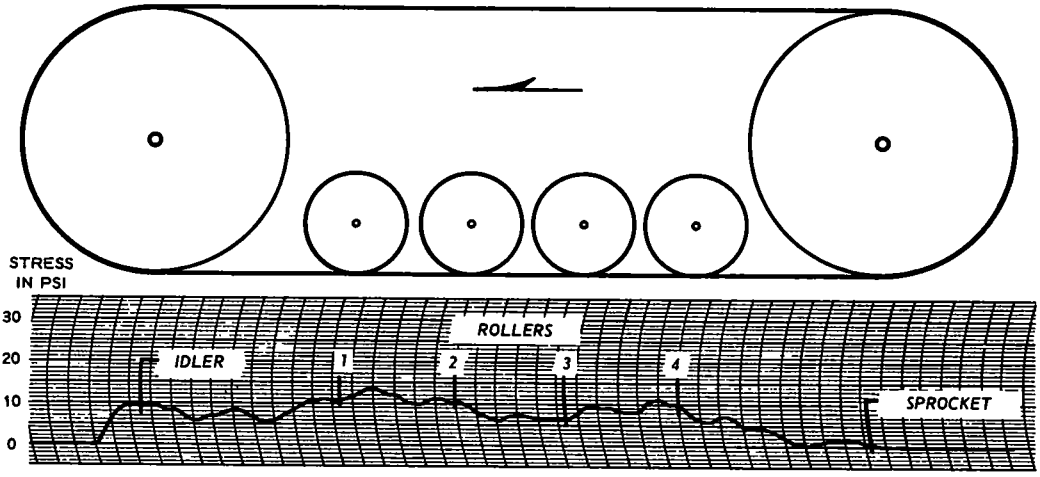

Figure 12. Stress recorded under D4, cell EP93, 6-in. depth, test 2, second pass.

Comparison with Elastic Theory

To provide some basis for estimating whether the measured stresses were reasonable, a theoretical computation of stresses was made for the cell position-load condition that existed on the last pass of each test. Computations were made using the Boussinesq solutions for the stresses in an isotropic, elastic, homogeneous mass of semi-infinite extent due to a static vertical load uniformly applied over the contact area. Although the assumptions involved are obviously crude for the case of soft, yielding soils under moving loads, it was believed that such comparisons were worthwhile.

In some instances the elastic theory appeared to provide at least a good working approximation of the stresses. For example, the dashed line drawn through the data points of Figure 9b represents the theoretical vertical stress due to a uniform circular load of an area equal to the tire contact area.

However, the measured stresses were generally greater than the computed stresses by a factor ranging from a little more than one to about four. Further, the ratio of the measured and computed stresses appeared to vary with the cell location. To study the manner in which the stress ratio (and ultimately that of the measured stresses) varied with the cell location, average values for depth, offset, and stress ratio were determined for similarly located cells for the tests with the rigid single wheel. The average depth of the cell is plotted against the average stress ratio for three offsets (0.0, 4.2, and 7.4 in.) and the average offset is also plotted against the average stress ratio for two depths (approximately 9 and 12 in.) in Figure 13. Although the trend of these data is not definitive, it indicates that the ratio of the measured to the computed stress is a function of the cell location. Furthermore, it indicates that the measured stresses follow a pattern other than that of the stresses computed from elastic theory. The data from tests conducted with the 600-lb load provide sufficient information for a direct comparison of computed and measured stress patterns in a portion of the stress field (Fig. 14). For the region for which data are available, this comparison shows that the stress induced in the soil is greater than that predicted by means of elastic theory.

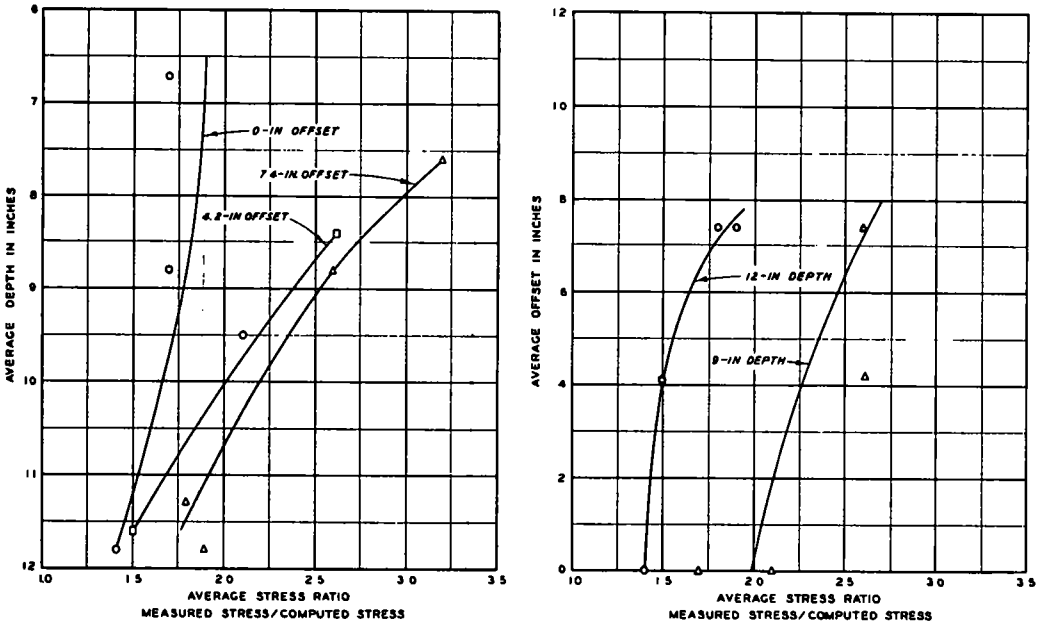

Figure 13. Effect of depth and offset on stress ratio.

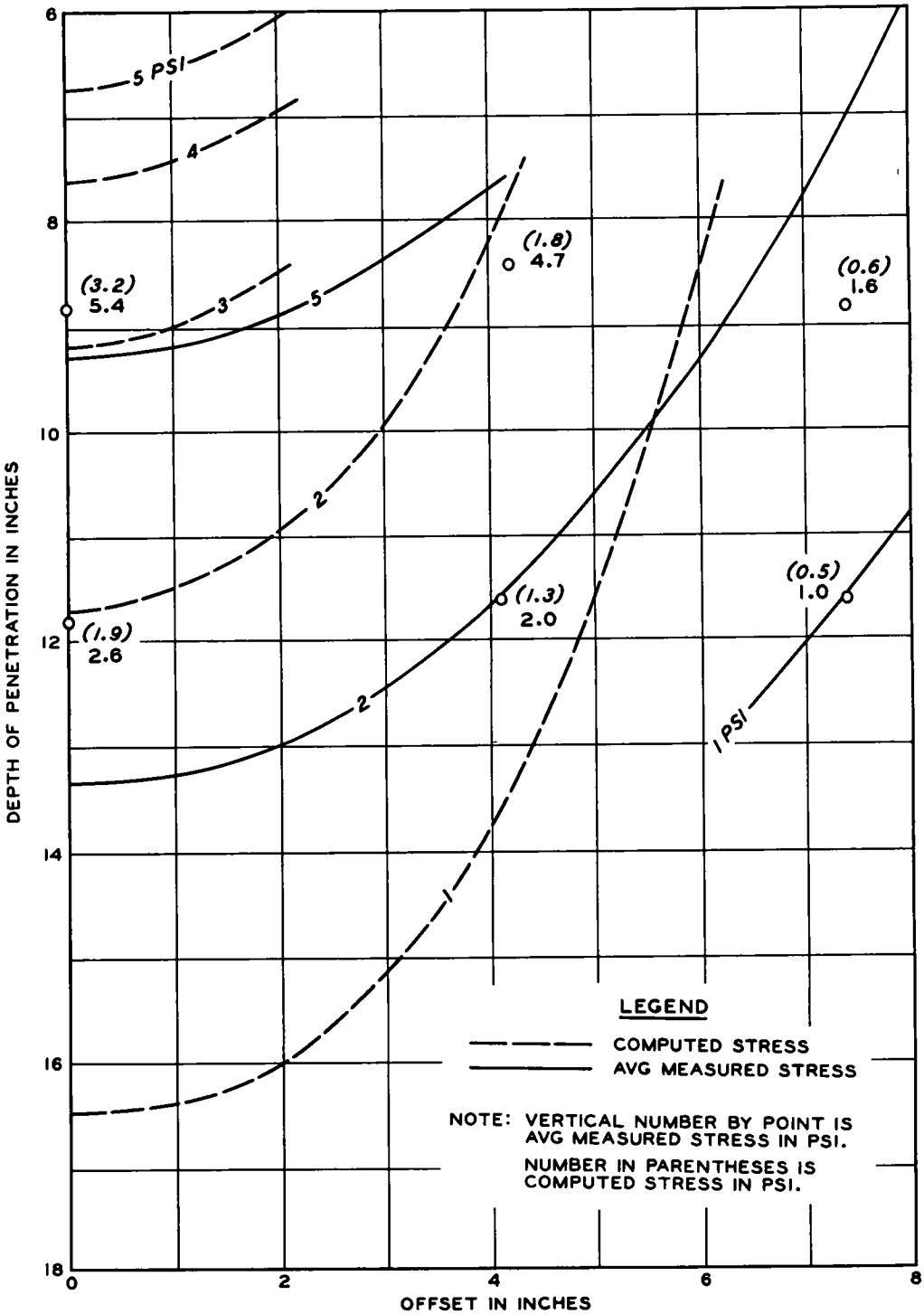

Figure 14. Distribution of vertical pressures in soil, 600-lb load.

SUMMATION

This study of stresses in yielding soils by means of pressure cells has not as yet produced any particularly useful results. It is believed, though, that much can be learned from this approach if some of the more perplexing problems can be solved. In particular, the very broad scatter of results must be narrowed. Previous work with pressure cells leads to the conclusion that from a purely mechanical standpoint a high degree of precision can be expected.

Probably much of the data dispersion encountered was due to nonuniformity of soil properties, particularly those created during cell placement. These should be susceptible of being minimized by carefully controlled preparation of the test soil and meticulous care during cell installation. Steps are being taken to improve techniques in this respect.

It would be useful to be able to locate each cell precisely at any interval during the course of the test To date, no one method of doing this has been very accurate, particularly for the smaller cells. With good fortune and minor movement of the cell, probing with a small-diameter stiff wire can be employed advantageously, but frequently the only accomplishment is serious disturbance of the soil. Probably a system based on reflected waves eventually will provide the required location-fixing ability.

Finally, more knowledge of the effect of soil properties on the response of embedded pressure cells, and of the effect of the shape of the cell on its response is needed.

REFERENCES

1. U. S. Army Engineer Waterways Experiment Station, CE, Technical Memorandum 3-323, "Investigations of Pressures and Deflections for Flexible Pavements": Report 1, "Homogeneous Clayey-Silt Test Section" (Mar 1951); Report 2, "Pilot Tests on New Four-Gage Cell" (Oct 1951); Report 3, "Theoretical Stresses Induced by Uniform Circular Loads" (Sept 1953); Report 4, "Homogeneous Sand Test Section" (Dec 1954).

2. U. S. Army Engineer Waterways Experiment Station, CE, "Trafficability of Soils, A Summary of Trafficability Studies Through 1955." Technical Memorandum 3-240, 14th Suppl., Vicksburg, Miss. (Dec 1956).

Use of Stress Loci for Determination of Effective Stress Parameters

R. YONG, Visiting Research Engineer, Armour Research Foundation of Illinois Institute of Technology, Chicago, and Assistant Professor of Civil Engineering, McGill University, Montreal, Canada; and
E. VEY, Supervisor, Soil Mechanics Research, Armour Research Foundation, and Professor of Civil Engineering, Illinois Institute of Technology

Recent investigations and studies have shown that the laboratory-measured values for internal friction and cohesion C for sensitive clays are much larger than the calculated field values. The need for a better correspondence in measured and calculated field values in such soils is evident. The study described herein was designed to investigate the use of stress loci for determination of the shear parameters not only for sensitive soils but also for normally consolidated clays, because it is realized that the state of stress in a soil specimen at any one condition of strain is an indication of the nature of stress resistance derived therein.

In consolidated undrained triaxial tests on both laboratory consolidated and field-undisturbed clays, the curve joining the points on the Mohr diagram representing shear and effective normal stress on the rupture plane at varying stages of strain has been used in this study to indicate the stress locus. By defining the friction parameter $\bar{\varphi}$ as that parameter in the shear stress vs normal stress region wherein the shear stress increases with the effective normal stress, and the cohesion parameter $\bar{C}$ as the parameter in the same region where the shear stress increases despite a decrease in the effective normal stress, it has been possible to arrive at values for these parameters which correspond to the difference measured by recent investigators. Using conventional methods involving effective stresses, the measured angle of friction for an illitic clay was 20^0. However, using the stress locus, this angle was found to be 10^0. Although $\bar{C}$ was found to be a function of the consolidation history for normally consolidated clays, its magnitude can also be determined from the stress locus and evaluated for the corresponding consolidation or overburden pressure.

•IN CONSOLIDATED undrained triaxial tests on fine-grained soils, pore pressure measurements taken during the period of tests reflect the effective stress condition within the soil specimen—assuming that effective stress is the difference between the total stress and the measured pore pressure. Under the application of a deviator stress, corresponding measured pore pressures can be used to indicate the effective stress condition on a prescribed plane at any one condition of axial strain. Casagrande and Hirschfeld (2), and Holtz and Ellis (4) among others have used this technique of data presentation to compare effective stress and pore pressure build-up under deviator stress application for various soil types and at varying confining pressures. Crawford (3) has used a slightly different technique to arrive at a stress locus, and in doing so, offers a method for interpretation of the effective stress parameters.

Inasmuch as there is reasonable doubt as to the interpretation and significance of the strength parameters (internal friction and cohesion) when applied to both

recompacted and undisturbed soils, it would seem most appropriate to use the stress locus as a means of observing the stress condition on a prescribed plane within a soil specimen, and to deduce therefrom the parameters giving rise to the components of soil strength. Recognizing that the definition of both "cohesion" and "friction" may not be semantically correct as used in soil testing, the physical significance of these terms and parameters may well be taken as descriptive of observed soil behavior. If the normal stresses and shear stresses on the surface of ultimate failure as obtained from triaxial data show that the component of shear resistance increases as the effective normal stress increases, it seems most reasonable to deduce that this constitutes a friction shear component. With this in mind, it is felt that the stress locus that describes the stress condition on a prescribed plane within a soil mass provides a very useful tool for use in interpretation of fundamental shear strength components or parameters.

The purpose of this paper is to present a method for interpretation of effective shear strength parameters giving rise to their respective strength components, based on a knowledge of the stress conditions on the failure plane during stress application. It is recognized, however, that the "friction" and "cohesion" parameters are primarily descriptive and that although the method described defines a technique for obtaining quantitative values for these parameters, it is understood that both may be operative over the entire range of shear resistance. However, in accordance with the definition of these parameters, the predominant shear component is used to define the corresponding operative parameter.

THE STRESS LOCUS

In general, the "stress-vector" technique used by Casagrande and Hirschfeld (2) has been used with certain deviations in selection of the failure plane and subsequent approximations following the initial stress locus determination. The stress locus defines, in terms of measured and calculated quantities, the shear and effective normal

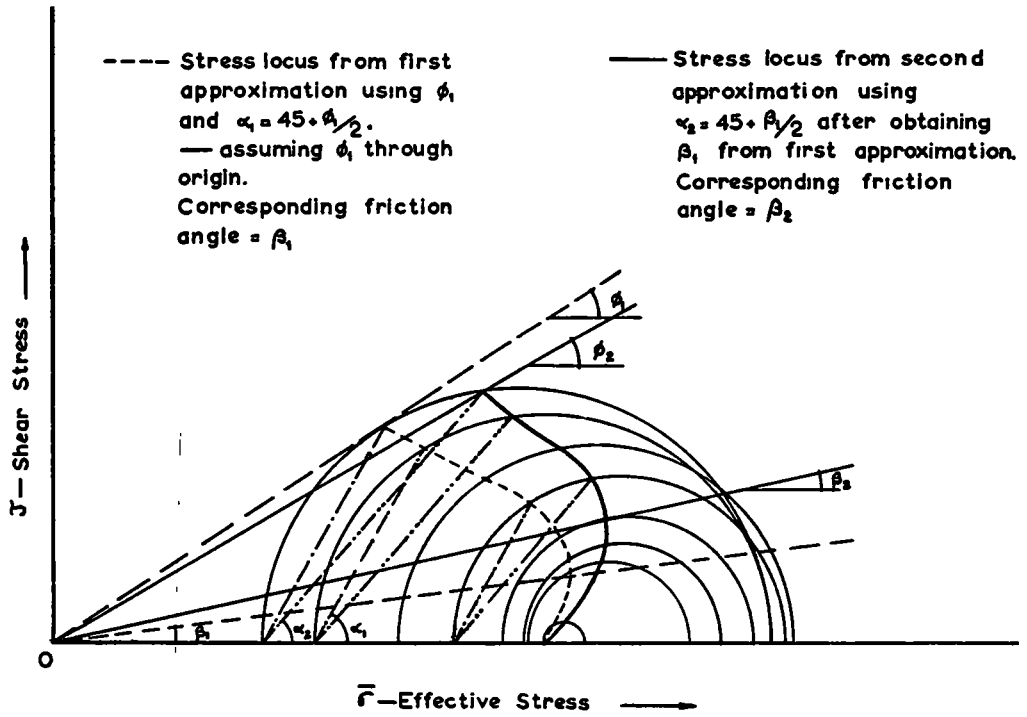

Figure 1. Stress locus from Mohr circles at varying strain conditions.

stresses on a prescribed plane. The dependency of stress on both pore pressure and strain can also be clearly seen in this system of presentation.

In the ordinary interpretation of the shear strength parameters of a cohesive soil, φ is taken as the slope angle of the rupture line derived from the envelope of failure, (Mohr's circles) and C is the intercept of the extended rupture line on the vertical shear stress axis. Such a rupture line depends on (a) the load under which the soil has been consolidated and (b) whether or not total stresses or effective stresses are used in plotting the Mohr's circles. If it is recognized that the shear strength of any normally consolidated clay soil increases with consolidation pressure from zero at zero consolidation pressure and that only effective stresses have meaning in this build-up of strength, then it is apparent that the true envelope of Mohr's circles must pass through the origin.

In the following discussion φ_1 (Fig. 1) is the angle that the rupture line makes with the horizontal. The point of tangency of the rupture line with the failure Mohr's circle defines the slope angle $\alpha_1 = 45^0 + \varphi_1/2$ of the plane in the specimen on which failure would occur if the shear strength could be attributed entirely to interparticle friction. If, however, this strength is partly derived from cohesion (developed from the consolidation pressures), φ_1 will not be the true friction angle and α_1 will not necessarily define the true failure plane. If now the shear stress vs effective normal stress curve on the α_1 plane is plotted over the range of stresses from $\overline{\sigma}_c$ (effective lateral stress) to the maximum σ_1 (effective axial stress), the stress locus (broken curve) is obtained. In examining the manner in which the shear stress on this plane changes with normal effective stress, it can be seen that the shear stress increases with normal stress to the point where the tangent to the curve is vertical. Beyond this point the shear stress increases as the normal effective stress decreases. A line through this point and the origin (slope β_1) defines a new friction angle which in turn defines a new failure plane (slope $\alpha_2 = 45^0 + \beta_1/2$). The stress locus for this new plane defines still another friction angle β_2. This process may be repeated to give other α angles but it can be shown that all additional α angles will lie between α_1 and α_2 and the additional β angles will not differ greatly from the β_2 angle. A new φ angle (φ_2) corresponding to α_2 is also shown. This is the slope of a line through the origin and the terminal point of the stress locus. If the total shear strength is actually composed partly of friction and partly of cohesion, neither φ_1 nor φ_2 is actually a true angle of internal friction. The angle that most nearly approximates a true friction angle is β and because successive approximations such as already described will yield a β not differing much from β_2 the latter may be taken as representing the proper friction angle or friction parameter $\overline{\varphi}$. The $\overline{C}$ is that part of the shear strength which is independent of the normal stress on the particular plane. In most cases, the $\overline{C}$ value will vary with the normal consolidation pressure σ_c. The particular values of $\overline{C}$ given in Figures 4, 5, 6, and 7, however, are for $\overline{\sigma}_c = 0$. At a particular $\overline{\sigma}_c$ the actual $\overline{C}$ would be the vertical distance from the $\overline{\varphi}$-plane to the φ-plane.

SAMPLE PREPARATION AND TEST PROCEDURE

Both laboratory consolidated and field undisturbed samples were used as test samples for the consolidated undrained triaxial tests. All laboratory samples (artificial soil) were consolidated from a slurry to a water content of about 45 percent and at a corresponding void ratio of about 1.3 in consolidation tubes provided with both end and side drainage. The solids used were illitic with a liquid limit of 39.0 and a plasticity index of 18.0 (94 percent of the particles were less than 105 μ in size), and a kaolinitic clay with a liquid limit of 70.2 and plasticity index of 29.4. The tube-consolidated soils were further consolidated in the triaxial cell at the predetermined cell pressure under incremental pressure loadings. Final water contents varied from 29 to 23 percent for the illite clay, and 44 to 49 percent for the kaolinite clay, depending on final cell pressure.

To reduce possible particle interaction arising from interparticle forces, artificial soil samples were also consolidated using ethylene glycol ($C'_2H_4(OH)_2$) as the pore fluid. In a clay-liquid system there exist attractive and repulsive forces between the particles. In general, the attractive forces are insensitive to system characteristics but the repulsive forces can be altered considerably depending on the system polarity

In replacing water with ethylene glycol in a soil-liquid system, the repulsive forces are reduced. Because ethylene glycol is less polar than water, this also permits the attractive forces to play a much larger role in the development of shear strength, allowing more contact between particles and thereby increasing the "frictional" contribution to strength. The purpose of the tests with ethylene glycol was therefore (a) to compare the shape of the stress locus curve with that obtained using water, (b) to see if the "frictional" part and "cohesive" part of the curve as previously described still existed, and (c) to compare the friction angles obtained in the two cases. The preparation procedure was similar to that used for samples with distilled water as the pore fluid. In this instance, ethylene glycol was also used in both the saturation and pore pressure line for the test series.

As still another test of the stress locus characteristics, any "undisturbed" samples of Chicago clay were tested in the same manner. These were obtained from freshly taken Shelby tube samples. The properties of this clay corresponded to those described by Peck and Reed (10). Because of the possibility of a slight precompression, the test samples were not fully consolidated in the triaxial cell prior to load application. Thus, it may be argued that $\bar{\varphi}$ obtained from this series may be somewhat low.

Because complications can arise as a result of partial and incomplete saturation of the test samples, all samples were allowed to take in pore fluid in the triaxial chamber under a low confining pressure —3 psi. Pore pressure response was determined as a function of cell pressure increase to ascertain the degree of saturation of the test sample. Both side filter strips and double membranes were used as standard procedure. A rate of loading of 0.001 in. per min was selected as a reasonable rate of strain loading corresponding to the results obtained by Osterberg and Perloff (9) and with due cognizance of the effect of other possible factors involved as suggested and discussed by Seed (12).

RESULTS AND INTERPRETATION

The results of the tests reported herein are not meant to be used specifically as quantitative data but to point out and highlight the role and application of stress loci in evaluation of the significant effective stress parameters. Because the technique involved defines the stress conditions on a predetermined plane, it is necessary to explain the significance of the stress locus in terms of components of shear strength. Following the method previously described for determination of the stress locus, Figure 2 shows the stress loci for two extreme conditions. These are the conditions defined primarily by the response of the pore pressure under application of the deviator stress.

In Figure 2, stress locus B represents the condition where there is no pore pressure response under deviator stress application. The specimen is consolidated in the cell to a consolidating pressure of $\bar{\sigma}_c$ before load application. When the load is applied, because pore pressure response is zero, $\bar{\sigma}_c$ is equal to $\bar{\sigma}_3$ (lateral pressure for shear test) at all times and hence remains constant

$$\bar{\sigma}_1 = \bar{\sigma}_3 + \Delta\sigma$$

in which $\Delta\sigma$ = deviator stress (because pore pressure μ is zero). The stress locus defined is coincident with the line determined from the tangent of the rupture envelope to the maximum deviator stress circle (not shown in the figure). The angle resulting therefrom is $45^0 + \varphi/2$. In tests conducted on saturated Ottawa sand at close to the critical void ratio, little or no pore pressure was recorded except very close to failure where condition of incipient failure creates irregular strains in the specimen. The stress loci drawn from these tests were similar to that defined by case B in the figure, except close to the rupture point. The total strength component operative over the entire stress region is then the friction stress component.

Stress locus A in Figure 2 defines the condition for full pore pressure response—assuming that such a condition can be achieved in an ideal case. Following consolidation under the consolidation pressure of $\bar{\sigma}_c$ any application of the deviator load results in a full response of the pore pressure. In consequence, $\bar{\sigma}_c = \bar{\sigma}_1$ = constant, and $\bar{\sigma}_3 = \bar{\sigma}_c - u$. Therefore, the condition defined indicated that φ=0, the rupture envelope for

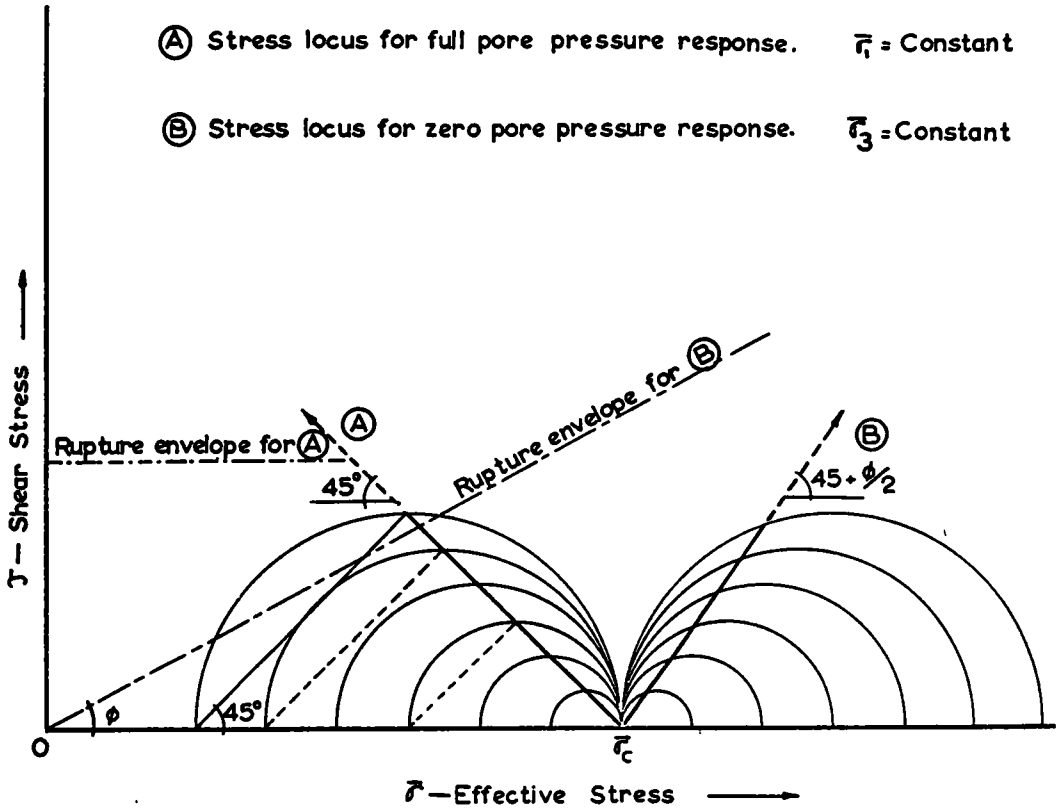

Figure 2. Stress loci for full pore pressure and zero pore pressure response.

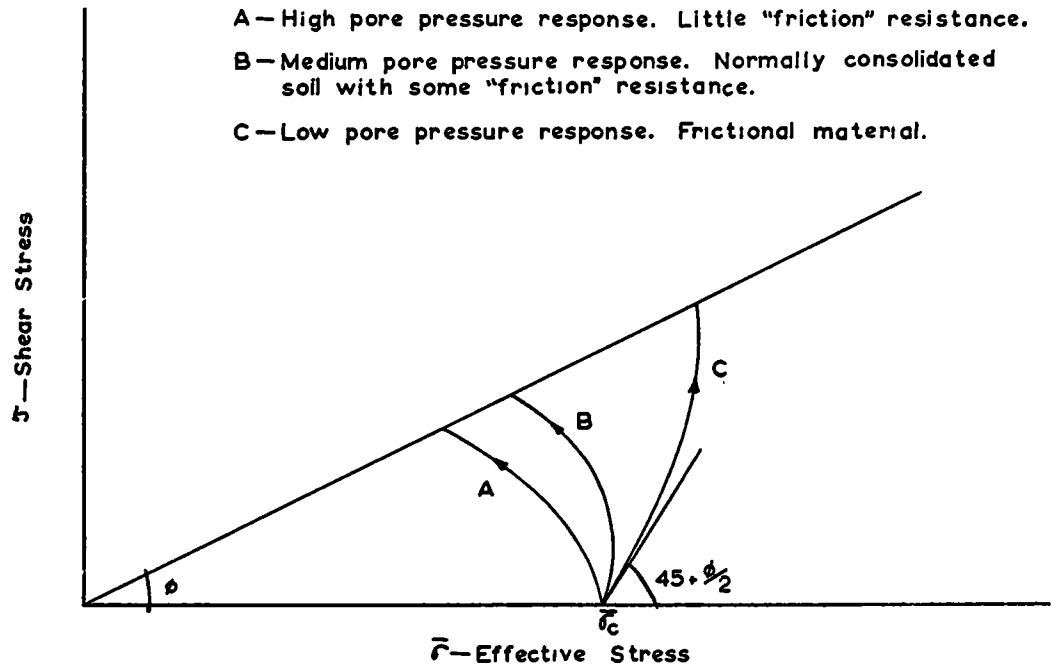

Figure 3. Stress loci for soils with varying pore pressure response.

case A, would be a horizontal line. In this instance, the inclination of the plane of failure is 45^0 and the stress locus defined is shown at 45^0 in the figure. Assuming that the ideal case for pore pressure response can be found, this would then indicate that the total shear strength component is the "cohesion" component.

Except for soils where pore pressure response is neither of the two extremes, the shear strength components will be operative throughout the entire test. Figure 3 shows the stress loci for soils with varying pore pressure response going from stress locus A, which is for a soil with a small frictional strength component and with high pore pressure response under load application, to stress locus B, which is for a soil of a higher frictional quality with a lesser pore pressure response, and final stress locus C illustrating the case for a still smaller pore pressure response and a much higher friction resistance component. Holtz and Ellis (4) have shown stress loci for artificial clay soils mixed with sand and gravel, and their results indicate the trend shown in cases A, B, and C in the figure. The higher the proportion of sand and gravel, the lesser is the pore pressure response and the more the stress locus trends from A to C, indicating the increasing influence of the friction strength component with proportional increases of sand and gravel.

The results of the consolidated undrained triaxial tests on both laboratory consolidated and natural soils are shown in Figures 4 through 7. Both the first and second approximations for the stress loci are shown.

In Figures 4 and 5, the soil used was illite clay and the variable component was the pore fluid. As expected, the shear strength for the illite clay with distilled water as its pore fluid was much lower than that of the same clay with ethylene glycol as its pore fluid—for corresponding densities and void ratios. Without going into the mechanism of particle interaction possibly arising as a result of interparticle forces, the argument can be resolved around the development of a higher friction strength component in the case of glycol in the absence of clay-water interaction. In comparing the friction angle φ between the two cases, there is a difference of about 2.5^0 between the φ established by the terminal points of the stress loci (and the tangents of the effective stress circles). $\varphi = 22^0$ for the illite-clay with glycol and $\varphi = 19.5^0$ for the same clay with distilled water. However, in making the comparison on the basis of the effective friction angle, defined by the maximum effective normal stress on the stress locus, the difference between the two $\bar{\varphi}$'s is 5^0; i.e., $\bar{\varphi} = 14^0$ and $\bar{\varphi} = 9^0$ for the illite clay with glycol and distilled water, respectively. The void ratios for the samples ranged from 0.83 at a cell pressure of 20 psi to 0.67 at a cell pressure of 56 psi. Variation in void ratio between companion samples was $\pm$ 0.02 at the same cell pressure following final consolidation in the cell and prior to load application.

The case for kaolinite is shown in Figure 6 where $\bar{\varphi}$ is reported as 11.5^0. In the test on Chicago clay, results show $\bar{\varphi}$ to be equal to 11^0 (Fig. 7). Peck and Reed (10) report the value of 11^0 for consolidated quick tests on a Chicago clay with slightly higher consistency limits and water contents. The result for the slow tests given in the same report was 20^0. The comparison is made here to show the use of the stress locus for evaluation of $\bar{\varphi}$. However, because there was a difference in consistency limits and natural water contents, presumably there would also be a small difference in the evaluated 'friction' angle.

The rupture envelopes for all soils were established by the terminal points of the stress loci. These in general defined a straight line for the same soil tested. The angle φ resulting from the establishment of the rupture envelope may be questioned in view of the technique used to obtain the second approximation for the stress locus as shown in Figure 1. However, the difference in φ values by the two procedures is relatively small. In Figure 8, only two cases are shown for the rupture envelopes drawn from the common tangent to the stress circles for illite clay with both types of pore fluid (glycol and distilled water). In comparing the effect of pore fluid on the friction angle φ in this figure with those in Figures 4 and 5, it can be seen that the percent difference is less than 1 percent. Although this correspondence may seem fortuitous, it can be shown that, by successive approximations for determination of the stress locus as shown in Figure 1, the final answer derived for φ will be identical with that shown in Figure 8. In this instance, the second approximation for stress locus determination has been found both adequate and sufficiently accurate.

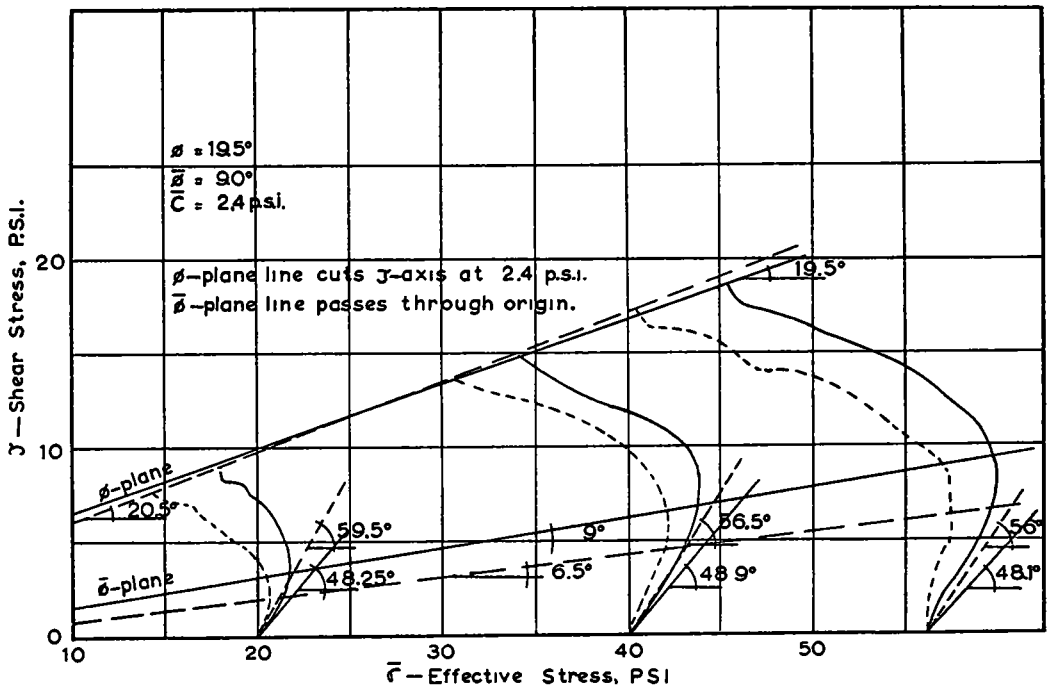

Figure 4. Stress loci for illite clay with distilled water.

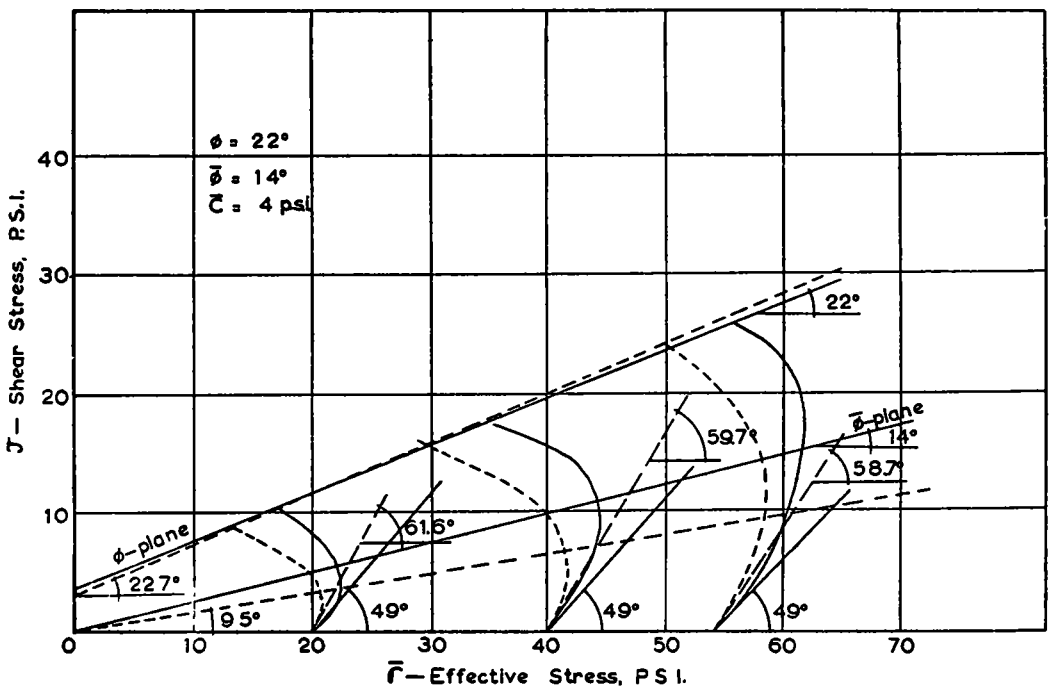

Figure 5. Stress loci for illite clay with $C_2H_4(OH)_2$.

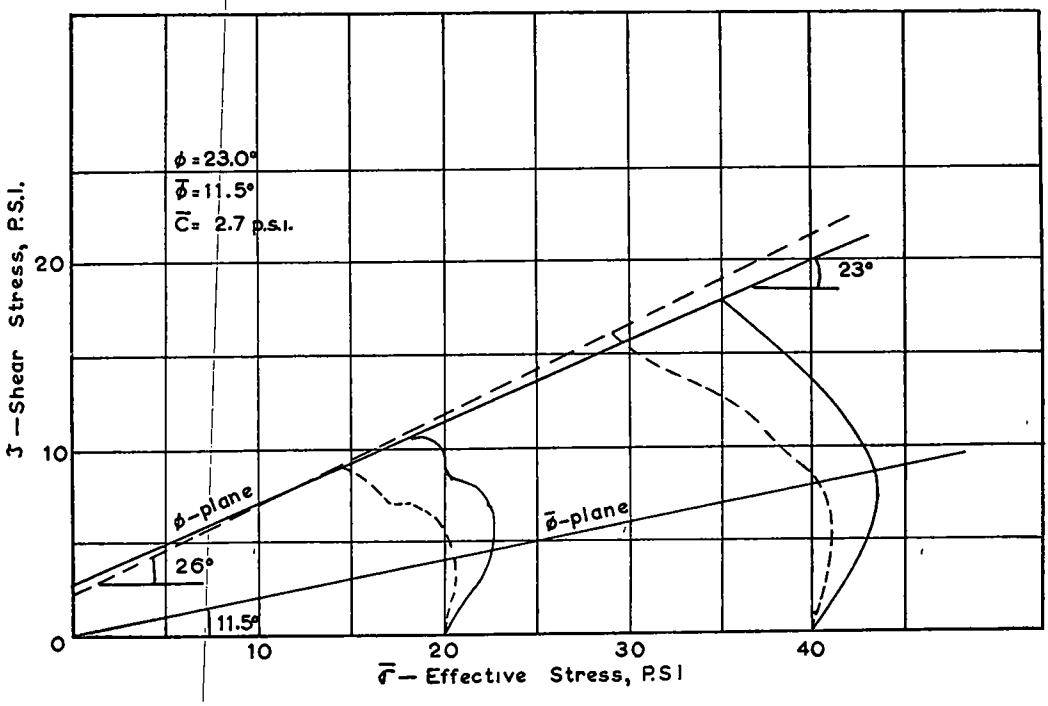

Figure 6. Stress loci for kaolinite clay with distilled water.

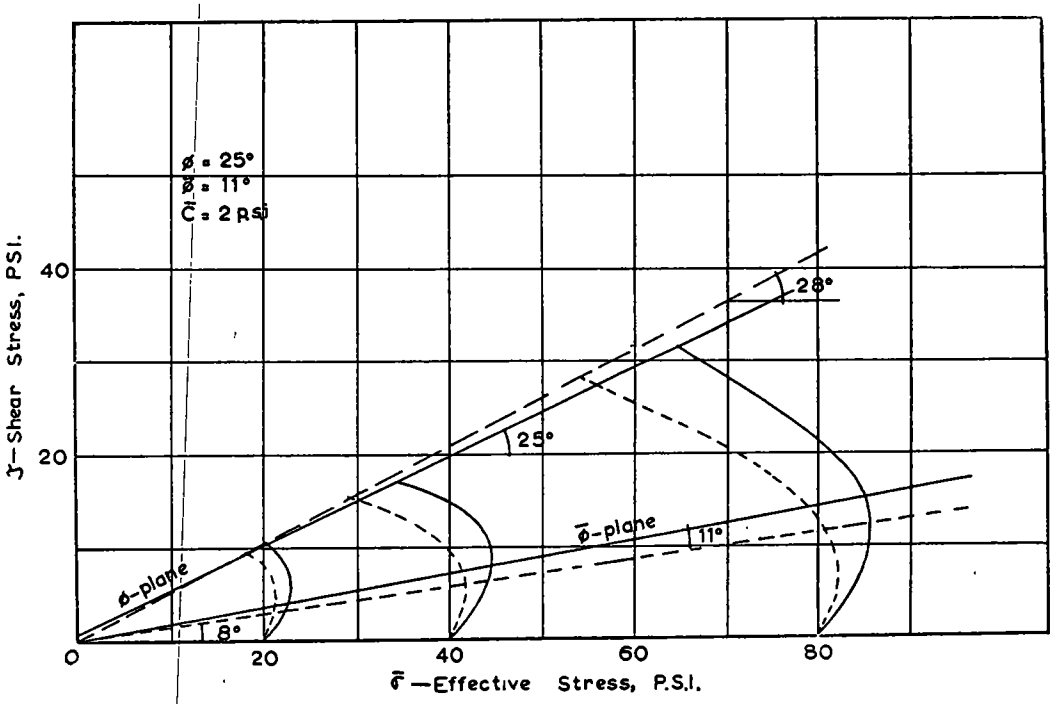

Figure 7. Stress loci for Chicago clay.

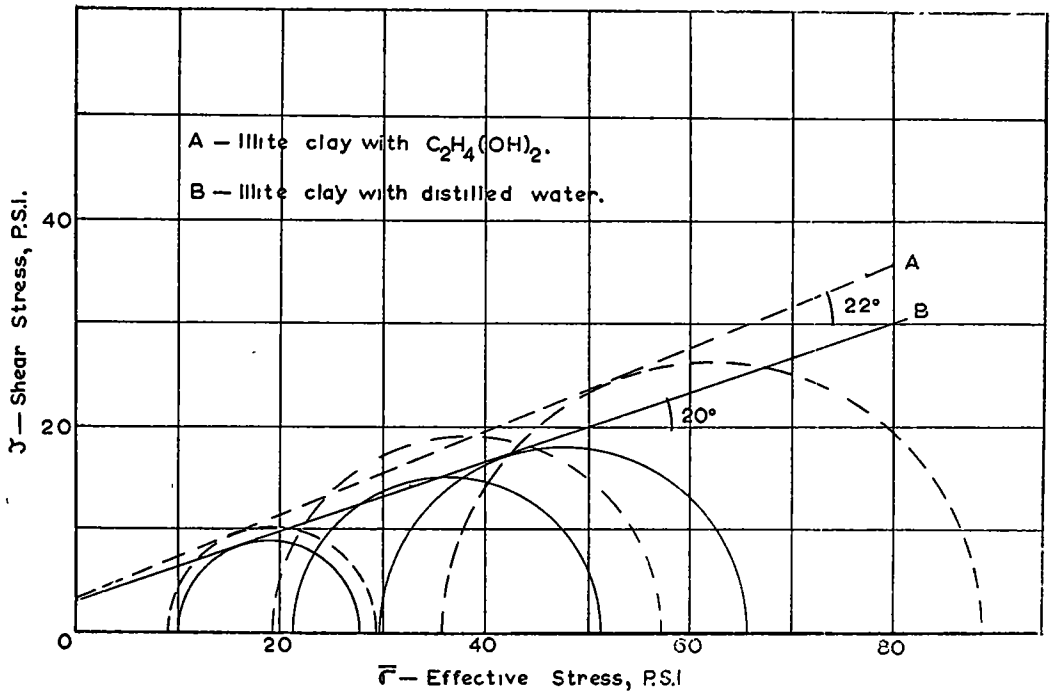

Figure 8. Effective stress circles for illite clay.

The maximum effective normal stress points on the stress loci for identical soils tested at varying confining pressure can be joined approximately by a straight line passing through the origin. The deviation from the straight line is slight.

SIGNIFICANCE OF STRENGTH PARAMETERS DERIVED FROM STRESS LOCI

It must be emphasized here that although both $\bar{\varphi}$ and $\bar{C}$ may be obtained from the stress loci, there is no possible way to define the actual boundaries of operation for these two parameters as limiting factors. Crawford (3) has shown that the friction angle varies with strain and increases as strain increases when measured in the conventional manner. In line with this, the cohesion parameter will also vary with strain. It is now well accepted that both these parameters are not constant during the entire test for measurement of shear strength, and it is further accepted that they are dependent on both pore pressure and strain—although it can be argued that strain may in turn be dependent to some extent on pore pressure.

The stress locus does not pretend to define the limits of operation of the parameters because it is well understood that both shear strength components are operative throughout the state of stress. Rather, it defines the relation between the shear stress and the effective normal stress for any one specimen subject to load application under the prescribed conditions. It is believed that the friction strength component increases rapidly in the initial stages of load application and reaches a peak while the cohesion strength component is still increasing. Beyond the peak friction component strength, total shear strength increases due to the continued increase of the cohesion strength component. This is shown in Figure 9. The stress locus in previous figures shows the shear stress increasing as effective normal stress increases (not necessarily as a linear function), to a point where shear stress increases while effective normal stress decreases. The friction strength component in the figure is drawn on this basis to interpret the variation of this component with strength. This does not necessarily mean a decreasing friction angle with increasing strength because the friction strength component is dependent on

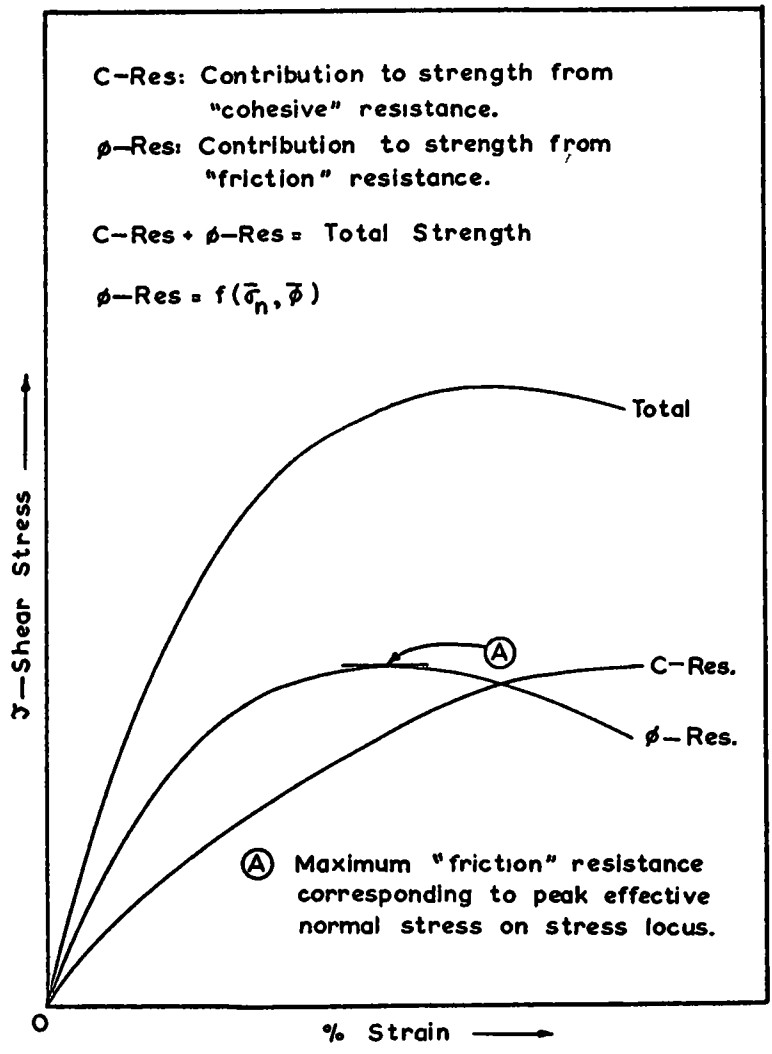

Figure 9. Strength parameter contribution to total strength.

both φ and effective normal stress. Schmertmann and Hall (11) also give data to show that φ increases with increasing strain as determined from their cohesion-friction-strain technique in which the pore pressure is controlled.

The total shear strength remains the same regardless of the method or technique used for interpretation of the strength component. Interpreting Crawford's (3) data on the basis of stress locus, $\bar{\varphi} = 9^0$ instead of 17^0 as reported. The soil considered in this reported study was a sensitive marine clay. As pointed out by Bjerrum (1) in conventional consolidated undrained triaxial tests on sensitive marine clay, the effective friction angle measured does not correspond to the effective friction angle calculated from the ratio of undrained shear strength to effective overburden pressure. Although laboratory tests gave values of effective friction angle ranging from 32^0 to 25^0 for increasing plasticity index, the calculated values for actual field conditions gave values of from 6^0 to 8^0. On this basis, the stress locus technique as applied to Crawford's data seems to bear out the value suggested by Bjerrum. However, whether this is the actual effective friction parameter seems to be more a question of definition.

For overconsolidated or partially saturated clay soils, the stress locus derived from the consolidated undrained test will give a characteristic "frictional" performance not unlike case C in Figure 3. The significance and interpretation of these loci will be discussed at a later date inasmuch as the present study is restricted to normally consolidated soils.

CONCLUSIONS

The stress loci technique used in this study shows the stress condition on a plane in the soil specimen at any one condition of strain. Although it is understood that the shear strength parameters are operative over the total stress range, a method is proposed here that defines the effective parameters, $\bar{C}$ and $\bar{\varphi}$, on the basis of their dominance in component strength contribution to total strength. By defining the effective friction angle $\bar{\varphi}$ in terms of a dependency on effective normal stress increase, a means for arriving at the parameter for normally consolidated soils is established.

In terms of the strength components, it is believed that the dominant component should define the operative parameter at its maximum point. The method suggested by this study has not been tested in terms of field application where it is believed verification or contradiction of the value of the parameters derived therefrom can be obtained.

ACKNOWLEDGMENTS

The work reported in this paper was carried out in the Soil Mechanics Laboratory of Armour Research Foundation of the Illinois Institute of Technology with Foundation support.

The authors wish to acknowledge the assistance of Raymond Rusin and Robert Rowe (both of Armour Research Foundation) in the performance of the laboratory tests. The graphs were drawn by Nathan Agensky of McGill University.

REFERENCES

1. Bjerrum, L., "The Effective Shear Strength Parameters of Sensitive Clays." Proc., 5th Conf. of Internat. Soc. of Soil Mechanics and Foundation Engineering (1961).

2. Casagrande, A., and Hirschfeld, R. C., "Investigation of Stress-Deformation and Strength Characteristics of Compacted Clays." Harvard Soil Mechanics Series, No. 61 (1960).

3. Crawford, C., "The Influence of Strain on the Shearing Resistance of Sensitive Clay." Paper, 64th Annual Meeting, ASTM (1961).

4. Holtz, W. G., and Ellis, W., "Triaxial Shear Characteristics of Clayey Gravel Soils." Proc. 5th Conf. of Internat. Soc. of Soil Mechanics and Foundation Engineering (1961).

5. Hvorslev, M. J., "Physical Components of the Shear Strength of Saturated Clays." ASCE Research Conf. on Shear Strength of Cohesive Soils (1960).

6. Lambe, T.W., "Compacted Clay." Symposium, Trans., ASCE Vol. 125, Pt. 1 (1960).

7. Leonards, G. A., "Strength Characteristics of Compacted Clay." Trans., ASCE, Vol. 120 (1955).

8. Mitchell, J. K., and Seed, H. B., "Discussion on 'Stress-Strain Characteristics of Compacted Clay under Varied Rates of Strain'." HRB Proc., 39: 616-618 (1960).

9. Osterberg, J. O., and Perloff, W. H., "Stress-Strain Characteristics of Compacted Clay under Varied Rates of Strain." HRB Proc., 39:605-615 (1960).

10. Peck, R. B., and Reed, W. C., "Engineering Properties of Chicago Subsoils." Univ. of Illinois Bull. 423 (1954).

11. Schmertmann, J. H., and Hall, J. R., "Cohesion After Non-Hydrostatic Consolidation." Jour. Soil Mechanics and Foundations, ASCE, 87: No. SM4 (1961).

12. Seed, H. B., Mitchell, J. K., and Chan, C. K., "The Strength of Compacted Cohesive Soils." ASCE Research Conf. on Shear Strength of Cohesive Soils (1960).

13. Warkentin, B. P., and Yong, R., "Shear Strength of Montmorillonite and Kaolinite Related to Interparticle Forces." Proc., 9th Nat. Conf. on Clays and Clay Minerals, Clays and Clay Minerals Series, Pergamon Press (1961).

Discussion

CHARLES C. LADD, Assistant Professor of Soil Engineering, Department of Civil Engineering, Massachusetts Institute of Technology.—There is no doubt that better methods need to be developed for relating the shear strength parameters in terms of effective stresses as measured by triaxial tests to those that describe actual strength behavior in the field. The parameters developed by the authors could be a step in the right direction. However, the interpretation of the physical significance that the authors have attached to these parameters is considered by the writer to be incorrect.

Referring to Figures 2 and 3, which show effective stress vector curves from consolidated undrained triaxial tests with pore pressure measurements, the authors state that if there is "zero" or "low pore pressure response" (in other words, Skempton's A factor is close to zero), the resistance to shear is primarily frictional in character because if "the component of shear resistance increases, it seems most reasonable to deduce that this constitutes a friction shear component." On the other hand, if there is a "full" or "high pore pressure response" (i.e., the A factor is close to unity), the material has little frictional resistance and hence the resistance must be predominately cohesional in character because the shear stress is increasing while the effective normal stress is decreasing.

Test data on a saturated Ottawa sand close to the critical void ratio are quoted to support the preceding argument. Because the vector curve showed an increasing effective normal stress as the shear stress increased (the A factor was very low), the "friction stress component" was, by definition, operative over the entire stress region. One cannot question that the strength of a sand is predominately frictional in character. However, if the authors had run a consolidated undrained test with pore pressure measurements ($\overline{CU}$ test) on a sample of loose sand, the proposed criteria for defining frictional behavior would be inconsistent. This is shown in Figure 10 which presents vector curves from $\overline{CU}$ tests on dense, medium, and loose specimens of a fine sand. The curves have been plotted from stress-strain data reported by Bjerrum, et al. (2). (The curves are not exact because the figure from which the data were scaled was very small. However, the general shapes of the curves are correct.) Although the strength of all three specimens is certainly frictional in character, the proposed criteria would define the strength as cohesional, cohesional and then frictional, and frictional for the loose, medium, and dense specimens, respectively.

Similar inconsistencies arise if the criteria are applied to clays. Vector curves from $\overline{CU}$ tests on normally consolidated and overconsolidated specimens of a plastic clay (P.I. = 40 percent) are shown in Figure 11. By the authors' criteria, the strength of the normally consolidated specimen, where A approaches unity, is predominately cohesional and that of the overconsolidated specimen, where A becomes negative, is predominately frictional. The Hvorslev parameters and hypotheses concerning the mechanism of shear strength in clays (for example, Lambe (4) and Ladd (3)) suggest, if anything, that the opposite is more plausible.

Although the writer disagrees with the interpretation that the authors have attached to their parameters, he feels that their analysis of strength via the shape of vector curves may develop into a most promising avenue of research. For example, $\overline{CU}$ tests by Bailey (1) have shown that leached samples of Boston blue clay that had been consolidated in sea water show very low friction angles at maximum stress difference and

(Data replotted from Bjerrum, et al, 1961)

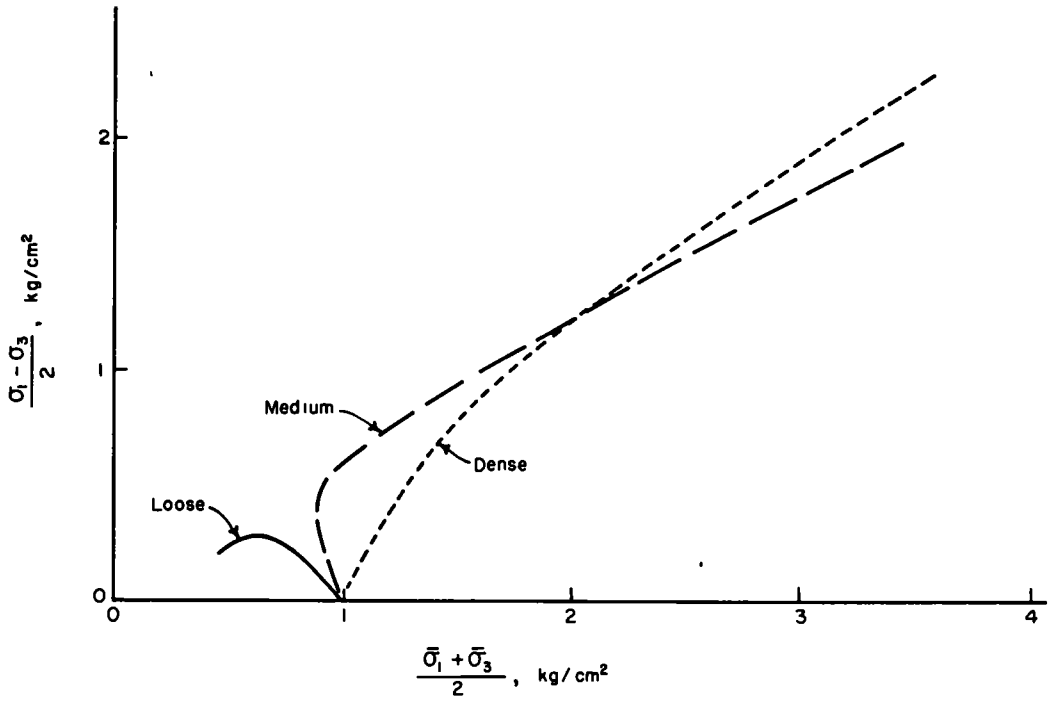

Figure 10. Vector curves from $\overline{CU}$ tests on a fine sand.

(Liquid Limit = 63%, Plasticity Index = 39%)

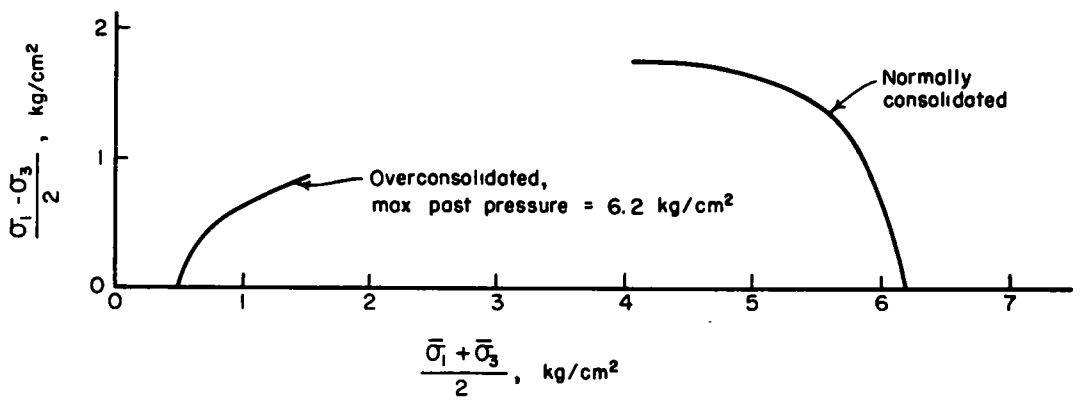

Figure 11. Vector curves from $\overline{CU}$ tests on Vicksburg buckshot clay.

marked decreases in strength at strains in excess of the strain at maximum stress difference. Such a soil might well exhibit a low friction angle in the field under conditions of undrained shear. (The samples were leached in the triaxial cells so that no disturbance occurred prior to shear.)

REFERENCES

1. Bailey, W. A., "Effects of Salt on the Shear Strength of Boston Blue Clay." B. S. Thesis, Dept. of Civil Engr., Mass. Inst. of Technol. (1961).

2. Bjerrum, L., Kringstad, S., and Kummeneje, O., "The Shear Strength of a Fine Sand." Proc., 5th Internat. Conf. on Soil Mech. and Found. Engr., 1:29 (1961).

3. Ladd, C. C., "Physico-Chemical Analysis of the Shear Strength of Saturated Clays." Sc.D. Thesis, Dept. of Civil Engr., Mass. Inst. of Technol. (1961).

4. Lambe, T. W., "A Mechanistic Picture of Shear Strength in Clay." ASCE Research Conf. on the Shear Strength of Cohesive Soils, p. 555 (1960).

R. YONG and E. VEY, Closure—The test results reported by Dr. Ladd for saturated sand and overconsolidated clays corroborate very well the current authors' findings of their initial study of the restrictions and limitations of the stress locus technique. The importance of this restriction was demonstrated in similar tests by the writers and evaluation procedures for overconsolidated and partially saturated clays. Included also, as a means for further definition of the nature of the effective stress parameters were tests on saturated sands and silts. Extreme care was taken in the paper to restrict the proposed method of evaluation to normally consolidated clays subjected to consolidated undrained triaxial tests.

The initial test results obtained from $\overline{CU}$ tests on various soil types showed that the stress locus can indeed vary over the entire range of forms shown in Figure 10 by Dr. Ladd for dense, medium, and loose fine sand. However, this same variation can be obtained with any soil type, depending on pore pressure response under load. In the case of fine sand, this response varies with the density at which the specimen was prepared. In the case of clay, it varies principally with prestress history, method of specimen preparation, and testing procedure. The effect of specimen preparation and testing procedure on the character of the stress locus has been well illustrated in other recent studies.

Because the technique proposed is essentially one that includes the variation of pore pressure coefficient A, it can be said that the stress locus is actually a measure of A for any particular specimen. Perhaps the significance of the stress locus is better viewed in this manner, because in the final analysis it is the performance of the specimen that is the object of strength evaluation studies. Based on the intrinsic dependency of the stress locus on pore pressure coefficient A, and on other recent studies it is fairly apparent that the stress loci shown in Figures 4 through 7 of the paper are acceptably those derived from normally consolidated clays. In particular, it is interesting to note from Henkel's studies that plotting his stress paths on the same basis as the stress loci demonstrated in the paper, the stress loci for normally consolidated and overconsolidated clays agree well with the current authors' suggestions. As stated in the paper, "For overconsolidated or partially saturated clay soils, the stress locus derived from the consolidated undrained test will give a characteristic 'frictional' performance not unlike case C in Figure 3."

To apply the working hypothesis to cases other than normally consolidated clays would be extending it beyond the defined limits of the test and the restrictions imposed by the writers. It is perhaps unfortunate that all the different varieties of stress loci were not included in the original presentation. However, it was purposely intended to restrict the paper to a consideration of normally consolidated clays and to defer consideration of both overconsolidated and partially saturated clays until more data are available.

A Rheological Analysis of Shear and Consolidation Of Saturated Clays

ADEL S. SAADA, Research Assistant, Princeton University

This study deals with "saturated clay," characterized by its dry density and moisture content. A change in the moisture content gives another material with other properties. On this material, the classical laws of rheology are applied and the behavior in shear and consolidation analyzed in their light. A quick analysis of the state of stress in a triaxial test shows that the shears due to the deviator of stresses form a circular cone tangent to the octahedral plane for any system of axes rotating around the axis of the sample.

Five series of tests show that in "saturated clay" the directions of maximum shear stresses and strains coincide and are independent of the stress at failure. This stress is not influenced by the isotropic component of the stress tensor, which causes the major part of the pore pressures. The tests show that the material has no true yield limit and that the curvature of the stress-strain diagram is influenced by the rate of strain at all stress levels. Finally, creep tests show that the rate of strain at the steady stage is dependent only on the value of the stress and independent of the load path.

The preceding results lead to the conclusion that a saturated clay is a viscoelastic material and that in its steady state of creep the laws of the theory of elasticity regarding the distribution of stresses are applicable. This opens the door to the wealth of information gathered in the study of high polymers. A general rheological model is given and analyzed, together with possible simplifications and the meanings and limitations of the various parameters.

•THE MECHANICAL properties of a soil are characterized by the internal friction and the cohesion. Rolling and sliding friction together with the resistance due to the geometry and relative position of the grains are usually gathered under the name of internal friction. True cohesion is explained as that part of the clay resistance due to the force of attraction which exists between the clay mineral particles. Little is known about the bond between the clay particles. If Terzaghi's assumption is accepted that a water shell surrounds each clay particle and is so firmly tied to it by electrochemical forces that it is nearly solid near the particle's surface, then it can be concluded that the shear strength in clays must be transmitted through the water shells separating the single grains. The cohesion is in this way determined by the strength of the adsorbed water. In modern literature, there is a great controversy concerning the rigidity and thickness of the adsorbed layer. However, it seems uncertain that a firm rigid bonding of the adsorbed water, if it exists, could endow the mass of saturated clay with true strength allowing for the existence of a true yield limit of practical significance.

This paper has as its subject the fundamental behavior of saturated clays on a phenomenological level. In other words, with awareness of the behavior and influence of each of the two solid and liquid soil phases, the author deals with the material "saturated clay" without trying to separate and recombine the effects of each phase. The paper considers that a change in the moisture content gives a different material with different mechanical properties.

The study is divided into three distinct but interrelated parts. The first part discusses tests conducted to establish whether the material could be classified as plastic or viscoelastic. Based on this classification, the second part gives rheological models in shear and in consolidation and indicates a method of analyzing test results for both cases. The third part discusses some implications of the study and proposes a method of design appropriate to the type of material as classified in the first part.

The symbols used throughout this paper are defined in Appendix B.

CLASSIFICATION OF SATURATED CLAY

In spite of their structural complexity, engineering materials may, with fair approximation, belong to either of the two types defined in terms of the characteristic differences in their inelastic deformation (7, 8):

1. The plastic materials. Here the deformational response to applied forces beyond the elastic or yield range results in permanent changes within the aggregate structure. Up to the elastic or yield limit the material can either store, reversibly and indefinitely, a certain quantity of energy, or it can withstand a certain level of stress without continuing deformation. Beyond this limit, yielding and/or work hardening occurs and the capacity of storing energy is maintained or increased; also, the effect of past stress is pronounced and permanent and does not vanish with time. Materials whose plastic behavior is dictated by a Coulomb type of plasticity ($\tau = \sigma \tan \varphi$) have a yield limit (shear strength) that increases with the increase of the compressive normal stresses. Thus, an increase of the volumetric stresses acting on these materials results in a proportional increase of the shear strength.
2. The viscoelastic materials. Here the dissipation of the applied energy depends not only on the material itself, but also on the rate at which work is done by the load. Volumetric compressive stresses have a small effect on the shear behavior, because viscosity increases very slowly with the increase of the normal stresses. The curvature of the stress-strain diagram at a definite stress level varies with the momentary strain rate. The material can store a certain amount of energy for a finite time, but this energy is dissipated with the relaxation of the induced shear stresses. In other words, flow occurs under any shear stress however small; also, the effect of load history vanishes with time.

State of Stress in a Triaxial Test

A state of stress is represented by a tensor. This tensor can always be considered as the result of the superposition of an isotropic (hydrostatic or volumetric) and a deviatoric one. In terms of the principal stresses (compression is considered positive and tension negative):

$$\begin{vmatrix} \sigma_1 & 0 & 0 \\ & \sigma_2 & 0 \\ & & \sigma_3 \end{vmatrix} = \begin{vmatrix} \sigma_m & 0 & 0 \\ & \sigma_m & 0 \\ & & \sigma_m \end{vmatrix} + \begin{vmatrix} S_1 & 0 & 0 \\ & S_2 & 0 \\ & & S_3 \end{vmatrix}$$

in which

$$\sigma_m = \frac{\sigma_1 + \sigma_2 + \sigma_3}{3}$$

is the mean or isotropic stress, and $S_i = \sigma_i - \sigma_m$ characterized by $\Sigma S_i = 0$ is the deviator. In any material, the isotropic component is the main cause of the volume changes and the deviatoric component is responsible for the flow and fracture of the material.

In a classical triaxial test, a cylindrical sample is subjected to an increasing vertical pressure and a constant lateral pressure ($\sigma_2 = \sigma_3$) until fracture occurs. The state of stress at any time can be decomposed in the following way into isotropic and devia-

toric components:

$$\begin{vmatrix} \sigma_1 & 0 & 0 \\ & \sigma_2 & 0 \\ & & \sigma_3 \end{vmatrix} = \begin{vmatrix} \sigma_m & 0 & 0 \\ & \sigma_m & 0 \\ & & \sigma_m \end{vmatrix} + \begin{vmatrix} S_1 & 0 & 0 \\ & -\frac{S_1}{2} & 0 \\ & & -\frac{S_1}{2} \end{vmatrix}$$

The Mohr circle representing this state of stress is shown in Figure 1. For the circle to represent the state of deviation alone, the origin of the axes is shifted from 0 to 0' with

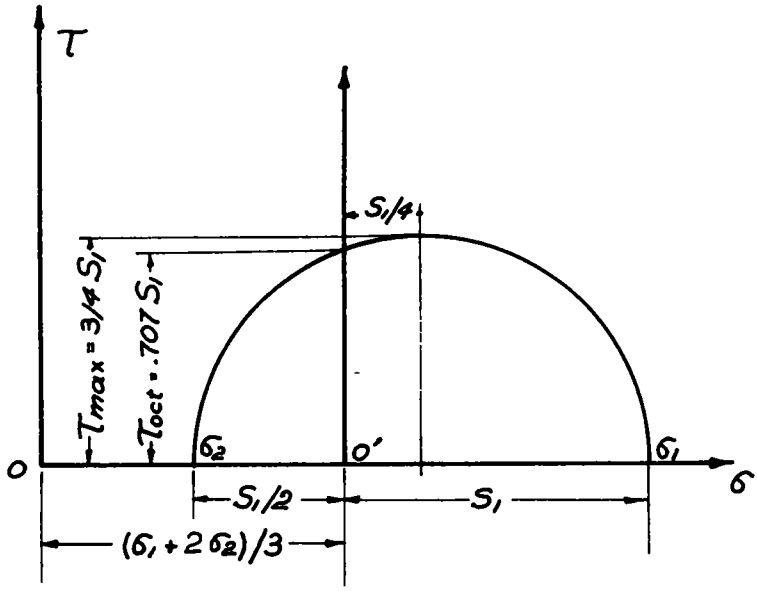

Figure 1. Mohr diagram for state of deviation in triaxial compression test.

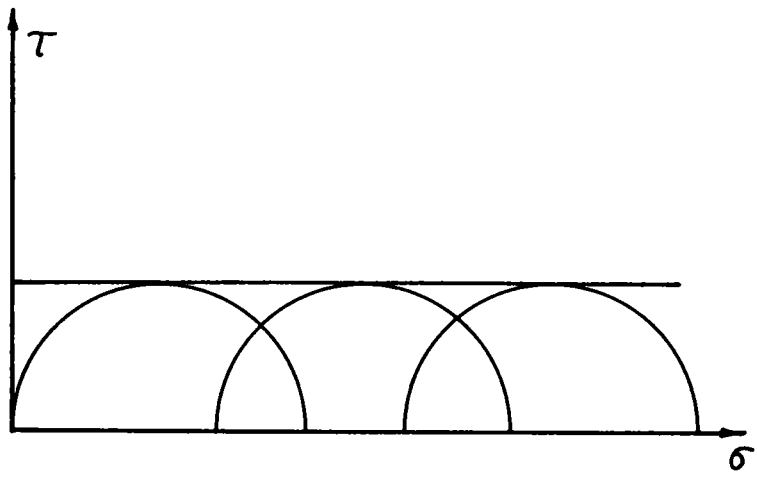

Figure 2. Mohr diagrams for constant volume saturated clay.

$$00' = \sigma_m = \frac{\sigma_1 + 2\sigma_2}{3}$$

A pure deviation can be applied to the material if the stress increments are made in a way such as to keep the isotropic component of the stress tensor constant. In a triaxial test, this is done by increasing the vertical pressure and decreasing the lateral pressure so that

$$\frac{\text{vertical stress increment}}{\text{lateral stress decrement}} = 2$$

In the range of small strains, volume changes due to the state of deviation can be neglected as being of the second order. However, with the increase in magnitude of the strains, these second order effects become important and result in pore pressures if the drainage is closed.

Experimental Investigation

A series of tests was made with a white kaolinite type of New Jersey clay designated by its trade name as Grantham clay. Its liquid limit is 77 percent, its plastic limit 32 percent. About 60 percent of the material is smaller than 2 μ. The material, in powder form, was mixed thoroughly with water, the mixture being in its natural state at about 95 percent of saturation. Complete saturation and specific moisture contents were obtained by triaxial consolidation under various volumetric stresses.

Effects of Volumetric Stresses and Rate of Strain on Shear Behavior.—Undrained triaxial tests on the same saturated clay material and under various lateral pressures are known to give similar stress-strain characteristics and Mohr circles at failure having the same diameter. These circles are located at different distances from the origin (Fig. 2) and correspond to the various values of the mean stress σ_m. Thus, in spite of an equal increase in the normal stresses on all the planes of the material being tested, the magnitude of the deviator of stresses at failure does not change.

The value of the maximum stress difference $(\sigma_1 - \sigma_3)$ increases with the rate of strain and the stress-strain curve moves towards smaller strains for higher strain rates. All plastic and viscoelastic materials are influenced by this variable; the difference is that this influence extends over the whole range of the stress-strain curve in viscoelastic material, and only on that part beyond the yield limit in plastic materials. Several identical samples with the same moisture content were tested in compression under various rates of vertical strain. In all cases and at all stress levels, the curvature of the stress-strain diagrams varies with the change of the rate of strain. Figure 3 shows the true stress, true strain diagram of two of the samples. The presence of a true elastic limit would have caused the two curves to coincide at the stress levels below this limit. If it exists, it is so small that it could not be recorded for the material under consideration.

Existence of a True Yield Limit.—Two types of tests are possible and were performed to find the level of shear stress that can be applied to the material without causing permanent deformations.

The first type is the relaxation test. In this test a certain deformation is applied to the sample and the decay of the induced stress measured with the time. A sample of 2.8-in. diameter, 7.4-in. height at a moisture content of 35.80 percent was given an initial axial deformation of 0.013 in. The axial stress was applied by means of a proving ring and the initially induced octahedral shear stress was 6.08 psi. The relaxation of the stress as indicated by the proving ring dial was accompanied by a slow creep of the material. Figure 4 shows the stress plotted against the logarithm of the time. It dropped to zero in a period of 56 days. The octahedral shear stress at failure for the same sample was 22.6 psi. The curve was expected to have an inflexion point beyond a value of the time equal to 2×10^4 min and theoretically the stress should have tended to its final value asymptotically. This, however, was not recorded.

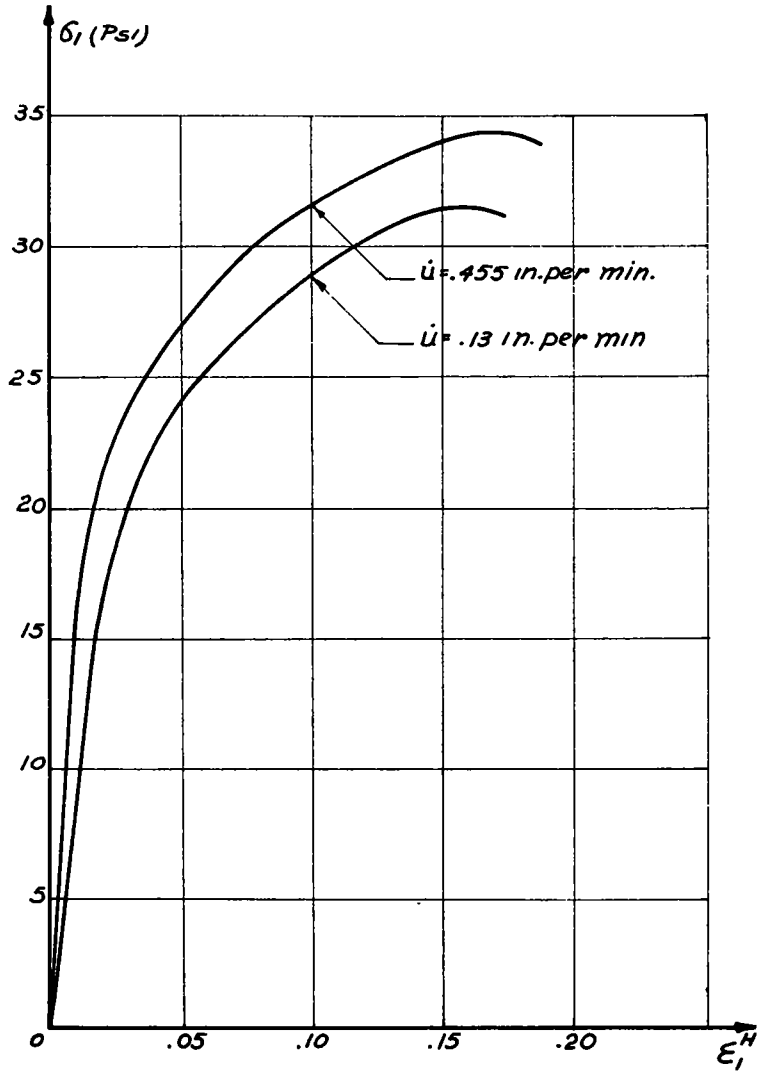

Figure 3. Influence of the rate of strain on the stress-strain curve ($\sigma_2 = \sigma_3 = 0$; moisture content = 36.60 percent).

The second type of test is the creep test. In this test a small, constant shear stress is applied for a period of time, then removed and the resulting rebound is measured. This rebound, for any stress smaller or equal to the yield limit, should bring complete strain recovery. A series of creep tests were performed under a certain number of deviators (6, 12, 18 psi) for a period of 24 hr. The deformations during this period and after the release of the stresses were measured (Fig. 5). The fact that a deviator equal to one-tenth of the deviator of fracture (60 psi) results in permanent deformation allows one to conclude that no true yield limit of practical significance exists in the considered material. At a later date, a creep test performed on the same type of clay, but at a higher moisture content, showed that even under a deviator of 1 psi, permanent flow occurred (Fig. 6). The deviator of fracture for this last material was 38 psi.

In summary these tests show that on the level of investigation, the material considered flowed under any shear stress and that it had no true yield limit.

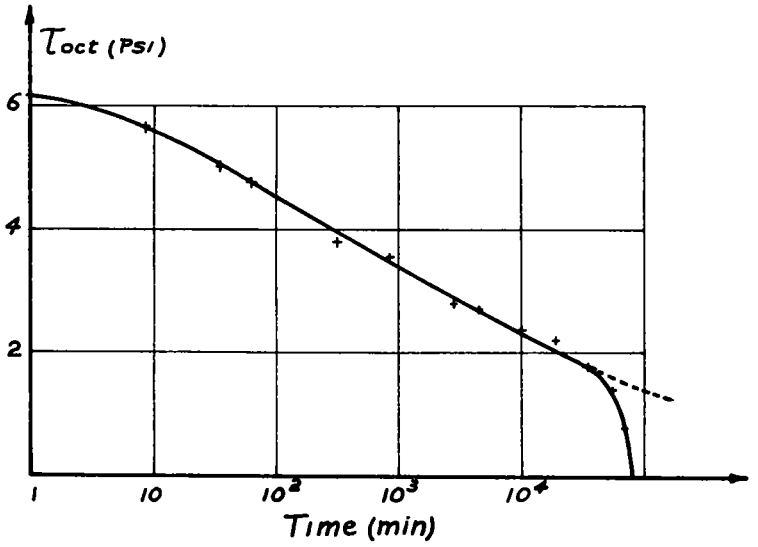

Figure 4. Decay of induced octahedral shear stress with time.

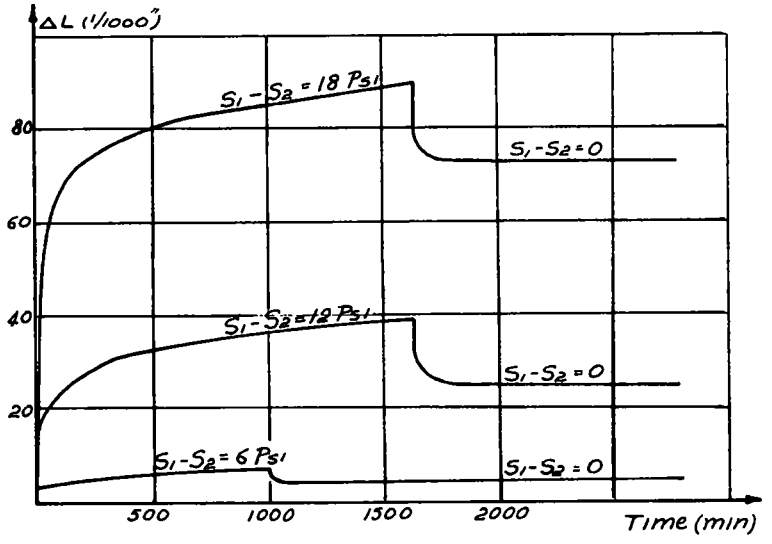

Figure 5. Creep under various deviators of stress.

Effect of Load Path on Strain-Time Characteristics. —The main aim of this group of tests was to study the effect of the load path on the steady state part of the creep curve. One of the principal characteristics of viscoelastic materials is that in a creep test, once a constant rate of strain is reached, it is only a function of the magnitude of the applied stress and independent of the load path. Three identical samples of 2.8-in. diameter and 7.4-in. height were subjected to various deviators (discussed later) for periods varying between 65 and 80 hr. Table 1 gives the sequence of loading. Results of these tests are shown in Figure 7. For all the curves an apparently instantaneous response, a retarded response, and a flow at a constant rate are present. Up to the

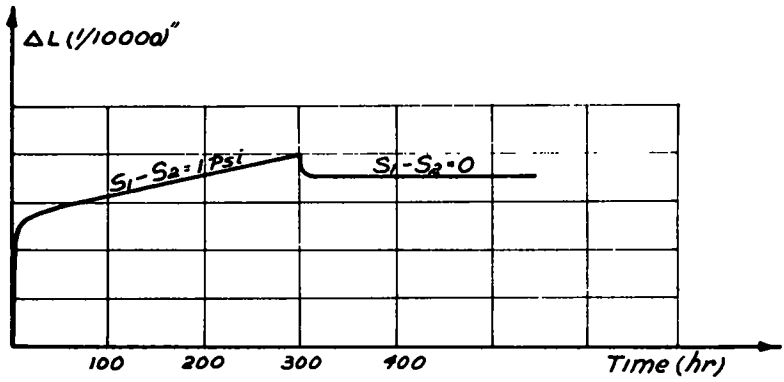

Figure 6. Creep under a deviator of 1 psi.

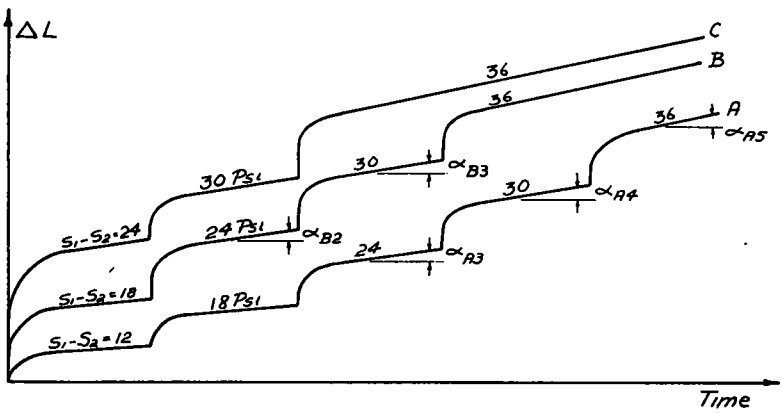

Figure 7. Independence of constant rate of strain from stress path.

TABLE 1

Sample	Applied Deviator (S_1 - S_2) (psi)								
A	12	18	24	30	36	42	48	54	60
B	18	24	30	36	36	42	38	54	60
C	24	30	36	36	36	42	48	54	60

deviator preceding fracture, the constant rate has been found to be dependent only on the total value of the deviatoric stress, and in Figure 7,

$$\alpha_{A2} = \alpha_{B1}$$

$$\alpha_{A3} = \alpha_{B2} = \alpha_{C1}$$

$$\alpha_{A4} = \alpha_{B3} = \alpha_{C2}, \text{ etc.}$$

Thus, the angles α describing the constant rate are independent of the rate of stress and the load path.

Summary.—To sum up the results of the experimental investigation, the material under consideration presents the following features in its shear behavior:

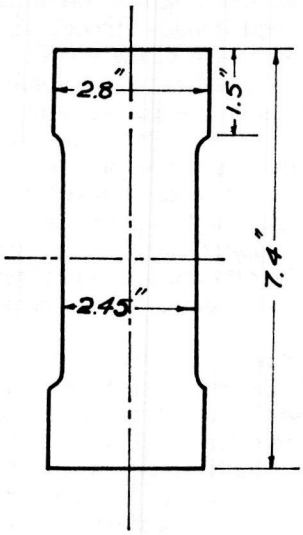

Figure 8. Shape of samples tested in pure deviation.

1. The deviatoric component of the strain tensor does not depend on the isotropic component of the stress tensor.
2. The curvature of the stress-strain diagram at all stress levels is affected by the rate of strain of the material.
3. The material flows under any shear stress.
4. The constant rate of strain in creep tests is independent of the load path and is a function of the stress alone.

These four items are the necessary and sufficient conditions for a material to be classified as "viscoelastic."

Possible Surfaces of Flow and Failure in Triaxial Compression Test

In an ideal linear viscoelastic material, the directions of maximum shearing stresses

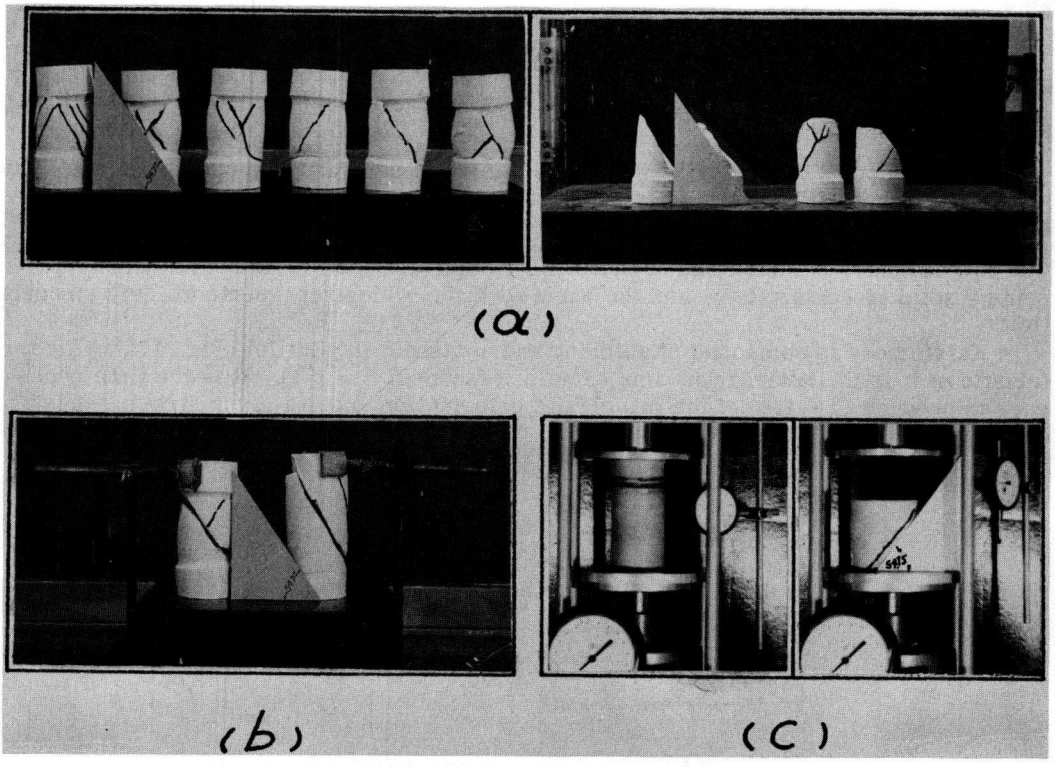

Figure 9. Fracture surfaces in triaxial compression tests.

and maximum shearing strains coincide. In such a material, failure would most probably occur along surfaces inclined at 45° to the horizontal (though viscoelastic considerations cannot be extended to failure). The isotropic component of the stress tensor acts normally and equally on all planes and would not favor any surface of fracture. The state of stress produced by the deviator alone gives on planes inclined at 45° a maximum shear equal to 0.75 S_1 (Fig. 1) and a normal stress equal to 0.25 S_1. Real viscoelastic materials are influenced to a very small extent by normal stresses and under a given deviator, failure might occur along surfaces subjected to a shear stress slightly smaller than the maximum and to a very small normal stress. In Figure 1, point A represents a plane on which the deviator of stresses gives a shear stress equal to approximately 94 percent of the maximum and a normal stress equal to zero. This plane is the octahedral plane and its inclination to the horizontal is equal to 54.75°. Thus, conical surfaces having this inclination are potential surfaces of flow and fracture.

A number of samples were turned down to the dimensions shown on Figure 8 to avoid end effects and tested in triaxial compression. In all the cases where no excessive bulging occurred before failure, the tangents to the surfaces of fracture make with the horizontal angles near 54.75° (Fig. 9a). In the case of cylindrical samples, the fracture starts at one of the ends because of the concentration of stresses, but it takes the direction of minimum shear resistance which seems to be that of the octahedral plane (Fig. 9b). Figure 9c shows one of the samples tested in an unconfined way with grease applied on both end plates. The sample kept a cylindrical shape (no rotation of principal axes) and the inclination of the surface of rupture was very near to the octahedral inclination.

The same tests were run on an illite type of clay called grundite clay at various moisture contents. The results were similar to those obtained for the kaolinite Grantham clay.

RHEOLOGY OF SHEAR

Models to illustrate viscoelastic behavior in shear are built up from combinations of two model elements:

1. A perfectly elastic spring to represent elastic deformations obeying Hooke's law.
2. A dashpot with a liquid obeying Newton's law of viscosity to represent viscous deformations.

The two simplest combinations of these two models are the Kelvin body, which represents a solid viscoelasticity, and the Maxwell body, which represents a liquid viscoelasticity.

A Kelvin body is composed of a spring and a dashpot in parallel (Fig. 10a). Characteristic of it is the retardation time (time of response) $\tau = \eta/G$. It is the time necessary to produce (1 - 1/e) of the full elastic deformation under a given stress. It is a

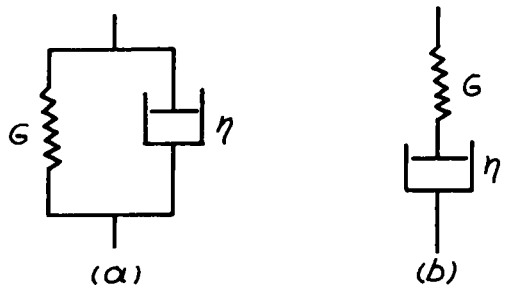

Figure 10. a) Kelvin body, b) Maxwell body.

sort of limit after which the strain tends to its final value at a very slow, decreasing rate.

A Maxwell body is composed of a spring and a dashpot in series (Fig. 10b). Characteristic of it is the relaxation time also defined as $\tau = \eta/G$. It is the time necessary for a stress to decay to 1/e of its original value while a constant strain is maintained. In a way, it is a time limit after which a sizeable decrease in the stress level is associated with a long and ever-increasing time (7, 17).

In both ideal bodies the relative importance of the elastic and the flow mechanisms apparently depends not only on the magnitude of G and η but also on the time scale of the experimental investigation. Either of the two mechanisms will tend to overshadow the other unless the time scale of the observations is of the order of magnitude of η/G, a circumstance that will allow the appearance of the composite nature of the deformation.

The behavior of a real material usually cannot be described by the two constants η and G of the ideal bodies However, the introduction of several such constants will permit reproduction of rather complex behavior.

Necessity for a Distribution of Retardation Times

The kind of isotropy that is present in the material is a statistical one When studying the deformational characteristics, the fact that each clay particle is surrounded by a hull of adsorbed water, whose viscosity varies between infinity and that of more or less free water, tends to complicate the problem when a factor of viscosity (23) is chosen in a quantitative analysis. An average value can always be chosen during the process of deformation, but this value would only be valid at a certain location of the material. There is a wide range of particle sizes in a clay soil, and the strength of the bonds between them is very highly influenced by these sizes and particularly by the spacing and geometric arrangement between the particles. When subjected to a stress, the material necessarily presents in its delayed response a wide range of retardation times. Theoretically, a retardation time implies complete recovery on release of the stress. Yet this will not be the case in clays. The delayed response that the creep curves of Figures 5 and 6 show is only partially recoverable and is accompanied by a continuous reorientation of the particles. A constant rate of deformation under a constant energy level (Figs. 5, 6, 7) denotes the establishment of a statistical equilibrium between a continuously applied energy and the dissipation that proceeds in small successive jumps and has the appearance of continuity. At this stage the rate of energy dissipation is only a function of the deviator of stresses and is given in terms of the octahedral variables by

$$W_D = \frac{3}{2}\frac{d}{dt}\int \tau_{oct}\, d\,\gamma^H_{oct} = \frac{3}{2}\frac{(\tau_{oct})^2}{2\eta} \qquad (1)$$

in which W_D is the rate of energy dissipation.

The condition of viscous flow is given by

$$\tau_{oct} = 2\eta\,\frac{d\,\gamma^H_{oct}}{dt} \qquad (2)$$

Model Representation of a Viscoelastic Saturated Clay

On the phenomenological level, any viscoelastic material presenting a whole spectrum of retardation times, whatever their origin, can be represented by n Kelvin bodies in series, with a Maxwell body to take care of any pure elasticity and pure viscous flow (Fig. 11a). For a constant deviatoric stress, the strain in such a model is given by (15)

$$e_{ij} = (S_{ij})_o\left[\frac{1}{2G_o} + \sum_{n=1}^{n}\frac{1}{2G_n}\left(1 - e^{-t/\tau_n}\right) + \frac{t}{2\eta_o}\right] \qquad (3)$$

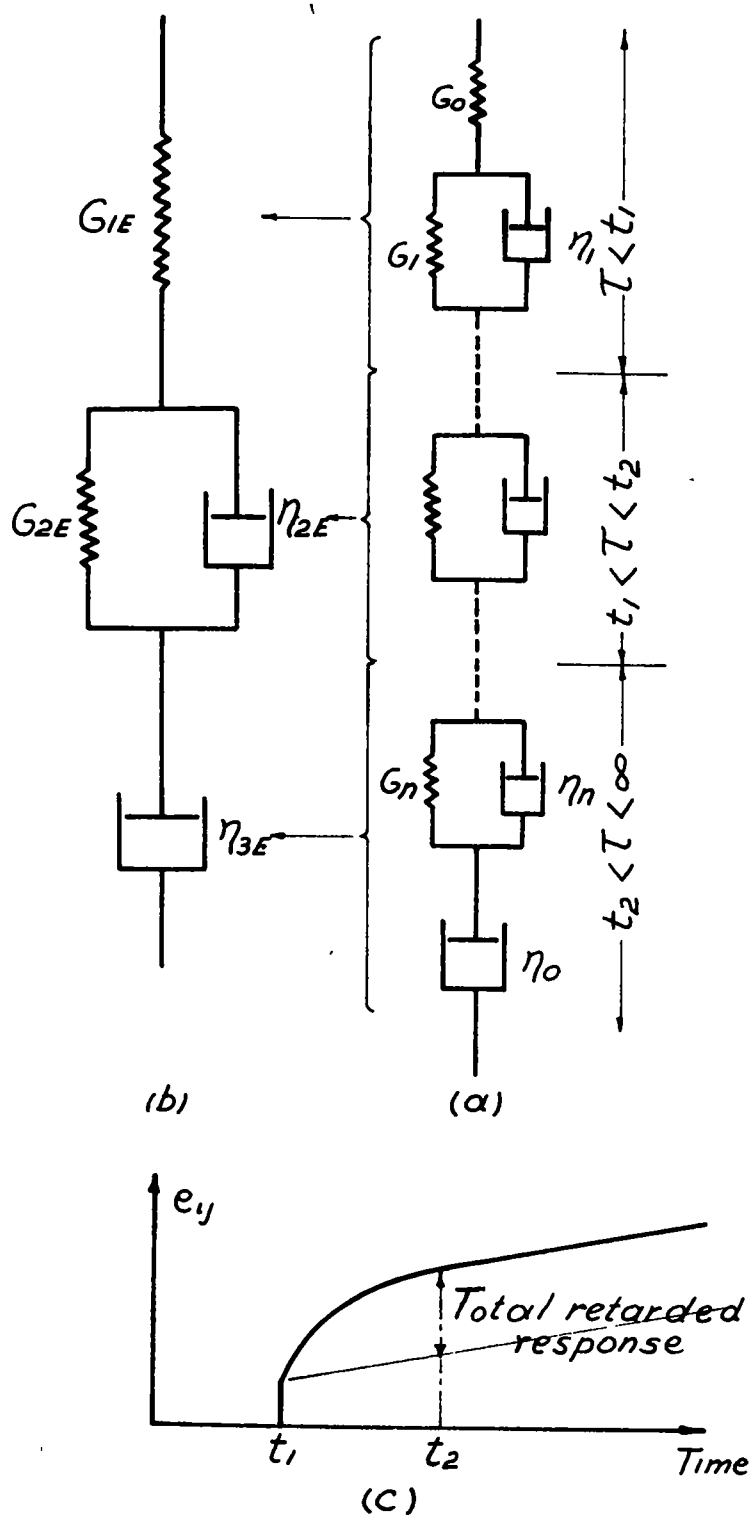

Figure 11. a) General model for a viscoelastic saturated clay in shear,
b) Four parameters experimental model (Burger's body),
c) Strain-time curve under a constant deviator of stress.

For a continuous distribution of retardation times, which can be assumed in clays;

$$e_{ij} = (S_{ij})_o \left[\frac{1}{2G_o} + \int_o^\infty \frac{J(\tau)}{2} (1 - e^{-t/\tau}) d\tau + \frac{t}{2\eta_o} \right] \quad (4)$$

where $J = 1/G$ is called the compliance of the Hooke element. Thus, the finite set of constants (J_n, τ_n) is now replaced by $J(\tau)$ which gives the amount of elastic compliance associated with the retardation time τ (the continuous parameter). This is referred to as a distribution of retardation times or distribution of compliances. This distribution should be obtainable from the experimental determination of the creep function:

$$\varphi(t) = \frac{2e_{ij}}{(S_{ij})_o} \quad (5)$$

but this presents considerable difficulties. Andrews (3) has proved that $J(\tau)$ can be obtained to a first approximation from the creep curve (Fig. 3) using the expression:

$$J(\tau) = \frac{d}{dt} \varphi(t) - \frac{1}{\eta_o} \quad (6)$$

Alfrey (1) has given a graphical method to obtain this distribution from the experimental creep curve (see Appendix A).

The model of Figure 11a has as an aim a qualitative description of the creep behavior under a particular stress. The phenomenological treatment of the problem is only interested in the resulting behavior which is materialized by the creep curve; the model must be considered as a whole, with all its elements acting together and giving a strain comparable to that of the material. Under a constant stress, each of the Kelvin bodies gives a simple exponential curve and the true deformational curve will keep the general exponential shape.

To approximate an experimental curve one does not need a continuous distribution of retardation times; in general, two or three elements are sufficient to approximate a creep curve of classical shape. The use of the continuous distribution greatly simplifies the computations and allows a relatively simple graphical construction to study the effects of mechanical variables on the properties of the material represented by the coefficients G and η.

Simplified Four-Parameter Empirical Model

Ideal creep curves should be determined over the complete time range from 0 to ∞. Experimentally it is difficult to determine the short-time response accurately; this means that the short-time behavior of the material will not show up. In terms of models, Kelvin bodies with a retardation time smaller than the smallest time observable experimentally (say, 1 or 2 sec) would behave as a pure spring (pseudo-elastic)(Figs. 11a, 11b). Kelvin bodies with retardation times falling within the time scale of the experimental investigation can be approximated by one Kelvin body with an average retardation time. Long retardation times appear as true flow (pseudo-flow) and can be approximated by a Newton element. Thus the simplest model to take the place of the most general one is the four-elements model known as the Burgers body (Fig. 11b). Each of the parameters of this model is followed by the letter E standing for experimental or empirical (1). Figure 11c shows the shape of its strain-time curve for a constant deviator $(S_{ij})_o$ (1, 6, 15, 16). The curve represents

$$e_{ij} = (S_{ij})_o \left[\frac{1}{2G_{1E}} + \frac{1}{2G_{2E}} (1 - e^{-t/\tau 2E}) + \frac{t}{2\eta_{3E}} \right] \quad (7)$$

About this empirical model the following may be said:

1. G_{1E} is the modulus of the Hooke element that replaces an element of ideal elasticity and a certain number of Kelvin elements with small retardation times. This modulus is by no means a constant, and its physical meaning does not go beyond the fact that it is related to the internal structure at the instant of application of the stress and during that period of response which seems to be instantaneous In general, the use of a Hooke element implies instantaneous response and complete reversibility, which is not at all the case when the internal structure changes continuously as a function of the stress and strain and their time derivatives. (Temperature is not considered.) If the distribution of $J(\tau)$ is known, G_{1E} is given by

$$\frac{1}{G_{1E}} = \int_{o}^{t_1} J(\tau)d\tau \tag{8}$$

t_1 being the smallest amount of time measurable. Actually from a creep test the only way to get G_{1E} is to divide $(S_{ij})_o$ by twice the instantaneous pseudo-elastic strain.

2. G_{2E} and η_{2E} are the parameters of that Kelvin body which takes the place of all the models whose retardation time falls between t_1 and t_2 (Fig. 11). If the distribution of $J(\tau)$ is known, then

$$\frac{1}{G_{2E}} = \int_{t_1}^{t_2} J(\tau)\, dt \tag{9}$$

in which t_2 is either the time at which the test is stopped (the curve becomes a straight line at infinity) or the time at which it is decided that the creep curve can be considered a straight line (steady state of creep). τ_{2E} can be given by a weighted mean value:

$$\tau_{2E} = \frac{\int_{t_1}^{t_2} \tau J(\tau)\, d\tau}{\int_{t_1}^{t_2} J(\tau)\, d\tau} \tag{10}$$

From a creep test G_{2E} is obtained by dividing $(S_{ij})_o$ by twice the total retarded response (Fig. 11c).

3. η_{3E} corresponds to all responses that appear to be true flow and can be obtained directly from the slope of a creep curve at the steady state. Theoretically it is given by

$$\eta_{3E} = \frac{1}{\frac{1}{\eta_o} + \int_{t_2}^{\infty} \frac{J(\tau)}{\tau}\, d\tau} \tag{11}$$

Limitations and Difficulties of a Model Representation

The previous model representations were inspired by the creep curve of the material under a particular stress and the presented physico-chemical considerations. The fact that only the over-all behavior of the model could be compared with the over-all behavior of the material was already emphasized. The author seeks to represent only an outside appearance by means of a series of "linear elements," an experimental curve to fit for a particular stress.

The previous rheological equations imply the constancy of the parameters G and η, and solutions of these equations given in classical treatises on rheology are valid only for linear viscoelastic behavior. This is not the case for saturated clays. The retardation times of the various Kelvin elements are not constant. Of course, no objection can be made to picking up a specific experimental creep curve, representing it by a series of linear Kelvin elements, and finding the distribution of retardation times, if it is remembered that what is deduced from that creep curve is not valid for any other state of stress even for the same material.

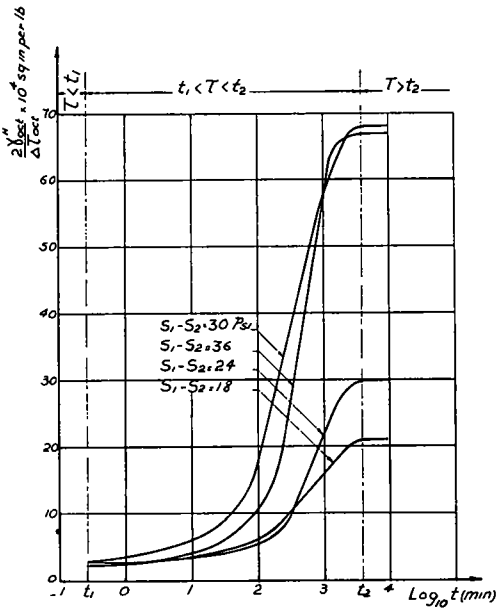

Figure 12. First step of Alfrey's construction to obtain distribution of the retardation times.

Effect of Stress Increase on Rheological Parameters

Eq. 4 can be written in terms of the octahedral variables:

$$\gamma^{H}_{oct} = (\tau_{oct})_o \left[\frac{1}{2G_o} + \int_o^{\infty} \frac{J(\tau)}{2} (1 - e^{-t/\tau}) \, d\tau + \frac{t}{2\eta_o} \right] \quad (12)$$

The creep function $\Phi(t)$ becomes

$$\varphi(t) = \frac{2\gamma^{H}_{oct}}{(\tau_{oct})_o} = \left[\frac{1}{G_o} + \int_o^{\infty} \frac{J(\tau)}{2} (1 - e^{-t/\tau}) \, d\tau + \frac{t}{\eta_o} \right] \quad (13)$$

The distribution of retardation times can thus be obtained by Alfrey's method for different values of $(\tau_{oct})_o$ if the creep curves are plotted in terms of γ^{H}_{oct}. This has been done for the creep curves of Sample A (Fig. 7) for $S_1 - S_2$ = 18, 24, 30, and 36 psi. The deviator increments were 6 psi corresponding to τ_{oct} = 2.82 psi.

The sigmoidal curves giving the relation between

$$\frac{2\gamma^{H}_{oct}}{\Delta\tau_{oct}}$$

and $\log_{10} t$ are shown in Figure 12, and the distribution of retardation times for the various stress states on Figure 13. The latter figure shows clearly that the distribution

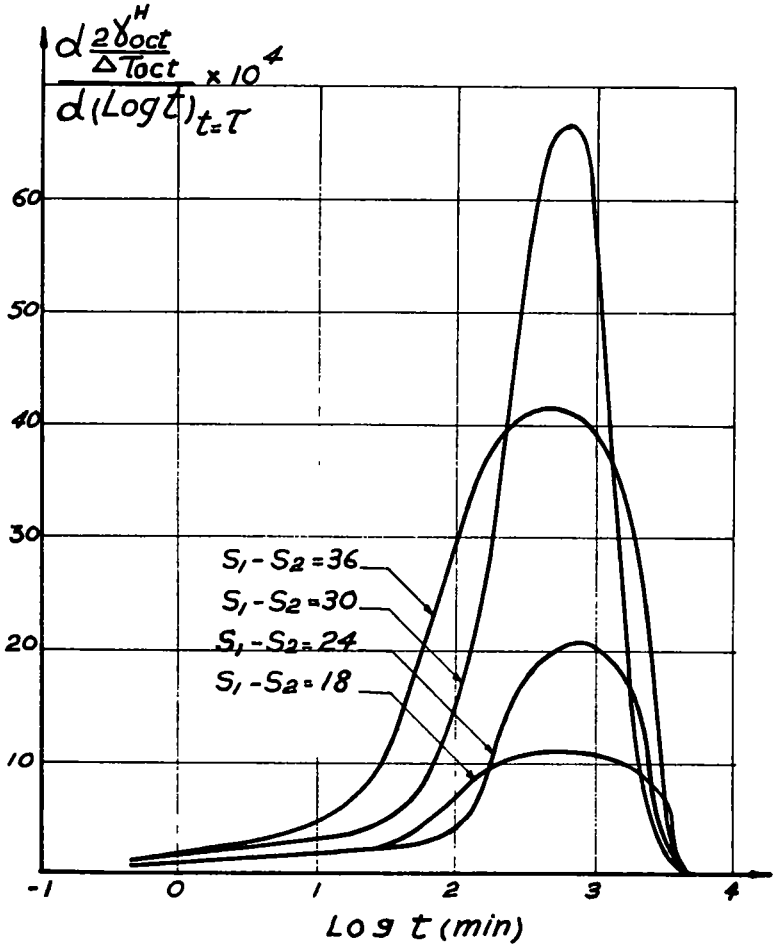

Figure 13. Distribution of retardation times under various deviators of stress.

of compliances for different retardation times, although keeping the same general shape of a Gauss curve, varies for different stress increments. For a linear viscoelastic material all the curves in this figure would coincide. The area under each of these curves corresponds to the value of J_{2E} of the empirical model. The most important compliance for the different stress levels corresponds to the same value of the retardation time.

Effect of Change in Moisture Content on Rheological Parameters

An increase of the moisture content has been found to produce a much wider distribution of retardation times under a given stress. It causes the whole spectrum to shift towards smaller retardation times. The coefficient G_{1E} changes rapidly because a certain number of mechanisms that are retarded at low moisture content become instantaneous at a higher one, and some in the pseudo-flow category pass into the retarded one. On the other hand, the viscous resistance to changes within the group of mechanisms classified as flow decreases together with the true, giving as a final result a net decrease in the viscosity for the apparent steady stage of flow. (Thus, η_{3E} decreases.)

General Remarks on Rheological Approach in Shear

The previous analysis is based on the behavior of one material, namely kaolinite Grantham clay. Even though no extrapolation to other materials can be made, the analysis may shed some light on the general approach to the shear problem.

Clays have been represented since 1931 (29) by a Bingham body, and statements are often made that they have a yield limit. It seems strange, however, that in the present case a material that belongs to a group classified as very stiff (28) (q_u = 38 psi) did flow under a deviator of 1 psi. It is the opinion of the author that, at least for normally consolidated clays, the importance of the yield limit has been exaggerated.

Overconsolidated saturated clays may require a certain level of stress to overcome possible interlocking effects. Through a phenomenon similar to work hardening, additional strength could be mobilized to stop deformations under a given stress (28). However, it is possible that beyond a certain limit necessary to overcome this interlocking the materials might behave as a viscoelastic material. This necessarily introduces dilatancy, and the volume changes would be a function of the degree of the overconsolidation.

In the case of highly overconsolidated clays, dilatancy phenomena become very important. The material is in general very brittle and the validity of a viscoelastic analysis similar to the one presented becomes questionable.

RHEOLOGY OF CONSOLIDATION

Distribution of Volumetric Relaxation and Retardation Times

In consolidation, the material changes continuously. For a given external volumetric stress, the problem can be stated in terms of either the decay of the induced pore pressure or the volumetric strains in the material.

If the problem is stated in terms of the induced pore pressures, the phenomena involved are relaxation ones. Near the drainage surfaces, the induced pore pressures relax instantaneously. The relaxation times vary from point to point and at each instant. This is due to the various lengths of the flow paths to the drainage boundaries, the range of viscosities around each solid particle, and the continuous change in the permeability of the material. The phenomenological approach does not attempt to separate the effects of these variables on the relaxation of the pore pressures; it simply considers that there exists a whole spectrum of relaxation times which is generated during the decay of the pore pressures. This spectrum can be obtained from the relaxation curve (1) and is only valid for one particular state of external volumetric stress. The pore pressures tend asymptotically to zero (Fig. 14).

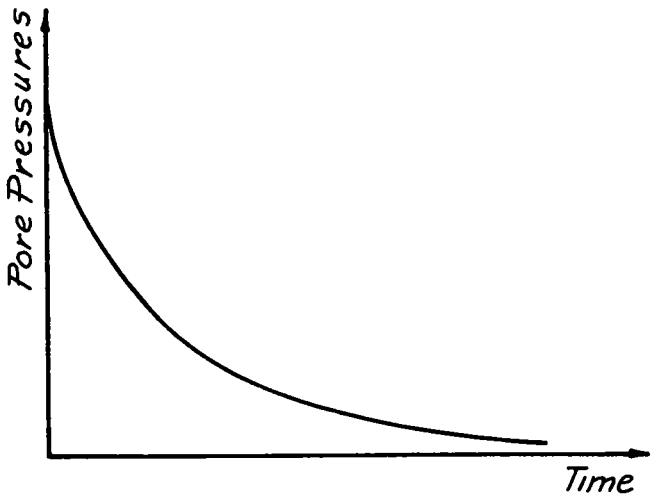

Figure 14. Decrease of pore pressures with time under given volumetric stress.

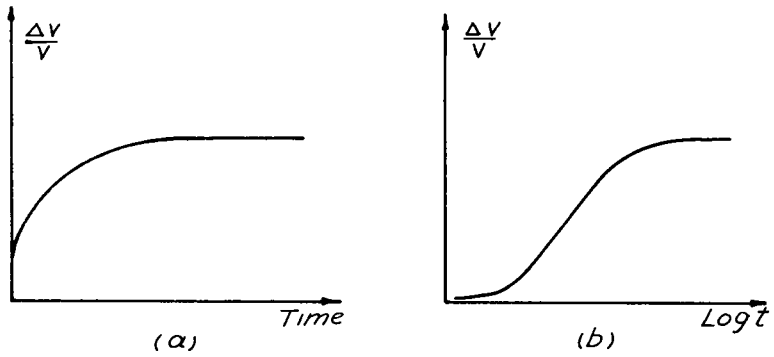

Figure 15. Volume changes with time under given volumetric stress in triaxial consolidation test.

If the problem is stated in terms of the volumetric strains, the phenomena involved are retardation ones. Instantaneous and retarded responses appear for the same reasons as in the previous approach. The distribution of retardation times can be obtained from a volumetric creep curve and is only valid for one state of stress The strain-time curve has a horizontal asymptote, as volumetric stresses do not cause unlimited flow (Figs. 15a, 15b).

Model Representation

In consolidation, the problem is in general expressed in terms of volume changes The model discussed in this section deals with retardation phenomena alone.

A material that exhibits in its volumetric behavior a whole spectrum of retardation times and no unlimited flow can be represented by n Kelvin bodies in series with a Hooke element to simulate any instantaneous deformation (Fig. 16). By analogy with Eq. 3 the volumetric strain in such a model can be written:

$$\epsilon_m^H = (\sigma_m)_o \left[\frac{1}{3K_o} + \sum_{n=1}^{n} \frac{1}{3K_n} \left(1 - e^{-t/\tau_{nv}}\right) \right] \tag{14}$$

in which K_n is the elastic bulk modulus (the spring constant), μ_n is the volumetric viscosity, and $\tau_{nv} = \mu_n/K_n$ is the volumetric retardation time.

For a continuous distribution of retardation times Eq. 14 becomes:

$$\epsilon_m^H = (\sigma_m)_o \left[\frac{1}{3K_o} + \int_o^{\infty} \frac{J_v(\tau_v)}{3} \left(1 - e^{-t/\tau_v}\right) d\tau_v \right] \tag{15}$$

in which $J_v = 1/K$ is the volumetric compliance of the Hooke element. The distribution of the volumetric compliances can be obtained from the experimental determination of the creep function:

$$\Phi_v(t) = \frac{3\epsilon_m^H}{(\sigma_m)_o} \tag{16}$$

by means of Alfrey's graphical method. The distribution will vary from one state of stress to the other

As in the case of shear, simplifications can be made in the model representation. The simplest model to take the place of the most general one is the three-element

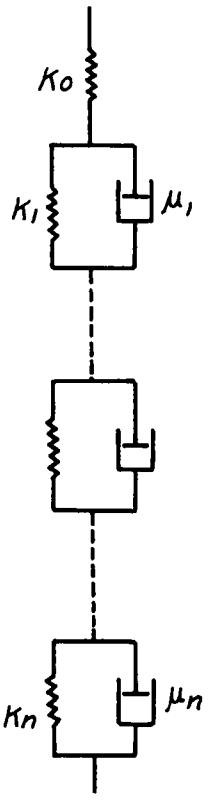

Figure 16. General model for clay consolidating under given volumetric stress.

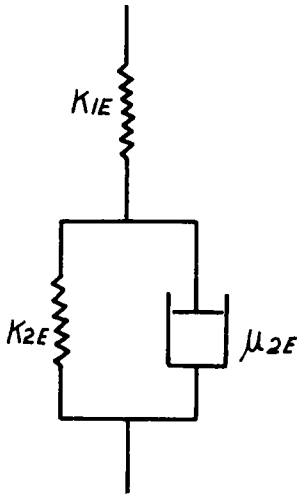

Figure 17. Three-element experimental model.

model composed of a Hooke and Kelvin body in series (Fig. 17). The remarks made earlier about the parameters of the empirical model in shear and the limitations of a model representation apply in the case of consolidation. However, there is no flow term equivalent to η_{3E}.

General Remarks on Rheological Approach in Consolidation

In a classical consolidation test, stress increments follow at certain regular intervals and in general act during a period of 24 hr. For each load stage it is customary to plot the volumetric deformations or the strains vs the logarithm of the time (Fig 15b). This is the first step of Alfrey's construction to obtain the distribution of retardation times. The slope of this curve for different values of $(\log t)_{t=\tau_V}$ gives a bell-shaped curve which is the required distribution (Fig. 18). The area under this curve represents the total deformability Each stress increment is associated with a different distribution. If, in all cases, the area S_2 falling beyond $\log_{10}$ 1,440 min = 3.158 (Fig. 18) is negligible, the final e vs log p curve would be a good representation of the behavior of the material under volumetric stresses. The accuracy decreases if the area S_2 increases. In other words, a classical test is valid for those clays whose spectrum of retardation times, under the considered stresses, is mostly shorter than 24 hr.

Another point of importance is that of the "secondary consolidation." There is sometimes a basic misunderstanding of the problem Both viscous flow due to shear and volumetric deformations corresponding to the existence of a spectrum of retardation times are often gathered under the same name. What shows up in a laboratory triaxial consolidation test as secondary consolidation is the result of volumetric retardation times larger than 24 hr. The process is hydrostatic, decreases, and is bound to stop. The secondary consolidation part of the experimental curve must finally reach a horizontal asymptote. As for the constant rate of settlement of buildings (5, 28, 29), it finds its direct explanation in the section on "Experimental Investigation," in which a saturated clay has been proved to exhibit a constant rate of strain which is a function of the stress alone.

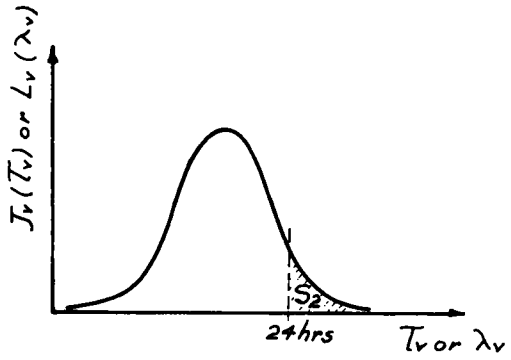

Figure 18. Distribution of retardation times in consolidation.

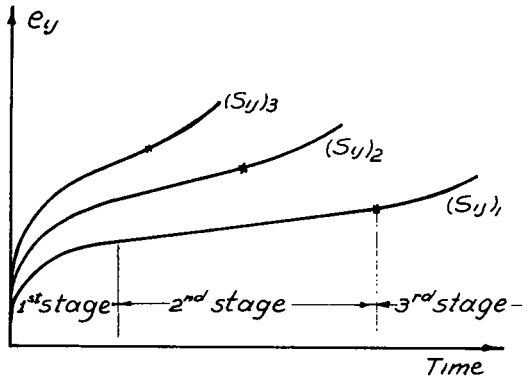

Figure 19. Creep stages under various deviators of stress.

PRACTICAL APPLICATIONS

Determination of the Shear Stress at Fracture

In this study, a line has been drawn between volumetric effects and deviatoric ones. Volumetric stresses cause consolidation and changes in the composition of the material (i.e., in the moisture content) but they do not result in permanent flow. Deviatoric stresses are responsible for flow and fracture. If the two effects are considered separately, to each material composition is attached a certain deviator of fracture under given testing conditions. The deviator of fracture can be obtained by means of one single unconfined compression test (Figs. 1, 2). This, however, would not allow for any sizable creep to take place.

If a saturated clay behaves as a viscoelastic material, creep phenomena must be considered Fracture is associated with the deformation as well as with its time derivative (Fig. 19). Under a given deviator, deformations will, in general, occur at a rapidly decreasing rate (primary creep) until a state of dynamic equilibrium is reached. At this stage the distortional energy applied to the material is dissipated at a constant rate given by Eq. 1. Deformation reaches a limit at the point of fracture. When this limit is reached, the continuity of the transformation from mechanical potential into heat energy is broken. Separation starts at points where the mechanism of coherent place change of particles is not available for the release of the potential energy of the applied forces (38). The disruption of a certain number of bonds increases the energy accumulated in the remaining ones (third stage of creep). Fracture is thus a chain reaction process that can be accelerated by higher stresses (Fig. 19).

Distribution of Stresses in Saturated Clay Soils

In a viscoelastic material, the amount of deformation or strain is not a direct indication of the stress. In the discussion of the effect of stress increase in rheological parameters, the material under consideration was shown to be nonlinear in its retarded response. Also, if the rate of strain at the steady state part of the creep curve is plotted vs the applied shear stress, the resulting curve is far from being a straight line (non-Newtonian). Thus, nonlinearity seems to extend throughout the viscoelastic behavior. Hence, Boltzmann's principle of superposition, as well as the elastic-viscoelastic analogy (1), cannot be applied.

In a semi-infinite medium, a stress distribution computed by means of the theory of elasticity would only be an approximation of unknown magnitude. As Tschebotarioff (30, p. 205) states,

> Nevertheless, observations on the behavior of soils indicate that the Boussinesq solutions can be applied with reasonable accuracy to cohesive soils and even, with some limitations, to granular soils, such as sand.

Regarding the value of Poisson's ratio ν which is used in computing the lateral stresses, thus in determining the value of the maximum shear stress, he says,

> Thus the possible variation of τ'_{max} because of uncertainties in the value of the Poisson ratio of soils is negligible and does not exceed 15 per cent.

The validity of a stress distribution based on the theory of elasticity during the constant rate of creep will be assumed in the following section.

On the Foundation of Structures on Saturated Clay Soils

If a saturated clay is treated as a viscoelastic material, the amount of vertical settlement due to creep might be used advantageously to determine the allowable pressures acting on a foundation. Such an analysis can at this stage of development be made for a constant volume material, and the creep would be due to the effects of the deviator of stresses alone. The procedure would be as follows:

Under the center of a given foundation, the distribution of stresses can be computed by means of Newmark's charts with a Poisson ratio of 0.5. Undisturbed samples taken at various depths under the foundation are then submitted in the laboratory to the same deviator of stress or the same octahedral shear stress as computed, and the rate of permanent vertical strain $d\epsilon_{1/dt}$ is deduced from a constant volume creep test (Fig. 20). This rate of strain is then plotted against the depth Z (Fig. 21) and the area between the resulting curve and the Z-axis represents an upper limit to the rate of settlement of the foundation due to creep. The following two points are to be noticed:

1. In the field the loads are applied gradually, but a laboratory test would not have to go through the various loading stages, because in a viscoelastic material the effect of the rate of stress vanishes with time (Fig. 20).

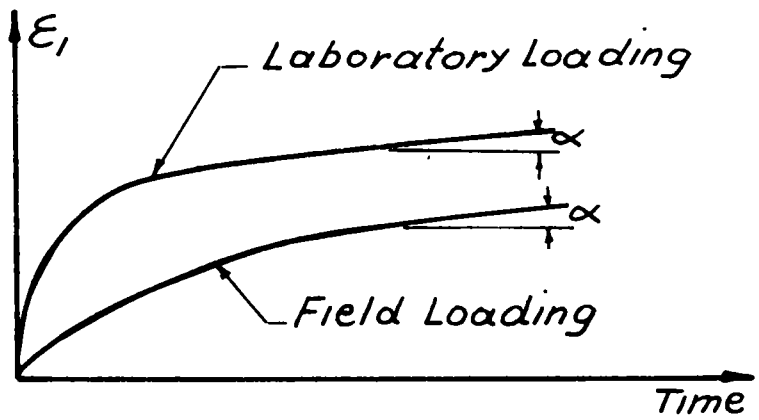

Figure 20. Determination of constant rate of vertical settlement from laboratory creep test under given maximum or octahedral shear stress.

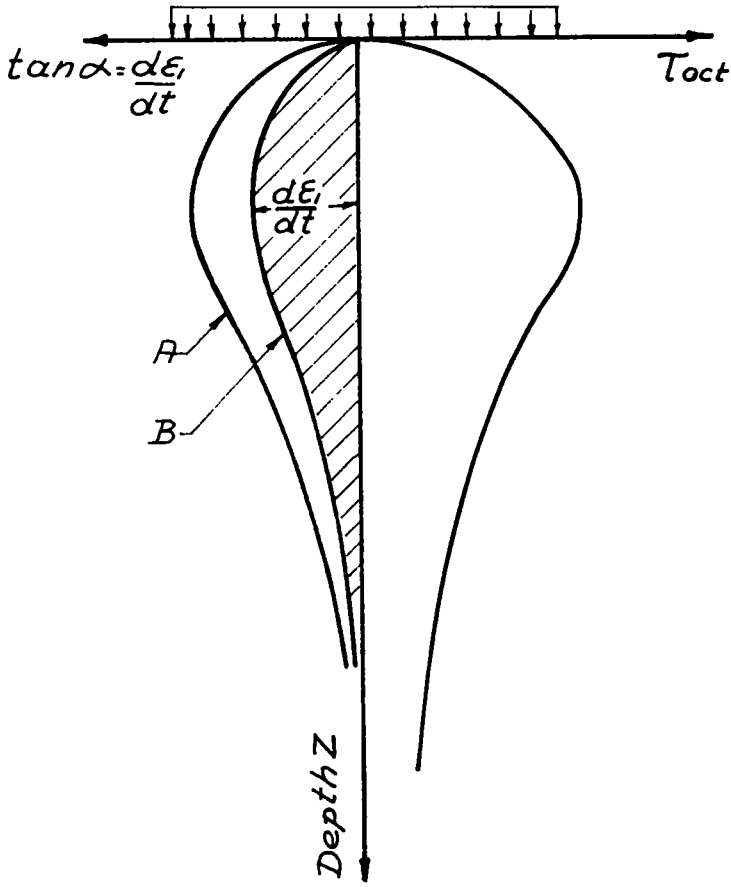

Figure 21. Rate of vertical settlement due to creep.

2. The distribution of stresses according to the theory of elasticity is assumed to be valid and the foundation is considered perfectly flexible.

In the previous analysis, the constancy of the moisture content in the material is assumed. Under the given stresses the material consolidates and its rate of creep under the same deviator decreases. One can make an initial analysis for an initial moisture content (Curve A, Fig. 21) and one for a final moisture content (Curve B, Fig. 21). For the latter, the material will have first to be consolidated in a triaxial cell, then subjected in an undrained condition to the computed deviator. All the curves representing the rate of settlement due to creep for intermediate values of the moisture content would be enclosed between Curves A and B.

The rate of settlement as given by the area between Curve B and the Z-axis should not exceed the tolerable rate of settlement.

For most clays, settlements due to consolidation will overshadow those due to creep, and it is only when consolidation is mostly finished that creep starts to be noticed. In the case of peat, however, creep phenomena are predominant and the presented method will be of value in estimating the allowable pressure on a foundation.

CONCLUSION

This paper has attempted to bring out the basic ideas behind a viscoelastic rheological analysis in shear as well as in consolidation. Mechanistic models and their limita-

tions have been presented and discussed. The separate treatment of volumetric and deviatoric phenomena avoids the measurement of pore pressures in the laboratory. This, however, does not imply that in the field their measurement is not necessary. They are the easiest way to know how the moisture content changes; in other words, how the material changes. A method of design based on creep has been proposed, and it appears that it can fruitfully be used, together with the theory of consolidation, to predict buildings settlements. The method, however, does not contain any stability criteria. This point requires extensive testing and is currently being investigated.

It is hoped that this study will help bring a better understanding of the deformational characteristics of saturated clays.

ACKNOWLEDGMENTS

Research was conducted in the Department of Civil Engineering of Princeton University as a part of a program sponsored by the Geophysics Branch of the Office of Naval Research under the direction of Werner E. Schmid. Acknowledgment is also made to Hans F. Winterkorn for his interest in this work, his aid, and his critical appraisal of the paper; and to the Civil Engineering Department of Princeton University for defraying some expenses.

REFERENCES

1. Alfrey, T., "Mechanical Behavior of High Polymers." Interscience Publishers (1948).
2. Andrade, N. da C , Proc., Royal Society, A 90 (1914).
3 Andrews, Industr. Eng. Chem., Annal 44 (1952).
4. Bishop, A. W., and Henkel, D. J., "The Measurement of Soil Properties in the Triaxial Test." Edward Arnold, London (1957).
5. Bernatzik, W., "Baugrund und Physik." Zurich, p. 234 (1947).
6. Casagrande, A., and Wilson, S. D., "Effect of Rate of Loading on the Strength of Clays and Shales at Constant Water Content." Geotechnique, 2: 251-263 (1950).
7. Freudenthal, A. M., "Inelastic Behavior of Engineering Materials and Structures." Wiley (1950).
8. Freudenthal, A. M., "Structural Engineering Aspects." Building Materials, Reiner (Ed.), North Holland Publishing Co., Amsterdam, pp. 64-121 (1954).
9. Geuze, E. C. W. A., and Tan, T. K., "The Mechanical Behavior of Clays." Proc., 2nd Internat. Congress on Rheology, V. G. W. Harrison (Ed.), Academic Press, New York, pp. 247-259 (1954).
10. Geuze, E. C. W. A., and Tan, T. K., "The Shearing Properties of Soils." Geotechnique, 2: 141-161 (Dec. 1950).
11. Habib, P., "La Resistance au Cisaillement des Sols." Thesis, La Documentation Technique du Batiment et des Travaux Publics, Paris (1953).
12. Housel, W. S., "The Shearing Resistance of Soils—Its Measurement and Practical Significance." Symposium on Shear Testing of Soils, ASTM Proc., 39: 1084-1099 (1939).
13. Hvorslev, M. J., "Physical Components of the Shear Strength of Saturated Clays." ASCE Research Conf. on Shear Strength of Cohesive Soils, Boulder, Colo. (June 1960).
14. Nadai, A.,"Theory of Flow and Fracture of Solids." McGraw-Hill (1950).
15. Newmark, N. M., "Influence Charts for Computation of Stresses in Elastic Foundations." Univ. of Illinois, Urbana (1942).

16. Reiner, M., Amer. Jour. Math, Vol. 67 (1945).

17. Reiner, M., "Rheology." Handbuch der Physik; Springer, Berlin, 6: 443-550 (1958).

18. Reiner, M., "Twelve Lectures on Theoretical Rheology." North Holland Publishing Co., Amsterdam (1949).

19. Rutledge, P. C., "Review of the Cooperative Triaxial Research Program of the War Department, Corps of Engineers." Soil Mechanics Fact Finding Survey, Progress Report: Triaxial Shear Research and Pressure Distribution Studies on Soil, U. S. Corps of Engineers, Mississippi River Concession (April 1947).

20. Schiffman, R. L., "Consolidation of Soil Under Time-Dependent Loading and Varying Permeability." HRB Proc., 37: 584-617 (1958).

21. Schiffman, R. L., "The Use of Viscoelastic Stress-Strain Laws in Soil Testing." Soils 1959 ASTM St P 254, Philadelphia (1959).

22. Schmid, W. E., and Klausner, Y., "Rheological Shear and Consolidation Behavior of Clay Soils." Progress Report to the Office of Naval Research, Princeton University (1960).

23. Schmid, W. E., "The Permeability of Soils and the Concept of a Stationary Boundary Layer." ASTM Proc., 57: 1195-1218 (1957).

24. Schmid, W. E., "New Concepts of Shear Strength for Clay Soils." Paper, Annual Meeting, ASCE, New York (Oct. 1961).

25. Sherif, M. A., "The Lateral Strain During Triaxial Testing." M.Sc. Thesis in Civil Engineering, Arizona State University (1961).

26. Skempton, A W., and Bishop, A. W., "Soils, Their Elasticity and Inelasticity." Chapter 10 in "Building Materials," M Reiner (Ed.), Interscience Publishing Co. (1954).

27. Tan, Tjong Kie, "Structure Mechanics of Clays." Academia Sinica, Harbin, China, (1947).

28. Terzaghi, K., and Peck, R. B., "Soil Mechanics in Engineering Practice." Wiley (1948).

29. Terzaghi, K., "The Static Rigidity of Plastic Clay." Jour. Rheol., 2: 253 (1931).

30. Tschebotarioff, G. P., "Soil Mechanics, Foundations and Earth Structures." McGraw-Hill (1951).

31. Waidelich, W. C., "Physico-Chemical Factors Influencing the Consolidation of Soils." M.Sc. Thesis in Civil Engineering, Princeton University (May 1957).

32. Westergaard, H. M., "A Problem of Elasticity Suggested by a Problem in Soil Mechanics." Contributions to the Mechanics of Solids, Stephen Timoshenko 60th Anniversary Volume, Macmillan (1938).

33. Winterkorn, H. F., and Moorman, R. B., "A Study of Changes in Physical Properties of Putnam Soil Induced by Ionic Substitution." HRB Proc., 21: 415-434 (1941).

34. Winterkorn, H. F., "Tensile and Compressive Strength on Homoionic Dry Soil Specimens. " Appendix C, ERDL Project 1953 to Pennsylvania State College, pp. 188-189 (1953).

35. Winterkorn, H. F., "Macromeritic Liquids." Symposium on Dynamic Testing of Soils, ASTM, pp. 77-99 (1953).

36. Winterkorn, H. F., "The Science of Soil Stabilization." HRB Bull. 108, 1-24 (1955).

37. Winterkorn, H. F., "Soil Water Interaction and Water Conduction in Soils." Princeton Univ. Conf.—Water Supply, pp. 43-84 (Jan. 1958).

38. Winterkorn, H. F., "Soil Mechanics." McGraw-Hill Encyclopedia of Science and Technology, 12: 449-458 (1960).

39. Winterkorn, H. F., "The Scientific Foundations of Soil Engineering." Princeton University (1960).

Appendix A

Approximate graphical method to determine the distribution of retardation times from a creep curve

In the study of $J(\tau)$ it is preferable to express J in terms of $\ln\tau$. Creep tests may extend for months, and the logarithmic scale is a very convenient one in such cases. If

$$K(\tau) = \tau J(\tau) \tag{17}$$

and if $K(\tau)$ is plotted against $\ln\tau$, an area under this curve is exactly equal to the area under $J(\tau)$ vs τ.

$$\int_{\tau_1}^{\tau_2} J(\tau)\, d\tau = \int_{\ln\tau_1}^{\ln\tau_2} K(\tau)\, d \ln\tau \tag{18}$$

if $\ln\tau = \lambda$, then

$$K(\tau) = \tau J(\tau) = e^{\lambda}\left[J(e^{\lambda})\right] = L(\lambda) \tag{19}$$

The distribution of the function $L(\lambda)$ is completely equivalent to that of $J(\tau)$. Thus the distribution of the elastic deformability J among the various retardation times can be represented either by a plot of $J(\tau)$ vs τ or by $L(\lambda)$ vs λ. The total deformability possessing a retardation time in the range between τ_1 and τ_2 is given by the area under either of these curves between the two values of the abscissa.

In terms of $L(\ln\tau)$ the amount of elastic deformability possessing a retardation time between the limits of τ_1 and τ_2 is given by

$$\left[J\right]_{\tau_1}^{\tau_2} = \int_{\ln\tau_1}^{\ln\tau_2} L(\ln\tau)\, d \ln\tau = \int_{\ln\tau_1}^{\ln\tau_2} L(\lambda)\, d\lambda \tag{20}$$

The following method gives an approximation to $J(\tau)$. An approximation is derived to the function $L(\log \tau)$ in which

$$L(\log \tau)\, d \log \tau = J(\tau)\, d\tau \tag{21}$$

(Because only the integral of this quantity is relevant for computation, the change in the independent variable ($\ln\tau$ to $\log \tau$) is immaterial.)

The steady flow component is first subtracted of the creep curve and the rest is plotted as $\frac{2e_{ij}}{(S_{ij})_o}$ vs log t. When the slope of this curve is determined and plotted against $(\log \tau)_{t=\tau}$, this curve which can be called L' ($\log \tau$) is a fair approximation to the actual distribution function $L(\log \tau)$. L'($\log \tau$) fails to show sharp discontinuities in $L(\log \tau)$ but reproduces the general contour. If $L(\log \tau)$ is a smooth distribution (which in general is the case for clay), L' ($\log \tau$) is a good approximation.

The area under the curve is exactly equal to the value of J_{2E}.

Appendix B

NOTATIONS

D = diameter of solid particles.
E = subscript standing for experimental or empirical.
e = base of Napierian logarithm—void ratio.
e_{ij} = deviator of strains.
G = specific gravity of solid particles—shear modulus—spring constant in shear.
H = superscript standing for Hencky.
i = subscript (1, 2, 3).
j = subscript (1, 2, 3).
J = compliance of Hooke's body = 1/G.
K = elastic bulk modulus—spring constant in consolidation.
L = length of sample.
ln = Napierian logarithm.
log = common logarithm.
m = subscript standing for mean.
S_{ij} = deviator of stresses.
t = time.
u = vertical deformation.
v = stands for volumetric.
w = moisture content.
W = energy.
(X, Y, Z) = trirectangular coordinates.
α = angle determining the constant rate of flow in a creep test.
γ_{oct}^{H} = octahedral shearing strain in the Hencky measure.
Δ = increment.
$\lambda = \ln\tau$.
η = viscosity of the Newton body in shear.
μ = viscosity of the Newton body in consolidation.
ν = Poisson ratio.
$\sigma_m = \sigma_{oct}$ = mean stress equal to the octahedral normal stress.
σ_i = principal stresses.
τ = retardation time—shear strength in Coulomb's equation: $\tau = \sigma \tan \Phi$.
τ_{oct} = octahedral shear stress.
φ = angle of internal friction.
$\varphi(t)$ = creep function.
ϵ_i = principal strains.
ϵ_m = mean strain.

Discussion

ROBERT L. SCHIFFMAN, Associate Professor of Soil Mechanics, Rensselaer Polytechnic Institute—This paper presents an interesting review of the rheological literature, especially where it concerns infinite spectrum models. It is worthwhile to see, in the soil mechanics literature, the reproduction of analyses that have established themselves in other disciplines. One must be cautious, however, in the making of an interdisciplinary transposition to be complete and to maintain the physical basis for such a move.

The author used a phenomenological analysis, in which he considered the total behavior of a two-phase material (solid and water) with minimal consideration of the influence and interactions of each phase.

It is the writer's opinion that this approach is of limited usefulness and does not add to a fundamental knowledge of soil behavior.

This discussion takes up four topics of the author:

1. Treatment of consolidation.
2. Statements concerning the necessity and sufficiency for defining a material as viscoelastic.
3. Statements concerning a yield limit.
4. Conclusion concerning the need for laboratory pore pressure measurements.

The author uses a multispectrum model to analyze the volumetric behavior of a saturated clay. Because he does not attempt to analyze the physical implications of the rheological parameters, one must consider the proposed method of analysis as being empirical.

An empirical approach, such as this one, may well be justified if it enables the solution of soil engineering problems in a more accurate fashion than is presently available. It would be enlightening if the author would present an example (taken from the field) in which his method can be quantitatively compared to other, relatively standard, procedures. Such an example would be of interest where the effects are both of a primary and secondary nature.

The author refers to situations in which there is a constant rate of settlement. Although there may be examples of structures settling at a constant rate, the vast majority of observed secondary compression effects show a linear settlement log t plot. These case records show that the settlements occur at a decreasing rate.

As a theoretical treatment of consolidation, the author's use of rheological models does not shed any light on the physics of the process. The author gathers together total behavior in a parametric model. As such this analysis makes no distinction between fluid and solid behavior and their various components.

From a macroscopic point of view, the process of consolidation is possibly the best understood of all phenomena in soil mechanics. This understanding comes about by the analysis of component behavior and the assessment of deviations from idealized conditions.

The theory of consolidation is a rigorous theory built on a finite set of physical idealizations. The physics of the theory as postulated by Terzaghi (41) considered volume changes as an ideal one-dimensional situation. As such, the vertical strain and the dilatation are coincident. The stated physical assumptions are

1. The soil is fully saturated.
2. The soil components (water and solid) are incompressible.
3. Darcy's law is valid.
4. The coefficient of permeability is constant throughout the process of consolidation.
5. The time delay in consolidation is due only to the permeability of the soil. Time rates of consolidation are thus controlled by the rate of water expulsion.

On the basis of these assumptions, the well-known consolidation pore pressure results:

$$C_v \frac{\partial^2 u}{\partial z^2} = \frac{\partial u}{\partial t} \tag{22}$$

More generalized consolidation theories as established by Florin (42) and Biot (43, 44) have extended the original work of Terzaghi to three-dimensional compression. Eq. 22 and the conditions preceding it become a special case of the general theory.

The general three-dimensional theory of consolidation is based on small strain, small velocity theory. The saturated soil mass is considered a two-phase continuum. The soil structure is represented by a linear elastic material, and the water phase is represented by an incompressible, Newtonian fluid, which does not develop strain components. The entire soil mass is of spatially uniform density. For an isotropic system (a restriction also imposed by the author) the effective stress-strain relations follow the linear theory of elasticity:

$$\sigma'_{ij} = \frac{2\nu G}{1 - 2\nu} \Delta \delta_{ij} + 2G \epsilon_{ij} \tag{23a}$$

$$\Delta = \epsilon_{xx} + \epsilon_{yy} + \epsilon_{zz} \tag{23b}$$

in which

σ'_{ij} = effective stress tensor,
Δ = dilatation,
δ_{ij} = Kronecker delta,
G = shear modulus of soil structure,
ν = Poisson's ratio of soil structure,
ϵ_{ij} = strain tensor.

Because the fluid components produce no strains, the strain tensor (ϵ_{ij}) in the effective stress-strain relation is the strain tensor for the soil mass.

The fluid phase behaves according to the Navier-Stokes equations for steady flow. The flow equation follows Darcy's law. It is assumed that the soil is isotropic with respect to flow.

$$v_i = \frac{k}{\gamma_w} \frac{\partial u}{\partial x_i} \tag{24}$$

in which

v_i = velocity vector,
x_i = coordinate component,
k = coefficient of permeability,
γ_w = unit weight of water,
u = pore pressure.

Eqs. 23 and 24 form the equations governing the material properties of the system within the general idealizations imposed on the mass. The component portions are coupled by the effective stress relationship:

$$\sigma_{ij} = \sigma'_{ij} + u\,\delta_{ij} \tag{25}$$

in which

σ_{ij} is the total stress tensor.

The soil mass must be in equilibrium and must satisfy the law of conservation of mass. As such, the soil mass is governed by the stress equilibrium and the continuity equations:

$$\frac{\partial \sigma'_{ij}}{\partial x_j} - \frac{\partial u}{\partial x_j} + F_i = 0 \tag{26a}$$

$$\frac{\partial v_i}{\partial x_i} = \frac{\partial \Delta}{\partial t} \tag{26b}$$

If, in a given boundary value problem, only the pore pressure were of concern, then Eq. 26b with appropriate boundary and initial conditions would suffice to define the problem. As shown by Gibson and Lumb (45) the general three-dimensional pore pressure equation for time-independent total stress is

$$\frac{k}{\gamma_w} \nabla^2 u = \frac{3(1-2\nu)}{2G(1+\nu)} \frac{\partial u}{\partial t} \tag{27}$$

In ideal one-dimensional consolidation, the lateral strains vanish and there are no shears across vertical planes. The pore pressure equation for time-independent total stress is then

$$\frac{k}{\gamma_w} \frac{\partial^2 u}{\partial z^2} = \frac{1-2\nu}{2G(1-\nu)} \frac{\partial u}{\partial t} \tag{28}$$

For an incompressible soil structure ($\nu = 0.5$) the pore pressure equation does not exhibit time delay, and thus the consolidation will be instantaneous. In this case the solution becomes trivial because there is no consolidation. The solution for (u) is not trivial, as it is the incompressible pressure distribution in the soil mass.

Because the physical system and the resulting mathematical relationships conform exactly to Terzaghi's theory when reduced to one dimension, the preceding theory is defined as the three-dimensional theory of primary consolidation.

Rheologically, the pore pressure dissipation in primary consolidation can be represented by a spring and dashpot model. The elasticity of the model, represented by a spring, physically represents the elastic soil structure. The viscosity of the model, represented by a dashpot, represents the water viscosity. The physical and mathematical system described requires that the pore pressure dissipation be represented by a Maxwell model (46)(Fig. 10b).

The rheological model just described, like all rheological models, is purely a mechanical analogue to a physical phenomenon. In this case, it is an "exact" analogue, because the differential equation and initial condition governing the model are identical to the differential equation and initial condition governing the physical phenomenon. Any other rheological analysis of pore pressure in primary consolidation, based on the physical conditions outlined, must be considered as ad hoc and thus empirical.

This analysis only considers an elastic soil structure phase and an incompressible, viscous water phase. A distinction is understood to exist between the soil particles and the soil structure. Whereas the particles are considered incompressible, the soil structure is viewed as a system of soil particles connected by springs. Using this physical approach one can logically consider volumetric changes as equivalent to changes in moisture content.

Biot's analysis considered a compressible water phase. Inasmuch as this condition is of little importance in saturated clays it is not considered in this discussion.

Secondary consolidation has come to mean, by usage, the inclusion within the effective stress-strain relationships of a viscosity effect. Proposed analytical theories of secondary consolidation have universally used a linear viscoelastic effective stress-strain relationship. A generalized form of such a relationship for an isotropic material is

$$\sum_{n=0}^{n} A_n \frac{\partial^n \sigma'_{ij}}{\partial t^n} = \sum_{m=0}^{m} B_m \frac{\partial^m \epsilon_{ij}}{\partial t^m} \tag{29}$$

In Eq. 29 the coefficients (A_0) and (B_0) represent the elastic constants of the soil structure. All the other physical assumptions of primary consolidation are the same in secondary consolidation.

As presented in this discussion, secondary consolidation is considered to occur simultaneously with the primary phase. This concept was used by Taylor (47) in theory B, in which he demonstrated, both theoretically and experimentally, that one-dimensional secondary consolidation could be approximately represented by a Kelvin model (see Fig. 10a) in the effective stress-strain relations.

Because the theory is a small strain, small velocity, linear, isotropic theory, it is

permissible to separate the effective stress-strain relations into deviatoric and volumetric components. An analysis of Taylor's theory B shows that the volumetric effective stress dilatation relationship is elastic. The deviatoric effective stress-strain rate relationship is Newtonian (46). Rheologically, one spring (volume change) and one dashpot (deviator) couple in the one-dimensional effective stress-strain relations in parallel to form a Kelvin model.

Although Taylor, in 1942, did not use the definitions used in this discussion, the mathematics of the analysis prove that the relationships described are the same as Taylor's.

Ishii (48), Tan (49, 50, 51), and Gibson and Lo (52) have analyzed another theory. This theory considers the volumetric effective stress-dilatation relationship to be elastic. The deviatoric effective stress-strain relationship has the mathematical structure of a Kelvin model coupled in series with a spring.

Lo (53) and Murayama (54) have considered changes in the microscopic structure during secondary consolidation by introducing a yield limit in the effective stress-strain relationship. Biot (55, 56) has developed a general mathematical structure for a three-dimensional analysis of secondary consolidation for isotropic and anisotropic media.

The theories and analyses cited are far from complete. However, they form significant steps in the development of a theoretically sound and experimentally valid method of analysis. In these cases the principles of rheology were used to develop the basic effective stress-strain relations, using physical concepts of behavior and/or experimental evidence. Once the rheology of the volume change and deviator of the solid phase was developed, the model analysis of secondary consolidation was based completely on the laws of mathematics and continuum mechanics.

The previous discussion was devoted to the subject of linear theories of secondary consolidation as they existed at the time of this discussion. It is not to be implied that these are the only effects. In actuality, secondary effects come about because of the nonlinearity of the effective stress-strain relations; the inelasticity of the soil structure; pore pressure effects in shear; the errors induced by using small strain theory; the nonlinearity of fluid flow relations, such as variations in permeability with hydraulic gradient The term "secondary" is not to be interpreted as second order. Many of the effects mentioned are of major significance in soil behavior. For example, the development of pore pressures during shear, though arbitrarily defined as a secondary effect, is of major significance in the development of knowledge of soil behavior.

The point is that by going through a methodical, careful, step-by-step analysis, one can analyze each idealization in turn and proceed to build theories and methods of analysis that will have general applicability. The author's analysis, based on his Eqs. 14 and 15, place permeability, viscosity of the soil structure, and the boundary conditions of the test in an arbitrary volumetric compliance, which then loses its physical meaning.

The author states four conditions which he states are necessary and sufficient for a material to be classified as viscoelastic. Inasmuch as a statement of necessary and sufficient conditions is derived from mathematical logic it must be viewed in that light. The author states, by claiming necessity and sufficiency, that a material is viscoelastic if and only if the four conditions listed are met (57).

The fourth condition requires that the constant rate of strain in creep be independent of the load path and be only a function of the stress. The "constant rate of strain" portion of this statement eliminates a Kelvin model from the author's classification of viscoelastic materials. The strain rate of a Kelvin model in creep (constant load) will be an exponential function of time, and thus is not constant. Inasmuch as Kelvin materials are considered viscoelastic, one can only conclude that the author's statement of necessity and sufficiency is incorrect.

Though precision and rigor are always important and should be inherent in every paper, it would appear, however, that the author has carried this attempt to extremes that would eliminate his own analysis of consolidation from the realm of viscoelasticity.

The author concludes from his experiments that the soil he studied did not exhibit a true yield limit of practical importance. Further, he states the belief that the "importance of the yield limit has been exaggerated."

Three questions are raised here. First, is the author justified in making the statement concerning the existence of a yield limit for the soil tested? Second, can this statement be generalized to normally consolidated clays? Finally, what is the importance of the yield limit?

It is the writer's opinion that the first two questions must be answered in the negative on the basis of the evidence given in the paper. Possibly, the author's position would be clearer if the data presented in Figures 4, 5, 6, and 7 were re-analyzed.

Figure 4 presents a relaxation-type test. It is apparent from the author's description of the test and the sharp stress drop-off at 56 days that the strain during the test did not remain constant. To present a complete picture capable of independent analysis, the author should present a strain-time record. It would appear that the test used a "soft" proving ring which permitted strain changes along with stress relaxation.

The author presents creep test data in Figures 5, 6, and 7. The graphical manner in which the data were presented, the limited test description, and the lack of sufficiently complete information on sample preparation make it difficult to analyze the author's data and thus to accept his conclusions. Information on the following points seems necessary:

1. Method of sample preparation and information on sample homogeneity at the time of the test; in particular, the measured degree of saturation during the creep tests, and the state of prestress induced by the triaxial consolidation.
2. The measured effect of volumetric stress on shear behavior. The author refers to strength behavior in undrained tests. What data does he have on the stress behavior?
3. Data points on the creep plots.
4. Moisture content data, including changes in moisture content with creep and moisture content distributions within a sample during creep or at least at the end of the test.

The concept of a yield limit in the rheological literature has a distinct meaning. It is defined as the intercept on the stress axis of a strain rate-stress plot (rheological diagram) resulting from a series of creep tests. The yield limit is thus a state of stress that defines a boundary between no flow (zero strain rate) and flow. Test results reported by Bingham (58), Geuze (9, 59), Tan (51), Haefeli (60), De Josselin de Jong (61), and Murayama (62) have all found that a yield limit exists for saturated clays.

It was the writer's tentative belief in 1959 (21) that there was some doubt as to the existence of a yield limit. Factual knowledge and experience gained subsequent to 1959 has convinced the writer that the preponderance of evidence points towards the existence of a yield limit.

Because the author does not provide data points and a precise graph, it is not possible to construct a rheological diagram and thus verify the author's statements concerning the existence of a yield limit.

Assuming that the author can justify his statements about a yield limit it is doubtful that his conclusion regarding its importance can be documented. A single test series on artificially prepared samples is insufficient to generalize for undisturbed soil. In the writer's experience in the Netherlands, it has been found that many of the soils used in dike and embankment cores have a yield limit of up to 40 percent of the shear strength. In analyzing conventional Dutch practice, one would find that, in many cases, the factors of safety are such that the working shear stresses are at, or slightly below, the yield limit. Geuze (59) has suggested that, in these cases, the yield limit can be used to provide a no-flow analysis.

The author recommends an analysis of foundation settlements based on a constant volume basis (Poisson's ratio of 0.5). He then correctly states that the creep (settlement under constant load) would be due only to the deviator components. If this analysis were carried to its conclusion, there would be no settlement due to consolidation, as the theory of three-dimensional consolidation has as its limiting condition, instantaneous deformation at Poisson's ratio of 0.5 (63). The author attempts to correct this inconsistency by performing an analysis at an initial and a final moisture content. By this method, the best that the author can achieve are upper and lower bounds of the settlement rate. The author determines the settlement rate at an alleged initial and final time in the consolidation process. It thus does not appear possible to integrate the settlement rate to provide time-settlement predictions. Were he to test at sufficient

intermediate moisture contents to provide a reasonable estimate of time-settlement data, the amount and length of testing required would be prohibitive.

The author's method of obtaining an initial analysis (curve A, Fig. 21) is not truly initial. He does not state whether his test is consolidated undrained or unconsolidated undrained. If it is the latter, then the measured strain-rate is not truly an initial one, but one taken at some time after settlement has started. If it is the former, then the process of consolidation will additionally alter the point in prototype time at which the creep rate is calculated.

The last paragraph in the section on practical applications appears to negate much of the author's previous writing in this paper. In this paragraph the author indicates that his creep analysis is of minor importance for most clays but will be of value in the analysis of "peat." The tests are confined to one clay. Considering the fact that the term "peat" covers a wide variety of soil types, it appears doubtful that the author's single series of tests on an inorganic clay can be so broadly extended. Peats vary from highly fiberous open-structured materials that show practically instantaneous settlements to colloidal gels with creep effects only. In the writer's experience some peats have shown substantial changes in moisture content under both volume change and deviator stress, whereas other deposits have shown substantial volumetric and deviatoric strains without change in moisture content.

The author makes a point in his conclusion that the separate treatment of volume change and deviator components permits laboratory analysis without pore pressure measurements. His thesis seems to be built on the predication that moisture content is, at least, the most predominant influence in soil behavior, and furthermore, that during shear creep the moisture content remains unchanged.

The author's analysis is the logical conclusion arrived at by considering the soil mass as a linear viscoelastic continuum exhibiting small strains and small velocities. The only modification to this theory in the author's hypothesis is that the shear properties remain constant at a constant moisture content but will vary from moisture content to moisture content. This would be a justification for running undrained creep shear tests to obtain the creep rate.

The author's basic proposition is that if the volume is held constant during a pure deviator test the shear properties will remain constant. Using this proposition along with small strain, small velocity, linear, continuum theory, he is then free to separate volumetric and deviatoric components and to analyze laboratory tests on a total stress basis.

Two points of view can be brought to bear on this proposition. From the microscopic point of view, a saturated clay is a system of discrete particles in an electrochemical, nonconservative force field. As such the over-all material properties will constantly change, under stress, due to changes in particle orientation and changes in interparticle forces. From the macroscopic point of view, the material property relationships can be considered nonlinear, and thus the uncoupling of shear and deviator is not strictly permissible.

Pore pressures occur in undrained shear tests and affect the shear behavior. This measured effect is evidence of the interactions between shear and volume change. The effective stress principle and analyses using pore pressure parameters (64) can be viewed as reasonable linearizing modifications to the uncoupled volume change and deviator mechanics, for the purpose of considering interactions between these two components.

The interaction of volume change and deviatoric components is not a phenomenon unique to soil mechanics. The literature discussing the rheology of polymers has recognized this effect for several years. "Weissenberg" or "normal stress effects" recognizes that in shear a polymer will develop normal stresses that are functions of the shear strain.

It is appealing to ignore pore pressures and examine everything on a total stress basis, even if confined to the laboratory. The soil mechanics literature for the past 40 years has devoted major sections to this thesis. The pendulum has swung back and forth. The literature shows that advances in fundamental knowledge and engineering practice have almost exclusively stemmed from methods and analyses that consider and

measure pore pressures. At this time there is probably greater activity in the laboratory and in practice devoted to measuring pore pressures and pore pressure effects than ever before. Pore pressures play an important role in the stress-strain-time behavior of soil and in the strength of a soil. To advocate ignoring pore pressures, at any time, would be to advocate ignoring a basic material property.

The laws of continuum mechanics and rheologic principles are extremely useful tools in the analysis of soil mechanics problems. In the development of theories and practical approaches, however, the mechanics of the system must conform to known or reasonable approximations of physical reality.

REFERENCES

41. Terzaghi, K., "Theoretical Soil Mechanics." Wiley, pp. 265-272 (1943).

42. Florin, V. A., "On the Problem of Hydrodynamic Stresses in a Soil Mass." Pamphlet of Glavgidroenergostroy, Leningrad (1938) (In Russian).

43. Biot, M. A., "General Theory of Three-Dimensional Consolidation." Jour. Appl. Physics, 12: 155-164 (Feb. 1941).

44. Biot, M. A., "General Solutions to the Equations of Elasticity and Consolidation for a Porous Material." Jour. Appl. Mechanics, 78: 91-96 (March 1956).

45. Gibson, R. E., and Lumb, P., "Numerical Solution of Some Problems in the Consolidation of Clay." Proc. Inst. of Civil Engineers, Pt 1, 2: 182-198 (March 1953).

46. Schiffman, R. L., "The Effect of Material Properties on Consolidation and Secondary Compression." Paper, Annual Conv., ASCE, New York (Oct. 1961).

47. Taylor, D. W., "Research on Consolidation of Clays." Mass. Inst. Technol., Serial 82 (Aug. 1942).

48. Ishii, Y., "General Discussion." Symposium on Consolidation Testing of Soils, ASTM, STP 126, pp. 103-109 (1951).

49. Tan, T. K., "Three Dimensional Theory on the Consolidation and Flow of the Clay Layers." Scientific Sinica, China, 6: No. 1, pp. 203-215 (1957).

50. Tan, T. K., "Secondary Time Effects and Consolidation of Clays." Academia Sinica, Harbin, China (1957).

51. Tan, T. K., "Onderzockingen Over de Rheologische Eigenschappen Van Klei." Ph.D. Thesis, Delft Technological University, Netherlands (1954).

52. Gibson, R. E., and Lo, K. Y., "A Theory of Consolidation for Soils Exhibiting Secondary Compression." Acta Polytechnica Scandinavica, 296/1961, Ci 10. Also Norwegian Geotechnical Institute Publication 41 (1961).

53. Lo, K. Y., "Secondary Compression of Clays." ASCE, Jour. Soil Mechanics and Foundations Div., Paper 2835, pp. 61-87 (Aug. 1961).

54. Murayama, S., and Shibata, T., "On the Secondary Consolidation of Clay." Proc., 2nd Japan Congress on Testing Materials, pp. 178-183 (1959).

55. Biot, M. A., "Theory of Deformation of a Porous Visco-elastic Anisotropic Solid." Jour. Appl. Physics, 27: 459-467 (May, 1956).

56. Biot, M. A., "Mechanics of Deformation and Acoustic Propagation in Porous Media." Jour. Appl. Physics, 33: 1482-1498 (Apr. 1962).

57. Jeffreys, H., and Jeffreys, B. S., "Methods of Mathematical Physics." 3rd Ed., Oxford Press (1956).

58. Bingham, E. C., "Fluidity and Plasticity." New York (1922).

59. Geuze, E. C. W. A., "The Effect of Time on the Shear Strength of Clays." Paper, ASCE Conv., New Orleans, La. (March 1960).

60. Haefeli, R., "Creep Problems in Soils, Snow and Ice." Proc., 3rd Internat. Conf. on Soil Mechanics and Foundation Engineering, 3: 238-251 (1953).

61. De Josselin de Jong, G., and Geuze, E. C. W. A., "A Capacitive Cell Apparatus." Proc., 4th Internat. Conf. on Soil Mechanics and Foundation Eng., 1: 52-55 (1957).

62. Murayama, S., and Shibata, T., "On the Rheological Characters of Clay, Part I." Disaster Prevention Research Institute, Bull. 26, Kyoto University, Japan (Oct. 1958).

63. McNamee, J., and Gibson, R. E., "Plane Strain and Axially Symmetric Problems of the Consolidation of a Semi-Infinite Clay Stratum." Jour. Mech. and Appl. Math., 13: Pt 2, pp. 210-227 (1960).

64. Lambe, T. W., "Pore Pressures in a Foundation Clay." ASCE, Jour. Soil Mechanics and Foundations Div., Paper 3097, pp. 19-47 (Apr. 1962).

ADEL S. SAADA, Closure— Professor Schiffman's discussion reveals little that is new. It reiterates the well-known Terzaghi theory of consolidation (41) and classical concepts of continuum mechanics (65) as understood by the discusser. It will be shown herein that in many instances this understanding is in conflict with the most fundamental definitions on which these theories are built. Although the author fails to see the reason why these theories are restated in such great detail in a discussion, there are no disagreements as long as they are faithful copies of the original statements.

Exception is taken, however, to any adumbrations by the discusser; for example, in the discussion on consolidation: "The soil structure is represented by a linear elastic material, and the water phase is represented by an incompressible, Newtonian fluid, which does not develop strain components.... For an isotropic system (a restriction also imposed by the author) the effective stress-strain relations follow the linear theory of elasticity." Although the author finds the idea of a Newtonian fluid that flows but does not develop strain components rather unusual, he does not understand how anyone would be led to make the second statement. Isotropy and linear elasticity are two properties that have nothing in common, and the first does not imply the second.

A few sentences later, there is the following statement in the discussion: "The fluid phase behaves according to the Navier-Stokes equations for steady flow." Steady flow is defined as a flow in which the velocity at any given point does not change with time. Yet, the essence of the Terzaghi theory of consolidation is that the pore pressure gradient changes with time, a thing that changes pore water velocities from instant to instant.

Regarding the author's treatment of consolidation, the discusser does not seem to realize that in essence the same operations as in Terzaghi's analysis are applied. The modulus of volume change m_v in Terzaghi's theory is obtained from an experimental curve; so is the modulus of the spring if Figure 16 is reduced to one Kelvin body. One is the inverse of the other. The general case of a distribution of retardation times is presented in this study. The phenomenon can be expressed as accurately as one wants by increasing the number of models. The various compliances and dashpot viscosities can easily be obtained by means of Alfrey's construction shown in Figure 18.

Regarding the discusser's statement that a majority of observed secondary compression effects show a linear settlement on an e-log p plot, the discusser is referred to the two last paragraphs of the section "General Remarks on Rheological Approach in Shear" and to several references (5, 9, 28, 29).

The dissipation of pore pressures can be represented by a Maxwell body, as can be any system of relaxing stresses. However, the statement that in this particular model the spring physically represents the elastic soil structure and that the dashpot represents the water viscosity is incorrect. The establishment of the equation governing the behavior of a Maxwell body is based on the fact that the same stress acts on the spring and

the dashpot, whereas in Terzaghi's theory the stresses are transmitted from the liquid to the solid phase. All that can be said is that under an externally applied stress, the process of relaxation of the pore pressures due to the expulsion of the water can be compared to the relaxation of the stresses in the spring of a Maxwell body because of the presence of the dashpot.

Also, the second sentence in the discusser's statement "The rheological model just described, like all rheological models, is purely a mechanical analogue to a physical phenomenon. In this case, it is an 'exact' analogue, because the differential equation and initial condition governing the model are identical to the differential equation and initial condition governing the physical phenomenon" is again incorrect. How the discusser has reached this conclusion is not known. However, if he has done so by applying a Fourier sine transform to the heat transfer equation as he did in his paper (46), it must be pointed out that this is mathematically if not logically incorrect. The equations describing a behavior in a transform domain must first be inverted before any meaningful comparison can be made with other equations in the real domain.

The author has warned against possible misunderstanding in the use of rheological models. When a spring is used either in this paper or in the Kelvin body "representing" Terzaghi's theory, it simply takes the place of a certain compliance or compressibility. It does not mean that the material is elastic in the sense defined in classical mechanics (7, 65) and is much less linear (1). For a given stress increment, Terzaghi assumes that the relation between the void ratio and the effective stress is a straight line (66, pp. 221), but the slope of this line and the coefficient of volume change m_v vary from one increment to another. Kelvin's body is merely a convenient way to illustrate the process of transmission of pressure from the liquid phase to the solid one (66). An examination of any e log P diagram shows that a consolidating clay behaves neither as an elastic nor as a linear material under successive states of stress.

Regarding the "proposed" analytical theories of secondary consolidation which have used a linear viscoelastic effective stress-strain relationship, the author has never heard of any experimental investigation that, while attempting to prove these theories, came out with constant parameters under the various stresses. This is a necessary condition for any viscoelastic body to be classified as linear.

As for the analysis of Taylor's theory B by the discusser, it is incorrect. Taylor has attempted to add to Terzaghi's theory the effects of a plastic resistance assumed proportional to the rate of strain. Both the modulus of volume change in Terzaghi's theory and the factor of proportionality ($\bar{\eta}$) in the plastic resistance vary from one effective stress to another. The relation between effective stresses and measured strains in Taylor's theory involves small strains but it is not linear.

Taylor did not mention that his combination of effects had anything to do with a Kelvin body, though he was familiar with such a body (66). The idea of representing the volumetric behavior of a material by a fraction of a Kelvin body and the deviatoric behavior by another fraction probably did not occur to him because it is evident that such an attempt can only lead to an absurdity. However, assuming for a moment with the discusser that the volumetric effective stress-dilatation relationship is elastic and that the deviatoric effective stress-strain relationship is Newtonian, then the discusser concludes: "Rheologically, one spring (volume change) and one dashpot (deviator) couple in the one-dimensional effective stress-strain relations in parallel to form a Kelvin Model." Such rheology is not Taylor's. How can a material classified as elastic under volumetric stresses and Newtonian (in other words, a liquid) under deviatoric stresses become a viscoelastic solid (see "Rheology of Shear") under combined stresses? Certainly, drawing a spring and a dashpot and joining them by two straight lines does not have the power of transforming the material from a liquid to a solid state. Any possibility of a misinterpretation from the author's side is eliminated by the discusser's statement: "... the mathematics of the analysis prove that the relationships described are the same as Taylor's." The mathematics of Taylor has no relationship with that of a Kelvin body.

The subsequent paragraphs in the discussion up to the point where the discusser considers the four conditions for viscoelasticity form a bibliographical revue that does not appear to be pertinent. Also, at least two references (52, 53) show that the material is not linear.

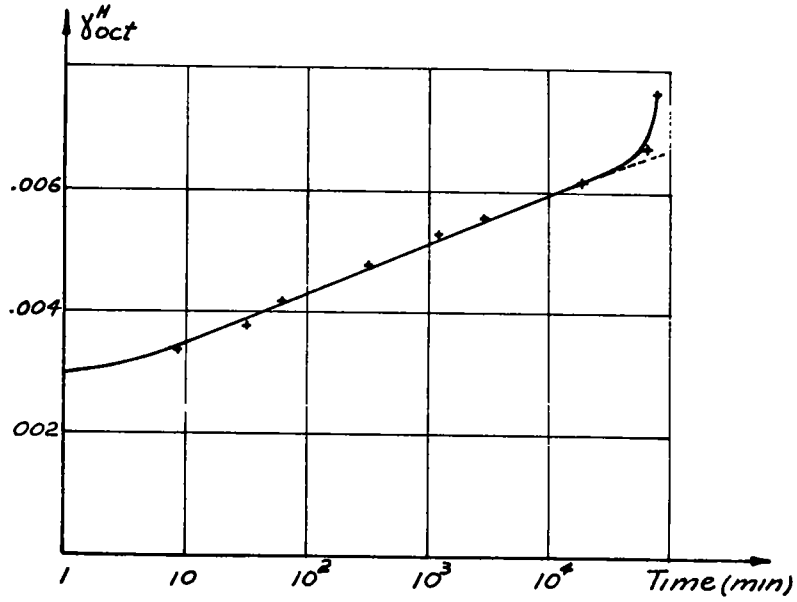

Figure 22. Strain-time relation under decreasing stress.

When analyzing the items that led the author to classify the material as viscoelastic under deviatoric stresses, the discusser appears to have concentrated solely on the final paragraph of the section "Existence of a Tone Yield Limit." He seems to have overlooked the creep tests that led to that statement, the reason for which they were performed, and most important, the fact that the first section in the paper states that for viscoelastic materials the effect of load history vanishes with time. The constant rate of strain, when present, must be a function of the stress alone. The statement in question is a result of the creep tests and does not present any ambiguity when looked at as such. Any ambiguity that may exist is only a temporary one, because shortly thereafter in the section "Rheology of Shear" it is stated that a Kelvin body represents a solid viscoelasticity and a Maxwell body represents a liquid viscoelasticity. Also, the general model to represent the behavior of the material in shear and to fit the performed tests is given in Figure 11 which represents a liquid type of visocelasticity. The author's treatment of consolidation contains several statements classifying the phenomenon as belonging to the solid viscoelasticity class; for example, under "Rheology of Consolidation," the first subsection states: "The strain-time curve has a horizontal asymptote, as volumetric stresses do not cause unlimited flow (Figs. 15a, 15b)"; and the second subsection states: "A material that exhibits in its volumetric behavior a whole spectrum of retardation times and no unlimited flow can be represented by n Kelvin bodies in series ... (Fig. 16)."

The remarks about precision and rigor, as well as those about the elimination of consolidation from the realm of viscoelasticity could have been avoided if the discusser had not overlooked what is before as well as what is after item 4. The author believes that reasonings based on mathematical logic should be made after and only after a thorough examination of the material to be analyzed.

Regarding the experimental investigation, Figures 5 and 6 represent exact, to-scale deformation time curves obtained by joining experimental points. The graphical manner in which these data are presented conforms to the style of the Highway Research Board. Figure 7 has been presented in a schematic way; if it were presented in an exact way, the inclination of the steady state part of the creep curves would not appear at all The data points of these tests were used to establish the distribution of retardation times and to classify the material as nonlinear (Figs. 12, 13).

The strain-time curve related to Figure 4 was not presented because the author did

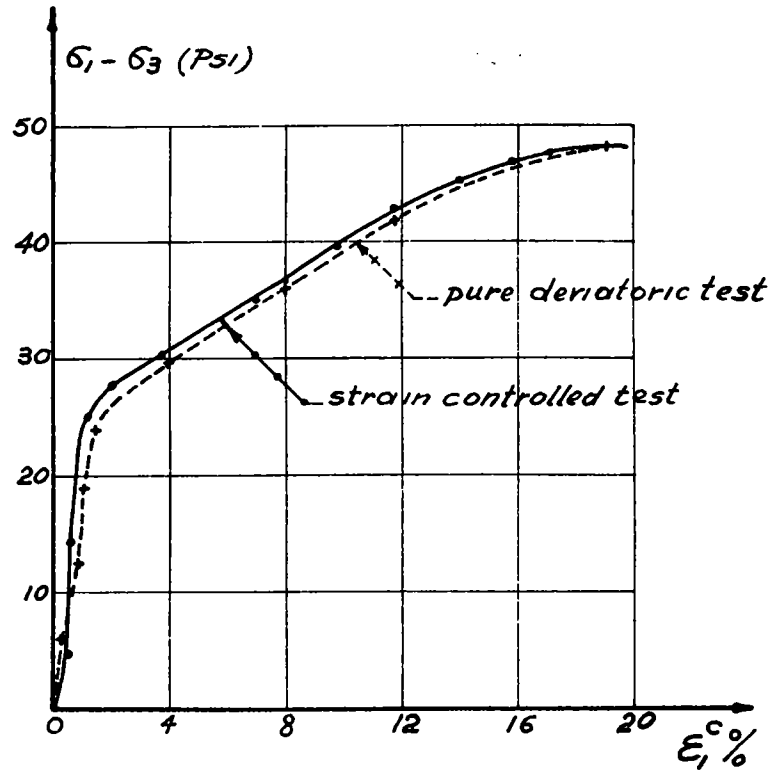

Figure 23. Stress-strain relations for a material consolidated under 35 psi.

not think any particular information could be deduced from it. This curve is not a creep curve because it represents the deformation of the material under a decreasing stress (it is given in Fig. 22). It was pointed out under "Existence of a Tone Yield Limit" that the drop of stress after 56 days was not expected. Many reasons could be given for this sudden drop, but if it is to be attributed to the proving ring, it would be due to its stiffness, not to its softness as stated by the discusser.

The sample preparation has been fully described in the section "Experimental Investigation": the consolidation pressure for the creep tests was 55 psi. Saturation was checked at the end of each test performed in this investigation and found close to 100 percent within the range of accuracy of slide rule computation.

The fact that for a saturated clay the shear behavior is not influenced by the volumetric component of the stress tensor is not new. Habib (11) presents a number of stress-strain diagrams for samples consolidated at the same volumetric pressure and tested under various lateral pressures. These curves nearly coincide. In this study, and for the material used, Figure 23 shows two extreme cases. Two identical samples were consolidated under a volumetric stress of 35 psi and brought to failure in a period of 6 min, one at a constant rate of deformation and the other in a pure deviatoric way keeping σ_m constant The two stress-strain curves nearly coincide.

The request for data in the discusser's point 4 is unexpected. All the tests in shear were undrained tests. The whole approach in shear in this study (see introduction) is based on the concept that a change in moisture content gives a different material with different properties. As for the distribution of moisture content within the sample during creep, the author does not know any method of obtaining it. In this study, the moisture content was considered to be evenly distributed in the samples, as is usually done. Its value for the three creep tests was 34.30 ± 0.1 percent.

As to the question of the yield limit, the author concludes that the definition given in

the first section has been overlooked. This definition is the usual one given in mechanics of material (7). Though being an intercept on a flow diagram, the concept of yield limit implies either no deformation at all or complete reversibility. A flow diagram is not necessary to determine the existence of a yield limit. In this study, a stress difference of 1 psi produced a deformation such that only a small fraction of it was recoverable. This is enough to state that, if a yield limit exists, it is smaller than 1 psi and of no practical importance considering an unconfined compressive strength of 38 psi. A flow diagram is a convenient way of representation, but the tendency to extrapolate a flow curve to its point of intersection with the stress axis is a common, but highly questionable, procedure.

Also, concerning the list of authors who have all found that a yield limit exists for saturated clay, there is the matter of their own definition of such a limit, the way they confirmed it experimentally, and its importance relative to the consistency of the material. As often happens, authors do not all use the same definition and do not come to their conclusion through a unanimously approved testing technique. Although Bingham (58) used a capillary method—see remarks of Terzaghi (29)—Geuze (9, 59) found a level of stress at which no deformation could be detected, and Heafeli (60) extrapolated a line on a flow diagram. As for de Josselin de Jong and Geuze (61), if they did demonstrate the existence of a yield limit, they do not seem to have followed either the definitions or the methods used in the two previous references. When these studies are considered from the same datum line, the term "all" does not carry the same weight anymore.

The discussion related to the suggested method of analyzing the settlement due to "creep" does not appear related to this paper. The discusser seems to have understood that the author suggests computing the total settlements of buildings by means of creep tests alone and he has based his discussion on such an understanding. It has been made clear, however, in this paper that consolidation is a volumetric process mainly due to volumetric stresses and synchronous with water expulsion. The remarks about the water expulsion which is bound to stop and the constant rate of settlement which cannot be due to water expulsion seem to the author sufficient indication that it is the effect of the shear stresses on what is called secondary consolidation that is being analyzed. To obtain curves like those in Figure 21, only the steady part of the creep curve is considered. This seems sufficient to show that the author is concerned with what happens after the process of water expulsion is nearly terminated or when it cannot account for all the observed settlement In the section "On the Foundation of Structures on Saturated Clay Soils," it is only a question of deviator of stresses and rate of settlement due to creep. Indeed, the deviator of stresses causes secondary volume changes, but when the settlements due to shear occur at a rate of ½ or 1 in. per year, it seems permissible to ignore these secondary volumetric effects. The previous analysis can find its direct and indirect experimental proof in the same references the discusser presents to make his points. Taylor (47) presents data showing that practically no hydrostatic excess pressure exists in his samples during secondary compression; in other words, no volume changes occur. He recognizes the necessity of attributing it to remolding caused by shear strains, and remarks that it is more pronounced in a unidimensional than in a three-dimensional compression where the disturbance of the soil structure is less. As a result, he postulated a law (theory A) which does not depend on permeability. Gibson and Lo (52, p. 11) refer to experimental evidence obtained by Taylor, Koppejan, and Geuze and state that these authors pointed out that secondary compression takes place at a time when the excess pore water pressure is practically negligible. The experimental work of these authors indicates the validity of the principle of dividing secondary consolidation into a volumetric component accounting for the slow and decreasing expulsion of water and a deviatoric component accounting for permanent, nearly constant rate flow. To evaluate the settlements due to shear at the end of the process of water expulsion, it is stated in the same section that the samples taken at various depths have to be first consolidated under the computed volumetric stresses and only then subjected to the deviator (curve B, Fig. 21).

Regarding the last paragraph of the section just mentioned, the author fails to find where he stated that his creep analysis was of minor importance for most clays. When two phenomena occur together (in this case, consolidation and creep), one can overshadow

the other for a period of time without the latter being of minor importance. An example in elementary rheology is given by a Maxwell body under a sudden imposed stress.

As for the experience of the discusser related to peat, the author has never heard of any "saturated" peat or other type of clay that could show substantial volumetric strains without changes in water content, considering the extremely high pressures needed to compress both phases without any losses.

Following this comes another statement: "The author's analysis is the logical conclusion arrived at by considering the soil mass as a linear viscoelastic continuum exhibiting small strains and small velocities." This entire paper is aimed mainly at discussing the nonlinearity of the material. Sections on the model and the effects of stress increase and change in moisture content on rheological parameters contain almost nothing but statements pointing to this nonlinearity. Figures 12 and 13 show it as clearly as possible Finally, the first paragraph of the section "Distribution of Stresses in Saturated Clay Soils" further discusses the nonlinearity of the material.

The end of the discussion is a criticism of the approach that attaches a shear strength to each moisture content and a stand in favor of pore pressure measurements in the laboratory. The fact that, in an undrained test on a saturated clay, pore pressures occur has never been denied by the author. Whether these pore pressures affect the shear behavior is another question. When in an undrained test on a saturated clay the imposed volumetric stress is changed, the pore pressures change by the same amount. Yet the Mohr circles at failure keep the same diameter (Fig. 2), (4, 11, 19, 26, etc.). The stress-strain curves, also, are hardly affected by this change in pore pressures (Fig. 23), (11). In other words, for given moisture contents, the shear behavior is not affected by the changes in pore pressures. Unless the expression "shear behavior" has a meaning other than ultimate strength and stress-strain relationship, the previous statement is true and has been established experimentally at least since 1947 (19), whether the strains are small or not.

No attempt will be made to discuss the pros and cons of pore pressure measurements in the laboratory and consequently the validity of the Mohr-Coulomb failure criterion in this closure. The author would like to point out, however, that the discusser's statement: "To advocate ignoring pore pressure, at any time, would be to advocate ignoring a basic material property," should have been accompanied by his definition of the term "material property." The pendulum has indeed swung back and forth, but never as far back as promoting pore pressures to this rank. Pore pressures are as much a material property as are the stresses induced in the cement of a piece of concrete under testing.

The measurement of pore pressures in the laboratory will keep its present important status as long as the Mohr-Coulomb failure criterion is used and as long as one ignores the fact that it is the water that is at the origin of the electrochemical forces binding the soil particles and that, like the cement in concrete, it is an inherent part of the material. A change in the moisture content gives another material with other properties.

In conclusion, it is not a simple difference of opinion that separates the writer and the discusser. It is a total and complete disagreement on most of the definitions and basic concepts of rheology and the way they are to be applied. This disagreement extends to the understanding and interpretation of existing results and theories and the conclusions that can be drawn from them. The author hopes that this exchange will result in a better understanding of the possible uses and limitations of rheology in the study of saturated clays

REFERENCES

65. Sokolnikoff, J. S., "The Mathematical Theory of Elasticity." McGraw-Hill (1946).

66. Taylor, D., "Fundamentals of Soil Mechanics." Wiley (1948).

Vertical Stresses in Subgrades Beneath Statically Loaded Flexible Pavements

GEORGE F. SOWERS and ALEKSANDAR B. VESIC, Respectively, Professor and Associate Professor of Civil Engineering, Georgia Institute of Technology

Full-scale static load tests have been made of single, dual, and dual tandem truck tire loads on flexible pavements to determine the stress distribution in the subgrade and the relative load spreading ability of different base course materials now in use by the Georgia Highway Department.

The measured stresses below topsoil and soil bound macadam base pavements are comparable to those computed by the Boussinesq theory. The measured stresses below the sand asphalt are comparable to or slightly more than those computed by the Boussinesq. The stresses found below the soil cement base are much lower than those given by Boussinesq and are comparable to the stresses found by the two layer elastic theories. Asphaltic concrete overlays reduce the stresses to the same degree as an equal thickness of the topsoil or soil bound macadam.

•THE RATIONAL DESIGN of any structural system, including pavements, requires a knowledge of the stresses induced by the imposed loads. However, little information is available regarding the stresses developed in the underlying soils by wheeled vehicles supported by pavements. The purpose of this research was to investigate the stresses produced in soil subgrades by wheel loads such as truck tires on flexible pavements.

A major function of any pavement is to spread the concentrated load delivered to it by the wheel sufficiently so that the stress ultimately transmitted to the underlying soil will not cause shear nor excessive deformation. The rigid pavement does this by beam or slab action. The flexible pavement system action is more complex—the load is spread through a mass of discrete particles that react like an elastic continuum when they are confined. The flexible pavement is composed of layers, all of which contribute to the load spreading, but some with more specialized functions. The surface resists the vertical and tractive loads as well as the wear of the wheels and provides a smooth roadbed. The base course is the main load spreading member. It is usually the thickest layer and the one that involves the greatest variety of materials and methods of construction. The subgrade, either natural soil or compacted fill, furnishes the ultimate support for the load. Some pavements include a subbase course that serves as a transition between base and subgrade. Resurfacing or overlaying with asphaltic concrete restores a damaged surface. It also adds another load-spreading layer to the pavement system.

Of course, the stresses at any point in the subgrade consist of combinations of shear and normal stress. Whether all the components of stress or only certain ones need be evaluated depends on the criteria established for pavement performance and design. The earliest methods of design were related to shear and shear failure in the subgrade; therefore, in these methods shear stresses have been considered the most important. Recent studies indicate that deflection may be the better index to design; and therefore, the vertical normal stress is of greatest significance. In this project, only the vertical normal stress has been investigated.

Although flexible pavements enjoy widespread use, little information has been available regarding the way in which vertical stresses are transmitted through them into the subgrade. Various simple assumptions have been proposed. One such method assumes

that the wheel is concentrated at a point on the pavement surface. The vertical component of the load spreads uniformly over an area defined by a cone whose vertex is at the pavement surface and whose sides slope at 45° with the vertical. A second method assumes the contact area of the tire to be a circle and the vertical component of the load is spread uniformly over an area defined by the frustum of a cone whose upper base is the circle of tire contact and whose sides slope at an angle of 30° with the vertical.

Various elastic theories have also been proposed for evaluating subgrade stresses beneath pavements. In all of these the pavement is represented by a simplified model whose physical properties can be described mathematically. The stresses in the model are analyzed by the laws of mechanics and assumed to be the same as those in the real pavement it represents. Certainly their validity depends on how accurately the model represents the real pavement.

Few data are available to confirm or reject any of the proposed theories for determining vertical stresses in the subgrade. One purpose of this investigation was to compare the measured stresses beneath pavements with those computed theoretically and if possible verify the theoretical methods.

The loads encountered in highway work are predominantly moving and vertical (except at points of braking and acceleration). The rate varies from a standstill to 70 mph or more. However, present knowledge of the behavior of soils and similar fragmental materials indicates that maximum deflections and stresses are more likely to occur with sustained load rather than rapidly changing load. Therefore, only static loading was investigated experimentally.

Theoretical Stress Distribution

The analysis of stress distribution in loaded soil masses or pavements is, generally, a problem that is being solved, for ideal materials, by the theory of elasticity.

The basic solution of this problem is the well-known Boussinesq solution (1) for a single, vertical point load acting on the horizontal surface of a semi-infinite, homogeneous, isotropic, elastic solid. This solution was extended to the case of load uniformly distributed over any finite area by Love (2). Particular solutions have been worked out, evaluated and presented in tables or graphs by many authors. The work

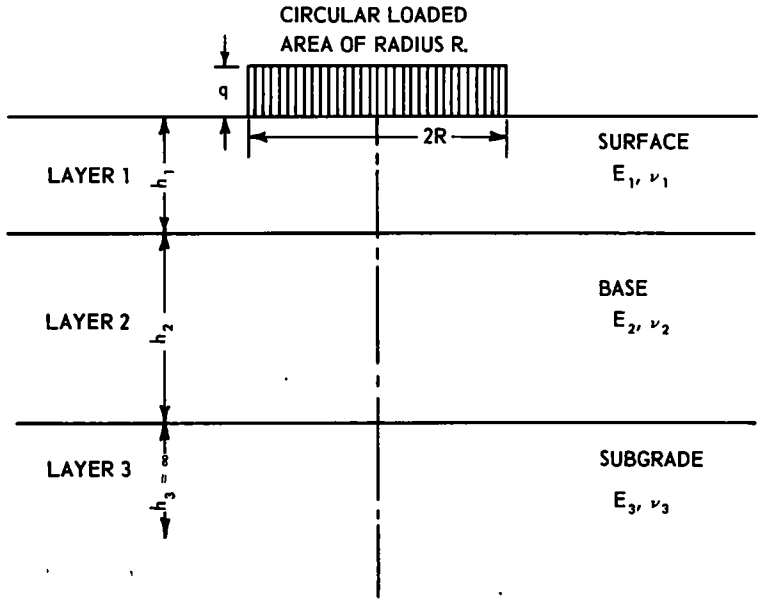

Figure 1. Flexible pavement system.

by Steinbrenner (3), Newmark (4, 5), Fadum (6), Fergus and Miner (7), Foster and Ahlvin (8), and Deresiewicz (9) should be cited as perhaps the most important for stress evaluation in pavements.

A semi-empirical modification of the Boussinesq solution by introduction of the concentration index has been proposed by Griffith (10) and Fröhlich (11) for semi-infinite soil masses that are nonhomogeneous in a vertical direction or nonisotropic. Their work was further extended by Ohde (12).

The stress distribution in semi-infinite, homogeneous, orthotropic solid, having different deformation moduli in horizontal and vertical directions was investigated by Buisman (13), Wolf (14), Jelinek (15, 16, 17) and Koning (18). Buisman also investigated the case of an orthotropic and nonhomogeneous mass having a modulus of deformation linearly increasing with depth. The problem of a semi-infinite solid reinforced by horizontal perfectly flexible membranes was solved by Westergaard (19) and integrated by Fadum (6).

Of particular interest for stress distribution in pavement systems is the problem of a multi-layered elastic solid (Fig. 1). The basic solution of this problem is that found by Burmister for a circular, uniformly distributed load at the surface of a two-layer system (20). This solution was extended by the same author to the case of a three-layer system (21) and generalized by Schiffman for any case of surface loading (22). Numerical evaluation of stresses in a two-layer system was performed by Fox (23) and Hank and Scrivner (24). Evaluation of stresses at the interfaces of a three layer system was made by Acum and Fox (25). All mentioned evaluations of stresses were performed for points beneath the center of the loaded circular area only.

Previous Experiments

The mentioned theories of stress distribution are based on several simplifying assumptions which, to a greater or lesser degree, always deviate from the real behavior of materials. Assumptions are made, for instance, that the materials are perfectly elastic and have linear relationship between stresses and strains defined, generally, by constant Young's moduli E and Poisson's ratios ν. However, soils and other pavement materials are only partly elastic and do not have linear stress-strain relationship. Neither E nor ν are constant but vary with the applied load. Both E and ν may have quite different values in tension than in compression (many soils and base materials have practically no tensile strength at all). Also, most solutions are based on assumption of perfect homogeneity and isotropy of different layers. Whereas pavement layers are usually reasonably homogeneous, they normally possess a structural aniostropy. Subgrades often display a decrease of compressibility with depth; they also may be stratified or laminated.

Consequently, discrepancies have to be expected between theoretical and actual stress in loaded soil masses or pavement systems. Several investigators have undertaken so far the task of checking to what extent the actual stresses follow the stress pattern indicated by the theories.

The early investigations of this kind, made on homogeneous sand fills in large boxes (26 to 31) as well as on layered pavement models (32), gave somewhat misleading results concerning the concentration of stresses under the applied loads, as compared with the Boussinesq theory for homogeneous solids. Namely, due to the limited dimensions of test boxes, the bottom acted as a rigid base and caused additional stress concentration.

Thorough experimental studies of stress distribution in homogeneous silt and sand masses were made at the Waterways Experiment Station at Vicksburg, Miss. (33, 34, 35). It was found that the pattern of measured stresses for both kinds of homogeneous soil followed closely the general shape indicated by the Boussinesq theory. There was somewhat higher concentration of stresses under the loads, particularly in sand; however, the use of the Fröhlich concentration index did not improve the agreement between the theoretical and measured stresses.

Experimental studies were made by McMahon and Yoder (36) on stress distribution in homogeneous clay as well as in a two-layered mass consisting of crushed stone base of variable thickness and a clay subgrade. This investigation showed within the homo-

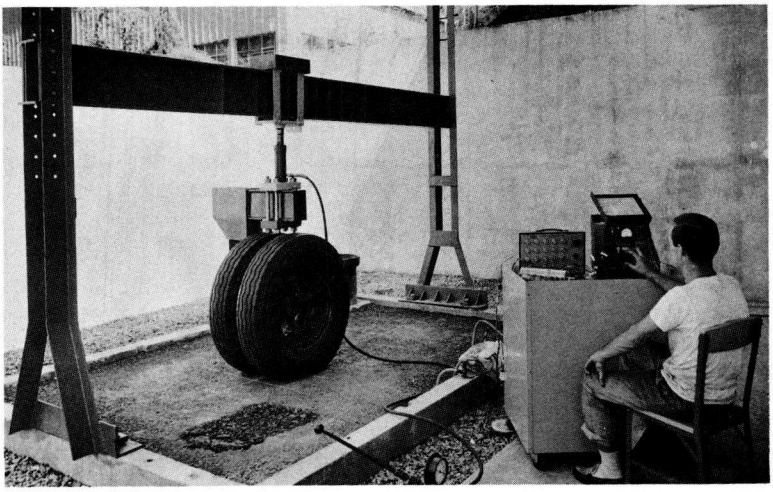

Figure 2a. Pavement load test in progress.

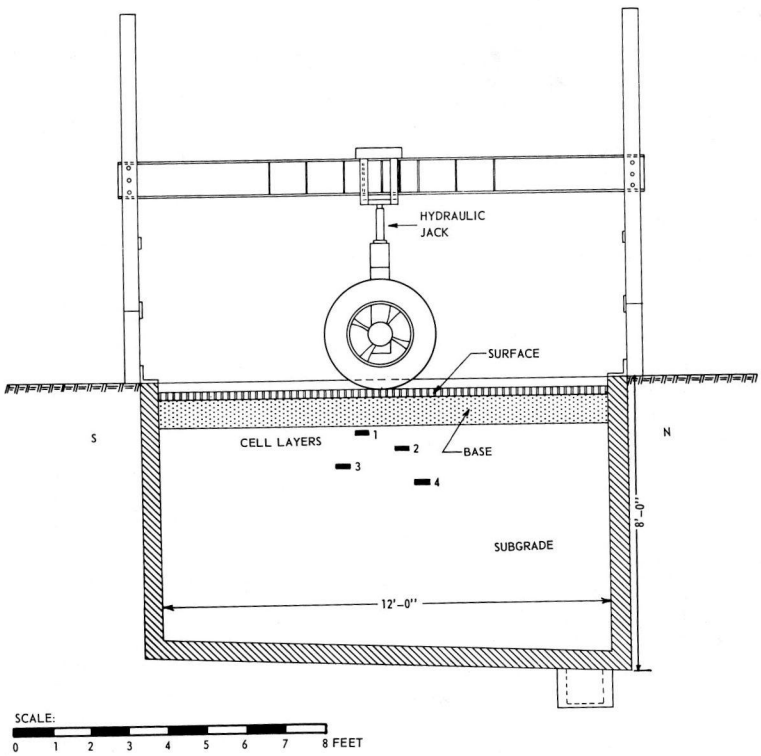

Figure 2b. Cross-section of the test pit showing position of layers of pressure cells and the loading equipment.

geneous clay mass a stress pattern close that predicted by the Boussinesq theory. At the same time the stresses in the two-layered system were somewhat reduced directly under the interface; however, only with a distance not greater than the radius of the loaded plate. Nevertheless, stresses were considerably higher than those predicted by the Burmister two-layer theory, and in general closer to values obtained by the Boussinesq theory for homogeneous soil.

TEST APPARATUS

Full-scale models of flexible pavement systems, including the subgrade, were constructed in a test pit. Static loads were applied to the pavement by truck tires and the vertical stresses in the subgrade were measured by pressure cells.

Test Pit and Load Frame

To control moisture content changes in the subgrade the entire model was built in a test pit (Fig. 2a and 2b). The inside dimensions are 8 ft wide, 7 ft deep and 12 ft long, so that the volume of the model was 25 cu yd. At a 9,000-lb wheel load the approximate diameter of the tire contact area was 11 in. The depth and width of the pit were 7.6 and 8.7 diameters respectively which means that the rigid boundary effects should not be significant A steel frame, fastened to the ends of the pit with a heavy beam spanning the centerline, furnished the reaction for loading the tires.

A hydraulic jack mounted beneath a carriage riding on the beam supplied the load. The load was measured by the hydraulic pressure with a calibration error of less than 2 percent.

Wheel Assemblies

Single, dual, and dual tandem wheel assemblies were employed, with 9- by 20-in. heavy duty truck tires inflated to pressures between 70 and 90 psi. These tires are designed for a maximum load of 9,000 lb each although they are occasionally overloaded in practice. The tire spacings were 10.5 in. center to center in the dual configuration

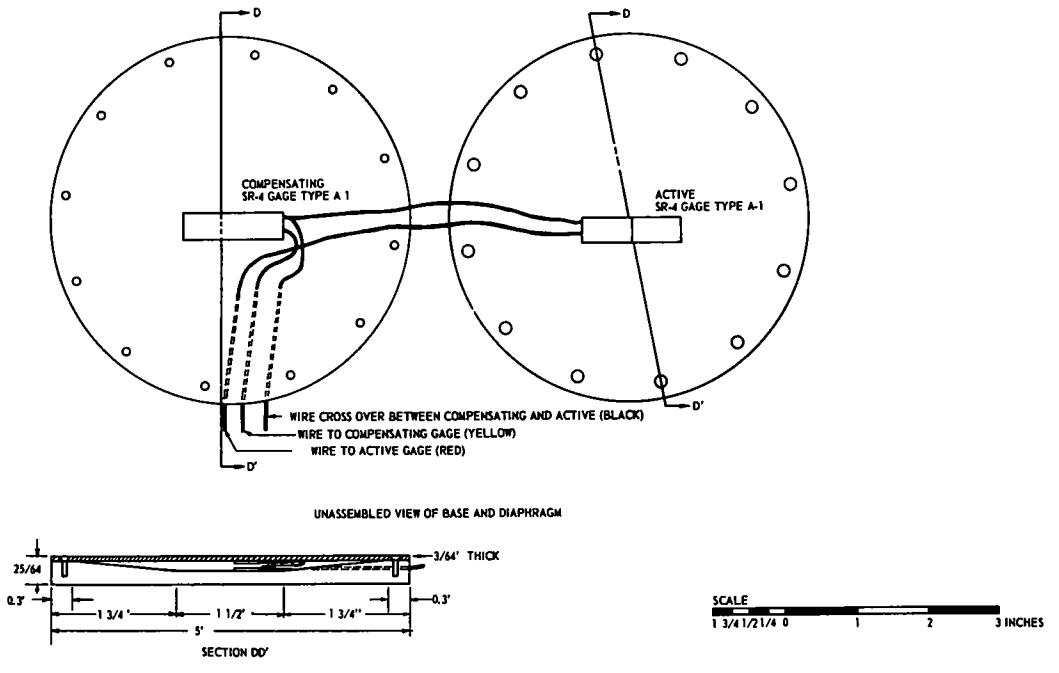

Figure 3. Typical pressure cell.

and 54 in. axle to axle in the dual tandem. These are standard spacings in U. S. Highway trucks.

Pressure Cells

A simple diaphragm type pressure cell (Fig. 3) previously developed in the Georgia Tech soil laboratory was employed to measure the vertical normal stresses in the subgrade. It consists of an elastic membrane (a thin disk of aluminum) fixed at its perimeter to a thicker circular base plate. The membrane responds to normal stresses by bending and stretching slightly. A SR-4 electrical strain gage, bonded to the membrane, measures the strain induced by the pressure. A second compensating gage is mounted in the base plate at a point where it undergoes little strain under load. The individual gages are internally waterproofed with petrosene wax. The entire assembled cell, with its vinyl-insulated lead wires, is waterproofed by dipping in a solvent-type vinyl cement, From three to four coats of the cement provide a waterproof, flexible jacket that can resist immersion in water for a month or more. Three different cell diameters were used (4, 5, and 6 in.) with diaphragms 0.19 and 0.12 in. thick to provide a range in sensitivities. The cells were 0.4 in. thick or less. The cell diameter to thickness ratios were between 10 and 15 which minimized the variable effects of soil arching over the deflecting diaphragms.

Each cell was individually calibrated by the application of a uniform pressure by means of an air-loaded rubber membrane in a soil-filled calibration chamber. Initially the cells were calibrated completely surrounded by subgrade soil compacted to the same density as in the test section. Comparative tests, however, showed that virtually the same results were obtained for pressures within the middle range for each cell if the cell were placed on a surface of compacted soil and loaded directly with the rubber membrane. Subsequent calibration was performed in this manner.

From 25 to 30 cells were employed, arranged in 4 (or 3) straight lines perpendicular to the axis of the pit, with each line at a different depth below the surface and at a different position along the pit axis. In this way no cell was directly below another so as to minimize any arching or load concentration caused by their rigidity. The exact depths varied from test to test. In the first series, on the topsoil base, the upper layer was in the base at a depth of 9 in. below the surface, and the remainder in the subgrade at depths of 15.7, 27.6, and 45.6 in. below the surface or respectively 0.8, 1.4, 2.5, and 4.1 diameters (based on an equivalent circular 9,000-lb wheel load). In the remainder of the tests the upper cell layer was in the subgrade, just below the base course at a depth of 11 to 13 in. (1 to 1.2 diameters) with a 3-in. asphaltic surface or 15 in. (1.4 diameters) with a 6-in. asphaltic surface. The other layers were at depths of about 17, 23, and 29 in. (1.5, 2.1, and 2.7 diameters) with a 3-in. asphaltic surface and correspondingly greater depths with the 6-in. thick surface. The exact depths for each test series are shown on the plots of the test results.

PAVEMENTS SYSTEMS

The pavement systems tested were typical of those currently employed by the Georgia State Highway Department. The subgrade soil for all tests was a micaceous sandy silt, a residual material derived from granite gneiss This type of soil is widespread in the northern half of the State and is characterized by a low resistance to deformation, particularly under load. It is far from an ideal subgrade and is typical of the poorer materials in the State on which roads must be built. Four types of bases were used: topsoil, (silty, well-graded sands from two locations in Central Georgia); soil-bound macadam consisting of 40 percent by weight of the topsoil and 60 percent by weight of size 467 crushed granite; soil cement, consisting of 4 percent by weight Type 1 portland cement and 96 percent of the soil-bound macadam; and sand asphalt, a uniform subangular quartz sand with 5 percent RC-3 cut-back asphalt.

Standard laboratory tests were run on all these materials to determine their physical properties. Because of the coarse aggregate size it was impossible to run the ordinary compaction test on the soil-bound macadam and soil-cement macadam materials. These materials were compacted in an 8-in. diameter by 16-in. high mold in 2-in. layers by

a 5.5-lb hammer filling 12 in. using sufficient blows on each layer to provide the same 12,400 ft-lb per cu ft as in the Standard AASHO test. The physical properties of these materials are summarized in Table 1. The surface in all cases was a plant mix asphaltic concrete.

Pavement Construction

Different combinations of base, base thickness and pavement thickness were tested as summarized in Table 2. The initial work employed 8-in. thick base courses and

TABLE 1

PROPERTIES OF SUBGRADE AND BASE MATERIALS

Material	Description	Liquid Limit	Plastic Index	Percent Passing No. 10	Percent Passing No 200	Maximum Density[a] (pcf)	Class.
Silt subgrade	Micaceous fine sandy silt	45	8	98-100	36-40	95-97	A-5
Topsoil	Silty, well-graded sand	14 5	0	98	12-15	128	A-1
Soil-bound macadam	Subangular to angular granite gneiss (sizes 467)[b] 60 percent; 40 percent topsoil			40	6-8	131	
Soil cement	4 percent Type 1 cement, 96 percent soil-bound macadam above					135	
Sand asphalt	Uniform subangular quartz sand 95 percent, 5 percent RC-3 cutback asphalt	0	0		0	105	A-3[c]
Asphaltic concrete	Plant Mix, 5 percent Bitumen					140	

[a] Std ASTM D 698-58T Method C for sand, topsoil, mica silt. For others a special compaction test was employed (see text)

[b] ASTM D 448

[c] Sand alone.

TABLE 2

TEST CONDITIONS

Test Series	Subgrade Soil	Surface-Plant Mix Asphalt Conc Thickness (in)	Base Course Composition	Base Course Thickness (in)	Loading Wheel	Loading Total Load (kips)
I	Mica silt	3	Topsoil I	8	Single	5, 9, 13.5
					Dual	5, 9, 13 5, 18
					Dual tandem	18, 27, 36
II	Mica silt	3	Soil-bound macadam	8	Single	5, 9, 13 5
					Dual	9, 13 5, 18
III	Mica silt	3	Soil-cement macadam	8	Single	5, 9, 13 5
					Dual	9, 13 5, 18
IV-1	Mica silt	3	Sand asphalt	8	Single	5, 9, 13 5
					Dual	9, 13 5, 18
IV-2	Mica silt	6[a]	Sand asphalt	8	Single	5, 9, 13 5
					Dual	9, 13 5, 18
V-1	Mica silt	3	Topsoil II	8	Dual	9, 13.5, 18
V-2	Mica silt	6 5[a]	Topsoil II	8	Single	8 5, 12 5, 17
					Dual	9, 13 5, 18
VI-1	Mica silt	3	Soil-cement macadam	6	Single	5, 9, 13 5
					Dual	9, 13.5, 18
VI-R	Mica silt	3	Soil-cement macadam	6	Single	13 5[b]
VI-2	Mica silt	6 5[a]	Soil-cement macadam	6	Single	5, 9, 13 5
					Dual	9, 13 5, 18
VI-F	Mica silt	6 5[a]	Soil-cement macadam[c]	6	Dual	9, 13 5, 18

[a] 3-in overlay

[b] 1,000 cycles

[c] Subgrade and base inundated

3-in. asphaltic concrete surface courses (laid in two layers). Later tests included 3- to 3.5-in. thick asphaltic concrete overlays on the 3-in. surfaces, as well as 6-in. base thickness.

The subgrades were constructed in accordance with the current Georgia Highway Department practice for embankments. The lower 3 ft was compacted to 90 percent of the maximum density as specified by ASTM D-698 - 58T - C Compaction test and to the upper 3 ft to a density of between 95 and 100 percent of the same maximum. Both were tamped in 2-in. thick layers with a gasoline-driven dynamic device, the "Jay Tamp" at a moisture content equal to or slightly below the optimum. The topsoil and sand asphalt base courses were compacted to 100 percent of the ASTM D698-58T-C max.; the soil-bound macadam and the soil-cement macadam were compacted to 100 percent of the maximum density found on the large compaction molds. The asphaltic surface was compacted with the Jay Tamp in 1.5-in. thick layers to as great a density as possible. Tests of cores from one series showed a mean density of 131 pcf which is slightly less than that obtained by rolling the same mix on a highway job.

Engineering Properties of Pavement Components

Tests were run on each of the pavement components to determine their modulus of elasticity and strength properties. Triaxial shear tests were made of all the materials in which both stress-strain characteristics and stresses at failure were determined. The tests of the subgrade, topsoil, and sand asphalt were run on both laboratory specimens compacted in a 4-in. diameter 8-in. high mold and on undisturbed samples cut

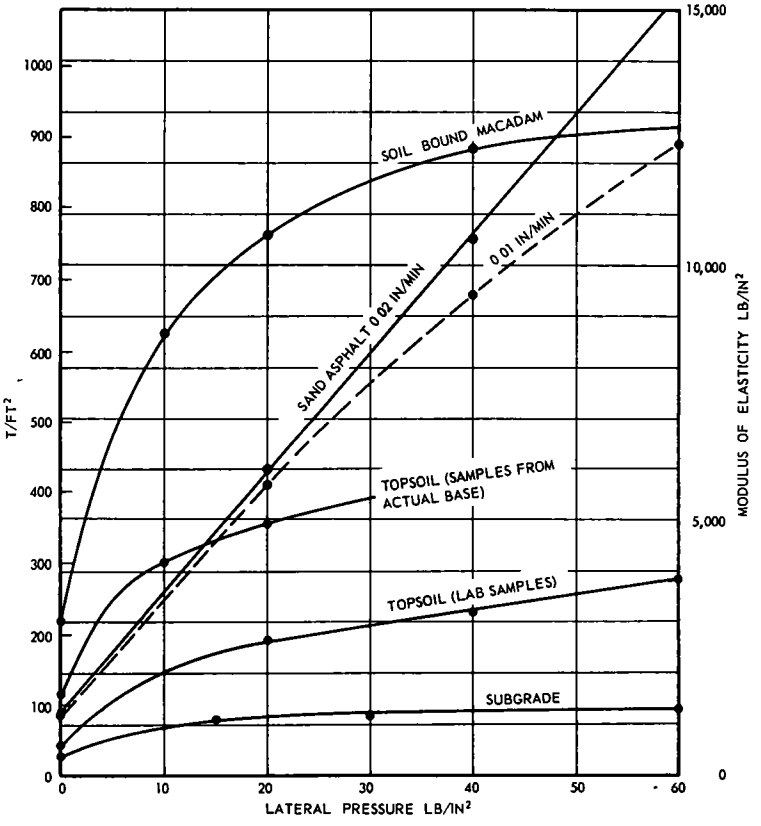

Figure 4a. Modulus of elasticity, E, of base and subgrade materials obtained by triaxial tests at different confining pressures.

from the test section. The tests on the soil-bound macadam were made on specimens compacted in the 8-in. diameter 16-in. high mold in the laboratory. All were tested in a large triaxial cell with interchangeable 4-, 6-, and 8-in. diameter sample bases. In all cases the undrained (quick) procedure was used, with a constant axial deformation rate of 0.02 in. per min. The sand asphalt was also tested at a rate of 0.01 in. per min to determine whether shear rate had any effect on its deformation properties. It was tested at temperatures comparable to those measured in the base course at the time of stress measurement. The elasticity test results are shown in Figures 4a, 4b, 5a, and 5b. They show the initial or tangent modulus of elasticity of each material as a function of the minor principal stress and the ratio of the modulus of elasticity of the base to that of the silt subgrade at equal minor principal stresses. The strength and elasticity data are summarized in Table 3.

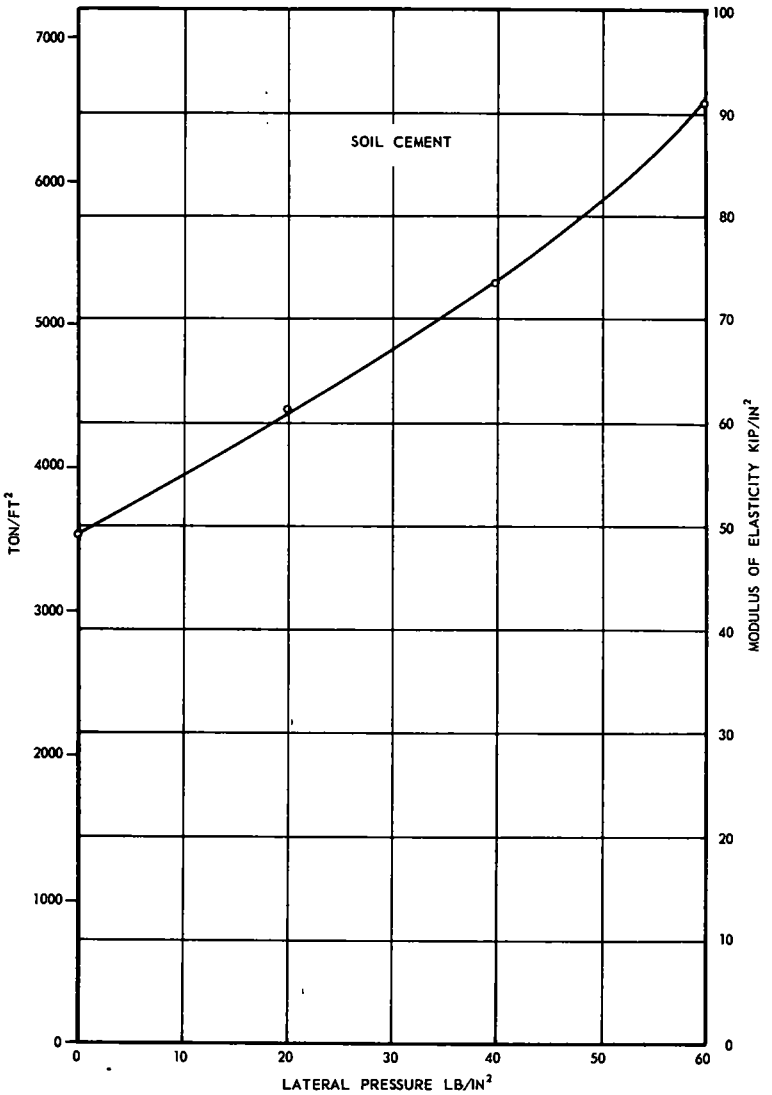

Figure 4b. Modulus of elasticity, E, of soil cement base material obtained by triaxial tests at different confining pressures.

TABLE 3

STRENGTH AND DEFORMATION CHARACTERISTICS OF MATERIALS

Material	Weight (pcf)	Water Content (%)	Strength Characteristics		Deformation Characteristics from Triaxial Tests								Elastic Modulus from Plate Load Tests (psi)	Tangent Modulus from CBR Tests (psi)		CBR Value	
					Elasticity Modulus (psi)				Strain at Failure (%)								
			c (psi)	ϕ (°)	At 0 Psi	At 20 Psi	At 40 Psi	At 60 Psi	At 0 Psi	At 20 Psi	At 40 Psi	At 60 Psi		No Surcharge	0.40-Psi Surcharge	No Surcharge	0.40-Psi Surcharge
Subgrade	79 1	26 8	9 0	23	328	1,104[a]	1,160[b]	1,346	2 5	13.7	14 3	17.6	1,300	691	1,237[c]	3 4	4.2
Topsoil samples																	
From actual base	121.2	10 2	20 2	33	1,640	4,910	4,800	-	4 9	6 3	8 2	-	10,400[d]	4,400	6,650	29.1	44 1
Prepared in laboratory	123 0	10 6	5 1	33	545	2,700	3,140	3,970	3 8	10 4	13 2	23.9	-	-	-	-	-
Soil-bound macadam	131 1	3 9	2 5	37	2,940	10,520	12,360	-	0 6	2 9	8 2	-	11,200[d]	12,660	-	34 5	-
Soil cement	134 5	3.5	51 3	50	49,400	61,500	74,000	91,000	0.8	0.7	0 9	0.9	130,000	-	-	-	-
Sand asphalt																	
0.02 in./min loading rate	103 4	8 5	2 2	35	1,245	5,970	10,520	15,380	1.4	4.8	4 4	5.9	5,590	2,370	3,820	9.2	19 3
0 01 in /min loading rate	105.2	8 8	1 0	33	1,080	5,670	9,450	12,350	2 9	6.2	8.2						

[a]At 15 psi. [b]At 30 psi. [c]Surcharge 0 80 psi [d]With 3 in of pavement above

The modulus of elasticity curves all show an increase in E with an increase in confining pressure. The curve for the sand asphalt shows a continuing, nearly linear increase, whereas for the others E increases rapidly at low pressures but approaches a constant of higher pressures. The ratios of the E of the base to the E of the subgrade, however, are nearly constant regardless of confining pressure for all except the sand asphalt base. For the latter, the ratio increases with increased confinement. These variations in E are significant because most theoretical analyses, including the Boussinesq and the two-layer and three-layer theories assume that E is a constant that is independent of confinement.

Two types of in-place tests were conducted on the pavement components—California Bearing Ratio (CBR) and plate load tests. The CBR tests were made on the upper surfaces of the subgrade and base courses using the standard methods of the Corps of Engineers with a nominal surcharge load equivalent to 3 in. of pavement.

Plate load tests were made on the subgrade, all base courses, and the surface course for all but the sand-asphalt base pavement. An 18-in. diameter plate was employed that was rigidly reinforced so as to have negligible deflection.

An effective modulus of elasticity was computed from each CBR and plate load test using the theory of the deflection of a rigid circular load on an elastic medium. The plate load modulus of elasticity data for the base courses were computed from the two layer elastic theory using the elastic modulus of the subgrade as computed from the subgrade load tests. The results of these computations, which must be considered as rough indications at best, are also given in Table 3.

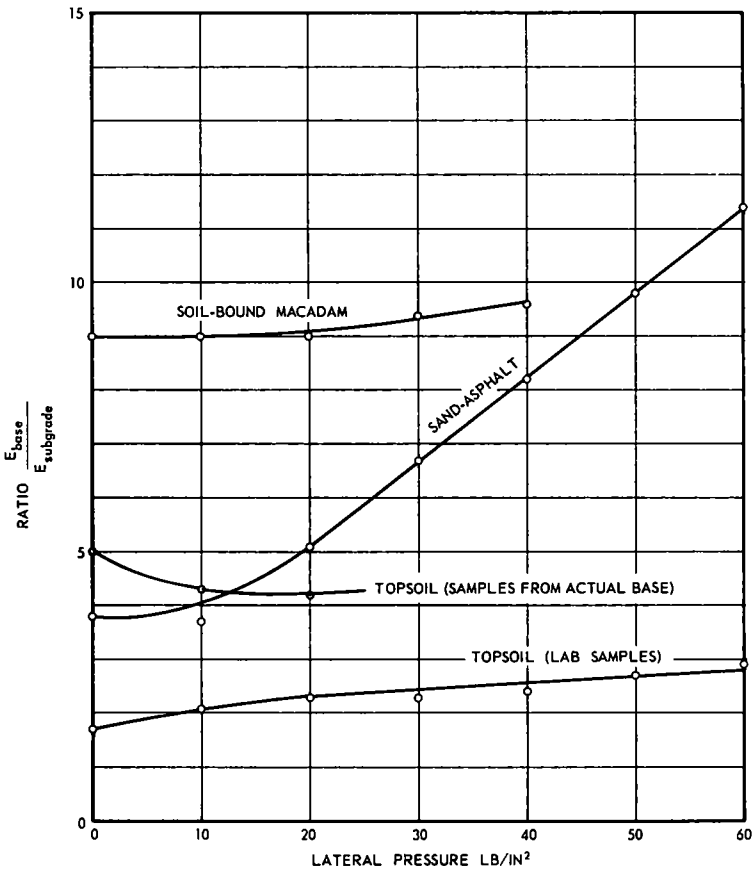

Figure 5a. Ratio of modulus of elasticity of base material to subgrade soil at different confining pressures.

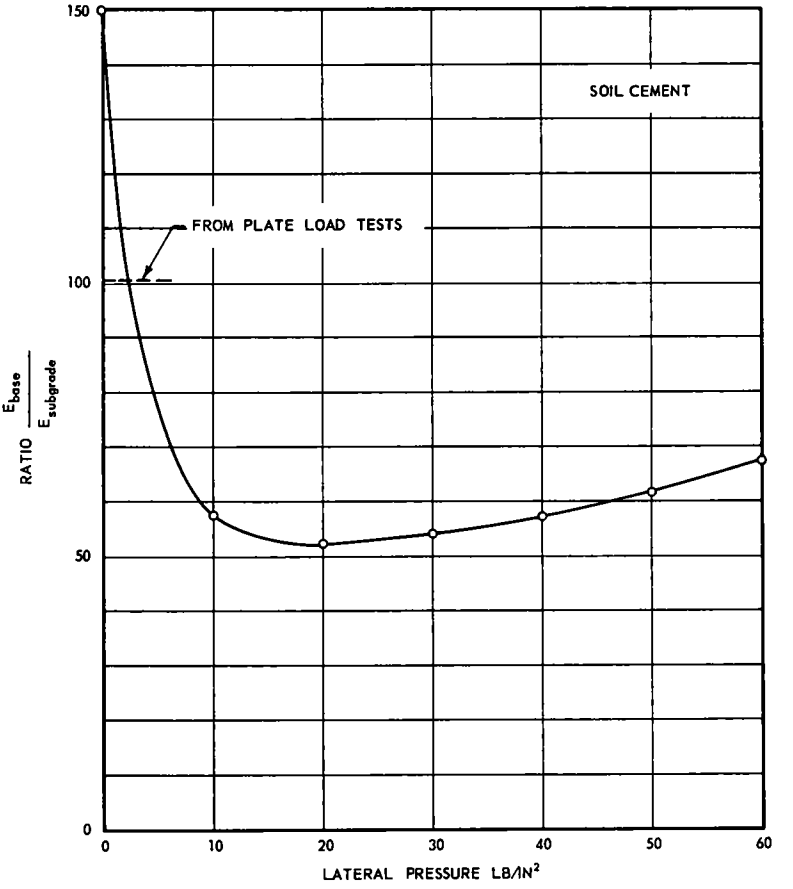

Figure 5b. Ratio of modulus of elasticity of soil cement base to subgrade at different confining pressures.

WHEEL LOAD-SUBGRADE STRESS TESTS

The full-scale model tests of truck tires on the pavement included more than sixty combinations of load, wheel configuration, and pavement design. In general the single tire was subjected 5, 9, and 13.5 kips equivalent to 10-, 18- and 27-kip axle loads and the dual tires were subjected to 9, 13.5, and 18 kips total or 18, 27, and 36 kips per axle. The range selected includes the legal loads permitted in many States and anticipates possible larger maximum loads of the future.

Tire Contact Area

The tire selected is designed for a maximum load of 9,000 lb at an inflation pressure between 80 and 90 psi. The size and shape of the tire contact was determined for loads of 4,500, 6,750, 9,000, and 13,500 lb in order to compute the stresses in the soil theoretically. The tire prints and the load-contact pressure curve are shown in Figures 6 and 7. The prints show a nearly circular contact at one-half the design tire load and a rectangle whose length is 2.5 times the width for 1.5 times the design tire load.

Test Procedure

Each load was placed on the pavement of ten different positions on the longitudinal

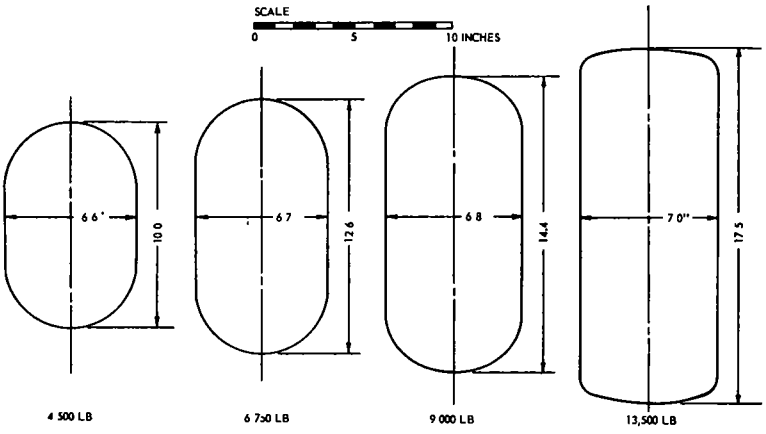

Figure 6. Typical tire prints for new 9 x 20 truck tire inflated to recommended pressure of 86 psi.

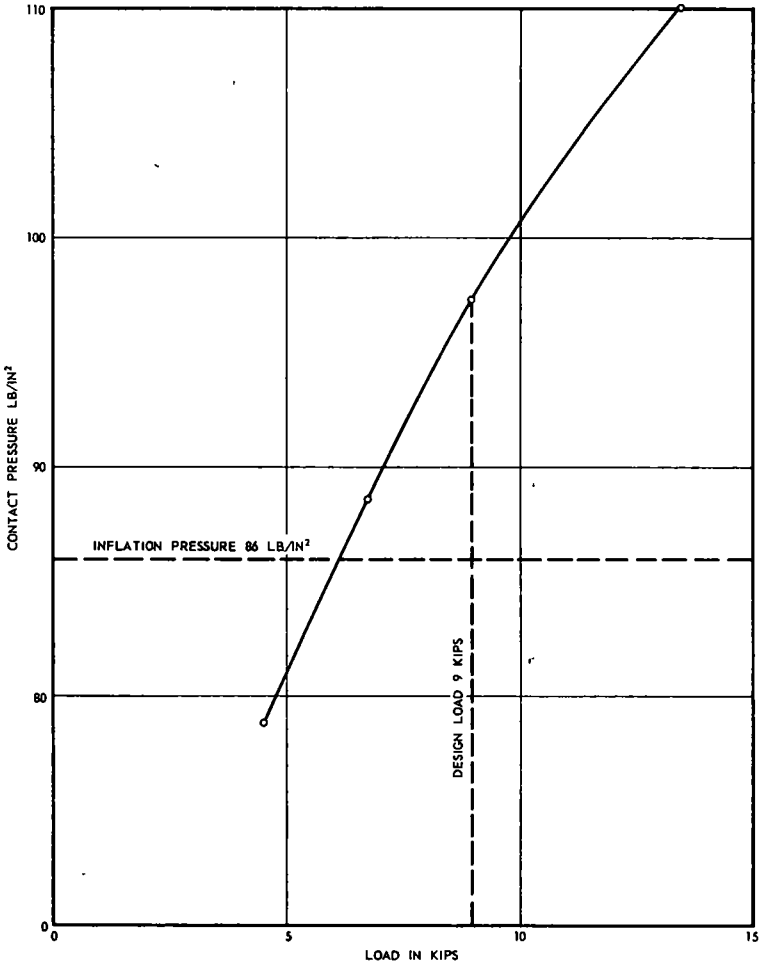

Figure 7. Variation of average contact pressure of a 9 x 20 truck tire as a function of tire load, at recommended inflation pressure of 86 psi.

axis of the pit—center, 3, 6, 12, 24 in. each side of center, and 36 in. north of the center. The vertical pressures were measured by each cell in each position. The results are shown graphically on the attached charts. They are plotted with vertical stress as a function of distance from the center of the load, regardless. The variable positioning of the tire made it possible for each cell to contribute more than one point to the curve. Only the center pressure with a distance from the load of 0 was measured by one cell alone at each depth. At least two and sometimes five sets of identical independent loadings and stress measurements were made for each tire load. All the individual stress measurements are plotted rather than averages to show the range of variability in the readings. In this paper only the data for the 9, 000-lb single tire

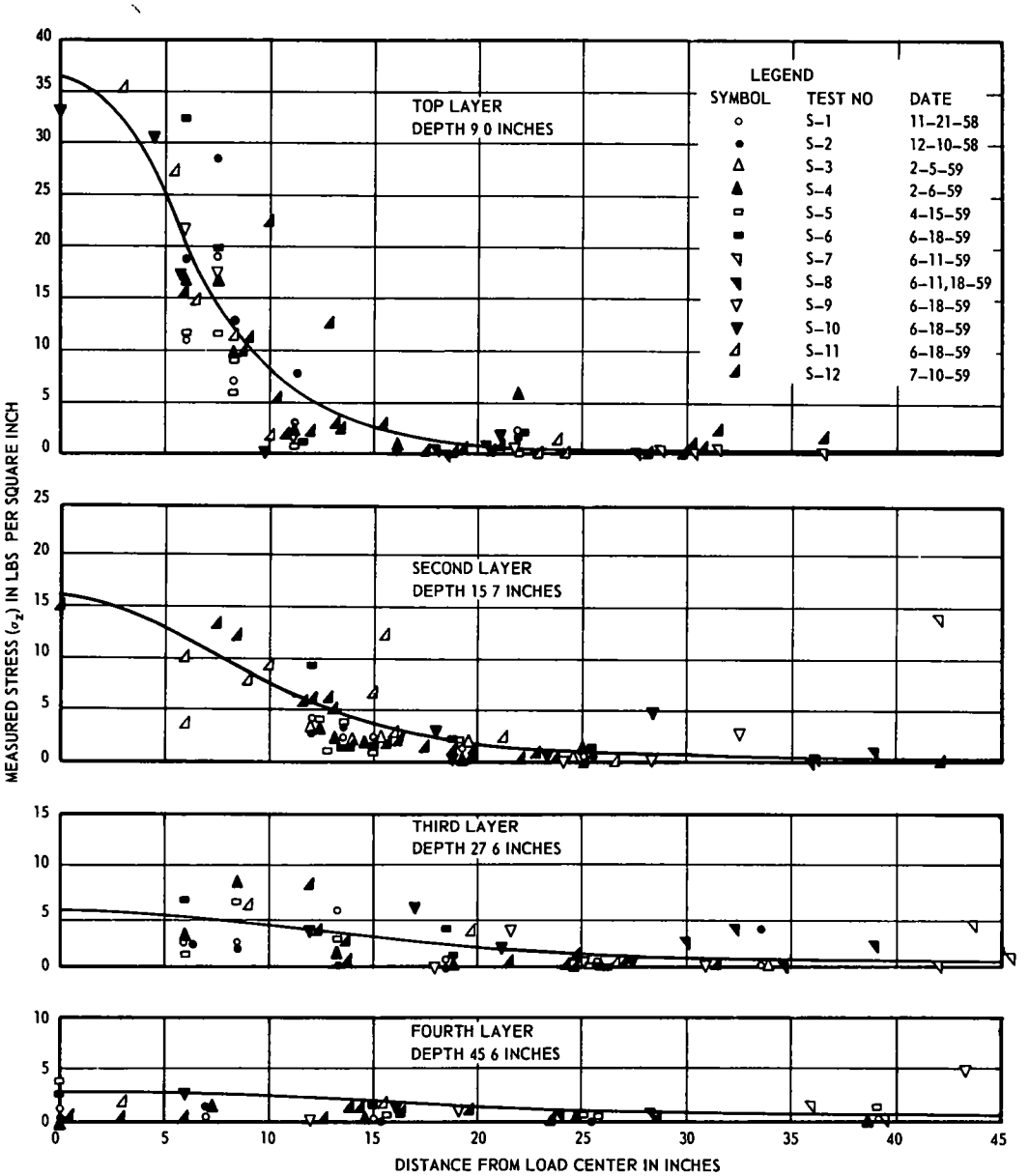

Figure 8. Measured stresses; single load 9,000 lb topsoil I base 8 in. thick; 3-in. surface. Solid line is Boussinesq stress distribution.

and the 13,500-lb dual are included. The data from the other loads are in direct proportion.

Theoretical Stresses

The theoretical stresses for each loading were computed from the load-tire contact area data using an equivalent rectangular or circular loaded area. The Boussinesq analysis of a semi-infinite homogeneous isotropic elastic solid was used for all. In addition the two-layer theory was employed for the soil-cement pavements by assuming that the modulus of elasticity of the asphaltic concrete surface was the same as that of the soil cement. Three different ratios of the elasticity of the upper layer to that of the lower layer were assumed: 1 to 1 (which is the same as the Boussinesq), 10 to 1,

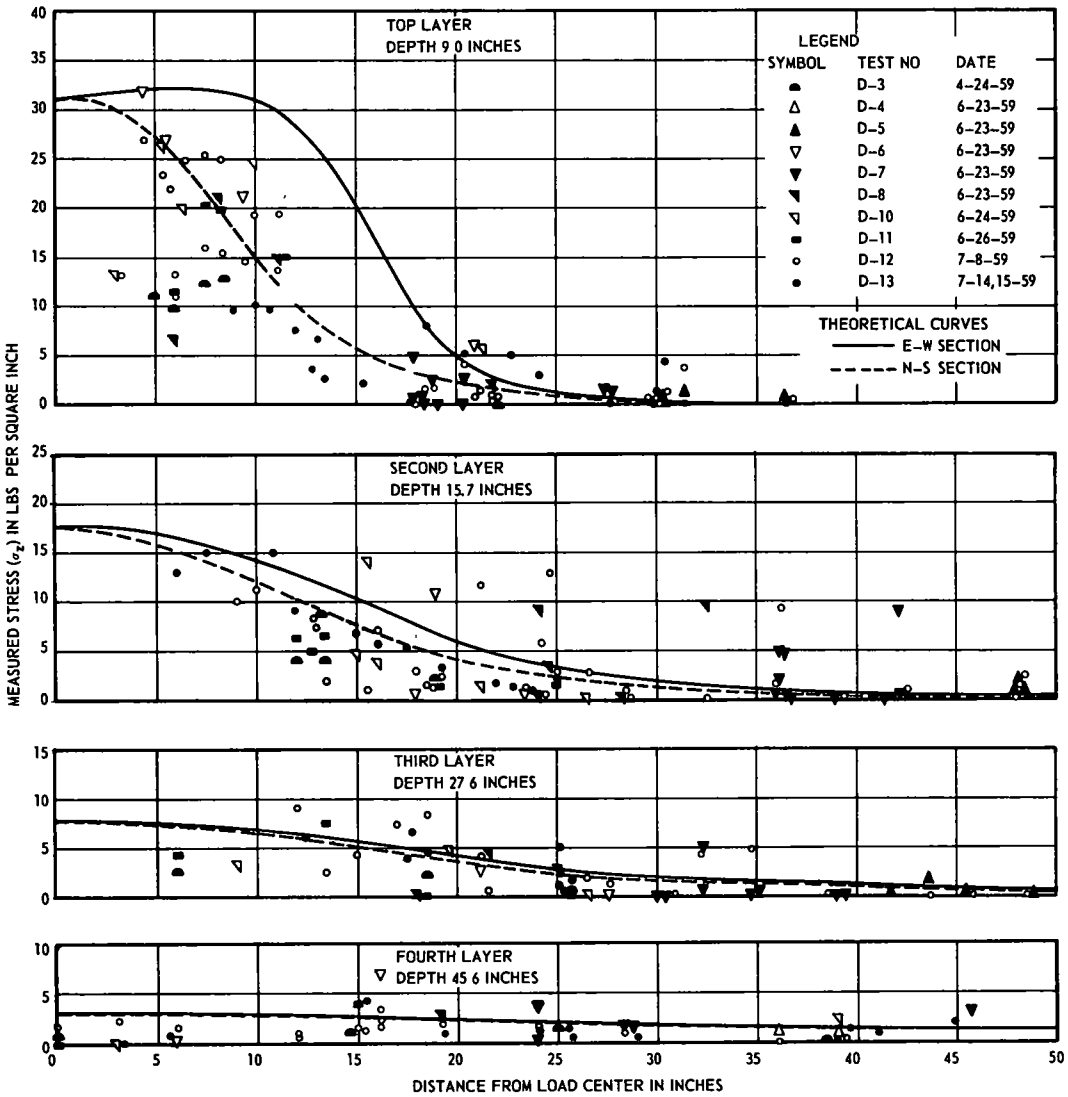

Figure 9. Measured stresses; dual load 13,500 lb topsoil I base 8 in. thick; 3-in. surface. Solid line is Boussinesq stress distribution parallel to axle; dotted line is Boussinesq stress perpendicular to axle.

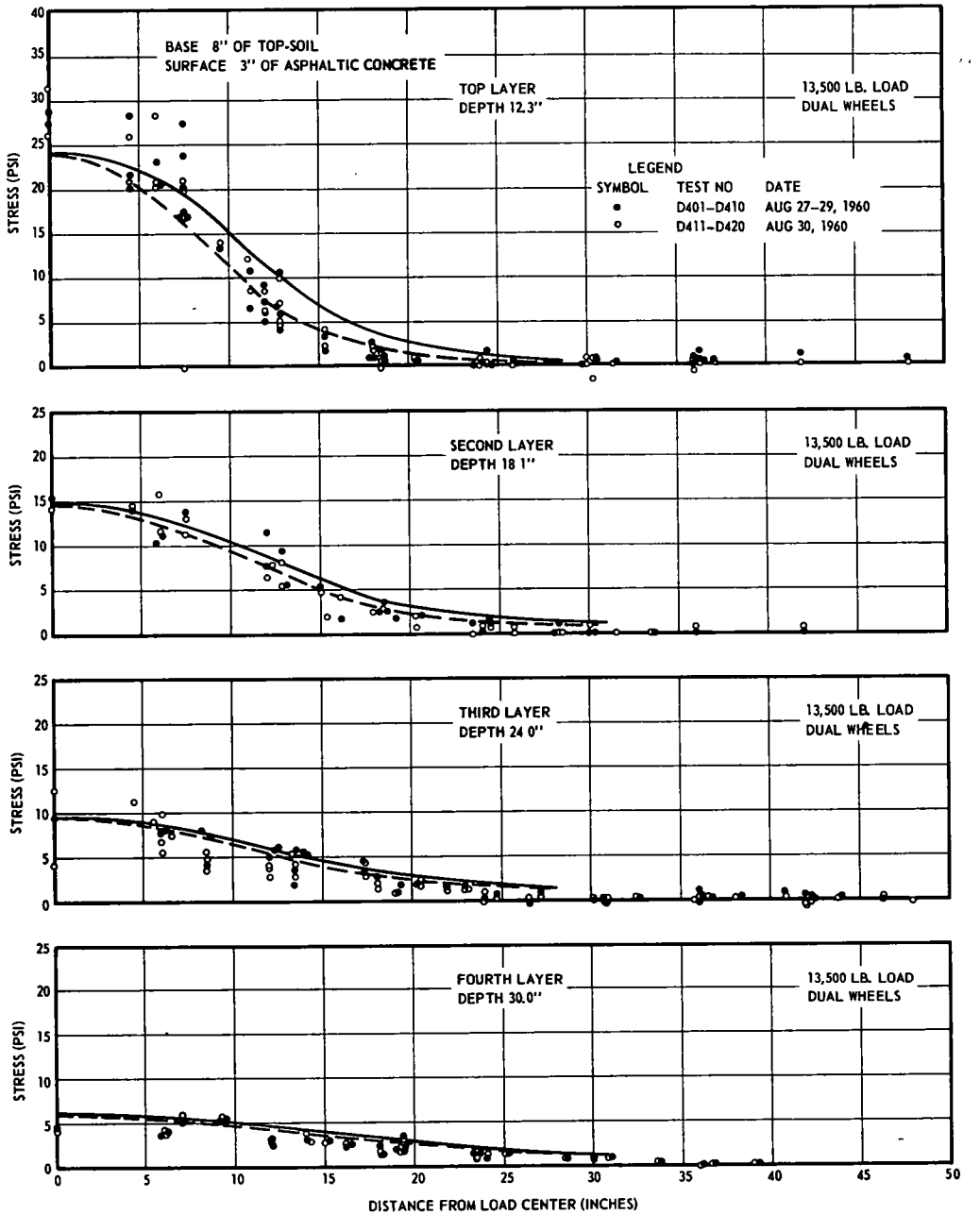

Figure 10. Measured stresses; dual load 13,500 lb topsoil II base 8 in. thick; 3-in. surface.

and 100 to 1. The stress computations for the dual tires were made in two directions: (a) along the axis of the pit—in the direction of wheel travel; and (b) on the line of the axle at right angles to the direction of wheel travel. (The actual stress measurements include both these directions and many others in between, and are not differentiated in the graphical presentation.) The theoretical stress distribution is shown in Figures 8 through 26 by the continuous curves. In the dual-tire results, the solid curve represents the stress distribution in line with the axle and the dashed curve at right angles to the axle.

Topsoil Base Pavements

The measured vertical stresses for the topsoil base pavement systems are shown in Figures 8 through 12 as individual points on the graphs. They show that the vertical

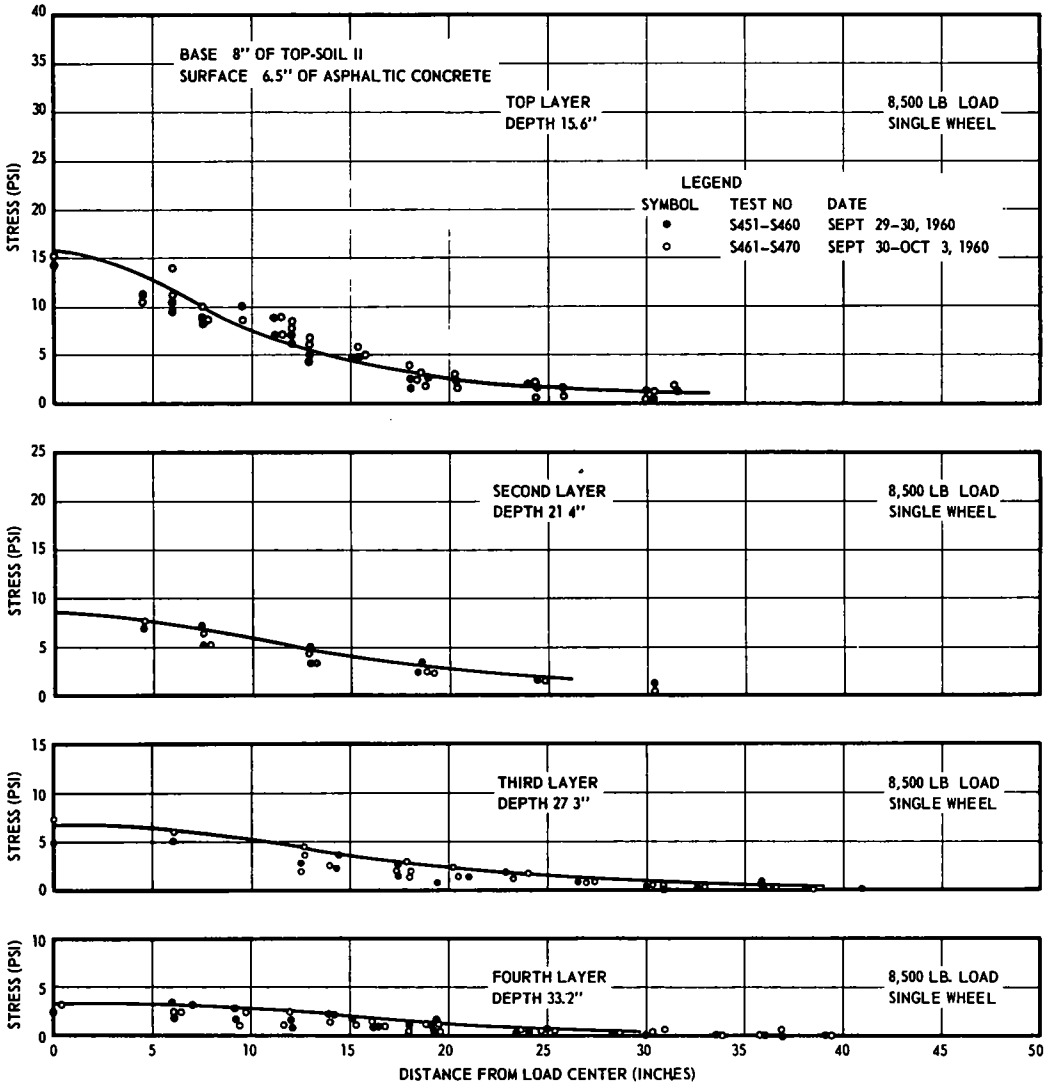

Figure 11. Measured stresses; single load 8,500 lb topsoil II base 8 in. thick; 3-in. asphaltic concrete surface and 3.5-in. asphaltic concrete overlay.

pressures in the subgrade decrease rapidly with increasing depth The pressure distribution is seen to be close to that given by the Boussinesq theory. The maximum pressure in the subgrade, under the center of the load is equal to the Boussinesq for Topsoil I and equal to or slightly greater (up to 15 percent more) for Topsoil II. For the topsoil subgrades, therefore the Boussinesq theory, based on a semi-infinite homogeneous isotropic elastic mass, is found to be a reasonably accurate representation. This is somewhat surprising because the ratio of the modulus of elasticity of the base to the subgrade is 3 to 4 which, by the two layer theory, should yield slightly lower stresses directly beneath the center of the load. Two factors are undoubtedly responsible. First, in order for the two layered theory to be theoretically valid, there must be tensile stresses in the interface between the two layers. The Mohr envelopes show a cohesion of only 15 psi for the topsoil (based on a curved envelope) or 20 psi (based on an approximate straight line) for the samples taken from the model pavement and 5

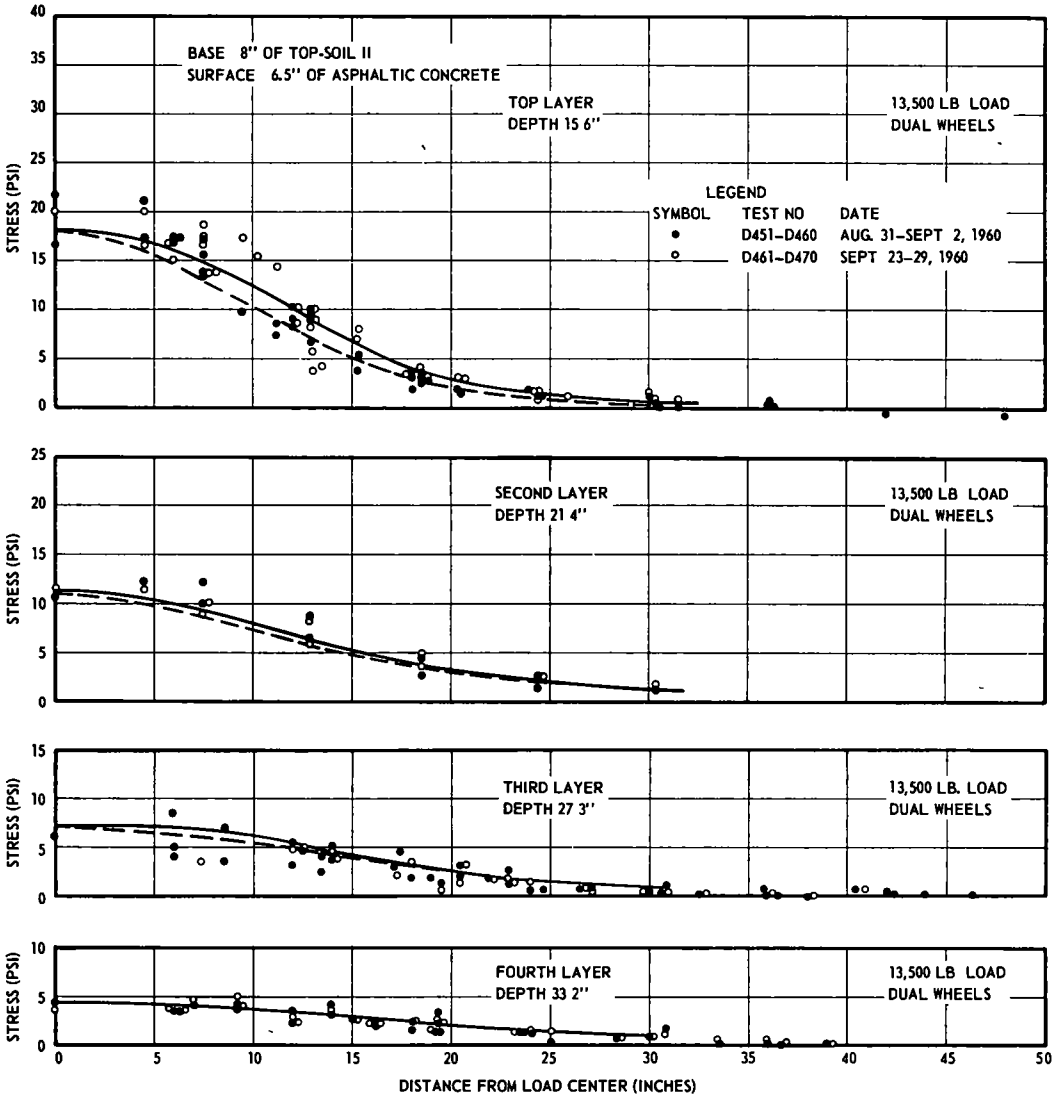

Figure 12. Measured stresses; dual load 13,500 lb topsoil II base 8 in. thick; 3-in. thick asphaltic concrete surface with 3.5-in. thick asphaltic concrete overlay.

psi for the laboratory compacted samples. The cohesion in the subgrade is 9 psi. Neither material, therefore, is capable of resisting much tension, which invalidates, to some degree, the two-layer theory. Second, neither modulus of elasticity is a constant although both the two-layer theory and the Boussinesq theory assume unchanging E values. It is possible the increase in E with increasing confinement causes a stress concentration, as noted by Griffith and Fröhlich, and partially offsets the gain in load spreading produced by the more rigid base. However, it also may be argued that the ratio of the E of the base to that of the subgrade is nearly constant so that the variation in E with confinement is not so significant. A theoretical analysis of the effects of varying E would be instructive, but is not available.

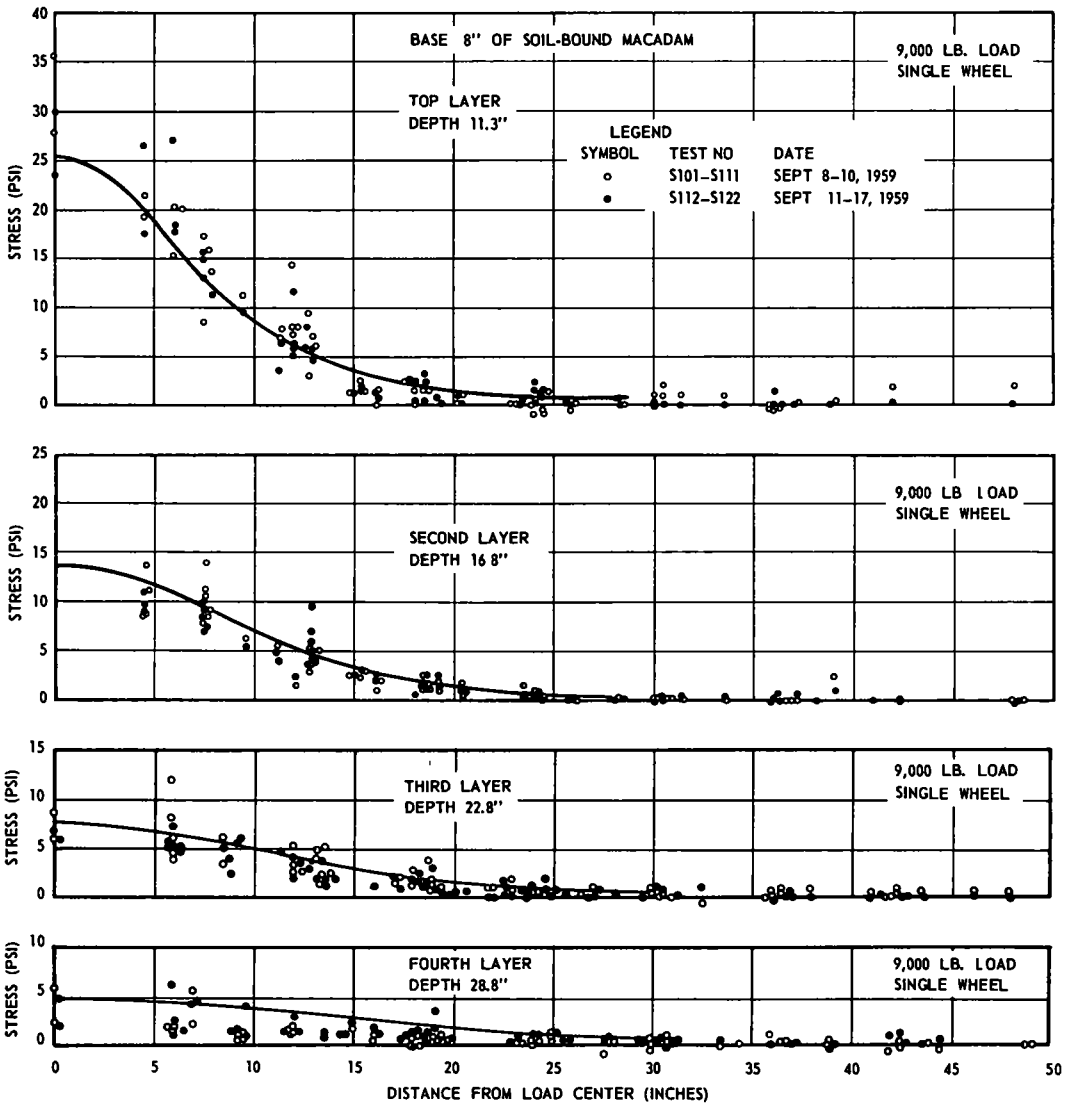

Figure 13. Measured stresses; single load 9,000 lb soil-bound macadam base 8 in. thick; 3-in. asphaltic concrete surface.

Soil-Bound Macadam Base Pavements

The test results for the wheel loads on the macadam base pavement are shown in Figures 13 and 14. The results are almost identical to those of the topsoil base—a marked decrease in vertical stress with increasing depth and a pressure distribution that is very close to that given by the Boussinesq theory. The modulus of elasticity data (Fig. 5a) shows that the soil-bound macadam base has a modulus of elasticity 9 times that of the subgrade. According to the two-layer elastic theory the stresses in the upper surface of the subgrade should be slightly less than one-half the measured vertical stresses (or slightly less than one-half the Boussinesq). As in the case of the topsoil base, two factors appear responsible. First, the cohesion of the soil-bound macadam is only 2 psi which with its high angle of friction means negligible tensile resistance. Tensile cracks develop at the bottom of the base course along the interface

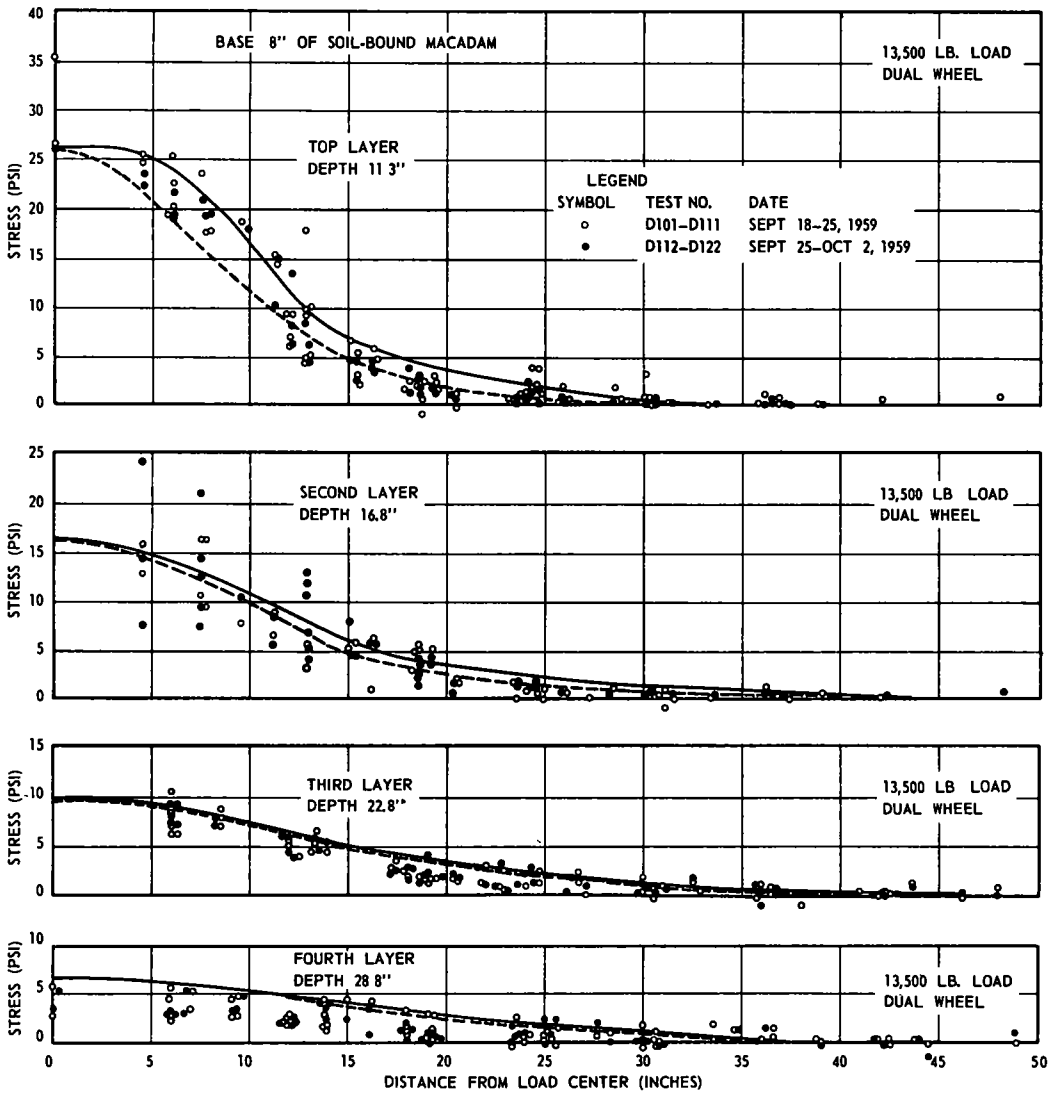

Figure 14. Measured stresses; dual load 13,500 lb soil-bound macadam base 8 in. thick; 3-in. asphaltic concrete.

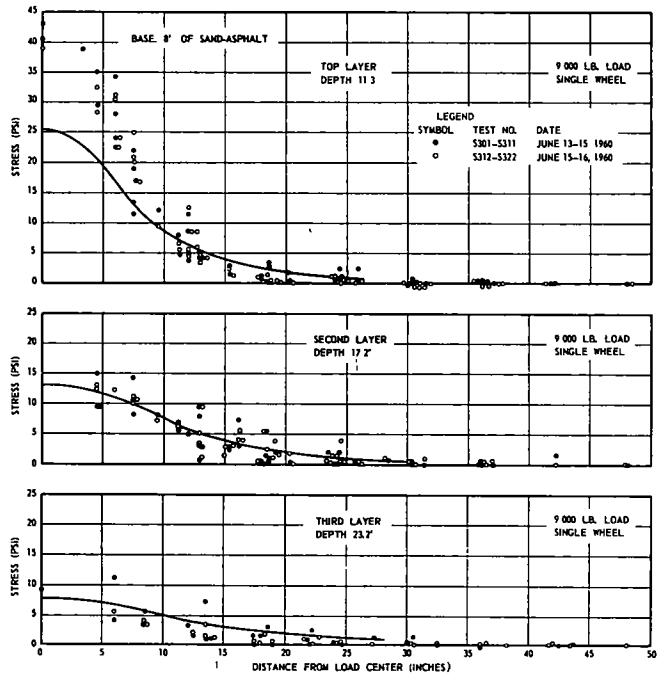

Figure 15. Measured stresses; single load 9,000 lb sand-asphalt base 8 in. thick; 3-in. thick asphaltic concrete surface.

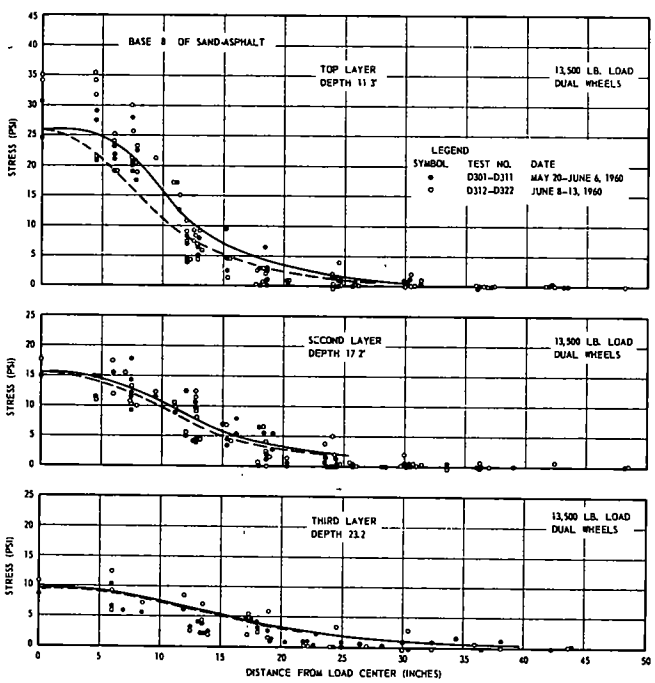

Figure 16. Measured stresses; dual load 13,500 lb sand-asphalt base 8 in. thick; 3-in. thick asphaltic concrete surface.

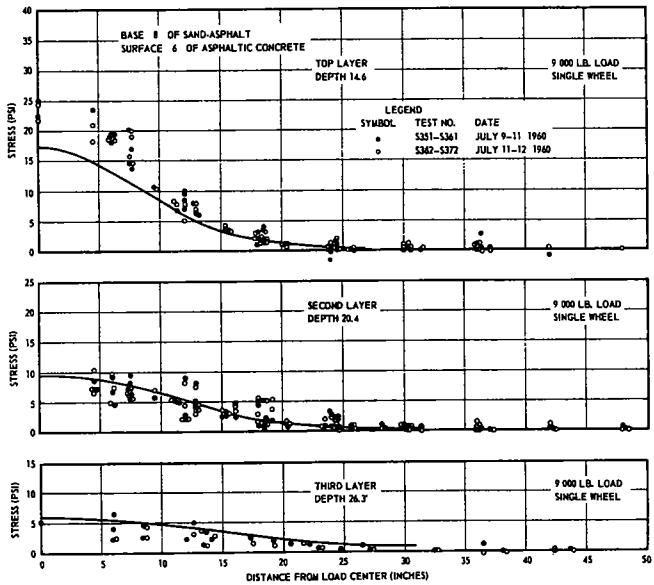

Figure 17. Measured stresses; single load 9,000 lb sand-asphalt base 8 in. thick; 3-in. asphaltic concrete surface with 3-in. asphaltic concrete overlay.

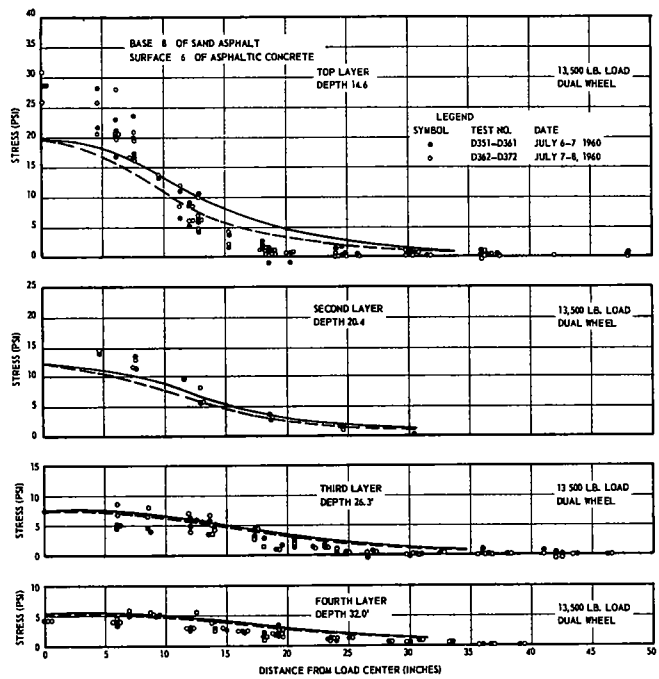

Figure 18. Measured stresses; dual load 13,500 lb sand-asphalt base 8 in. thick; 3-in. asphaltic concrete surface and 3-in. asphaltic concrete overlay.

TABLE 4
RATIOS OF MAXIMUM MEASURED STRESSES

	Single Tire		Dual Tire	
Load (lb)	3-In. Surf.	6-In. Surf.	3-In. Surf.	6-In. Surf.
5,000	1.72[a]	1.52[a]	---	---
9,000	1.61	1.42	1.31[a]	1.33[a]
13,500	1.38[a]	1.23[a]	1.23	1.36
18,000	---	---	1.25[a]	1.32[a]
Avg.	1.57	1.39	1.26	1.34

[a]Not shown in the figures included with this report.

which destroy the continuity of the elastic layer and invalidate the theory. Second, the modulus of elasticity increases with increasing confining pressures, although the ratio of the E of the base to that of the subgrade is nearly constant. The result may be a stress concentration that offsets the gain in load spreading of the more rigid base, as also may be in the case of the topsoil.

Sand Asphalt Base

The stresses beneath the pavements with sand asphalt bases on the micaceous silt subgrade are shown in Figures 15 through 18. Although all the tests show a marked reduction in vertical stresses with increasing depth, the maximum vertical stress directly under the load center and 0.3 in. below the base-subgrade interface was found to be considerably greater than that at an equivalent location in the topsoil and soil-bound macadam base pavements. The ratios of these maximum measured stresses just below the interface to the theoretical stresses as computed by the Boussinesq theory at the same point are given in Table 4. As can be seen, the ratios are greater for the single tire than for the dual and for the smaller loads than for the larger ones. Deeper in the subgrade (6 in. below the interface) the measured stresses are approximately the same as those computed by the Boussinesq theory.

The modulus of elasticity data (Fig. 5a) show that the E of the sand asphalt base is 4 or more times that of the subgrade and on that basis it would be presumed that the subgrade stresses, in accordance with the two-layer theories would be appreciably less than those computed by the Boussinesq theory. Instead, they are considerably greater. The Griffith-Fröhlich theories demonstrate that in a material whose modulus of elasticity increases in direct proportion to the confining pressure there is a concentration of stress immediately below the load. A concentration factor of 4 in the G-F equations (which has been verified by limited tests of cohesionless sands) gives a maximum stress 1.33 times the Boussinesq; a concentration factor of 5 gives a maximum stress 1.63 times the Boussinesq. Of all the base materials tested, the sand asphalt has a modulus of elasticity that most nearly resembles that of a cohesionless sand—a nearly linear increase of E with increasing confining pressure. Further, it is the only base material in which the ratio of the base E to the subgrade E increases substantially with increasing pressure. It is the authors' opinion that the stress concentration found just below the interface of the sand asphalt base is similar to the stress concentration described by the Griffith-Fröhlich equations. Deeper in the elastic subgrade, the stresses return to the Boussinesq as might be expected.

Soil-Cement Bases

The test results for the 8-in. soil-bound macadam cement are given in Figures 19 and 20, and the 6-in. soil-bound macadam cement in Figures 21 through 26. The stresses in the subgrade are considerably less than those found below the topsoil, soil-bound macadam, and sand-asphalt bases. The reduction is greater beneath the 8-in. thick base than the 6-in. thick base as might be expected. Each graph shows the stresses

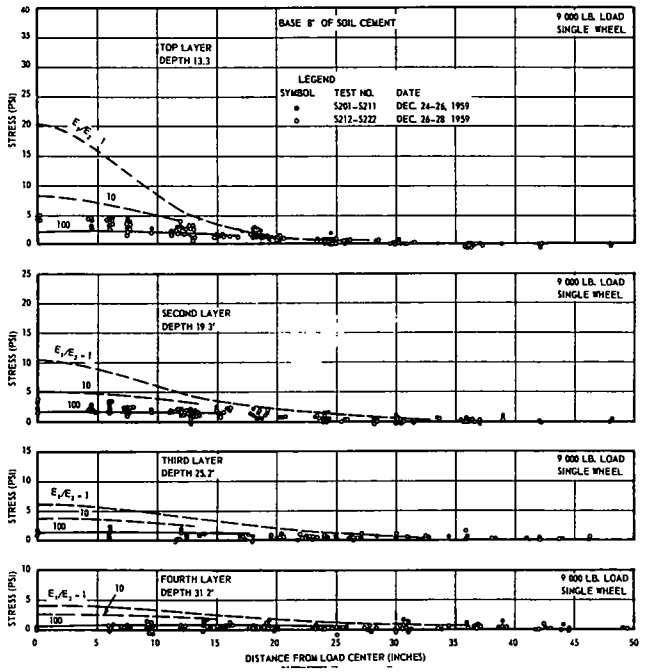

Figure 19. Measured stresses; single load 9,000 lb soil-cement base 8 in. thick; 3-in. asphaltic concrete surface. Curves are for theoretical stresses computed by the two layer theory, for different elasticity ratios; upper curve is equivalent to Boussinesq distribution.

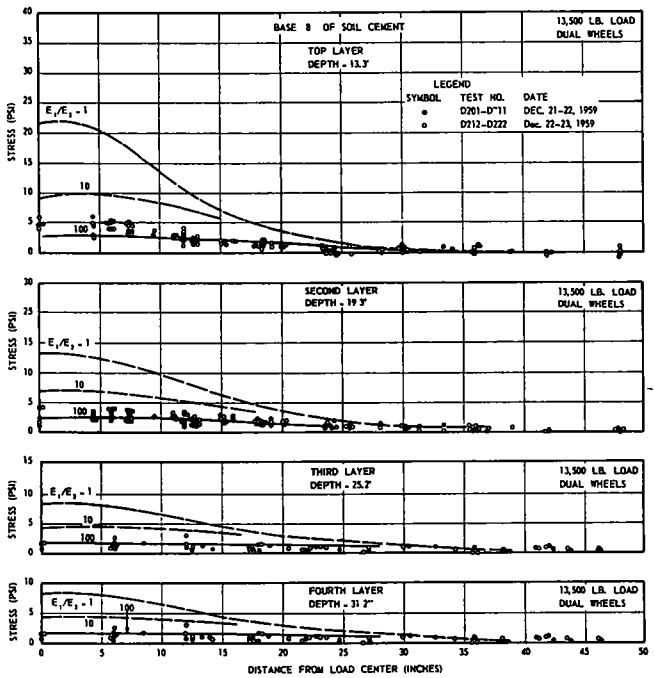

Figure 20. Measured stresses; dual load 13,500 lb soil-cement base 8 in. thick; 3-in. asphaltic concrete surface.

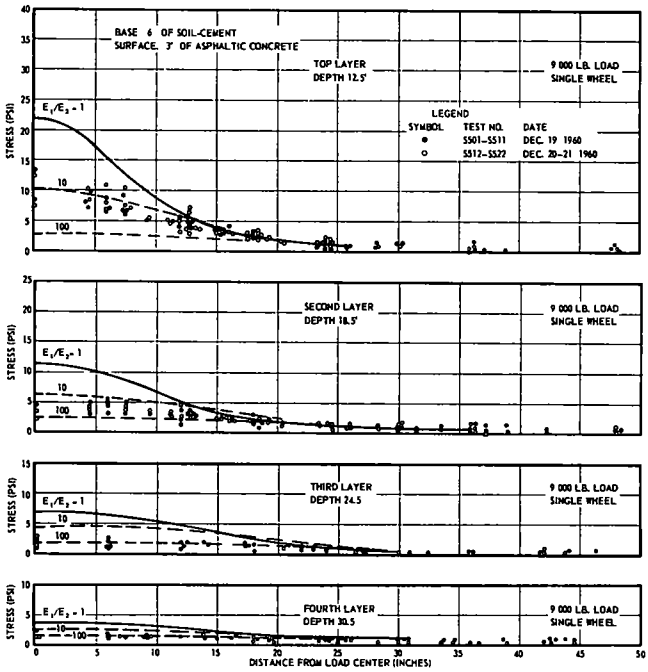

Figure 21. Measured stresses; single load 9,000 lb 6-in. soil-cement base; 3-in. asphaltic concrete surface.

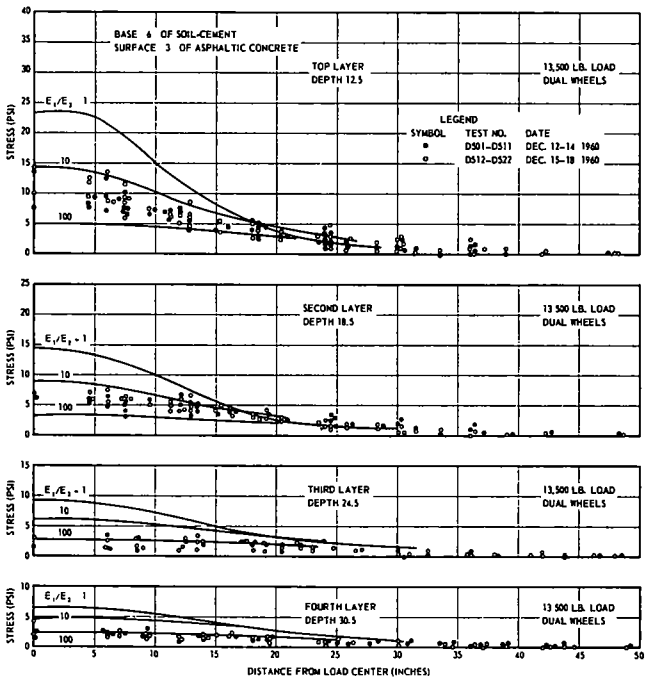

Figure 22. Measured stresses; dual load 13,500 lb 6-in. soil-cement base; 3-in. asphaltic concrete surface.

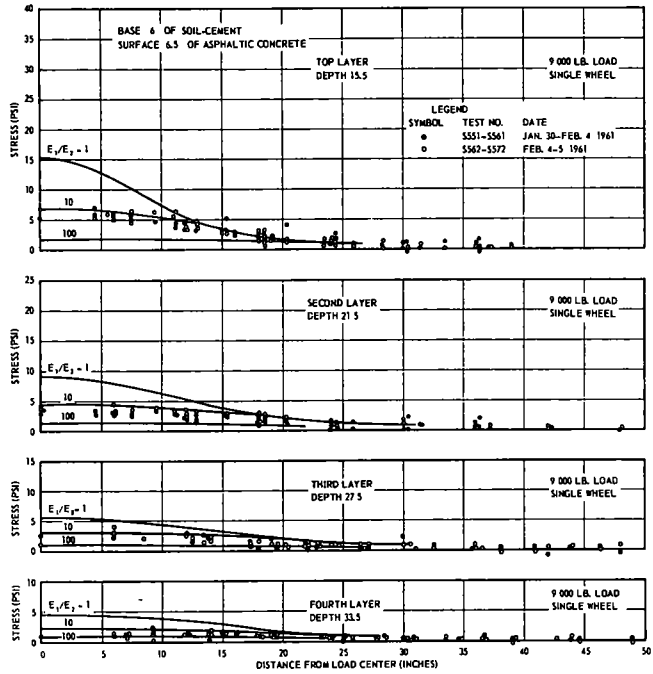

Figure 23. Measured stresses; single load 9,000 lb 6-in. soil-cement base; 3-in. asphaltic concrete surface and 3.5-in. asphaltic concrete overlay.

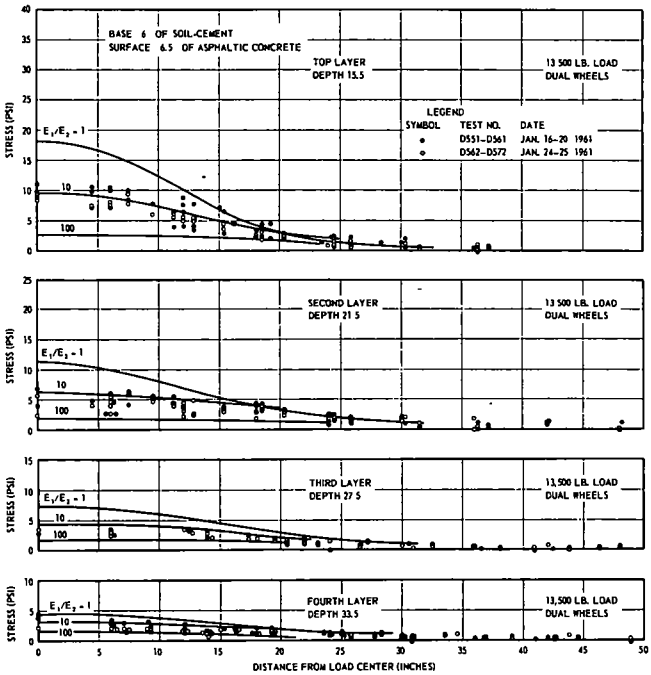

Figure 24. Measured stresses; dual load 13,500 lb 6-in. soil-cement base; 3-in. asphaltic concrete surface and 3.5-in. asphaltic concrete overlay.

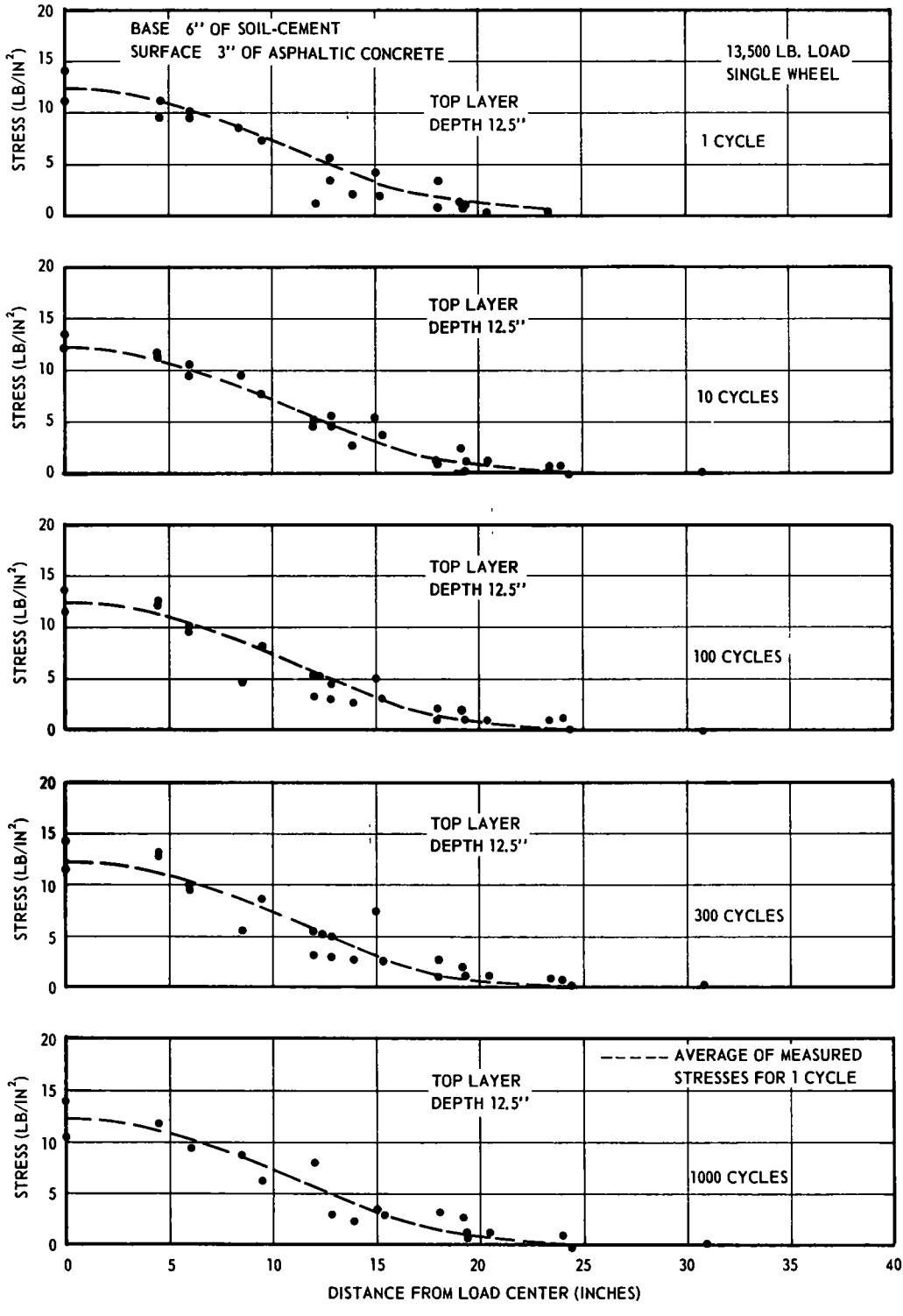

Figure 25. Measured stresses; repeated single wheel load 13,500 lb on 6-in. soil-cement base; 3-in. thick asphaltic concrete surface. Curve is average of measured stresses for one load cycle.

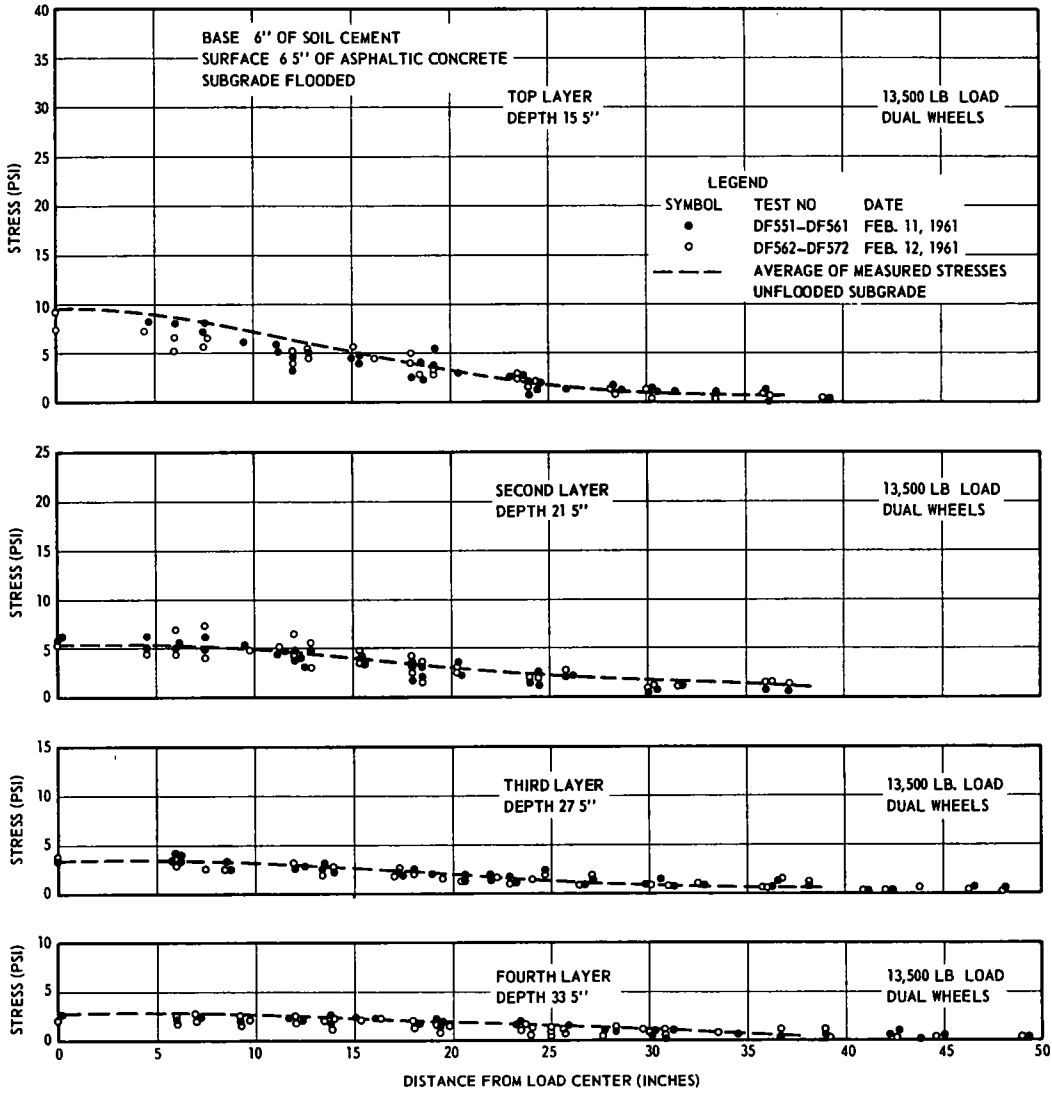

Figure 26. Measured stresses; dual load 13,500 lb 6-in. soil-cement base; 3-in. thick asphaltic concrete surface and 3.5-in. asphaltic concrete overlay, subgrade flooded. Curves are average measured stresses in unflooded subgrade.

TABLE 5

Base	E (ksi)		ΔE (ksi)	Increase (%)
	At 0 Psi	At 20 Psi		
Topsoil (actual)	1.6	4.9	3.3	206
Soil-bound macadam	3.0	10.6	7.6	254
Sand asphalt	1.2	5.8	4.6	384
Soil cement	49	62	13	26

computed by the two-layer elastic theory by assuming that the asphaltic surface has the same modulus of elasticity as the base. This is not strictly valid because the asphaltic concrete is less rigid than the soil cement, but it will serve as an index for comparison. The stresses beneath the 8-in. thick soil cement base (where the base thickness is 73 percent of the total pavement) are between those computed for a ratio of base E to subgrade E of 10 and those for a ratio of 100. The laboratory tests (Figs. 5, 6) show an E ratio of 100 or more for very small confining pressures dropping to about 55 for confining pressures between 10 and 40 psi. Plate load tests on the base found a ratio of 100 (computed by the elastic layer theory). Because the surface is not as rigid as the base, the effective ratio would appear to be 50 or slightly less which agrees with the test results.

The results for the 6-in. base and 3-in. surface are equivalent to an elasticity ratio between 10 and 100, but closer to 10. This is to be expected because the less rigid surface is one-third the total pavement thickness. The measured stresses with the 6-in. base and 6-in. thick surface correspond to a slightly lower elasticity ratio, approximately 10. These differences are to be expected because the effective rigidity of the pavement (base plus surface) becomes less as the proportion of surface to base increases.

The agreement between the measured stresses and the stresses computed by the two-layered elastic theory for the soil cement tends to verify the authors' explanation of the lack of validity of the layered theory for the other bases. The shear tests show that the soil cement is capable of withstanding appreciable tensile stresses, whereas the others are not. In addition, the modulus of elasticity of the soil cement, while increasing with increasing confining pressure, does not change as much relatively as the others. This can be seen by the percentage increase of E with respect to E measured at 0 confining pressure produced by increasing the confining pressure from 0 to 20 psi (Table 5).

Repeated Load-Soil Cement Base

Some concern was felt about the continued load-spreading efficiency of the soil cement after repeated loading. It has been observed that soil-cement pavements tend to develop hair cracks that divide the surface into large polygonal blocks. To investigate this possibility the 6-in. thick soil cement base 3-in. surface pavement was subjected to 1,000 cycles of load-unload with the 13,500-lb single tire. In employing this gross overload on a single tire, equivalent to a 27,000-lb axle, it was hoped to magnify any effects of base cracking. The results (Fig. 25) show no change of stresses in the subgrade 3 in. below the subgrade-base interface.

Effect of Inundation

All the tests had been made with the moisture content of the soil subgrade and the base near the respective optimum moistures Holes were drilled through the 6-in. base soil cement, 6.5-in. surface pavement, and through the entire depth of the subgrade. These were filled with water and kept full so as to inundate the subgrade and base. Moisture tests made at regular intervals in observation holes between the inflow holes showed an increase in saturation from the original value of about 75 percent to an average of 96.5 percent in one week, after which it remained constant. Tests were conducted with dual wheels and loads of 9,000, 13,500, and 18,000 lb. The results (data for the 13,500-lb load are given in Figure 26) showed possibly a slight reduction in the stresses just below the subgrade-base interface. Because inundation caused a small reduction in the modulus of elasticity of the subgrade but little change in the soil-cement base, the elasticity ratio was increased. Theoretically, the stress should have decreased slightly, and the tests verify it.

Effect of Overlay

A number of the pavement systems were tested with both 3- and 6-in. thick asphaltic surfaces to determine the load spreading effects of a 3-in. thick overlay. The results can be seen by comparing the graphs of the 3- and 6-in. surfaces for the topsoil II, sand asphalt, and 6-in. soil-cement base pavements. They show that the overlay causes a

stress reduction slightly less than that produced by an equal thickness of a homogeneous, isotropic elastic solid. In other words, the stress reduction was comparable to that produced by an equal thickness of topsoil or soil-bound macadam base and somewhat more effective than that of an equal thickness of sand asphalt.

ACKNOWLEDGMENTS

This work has been sponsored by the Georgia State Highway Department and the U. S. Bureau of Public Roads, through the Engineering Experiment Station of the Georgia Institute of Technology. The authors are indebted to C. E. Hedges, W. H. Johnson, F. Chabrol, C. E. Snepp, W. L. Boyd, A. Schwartz, and D. Wheeless, Graduate Research Assistants, for their part in these investigations.

REFERENCES

1. Boussinesq, J., "Application des Potentiels a l'Etude de l'Equilibre et du Mouvement des Solides Elastiques." Gauthier-Villars, Paris (1885).
2. Love, A. E. H., "The Stress Produced in a Semi-Infinite Body by Pressure on Part of the Boundary." Phil. Trans. Roy. Soc., Series A, 228:377-420 (1928).
3. Steinbrenner, W., "Tafeln zur Setzungsberechung." Die Strasse, Vol. 1 (1934).
4. Newmark, N. M., "Influence Charts for Computation of Stresses in Elastic Foundations." Univ. of Illinois Eng. Exp. Sta. Bull. 338 (1942).
5. Newmark, N. M., "Influence Charts for Computation of Vertical Displacements in Elastic Foundations." Univ. of Illinois Eng. Exp. Sta. Bull. 367 (1947).
6. Fadum, R.E., "Influence Values for Vertical Stresses in a Semi-Infinite Solid Due to Surface Loads." Harvard Univ. (1941).
7. Fergus and Miner, "Distributed Loads on Elastic Foundation." HRB Proc. 34: 582-597 (1955).
8. Foster and Ahlvin, "Stresses and Deflections Induced by a Uniform Circular Load." HRB Proc., 33: 467-470 (1954).
9. Deresiewicz, H., "The Half-Space Under Pressure Distributed over an Elliptical Portion of Its Plane Boundary." Trans. ASME, Jour. Appl. Mech. (1960).
10. Griffith, J. H., "The Pressures Under Substructures; Engineering and Contracting." 1:113-119 (1929)..
11. Fröhlich, O.K., "Druckverteilung im Baugrunde." J. Springer, Berlin (1934).
12. Ohde, J., "Zur Theorie der Druckverteilung im Baugrunde." Der Bauingenieur, 20:451-459 (1939).
13. Buisman, A. S., "Druckverdeeling in Bouwgrond in Verband met Ongelijke Samendrukbaarheid in Horizontale en Verticale Richting." De Ingenieur, 47: B175-180 (1932).
14. Wolf, K., "Ausbreitung der Kraft in der Halbebene und im Halbraum bei Anisotropem Material." Zeitschift Angew. Math. und Mech., 15:249-254 (1935).
15. Jelinek, R., "Der Boden als Querisotropes Medium." Abhandlungen über Bodenmechanik und Grundbau, E. Schmidt, Berlin, pp. 19-24 (1948).
16. Jelinek, R., "Die Kraftausbreitung im Verallgemeinerten Ebenen Spannungszustand für Querisotrope Böden." Abhandlungen über Bodenmechanik und Grundbau, E. Schmidt, Berlin, pp. 24-27 (1948).
17. Jelinek, R., "Die Kraftausbreitung im Halbraum für Querisotrope Böden." Abhandlungen über Bodenmechanik und Grundbau, E. Schmidt, Berlin, pp. 28-33 (1948).
18. Koning, H., "Stress Distribution in a Homogeneous, Anisotropic, Elastic Semi-Infinite Solid." Proc., 4th Int. Conf. Soil Mech. and Found. Engrg. London, 1:335-338 (1957).
19. Westergaard, H. M., "A Problem of Elasticity Suggested by a Problem in Soil Mechanics, Soft Material Reinforced by Numerous Strong Horizontal Sheets, Contribution to Mechanics of Solids." Stephen Timoshenko 60th Anniversary Volume, MacMillan (1938).

20. Burmister, D. M., "The Theory of Stresses and Displacements in Layered Systems and Application to the Design of Airport Runways." HRB Proc., 23: 126-148 (1943).
21. Burmister, D. M., "The General Theory of Stresses and Displacements in Layered Systems." Jour. Appl. Physics, 16: 296-302 (1945).
22. Schiffman, R. L., "The Use of Integral Transforms in the Solutions of Three-Layer Soil Problems." (Unpublished).
23. Fox, L., "Computation of Traffic Stresses in a Simple Road Structure." Road Research Laboratory (England), Road Research Paper 9, London (1948). Also, Proc. Sec. Inf. Conf. Soil Mech. and Found. Engrg., 2: 236-246.
24. Hank and Scrivner, "Some Numerical Solutions of Stresses in Two and Three Layered Systems." HRB Proc., 28: 457-468 (1948).
25. Acum, W. E. A., and Fox, L., "Computation of Load Stresses in a Three-Layer Elastic System." Geotechnique, 2: No. 4, pp. 293-300 (1951).
26. Steiner, "Handbuch der Ingenieurwissenschaften." Der Bruckenbau, Leipzig 2: 195, (1882).
27. Strohschneider, O., "Elastische Druckverteilung und Drüchüberschreitung in Schüttungen." Sitz. Berichte der K. K. Akad. Wiss. Wien, 121: 301 (1912).
28. Moyer, J. A., "Distribution of Vertical Soil Pressure." Eng. Record, 69: 608 (1914) and 71:330 (1915).
29. Enger, M. L., "High Unit Pressures Found in Experiments on Distribution of Vertical Loading Through Sand." Eng. Record, 73: 106 (1913).
30. Goldbeck, A. T., "Distribution of Pressures Through Earth Fills." Proc. ASTM, 17: 640 (1917).
31. Kögler, F., and Scheidig, A., "Druckverteilung im Baugrunde." Bautechnik, 5: 418 (1927); 6: 205 (1928); 7: 268 (1929).
32. Spangler, M. G., and Ustrud, H. O., "Wheel Load Stress Distribution Through Flexible Type Pavements." HRB Proc., 20: 235-257 (1940).
33. Waterways Experiment Station, "Investigations of Pressures and Deflections for Flexible Pavements." Report 1, Homogeneous Clayey-Silt Test Section, Vicksburg, Miss. (1951).
34. Waterways Experiment Station, "Investigations of Pressures and Deflections for Flexible Pavements." Report 4, Homogeneous Sand Test Section, Vicksburg, Miss., (1954).
35. Turnbull, W., Maxwell, A. A., and Ahlvin, R. G., "Stress Distribution in Homogeneous Soil Masses." Proc., 5th Int. Conf. Soil Mech. and Found. Engrg., Paris, 2: 337-345 (1961).
36. McMahon, T. F., and Yoder, E. J., "Design of a Pressure-Sensitive Cell and Model Studies of Pressures in a Flexible Pavement Subgrade." HRB Proc., 39: 650-682 (1960).

Discussion

ROBERT L. SCHIFFMAN, Associate Professor of Soil Mechanics, Rensselaer Polytechnic Institute—It is gratifying to see experiments directed towards the validity of layered system analyses. All too often, theories are accepted or rejected without adequate experimental evidence. On the other hand, the interpretation of the experiment must always consider the alteration of the theory due to the measuring instruments.

The experimental results presented showed a general trend of normal stresses being in excess of the layered theory. The system tested was geometrically a three-layer system. For most cases the recorded results were in the range of, or higher than, the homogeneous analysis of Boussinesq. In the case of the soil-cement bases, the stresses were compared to a two-layer theory. The actual geometry, a three-layer theory, would produce stresses of smaller magnitude than actually recorded in all cases.

A general conclusion can be drawn that the measured normal stresses were, on the whole, higher than the predications of the appropriate theory being tested.

An interpretation of this conclusion can fall into two patterns. In the first instance, one is tempted to conclude that the theories use gross idealizations of field conditions

and thus are insufficient to predict pavement behavior. It is possible to judge this interpretation by considering the effects of an improved theory. In a linear elastic theory, two major considerations can be the effect of adhesive restraints between the tire and the pavement (1) and the effect of anisotropy (2). These two influences would tend to reduce the theoretical stresses, and thus increase the deviation between theory and experiment. The influences of nonlinear stress-strain properties and "large" strains are more difficult to access. The Vicksburg tests (3), however, have indicated that these influences do not seriously affect the magnitude and distribution of normal stresses.

The result of an "improved" theoretical analysis would thus give greater "errors" than are presented. Inasmuch as every physical phenomenon must have a theoretical description (known or unknown), the reasons for the difference between theory and experiment must be sought, elsewhere than in the analysis of the assumptions of the theory.

A second interpretation is that the experiment performed does not geometrically conform to the theory tested. It is the writer's opinion that the experimental set-up was sufficiently geometrically different from the theories tested to cast doubt on the comparisons used. The gages used, with relationship to the surrounding soil are, in fact, rigid inclusions in the soil mass. The inclusion effect will produce higher stresses at the gage than the corresponding "non-inclusion" theory. The fact that there were several gages in a line would accentuate the effect. The inclusion effect for a line of gages can crudely be compared to the stresses at a rigid boundary. Biot's (4) analysis for a single layer with a rigid boundary underlying the elastic layer shows that the normal stresses (particularly under the load) are substantially higher than the corresponding Boussinesq stresses.

It is the writer's interpretation that the deviations between the experimental results and the theory used are largely due to the influence of the gage as a rigid inclusion in a layered system.

The inclusion effect is one that will affect all stress measurement work. It is a most difficult problem, because the effect depends on the type of gage, the geometry of the gage, the gage characteristics the gage spacing, etc. It is a problem that must be solved, however, if one wishes to evaluate the validity of stress distribution theories for soil.

This discussion is not intended to criticize the excellent experimental data obtained by the authors. It is hoped that the discussion will provide a possible explanation for the lack of agreement between the theories used and the experiments reported. Furthermore, it is hoped that this discussion will point up certain deficiencies in the theoretical knowledge which make an assessment of layered system theories difficult. If and when layered system theories with inclusions are developed, the authors' data will provide an excellent means of evaluating the theory.

REFERENCES

1. Schiffman, R. L., "The Influence of Adhesion on the Stresses and Displacements in an Elastic Semi-Infinite Solid." Rensselaer Polytechnic Institute Report N 11/9 (March 1962).
2. Koning, H., "Stress Distribution in a Homogeneous, Anisotropic, Elastic Semi-Infinite Solid." Proc., 4th Int. Conf. on Soil Mech. and Found. Eng., 1: 335-338 (1957).
3. Turnbull, W. J., Maxwell, A. A., and Ahlvin, R. G., "Stresses and Deflections in Homogeneous Soil Masses." Proc., 5th Int. Conf. on Soil Mech. and Found. Eng., 2: 337-345 (1961).
4. Biot, M. A., "Effect of Certain Discontinuities on the Pressure Distribution in a Loaded Soil." Physics, 6: 367-375 (1935).

GEORGE F. SOWERS and ALEKSANDAR B. VESIC, Closure—In his discussion Professor Schiffman expressed the opinion that the reasons for the differences observed between the theoretical and experimental values of stresses in the pavements tested must be sought not in the analysis of the assumptions of the theory but in the effect of rigidity of cells included in a layered system. He based his conclusions on the premise that

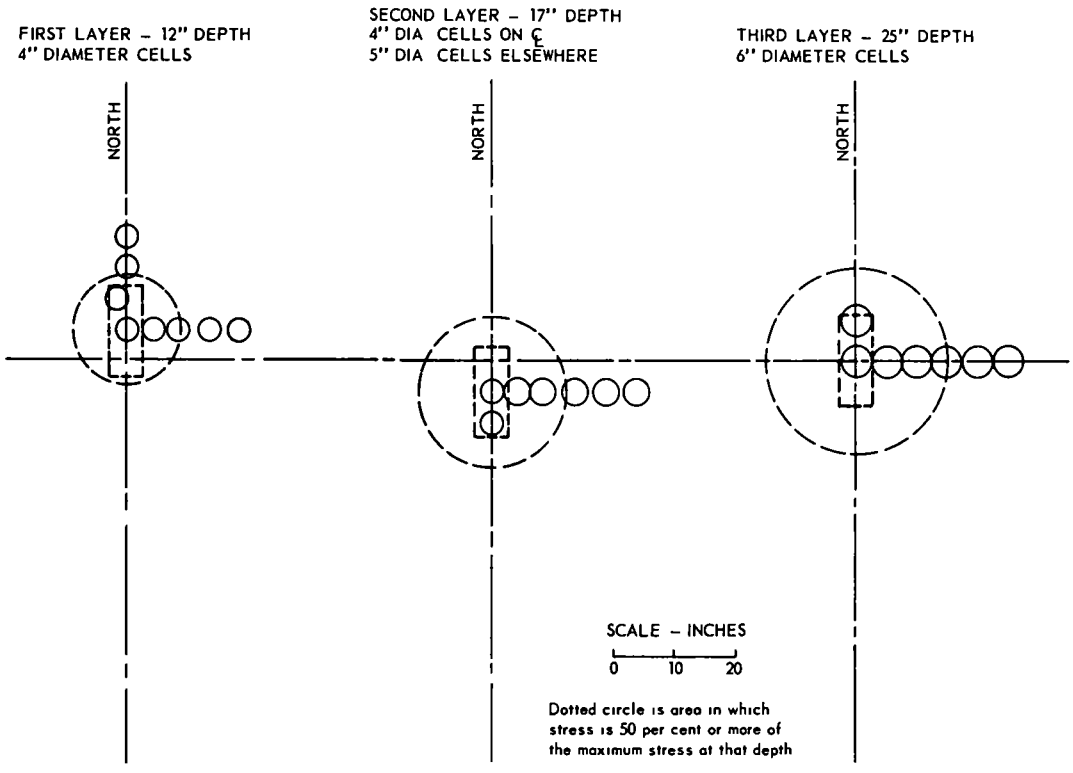

Figure 27. Pressure cell layout test series -600 showing imprint of single wheel under 13,500 lb.

two major factors not considered in the theory should be the adhesion between the tire and pavement and the anisotropy of the pavement materials. However, he does not consider one of the basic assumptions of the layered soil theory—constant modulus, E, equal in both tension and compression and independent of strain.

An analysis of lateral stresses in an ideal two-layer system shows that the upper layer (Fig. 27) will have tension at the interface as soon as $E_1/E_2 > 1.5$ and that, in the cases tested, tension should be of the order of 30 psi in the flexible bases and of the order of 60 psi in the soil-cement base. The tensile strength of the flexible bases was most likely not higher than 5 psi.

How much effect on stress distribution this lack of tensile strength will have has not yet been rigorously investigated. In support of the authors' conclusions, it should be mentioned that Ruckli (37) reports, for a two-layer system with $E_1/E_2 = 10$ and $h_1 = 12$ in. (data very close to authors' test conditions), a stress concentration factor n (after Fröhlich) of 2.82, which is quite close to the Boussinesq case (n=3) and would mean a reduction under the load of only 6 percent compared to Boussinesq stresses.

Professor Schiffman believes that the tests did not conform to the theories in that the pressure cells were rigid inclusions that produced stress concentrations at the point of stress measurement. It is his opinion that the rigid cells were responsible for the differences between the test data and the theoretical stresses.

Stress concentration due to cell rigidity is a fault of all pressure cells. It may be minimized by making the cell as small as possible compared to the volume of soil undergoing stress and by minimizing the ratio of cell thickness to cell diameter. The cells employed in these tests were far smaller in diameter than those of the U. S. Waterways Experiment Station to whose test results Professor Schiffman refers.

Furthermore, the ratio of cell thickness to diameter was less than 1/10, as small as those of the USWES. The cells were individually calibrated in soil so that the cali-

bration would reflect the effect of cell rigidity. Also, if there were any significant stress concentrations due to cell rigidity, it would be apparent in the tests on soil-cement base as it was in the other flexible bases. Therefore, the authors doubt that stress concentration at the cells was a significant source of the stress difference.

A second effect of cell rigidity brought out by Professor Schiffman is the rigid boundary effect as described by Biot. Biot investigated the stresses on an infinitely rigid boundary of infinite lateral extent beneath an elastic layer of finite thickness. The vertical stress directly beneath the load was 1.56 times the Boussinesq stress, if a perfectly rough interface is assumed. The authors do not believe that the pressure cells, arranged close together in a line, resemble the Biot condition. First, the area covered by the group of cells at any one depth is a small fraction of the area in which the vertical stress is one-half or more of the maximum stress, as shown in Figure 27. Second, the cells are individually free to tilt or deflect downward in the subgrade soil rather than being rigidly supported.

The authors contend that the test results for the soil-cement base, which are in agreement with the layered theory, demonstrate that the stress measurement system is not the cause of the lack of agreement between the layered theory and certain of the test results. Instead, it is the inappropriate use of the layered theory that is at fault.

A few additional comments should be of interest concerning some of Professor Schiffman's remarks. Stating that the asphaltic surface, the soil-cement base, and the subgrade form a three-layer system, he suggests that the theoretical stresses are even less when computed by the three-layer theory than by the two-layer theory, and that the authors' test results for soil-cement bases, therefore, exceed the theoretical stresses. The authors would agree with this suggestion if the asphaltic surface were significantly more rigid than the soil-cement base. However, the modulus of deformation of the asphaltic concrete tested at corresponding temperature was only about 20 percent of that of the base. It can be shown that under such conditions the theoretical stresses computed by the three-layer theory should be approximately 8 percent greater than that computed by the authors using the two-layer theory and assuming the surface course and the base to have the same modulus. The authors, therefore, must reaffirm their conclusion that the soil cement base test results are in substantial agreement with the layered theory.

The writer also contends that the effect of anisotropy would be to reduce stresses, as compared with those in an isotropic medium and that the differences between the measured stresses and those computed by the layered soil theory would therefore be even greater. It should be mentioned that anisotropy of materials does not necessarily reduce the σ_z stresses. As it has been shown by Buisman (13) the effect of anisotropy depends on the ratio of the moduli of deformation of the soil in horizontal and vertical directions, E_h/E_v. If $E_h/E_v < 1$, an increase of σ_z stresses has to be expected. However, an E_h/E_v ratio as low as 0.4 brings an increase of only 30 percent compared to the case of isotropic materials, whereas the measured stresses are several hundred percent higher than those obtained for isotropic layered solids.

The authors wish to thank Professor Schiffman for his discussion and hope he will continue his extension of the layered theory into real situations.

REFERENCE

Ruckli, R., "Discussion on Pavement Bearing Capacity Computed by Theory of Layered Systems." Trans., ASCE, 116: 767 (1951).

Lateral Stability of Rigid Poles Subjected to a Ground-Line Thrust

ROBERT L. KONDNER, Civil Engineering Department, Technological Institute, Northwestern University; and
GORDON E. GREEN, Shannon and Wilson, Consulting Engineers, Seattle

Functional relationships are developed for the load-deflection characteristics of rigid, vertical poles, embedded in sand, subjected to a horizontal ground-line thrust and ground-line couple-moment. The study is based on nondimensional techniques and the physical variables included in the theoretical analysis are the ground-line deflection, depth of embedment, geometry of the pole cross-section, ground-line thrust, couple-moment at the ground-line, time of loading, and soil parameters. The soil parameters used are the density, angle of internal friction, and flow viscosity of sand. Nondimensional techniques in conjunction with small-scale model studies are used to determine the interrelationship among these physical variables for a pole embedded in a dense, uniform, fine dune sand of constant properties and subjected to a horizontal ground-line thrust only. Prediction equations are given from which the load-deflection characteristics of a prototype pole might be determined. A failure criterion relating the ultimate ground-line thrust to the pole geometry and examples are given.

•POLES subjected to lateral loads are used extensively by utilities, railroads, highway departments, and outdoor advertising agencies. The lateral stability of a pole has, to date, defied any altogether satisfactory analysis although numerous authors have attempted to solve the problem both analytically and empirically. At present, design is usually based on past experience, empirical formulas, or inadequate theoretical analyses founded on unrealistic assumptions. To obtain a rigorous solution to the problem of a partially embedded pole, certain systems of equations must be solved. The solution must satisfy the equilibrium equation, compatibility equations, and boundary conditions. Any solution will depend on the form of the stress-strain-time relationships used for the soil, and herein lies the difficulty. In general there are no stress-strain-time relationships available for soils.

This investigation was aimed at describing the phenomena of pole-soil behavior by determining the relationships among the physical variables involved through a semi-empirical approach utilizing dimensional analysis and small-scale model experiments on sand. The methods of dimensional analysis which have proved successful in other fields with regard to model-prototype studies were used in an attempt to achieve a coherent rational order to the study. It has been shown by Kondner (1, 2, 3, 4) that the use of these methods in soil mechanics is advantageous. Model tests have great flexibility with regard to the number of variables and conditions that can be studied in a given time. They should however be correlated with field experience.

A pole or short pile is essentially a partially embedded rigid member whose lateral deflections, under load, are primarily due to rigid body motions. It is assumed that flexural failure of the pole does not occur and that failure of the soil may be assumed to have occurred when the angle of inclination θ of the pole with the vertical becomes excessive.

The research reported in this paper involved a study of the following factors:

1. The development of a theoretical, nondimensional, functional form of the parameters involved in the load-deflection-time relationship for a laterally loaded single pole partially embedded in sand. This includes both horizontal ground-line thrust and ground-line couple-moment.
2. The design and calibration of a model to perform tests on poles embedded in sand of constant properties which are subjected to a horizontal ground-line thrust only.
3. Tests on the model to determine the load-deflection-time relationship involved, considering (a) reproducibility of test results, (b) influence of creep phenomena to determine a suitable loading rate, (c) effect of varying the loading rate on the load-deflection relationship, and (d) effect of varying the diameter and depth of embedment of the pole on the load-deflection-time relationship.
4. An analysis of the model test results to develop an empirical equation relating the physical variables involved.
5. Construction of nomographs to predict (a) failure loads and (b) load-deflection relationships for a pole embedded in dense dry sand having constant properties and subjected to a horizontal ground-line thrust.

Although the general pole problem containing thrusts and couple-moments has been functionally formulated for both cohesive and cohesionless soils, the primary emphasis of the present paper deals with only one phase of the problem, ground-line thrusts and sand, and as such is the first of a series of papers on the general problem. Future papers will deal with couple-moments and superposition principles in sands and clays as well as ground-line thrusts in clays. In addition, the study presented herein deals only with a very dense, uniform sand having a constant dry density of 107 pcf. Preliminary tests indicate that the important soil parameter effecting the load-deflection response of poles partially embedded in sands is the relative density of the sand. Relative density effects will be studied in the near future.

EXISTING INFORMATION

Beginning in the early 1920's a relatively large number of papers have appeared that attempt to solve the laterally loaded single pole problem. According to Prakash (5), the majority of analytical solutions are based on one or more of the following assumptions:

1. The maximum resistance to deformation of the soil at any depth is equal to Rankine's passive earth pressure or the difference between Rankine's active and passive earth pressures at that depth.
2. To develop passive resistance there must be movement (however small) of the pole compressing the ground in front of it.
3. The intensity of passive resistance developed is proportional to the amount of lateral displacement.
4. The intensity of the passive resistance developed is proportional to the depth below the ground-line.

In addition, individual authors have made further assumptions, particularly with respect to the shape of the pressure distribution diagram. An excellent annotated bibliography by Chang (6) concerning laterally loaded piles contains a chronological summary of the literature up to 1958, which includes poles as a subsection. The more extensive work by Prakash (5) contains a fairly complete review confined to the behavior of partially embedded poles subjected to lateral loads. In view of the availability of these two papers, it is not proposed to submit an extensive review of previous authors' work. This review will confine itself to some of the more recent trends and their implications.

There is no clear agreement in the literature as to a definition of the problem. Most authors assume a vertical pole with a horizontal load applied above the ground-line whereas Prakash (5) has considered the additional effect of a vertical load and an initial inclination of the axis of the pole. Considering the difficulty of the pole-soil

interaction, it would seem rational to study the simplified cases first and build up to the more general pole system.

The rotation of a laterally loaded pole requires that large deformations occur near the ground surface, where the soil is least capable of offering resistance. Therefore, the soil near the ground surface will probably nearly always be in a "plastic" state when resisting a laterally loaded pole. At some depth below the ground surface the soil behavior becomes nearly elastic. Thus, according to Prakash (5) a combination of elastic and plastic soil behavior should be accounted for in an analysis of a laterally loaded pole. According to Terzaghi (7) the deformation characteristics of a stiff clay are more or less independent of depth. However, the strength characteristics of clay soils may increase or decrease with depth, depending on the geographical location and climate, so that no general rules may be formulated. In connection with clay, on account of progressive deflection under constant load (a creep effect), the deformation increases and the soil modulus function varies with time—both approaching ultimate values. Ideally, these ultimate values should be used in the analysis. In a cohesionless sand the values of the deformation and the soil modulus are supposedly independent of time, but the soil modulus increases approximately in simple proportion to depth. According to Czerniak (8), the analysis is further complicated because the sand may fill the space left as the pole moves, thus preventing its returning to the vertical position upon removal of the overturning forces. An analytical solution of the laterally loaded pole is hence stymied by the unknown soil stress-strain-time relation which is herein called the soil modulus function. Present trends in analytical studies favor an increase in the soil modulus function in direct proportion to depth for sands:

$$k_x = k_h x \tag{1}$$

in which

k_x = soil modulus function at depth x,

k_h = constant of horizontal subgrade reaction function, and

x = depth below ground level.

For cohesive soils Palmer and Thompson (9) consider that:

$$k_x = k_h \frac{x^n}{L} \tag{2}$$

in which

L = depth of embedment and

k_h = constant

adequately describes the variation of soil modulus with depth and they indicate that the values for n must be determined by applying the method to check various field data.

Matlock and Reese (10) attempted to derive generalized solutions for laterally loaded piles, treating the rigid pole as a particular case. They considered the nonlinear force-deformation-depth characteristics of the soil by means of the repeated application of elastic theory. The soil modulus constants were adjusted for each successive trial until satisfactory compatibility was obtained between the predicted behavior of the soil and the load-deflection relationships required by the pole. In the final trial, in a series of iterative approximations, the final variation in soil modulus could assume any form with respect to distance along the pole. If it were required that the soil modulus values be adjusted independently at each depth considered, then, in practice, a solution for any particular pole problem required the use of a digital computer. The author gave nondimensional general solutions that could be computed for any desired form of variation of soil modulus with respect to depth. However, the two general forms of soil modulus function, the power form,

$$E_s = kx^n \tag{3}$$

and the polynomial form,

$$E_s = k_o + k_1 x \tag{4}$$

which the authors considered suitable are perhaps oversimplifications and may not be sufficiently sensitive to characterize the soil-pole interaction.

In an attempt to circumvent the soil modulus-depth-deflection-time relationship problem, it was believed that the behavior of the soil could be defined by parameters that could be more easily measured and controlled than the soil modulus. This, in conjunction with a semiempirical approach making use of small-scale model experiments, designed and constructed on the basis of the methods of dimensional analysis, seems to be a feasible method of attacking the problem.

THEORETICAL ANALYSIS

To describe a physical phenomena it is necessary to define it in terms of a finite number of physical quantities or parameters. Dimensional analysis offers an easy way to formulate such a description in functional form. The method of dimensional analysis as used to formulate relationships between physical quantities can be briefly summarized as follows. If there are m physical quantities containing n fundamental units, which can be related by an equation, then there are (m-n), and only (m-n), independent, nondimensional parameters (called π-terms) such that the π-terms are arguments of some indeterminate, homogeneous function $\varkappa$:

$$\varkappa\ (\pi_1, \pi_2, \pi_3, \ldots, \pi_{m-n}) = 0. \tag{5}$$

An important part of the dimensional analysis is the choice of the physical quantities involved. Once this is accomplished, a methodical process is used to obtain the π-terms contained in the functional formulation. The functional formulation is the extent to which dimensional analysis is useful. The explicit form of the functional relation must then be determined experimentally.

To keep the explicit form of the functional relation as simple as possible, only the more important variables should be considered. If the number of variables considered is too large, the practical usefulness of the results may be greatly impaired. In addition, the difficulties involved in the separation of the nondimensional parameters in the experimental determination of the explicit nature of the functional relation will be quite formidable. However, should important variables that may logically influence the phenomenon be omitted, the experimental phase may be simple, but the results may be incomplete or erroneous.

The analysis of a laterally loaded pole embedded in the ground is a static problem. The boundary forces have a predominating influence in the problem rather than the body forces and the latter will be neglected in the subsequent analyses. The general methods of dimensional analysis have been described elsewhere (11, 12) and are repeated here. The particular problems encountered in the soil mechanics field when applying this tool have been described by Kondner (1) and his techniques are freely drawn on in the analyses where considered desirable.

It is assumed that the material constants needed to describe the deformation characteristics of the sand are implicit in the dry density, angle of internal friction, and "viscosity" of the sand. The term "viscosity" refers to the time-dependent deformation characteristics that were observed in the experimental program. It has been previously noted that the relative density is thought to be an important soil parameter, but is by definition nondimensional and can be added to the functional relationship when convenient. For the present study the relative density was held constant and hence is not specifically included as a variable. A future test series will be conducted in which various relative densities will be studied.

The physical quantities considered in this study are given in Table 1. A force, length, and time system of fundamental units has been used. Because there are ten physical quantities and three fundamental units, there must be seven independent,

TABLE 1

PHYSICAL QUANTITIES CONSIDERED IN THE DIMENSIONAL ANALYSIS OF A RIGID POLE EMBEDDED IN SAND

Quantity	Symbol	Fundamental Unit
Deflection at ground-line	y	L
Depth of embedment	L	L
Cross-sectional area of pole	A	L^2
Perimeter of pole	C	L
Thrust at ground-line	F	F
Moment at ground-line	M	FL
Dry density of sand	γ	FL^{-3}
Angle of internal friction	ϕ	$F^\circ L^\circ T^\circ$
Viscosity of sand	η	$FL^{-2}T$
Time of loading	t	T

nondimensional π-terms. These π-terms can be methodically obtained by choosing three physical quantities that contain all three fundamental units and cannot be formed into a nondimensional parameter by themselves (for example, F, t, and L), and combining them with each of the remaining quantities one at a time. As an example, combining them with γ,

$$\pi = F^{\alpha} \cdot t^{\beta} \cdot L^{\rho} \cdot \gamma^{\lambda} = F^{\circ} L^{\circ} T^{\circ} \tag{6}$$

Substituting the fundamental units of each of the physical quantities involved into Eq. 6,

$$(F)^{\alpha} \cdot (T)^{\beta} \cdot (L)^{\rho} \cdot (FL^{-3})^{\lambda} = F^{\circ} L^{\circ} T^{\circ} \tag{7}$$

Equating exponents of the fundamental units,

$$\begin{aligned} \alpha + \lambda &= 0, \\ \beta &= 0, \text{ and} \\ \rho - 3\lambda &= 0 \end{aligned} \tag{8}$$

Solving Eq. 8 by letting $\alpha = 1$ gives

$$\alpha = 1 \ , \ \beta = 0 \ , \ \rho = -3 \ , \text{ and } \lambda = -1 \tag{9}$$

Thus, the π-term under consideration is

$$\pi = \frac{F}{\gamma L^3} \ . \tag{10}$$

By repeating this process for the other physical quantities involved, the following nondimensional parameters can be obtained:

$$\bar{\pi}_1 = \frac{y}{L}, \ \bar{\pi}_2 = \frac{A}{L^2}, \ \bar{\pi}_3 = \frac{C^2}{L}, \ \bar{\pi}_4 = \frac{M}{FL}, \qquad \bar{\pi}_5 = \frac{F}{\gamma L^3} \quad \bar{\pi}_6 = \phi \ , \text{ and } \bar{\pi}_7 = \frac{Ft}{L^2 \eta} \tag{11}$$

Because a requirement of the function $\varkappa$ is that it shall consist of independent, non-

dimensional parameters, there is nothing unique about these forms of the π-terms. It is therefore possible to transform the π-terms algebraically in any way desired so long as the final π-terms are nondimensional and independent. The final form is chosen so as to group desired physical quantities together in the most meaningful form; in particular with regard to the form of the experimental data. This implies that each term shall preferably contain one and only one physical quantity having a predominating effect on the function $\varkappa$.

By algebraically transforming Eq. 11 the following form of the π-terms was obtained:

$$\pi_1 = \frac{y}{L}, \quad \pi_2 = \frac{C}{L}, \quad \pi_3 = \frac{C^2}{A}, \quad \pi_4 = \frac{F}{\gamma AL}, \qquad (12)$$

$$\pi_5 = \frac{\gamma tc}{\eta}, \quad \pi_6 = \frac{M}{\gamma AL^2}, \quad \pi_7 = \phi$$

The π-terms of Eq. 12 may be substituted into Eq. 5 to obtain the functional relationship which can be rewritten

$$\frac{y}{L} = \varkappa\left[\frac{C}{L}, \frac{C^2}{A}, \frac{F}{\gamma AL}, \frac{\gamma tC}{\eta}, \frac{M}{\gamma AL^2}, \phi\right] \qquad (13)$$

In Eq. 13 and hereafter the symbol $\varkappa$ denotes "some function of," but not necessarily the same function for, each equation. This notation is used to avoid the use of numerous subscripts and superscripts as a means of differentiating between the equations.

The physical interpretation of the π-terms contained in Eq. 13 is as follows. The dependent variable is the term y/L which is called the deflection ratio. This term is the ratio of the horizontal surface deflection to the depth of embedment. Shape effects are given by C^2/A which is the characteristic shape factor of the pole. For a circular cross-section of any size, the shape factor is equal to 4π ($\pi = 3.1416$), and for a square shape the value is 16. The term C/L is a geometric factor pertaining to the distribution of the cross-section area of the pole and is called the slenderness ratio. The term $F/\gamma AL$ is the ratio of the applied force to the resisting force and is called the thrust strength ratio. The term $M/\gamma AL^2$ is the ratio of the applied moment to the resisting moment and is called the moment strength ratio. Creep effects are included in the term $\frac{\gamma tC}{\eta}$ which is considered to be the ratio of the time of loading to a characteristic relaxation time of the soil. The angle of internal friction (ϕ) is, by definition, a nondimensional strength factor.

Similitude requirements have been previously discussed by numerous authors including Kondner (1) and is repeated in this paper.

Frequently, tests that appear to be different because of different values of the physical quantities involved are in reality duplicate tests giving the same results when examined in nondimensional form. The reason for this is that in the search for an explicit relation expressing a physical phenomenon, it is the values of the nondimensional parameters, which are the new variables, that are important and not simply the magnitudes of the individual physical quantities. Thus, many of the results given by the field tests, conducted in a conventional dimensional form, are simply isolated parts or subspaces of the general nondimensional formulation (vector space).

MODEL DESIGN AND PRELIMINARY TESTS

Some of the important advantages of model tests vs field tests are that the former are more flexible, simpler to execute, relatively inexpensive and the variables are capable of more rigid control. They do however require correlation with field tests because unknown scale factors may be present which, if ignored, can lead to completely erroneous conclusions. Although the authors have formulated the functional relationships for the pole problem with both cohesive and cohesionless soils, it was considered advisable to conduct the initial experimental phase using sand rather than clay as the

soil medium for the following reasons. Sand properties are easier to control in the laboratory than those of clay and the time effects are generally considered to be less complex. Because good field test data on sand appears to be lacking, it was hoped that sometime later field tests could be conducted on sand using the model test results as a guide.

The model scale must be chosen so that the elements of the model can be easily manipulated (e.g., loads), and deflections simply measured.

Because the general pole problem containing both applied thrust and applied moment is quite difficult, it was decided to separate the two effects contained in Eq. 13; namely, the horizontal ground-line thrust F and the couple-moment at the ground-line M as follows:

$$\frac{y}{L} = \varkappa \left[\frac{C}{L}, \frac{C^2}{A}, \frac{F}{\gamma A L}, \frac{\gamma t C}{\eta}, \phi \right] \tag{14}$$

$$\frac{y}{L} = \varkappa \left[\frac{C}{L}, \frac{C^2}{A}, \frac{M}{\gamma A L^2}, \frac{\gamma t C}{\eta}, \phi \right] \tag{15}$$

By performing separate tests using (a) horizontal ground-line thrust only, (b) applied couple-moment only, and (c) thrust and bending moment combined; the data analysis can be simplified because in (a) and (b) the number of π-terms is reduced by one. Then from (a), (b), and (c) the principle of superposition can be checked. However, the scope of the model test study subsequently reported in this paper is confined to tests using a horizontal ground-line thrust only. A range in pole diameters of from ½ to 1½ in. and of embedments from 3 to 5½ in. was chosen. The couple-moment and combined studies are being conducted and will be reported in the future.

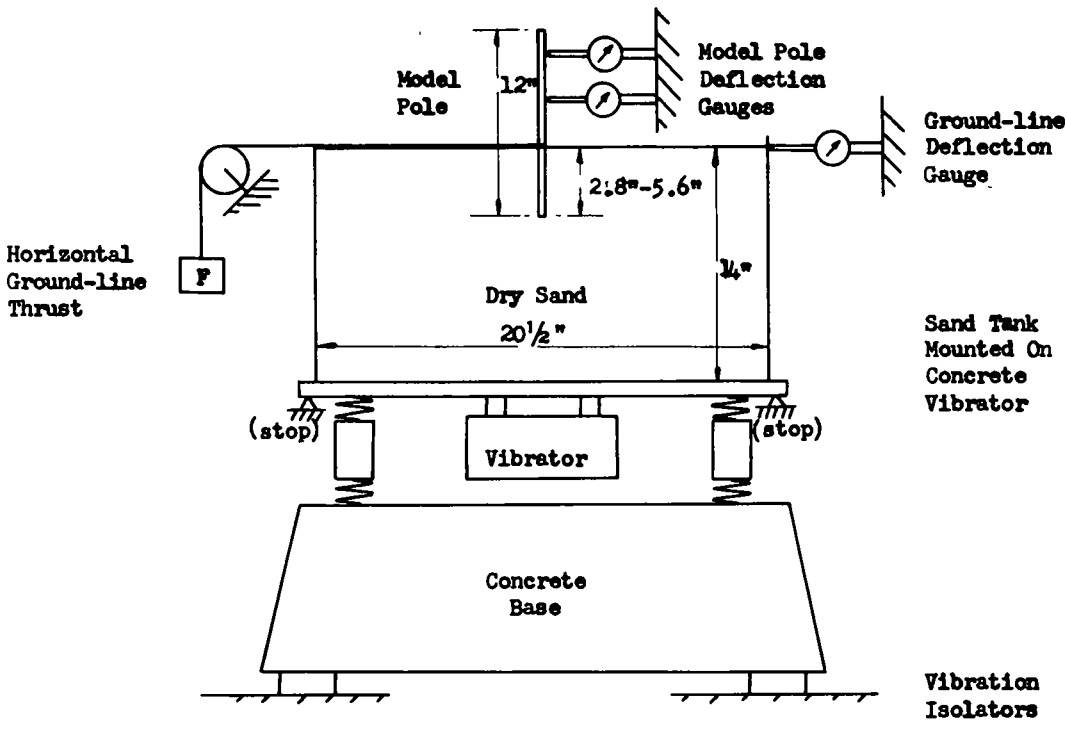

Figure 1. Model pole apparatus.

TABLE 2

PROPERTIES OF MODEL POLES

Pole No.	Material	Diameter (in.)	Area A (sq in.)	Weight (g)	Perimeter C (in.)
1	Aluminum	0.501	0.197	30	1.573
2	Aluminum	0.626	0.307	62	1.966
3	Steel	0.707	0.393	143	2.221
4	Steel	0.927	0.674	216	2.911
5	Steel	1.248	1.222	229	3.921
6	Steel	1.515	1.801	478	4.755

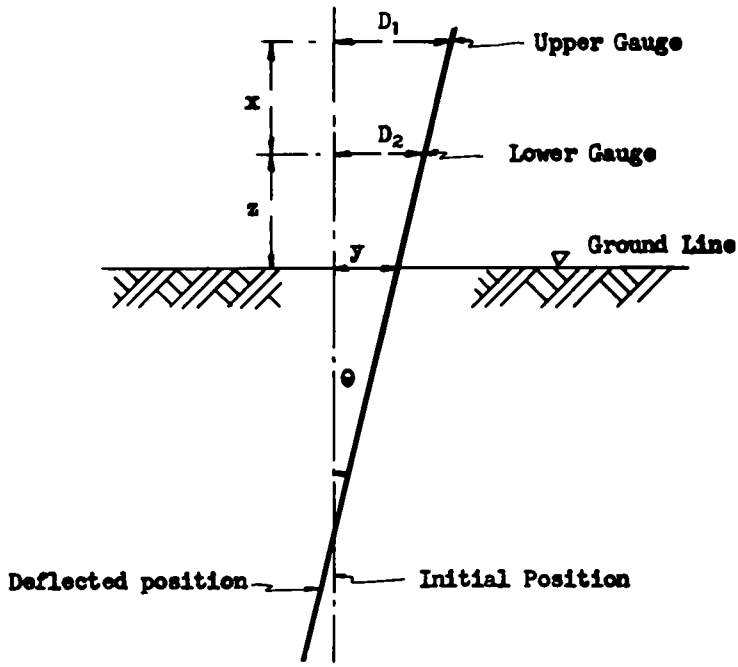

$$\frac{D_1 - D_2}{x} = \frac{D_2 - y}{z}$$

$$\therefore y = D_2 - \frac{z}{x}(D_1 - D_2)$$

if $x = z$

$$y = 2D_2 - D_1$$

Figure 2. Gauge set-up equation for ground-line deflection.

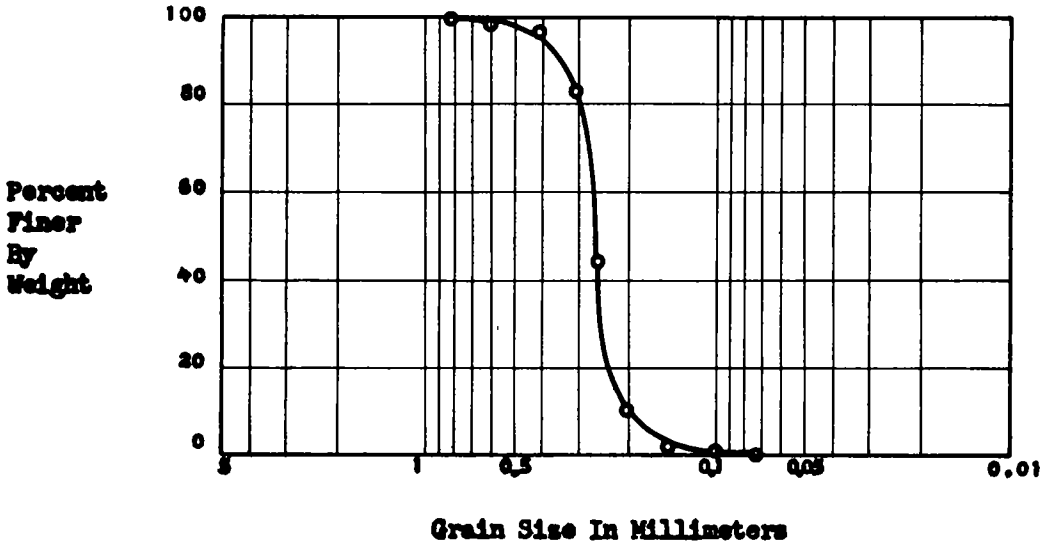

Figure 3. Grading curve for sand used in model.

The model pole apparatus used in the study is shown in Figure 1. A cut-down oil drum welded to a vibrating table-type concrete vibrator mounted on a heavy concrete base was used. To minimize the effect of building vibrations, the concrete base was supported on rubber blocks. The tank contained 330 lb of dry sand vibrated to as dense a state as possible. The model pole embedded in the sand was loaded by hanging weights on a cord attached to the pole at the ground-line and passing over a light pulley. The model poles consisted of 12-in. lengths of polished aluminum or steel tube, plugged at the lower end. Properties of these tubes are given in Table 2. The ground-line deflection of the pole was determined by measuring (a) the deflection at two points above ground level, from which the apparent ground-line deflection could be extrapolated, (see Fig. 2), and (b) a small correction due to the horizontal deflection of the tank relative to the two pole dial gauges. Gauges reading to 1/1, 000 in. were used for all tests except two where 1/10, 000-in. gauges were required. The sand used in the tank was a uniform fine dune sand from Wolf Lake, Ind., provided through the courtesy of the Raymond Concrete Pile Company, Chicago. The sand had a grading as shown in Figure 3 and was air-dried in the laboratory to a moisture content of about ¼ percent. For a dense state (i.e., density = 108 pcf) this sand had an angle of internal friction, ϕ, of 37°, as determined from a series of triaxial compression tests. Subsequent to extensive initial vibration the density of the sand in the tank remained constant at 107 pcf. The volume of the sand in the tank was determined from a calibration curve obtained by filling the tank with water and weighing it.

For the experimental data to be of any value the variables measured must truly represent the phenomena. Thus, in particular, the measured forces and deflections must be accurate.

It was found necessary to remove the springs from the pole dial gauges because the magnitude of the gauge spring force was high relative to the applied pole loads. The dial gauge arms were secured to the pole by elastic bands. It was also observed during the tests that the apparatus was very sensitive to vibrations transmitted to it through the floor. Heavy footsteps 3 to 4 ft away from the tank were sufficient to cause the dial gauge readings to "jump" a significant amount.

Because it was thought that the load rate might have a major effect on the shape of the load-deflection curve, similar tests under varying load rates were performed. The load rate was varied from 75 g per 2 min to 300 g per 2 min for constant C and L values in tests 4D, 4D/1, 4D/2, and 4D/3. The nondimensional plot of these data is shown

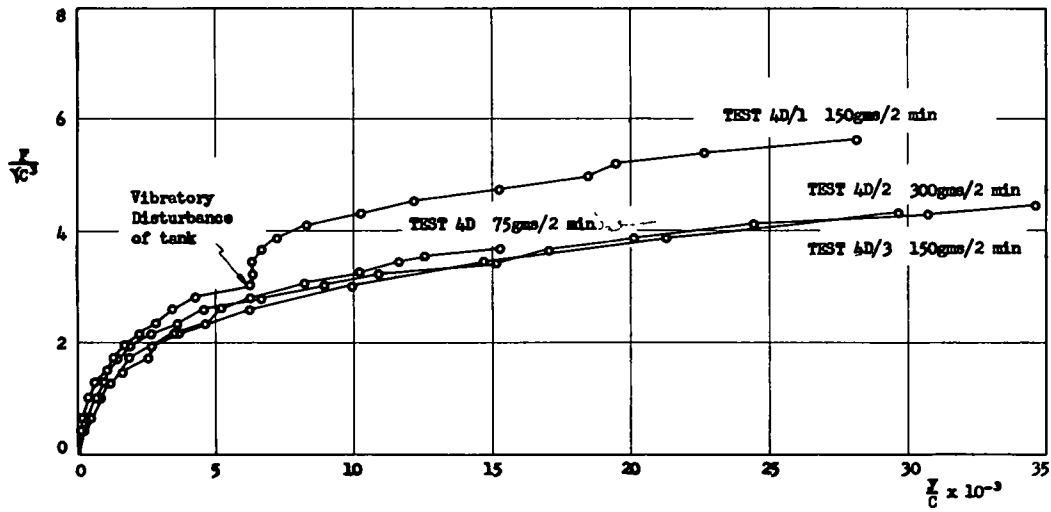

Figure 4. Nondimensional plot of $\frac{F}{\gamma C^3}$ versus $\frac{y}{C}$ for a constant value of $\frac{C}{L}$ = 0.6, for a varying load rate.

in Figure 4. The latter part of test 4D/1 was disturbed by accidental vibration of the tank. The three remaining curves for load rates of 75, 150, and 300 g per 2 min lie along the same line. This implies that, within this range, the rate of application of the load has no significant effect on the resulting $F/\gamma C^3$ vs y/C curves. Hence, although the value of the term $\gamma tC/\eta$ did not remain constant for the changing load rate, its influence was of little importance. Preliminary experiments suggested that the deflection under a given load increment was a time-dependent function; i.e., a creep phenomenon of some type. To investigate this, creep tests were conducted using 1/10,000-in. dial gauges instead of the normal 1/1,000-in. gauges used in all other tests. A typical result of such a creep test is shown in Figure 5. In this test, load increments of 75 g were applied at 5-min intervals until a total of 525 g was applied. Then on application of the next 75-g increment the deflections were measured at 1-min intervals for 15 min, whereupon 75 g increments were again applied at 5-min intervals up to a total of 900 g at which point a second 15-min creep test was performed. From the results of this and similar tests the following is concluded. When a load increment is applied, there is an initial sharp linear increase in deflection with time. After approximately 2 min, the slope of the line decreases sharply and the deflection continues at a much lower rate finally tending toward an ultimate value for a sufficiently large time. It was found that the slope of the upper part of the curve increases for an increase in applied load. Assuming that one need be concerned only with the initial deflections and can neglect the large time part of the deflection vs time curve, a load increment time interval of 2 min should prove satisfactory. Thus, load rate and creep tests indicate that the effects of the term $\gamma tC/\eta$ can be minimized.

TEST RESULTS

In using dimensional analysis to assist in interpreting the experimental data, one of the major problems is the choice of the exact form of the nondimensional groups. Because there are ten physical quantities and three fundamental units, the maximum number of dimensionless groups that can be obtained without considering powers is 210. Guided by previous work, experience, and preliminary results, a suitable form is selected. The effects of the variables must, if possible, be concentrated in individual π-terms so that phenomenological variations can be separated. The form of the nondimensional, functional relationship given by Eq. 14:

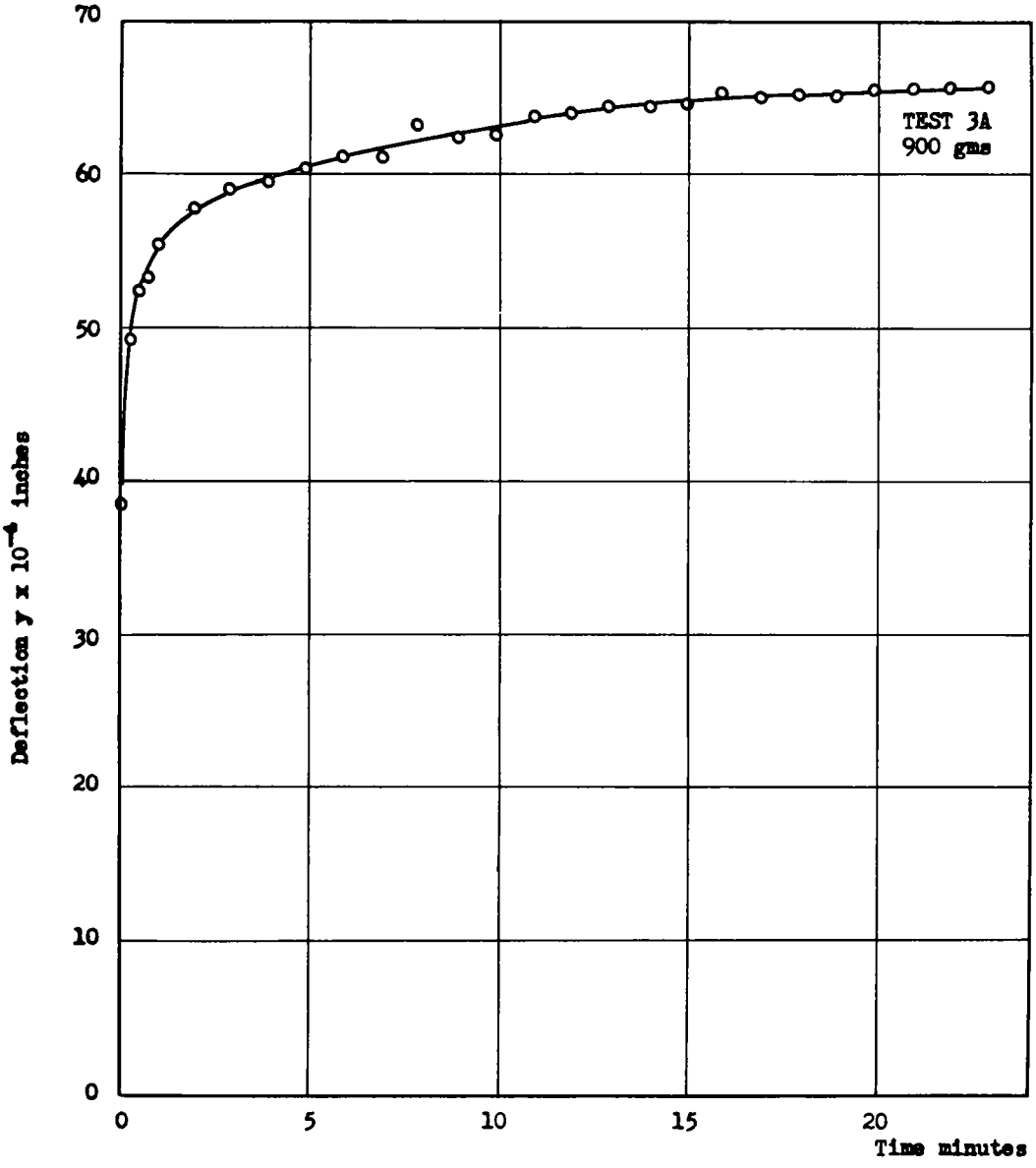

Figure 5. Plot of deflection y vs time for creep test, for a constant value of $\frac{C}{L} = 0.56$.

$$\frac{y}{L} = \varkappa\left[\frac{C}{L}, \frac{C^2}{A}, \frac{F}{\gamma AL}, \frac{\gamma tC}{\eta}, \phi\right] \tag{16}$$

can be algebraically transformed by forming the ratios

$$\frac{y/L}{C/L} = \frac{y}{C} \quad \text{and} \quad \frac{F/\gamma AL}{C/L.C^2/A} = \frac{F}{\gamma C^3}, \tag{17}$$

and replacing y/L and $F/\gamma AL$ to maintain independence of the π-terms. Thus, Eq. 16 may be rewritten

$$\frac{y}{C} = \varkappa\left[\frac{C}{L}, \frac{C^2}{A}, \frac{F}{\gamma C^3}, \frac{\gamma tC}{\eta}, \phi\right] \tag{18}$$

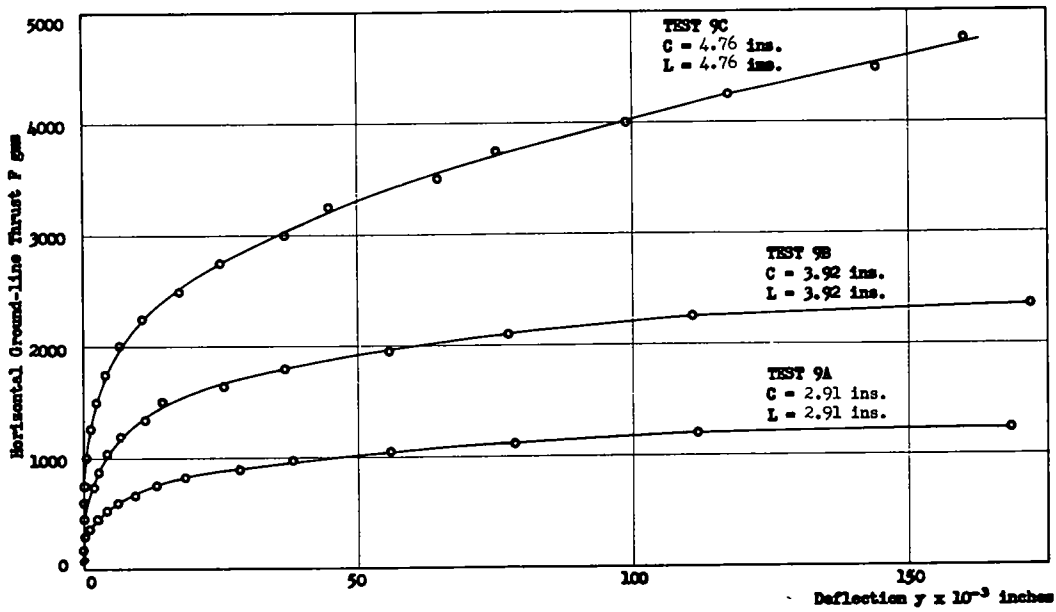

Figure 6. Plot of horizontal ground-line thrust F vs deflection y for a constant value of $\frac{C}{L} = 1.0$.

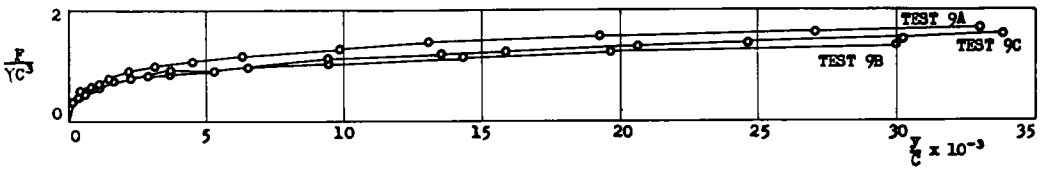

Figure 7. Nondimensional plot of $\frac{F}{\gamma C^3}$ vs $\frac{y}{C}$ for a constant value of $\frac{C}{L} = 1.0$.

In Eq. 18 the nondimensional term C^2/A is a constant equal to 4π for circular poles and its effect can be eliminated from the functional relationship because circular poles were used throughout the tests reported. The nondimensional term ϕ is a constant because the density, γ, of the sand is constant, and may also be eliminated from the functional relationship. It has been shown that the effects of the nondimensional term ytC/η can be minimized and therefore assumed to have a negligible influence on the function relationship. Hence, it may be eliminated. Thus, Eq. 18 may be rewritten

$$\frac{y}{C} = \varkappa\left[\frac{C}{L}, \frac{F}{\gamma C^3}\right] \tag{19}$$

To illustrate the advantages of presenting the experimental results in nondimensional form, data from Tests 9A, 9B, and 9C, for pole diameters of 0.927, 1.248, and 1.515 in. and embedded lengths of 2.91, 3.92, and 4.76 in. respectively were plotted in the conventional manner. Figure 6 is a plot of horizontal ground-line thrust F vs deflection y for the three tests. The seemingly important yet different influence of diameter and embedded length on the results are noteworthy. Because the C/L ratios for these three tests were constant, the data may also be plotted nondimensionally and reference to Figure 7 shows that they follow essentially the same curve.

An extensive program of tests were conducted for C/L values of 0.4, 0.6, 0.8, 1.0, and 1.2. The loading rate was varied to give approximately the same over-all time of

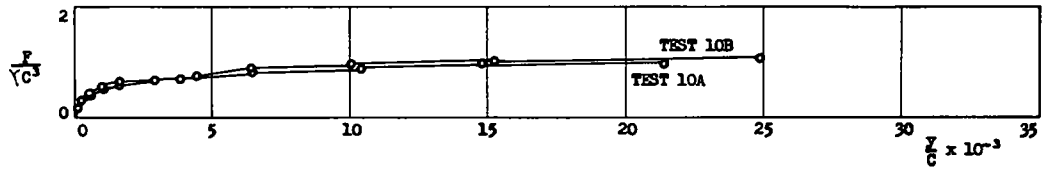

Figure 8. Nondimensional plot of $\frac{F}{\gamma C^3}$ vs $\frac{y}{C}$ for a constant value of $\frac{C}{L}$ = 1.2.

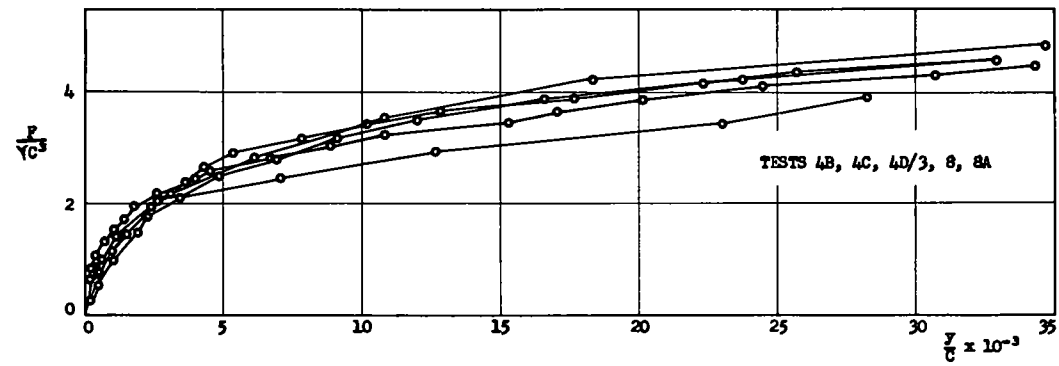

Figure 9. Nondimensional plot of $\frac{F}{\gamma C^3}$ vs $\frac{y}{C}$ for a constant value of $\frac{C}{L}$ = 0.6.

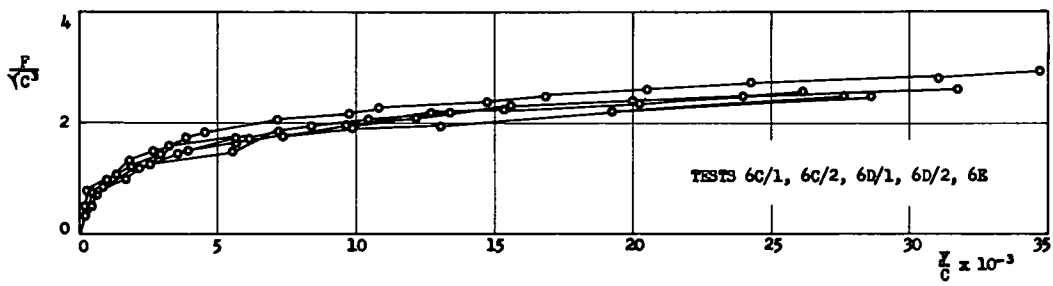

Figure 10. Nondimensional plot of $\frac{F}{\gamma C^3}$ vs $\frac{y}{C}$ for a constant value of $\frac{C}{L}$ = 0.8.

loading to failure in all tests. The nondimensional plots of these data appear in Figures 7 through 11 inclusive. In each test, a load increment was applied and the pole allowed to deflect, the gauge readings being recorded immediately before the application of the next load.

The maximum depth of embedment used in the tests was 5.6 in. For the plotted data the "scatter" is greatest for a C/L value of 0.4; i.e., for the smaller depths of embedment which exhibited the largest time effects. Figure 11 shows that this is true "scatter" and not a phenomenological difference. Thus, although tests 5A and 5A/1 were performed under apparently identical conditions their plots are different. As the C/L value increases from 0.4 to 1.2 the slight disparity between supposedly similar curves is reduced.

Although the load application rate was varied, the rate of stress application was not necessarily constant. In order to obtain a unique relationship between y/C, C/L and $F/\gamma C^3$ a constant value of $\gamma tC/n$ would have been required for the data included in each of Figures 7 through 11. Theoretically this could have been done by varying the loading

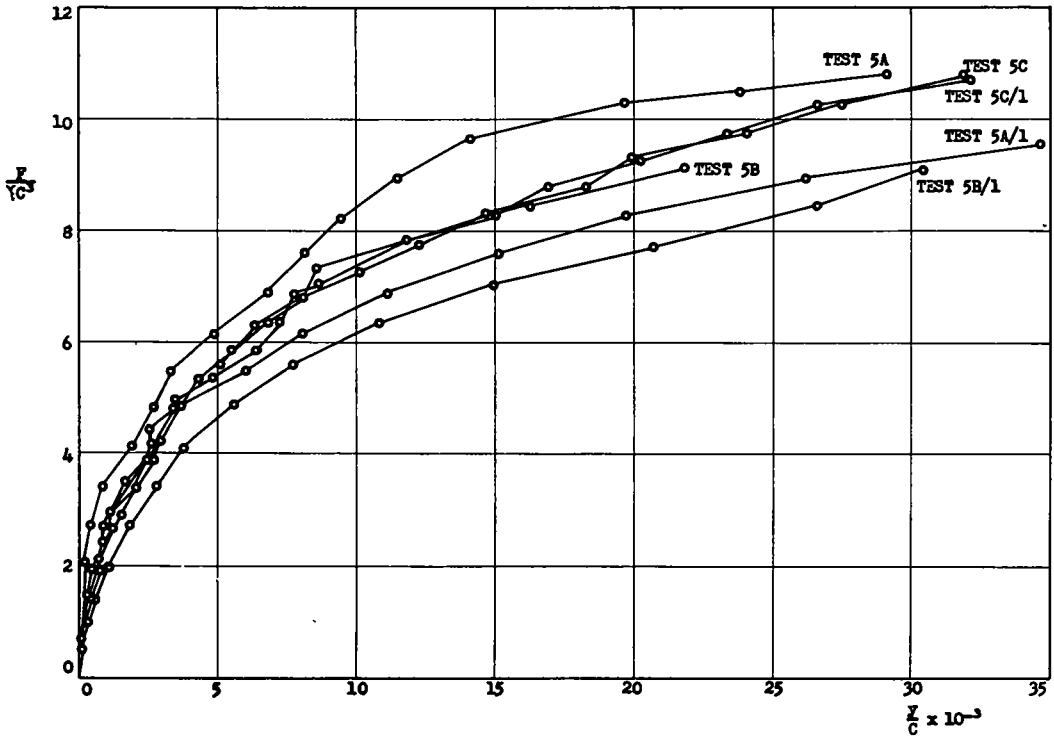

Figure 11. Nondimensional plot of $\frac{F}{\gamma C^3}$ vs $\frac{y}{C}$ for a constant value of $\frac{C}{L} = 0.4$.

rate for each test either by varying the load increment or by changing the time interval of loading. Unfortunately the field of soil mechanics has not yet reached a state of development where such loading rates can be predicted. Thus the "scatter" in the figures is probably due to time effects as well as experimental error, although as previously stated the effects of $\gamma tC/\eta$ were supposedly minimized.

If the soil is assumed to have failed when the angle of inclination θ of the pole with the vertical exceeds 5° (i.e., when $\tan\theta \geq 0.1$), Figure 2 shows, for x = z = 3 in., failure may be assumed to have occurred if

$$\tan\theta = \frac{D_1 - D_2}{3} \geq 0.1 \qquad (20)$$

i.e., if $D_1 - D_2 \geq 3,000 \times 10^{-4}$ in. because at no time did the difference in gauge readings exceed 0.3 in. one is justified in taking the whole of the $F/\gamma C^3$ vs y/C curve and basing a failure criterion on the asymptotic $F/\gamma C^3$ limit of the curve.

The shape of the thrust strength ratio vs deflection ratio curve is that of a nonlinear-type material. The curve tends asymptotically to an upper limit of the thrust strength ratio and had the load increment been reduced in this region it would have been possible to obtain higher points on the curve. However, the range of values actually covered is considered quite adequate. The nonlinearity of the thrust strength ratio vs deflection ratio indicates that the superposition principle is probably not valid. This would not agree with the use of a soil modulus approach. The degree of nonlinearity remains to be tested.

EXPLICIT FORM OF FUNCTIONAL RELATIONSHIP AND DEVELOPMENT OF NOMOGRAPHS

The experimental data plotted in Figures 7 through 11 in nondimensional form were used to develop an empirical relationship relating the three π-terms of Eq. 19. Mean curves were drawn through the experimental curves and appear in Figure 12. By replotting these mean curves on a semi-logarithmic scale, near straight lines were obtained as shown in Figure 13. The curves were further straightened out by replotting in the form log $(y/C + \bar{A})$ vs $F/\gamma C^3$, as shown in Figure 14, to give a two-constant curve of the type

$$\frac{y}{C} = \bar{A}\left[e^{B\frac{F}{\gamma C^3}} - 1\right] \tag{21}$$

in which $\bar{A}$ and B are constants. The value of $\bar{A}$ is given by the intercept of the line on the log $(y/C + \bar{A})$ axis for $F/\gamma C^3 = 0$. By plotting values of this intercept against C/L an equation relating $\bar{A}$ and C/L was found:

$$\bar{A} = 0.7 - 0.5\frac{C}{L} \tag{22}$$

A plot of this data appears in Figure 15.

By plotting values of the slope of the lines in Figure 14 (the constant B) against C/L on a logarithmic scale as shown in Figure 16, an equation relating B and C/L was found:

$$B = 3.28\left(\frac{C}{L}\right)^{-2.24} \tag{23}$$

Therefore, the empirical equation relating the three π-terms $F/\gamma C^3$, y/C, and C/L may be written:

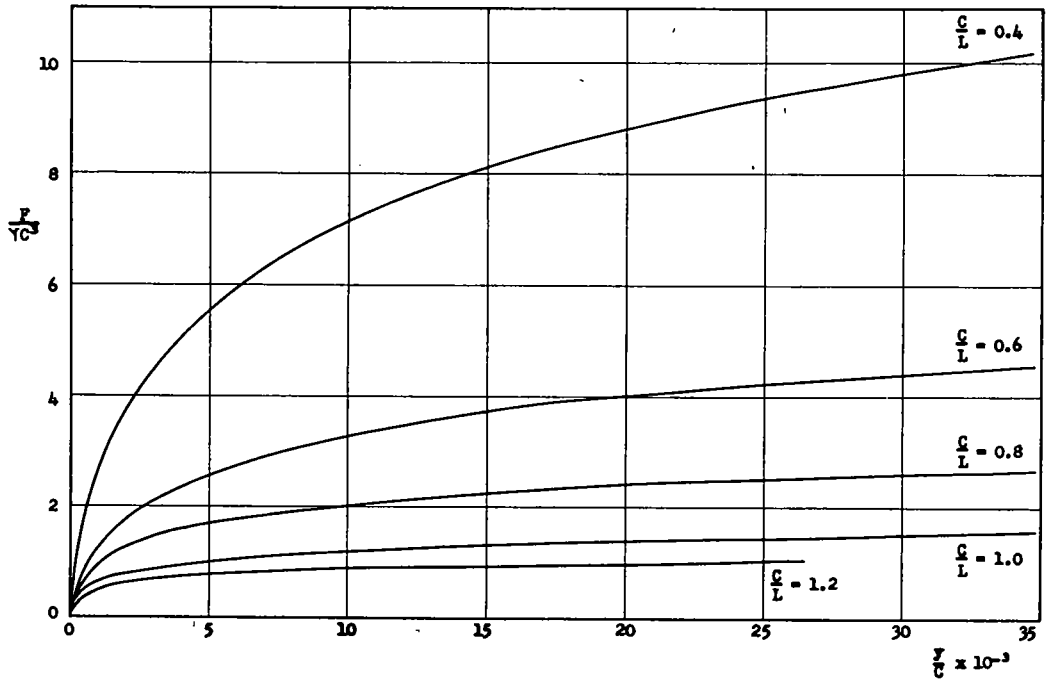

Figure 12. Nondimensional plot of $\frac{F}{\gamma C^3}$ vs $\frac{y}{C}$ mean curves to experimental data for $\frac{C}{L}$ = 0.4 - 1.2.

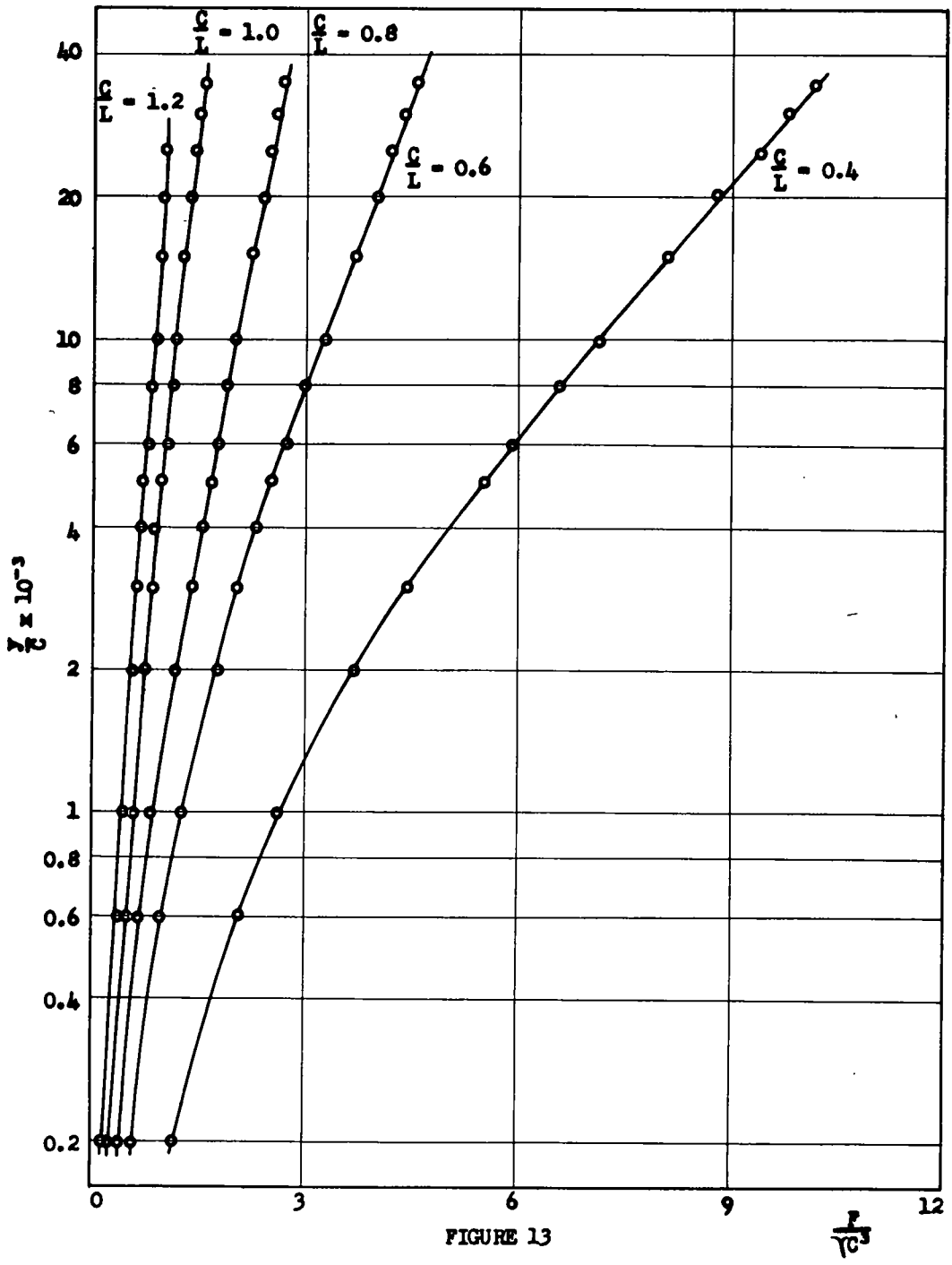

Figure 13. Nondimensional plot of $\frac{F}{\gamma C^3}$ vs $\frac{Y}{C}$ mean curves to experimental data for $\frac{C}{L}$ = 0.4 - 1.2.

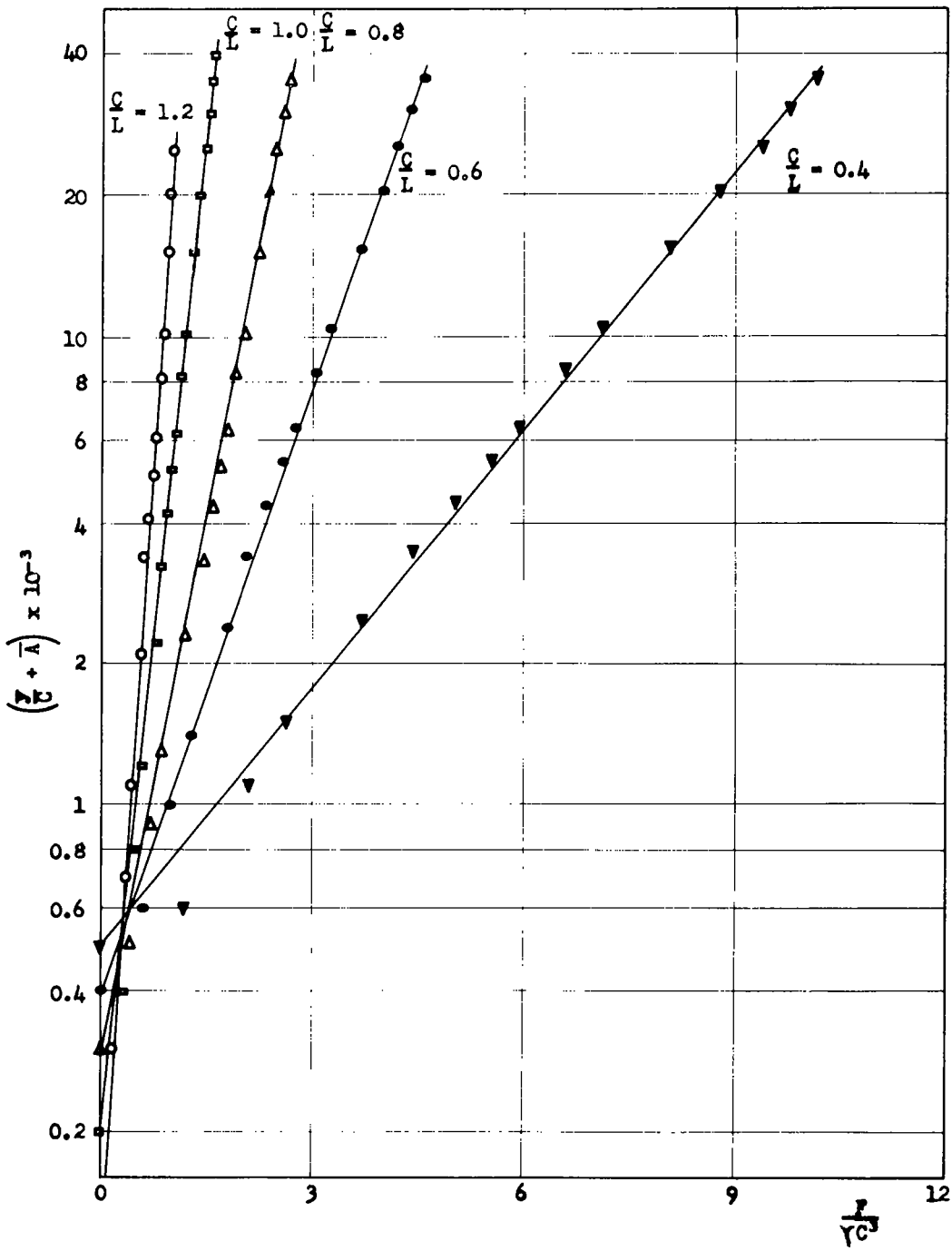

Figure 14. Nondimensional plot of $\frac{F}{\gamma C^3}$ vs $\left[\frac{y}{C} + \bar{A}\right]$ mean curves to experimental data for $\frac{C}{L} = 0.4 - 1.2$.

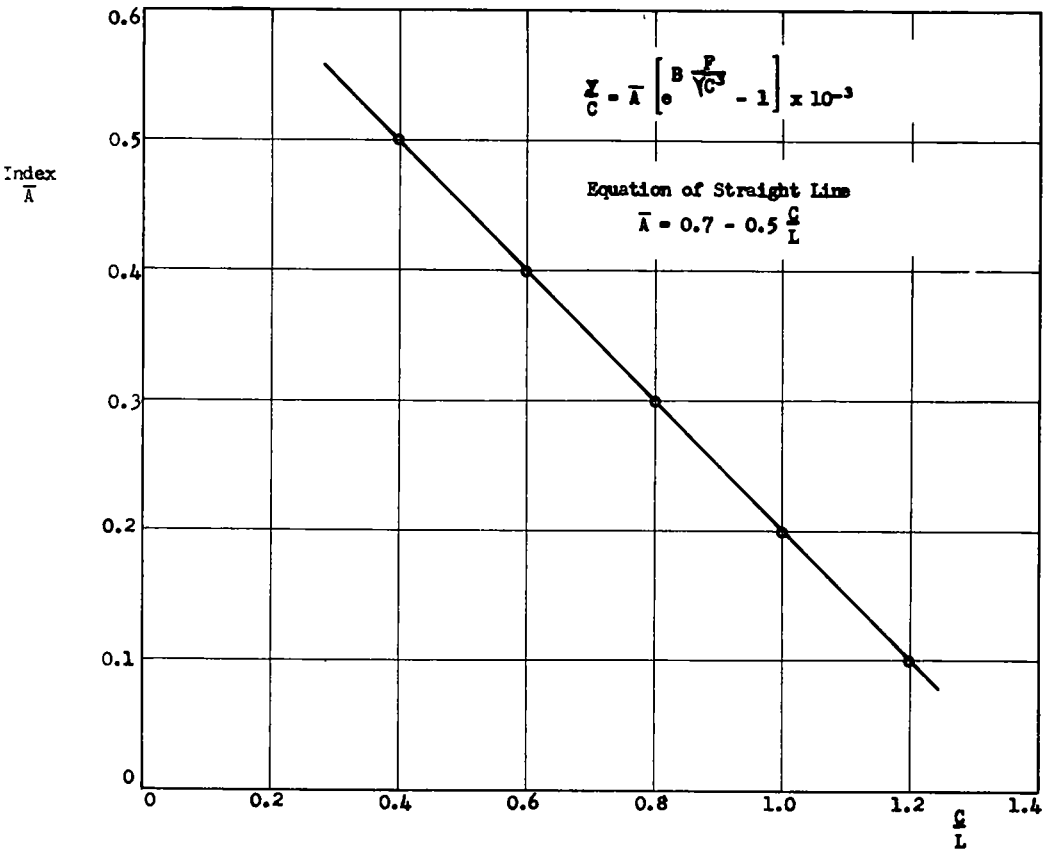

Figure 15. Plot of index $\bar{A}$ vs $\frac{C}{L}$.

$$\frac{y}{C} = \left(0.7 - 0.5\frac{C}{L}\right)\left[e^{3.28\left(\frac{C}{L}\right)^{2.24}\frac{F}{\gamma C^3}} - 1\right] \times 10^{-3} \qquad (24)$$

Alternatively Eq. 24 may be rewritten to give $F/\gamma C^3$ in terms of y/C and C/L:

$$\frac{F}{\gamma C^3} = 0.70\left(\frac{C}{L}\right)^{-2.24} \log_{10}\left[\frac{\frac{y}{C} \times 10^3}{0.7 - 0.5\frac{C}{L}} + 1\right] \qquad (25)$$

A nomograph for Eqs. 24 and 25 has been computed and appears in Figure 17. The five curves are almost identical with the mean curves of Figure 12, indicating satisfactory curve fitting. Although Eqs. 24 and 25 and Figure 17 only apply for values of y/C up to approximately 50×10^{-3}, the complete practical range is included since $y/C = 50 \times 10^{-3}$ is well in the range of failure or instability.

In an effort to develop an equation for the ultimate strength ratio, independent of the deflection ratio; a graph of the ultimate value of $F/\gamma C^3$ vs C/L was plotted in Figure 18. For values of C/L less than about 0.4, the curve tends asymptotically to infinity and the pole becomes a flexible pile. According to Czerniak (8) a pole is a pile "whose embedded depth does not exceed ten times its least lateral dimension." For a C/L value of

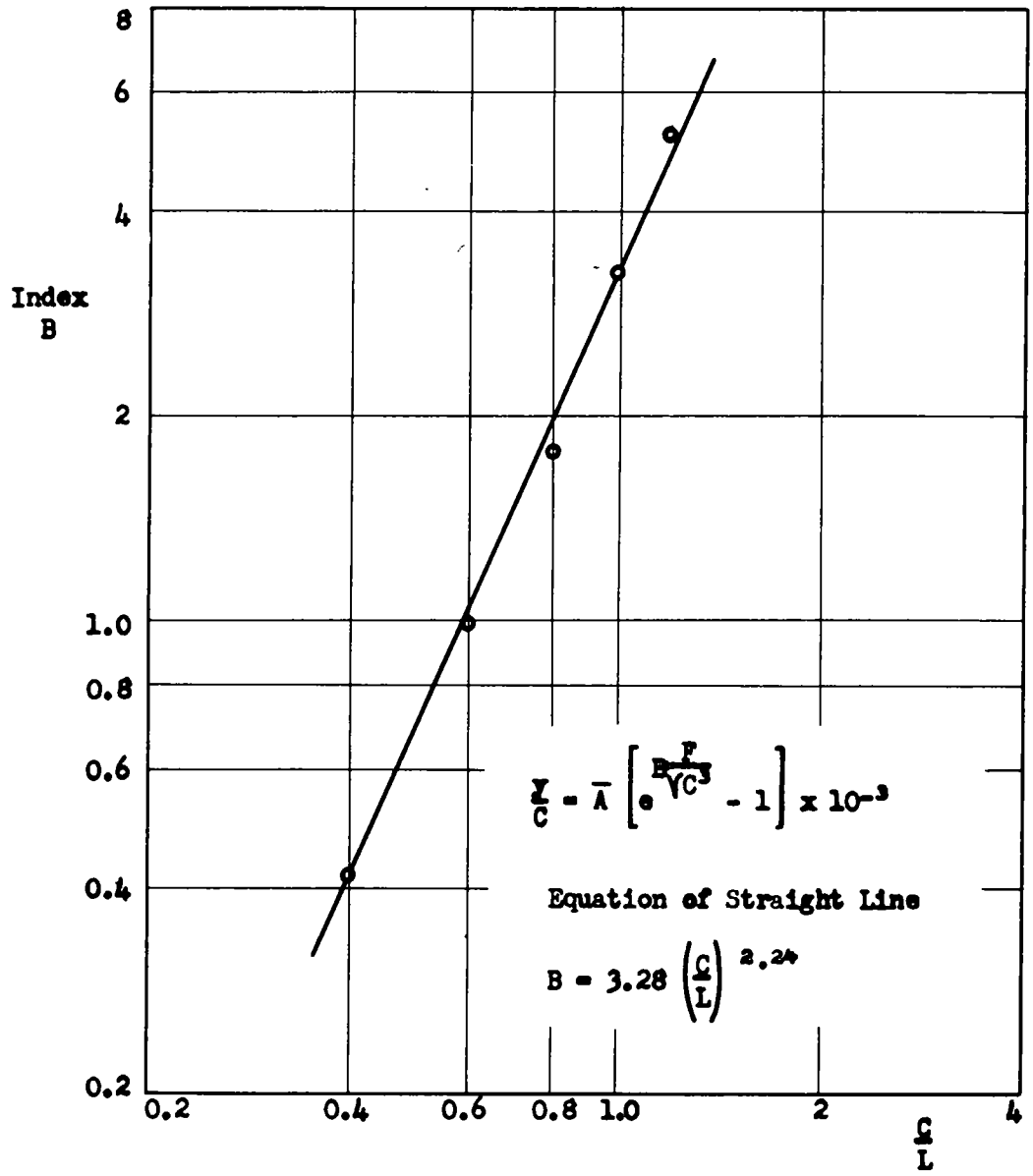

Figure 16. Plot of index B vs $\frac{C}{L}$.

0.4, the embedded length is 7.5 times the diameter. This is a relatively crude working rule inasmuch as no account is taken of the moment of inertia of the pole. Matlock and Reese (10) introduce the concept of a "maximum depth coefficient" to define a pile-pole criterion. This coefficient is related to the stiffness of the pile but is of such a complex nature that it appears to be difficult to relate it to the pole-soil interaction under investigation. This discussion of C/L is not an attempt to define a pole or pile, but is only intended as a qualitative discussion of the seemingly asymptotic nature for the small and large values of C/L given in Figure 18.

For values of C/L greater than 1.5 or 2, the strength ratio is very small and the resistance to deformation becomes very small. This corresponds to the case of a

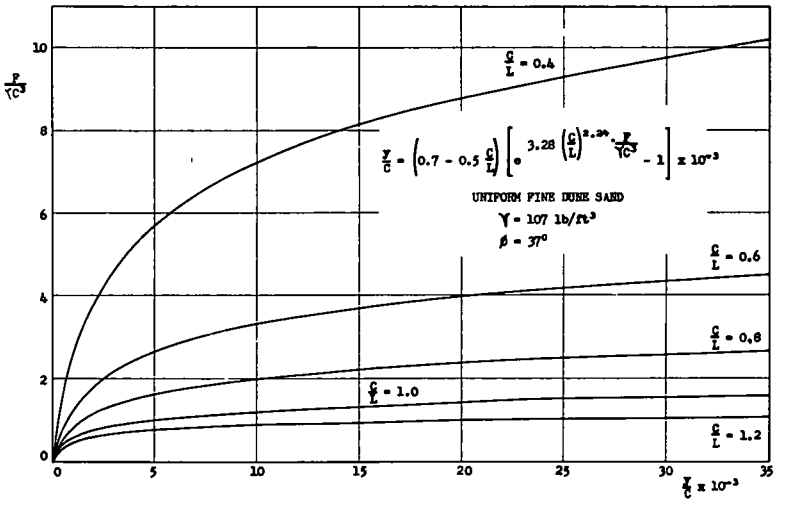

Figure 17. Nomograph relating $\frac{F}{\sqrt{C^3}}$, $\frac{Y}{C}$, and $\frac{C}{L}$.

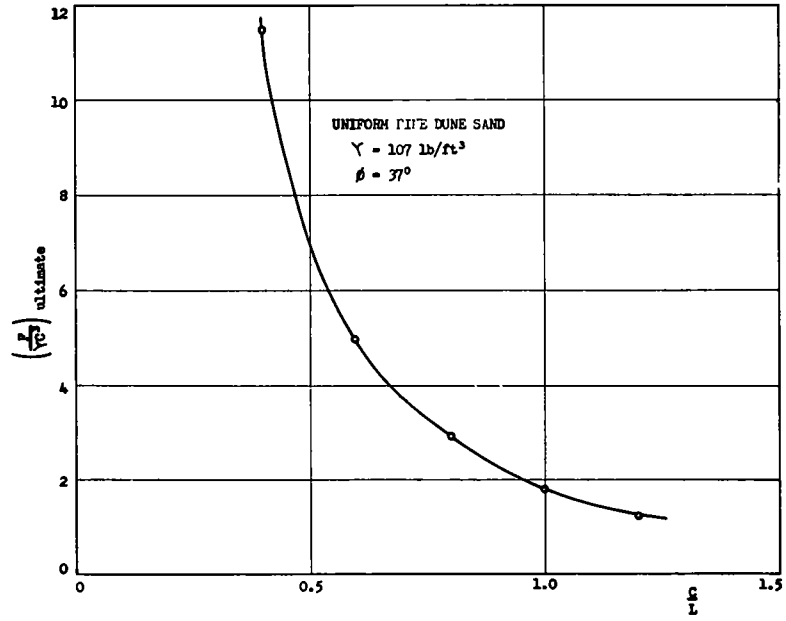

Figure 18. Plot of $\left(\frac{F}{\sqrt{C^3}}\right)$ ultimate vs $\frac{C}{L}$.

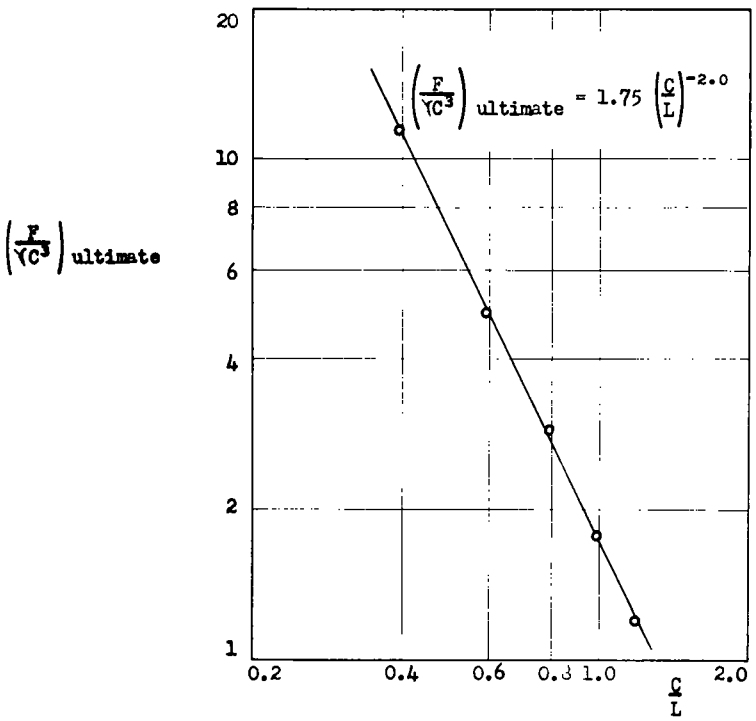

Figure 19. Plot of $\left(\frac{F}{\gamma C^3}\right)$ ultimate vs $\frac{C}{L}$.

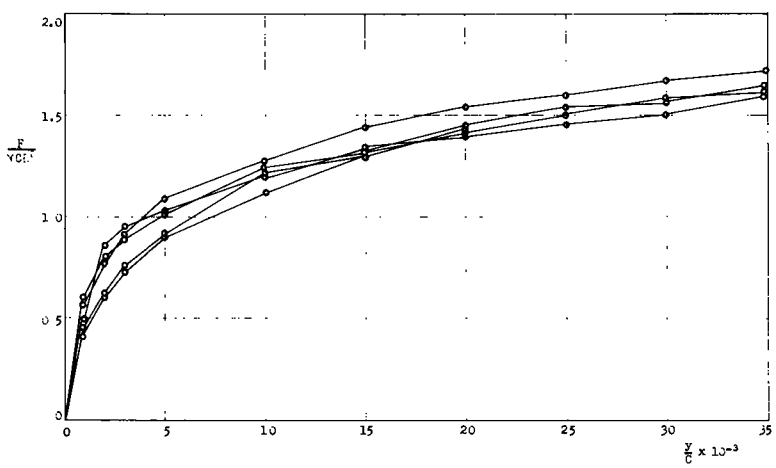

Figure 20. Nondimensional plot of $\frac{F}{\gamma CL^2}$ vs $\frac{V}{C}$ for $\frac{C}{L}$ = 0.4 - 1.2.

footing, with a horizontal applied load, in which the vertical forces, both body and applied, are very small and hence the frictional resistance is very small.

By replotting the data of Figure 18 on a logarithmic scale a straight line was obtained, the equation of which was

$$\left(\frac{F}{\gamma C^3}\right)_{\text{ultimate}} = 1.75 \left(\frac{C}{L}\right)^{-2} \tag{26}$$

which may be written

$$\left(\frac{F}{\gamma CL^2}\right)_{\text{ultimate}} = 1.75 \tag{27}$$

in which $F/\gamma CL^2$ is a stability number for the pole problem under consideration. A plot of these data appears in Figure 19. The empirical Eq. 27 is relatively simple and gives the ultimate ground-line thrust, F, directly.

The nondimensional form of Eq. 27 suggests a more optimum form for the functional relationship given by Eq. 19. This can be obtained by multiplying $F/\gamma C^3$ by $(C/L)^2$ to get the new term $F/\gamma CL^2$ and by dropping $F/\gamma C^3$ to maintain independence. Thus,

$$\frac{y}{C} = \varkappa \left[\frac{F}{\gamma CL^2} , \frac{C}{L} \right] \tag{28}$$

The mean curves to the experimental data previously given have been replotted in the form of $F/\gamma CL^2$ vs y/C for a range of C/L varying from 0.4 to 1.2 in Figure 20. Although the functional form of Eq. 19, as plotted in Figure 12, indicates a dependence on C/L, the form given by Eq. 28 and shown in Figure 20 indicates that the effects of the depth of embedment have been "lumped" into the term $F/\gamma CL^2$ and, except for experimental error, C/L has a negligible influence on the results. This permits the obtaining of a simpler, although more approximate, equation relating the variables of Eq. 28. Considering the mean curve to be independent of C/L, Eq. 19 may be rewritten:

$$\frac{y}{C} = \varkappa \left[\frac{F}{\gamma CL^2} \right] \tag{29}$$

in which the effect of C/L is negligible and may therefore be eliminated.

By replotting the curves on a semi-logarithmic scale, a near straight line was obtained as shown in Figure 21. The curve was further straightened out by replotting in the form log (y/C + A') vs $F/\gamma CL^2$, as shown in Figure 22, to give a two-constant curve, whose equation was

$$\frac{y}{C} = 0.2 \left(e^{3.20 \frac{F}{\gamma CL^2}} - 1 \right) \tag{30}$$

The value of A' is given by the intercept of the line on the log (y/C + A') axis for $F/\gamma CL^2 = 0$.

Alternatively Eq. 30 may be rewritten to give $F/\gamma CL^2$ in terms of y/C:

$$\frac{F}{\gamma CL^2} = 0.72 \log_{(10)} \left[5{,}000 \frac{y}{C} + 1 \right] \tag{31}$$

A nomograph for Eqs. 30 and 31 has been computed and appears in Figure 23. The curve is almost identical to a mean curve of Figure 20 indicating satisfactory curve fitting.

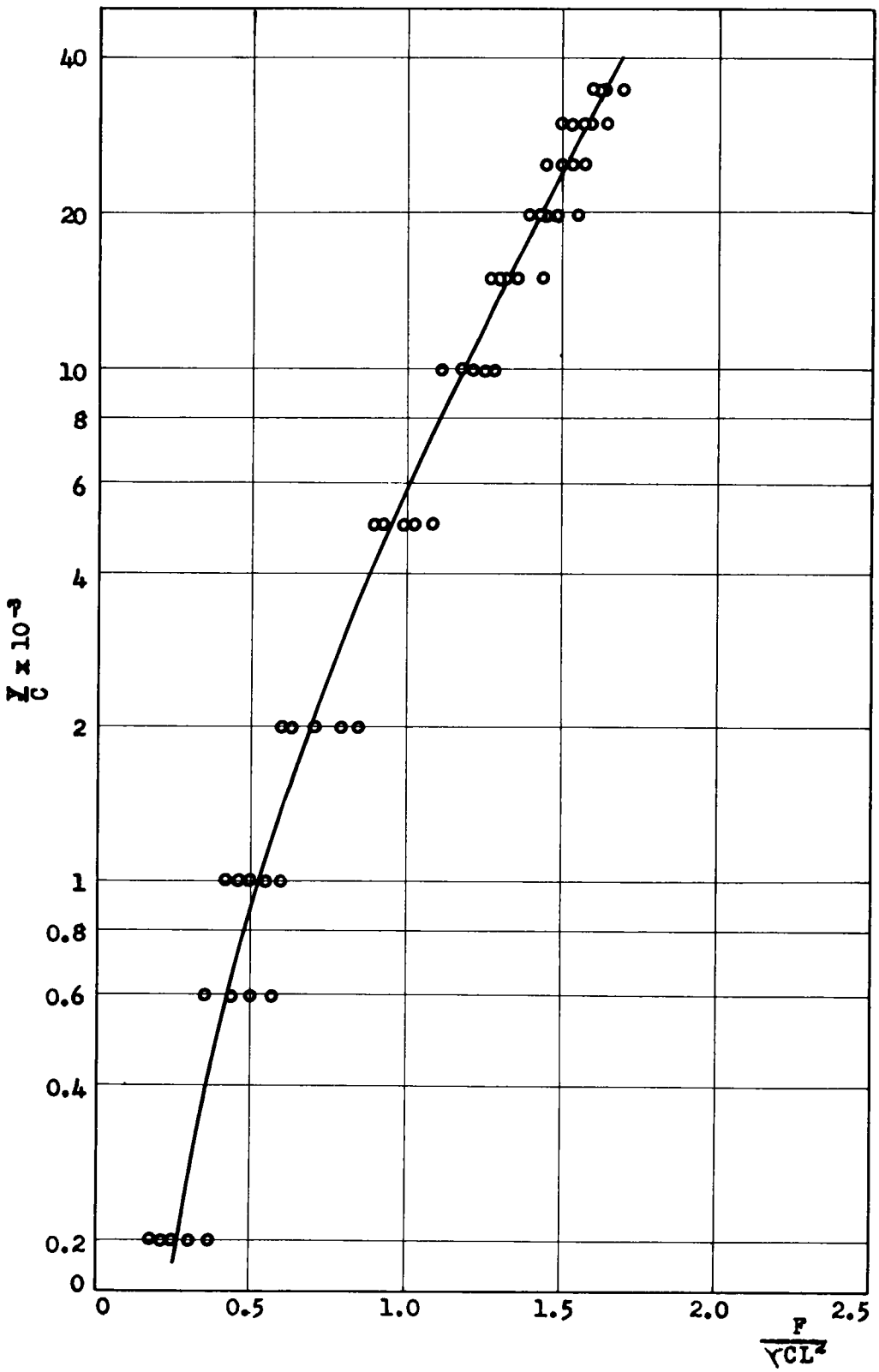

Figure 21. Nondimensional plot of $\frac{F}{\gamma CL^2}$ vs $\frac{y}{C}$ for $\frac{C}{L}$ = 0.4 - 1.2.

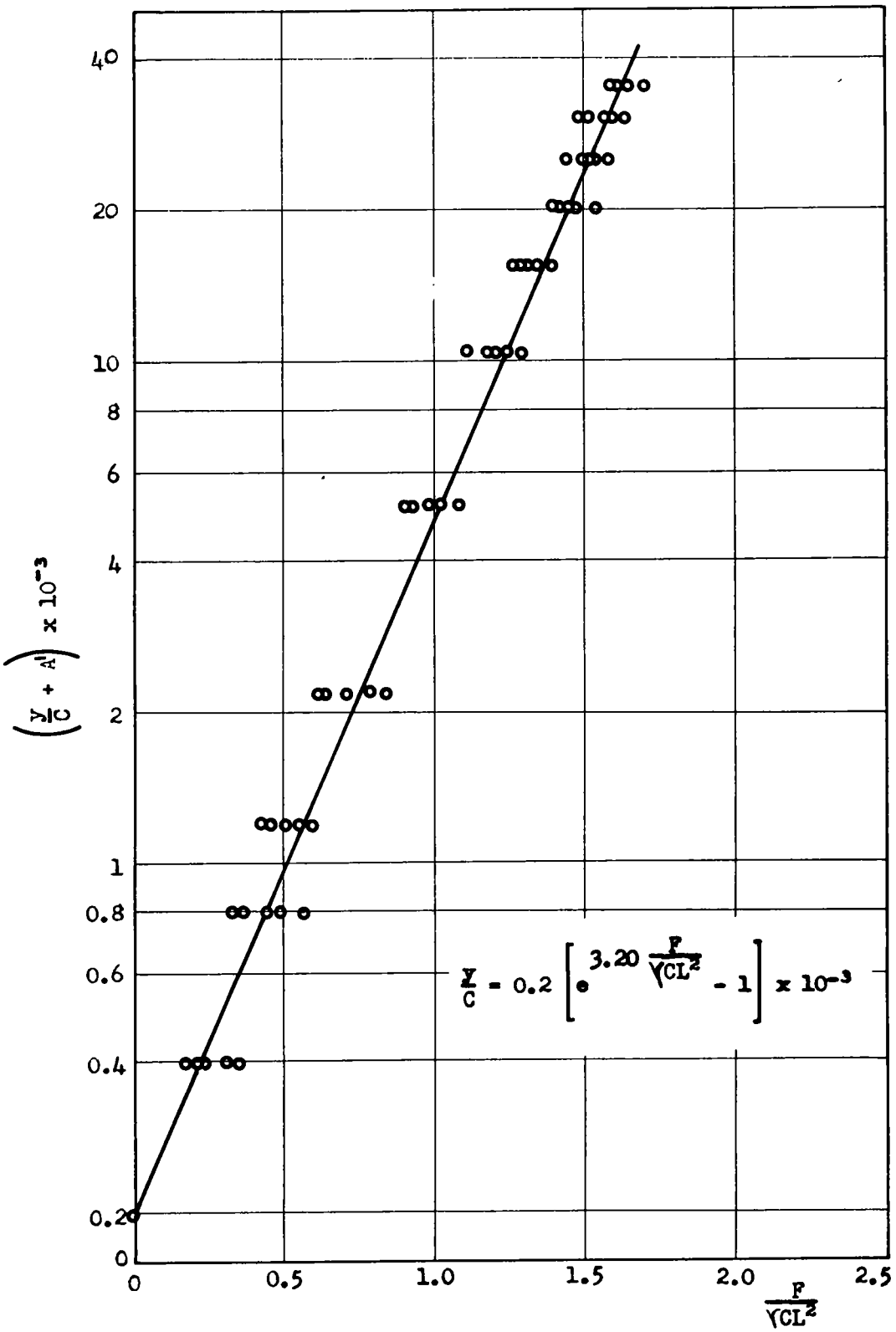

Figure 22. Nondimensional plot of $\frac{F}{\gamma CL^2}$ vs $\left(\frac{y}{C} + A'\right)$ for $\frac{C}{L}$ = 0.4 - 1.2.

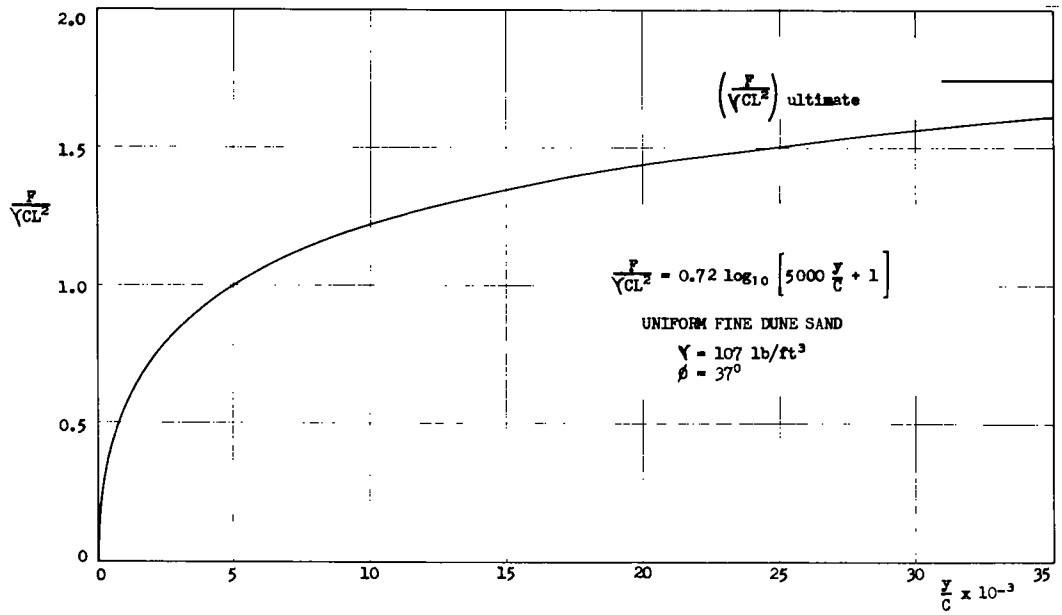

Figure 23. Nomograph relating $\frac{F}{\gamma CL^2}$ and $\frac{y}{C}$.

Referring to Figure 12, the maximum values of $F/\gamma C^3$ occur for a value of y/C of approximately 50 x 10^{-3}. Substituting this into Eq. 31 gives

$$\frac{F}{\gamma CL^2} = 0.72 \log 251 = 1.75 \qquad (32)$$

which is identical with Eq. 27, obtained by considering the ultimate values only. From this it may be inferred that the mathematical forms of Eqs. 27, 30, and 31 are compatible with one another.

In summary, although the general functional relationship for the problem has been developed, this paper deals primarily with the horizontal ground-line thrust on a pole embedded vertically in a uniform fine sand. The effects of pure couple-moments and superposition for both clays and sands are being investigated as well as the effects of soil type, density, and consistency. It is hoped that full-scale tests will be conducted in the future to correlate field response with the model study. The following examples are given to show the possible use to which model results may some day be applicable.

EXAMPLES

In the first example it has been assumed that the model test results may be applied directly to a field prototype so as to determine the order of magnitude of the field test results.

Given: A 10 ¾-in. circular steel pole was embedded in a uniform fine dune sand, density 107 pcf, $\phi = 37°$, and was subjected to a horizontal ground-line thrust.

Required: (a) The ultimate load for an embedment of 4 ft 6 in.
(b) The factor of safety for an applied load of 3 tons.
(c) The ground-line deflection in (b).
(d) An estimate of the ultimate deflection in (a).

Solution: $C = 10\ ¾ \times \pi = 33.8$ in. $= 2.82$ ft
$L = 54$ in. $= 4.5$ ft
$\frac{C}{L} = 0.63$

(a) From Figure 18,

$$\text{for } \frac{C}{L} = 0.63; \left[\frac{F}{\gamma C^3}\right]_{\text{ultimate}} = 4.45,$$

$$F_{\text{ultimate}} = 4.45\,\gamma C^3$$

$$= 4.45 \times \frac{107}{2000} \times (2.82)^3$$

$$= 5.35 \text{ tons}$$

Alternatively, using the pole stability number of Eq. 27

$$\left[\frac{F}{\gamma CL^2}\right]_{\text{ultimate}} = 1.75$$

$$F_{\text{ultimate}} = 1.75\,\gamma CL^2 = 1.75 \times \frac{107}{2000} \times 2.82 \times (4.5)^2$$

$$= 5.35 \text{ tons}$$

(b) Factor of safety $= \frac{5.35}{3} = 1.78$

(c) $$\frac{F}{\gamma CL^2} = \frac{3 \times 2000}{107 \times 2.82 \times (4.5)^2} = 0.98$$

from Figure 23

$$\text{for } \frac{F}{\gamma CL^2} = 0.98\ ;\ \frac{y}{C} = 4.7 \times 10^{-3}$$

$$\therefore\ y = 4.7 \times 33.8 \times 10^{-3} = 0.16 \text{ in.}$$

Alternatively,

$$\frac{F}{\gamma C^3} = \frac{3 \times 2000}{107 \times 2.82^3} = 2.50$$

from Figure 17

$$\text{for } \frac{F}{\gamma C^3} = 2.50\ ;\ \frac{C}{L} = 0.63\ ;\ \frac{y}{C} = 4.7 \times 10^{-3}$$

$$\therefore\ y = 0.16 \text{ in. (as before)}$$

(d) an estimate of the ultimate deflection may be determined from

$$\left(\frac{y}{C}\right)_{\text{ultimate}} \approx 50 \times 10^{-3}$$

$$y_{\text{ultimate}} \approx 50 \times 33.8 \times 10^{-3}$$

$$\approx 1.70 \text{ in.}$$

The first example could have been presented as a design problem rather than one of analysis.

Given: A 10 ¾-in. circular steel pole is to be embedded in a uniform fine dune sand, density 107 pcf, $\phi = 37^\circ$, and subjected to a horizontal ground-line thrust of 3.0 tons.

Required: (a) The depth of embedment for a factor of safety of 1.78 against failure.
(b) The ground-line deflection in (a).

Solution: $C = 10\ \frac{3}{4} \times \pi = 2.82 \text{ ft} = 33.8 \text{ in.}$

$$F_{\text{design}} = 1.78 \times 3 = 5.35 = F_{\text{ultimate}}$$

(a) from Figure 18

$$\text{for}\left[\frac{F}{\gamma C^3}\right]_{\text{ultimate}} = \frac{5.35 \times 2000}{107 \times (2.82)^3} = 4.45$$

$$\frac{C}{L} = 0.63$$

$$\text{Therefore, } L = \frac{C}{0.63} = \frac{2.82}{0.63} = 4.5 \text{ ft}$$

Alternatively, use of the pole stability number of Eq. 27 gives

$$\left[\frac{F}{\gamma CL^2}\right]_{\text{ultimate}} = 1.75$$

$$L = \sqrt{\frac{F_{\text{ultimate}}}{1.75\gamma C}} = \sqrt{\frac{5.35 \times 2,000}{1.75 \times 107 \times 2.82}} = 4.5 \text{ ft}$$

(b) from Figure 23

$$\text{for } \frac{F}{\gamma CL^2} = 0.98$$

$$\frac{y}{C} = 4.7 \times 10^{-3}$$

Therefore, $y = 4.7 \times 33.8 \times 10^{-3} = 0.16$ in.

CONCLUSIONS

1. For a model pole embedded in a very dense sand having constant properties the following theoretical, functional relationship has been developed to describe the phenomena:

$$\frac{y}{L} = \varkappa\left[\frac{C}{L}, \frac{C^2}{A}, \frac{M}{\gamma AL^2}, \frac{F}{\gamma AL}, \frac{\gamma tC}{n}, \phi\right] \tag{13}$$

2. For a model pole embedded vertically in a very dense uniform fine dune sand, density 107 pcf and angle of internal friction 37°, subject to a horizontal ground-line thrust:

(a) Variation in the diameter and depth of embedment of the pole resulted in different load-deflection curves. When the data were then plotted non-dimensionally in terms of $F/\gamma C^3$ vs y/C, a series of curves for differing C/L values resulted. These could be further approximated to a single curve for $F/\gamma CL^2$ vs y/C.

(b) A series of nomographs were constructed giving: 1. A relationship between the thrust strength ratio, $F/\gamma C^3$; the deflection ratio, y/C; and the slenderness ratio, C/L:

$$\frac{F}{\gamma C^3} = 0.70\left(\frac{C}{L}\right)^{-2.24} \log_{10}\left[\frac{\frac{y}{C} \times 10^3}{0.7 - 0.5\frac{C}{L}} + 1\right] \tag{25}$$

2. A slightly simplified, but more approximate, relationship between a "modified" thrust strength ratio, $F/\gamma CL^2$; and the deflection ratio, y/C:

$$\frac{F}{\gamma CL^2} = 0.72 \log_{10}\left[5,000\frac{y}{C} + 1\right] \tag{31}$$

3. A failure criterion relating the ultimate thrust strength ratio, $(F/\gamma C^3)_{\text{ultimate}}$; and the slenderness ratio, C/L; which may be written in the form of a stability number:

$$\left(\frac{F}{\gamma CL^2}\right)_{\text{ultimate}} = 1.75 \tag{27}$$

3. The use of dimensional analysis in interpreting the data permits the reducing of them to a relatively simple form, for which empirical equations may be developed. Conventional methods result in numerous disconnected "bits" of information.

4. Because there have been no field tests to correlate with the model study, caution is recommended regarding the use of the model response for prototype considerations. However, the model test results can be of considerable value with regard to providing an insight into the actual field response of prototype structures.

ACKNOWLEDGMENTS

The authors wish to express their appreciation to Jorj O. Osterberg, Professor of Civil Engineering, Northwestern University, for his assistance in obtaining the soil and experimental apparatus as well as his general encouragement.

The sand was provided through the courtesy of the Raymond Concrete Pile Company, Chicago.

REFERENCES

1. Kondner, R. L., "Non-Dimensional Approach to the Vibratory Cutting, Compaction and Penetration of Soils." Johns Hopkins Univ., Department of Mechanics, Tech. Report 8 (Aug. 1960).
2. Kondner, R. L., and Edwards, R. S., "The Static and Vibratory Cutting and Penetration of Soil." HRB Proc., 39:583-604 (1960).
3. Kondner, R. L., and Krizek, R. J., "A Non-Dimensional Approach to the Static and Vibratory Loading of Footings." HRB Bull. 277, 37-60 (1960).
4. Kondner, R. L., "Bearing Capacity of Friction Pile Groups in Cohesive Soil." Jour. Soil Mechanics and Foundations Division, ASCE (To be published).
5. Prakash, S., "A Review of the Behavior of Partially Embedded Poles Subjected to Lateral Loads." M.S. Thesis, University of Illinois (1960).
6. Chang, Y. C., "Annotated Bibliography of Lateral Loads on Piles." University of Illinois Report for Illinois Cooperative Highway Research Program (1960).
7. Terzaghi, K., "Evaluation of Coefficients of Subgrade Reaction." Geotechnique, Vol. 4 (Dec. 1955).
8. Czerniak, E., "Resistance to Overturning of Single, Short Piles." ASCE Proc., Vol. 83, Jour. Structural Division, Paper 1188, ST2 (March 1957).
9. Palmer, L. A., and Thompson, "The Earth Pressure and Deflection Along the Embedded Length of Pile Subjected to Lateral Thrust." Proc. 2nd Internat. Conf. on Soil Mechanics and Foundation Engineering, Vol. 5.
10. Matlock, H., and Reese, L. C., "Generalized Solutions for Laterally Loaded Piles." ASCE Proc., Vol. 86, Jour. Soil Mechanics and Foundations Division, Paper 2626, SN5 (Oct. 1960).
11. Langhaar, H. L., "Dimensional Analysis and Theory of Models." Wiley (1951).
12. Bridgman, P. W., "Dimensional Analysis." New Haven (1931).

Three-Dimensional Consolidation

J. A. DE WET, Research Officer, National Building Research Institute, South African Council for Scientific and Industrial Research, Pretoria

The one-dimensional theory of Terzaghi can be extended to three dimensions if the initial distribution of pore water pressures is known. This theory is similar to that of Biot with the exception that the normal strains are not defined during consolidation other than by the general conditions of compatibility of strain. Only the volumetric strain is prescribed. Experimental evidence is presented in favor of the former approach, and a complete solution, including stability analysis, is made of a consolidating rigid circular footing using the generalized Terzaghi theory.

A study is also made of secondary compression which is shown to be due to variations in the coefficient of permeability. The bulk modulus or coefficient of compression is shown to be very nearly constant, in spite of variation of the Poisson ratio during consolidation, and is proportional to the average permeability.

• THIS PAPER presents experimental evidence that the space distribution of pore water pressures, caused by an applied load, is independent of the strain field and is very nearly equal to the normal stress on octahedral planes. Small pore pressures are caused by the reorientation of particles which follows after shearing strain, but these are shown to be negligible in the field. If Darcy's law is valid with a constant coefficient of permeability, then the dissipation of pore pressure is governed by the classical equation like that for the diffusion of heat in solids, and therefore, the pore pressure history can be traced if the initial distribution is known. This is given by the theory of elasticity which is shown to be applicable to soils if the shear stress-strain curve is linearized. The bulk modulus relating a normal strain to a normal stress is shown experimentally to be constant over a reasonable stress increment, although Poisson's ratio varies during the consolidation of a saturated clay—from 0.5 to approximately 0.4.

The strain in the vertical direction (i.e., settlement) can be split into a component due to shearing stress only, which will be almost instantaneous for practical footings, and a component due to normal stress only, which will be time dependent and for a saturated soil will have to await the expulsion of the pore water (coincident with dissipation of pore pressure). Only the latter is defined as consolidation and the resulting normal strains are independent of the conditions of drainage in full accord with the theory of elasticity. But both settlements can be evaluated if the average shear modulus and the bulk modulus are known. As an illustration, the complete solution is given for a cylindrical footing on a semi-infinite layer for both a constant load and a variable load, with an analysis of the stability of the footing.

It is apparent that it is unnecessary to consider consolidation as an elastic problem with a variable body force as done by Biot (1) in 1941, when he derived equations identical to the elastic equations used to compute secondary effects due to a nonuniform temperature distribution. Cryer, in a note as yet unpublished, has shown that, for small values of the Poisson's ratio ν, these equations can lead to a pore pressure σ at the center of a clay sphere, equal to 157 percent of a hydrostatic pressure σ_0 round the sphere (there being no shearing stresses). No such increases have been observed during tests conducted by the author of the present paper. The pore pressure is always equal to the hydrostatic pressure as predicted by the classical theory of Terzaghi (2).

This case corresponds to a solution of Biot's equations for Poisson's ratio $\nu = 0.50$, when the solutions of Biot are also solutions of the generalized Terzaghi Theory. This method outlined for the treatment of three-dimensional consolidation is also identical to that of Terzaghi and is considerably simpler mathematically than that of Biot.

The reason why Biot's equations predict a possible pressure increase is because his fundamental stress-strain relations are of the form

$$\epsilon_x = \frac{\sigma_x}{E} - \frac{\nu}{E}(\sigma_y + \sigma_z) + \beta\sigma \tag{1a}$$

$$\epsilon_y = \frac{\sigma_y}{E} - \frac{\nu}{E}(\sigma_x + \sigma_z) + \beta\sigma \tag{1b}$$

$$\epsilon_z = \frac{\sigma_z}{E} - \frac{\nu}{E}(\sigma_x + \sigma_y) + \beta\sigma \tag{1c}$$

in which σ_x, σ_y, and σ_z are normal stresses on the soil element, σ is the pore water pressure, and β, ν, E are elastic constants. These equations imply that a change in the pure water pressure affects each normal strain in the same way or, conversely, a strain must cause a pore pressure change in a unique manner. That such is not the case is shown by experimental results described later and illustrated by Figure 2. The distribution of pore pressures at the center of a consolidating sample, with volume change ΔV as shown by the curve 2, was found to be unaffected whether there was a lateral strain ϵ_r equal to the vertical unit strain ϵ_v, or no lateral strain whatever, whereas the normal stresses $\sigma_z = \sigma_1$ and $\sigma_x = \sigma_y = \sigma_z$ were nearly the same in both cases. Apparently the only certainty about a consolidating soil is that there is a reasonably constant bulk modulus (i.e., that there will be a volumetric strain with a pore pressure change), but the individual normal strains cannot be prescribed other than by the rather wide conditions of compatibility. This point is further illustrated by Figure 3, which shows that the volumetric strain is virtually the same for a confined and unconfined sample, although in the former case the strain is necessarily all in the vertical direction, whereas the latter was characterized by isotropic unit strains (being the same in the three coordinate directions).

The main error in the extended Terzaghi approach rests in the so-called phenomenon of "secondary compression," defined as consolidation that does not follow the time behavior predicted by the simple diffusion equation with constant coefficients. This phenomenon is shown experimentally to be due to variations in the coefficient of permeability which are present at the small pressure gradients in the latter stages of consolidation; this is in direct confirmation of an hypothesis by Schiffman (3). The average coefficient of consolidation C_v was found for intervals in an interrupted consolidation test and these values were used in a numerical solution of one-dimensional consolidation by a method also mentioned by Schiffman (3). This numerical solution provides a far better fit to laboratory consolidation curves and, using this fit, it was possible to show that the coefficient of consolidation was practically independent of the loading sequence in the virgin range.

If the soil is partially saturated, there will still be consolidation, but the pore water pressure σ will only be some fraction α of the octahedral stress σ_G on a soil element at the moment of application of the load, and, according to a thermodynamic relationship derived by Coleman and Croney (4), the volume change ΔV of the soil element will be the same fraction α of ΔV_m, the quantity of water expelled. Therefore, the settlement due to consolidation can still be determined if α and the relation between a change in the water pressure and a corresponding change in ΔV_m are known. The latter is given numerically by the slope of the pF moisture content curve, if the pF is converted to a natural scale of pressure.

APPARATUS AND SAMPLES

Most of the experimental evidence was obtained from a large triaxial machine which was adapted as a three-dimensional consolidometer without side friction and without any

shear stresses (see Fig. 1). Provision was also made for measuring the pore pressures in the center of the sample by means of a pore pilot, which consisted of a flat, hollow brass tube roughly 1 ½ in. long by ¼ in. wide, with a smaller aperture at the end covered by 200-mesh wire. The press remeasuring device was extremely simple, consisting merely of the movement of a slug of mercury against air entrapped at the end of a sealed glass tube (0.4-mm bore). The air volume changes were very small (of the order of 10^{-4} cu in.) and so were measured by micrometer. The system could be calibrated by exerting pressure on the reservoir connected to the water lines. By using flexible Saran tubing it was possible to insert the pore pilot while water was dripping through its end in order to ensure both a thorough de-airing as well as a direct contact between the soil water and the water in the measuring assembly.

Loads could be applied to the cylindrical sample (height and diameter 3 in.) either by a cell pressure or a vertical load, or both. In the former case, it was necessary to ensure contact of the loading bar with the top of the sample by observing the "response" of an ammeter connected to a measuring bridge which was in balance with a linear variable differential transformer attached to a diaphragm on the base of the cell.

Deformations could therefore be registered either by the vertical dial gauge d or by volume changes dV of castor oil in the right hand tube connected to the cell. The sample was insulated from the oil by means of a thin rubber membrane provided with a nipple

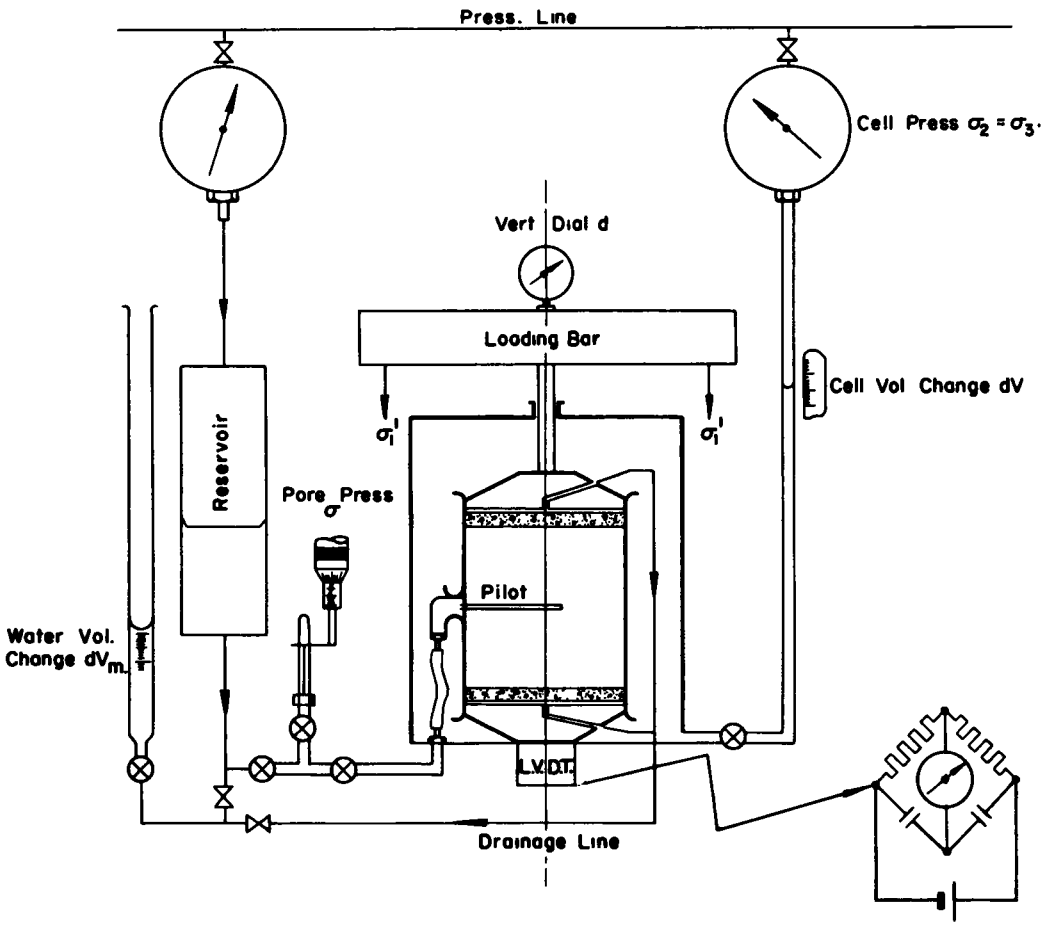

Figure 1. Modified triaxial compression apparatus.

for the pore pilot insertion. These volume changes could be correlated with the quantity of water dV_m expelled from the sample. If $dV_m = dV$, the sample was defined as saturated. It was also possible to close the drainage line at any time during a test and to block effectively any further consolidation. Where radial drainage was also desired, a layer of coir was placed between the circumference of the sample and the rubber membrane, and air was expelled by circulation from the water reservoir (see Fig. 1).

The samples tested in this apparatus were prepared of finely-ground Ball clay from a neighboring pottery and mixed with water under a vacuum, extruded in cylindrical form, and then allowed to adsorb further moisture in an atmosphere at 100 percent humidity until a moisture content of 39 percent was attained. It was found that these samples satisfied the criterion for 100 percent saturation when tested in the virgin range.

SUMMARY OF TEST RESULTS

These results are aimed mainly at showing that the behavior of soil during consolidation is largely elastic, especially in regard to the prediction of pore pressures. These pressures are shown to be independent of any strains that may occur due to expulsion of water; therefore, their description is governed by flow rates only, and can be evaluated by the Terzaghi diffusion equation (to the approximation of assuming a constant coefficient of permeability). A linear relationship is shown to hold between volumetric strains and the water pressure changes and these strains are independent of the water flow paths, so that any resulting settlement is given by the equations of elasticity. All tests were on saturated clay samples.

Figure 2 shows the results of three consolidation tests on cylindrical samples where pore pressures at the center were measured. Two tests appear on curve 2 for vertical drainage only; one was conducted using a consolidometer ring so that the radial strain ϵ_r was zero, and the second was free to strain in both coordinate directions under the ambient pressure, and it was found that the horizontal unit strain $\epsilon_r = \frac{u_r}{r_0}$ was equal

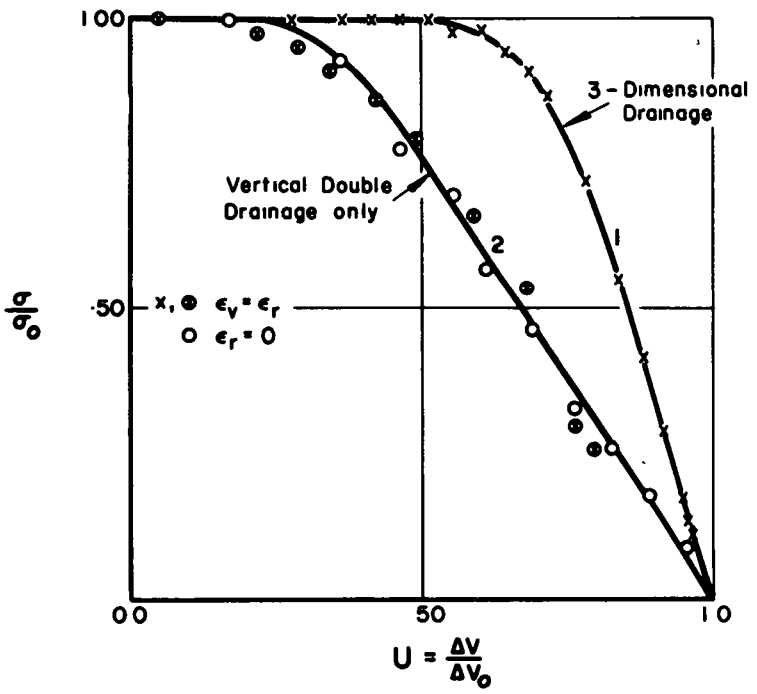

Figure 2. Relationship between pore pressure and strain during consolidation.

to the vertical unit strain

$$\epsilon_z = \frac{u_z}{h} = \frac{u_z}{2r_o} \tag{2}$$

in which r_o is the sample radius and h the sample height. The unit strains appear in the simple integrated form because it can be shown that the stresses are all constant throughout the cylinder, if there is no friction on the end plates. Then, if ΔV_o is the total volume change the degree of consolidation is $U = \frac{\Delta V}{\Delta V_o}$ and it is apparent that the variation of pore pressure with U is unaffected by the strain and falls very close to the solid line, which is a solution of the diffusion equation for vertical drainage alone. On the other hand, curve 1 is for both radial and horizontal drainage (when again the experimental points correspond to a theoretical solution) but ϵ_r was measured equal to ϵ_z so that the strain picture is independent of the drainage conditions. From the very close correspondence of the measured pressures with those predicted, it would seem that this phase of the consolidation theory is satisfactory. "Secondary" effects only appear in the relation between and at the time when variations in the coefficient of permeability play their part.

In the laboratory, only the vertical displacement u_z was measured so that the horizontal displacement u_r had to be evaluated by subtracting volume changes dV_u in the vertical direction from the total volume change dV. It was found that dV_u was equal to $\frac{dV}{3}$, signifying the equality of the unit strains ϵ_r, ϵ_θ, and ϵ_z.

The distribution of volumetric strain $\frac{\Delta V}{V}$ is compared for the two cases of lateral confinement and no lateral confinement in Figure 3 which shows that, for the same load increment on identical samples, the total volume change is the same, even though in

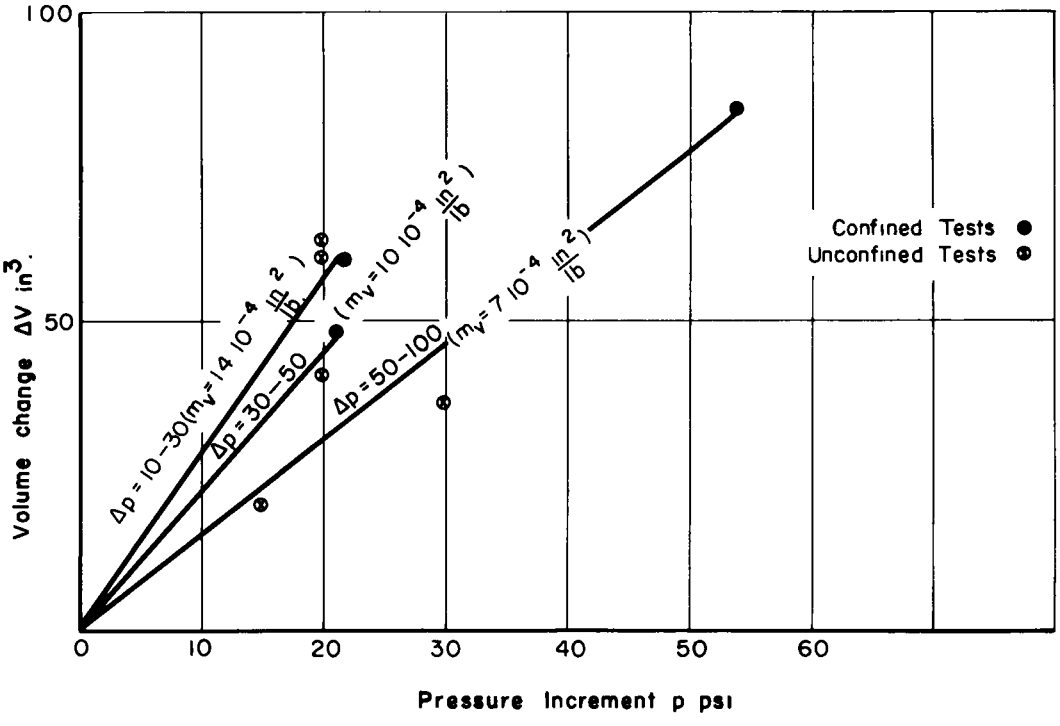

Figure 3. Volume changes for confined and unconfined consolidation.

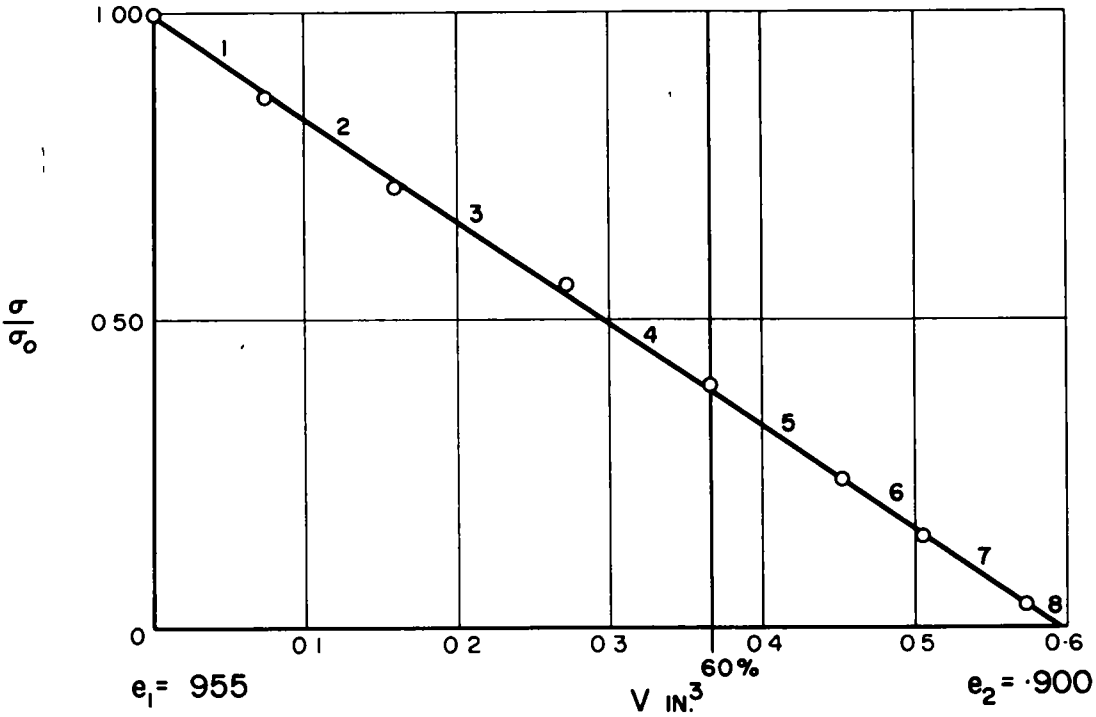

Figure 4. Relationship between pore pressure and volume change during consolidation.

the former case (corresponding to a conventional one-dimensional consolidation test) all of the volume change is confined to the vertical direction only. Of course, in three-dimensional consolidation the vertical volumetric strain is only $\frac{1}{3}\frac{\Delta V}{V}$, so that a one-dimensional test would overestimate the bulk modulus $B = p/\frac{\Delta V}{V} = \frac{1}{m_y}$, although there is likely to be some settlement due to shearing strain.

To measure the fall of pore water pressure with volume change due to expulsion of water, consolidation was interrupted (by closing the drainage line) until the pressure σ had attained a uniform value throughout the sample. During a vertically drained test under an ambient pressure of 20 psi this was done seven times, and the plot of the pressures against the volume change (Fig. 4) shows that the bulk modulus for a given load increment is constant as postulated by Terzaghi and Schiffman.

The intervals are numbered because each time the drainage line was reopened there was a new consolidation test under a reduced load. The results of these tests are plotted in Figure 6, referred to later.

In all of the experiments mentioned so far, the initial value of the pore water pressure σ_0 was found to be equal to the cell pressure p. In other words, all of the average normal stress was being carried by the pore fluid, which is one of the fundamental assumptions of consolidation theory for saturated soils. But this means a value of Poisson's ratio $\nu = \frac{1}{2}$, the Poisson's ratio of a fluid, and under these conditions no volume changes are theoretically possible because

$$B = \frac{1}{m_v} = \frac{p}{\frac{\Delta V}{V}} = \frac{E}{3(1 - 2\nu)} \qquad (3)$$

To study the behavior of the Poisson's ratio during consolidation, a thin-walled (thickness = $\frac{1}{20}$ in.) stainless-steel consolidometer ring was fitted with strain gauges

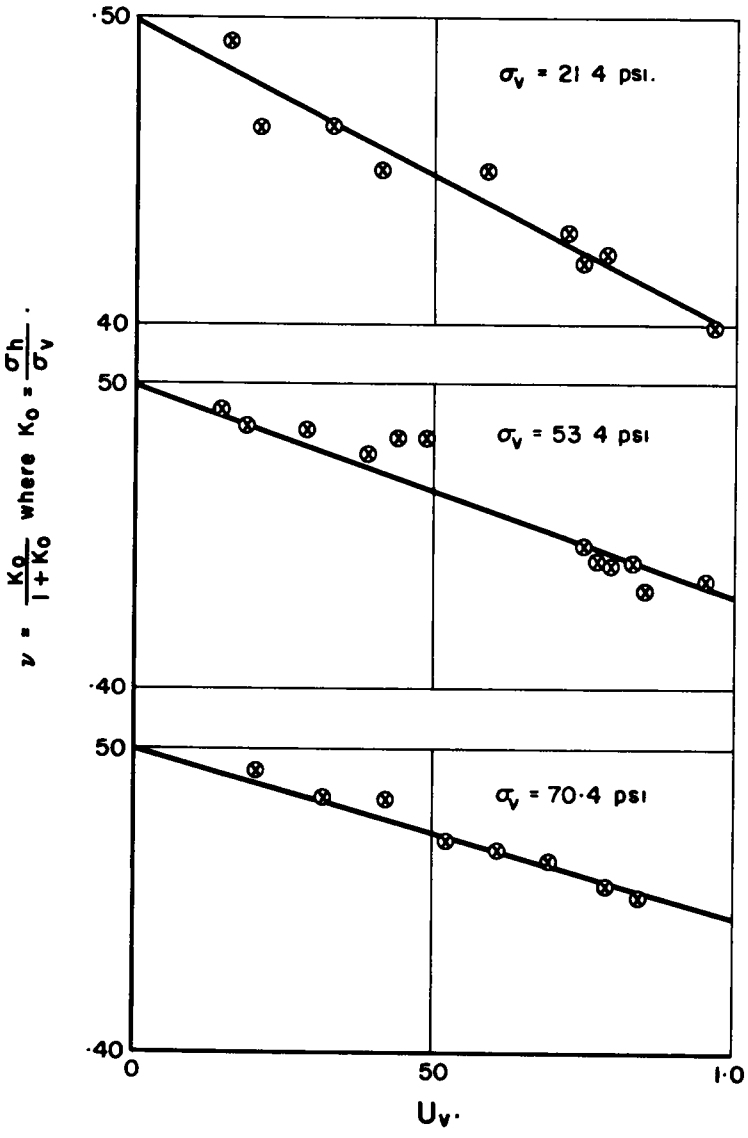

Figure 5. Variation of Poisson's ratio during consolidation.

and circumferential strains measured during the progress of the test. Thus, the hoop stress and the ratio $K_o = \frac{\nu}{1-\nu}$ of vertical to lateral stress could be determined and hence ν. The relationship of ν to degree of consolidation U_V is shown in Figure 5, and Poisson's ratio appears to decrease linearly from a value of 0.500 to a value of about 0.400. Because B remains constant during consolidation (Fig. 4), this must mean that the modulus E changes proportionately.

The loads are cumulative; that is to say, when σ_V = 53.4 psi was applied, the sample was already subjected to a stress of σ_V = 21.4 psi, and the stress of 70.4 psi was in addition to an existing stress of 75 psi.

ONE-DIMENSIONAL CONSOLIDATION WITH VARIABLE PERMEABILITY

It was possible to determine how the coefficient of consolidation

$$c_v = \frac{k}{\gamma_w m_v} = \frac{kB}{\gamma_w} \qquad (4)$$

varied with the degree of consolidation U_v, from the results of the interrupted test used for the construction of Figure 4. Figure 6 shows the degree of consolidation against the square root of the time for the succession of partial consolidation tests 1 to 8 which occurred each time the drainage line was reopened. It can be shown that, if the coefficient of permeability is a function of the void ratio, there will always be a linear relationship between the degree of consolidation and the square root of the time for small values of the latter (5). The coefficient c_v is then given initially (6, p. 234) by

$$T = \frac{c_v t}{H^2} = \frac{\pi}{4} U_v^2 \quad (U_v < 60\ \%) \qquad (5)$$

in which $U_v = \frac{\partial V_m}{\Delta V_m}$ if ΔV_m is the total amount of water expelled in one partial test. H is the length of the longest drainage path; i.e., one-half the sample height in double drainage. The values of c_v calculated from Eq. 5 and the initial slope $\frac{dU_v}{dt^{1/2}}$ are plotted in Figure 7 which is an experimental determination of the variation of the coefficient of consolidation with degree of consolidation.

The reason why all the lines of Figure 6 do not pass through the origin may be attributed to the time lag in the horizontal displacement u_r, because, as soon as the drainage

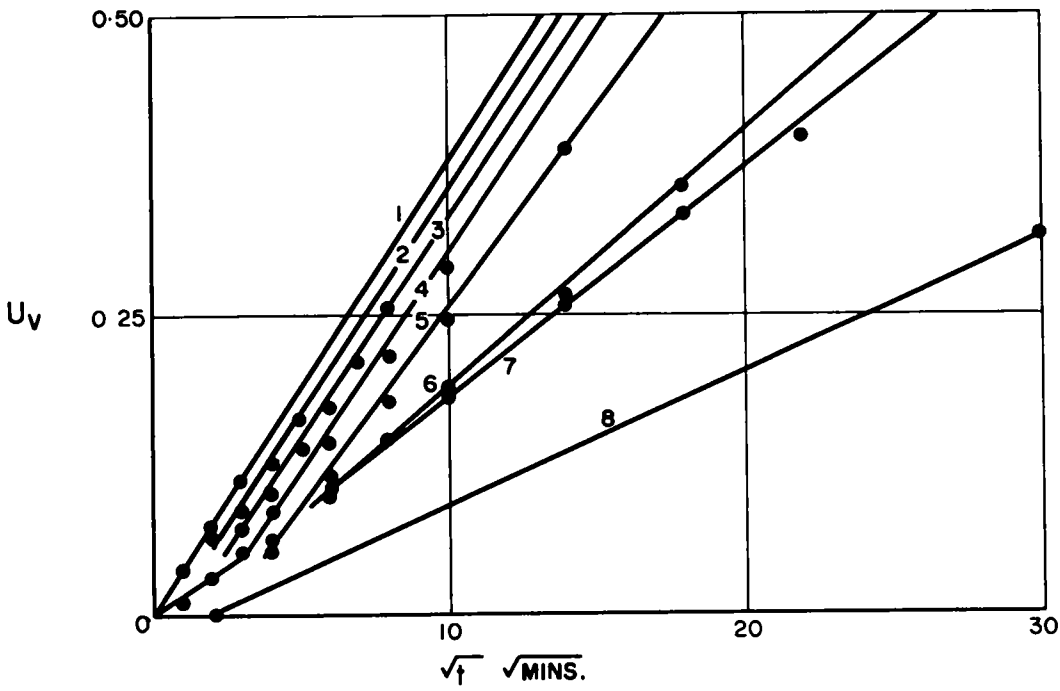

Figure 6. Interrupted consolidation tests.

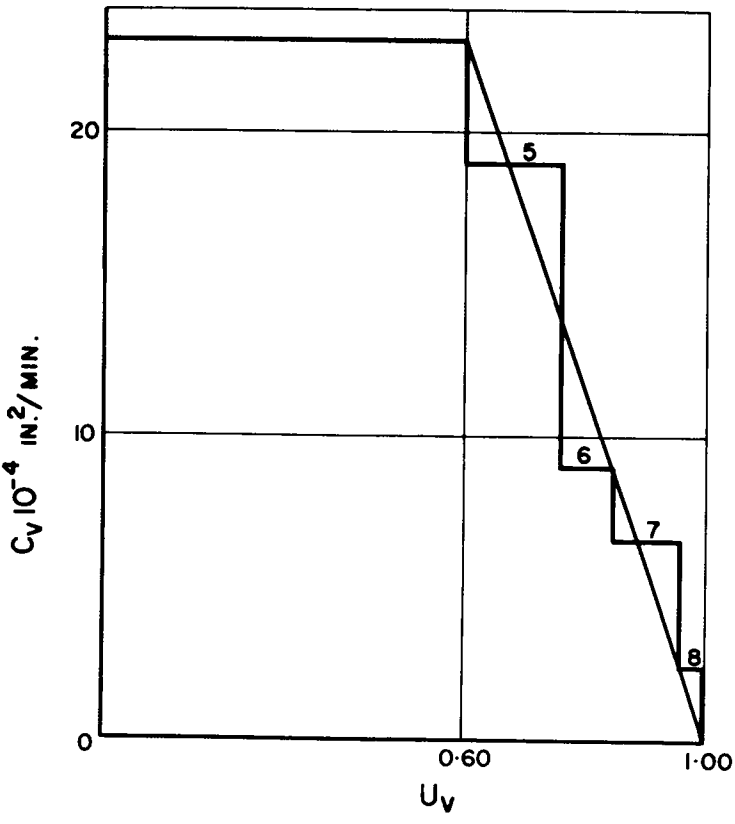

Figure 7. Variation of diffusion coefficient during consolidation.

cock was opened, the water flow was accounted for by the vertical displacement only.

According to Eq. 4, the fact that c_v falls approximately linearly after a degree of consolidation of 60 percent must mean that the permeability decreases with the small gradients present at the end of consolidation, because it has already been shown that the bulk modulus B remains a constant for that increment. In fact, the permeability will probably be a function of the distance as well as of the time, but, because this function is not known, a numerical procedure similar to that mentioned by Schiffman (3) was used for incorporating the results of Figure 7 into an approximate solution of one-dimensional consolidation with secondary effects.

The coefficient of consolidation was assumed to remain constant over a finite time interval and the pore water pressure distribution at the end of the previous time increment was used as the initial condition for a finite difference solution with the new, smaller coefficient.

The equation of consolidation in one dimension is

$$\frac{\partial \sigma}{\partial t} = c_v \frac{\partial^2 \sigma}{\partial z^2} \tag{6}$$

which may be written in the finite difference form (7, ch. 10):

$$\sigma_m^+ = \sigma_m + \frac{c_v \partial t}{(\partial z)^2} \left(\sigma_{m+1} - 2\sigma_m + \sigma_{m-1} \right) \tag{7}$$

The space variable z is divided into a number of equal intervals ∂z, and σ_{m+1}, σ_m, and σ_{m-1}, are the pore pressures at the nodal points $(m+1)\partial z$, $m\partial z$ and $(m-1)\partial z$

respectively, at the time $t = n\partial t$; σ_m^t being the value of the pore pressure at the time $(n+1)\partial t$.

Because, according to Figure 7, the coefficient of consolidation remains constant until $U_v = 60$ percent, the pore pressure distribution at this point was given by the exact solution of Eq. 6.

$$\sigma(z, T) = \frac{4\sigma_0}{\pi} \sum_{n = 1,3,5\ldots}^{\infty} \frac{1}{n} \sin \frac{n\pi z}{2H} e^{-\frac{1}{4}n^2\pi^2 T} \tag{8}$$

At $U_v = 60$ percent, $T = 0.300$ (Eq. 5) so that σ could be evaluated at the nodal points $0, \frac{H}{5}, \frac{2H}{5}, \frac{3H}{5}, \frac{3H}{5}, \frac{4H}{5}$, and H, the σ-values at reflected points being given by symmetry. The solution was then generated from Eq. 7 but with a smaller value of c_v given by

$$\frac{c_v}{c_v} = \frac{(1 - U_v)}{0.40} \tag{9}$$

in which c_{v_0} is the initial value of $c_v (U_v \leq 60$ percent). The independent variable $(1-U_v) = \frac{\bar{\sigma}}{\sigma_0}$ could be readily evaluated by finding the average pressure $\bar{\sigma}$ from the computed nodal values by the use of Simpson's rule, and then the next step carried through, starting with the previously computed pressure distribution and the boundary condition $\sigma = 0.00$ at $z = 0$, with symmetry about the center $\frac{z}{H} = 1.00$. Generally, $\frac{c_v \sigma t}{(\delta z)^2} \leq \frac{1}{2}$ to ensure convergence of the method.

Figure 8 shows the degree of consolidation as a function of the time factor T when

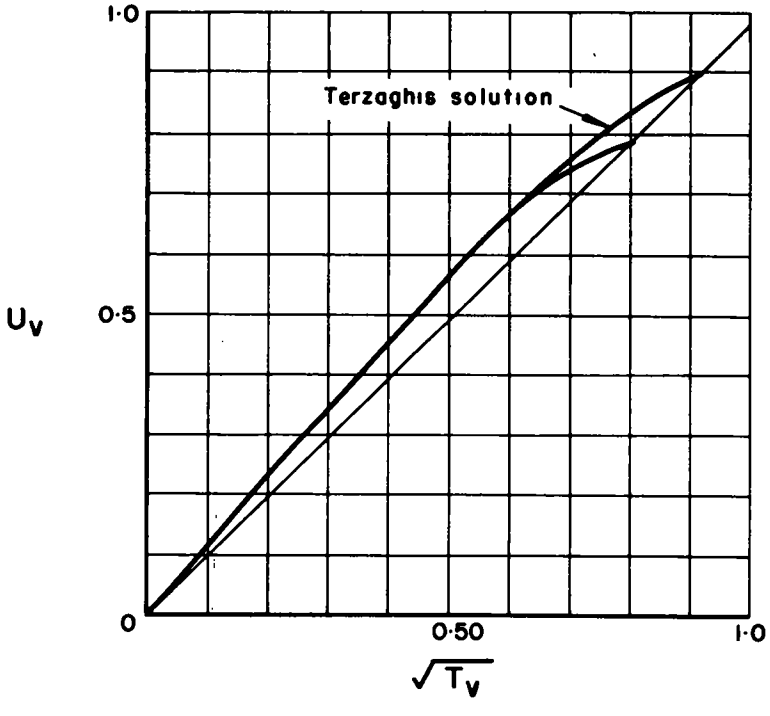

Figure 8. One-dimensional consolidation with variable diffusion coefficient.

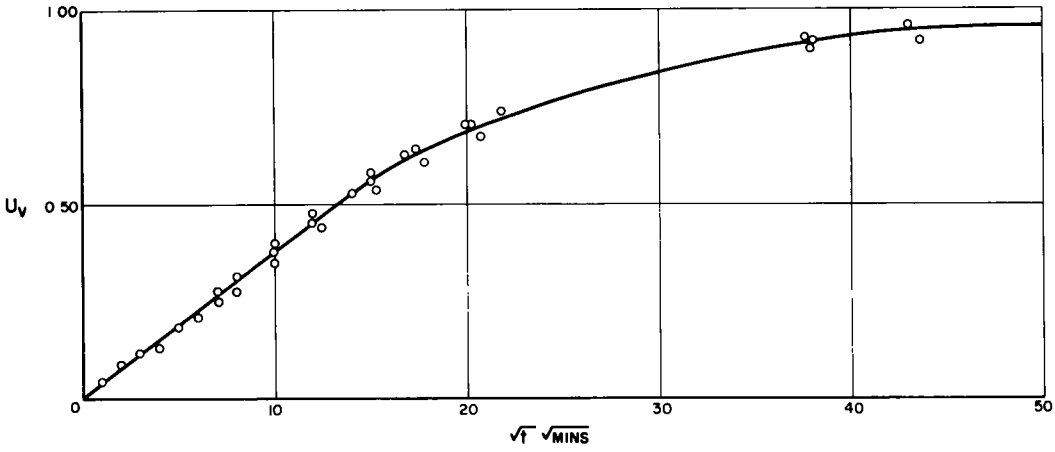

Figure 9. Independence of c_v with loading history in the virgin range.

secondary effects due to permeability changes are taken into account. Any "secondary compression" resulting from shearing strains was effectively eliminated from Figure 6 by consolidating the sample with only a cell pressure so that the Mohr circle of stress would be simply a point. This, however, is not generally the case in a consolidometer ring because, with the change in Poisson's ratio during consolidation (Fig. 5), the lateral pressures will decrease so that shearing stresses must inevitably be present.

A fitting method for the new consolidation curve is readily given by an adaptation of the "square root of time" method developed by Taylor (6, p. 238) where the intersection of a line with 1.15 times the slope of the linear portion of the curve is alleged to give the point of 90 percent consolidation. Allowing for variations in permeability, this intersection is only about 78 percent, and the final volume change may be taken as approximately $\frac{10}{7.8}$ times the volume change given by the point of intersection. Figure 9 shows the consolidation of four different double drainage tests fitted by this method. These tests were all in the "virgin" range and covered a pressure range of from 10 to 80 psi; however, they all fall about the same curve, which indicates that the average coefficient of permeability must change in phase with the bulk modulus (so as to preserve a uniform value of the coefficient of consolidation). There is some variation in B as is shown by Figure 10 which is the compression curve for the test series. (The results of tests 2, 3, 8, and 14 appear in Figure 9.)

THREE-DIMENSIONAL CONSOLIDATION IN THE FIELD

The strains caused in a soil by the hydrostatic pressure $p = \sigma_0$ have been discussed, and it has been shown that these volumetric strains are proportional to the pressure and independent of the conditions of drainage, but dependent on the time, according to a law governed by the solution of the equation for diffusion of pore pressure. Therefore, the normal strains may be considered as a problem of delayed elastic response. Because the pore pressures are independent of the strain, the time variation can be found by a solution of the classical diffusion equation with the pressure as the dependent variable. The only approximation is the assumption that the coefficient of permeability remains constant, but this is shown to be important only in the latter stages of consolidation when a decrease of the permeability has the effect of slowing down the process.

In general, a soil element will not be subjected to a uniform ambient pressure p but rather to three normal stresses σ_x, σ_y, σ_z and three shearing stresses τ_{xy}, τ_{yz}, τ_{zx}. However, if each normal component is resolved into two parts

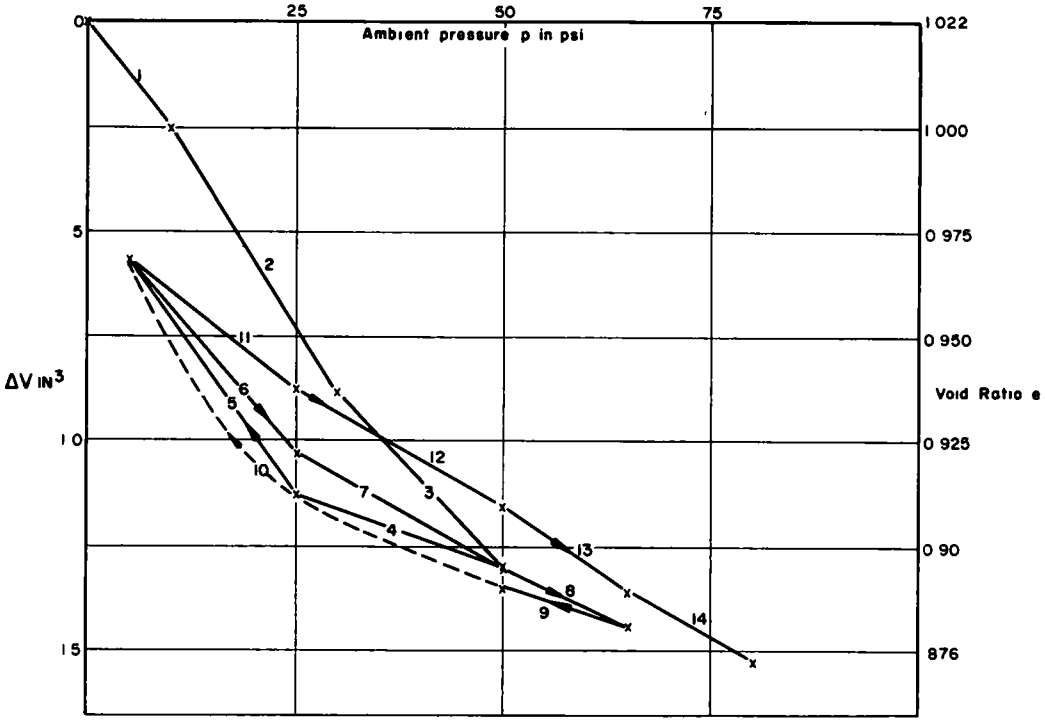

Figure 10. Compression curve for triaxial consolidation with vertical drainage.

$$\sigma_x = \sigma_x^1 + p \tag{10a}$$

$$\sigma_y = \sigma_y^1 + p \tag{10b}$$

$$\sigma_z = \sigma_z^1 + p \tag{10c}$$

in which p = average of the normal stress = $\frac{1}{3}$ $(\sigma_x + \sigma_y + \sigma_2)$, then $\frac{\Delta V}{V} = \frac{p}{B}$, and therefore, the deviator stresses σ_x^1, σ_y^1, σ_z^1 can cause no volume change, only shear distortion. If the soil grains are incompressible, then all volume changes must take place due to outflow under the gradient of the initial pore pressure σ_0 so that this pressure would appear to be equal to the pressure p. This concept agrees with the initial condition

$$\nabla^2 \sigma_0 = 0 \tag{11}$$

which must govern the distribution of σ_0 if there is no volume change just after the application of the load (corresponding to $\nu = \frac{1}{2}$). The condition (Eq. 11) is that postulated by Biot (1).

Now the conditions of compatibility, as shown by Timoshenko (8, ch. 7), require that p should also satisfy the Laplacian (Eq. 11) and, in fact, this is the only stress that does obey this simple equation, so again there is an equivalence between p and σ_0.

It has been found in the laboratory that shearing strains are also responsible for a build-up of pore water pressure (9). During a combined consolidation and shear test performed by the author under conditions of three-dimensional drainage, the pressure σ_0 reached a value of about 1.10 p (p is the ambient or cell pressure all round the sample). However, the stress conditions in the laboratory are arbitrary and probably artificial, and the amount of pressure increase depends on the degree of particle reorientation and, therefore, on the strain and stress history. It is even possible to get a pressure decrease caused by shearing strain if the clay has been preconsolidated and then rebounded to a

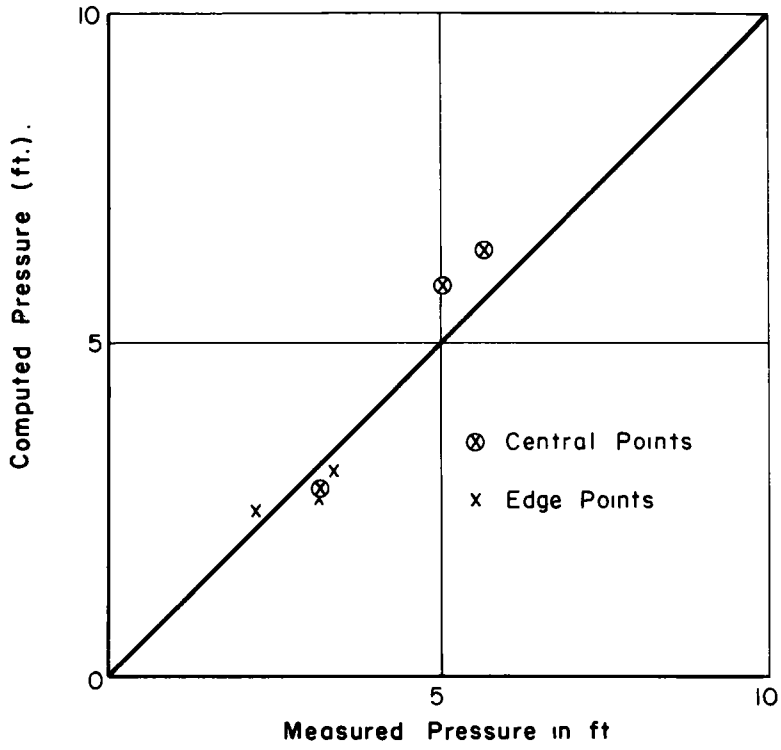

Figure 11. Comparison of measured and computed pore pressures under a circular tank.

smaller void ratio. Therefore, pore pressure changes caused by shearing stresses are notoriously difficult to assess and probably play a small part in the stress distributions present under footings.

The pore pressures σ_0 were measured under a large cylindrical oil tank on the Isle of Grain by Gibson and Cooling (10) so that it is possible to compare these pressures with pressures calculated on the assumption that

$$\sigma_0 = p = \tfrac{1}{3}(\sigma_x + \sigma_y + \sigma_z) = \tfrac{1}{3}(\sigma_1 + \sigma_2 + \sigma_3) \qquad (12)$$

The value of p may be readily computed under the center and under an edge of a uniformly loaded circular area on a semi-infinite foundation by integrating the solution for a point load (8, ch. 11). These computed values are compared in Figure 11 with measured values at depths of 15, 20, and 60 ft below the edge of the tank and on the centerline.

The agreement is remarkably good when it is considered that the tank was underlain by soft blue clay and below this by a thick bed of gray laminated sandy clay. Values plotted in Figure 11 come from both of these strata.

Therefore, the initial distribution of σ may be assumed given by Eqs. 11 and 12, and follow the development of $\sigma(t)$ by a solution of the three-dimensional diffusion equation subject to this initial condition. However, the ultimate settlement w at $t = \infty$ will also include shear settlement but, fortunately, the settlement w_c due to consolidation, and the settlement w_s due to shearing stresses, may be separated because the stress-strain relations (8, Introduction) may be written

$$\epsilon_z = \frac{\partial w}{\partial z} = \frac{1}{2G}(\sigma_z - \sigma_0) + \frac{\epsilon}{3} \qquad (13)$$

ϵ is the volumetric strain equal to $\frac{dV}{V}$ or $\frac{\sigma_0}{B}$, so integrating Eq. 13:

$$w = \frac{1}{2G} \int_0^\infty (\sigma_z - \sigma_0)dz + \frac{1}{3B} \int_0^\infty \sigma_0 dz \qquad (14)$$

$$= \quad w_z \quad + \quad w_c$$

It is apparent that the volume change in the vertical direction is only one-third of the total volume change indicated by the results in Figure 3. The settlement due to shearing stress will probably be almost instantaneous and corresponds to what is generally termed the "elastic settlement" whereas that due to consolidation will take time to complete.

Therefore, to estimate the total settlement, it is essential to know both the bulk and the shear modulus. The latter does not have a constant value because soil is plastic; that is, the shearing strain is a function of the time as well as of the stress. Thus, to use elastic theory for predicting shearing stress, the stress-strain curve must be linearized. A theory for the behavior of soil under a shearing stress τ has been developed in a companion paper by the author, still to be published, and a method of linearization is given (see also 16). This consisted of choosing a modulus G such that the strain energy $\frac{1}{2}\frac{\tau^2}{G}$ was identically equal to the area $\int \tau d\gamma$ under the nonlinear stress-strain curve. It turns out that this modulus can be obtained either from one-half the initial slope of the stress-strain curve in a constant rate of strain test or from one-half the slope $\frac{\tau d(\log_e t)}{d\gamma}$ of the latter stages of a constant load test where τ is the applied stress, and the strain γ is plotted against the natural logarithm of the time $\log_e t$. For a limited number of tests conducted on the saturated "Ball" pottery clay, G was found to be less than or equal to ½ B.

CONSOLIDATION OF A RIGID CIRCULAR FOOTING ON A SEMI-INFINITE FOUNDATION

The complete elastic solution for a circular punch on a semi-infinite medium has been derived by Sneddon (11) using the method of Hankel transforms to reduce the biharmonic for the stress function to an ordinary differential equation in terms of the depth z. This may then be integrated and the constants of integration found by also expressing the boundary conditions in terms of their Hankel transforms.

The two stresses of interest for evaluation of the settlement are given by

$$\sigma_0 = -\frac{(1+\nu)}{3} = -\frac{p}{2} J_1^0 \quad \text{if } \nu = \tfrac{1}{2} \qquad (15)$$

and

$$\sigma_z = -\frac{p}{2}(J_1^0 + \zeta J_2^0) \qquad (16)$$

in which $\pi a^2 p = P$ if P is the total load in pounds carried by the footing of radius a, and the integrals of Bessel functions J_1^0 and J_2^0 may be put in terms of the coordinates $\zeta = \frac{z}{a}$ and $\rho = \frac{r}{a}$ by

$$J_1^0 = R^{-1} \sqrt{\frac{R - (\rho^2 + \zeta^2 - 1)}{2}} \qquad (17a)$$

$$J_2^0 = R^{-3} \left[(\zeta^2 - \rho^2 + 1) \sqrt{\frac{R + (\rho^2 + \zeta^2 - 1)}{2}} + \zeta(\rho^2 + \zeta^2 + 1) \sqrt{\frac{R - (\rho^2 + \zeta^2 - 1)}{2}} \right] \qquad (17b)$$

in which

$$R^2 = (\rho^2 + \zeta^2 - 1)^2 + 4\zeta^2$$

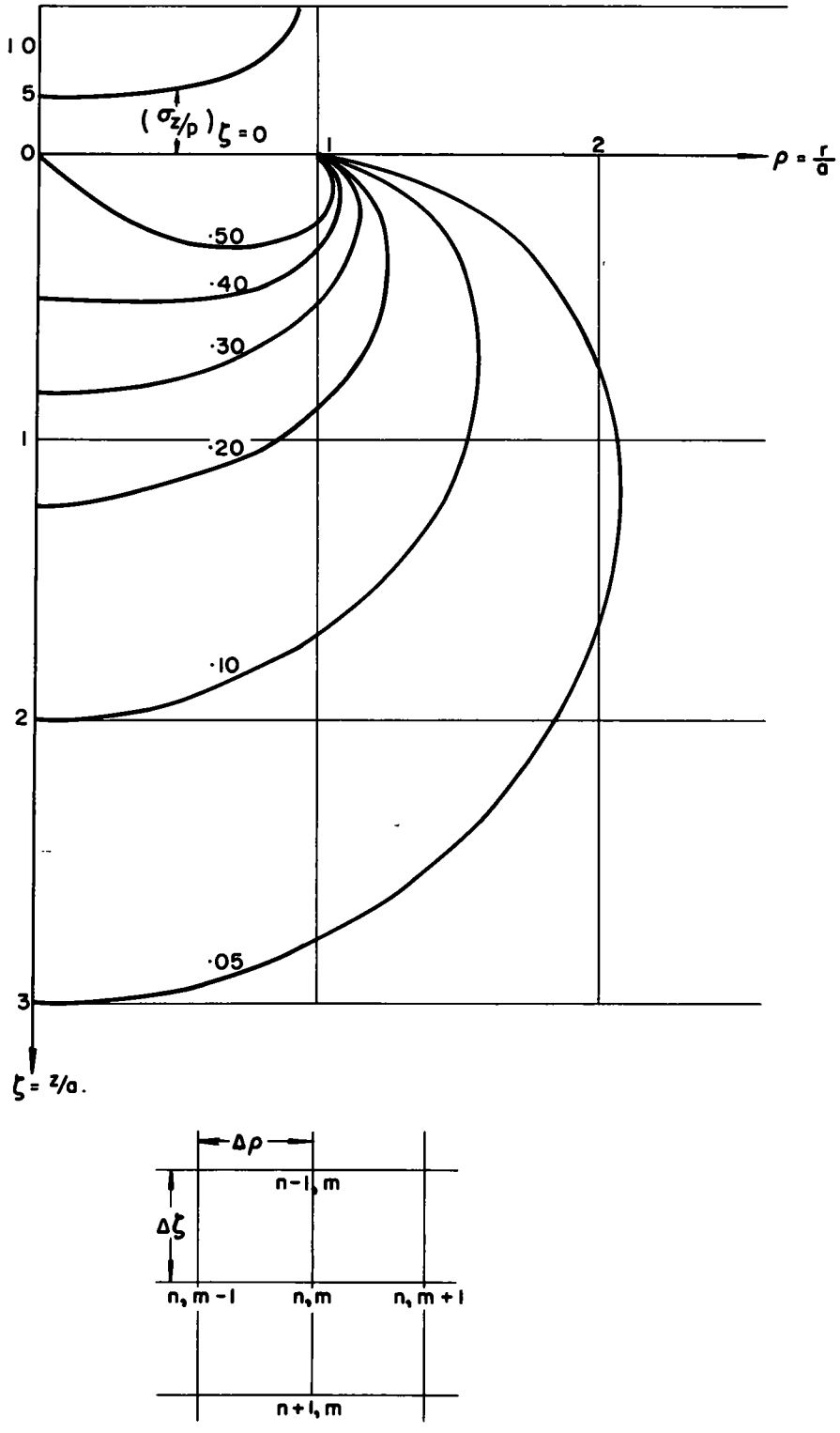

Figure 12. Initial distribution of pore pressure $\frac{\sigma}{\rho}$ under a circular punch.

Then, at the instant of application of P and before there is any time for drainage to take place, the Poisson's ratio $\nu = \frac{1}{2}$ and the initial distribution of pore pressure σ_0/p is shown in Figure 12 by equipotential contours.

At this point it may be assumed that most of the shear settlement w_τ takes place and, from Eq. 14 and 16

$$w_\tau = \frac{ap}{4G} \int_0^\infty \zeta J_2^0 \, d\zeta \tag{18a}$$

or

$$w_\tau = \frac{1}{8G} \cdot \frac{\rho}{a} \quad \text{if } \rho = r = 0 \tag{18b}$$

Eq. 18b gives the shear settlement down the axis of symmetry (which must be the same for the whole rigid footing). This is the so-called "elastic settlement."

Again from Eqs. 14 and 15, the ultimate settlement under the footing due to consolidation is given by

$$w_c = \frac{(1+\nu)ap}{9B} \int_0^\infty J_1^0 \, d\zeta \tag{19a}$$

$$= \frac{(1+\nu)}{18B} \cdot \frac{\rho}{a} \quad \text{if } \rho = r = 0 \tag{19b}$$

which implies that, in general, this settlement is less than the instantaneous elastic settlement caused by shear. The conclusion has been anticipated by de Josselin de Jong (12), who found a solution of Biot's equation for a uniformly loaded circular area. In the same reference, de Josselin de Jong showed that the retardation of compressive strain by the enclosed water had no great influence on the way in which the superfluous water could escape; i.e., whether the base of the footing was impervious.

A numerical solution was found for the three-dimensional consolidation equation subject to the initial condition (Eq. 15) and the boundary condition $\frac{\partial \sigma}{\partial \zeta} = 0, \; -1 \le \rho \le 1$, corresponding to an impervious base. Use was made of the finite difference approximation for radial symmetry suggested by Hart et al. (13) of the equation $c_v V^2 \sigma = \partial \sigma / \partial t$ which becomes

$$\sigma_{n,m}(T + \Delta T) = \tfrac{1}{4}\left[\left(1 - \frac{1}{2m}\right) \sigma_{n,m-1} + \sigma_{n+1,m} + \left(1 + \frac{1}{2m}\right)\sigma_{n,m+1} + \sigma_{n-1,m}\right] \tag{20}$$

The integers n, m refer to nodal points on a grid with equal spacing $\Delta\rho = \Delta\zeta = \Delta$ (see Fig. 12); that is, the coordinates ρ and ζ of the point n, m are $\rho = m\Delta\rho$; $\zeta = n\Delta\zeta$. T is a time factor numerically equal to $c_v t$, and $\frac{\Delta T}{\Delta^2}$ was chosen as $\frac{1}{4}$. This means that if a distance of 0.20 was chosen in the grid, ΔT would equal 0.01, so that over one hundred time increments had to be used before the pressure under the center fell to less than one-tenth of its initial value.

To study the pore pressure configurations as consolidation proceeded, the total dimensions of the grid were $\rho = 14\Delta$ and $\zeta = 18\Delta$ (= 0.20). This meant that almost 300 stresses were evaluated for each time increment and, because the foundation was considered semi-infinite, the stress values around the edges had to be determined by using the previous stresses and assuming a linear change over $\Delta\rho$ and $\Delta\zeta$. All of this work was done on a Stantec ZEBRA computer. Also, in the case of anisotrophy the coordinate ρ must be replaced by $\sqrt{\frac{c_v}{c_r}}\,\rho$, where c_v and c_r are the coefficients of consolidation in the vertical and radial directions respectively, but the same solution may be used.

The pore water pressures fall very rapidly near the edges of the footing as shown by the contours of equal pressure, in Figure 13, corresponding to a degree of consolidation U = 0.05. This is a great advantage for the stability of the footing, because the

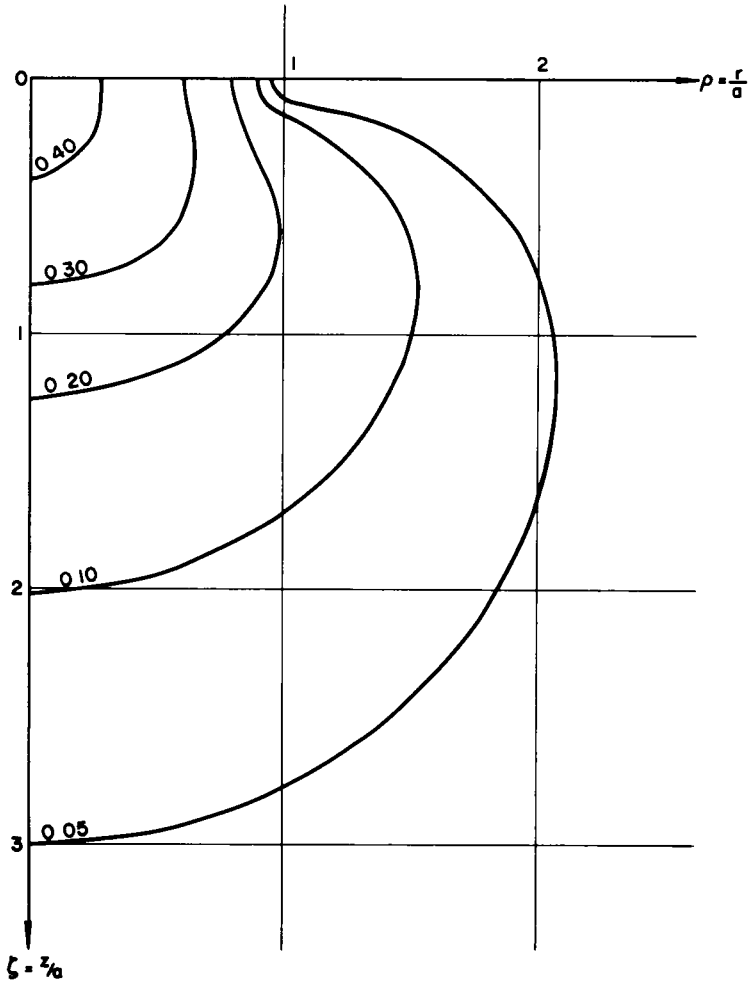

Figure 13. Pore pressures $\frac{\sigma}{\rho}$ at 5 percent consolidation.

the shearing stresses are greatest in this region (Fig. 14) and a fall in pressure means a decrease in volume and therefore a strength increase.

The stresses shown in Figure 14 are the complementary stresses to the pore pressure σ; that is, they are the shearing stresses acting on the same planes as the normal stress σ_G. These are the eight octahedral planes at 45° to the three principal planes. The octahedral shearing stress τ_G is very nearly equal to the maximum shearing stress τ_m and may be found from a three-dimensional Mohr circle (14). It is proportional to the second invariant of the deviator stress tensor J_2^1; i.e.,

$$\tau_G = (\tfrac{2}{3} J_2^1)^{1/2} \tag{21a}$$

$$= \sqrt{\tfrac{2}{3}} \left\{ \tfrac{1}{6} \left[(\sigma_x - \sigma_y)^2 + (\sigma_y - \sigma_z)^2 + (\sigma_z - \sigma_y)^2 \right] + \tau_{xy}^2 + \tau_{yz}^2 + \tau_{zx}^2 \right\}^{1/2} \tag{21b}$$

$$= \tfrac{1}{3} \left[(\sigma_1 - \sigma_2)^2 + (\sigma_2 - \sigma_3)^2 + (\sigma_3 - \sigma_1)^2 \right]^{1/2} \tag{21c}$$

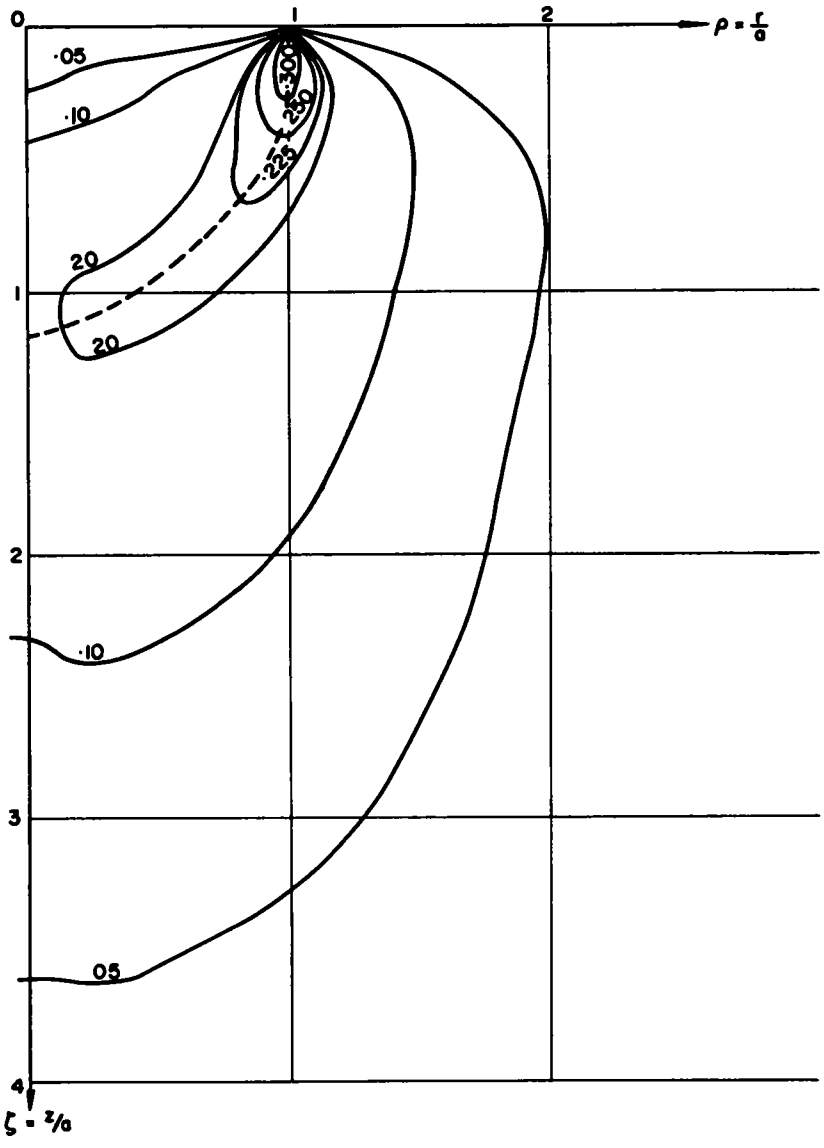

Figure 14. Octahedral shear stresses τ_G/p for $\upsilon = \frac{1}{2}$ under a circular punch.

if σ_1, σ_2, σ_3, are principal stresses. It has been shown that τ_G is the radius of the Mohr circle in a three-dimensional theory of failure (16).

According to this theory, which is an extension of the conventional Mohr Coulomb hypothesis, a fall in pressure of $\Delta\sigma_0$ is equivalent to a strength increase

$$\Delta\tau_G = \Delta\sigma_0 \sin\phi \tag{22}$$

in which ϕ is the central angle of the failure cone and is equal to about 20° for a Poisson's ratio of just over 0.40.

Figure 15 illustrates how the pore pressure falls with time for a column of soil below a footing edge (assuming that drainage is free at the edge). It is apparent that, by the time the soil is 5 percent consolidated (T = 0.10), there has been such a strength

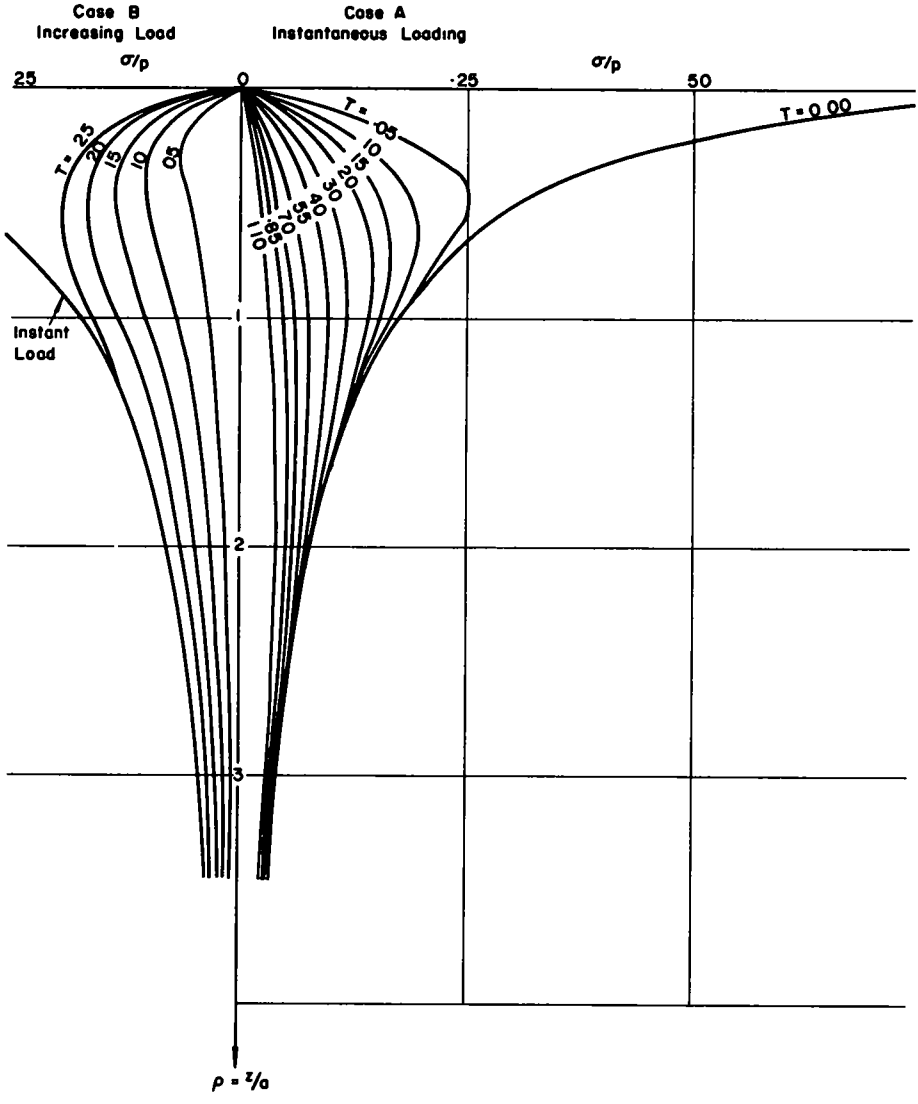

Figure 15. Isochrones under the footing edge.

increase in the regions of high shear ($\tau_G/p > 0.20$) immediately below the edge, that it is safe to say that the foundation will not fail in shear if it has been designed for a shear stress no greater than $\tau_G/p > 0.20$. Referring to Figures 12, 13, and 14, the roughly hemispherical basin-shaped surface on which τ_G/p reaches its maximum values coincides very closely with the surface on which σ/p also has a value of 0.20.

This important result is also true for a uniformly loaded circular area (p = constant) which corresponds to the flexible circular footing as distinct from the rigid footing where the unit load $(\sigma_z)_{z=0}$ is not constant but increases to infinity at the edges according to a parabolic law (see Fig. 12):

$$(\sigma_z)_{z=0} = -\frac{P}{2}\left(\frac{1}{1-\rho^2}\right)^{1/2}; \quad 0 < \rho < 1 \qquad (23)$$

The stress distributions caused by uniformly loaded areas on a semi-infinite medium were thoroughly investigated by Love (15) in 1929, and, in the case of the circular area,

the surface of maximum shear ($\tau m/p = 0.30$) coincides approximately with the surface where $\sigma/p = 0.40$, which is an oblate spheroid intersecting the axis of symmetry at $\zeta = 0.75$. For the uniformly loaded long wall, the two-dimensional case, the values $\tau m/p = 1/\pi$ and the values $\sigma/p = 0.500$ coincide exactly on the cylindrical surface with a diameter coincident with the base of the footing and intersecting the axis of symmetry at $\zeta = 1.00$ which is seen to be the most dangerous of all. It is, of course, considerably easier to find the countours of equal pore pressure (isochrones) than the contours where the shearing stress is a maximum.

In practice, the whole load $P = \pi a^2 p$ will not be applied at once, but in steps over the construction period. If a coefficient of consolidation indicated by Figure 9 is assumed, then, using Eq. 5, c_v for Ball clay $= 25 \times 10^{-4}$ in. per min $= 25 \times 10^{-3}$ sq ft per day is which is approximately the value Taylor gives for a Chicago clay (6, ch. 10). If one now imagines a circular footing of 10-ft diameter, the distance Δ between nodal points will be 0.20×5, or 1 ft, so that, because $c_v \Delta t/\Delta^2 = 1/4$, $\Delta t = 10$ days, which is the time corresponding to each computed time increment ΔT. Therefore, a construction period of 250 days will equal a value of 25 ΔT, or $T = 0.25$; that is, a degree of consolidation of about 25 percent if all of the load had been applied at once (see Fig. 16). Under these assumptions, less than one-half of the shearing load would have been applied at $T = 0.10$, but there would have still been considerable consolidation near the footing edge so that the foundation becomes even more stable (see Fig. 15).

In Figure 16, the pressures under the center of the punch have been plotted for various values of T. Because the settlement must await flow from the central regions, the degree of consolidation U at a given T could be evaluated from the area between the pressure curve for T and that for T = 0. The resulting functional relation is also shown in Figure 16 by curve A. Near the edges there is at first a much greater volume change but most of this is in the radial direction. It is only in the later stages of consolidation, when the pressure gradients are very small (as exemplified by Fig. 17), that the vertical unit strain ϵ_z will become approximately equal to $\epsilon/3$. This stage again approaches the elastic condition

$$\nabla z \, \epsilon = 0 \tag{24a}$$

$$\epsilon = \frac{\sigma_0}{B} \tag{24b}$$

which is the correct solution of Eq. 11 except that there has been a delay before the establishment of ϵ. Owing to the small gradients after 60 percent consolidation (Fig. 17), the rate of settlement becomes progressively slower and will probably follow an asymptotic relation, like the one sketched by de Josselin de Jong (12) for the settlement of the center of a flexible circular footing.

RIGID CIRCULAR FOOTING UNDER A VARIABLE LOAD

Next, a case coming nearer to practice, is considered in which the load is applied in 5 steps of p/5 over a construction period of 250 days ($T = 0.25$), such that these steps approximate a linear loading (see Fig. 16). The pore pressures under the footing can readily be obtained from the solution for an instantaneous loading of $p = \frac{P}{\pi a^2}$ by using simple superposition; that is, the pressure at any time T due to the previously applied loads is equal to the simple summation of the pressures that would have been observed at that instant (T) had each of the loads been applied independently. Mathematically, this can be expressed by writing (T - t) for T if T = t is the time at which a given load is applied; thus for this case if (T - t) is positive, then

$$\sigma(T) = \frac{p}{5}\left[\sigma(T - 0.05) + \sigma(T - 0.10) + \sigma(T - 0.15) + \sigma(T - 0.20) + \sigma(T - 0.25)\right] \tag{25}$$

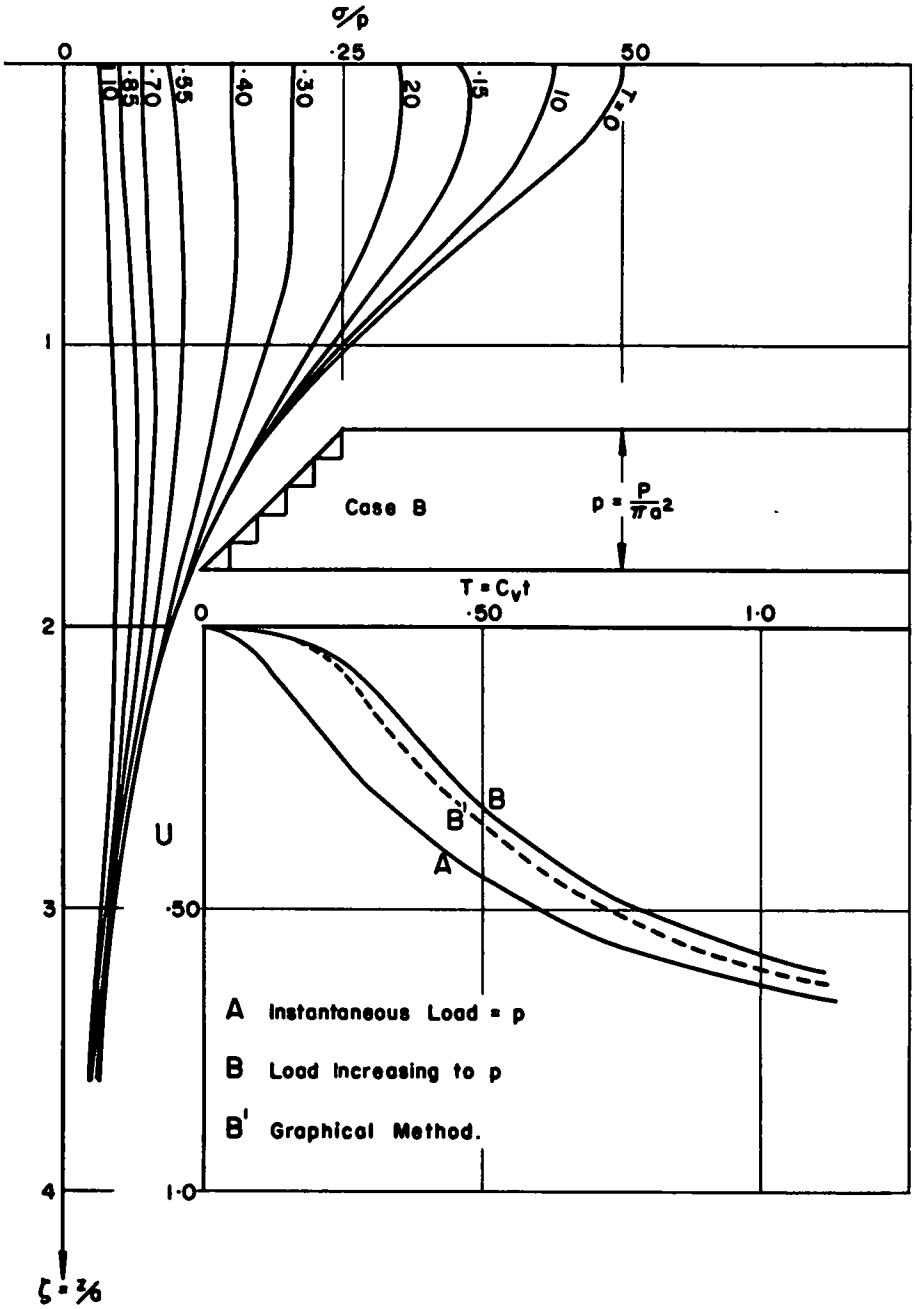

Figure 16. Isochrones on the axis of symmetry for instantaneous loading.

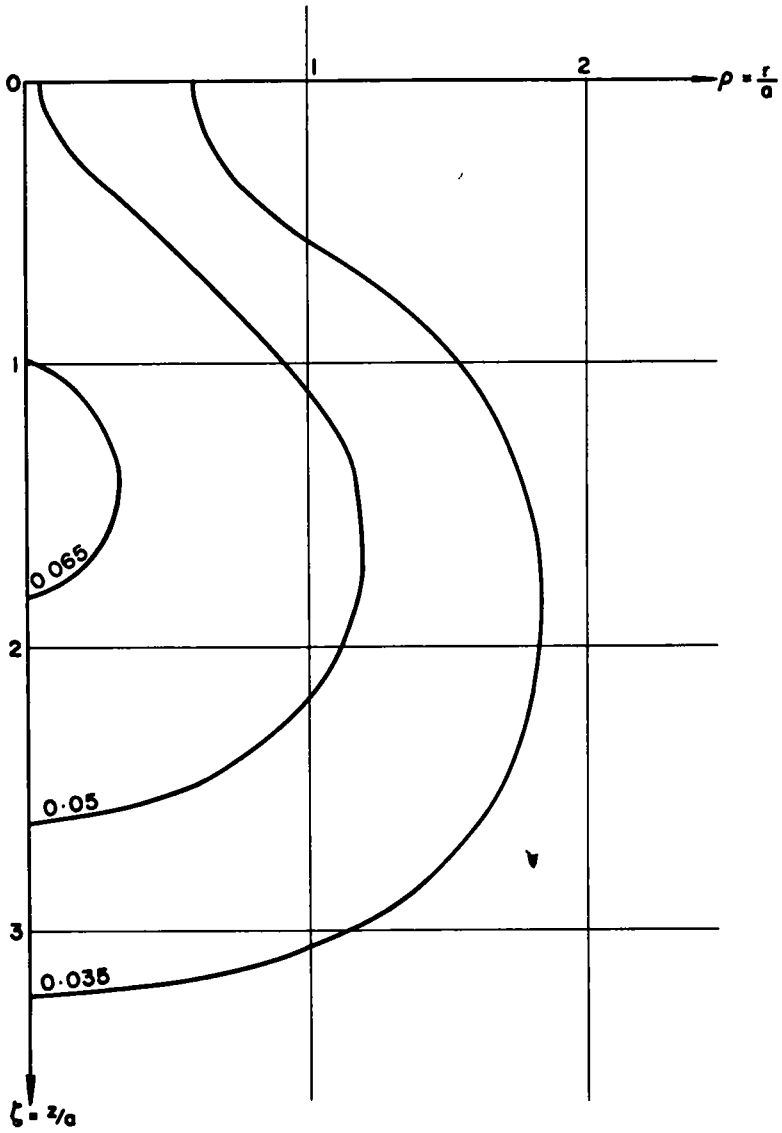

Figure 17. Pore pressures $\frac{\sigma}{p}$ at 60 percent consolidation.

at any point of the grid under the footing. (During the actual loading period, negative values of T - t_i are taken as zero because the loads at t_i have not yet been applied.)

Values of σ were computed using Eq. 25 under the center of the footing as well as under an edge, and the results plotted in Figure 18 and on the right-hand side of Figure 15. It is apparent that there will be greater stability as can be appreciated by comparing the pore pressure distribution at T = 0.25 corresponding to full loading in case B with the curve at T = 0.00 giving full load for case A (see Fig. 15). The difference is a measure of the degree of consolidation U_E which is particularly significant in the region of high shear stress shown by Figure 14 (numerically, U_E = 36 percent).

Again, from a comparison of Figures 16 and 18 it is apparent that the region most affected by the varying load is that at low depths. The time consolidation curve computed from the areas given by Figure 18 is shown in Figure 16 (curve B) and is seen to agree closely with a graphical determination derived from the instantaneous curve by the method outlined by Taylor (6, p. 290) which is shown dotted (curve B).

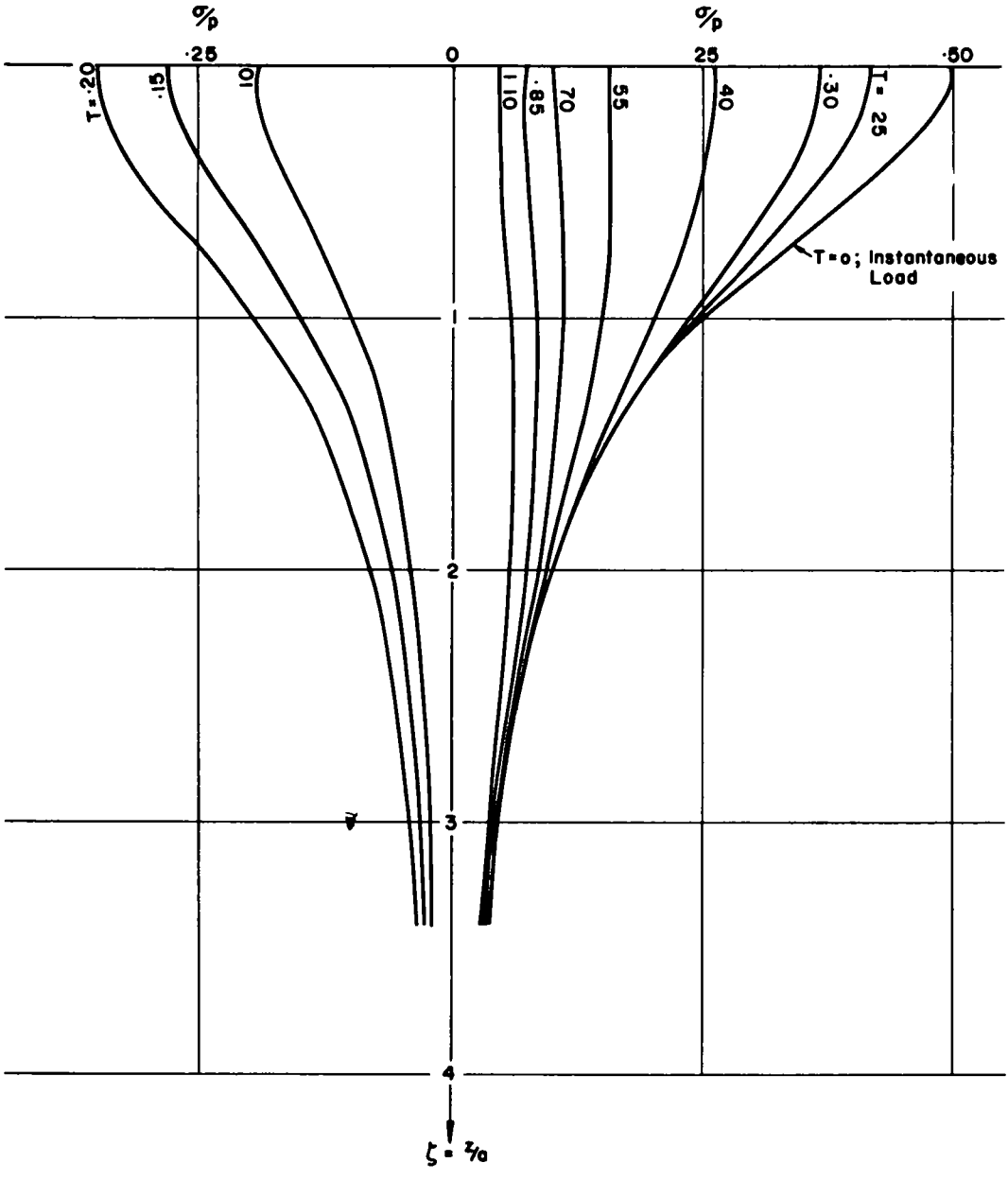

Figure 18. Isochrones on the axis of symmetry for a linearly increasing load.

CONCLUSION

At least one-half of the settlement of a footing is the so-called "elastic" or immediate settlement caused by shearing stresses, so that the actual shape of the time settlement curve due to consolidation is not of great importance when compared with the ultimate settlement that may be encountered after long periods. The estimation of this important quantity depends on sampling and testing procedures and Figure 10 may give a clue to a possible source of error. Tests 4 and 5 correspond to a rebound where the sample was allowed to absorb water in an attempt to copy natural conditions after an alleviation of pressure—this was also the case for test 9. However, during the second rebound

(test 10), the sample expanded in the absence of water as could possibly occur with a sampling technique. It is significant that the slopes of the recompression curves vary considerably. Tests 6, 7, and 8 tend to follow the rebound lines 4, 5, and 9, and 11, 12, and 13 fall far higher. In particular, the slope of 13 is 1½ times greater than that of test 8 which measures the true compressibility of the clay.

ACKNOWLEDGMENT

The author owes a substantial debt to the Department of Mathematical Analysis at the National Physical Research Laboratory, in particular to C. Cryer, who helped with the analysis and made important suggestions, and to J. Neetling for his aid in programing the consolidation problem for the computer. Also, P. Hall rendered valuable assistance in the computational work.

REFERENCES

1. Biot, M. A., "General Theory of Three-Dimensional Consolidation." J. Appl. Phys., 12:155 (1941).
2. Terzaghi, K., "Theoretical Soil Mechanics." Wiley (1943).
3. Schiffman, R. L., "Consolidation of Soil Under Time-Dependent Loading and Varying Permeability." HRB Proc., 37: 584-617 (1958).
4. Croney, D., Coleman, J. D., and Black, W. P. M., "Movement and Distribution of Water in Soil in Relation to Highway Design and Performance." HRB Special Report 40, 226-252 (1958).
5. McNabb, A., "A Mathematical Treatment of One-Dimensional Soil Consolidation." Quart. Appl. Math., Vol. 17, (Jan. 4, 1960).
6. Taylor, D. W., "Fundamentals of Soil Mechanics." Wiley (1948).
7. Crank, J., "Mathematics of Diffusion." Oxford (1956).
8. Timoshenko, S., "Theory of Elasticity." McGraw-Hill (1934).
9. Skempton, A. W., and Bjerrum, L., "A Contribution to the Settlement Analysis of Foundations on Clay." Geotechnique. 7: 4 (1957).
10. Cooling, L. F., "The Measurement of Pore-Water Pressure and Its Application to Some Engineering Soil Problems." R.I.L.E.M. Paper 18, Theme 1a, Symposium sur les Observations des Ourvrages Realises au Laboratorio Nacional de Engenheria Civil, Lisbon (Oct. 1955).
11. Sneddon, I. N., "Fourier Transforms." McGraw-Hill (1951).
12. de Josselin de Jong, G., "Application of Stress Functions to Consolidation Problems." Proc., 4th Internat. Conf. on Soil Mechanics and Found. Eng., 1: 320-323 (1957).
13. Hart, E. G., Kondner, R. L., and Boyer, W. C., "Analysis for partially Penetrating Sand Drains." Proc. Amer. Soc. Civ. Engrs., 84: S.M. 4 (Oct. 1958).
14. Seely, F. B., and Smith. J. O., "Advanced Mechanics of Materials." Wiley (1952).
15. Love, A. E. H., "The Stress Produced in a Semi-Infinite Solid by Pressure on Part of the Boundary." Phil. Trans., Series A, Vol. 228 (1929).
16. de Wet, J. A., "The Use of the Energy Concept in Soil Mechanics." Proc., 5th Internat. Conf. on Soil Mechanics and Found. Eng., 1: 403-407 (1961).

Tables of Stresses in Three-Layer Elastic Systems

A. JONES, "Shell" Research Ltd., Thornton Research Centre, Chester, England

The tables of values of stresses arising in a three-layer elastic system loaded over a circular area, published by Acum and Fox, have been extended to cover a wider range of parameters. Values of the vertical stresses at both interfaces are given, and are accurate to within 1 percent. The calculations were performed on the Ferranti Mark I* computer at Koninklijke/Shell Laboratorium, Amsterdam.

The work forms part of a program for the development of a method for the design of flexible roads.

•IN GENERAL, road design involves the determination of the thicknesses and elasticities of the various layers in the road structure to insure that the stresses and strains developed are within permissible limits. The present analysis assumes that the design is based on a knowledge of the stresses at the interfaces between the layers on the axis of symmetry below a circular loaded area.

The first analysis to take into account the different elastic properties of the various layers was given by Burmister (1) in 1943. In a series of subsequent papers (2) he derived expressions for the stresses and displacement in two- and three-layer systems. However, he did not publish any stress values and only a small number of values of the surface deflection at the centre of the loaded area for a two-layer system. Fox (3) produced extensive tables of stresses in two-layer systems in 1948, and in 1951 Acum and Fox (4) produced tables for the normal and radial stresses in three-layer systems at the intersections of the axis of symmetry with the interfaces. The tables in this paper form an extension, to a much wider range of the parameters, of those of Acum and Fox. (Stress and displacement values for one given system were published by Schiffman (5) in 1957).

The road system considered in this paper consists of three layers, as in Figure 1. The stresses that have been computed are listed in Table 1, where the numerical subscripts refer to the layer.

Throughout the tables it is assumed that Poisson's ratio is equal to 0.5 and that there is full friction at the interfaces. For convenience, the stresses are printed on the assumption that compression stress is positive.

Values of these stresses are given in Appendix A for all combinations of the following parameter values:

$E_1/E_2 = k_1 = 0.2, 2.0, 20.0, 200.0$
$E_2/E_3 = k_2 = 0.2, 2.0, 20.0, 200.0$
$a/h_2 = a_1 = 0.1, 0.2, 0.4, 0.8, 1.6, 3.2$
$h_1/h_2 = H = 0.125, 0.25, 0.5, 1.0, 2.0, 4.0, 8.0$

Each stress value is expressed as a fraction of the applied load. Stresses for all values of a_1 appear in a block and the blocks are arranged in groups of four in ascending order of k_2; these groups are arranged in order of k_1 and finally in sets in order of H.

The calculations were performed on the Ferranti Mark 1* computer at Koninklijke/Shell Laboratorium, Amsterdam. The machine program was written to calculate 36 stress values at the same time; viz., 6 stresses for each of 6 values of a_1. The infinite range of integration (see Appendix B) was truncated at such a point that the contribution from the omitted portion was negligible. The finite part of the range was then split into a number of equal intervals and the integrals were then evaluated over each interval

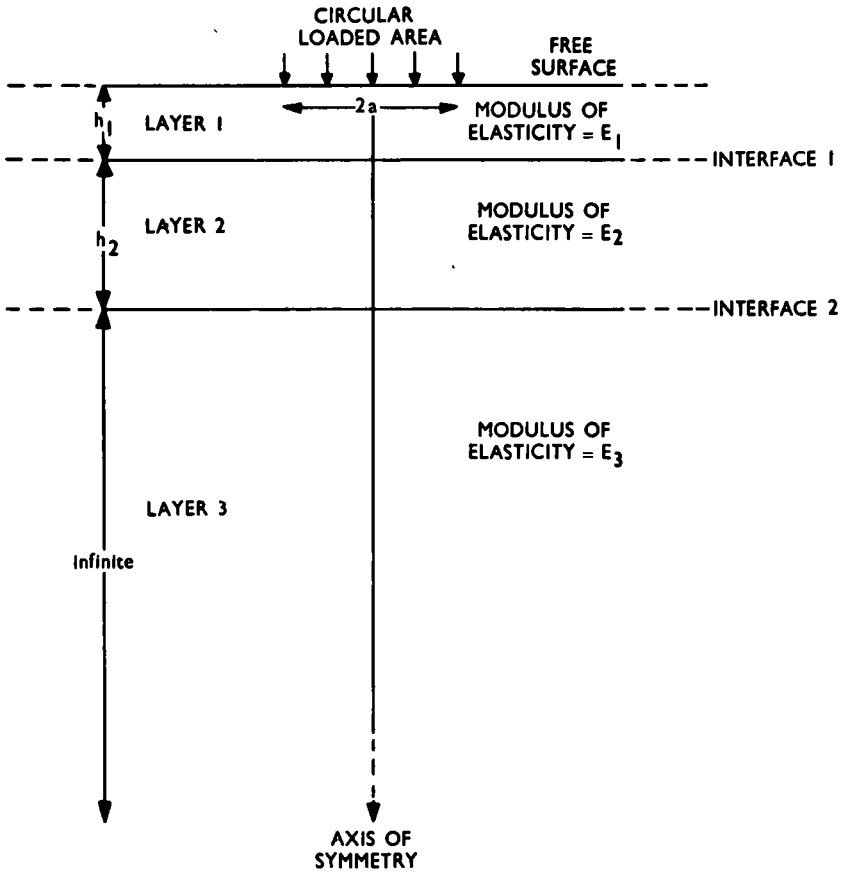

Figure 1. Structure of layered system.

TABLE 1

NOTATION FOR STRESSES GIVEN IN APPENDIX A

Stress	First Interface	Second Interface
Vertical	σ_{z_1}	σ_{z_2}
Vertical and radial (upper layer)	$\sigma_{z_1} - \sigma_{r_1}$	$\sigma_{z_2} - \sigma_{r_2}$
Vertical and radial (lower layer)	$\sigma_{z_1} - \sigma_{r_2}$	$\sigma_{z_2} - \sigma_{r_3}$

separately using a Gauss quadrature formula. Some difficulty was encountered near the origin due to the fact that the integrand had an essential singularity on the negative real axis, this was overcome by subdividing the first interval.

The following checks (which are perfect apart from a constant factor) were built into the computer program.

$$\sigma_{z_1} - \sigma_{r_1} = k_1 (\sigma_{z_1} - \sigma_{r_2}) \quad \text{(first interface)}$$

$$\sigma_{z_2} - \sigma_{r_2} = k_2 (\sigma_{z_2} - \sigma_{r_3}) \quad \text{(second interface)}$$

In most cases the two sides of these equations agreed to five significant digits but where this was not so the disagreement was still less than 1 percent. All numbers in the tables, however, are correct only to within one digit in the last decimal place printed.

As a further check some results were obtained for comparison with those of Acum and Fox. These are presented in Appendix C with the corresponding values from Acum and Fox's paper in brackets.

A typographical error was found in the published solution of Acum and Fox and was corrected before the tables were calculated.

A brief mathematical description of the problem is given in Appendix B, together with some notes on the assumptions involved in setting up the problem and the correct expressions for the stresses.

ACKNOWLEDGMENTS

The author wishes to record his gratitude for the assistance given by his colleagues in the production of the tables. He also wishes to thank the Management of Koninklijke/Shell Laboratorium for the use of the computer, and the Directors of "Shell" Research Limited for permission to publish this paper.

REFERENCES

1. Burmister, D. M., "The Theory of Stresses and Displacements in Layer Systems and Applications to Design of Airport Runways." HRB Proc., 23: 126-149 (1943). Discussion, pp. 144-148.
2. Burmister, D. M., "The General Theory of Stresses and Displacements in Layered Systems." J. Appl. Phys., 16: No. 2, pp. 89-96; No. 3, pp. 126-127; No. 5, pp. 296-302 (1945).
3. Fox, L., "Computation of Traffic Stresses in a Simple Road Structure." Department of Scientific and Industrial Research, Road Res. Tech. Paper 9 (1948).
4. Acum, W. E. A., and Fox, L., "Computation of Load Stresses in a Three-Layer Elastic System." Geotechnique, 2: 293-300 (1951).
5. Schiffman, R. L., Proc. 4th Internat. Conf. on Soil Mechanics and Foundation Engineering, London (1957).
6. Sneddon, I. N., "Fourier Transforms." McGraw-Hill (1951).

Appendix A

$H = 0.125$

$k_1 = 0.2$

a_1	σ_{z_1}	$\sigma_{z_1}-\sigma_{r_1}$	$\sigma_{z_1}-\sigma_r$	σ_{z_2}	$\sigma_{z_2}-\sigma_{r_2}$	$\sigma_{z_2}-\sigma_{r_3}$
						$k_2 = 0.2$
0.1	0.66045	0.12438	0.62188	0.01557	0.00332	0.01659
0.2	0.90249	0.13546	0.67728	0.06027	0.01278	0.06391
0.4	0.95295	0.10428	0.52141	0.21282	0.04430	0.22150
0.8	0.99520	0.09011	0.45053	0.56395	0.10975	0.54877
1.6	1.00064	0.08777	0.43884	0.86253	0.13755	0.68777
3.2	0.99970	0.04129	0.20643	0.94143	0.10147	0.50736
						$k_2 = 2.0$
0.1	0.66048	0.12285	0.61424	0.00892	0.01693	0.00846
0.2	0.90157	0.12916	0.64582	0.03480	0.06558	0.03279
0.4	0.95120	0.08115	0.40576	0.12656	0.23257	0.11629
0.8	0.99235	0.01823	0.09113	0.37307	0.62863	0.31432
1.6	0.99918	-0.04136	-0.20680	0.74038	0.98754	0.49377
3.2	1.00032	-0.03804	-0.19075	0.97137	0.82102	0.41051
						$k_2 = 20.0$
0.1	0.66235	0.12032	0.60161	0.00256	0.03667	0.00183
0.2	0.90415	0.11787	0.58933	0.01011	0.14336	0.00717
0.4	0.95135	0.03474	0.17370	0.03838	0.52691	0.02635
0.8	0.98778	-0.14872	-0.74358	0.13049	1.61727	0.03086
1.6	0.99407	-0.50533	-2.52650	0.36442	3.58944	0.17947
3.2	0.99821	-0.80990	-4.05023	0.76669	5.15409	0.25770
						$k_2 = 200.0$
0.1	0.66266	0.11720	0.58599	0.00057	0.05413	0.00027
0.2	0.90370	0.10495	0.52477	0.00226	0.21314	0.00107
0.4	0.94719	-0.01709	-0.08543	0.00881	0.30400	0.00402
0.8	0.99105	-0.34427	-1.72134	0.03259	2.67934	0.01340
1.6	0.99146	-1.21129	-6.05643	0.11034	7.35978	0.03680
3.2	0.99332	-2.89282	-14.46408	0.32659	16.22830	0.08114

H = 0.125

k_1 = 2.0

a_1	σ_{z_1}	$\sigma_{z_1}-\sigma_{r_2}$	$\sigma_{z_1}-\sigma_{r_2}$	σ_{z_2}	$\sigma_{z_2}-\sigma_{r_2}$	$\sigma_{z_2}-\sigma_{r_3}$
						k_2 = 0.2
0.1	0.43055	0.71614	0.35807	0.01682	0.00350	0.01750
0.2	0.78688	1.01561	0.50780	0.06511	0.01348	0.06741
0.4	0.98760	0.83924	0.41962	0.23005	0.04669	0.23346
0.8	1.01028	0.63961	0.31981	0.60886	0.11484	0.57418
1.6	1.00647	0.65723	0.32862	0.90959	0.13726	0.68630
3.2	0.99822	0.38165	0.19093	0.94322	0.09467	0.47335
						k_2 = 2.0
0.1	0.42950	0.70622	0.35303	0.00896	0.01716	0.00858
0.2	0.78424	0.97956	0.48989	0.03493	0.06647	0.03324
0.4	0.98044	0.70970	0.35483	0.12667	0.23531	0.11766
0.8	0.99434	0.22319	0.11164	0.36932	0.63003	0.31501
1.6	0.99364	− 0.19982	− 0.09995	0.72113	0.97707	0.48853
3.2	0.99922	− 0.28916	− 0.14461	0.96148	0.84030	0.42015
						k_2 = 20.0
0.1	0.43022	0.69332	0.34662	0.00228	0.03467	0.00173
0.2	0.73414	0.92096	0.46048	0.00899	0.13541	0.00677
0.4	0.97493	0.46583	0.23297	0.03392	0.49523	0.02476
0.8	0.97806	− 0.66535	− 0.33270	0.11350	1.49612	0.07481
1.6	0.96921	− 2.82859	− 1.41430	0.31263	3.28512	0.16426
3.2	0.98591	− 5.27906	− 2.63954	0.68433	5.05952	0.25298
						k_2 = 200.0
0.1	0.42925	0.67488	0.33744	0.00046	0.04843	0.00024
0.2	0.78267	0.85397	0.42698	0.00183	0.19043	0.00095
0.4	0.97369	0.21165	0.10582	0.00711	0.71221	0.00356
0.8	0.97295	− 1.65954	− 0.82977	0.02597	2.32652	0.01163
1.6	0.95546	− 6.47707	− 3.23855	0.08700	6.26638	0.03133
3.2	0.96377	−16.67376	− 8.33691	0.26292	14.25621	0.07128

H = 0.125

k_1 = 20.0

a_1	σ_{z_1}	$\sigma_{z_1}-\sigma_{r_1}$	$\sigma_{z_1}-\sigma_{r_2}$	σ_{z_2}	$\sigma_{z_2}-\sigma_{r_2}$	$\sigma_{z_2}-\sigma_{r_3}$
						k_2 = 0.2
0.1	0.14648	1.80805	0.09040	0.01645	0.00322	0.01611
0.2	0.39260	3.75440	0.18772	0.06407	0.01249	0.06244
0.4	0.80302	5.11847	0.25592	0.23135	0.04421	0.22105
0.8	1.06594	3.33600	0.16930	0.64741	0.11468	0.57342
1.6	1.02942	1.81603	0.09080	1.00911	0.13687	0.68436
3.2	0.99817	1.75101	0.08756	0.97317	0.07578	0.37890
						k_2 = 2.0
0.1	0.14529	1.81178	0.09059	0.00810	0.01542	0.00771
0.2	0.38799	3.76886	0.18844	0.03170	0.06003	0.03002
0.4	0.78651	5.16717	0.25836	0.11650	0.21640	0.10820
0.8	1.02218	3.43631	0.17182	0.34941	0.60493	0.30247
1.6	0.99060	1.15211	0.05761	0.69014	0.97146	0.48573
3.2	0.99393	- 0.06894	- 0.00345	0.93487	0.88358	0.44179
						k_2 = 20.0
0.1	0.14447	1.80664	0.09033	0.00182	0.02985	0.00149
0.2	0.38469	3.74573	0.18729	0.00716	0.11697	0.00585
0.4	0.77394	5.05489	0.25274	0.02710	0.43263	0.02163
0.8	0.98610	2.92533	0.14627	0.09061	1.33736	0.06687
1.6	0.93712	- 1.27093	- 0.06355	0.24528	2.99215	0.14961
3.2	0.96330	- 7.35384	- 0.36761	0.55490	5.06489	0.25324
						k_2 = 200.0
0.1	0.14422	1.78941	0.08947	0.00033	0.04010	0.00020
0.2	0.38388	3.68097	0.18405	0.00131	0.15781	0.00079
0.4	0.77131	4.80711	0.24036	0.00505	0.59391	0.00297
0.8	0.97701	1.90825	0.09541	0.01830	1.95709	0.00979
1.6	0.91645	- 5.28803	- 0.26440	0.06007	5.25110	0.02626
3.2	0.92662	-21.52546	- 1.07627	0.18395	12.45058	0.06225

H = 0.125

k_1 = 200.0

a_1	σ_{z_1}	$\sigma_{z_1}-\sigma_{r_1}$	$\sigma_{z_1}-\sigma_{r_2}$	σ_{z_2}	$\sigma_{z_2}-\sigma_{r_2}$	$\sigma_{z_2}-\sigma_{r_3}$
						k_2 = 0.2
0.1	0.03694	2.87564	0.01438	0.01137	0.00201	0.01005
0.2	0.12327	7.44285	0.03721	0.04473	0.00788	0.03940
0.4	0.36329	15.41021	0.07705	0.16785	0.02913	0.14566
0.8	0.82050	19.70261	0.09851	0.53144	0.08714	0.43568
1.6	1.12440	7.02380	0.03512	1.03707	0.13705	0.68524
3.2	0.99506	2.35459	0.01177	1.00400	0.06594	0.32971
						k_2 = 2.0
0.1	0.03481	3.02259	0.01511	0.00549	0.00969	0.00485
0.2	0.11491	8.02452	0.04012	0.02167	0.03812	0.01906
0.4	0.33218	17.64175	0.08821	0.08229	0.14286	0.07143
0.8	0.72695	27.27701	0.13639	0.27307	0.45208	0.22604
1.6	1.00203	23.38638	0.11693	0.63916	0.90361	0.45430
3.2	1.00828	11.87014	0.05935	0.92560	0.91469	0.45735
						k_2 = 20.0
0.1	0.03336	3.17763	0.01589	0.00123	0.01980	0.00099
0.2	0.10928	8.66097	0.04330	0.00509	0.07827	0.00391
0.4	0.31094	20.12259	0.10061	0.01972	0.29837	0.01494
0.8	0.65934	36.29943	0.18150	0.07045	1.01694	0.05085
1.6	0.87931	49.40857	0.24704	0.20963	2.64313	0.13216
3.2	0.93309	57.84369	0.28923	0.49938	4.89895	0.24495
						k_2 = 200.0
0.1	0.03307	3.26987	0.01635	0.00025	0.02809	0.00014
0.2	0.10810	9.02669	0.01513	0.00098	0.11136	0.00056
0.4	0.30639	21.56482	0.10782	0.00386	0.43035	0.00215
0.8	0.64383	41.39878	0.20949	0.01455	1.53070	0.00765
1.6	0.84110	69.63157	0.34816	0.05011	4.56707	0.02284
3.2	0.86807	120.95981	0.60481	0.15719	11.42045	0.05710

H = 0.25

k_1 = 0.2

a_1	σ_{z_1}	$\sigma_{z_1}-\sigma_{r_1}$	$\sigma_{z_1}-\sigma_{r_2}$	σ_{z_2}	$\sigma_{z_2}-\sigma_{r_2}$	$\sigma_{z_2}-\sigma_{r_3}$
						k_2 = 0.2
0.1	0.27115	0.05598	0.27990	0.01259	0.00274	0.01370
0.2	0.65109	0.12628	0.63138	0.04892	0.01060	0.05302
0.4	0.90404	0.14219	0.71096	0.17538	0.03744	0.18722
0.8	0.95559	0.12300	0.61499	0.48699	0.09839	0.49196
1.6	0.99703	0.10534	0.52669	0.81249	0.13917	0.69586
3.2	0.99927	0.05063	0.25317	0.92951	0.11114	0.55569
						k_2 = 2.0
0.1	0.27103	0.05477	0.27385	0.00739	0.01409	0.00704
0.2	0.66010	0.12136	0.60631	0.02893	0.05484	0.02742
0.4	0.90120	0.12390	0.61949	0.10664	0.19780	0.09890
0.8	0.94923	0.06482	0.32410	0.32617	0.56039	0.28019
1.6	0.99029	− 0.00519	− 0.02594	0.69047	0.96216	0.48108
3.2	1.00000	− 0.02216	− 0.11080	0.95608	0.87221	0.43610
						k_2 = 20.0
0.1	0.26945	0.05192	0.25960	0.00222	0.03116	0.00156
0.2	0.66161	0.11209	0.56045	0.00877	0.12227	0.00611
0.4	0.90102	0.08622	0.43111	0.03354	0.45504	0.02275
0.8	0.94012	− 0.07351	− 0.36756	0.11653	1.44285	0.07214
1.6	0.97277	− 0.40234	− 2.01169	0.33692	3.37001	0.16850
3.2	0.99075	− 0.71901	− 3.59542	0.73532	5.10060	0.25503
						k_2 = 200.0
0.1	0.27072	0.04956	0.24778	0.00051	0.04704	0.00024
0.2	0.65909	0.10066	0.50330	0.00202	0.18557	0.00093
0.4	0.89724	0.04243	0.21242	0.00791	0.70524	0.00353
0.8	0.93596	− 0.24071	− 1.20357	0.02961	2.40585	0.01203
1.6	0.96370	− 1.00743	− 5.03714	0.10193	6.82481	0.03412
3.2	0.97335	− 2.54264	−12.71320	0.30707	15.45931	0.07730

$H = 0.25$

$k_1 = 2.0$

a_1	σ_{z_1}	$\sigma_{z_1}-\sigma_{r_1}$	$\sigma_{z_1}-\sigma_{r_2}$	σ_{z_2}	$\sigma_{z_2}-\sigma_{r_2}$	$\sigma_{z_2}-\sigma_{r_3}$
						$k_2 = 0.2$
0.1	0.15577	0.28658	0.14329	0.01348	0.00277	0.01384
0.2	0.43310	0.72176	0.36088	0.05259	0.01075	0.05377
0.4	0.79551	1.03476	0.51738	0.19094	0.03842	0.19211
0.8	1.00871	0.88833	0.44416	0.54570	0.10337	0.51687
1.6	1.02425	0.66438	0.33219	0.90563	0.14102	0.70510
3.2	0.99617	0.41539	0.20773	0.93918	0.09804	0.49020
						$k_2 = 2.0$
0.1	0.15524	0.28362	0.14181	0.00710	0.01353	0.00677
0.2	0.42809	0.70225	0.35112	0.02783	0.05278	0.02639
0.4	0.77939	0.96634	0.48317	0.10306	0.19178	0.09589
0.8	0.96703	0.66885	0.33442	0.31771	0.55211	0.27605
1.6	0.98156	0.17331	0.08665	0.66753	0.95080	0.47540
3.2	0.99840	− 0.05691	− 0.02846	0.93798	0.89390	0.44695
						$k_2 = 20.0$
0.1	0.15436	0.27580	0.13790	0.00179	0.02728	0.00136
0.2	0.42462	0.67115	0.33557	0.00706	0.10710	0.00536
0.4	0.76647	0.84462	0.42231	0.02697	0.39919	0.01996
0.8	0.92757	0.21951	0.10976	0.09285	1.26565	0.06328
1.6	0.91393	− 1.22411	− 0.61205	0.26454	2.94860	0.14743
3.2	0.95243	− 3.04320	− 1.52160	0.60754	4.89878	0.24494
						$k_2 = 200.0$
0.1	0.15414	0.26776	0.13388	0.00036	0.03814	0.00019
0.2	0.42365	0.63873	0.31937	0.00143	0.15040	0.00075
0.4	0.76296	0.71620	0.35810	0.00557	0.57046	0.00285
0.8	0.91600	− 0.28250	− 0.14125	0.02064	1.92636	0.00963
1.6	0.88406	− 3.09856	− 1.54928	0.07014	5.35936	0.02680
3.2	0.89712	− 9.18214	− 4.59107	0.21692	12.64318	0.06322

H = 0.25

k_1 = 20.0

a_1	σ_{z_1}	$\sigma_{z_1}-\sigma_{r_1}$	$\sigma_{z_1}-\sigma_{r_2}$	σ_{z_2}	$\sigma_{z_2}-\sigma_{r_2}$	$\sigma_{z_2}-\sigma_{r_3}$
						k_2 = 0.2
0.1	0.04596	0.61450	0.03072	0.01107	0.00202	0.01011
0.2	0.15126	1.76675	0.08834	0.04357	0.00793	0.03964
0.4	0.41030	3.59650	0.17983	0.16337	0.02931	0.14653
0.8	0.85464	4.58845	0.22942	0.51644	0.08771	0.43854
1.6	1.12013	2.31165	0.11558	1.01061	0.14039	0.70194
3.2	0.99676	1.24415	0.06221	0.99168	0.07587	0.37934
						k_2 = 2.0
0.1	0.04381	0.63215	0.03162	0.00530	0.00962	0.00481
0.2	0.14282	1.83766	0.09188	0.02091	0.03781	0.01891
0.4	0.37882	3.86779	0.19339	0.07933	0.14159	0.07079
0.8	0.75904	5.50796	0.27540	0.26278	0.44710	0.22355
1.6	0.98743	4.24281	0.21213	0.61673	0.90115	0.45058
3.2	1.00064	1.97494	0.09876	0.91258	0.93254	0.46627
						k_2 = 20.0
0.1	0.04236	0.65003	0.03250	0.00123	0.01930	0.00096
0.2	0.13708	1.90693	0.09535	0.00488	0.07623	0.00381
0.4	0.35716	4.13976	0.20699	0.01388	0.29072	0.01454
0.8	0.68947	6.48948	0.32447	0.06741	0.98565	0.04928
1.6	0.85490	6.95639	0.34782	0.20115	2.55231	0.12762
3.2	0.90325	6.05854	0.30293	0.48647	4.76234	0.23812
						k_2 = 200.0
0.1	0.04204	0.65732	0.03287	0.00024	0.02711	0.00014
0.2	0.13584	1.93764	0.09638	0.00095	0.10741	0.00054
0.4	0.35237	4.26004	0.21300	0.00372	0.41459	0.00207
0.8	0.67286	6.94871	0.34743	0.01399	1.46947	0.00735
1.6	0.81223	8.55770	0.42789	0.04830	4.36521	0.02183
3.2	0.82390	10.63614	0.53181	0.15278	10.93570	0.05468

H = 0.25

k_1 = 200.0

a_1	σ_{z_1}	$\sigma_{z_1}-\sigma_{r_1}$	$\sigma_{z_1}-\sigma_{r_2}$	σ_{z_2}	$\sigma_{z_2}-\sigma_{r_2}$	$\sigma_{z_2}-\sigma_{r_3}$
						k_2 = 0.2
0.1	0.011139	0.866114	0.000433	0.005389	0.000090	0.004451
0.2	0.041180	2.771354	0.001357	0.022334	0.000357	0.017784
0.4	0.141196	6.883021	0.003415	0.090224	0.001365	0.068224
0.8	0.426o3	13.119664	0.006598	0.331785	0.004624	0.231118
1.6	0.94520	13.779134	0.006896	0.883371	0.010591	0.529555
3.2	1.10738	2.772901	0.001365	1.110259	0.008008	0.443037
						k_2 = 2.0
0.1	0.00909	0.896553	0.000483	0.002259	0.000407	0.000203
0.2	0.032669	3.110763	0.001554	0.011027	0.001611	0.000806
0.4	0.110584	8.337852	0.004189	0.044000	0.006221	0.003110
0.8	0.330477	18.895534	0.009478	0.114513	0.021860	0.110930
1.6	0.666786	31.118909	0.015595	0.342940	0.058553	0.029277
3.2	0.898447	23.898500	0.114493	0.884545	0.089191	0.044595
						k_2 = 20.0
0.1	0.000776	1.083738	0.000544	0.000065	0.000361	0.000043
0.2	0.002741	3.859448	0.001797	0.000257	0.003421	0.000171
0.4	0.008631	10.330923	0.005155	0.001014	0.013365	0.000663
0.8	0.023137	26.441442	0.013207	0.003844	0.049135	0.002457
1.6	0.046835	57.146409	0.028732	0.013143	1.553333	0.007692
3.2	0.071083	99.229034	0.049645	0.037342	3.660964	0.018048
						k_2 = 200.0
0.1	0.000744	1.119099	0.000596	0.000014	0.001311	0.000007
0.2	0.002616	4.000968	0.002005	0.000056	0.005223	0.000026
0.4	0.008141	11.996405	0.005982	0.000224	0.020551	0.000103
0.8	0.021293	32.997364	0.016487	0.000871	0.077534	0.000388
1.6	0.040876	82.777997	0.041390	0.003234	2.639622	0.001320
3.2	0.056613	189.137439	0.094687	0.011049	7.602287	0.003801

H = 0.5

k_1 = 0.2

a_1	σ_{z_1}	$\sigma_{z_1}-\sigma_{r_1}$	$\sigma_{z_1}-\sigma_{r_2}$	σ_{z_2}	$\sigma_{z_2}-\sigma_{r_2}$	$\sigma_{z_2}-\sigma_{r_3}$
						k_2 = 0.2
0.1	0.07943	0.01705	0.08527	0.00914	0.00206	0.01030
0.2	0.27189	0.05724	0.28621	0.03577	0.00804	0.04020
0.4	0.66375	0.13089	0.65444	0.13135	0.02924	0.14622
0.8	0.91143	0.15514	0.77571	0.38994	0.08369	0.41843
1.6	0.96334	0.13250	0.66248	0.72106	0.13729	0.68647
3.2	0.99310	0.06976	0.34879	0.89599	0.12674	0.63371
						k_2 = 2.0
0.1	0.07906	0.01617	0.08085	0.00557	0.01074	0.00537
0.2	0.27046	0.05375	0.26877	0.02190	0.04206	0.02103
0.4	0.65347	0.11770	0.58848	0.08222	0.15534	0.07767
0.8	0.89579	0.11252	0.56258	0.26429	0.47045	0.23523
1.6	0.94217	0.04897	0.24486	0.60357	0.90072	0.45036
3.2	0.99189	0.01380	0.06900	0.91215	0.94385	0.47192
						k_2 = 20.0
0.1	0.07862	0.01439	0.07196	0.00175	0.02415	0.00121
0.2	0.26873	0.04669	0.23345	0.00692	0.09519	0.00476
0.4	0.65188	0.09018	0.45089	0.02676	0.36003	0.01800
0.8	0.87401	0.01269	0.06347	0.09552	1.19151	0.05958
1.6	0.39563 −	0.24336 −	1.21680	0.28721	2.95409	0.14770
3.2	0.95392 −	0.53220 −	2.66100	0.66445	4.86789	0.24339
						k_2 = 200.0
0.1	0.07820	0.01243	0.06213	0.00041	0.03632	0.00018
0.2	0.26803	0.03912	0.19558	0.00163	0.14576	0.00073
0.4	0.64904	0.06006	0.30029	0.00643	0.56051	0.00280
0.8	0.86406 −	0.10447 −	0.52234	0.02436	1.06771	0.00984
1.6	0.36677 −	0.67154 −	3.35768	0.08540	5.77669	0.02388
3.2	0.89703 −	1.86126 −	9.30628	0.26467	13.63423	0.06817

H = 0.5

k_1 = 2.0

a_1	σ_{z_1}	$\sigma_{z_1}-\sigma_{r_1}$	$\sigma_{z_1}-\sigma_{r_2}$	σ_{z_2}	$\sigma_{z_2}-\sigma_{r_2}$	$\sigma_{z_2}-\sigma_{r_3}$
						k_2 = 0.2
0.1	0.04496	0.08398	0.04199	0.00903	0.00181	0.00906
0.2	0.15978	0.28904	0.14452	0.03551	0.00711	0.03554
0.4	0.44523	0.72313	0.36156	0.13314	0.02634	0.13172
0.8	0.83298	1.03603	0.51802	0.42199	0.07992	0.39962
1.6	1.05462	0.83475	0.41737	0.85529	0.13973	0.69863
3.2	0.99967	0.45119	0.22560	0.94506	0.10667	0.53336
						k_2 = 2.0
0.1	0.04330	0.08250	0.04125	0.00465	0.00878	0.00439
0.2	0.15325	0.28318	0.14159	0.01836	0.03454	0.01727
0.4	0.42077	0.70119	0.35060	0.06974	0.12951	0.06477
0.8	0.75633	0.96681	0.48341	0.23256	0.41187	0.20594
1.6	0.93447	0.70726	0.35363	0.56298	0.85930	0.42965
3.2	0.98801	0.33878	0.16939	0.88655	0.96353	0.48176
						k_2 = 20.0
0.1	0.04193	0.08044	0.04022	0.00117	0.01778	0.00089
0.2	0.14808	0.27574	0.13787	0.00464	0.07027	0.00351
0.4	0.40086	0.67174	0.33587	0.01799	0.26817	0.01341
0.8	0.69098	0.86191	0.43095	0.06476	0.91168	0.04558
1.6	0.79338	0.39588	0.19794	0.19803	2.38377	0.11919
3.2	0.85940	− 0.41078	− 0.20539	0.49238	4.47022	0.22351
						k_2 = 200.0
0.1	0.04160	0.07864	0.03932	0.00024	0.02515	0.00013
0.2	0.14676	0.26853	0.13426	0.00095	0.09968	0.00050
0.4	0.39570	0.64303	0.32152	0.00374	0.38497	0.00192
0.8	0.67257	0.74947	0.37474	0.01416	1.36766	0.00684
1.6	0.74106	− 0.02761	− 0.01381	0.04972	4.08937	0.02045
3.2	0.75176	− 1.88545	− 0.94273	0.15960	10.25631	0.05128

H = 0.5

k_1 = 20.0

a_1	σ_{z_1}	$\sigma_{z_1}-\sigma_{r_1}$	$\sigma_{z_1}-\sigma_{r_2}$	σ_{z_2}	$\sigma_{z_2}-\sigma_{r_2}$	$\sigma_{z_2}-\sigma_{r_3}$
						k_2 = 0.2
0.1	0.01351	0.16526	0.00826	0.00596	0.00098	0.00488
0.2	0.05079	0.58918	0.02946	0.02361	0.00386	0.01929
0.4	0.16972	1.66749	0.08337	0.09110	0.01474	0.07369
0.8	0.47191	3.23121	0.16156	0.31904	0.04967	0.24834
1.6	0.97452	3.54853	0.17743	0.82609	0.11279	0.56395
3.2	1.09911	1.27334	0.06367	1.08304	0.09527	0.47637
						k_2 = 2.0
0.1	0.01122	0.17997	0.00900	0.00259	0.00440	0.00220
0.2	0.04172	0.64779	0.03239	0.01023	0.01744	0.00872
0.4	0.13480	1.89817	0.09491	0.03993	0.06722	0.03361
0.8	0.35175	4.09592	0.20480	0.14419	0.23476	0.11738
1.6	0.70221	6.22002	0.31100	0.42106	0.62046	0.31023
3.2	0.97420	5.41828	0.27091	0.82256	0.93831	0.46916
						k_2 = 20.0
0.1	0.00990	0.19872	0.00994	0.00063	0.00911	0.00046
0.2	0.03648	0.72264	0.03613	0.00251	0.03520	0.00181
0.4	0.11448	2.19520	0.10976	0.00988	0.14116	0.00706
0.8	0.27934	5.24726	0.26236	0.03731	0.51585	0.02579
1.6	0.50790	10.30212	0.51511	0.12654	1.59341	0.07967
3.2	0.70903	16.38520	0.81926	0.35807	3.69109	0.18455
						k_2 = 200.0
0.1	0.00960	0.21440	0.01072	0.00013	0.01355	0.00007
0.2	0.03526	0.78493	0.03925	0.00054	0.05395	0.00027
0.4	0.10970	2.44430	0.12221	0.00214	0.21195	0.00106
0.8	0.26149	6.23424	0.31172	0.00331	0.79583	0.00398
1.6	0.45078	14.11490	0.70574	0.03070	2.67578	0.01338
3.2	0.57074	29.95815	1.49791	0.10470	7.61457	0.03807

H = 0.5

k_1 = 200.0

a_1	σ_{z_1}	$\sigma_{z_1}-\sigma_{r_1}$	$\sigma_{z_1}-\sigma_{r_2}$	σ_{z_2}	$\sigma_{z_2}-\sigma_{r_2}$	$\sigma_{z_2}-\sigma_{r_3}$
						k_2 = 0.2
0.1	0.00363	0.22388	0.00112	0.00256	0.00033	0.00163
0.2	0.01414	0.81903	0.00410	0.01021	0.00130	0.00648
0.4	0.05256	2.52558	0.01263	0.04014	0.00506	0.02529
0.8	0.18107	6.11429	0.03057	0.15048	0.01844	0.09221
1.6	0.53465	10.82705	0.05414	0.48201	0.05399	0.26993
3.2	1.04537	9.34212	0.04671	1.00671	0.08624	0.43121
						k_2 = 2.0
0.1	0.00215	0.26620	0.00133	0.00094	0.00128	0.00064
0.2	0.00826	0.98772	0.00494	0.00373	0.00509	0.00254
0.4	0.02946	3.19580	0.01598	0.01474	0.01996	0.00998
0.8	0.09508	8.71973	0.04360	0.05622	0.07434	0.03717
1.6	0.27135	20.15765	0.10079	0.19358	0.23838	0.11919
3.2	0.62399	34.25229	0.17126	0.52912	0.54931	0.27466
						k_2 = 20.0
0.1	0.00149	0.31847	0.00159	0.00023	0.00257	0.00013
0.2	0.00564	1.19598	0.00598	0.00094	0.01025	0.00051
0.4	0.01911	4.02732	0.02014	0.00372	0.04047	0.00202
0.8	0.05574	12.00835	0.06004	0.01453	0.15452	0.00773
1.6	0.13946	32.77028	0.16385	0.05399	0.53836	0.02692
3.2	0.30247	77.62943	0.38815	0.18091	1.56409	0.07820
						k_2 = 200.0
0.1	0.00133	0.37065	0.00185	0.00005	0.00387	0.00002
0.2	0.00498	1.40493	0.00702	0.00022	0.01544	0.00008
0.4	0.01649	4.86215	0.02431	0.00086	0.06118	0.00031
0.8	0.04553	15.33902	0.07670	0.00340	0.23698	0.00118
1.6	0.10209	45.93954	0.22970	0.01315	0.86345	0.00432
3.2	0.18358	128.13051	0.64065	0.04854	2.80877	0.01404

H = 1.0

k_1 = 0.2

a_1	σ_{z_1}	$\sigma_{z_1}-\sigma_{r_1}$	$\sigma_{z_1}-\sigma_{r_2}$	σ_{z_2}	$\sigma_{z_2}-\sigma_{r_2}$	$\sigma_{z_2}-\sigma_{r_3}$
						k_2 = 0.2
0.1	0.02090	0.00464	0.02320	0.00541	0.00128	0.00638
0.2	0.08023	0.01773	0.08865	0.02138	0.00503	0.02515
0.4	0.27493	0.05976	0.29878	0.08125	0.01903	0.09516
0.8	0.67330	0.13818	0.69092	0.26887	0.06192	0.30960
1.6	0.92595	0.15978	0.79888	0.60229	0.13002	0.65010
3.2	0.95852	0.09722	0.48612	0.82194	0.14348	0.71742
						k_2 = 2.0
0.1	0.02045	0.00410	0.02052	0.00356	0.00687	0.00343
0.2	0.07845	0.01561	0.07805	0.01410	0.02713	0.01357
0.4	0.26816	0.05166	0.25828	0.05427	0.10351	0.05175
0.8	0.65090	0.11111	0.55555	0.18842	0.34703	0.17351
1.6	0.88171	0.10364	0.51819	0.48957	0.79986	0.39993
3.2	0.94153	0.06967	0.34335	0.81663	0.99757	0.49879
						k_2 = 20.0
0.1	0.01981	0.00306	0.01529	0.00118	0.01591	0.00080
0.2	0.07587	0.01145	0.05726	0.00471	0.06310	0.00315
0.4	0.25817	0.03540	0.17702	0.01846	0.24396	0.01220
0.8	0.61544	0.05163	0.25817	0.06839	0.86114	0.04306
1.6	0.73884	− 0.07218	− 0.36091	0.21770	2.36054	0.11803
3.2	0.82936	− 0.25569	− 1.27847	0.53612	4.28169	0.21408
						k_2 = 200.0
0.1	0.01952	0.00214	0.01068	0.00028	0.02412	0.00012
0.2	0.07473	0.00777	0.03883	0.00110	0.09587	0.00048
0.4	0.25368	0.02076	0.10382	0.00436	0.37417	0.00187
0.8	0.59853	− 0.00538	− 0.02690	0.01679	1.36930	0.00685
1.6	0.73387	− 0.28050	− 1.40250	0.06020	4.23805	0.02119
3.2	0.70243	− 0.90965	− 4.54826	0.19189	10.36507	0.05183

$H = 1.0$

$k_1 = 2.0$

a_1	σ_{z_1}	$\sigma_{z_1}-\sigma_{r_1}$	$\sigma_{z_1}-\sigma_{r_2}$	σ_{z_2}	$\sigma_{z_2}-\sigma_{r_2}$	$\sigma_{z_2}-\sigma_{r_3}$
						$k_2 = 0.2$
0.1	0.01241	0.02186	0.01093	0.00490	0.00096	0.00478
0.2	0.04816	0.08396	0.04198	0.01943	0.00378	0.01890
0.4	0.17203	0.28866	0.14433	0.07496	0.01448	0.07241
0.8	0.48612	0.71684	0.35842	0.26193	0.04924	0.24620
1.6	0.91312	0.97206	0.48603	0.67611	0.11558	0.57790
3.2	1.04671	0.60091	0.30046	0.95985	0.12527	0.62637
						$k_2 = 2.0$
0.1	0.01083	0.02179	0.01090	0.00241	0.00453	0.00227
0.2	0.04176	0.08337	0.04169	0.00958	0.01797	0.00899
0.4	0.14665	0.28491	0.14246	0.03724	0.06934	0.03467
0.8	0.39942	0.71341	0.35670	0.13401	0.24250	0.12125
1.6	0.71032	1.02680	0.51340	0.38690	0.63631	0.31815
3.2	0.92112	0.90482	0.45241	0.75805	0.97509	0.48754
						$k_2 = 20.0$
0.1	0.00963	0.02249	0.01124	0.00061	0.00920	0.00046
0.2	0.03697	0.08618	0.04309	0.00241	0.03654	0.00183
0.4	0.12805	0.29640	0.14820	0.00950	0.14241	0.00712
0.8	0.33263	0.76292	0.38146	0.03578	0.51815	0.02591
1.6	0.52721	1.25168	0.62584	0.12007	1.56503	0.07825
3.2	0.65530	1.70723	0.85361	0.33669	3.51128	0.17556
						$k_2 = 200.0$
0.1	0.00925	0.02339	0.01170	0.00013	0.01319	0.00007
0.2	0.03561	0.09018	0.04509	0.00051	0.05252	0.00026
0.4	0.12348	0.31470	0.15735	0.00202	0.20609	0.00103
0.8	0.31422	0.83274	0.41637	0.00783	0.76955	0.00385
1.6	0.46897	1.53521	0.76760	0.02874	2.53100	0.01265
3.2	0.51161	2.76420	1.38210	0.09751	6.99283	0.03496

H = 1.0

k_1 = 20.0

a_1	σ_{z_1}	$\sigma_{z_1}-\sigma_{r_1}$	$\sigma_{z_1}-\sigma_{r_2}$	σ_{z_2}	$\sigma_{z_2}-\sigma_{r_2}$	$\sigma_{z_2}-\sigma_{r_3}$
						k_2 = 0.2
0.1	0.00417	0.04050	0.00202	0.00271	0.00039	0.00195
0.2	0.01641	0.15675	0.00784	0.01080	0.00155	0.00777
0.4	0.06210	0.55548	0.02777	0.04241	0.00606	0.03028
0.8	0.21057	1.53667	0.07683	0.15308	0.02198	0.10991
1.6	0.58218	2.77359	0.13868	0.49705	0.06327	0.31635
3.2	1.06296	2.55195	0.12760	1.00217	0.09906	0.49525
						k_2 = 2.0
0.1	0.00263	0.04751	0.00238	0.00100	0.00160	0.00080
0.2	0.01029	0.18481	0.00924	0.00397	0.00637	0.00319
0.4	0.03810	0.66727	0.03336	0.01565	0.02498	0.01249
0.8	0.12173	1.97428	0.09871	0.05938	0.09268	0.04634
1.6	0.31575	4.37407	0.21870	0.20098	0.29253	0.14626
3.2	0.66041	6.97695	0.34885	0.53398	0.65446	0.32723
						k_2 = 20.0
0.1	0.00193	0.05737	0.00287	0.00024	0.00322	0.00016
0.2	0.00751	0.22418	0.01121	0.00098	0.01283	0.00064
0.4	0.02713	0.82430	0.04121	0.00387	0.05063	0.00253
0.8	0.08027	2.59672	0.12984	0.01507	0.19267	0.00963
1.6	0.17961	6.77014	0.33851	0.05549	0.66326	0.03316
3.2	0.34355	15.23252	0.76163	0.18344	1.88634	0.09432
						k_2 = 200.0
0.1	0.00176	0.06733	0.00337	0.00006	0.00478	0.00002
0.2	0.00683	0.26401	0.01320	0.00022	0.01908	0.00010
0.4	0.02443	0.98346	0.04917	0.00088	0.07557	0.00038
0.8	0.06983	3.23164	0.16158	0.00348	0.29194	0.00146
1.6	0.14191	9.28148	0.46407	0.01339	1.05385	0.00527
3.2	0.22655	24.85236	1.24262	0.04911	3.37605	0.01688

$H = 1.0$

$k_1 = 200.0$

a_1	σ_{z_1}	$\sigma_{z_1}-\sigma_{r_1}$	$\sigma_{z_1}-\sigma_{r_2}$	σ_{z_2}	$\sigma_{z_2}-\sigma_{r_2}$	$\sigma_{z_2}-\sigma_{r_3}$
						$k_2 = 0.2$
0.1	0.00117	0.05507	0.00028	0.00097	0.00010	0.00051
0.2	0.00464	0.21467	0.00107	0.00388	0.00041	0.00203
0.4	0.01814	0.78191	0.00391	0.01538	0.00160	0.00801
0.8	0.06766	2.38055	0.01190	0.05952	0.00607	0.03037
1.6	0.22994	5.57945	0.02790	0.21214	0.02028	0.10140
3.2	0.62710	9.29529	0.04648	0.60056	0.04847	0.24236
						$k_2 = 2.0$
0.1	0.00049	0.06883	0.00034	0.00029	0.00035	0.00017
0.2	0.00195	0.26966	0.00135	0.00116	0.00138	0.00069
0.4	0.00746	1.00131	0.00501	0.00460	0.00545	0.00273
0.8	0.02647	3.24971	0.01625	0.01797	0.02092	0.01046
1.6	0.08556	8.92442	0.04462	0.06671	0.07335	0.03668
3.2	0.25186	20.83387	0.10417	0.22047	0.21288	0.10644
						$k_2 = 20.0$
0.1	0.00027	0.08469	0.00042	0.00007	0.00062	0.00003
0.2	0.00104	0.33312	0.00167	0.00028	0.00248	0.00012
0.4	0.00384	1.25495	0.00627	0.00110	0.00985	0.00049
0.8	0.01236	4.26100	0.02130	0.00436	0.03825	0.00191
1.6	0.03379	12.91809	0.06459	0.01683	0.13989	0.00699
3.2	0.08859	36.04291	0.18021	0.06167	0.45544	0.02277
						$k_2 = 200.0$
0.1	0.00021	0.10075	0.00050	0.00002	0.00037	0.00000
0.2	0.00082	0.39741	0.00199	0.00006	0.00347	0.00002
0.4	0.00298	1.51234	0.00756	0.00025	0.01331	0.00007
0.8	0.00893	5.28939	0.02645	0.00100	0.05403	0.00027
1.6	0.02065	17.01872	0.08509	0.00392	0.20250	0.00101
3.2	0.04154	52.23615	0.26118	0.01505	0.70098	0.00350

H = 2.0

k_1 = 0.2

s_1	σ_{s_1}	$\sigma_{s_1}-\sigma_{r_1}$	$\sigma_{s_1}-\sigma_{r_2}$	σ_{s_2}	$\sigma_{s_2}-\sigma_{r_2}$	$\sigma_{s_2}-\sigma_{r_3}$
						k_2 = 0.2
0.1	0.00540	0.00121	0.00604	0.00242	0.00060	0.00302
0.2	0.02138	0.00477	0.02386	0.00964	0.00240	0.01202
0.4	0.08209	0.01821	0.09106	0.03770	0.00939	0.04695
0.8	0.28150	0.06106	0.30531	0.13832	0.03422	0.17112
1.6	0.68908	0.13660	0.68299	0.40830	0.09826	0.49131
3.2	0.93103	0.12809	0.64493	0.73496	0.15705	0.78523
						k_2 = 2.0
0.1	0.00502	0.00098	0.00494	0.00180	0.00339	0.00170
0.2	0.01986	0.00389	0.01953	0.00716	0.01350	0.00675
0.4	0.07630	0.01485	0.07449	0.02815	0.05288	0.02644
0.8	0.26196	0.04977	0.24875	0.10523	0.19467	0.09733
1.6	0.63535	0.10924	0.54641	0.33075	0.57811	0.28905
3.2	0.87025	0.12296	0.61462	0.68388	1.00199	0.50100
						k_2 = 20.0
0.1	0.00444	0.00056	0.00282	0.00065	0.00825	0.00041
0.2	0.01756	0.00221	0.01105	0.00260	0.03286	0.00164
0.4	0.06706	0.00819	0.04097	0.01030	0.12933	0.00647
0.8	0.22561	0.02431	0.12153	0.03956	0.48595	0.02430
1.6	0.51929	0.03070	0.15352	0.13743	1.55804	0.07790
3.2	0.65700 −	0.00926 −	0.04632	0.37409	3.39883	0.16994
						k_2 = 200.0
0.1	0.00414	0.00032	0.00160	0.00015	0.01234	0.00006
0.2	0.01635	0.00124	0.00621	0.00058	0.04922	0.00025
0.4	0.06231	0.00436	0.02180	0.00231	0.19450	0.00097
0.8	0.20757	0.00955	0.04774	0.00905	0.74256	0.00371
1.6	0.45550 −	0.02172 −	0.10861	0.03363	2.52847	0.01264
3.2	0.48642 −	0.15589 −	0.77944	0.11105	6.69835	0.03349

$H = 2.0$

$k_1 = 2.0$

a_1	σ_{z_1}	$\sigma_{z_1}-\sigma_{r_1}$	$\sigma_{z_1}-\sigma_{r_2}$	σ_{z_2}	$\sigma_{z_2}-\sigma_{r_2}$	$\sigma_{z_2}-\sigma_{r_3}$
						$k_2 = 0.2$
0.1	0.00356	0.00545	0.00272	0.00216	0.00041	0.00203
0.2	0.01415	0.02155	0.01078	0.00861	0.00162	0.00809
0.4	0.05493	0.08266	0.04133	0.03386	0.00634	0.03172
0.8	0.19661	0.28226	0.14113	0.12702	0.02349	0.11744
1.6	0.55306	0.67844	0.33922	0.40376	0.07109	0.35545
3.2	0.96647	0.79393	0.39696	0.83197	0.12583	0.62913
						$k_2 = 2.0$
0.1	0.00250	0.00555	0.00278	0.00100	0.00188	0.00094
0.2	0.00991	0.02199	0.01099	0.00397	0.00750	0.00375
0.4	0.03832	0.08465	0.04231	0.01569	0.02950	0.01475
0.8	0.13516	0.29365	0.14683	0.05974	0.11080	0.05540
1.6	0.36644	0.75087	0.37542	0.20145	0.35515	0.17757
3.2	0.67384	1.17294	0.58647	0.51156	0.77434	0.38717
						$k_2 = 20.0$
0.1	0.00181	0.00652	0.00326	0.00025	0.00378	0.00019
0.2	0.00716	0.02586	0.01293	0.00099	0.01507	0.00075
0.4	0.02746	0.10017	0.05007	0.00394	0.05958	0.00298
0.8	0.09396	0.35641	0.17821	0.01535	0.22795	0.01140
1.6	0.23065	1.00785	0.50392	0.05599	0.78347	0.03917
3.2	0.37001	2.16033	1.08017	0.17843	2.13215	0.10661
						$k_2 = 200.0$
0.1	0.00164	0.00778	0.00389	0.00005	0.00542	0.00003
0.2	0.00647	0.03090	0.01544	0.00021	0.02163	0.00011
0.4	0.02470	0.12030	0.06014	0.00085	0.08578	0.00043
0.8	0.08326	0.43693	0.21847	0.00335	0.33214	0.00166
1.6	0.19224	1.32870	0.66434	0.01283	1.19190	0.00596
3.2	0.25526	3.40664	1.70332	0.04612	3.67558	0.01838

$H = 2.0$

$k_1 = 20.0$

a_1	σ_{z_1}	$\sigma_{z_1}-\sigma_{r_1}$	$\sigma_{z_1}-\sigma_{r_2}$	σ_{z_2}	$\sigma_{z_2}-\sigma_{r_2}$	$\sigma_{z_2}-\sigma_{r_3}$
						$k_2 = 0.2$
0.1	0.00134	0.00968	0.00048	0.00108	0.00014	0.00068
0.2	0.00533	0.03839	0.00192	0.00429	0.00055	0.00273
0.4	0.02100	0.14845	0.00741	0.01702	0.00216	0.01078
0.8	0.07950	0.52414	0.02621	0.06576	0.00820	0.04101
1.6	0.26613	1.41720	0.07085	0.23186	0.02740	0.13698
3.2	0.67882	2.38258	0.11913	0.63006	0.06384	0.31919
						$k_2 = 2.0$
0.1	0.00059	0.01219	0.00061	0.00033	0.00051	0.00025
0.2	0.00235	0.04843	0.00242	0.00130	0.00203	0.00101
0.4	0.00922	0.18857	0.00943	0.00513	0.00803	0.00401
0.8	0.03412	0.68382	0.03419	0.02023	0.03093	0.01547
1.6	0.10918	2.04134	0.10207	0.07444	0.10864	0.05432
3.2	0.29183	4.60426	0.23021	0.23852	0.30709	0.15354
						$k_2 = 20.0$
0.1	0.00033	0.01568	0.00078	0.00008	0.00094	0.00005
0.2	0.00130	0.06236	0.00312	0.00031	0.00374	0.00019
0.4	0.00503	0.24425	0.01221	0.00123	0.01486	0.00074
0.8	0.01782	0.90594	0.04530	0.00485	0.05739	0.00289
1.6	0.05012	2.91994	0.14600	0.01862	0.21190	0.01060
3.2	0.11331	7.95104	0.39755	0.06728	0.67732	0.03387
						$k_2 = 200.0$
0.1	0.00027	0.01927	0.00096	0.00002	0.00131	0.00001
0.2	0.00106	0.07675	0.00384	0.00007	0.00524	0.00003
0.4	0.00406	0.30182	0.01509	0.00028	0.02085	0.00010
0.8	0.01397	1.13555	0.05673	0.00110	0.08180	0.00041
1.6	0.03538	3.83254	0.19163	0.00431	0.30676	0.00153
3.2	0.06182	11.55403	0.57770	0.01644	1.04794	0.00524

$H = 2.0$

$k_1 = 200.0$

a_1	σ_{z_1}	$\sigma_{z_1}-\sigma_{r_1}$	$\sigma_{z_1}-\sigma_{r_2}$	σ_{z_2}	$\sigma_{z_2}-\sigma_{r_2}$	$\sigma_{z_2}-\sigma_{r_3}$
						$k_2 = 0.2$
0.1	0.00036	0.01350	0.00007	0.00033	0.00003	0.00015
0.2	0.00144	0.05366	0.00027	0.00130	0.00012	0.00058
0.4	0.00572	0.20911	0.00105	0.00518	0.00046	0.00232
0.8	0.02231	0.76035	0.00380	0.02038	0.00180	0.00901
1.6	0.08215	2.29642	0.01148	0.07675	0.00649	0.03244
3.2	0.26576	5.28589	0.02643	0.25434	0.01912	0.09562
						$k_2 = 2.0$
0.1	0.00011	0.01737	0.00009	0.00008	0.00009	0.00004
0.2	0.00045	0.06913	0.00035	0.00033	0.00036	0.00018
0.4	0.00179	0.27103	0.00136	0.00131	0.00142	0.00071
0.8	0.00685	1.00808	0.00504	0.00520	0.00553	0.00277
1.6	0.02441	3.27590	0.01638	0.02003	0.02043	0.01021
3.2	0.08061	9.02195	0.04511	0.07248	0.06638	0.03319
						$k_2 = 20.0$
0.1	0.00005	0.02160	0.00011	0.00002	0.00014	0.00001
0.2	0.00018	0.08604	0.00043	0.00007	0.00058	0.00003
0.4	0.00071	0.33866	0.00169	0.00030	0.00229	0.00011
0.8	0.00261	1.27835	0.00639	0.00119	0.00901	0.00045
1.6	0.00819	4.35311	0.02177	0.00467	0.03390	0.00170
3.2	0.02341	13.26873	0.06634	0.01734	0.11666	0.00583
						$k_2 = 200.0$
0.1	0.00003	0.02587	0.00013	0.00000	0.00019	0.00000
0.2	0.00012	0.10310	0.00052	0.00002	0.00075	0.00000
0.4	0.00047	0.40676	0.00203	0.00007	0.00300	0.00002
0.8	0.00165	1.54951	0.00775	0.00026	0.01183	0.00006
1.6	0.00445	5.43705	0.02719	0.00104	0.04515	0.00023
3.2	0.00929	17.58810	0.08794	0.00409	0.16107	0.00081

$H = 4.0$

$k_1 = 0.2$

a_1	σ_{z_1}	$\sigma_{z_1}-\sigma_{r_1}$	$\sigma_{z_1}-\sigma_{r_2}$	σ_{z_2}	$\sigma_{z_2}-\sigma_{r_2}$	$\sigma_{z_2}-\sigma_{r_3}$
						$k_2 = 0.2$
0.1	0.00139	0.00028	0.00141	0.00086	0.00023	0.00114
0.2	0.00555	0.00112	0.00562	0.00345	0.00091	0.00454
0.4	0.02198	0.00444	0.02220	0.01371	0.00360	0.01801
0.8	0.08435	0.01636	0.08428	0.05323	0.01394	0.06968
1.6	0.28870	0.05529	0.27647	0.19003	0.04909	0.24545
3.2	0.70074	0.11356	0.56778	0.51882	0.12670	0.63352
						$k_2 = 2.0$
0.1	0.00133	0.00026	0.00131	0.00071	0.00130	0.00065
0.2	0.00491	0.00104	0.00521	0.00283	0.00518	0.00259
0.4	0.01942	0.00412	0.02059	0.01126	0.02057	0.01028
0.8	0.07447	0.01574	0.07869	0.04383	0.07977	0.03989
1.6	0.25449	0.05311	0.26554	0.15904	0.28357	0.14178
3.2	0.62074	0.12524	0.62622	0.45455	0.75651	0.37825
						$k_2 = 20.0$
0.1	0.00087	0.00018	0.00090	0.00028	0.00325	0.00016
0.2	0.00346	0.00072	0.00358	0.00111	0.01298	0.00065
0.4	0.01367	0.00283	0.01417	0.00443	0.05159	0.00258
0.8	0.05207	0.01089	0.05444	0.01741	0.20134	0.01007
1.6	0.17367	0.03790	0.13949	0.06525	0.73322	0.03666
3.2	0.39955	0.10841	0.54203	0.20965	2.13666	0.10683
						$k_2 = 200.0$
0.1	0.00069	0.00019	0.00097	0.00006	0.00487	0.00002
0.2	0.00274	0.00078	0.00389	0.00024	0.01947	0.00010
0.4	0.01079	0.00309	0.01544	0.00095	0.07752	0.00039
0.8	0.04074	0.01199	0.05995	0.00373	0.30432	0.00152
1.6	0.13117	0.04352	0.21753	0.01456	1.13373	0.00567
3.2	0.26403	0.14445	0.72224	0.05161	3.59608	0.01798

$H = 4.0$

$k_1 = 2.0$

a_1	σ_{z_1}	$\sigma_{z_1}-\sigma_{r_1}$	$\sigma_{z_1}-\sigma_{r_2}$	σ_{z_2}	$\sigma_{z_2}-\sigma_{r_2}$	$\sigma_{z_2}-\sigma_{r_3}$
						$k_2 = 0.2$
0.1	0.00103	0.00123	0.00064	0.00078	0.00014	0.00071
0.2	0.00411	0.00511	0.00256	0.00312	0.00057	0.00284
0.4	0.01631	0.02022	0.01011	0.01241	0.00226	0.01129
0.8	0.06319	0.07722	0.03861	0.04842	0.00877	0.04384
1.6	0.22413	0.25955	0.12977	0.17617	0.03133	0.15666
3.2	0.60654	0.58704	0.29352	0.50917	0.08500	0.42501
						$k_2 = 2.0$
0.1	0.00057	0.00147	0.00074	0.00034	0.00065	0.00032
0.2	0.00223	0.00587	0.00293	0.00137	0.00260	0.00130
0.4	0.00905	0.02324	0.01162	0.00544	0.01032	0.00516
0.8	0.03500	0.08957	0.04479	0.02135	0.04031	0.02015
1.6	0.12354	0.31215	0.15603	0.07972	0.14735	0.07368
3.2	0.34121	0.81908	0.40954	0.25441	0.43632	0.21816
						$k_2 = 20.0$
0.1	0.00030	0.00201	0.00101	0.00008	0.00128	0.00006
0.2	0.00119	0.00803	0.00402	0.00034	0.00510	0.00026
0.4	0.00469	0.03191	0.01596	0.00134	0.02032	0.00102
0.8	0.01700	0.12427	0.06213	0.00532	0.07991	0.00400
1.6	0.06045	0.45100	0.22550	0.02049	0.29991	0.01500
3.2	0.14979	1.36427	0.68214	0.07294	0.97701	0.04885
						$k_2 = 200.0$
0.1	0.00023	0.00263	0.00131	0.00002	0.00180	0.00001
0.2	0.00091	0.01050	0.00525	0.00007	0.00720	0.00004
0.4	0.00360	0.04179	0.02000	0.00029	0.02870	0.00014
0.8	0.01360	0.16380	0.08190	0.00115	0.11334	0.00057
1.6	0.04409	0.60898	0.30449	0.00451	0.43251	0.00216
3.2	0.00323	1.98899	0.99449	0.01705	1.49306	0.00747

H = 4.0

k_1 = 20.0

a_1	σ_{z_1}	$\sigma_{z_1}-\sigma_{r_1}$	$\sigma_{z_1}-\sigma_{r_2}$	σ_{z_2}	$\sigma_{z_2}-\sigma_{r_2}$	$\sigma_{z_2}-\sigma_{r_3}$
						k_2 = 0.2
0.1	0.00042	0.00233	0.00012	0.00037	0.00004	0.00021
0.2	0.00166	0.00932	0.00047	0.00143	0.00017	0.00085
0.4	0.00663	0.03692	0.00185	0.00588	0.00068	0.00340
0.8	0.02603	0.14242	0.00712	0.02319	0.00266	0.01331
1.6	0.09718	0.49826	0.02491	0.08758	0.00983	0.04914
3.2	0.31040	1.31627	0.06581	0.28747	0.02990	0.14951
						k_2 = 2.0
0.1	0.00013	0.00312	0.00016	0.00010	0.00015	0.00007
0.2	0.00054	0.01245	0.00062	0.00039	0.00059	0.00029
0.4	0.00214	0.04944	0.00247	0.00154	0.00235	0.00117
0.8	0.00837	0.19247	0.00962	0.00610	0.00924	0.00462
1.6	0.03109	0.69749	0.03487	0.02358	0.03488	0.01744
3.2	0.10140	2.09049	0.10452	0.03444	0.11553	0.05776
						k_2 = 20.0
0.1	0.00005	0.00213	0.00021	0.00002	0.00025	0.00001
0.2	0.00021	0.01651	0.00083	0.00009	0.00099	0.00005
0.4	0.00083	0.06569	0.00328	0.00035	0.00396	0.00020
0.8	0.00321	0.25739	0.01287	0.00138	0.01565	0.00078
1.6	0.01130	0.95622	0.04781	0.00542	0.05993	0.00300
3.2	0.03258	3.10980	0.15549	0.02061	0.20906	0.01045
						k_2 = 200.0
0.1	0.00003	0.00515	0.00026	0.00000	0.00033	0.00000
0.2	0.00014	0.02056	0.00103	0.00003	0.00131	0.00001
0.4	0.00054	0.08191	0.00410	0.00008	0.00524	0.00003
0.8	0.00206	0.32231	0.01612	0.00030	0.02077	0.00010
1.6	0.00683	1.21587	0.06079	0.00120	0.08034	0.00040
3.2	0.01590	4.14395	0.20720	0.00468	0.28961	0.00145

$H = 4.0$

$k_1 = 200.0$

a_1	σ_{z_1}	$\sigma_{z_1}-\sigma_{r_1}$	$\sigma_{z_1}-\sigma_{r_2}$	σ_{z_2}	$\sigma_{z_2}-\sigma_{r_2}$	$\sigma_{z_2}-\sigma_{r_3}$
						$k_2 = 0.2$
0.1	0.00010	0.00334	0.00002	0.00010	0.00001	0.00004
0.2	0.00042	0.01333	0.00007	0.00039	0.00003	0.00016
0.4	0.00167	0.05295	0.00026	0.00157	0.00013	0.00065
0.8	0.00663	0.20621	0.00103	0.00625	0.00051	0.00256
1.6	0.02562	0.74824	0.00374	0.02427	0.00195	0.00975
3.2	0.09166	2.25046	0.01125	0.08799	0.00660	0.03298
						$k_2 = 2.0$
0.1	0.00003	0.00437	0.00002	0.00002	0.00002	0.00001
0.2	0.00011	0.01746	0.00009	0.00009	0.00009	0.00005
0.4	0.00042	0.06947	0.00035	0.00036	0.00036	0.00018
0.8	0.00168	0.27221	0.00136	0.00142	0.00144	0.00072
1.6	0.00646	1.01140	0.00506	0.00560	0.00553	0.00277
3.2	0.02332	3.23913	0.01645	0.02126	0.01951	0.00975
						$k_2 = 20.0$
0.1	0.00001	0.00545	0.00003	0.00000	0.00003	0.00000
0.2	0.00003	0.02178	0.00011	0.00002	0.00014	0.00001
0.4	0.00013	0.08673	0.00043	0.00003	0.00054	0.00003
0.8	0.00050	0.34131	0.00171	0.00031	0.00215	0.00011
1.6	0.00186	1.28773	0.00644	0.00124	0.00833	0.00042
3.2	0.00612	4.38974	0.02195	0.00483	0.03010	0.00150
						$k_2 = 200.0$
0.1	0.00000	0.00652	0.00003	0.00000	0.00004	0.00000
0.2	0.00002	0.02606	0.00013	0.00000	0.00017	0.00000
0.4	0.00007	0.10389	0.00052	0.00002	0.00068	0.00000
0.8	0.00025	0.40997	0.00205	0.00007	0.00269	0.00001
1.6	0.00086	1.56284	0.00781	0.00027	0.01049	0.00005
3.2	0.00225	5.48870	0.02744	0.00107	0.03866	0.00019

$H = 8.0$

$k_1 = 0.2$

a_1	σ_{z_1}	$\sigma_{z_1}-\sigma_{r_1}$	$\sigma_{z_1}-\sigma_{r_2}$	σ_{z_2}	$\sigma_{z_2}-\sigma_{r_2}$	$\sigma_{z_2}-\sigma_{r_3}$
						$k_2 = 0.2$
0.1	0.00035	0.00006	0.00028	0.00027	0.00007	0.00036
0.2	0.00142	0.00023	0.00113	0.00108	0.00028	0.00142
0.4	0.00566	0.00090	0.00449	0.00432	0.00113	0.00567
0.8	0.02240	0.00354	0.01769	0.01711	0.00449	0.02246
1.6	0.08589	0.01335	0.06673	0.06610	0.01725	0.08624
3.2	0.29318	0.04270	0.21350	0.23182	0.05907	0.29533
						$k_2 = 2.0$
0.1	0.00030	0.00008	0.00038	0.00023	0.00041	0.00021
0.2	0.00120	0.00030	0.00152	0.00091	0.00165	0.00083
0.4	0.00479	0.00121	0.00606	0.00364	0.00660	0.00330
0.8	0.01894	0.00480	0.02399	0.01446	0.02616	0.01308
1.6	0.07271	0.01841	0.09206	0.05601	0.10080	0.05040
3.2	0.24933	0.06307	0.31534	0.19828	0.35008	0.17504
						$k_2 = 20.0$
0.1	0.00016	0.00010	0.00049	0.00009	0.00105	0.00005
0.2	0.00065	0.00040	0.00198	0.00037	0.00421	0.00021
0.4	0.00260	0.00158	0.00790	0.00149	0.01679	0.00084
0.8	0.01026	0.00629	0.03143	0.00594	0.06664	0.00333
1.6	0.03926	0.02463	0.12314	0.02320	0.25871	0.01294
3.2	0.13335	0.09123	0.45615	0.08510	0.92478	0.04624
						$k_2 = 200.0$
0.1	0.00009	0.00015	0.00074	0.00002	0.00162	0.00001
0.2	0.00036	0.00059	0.00294	0.00008	0.00648	0.00003
0.4	0.00145	0.00235	0.01176	0.00032	0.02587	0.00013
0.8	0.00573	0.00938	0.04690	0.00127	0.10287	0.00051
1.6	0.02160	0.03710	0.18549	0.00503	0.40238	0.00201
3.2	0.06938	0.14226	0.71130	0.01912	1.48097	0.00740

H = 8.0

k_1 = 2.0

a_1	σ_{z_1}	$\sigma_{z_1}-\sigma_{r_1}$	$\sigma_{z_1}-\sigma_{r_2}$	σ_{z_2}	$\sigma_{z_2}-\sigma_{r_2}$	$\sigma_{z_2}-\sigma_{r_3}$
						k_2 = 0.2
0.1	0.00028	0.00028	0.00014	0.00024	0.00004	0.00022
0.2	0.00113	0.00111	0.00056	0.00096	0.00017	0.00087
0.4	0.00451	0.00444	0.00222	0.00384	0.00069	0.00347
0.8	0.01736	0.01752	0.00876	0.01522	0.00275	0.01373
1.6	0.06895	0.06662	0.03331	0.05900	0.01060	0.05298
3.2	0.24127	0.22014	0.11007	0.20949	0.03693	0.18466
						k_2 = 2.0
0.1	0.00013	0.00039	0.00020	0.00010	0.00020	0.00010
0.2	0.00053	0.00157	0.00079	0.00041	0.00078	0.00039
0.4	0.00213	0.00628	0.00314	0.00164	0.00311	0.00156
0.8	0.00844	0.02487	0.01244	0.00653	0.01237	0.00618
1.6	0.03269	0.09597	0.04798	0.02556	0.04802	0.02401
3.2	0.11640	0.33606	0.16803	0.09405	0.17138	0.08594
						k_2 = 20.0
0.1	0.00005	0.00061	0.00030	0.00002	0.00037	0.00002
0.2	0.00019	0.00242	0.00121	0.00010	0.00149	0.00007
0.4	0.00076	0.00967	0.00484	0.00040	0.00596	0.00030
0.8	0.00300	0.03845	0.01922	0.00159	0.02369	0.00118
1.6	0.01154	0.15010	0.07505	0.00630	0.09274	0.00464
3.2	0.04003	0.54942	0.27471	0.02409	0.34233	0.01712
						k_2 = 200.0
0.1	0.00003	0.00082	0.00041	0.00001	0.00052	0.00000
0.2	0.00011	0.00328	0.00164	0.00002	0.00206	0.00001
0.4	0.00042	0.01310	0.00655	0.00008	0.00825	0.00004
0.8	0.00167	0.05216	0.02608	0.00034	0.03287	0.00016
1.6	0.00629	0.20491	0.10245	0.00135	0.12933	0.00065
3.2	0.02030	0.76769	0.38384	0.00527	0.48719	0.00244

H = 8.0

k_1 = 20.0

a_1	σ_{z_1}	$\sigma_{z_1}-\sigma_{r_1}$	$\sigma_{z_1}-\sigma_{r_2}$	σ_{z_2}	$\sigma_{z_2}-\sigma_{r_2}$	$\sigma_{z_2}-\sigma_{r_3}$
						k_2 = 0.2
0.1	0.00012	0.00056	0.00003	0.00011	0.00001	0.00006
0.2	0.00047	0.00223	0.00011	0.00044	0.00005	0.00025
0.4	0.00190	0.00839	0.00044	0.00176	0.00020	0.00099
0.8	0.00754	0.03522	0.00176	0.00701	0.00079	0.00393
1.6	0.02947	0.13569	0.00678	0.02746	0.00306	0.01528
3.2	0.10817	0.47240	0.02362	0.10145	0.01105	0.05524
						k_2 = 2.0
0.1	0.00003	0.00079	0.00004	0.00003	0.00004	0.00002
0.2	0.00013	0.00316	0.00016	0.00011	0.00016	0.00008
0.4	0.00050	0.01260	0.00063	0.00043	0.00064	0.00032
0.8	0.00200	0.05007	0.00250	0.00170	0.00253	0.00127
1.6	0.00736	0.19496	0.00975	0.00673	0.00993	0.00496
3.2	0.02944	0.70709	0.03535	0.02579	0.03678	0.01839
						k_2 = 20.0
0.1	0.00001	0.00106	0.00005	0.00001	0.00006	0.00000
0.2	0.00004	0.00425	0.00021	0.00002	0.00025	0.00001
0.4	0.00014	0.01696	0.00085	0.00009	0.00100	0.00005
0.8	0.00056	0.06751	0.00338	0.00037	0.00398	0.00020
1.6	0.00217	0.26466	0.01323	0.00147	0.01565	0.00078
3.2	0.00791	0.98450	0.04922	0.00576	0.05892	0.00295
						k_2 = 200.0
0.1	0.00000	0.00133	0.00007	0.00000	0.00003	0.00000
0.2	0.00002	0.00531	0.00027	0.00000	0.00032	0.00000
0.4	0.00006	0.02122	0.00106	0.00002	0.00128	0.00001
0.8	0.00025	0.08453	0.00423	0.00008	0.00509	0.00003
1.6	0.00096	0.33268	0.01663	0.00032	0.02009	0.00010
3.2	0.00319	1.25614	0.06281	0.00125	0.07660	0.00033

H = 8.0

k_1 = 200.0

a_1	σ_{z_1}	$\sigma_{z_1}-\sigma_{r_1}$	$\sigma_{z_1}-\sigma_{r_2}$	σ_{z_2}	$\sigma_{z_2}-\sigma_{r_2}$	$\sigma_{z_2}-\sigma_{r_3}$
						k_2 = 0.2
0.1	0.00003	0.00083	0.00000	0.00003	0.00000	0.00001
0.2	0.00011	0.00330	0.00002	0.00011	0.00001	0.00005
0.4	0.00046	0.01320	0.00007	0.00044	0.00004	0.00018
0.8	0.00182	0.05242	0.00026	0.00175	0.00014	0.00072
1.6	0.00720	0.20411	0.00102	0.00693	0.00056	0.00282
3.2	0.02751	0.74013	0.00370	0.02656	0.00212	0.01058
						k_2 = 2.0
0.1	0.00001	0.00109	0.00001	0.00001	0.00001	0.00000
0.2	0.00003	0.00438	0.00002	0.00002	0.00002	0.00001
0.4	0.00010	0.01748	0.00009	0.00009	0.00009	0.00005
0.8	0.00041	0.06956	0.00035	0.00038	0.00037	0.00018
1.6	0.00162	0.27262	0.00136	0.00149	0.00145	0.00072
3.2	0.00625	1.01322	0.00507	0.00584	0.00547	0.00273
						k_2 = 20.0
0.1	0.00000	0.00136	0.00001	0.00000	0.00001	0.00000
0.2	0.00001	0.00546	0.00003	0.00001	0.00003	0.00000
0.4	0.00002	0.02181	0.00011	0.00002	0.00013	0.00001
0.8	0.00010	0.08687	0.00043	0.00008	0.00052	0.00003
1.6	0.00039	0.34202	0.00171	0.00032	0.00204	0.00010
3.2	0.00149	1.29190	0.00646	0.00127	0.00777	0.00039
						k_2 = 200.0
0.1	0.00000	0.00163	0.00001	0.00000	0.00001	0.00000
0.2	0.00000	0.00654	0.00003	0.00000	0.00004	0.00000
0.4	0.00001	0.02613	0.00013	0.00000	0.00016	0.00000
0.8	0.00003	0.10417	0.00052	0.00002	0.00063	0.00000
1.6	0.00013	0.41121	0.00206	0.00007	0.00249	0.00001
3.2	0.00047	1.56843	0.00784	0.00027	0.00957	0.00005

Appendix B

A MATHEMATICAL DESCRIPTION OF THE PROBLEM

A diagrammatic representation of the system was given in Figure 1. The system consists of a semi-infinite elastic solid bounded at the surface by two finite elastic layers of constant thickness. The surface is loaded uniformly over a circular area and so, if cylindrical polar coordinates (r, θ, z) are used, the stresses and strains in the system will be independent of the angle θ.

Assumptions

1. The Applicability of the Theory of Elasticity.—The materials involved are assumed to be homogeneous and isotropic, the stress/strain relationship to be linear and the modulus to be the same in compression as in tension.
2. Description of System.—The three layers are horizontal and have different elastic properties. The two upper layers are weightless and of infinite extent in the horizontal plane. The bottom layer is infinite in the horizontal plane and semi-infinite in the vertical plane.
3. Boundary Conditions.—The surface of the top layer is free of shear stress. Outside the circular loaded area the surface is free of normal stress and inside the load is uniformly distributed. All stresses and displacements are zero at infinite depth.
4. Continuity Conditions.—The three layers are continuously in contact and act together as a composite medium. At the interfaces the normal and shear stresses and the vertical and horizontal displacements must be the same in both layers.

TABLE 2

NOTATION FOR STRESSES

Stress	Symbol
Vertical normal	σ_z
Radial normal	σ_r
Circumferential normal	σ_θ
Shear	τ_{rz}

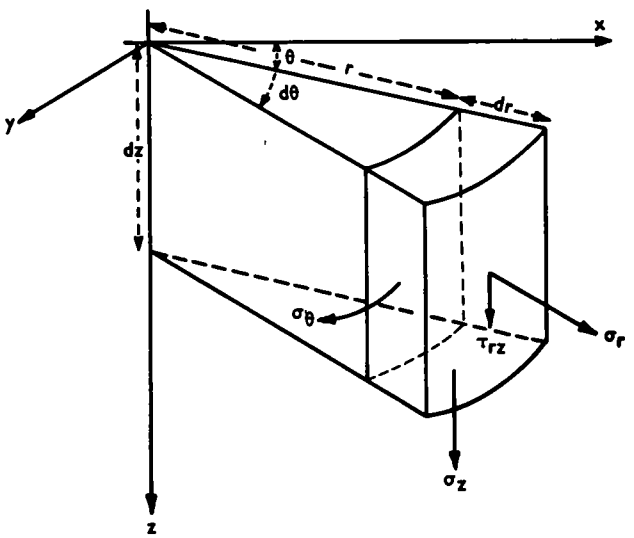

Figure 2. Components of stress in cylindrical co-ordinates.

5. Poisson's Ratio. —This is assumed to be equal to 0.5 in all three layers, the main reasons being that the algebra involved in developing the stress expression is considerably simplified. This value of Poisson's ratio corresponds to an incompressible medium.

Derivations of the Expressions for the Stresses in a Three-Layered System

The notation for the stresses is presented in Table 2. To take advantage of the symmetry of the problem cylindrical polar coordinates have been used. The components of stress are shown in Figure 2.

The equations of equilibrium are obtained by considering the total force for a small element in both the radial and vertical directions.

$$\frac{\partial \sigma_r}{\partial r} + \frac{\partial \tau_{rz}}{\partial z} + \frac{\sigma_r - \sigma_\theta}{r} = 0 \qquad (1a)$$

$$\frac{\partial \tau_{rz}}{\partial r} + \frac{\partial \sigma_z}{\partial z} + \frac{\tau_{rz}}{r} = 0 \qquad (1b)$$

(Because of the axial symmetry in the problem, $\tau_{r\theta}$ and $\tau_{\theta z}$ are zero, and there is no equilibrium condition for the θ-direction).

In the general three-dimensional case in rectangular coordinates, each of the six components of strain (three normal and three shear) may be expressed in terms of the three components of displacement. Thus these equations are not independent and three relationships exist between the six components of strain. These are called the compatibility conditions, and they may be expressed in terms of components of stress by using Hooke's law. In cylindrical polar coordinates with axial symmetry the compatibility conditions become

$$\nabla^2 \sigma_r - \frac{2}{r^2}(\sigma_r - \sigma_\theta) + \frac{1}{1+\mu}\frac{\partial^2}{\partial r^2}(\sigma_r + \sigma_\theta + \sigma_z) = 0 \qquad (2a)$$

$$\nabla^2 \sigma_\theta + \frac{2}{r^2}(\sigma_r - \sigma_\theta) + \frac{1}{1+\mu}\frac{1}{r}\frac{\partial}{\partial r}(\sigma_r + \sigma_\theta + \sigma_z) = 0 \qquad (2b)$$

where μ is Poisson's ratio and

$$\nabla^2 = \frac{\partial^2}{\partial r^2} + \frac{1}{r}\frac{\partial}{\partial r} + \frac{\partial^2}{\partial z^2}$$

is the Laplacian operator.

The components of stress and displacement may be expressed in terms of a stress function φ in such a way that Eqs. 1a and 1b are identically satisfied. These expressions are

Stress

$$\sigma_z = \frac{\partial}{\partial z}\left[(2-\mu)\nabla^2\varphi - \frac{\partial^2 \varphi}{\partial z^2}\right] \qquad (3a)$$

$$\sigma_r = \frac{\partial}{\partial z}\left[\mu\nabla^2\varphi - \frac{\partial^2 \varphi}{\partial r^2}\right] \qquad (3b)$$

$$\sigma_\theta = \frac{\partial}{\partial z}\left[\mu\nabla^2\varphi - \frac{1}{r}\frac{\partial \varphi}{\partial r}\right] \qquad (3c)$$

$$\tau_{rz} = \frac{\partial}{\partial r}\left[(1-\mu)\nabla^2\varphi - \frac{\partial^2 \varphi}{\partial z^2}\right] \qquad (3d)$$

Displacement

(vertical) $$w = \frac{1+\mu}{E}\left[(1-2\mu)\nabla^2\varphi + \frac{\partial^2 \varphi}{\partial r^2} + \frac{1}{r}\frac{\partial \varphi}{\partial r}\right] \qquad (3e)$$

$$\text{(horizontal)} \quad u = -\frac{(1+\mu)}{E} \frac{\partial^2 \varphi}{\partial r \partial z} \tag{3f}$$

in which E is the modulus of elasticity.

It may be shown quite easily that Eqs. 2a and 2b are satisfied provided φ is a solution of the biharmonic equation:

$$\nabla^4 \varphi = 0 \tag{4}$$

in which ∇^2 is again the Laplacian operator.

The problem is thus reduced to the solution of this partial differential equation subject to the boundary conditions at the surface, the interfaces and at infinite depth. The boundary conditions are expressed next; the numerical subscripts refer to the different layers.

Interface 1 ($z = -h_1$)	Interface 2 ($z = -h_1-h_2$)	
$\sigma_{z_1} = \sigma_{z_2}$	$\sigma_{z_2} = \sigma_{z_3}$	(normal stresses)
$\tau_{rz_1} = \tau_{rz_2}$	$\tau_{rz_2} = \tau_{rz_3}$	(shear stresses)
$w_1 = w_2$	$w_2 = w_3$	(vertical displacements)
$u_1 = u_2$	$u_2 = u_3$	(horizontal displacements)

$\tau_{rz_1} = 0$ ($z = 0$, surface free of shear stress)

$w_3 = u_3 = \sigma_{z_3} = \tau_{rz_3} = 0$ at infinite depth

$$\left.\begin{aligned} \sigma_z &= 1 \quad 0 \le r \le a \\ \sigma_z &= 0 \quad r > a \end{aligned}\right\} \quad \text{(surface loading)}$$

The radial stresses σ_r are not continuous across the interface because the horizontal displacements are equal; they are determined by the relevant modulus of elasticity.

The partial differential Eq. 4 may be solved by using the Hankel transform*. However, for purpose here the solution may be expressed in the following form.

The stress functions

$$\varphi_1 \quad \text{(top layer)} = J_o(mr)\left[(A_1 + B_1 z)\, e^{mz} + (C_1 + D_1 z)\, e^{-mz}\right]$$

$$\varphi_2 \text{ (middle layer)} = J_o(mr)\left[(A_2 + B_2 z)\, e^{mz} + (C_2 + D_2 z)\, e^{-mz}\right]$$

$$\varphi_3 \text{ (bottom layer)} = J_o(mr)\left[(C_3 + D_3 z)\, e^{-mz}\right]$$

satisfy Eq. 4 and the conditions at infinite depth**. The ten constants are evaluated by using the boundary conditions at the interfaces, the condition that the surface shear stress is zero and by assuming a stress distribution of the form:

*The Hankel transform $F(m)$ of order zero of the function $f(x)$ is given by

$$F(m) = \int_0^\infty xf(x)J_o(mx)dx$$

for details of the application of this transform to problems in three dimensional elasticity, see (6).

**$J_o(x)$ is the Bessel function of order zero.

$$\sigma_z\,(r,\ m) = -mJ_0(mr)$$

The final expressions for the stresses and displacements are then given by

$$\sigma_z = \int_0^a \int_0^\infty \sigma_z(r,\ m)\ r\ dr\ dm \tag{5a}$$

$$\sigma_r = \sigma_\theta = \int_0^a \int_0^\infty \frac{\sigma_r(r,\ m) + \sigma_\theta(r,\ m)}{2}\ r\ dr\ dm \tag{5b}$$

The total surface load is given by

$$\int_0^a \int_0^\infty \sigma_z(r,\ m)\ r\ dr\ dm$$

$$= -\int_0^a \int_0^\infty mr\ J_0(mr)\ dr\ dm = -\int_0^\infty aJ_1(am)dm = -1 \tag{6}$$

The final expressions for the stresses and displacements are obtained by substituting the stress functions φ into Eqs. 3a through 3f for the components of stress and then using the Eqs. 5a and 5b. The algebra involved is quite considerable but is simplified by assuming that Poisson's ratio is equal to 0.5 in all three layers. The expressions for the components of stress that appear in the tables are given next.

(1) First interface

$$\sigma_{z_1} = -(1-K)\int_0^\infty a_1 J_1(a_1 x)\ \frac{f_1(x)}{D(x)}\ dx$$

$$2\sigma_{r_1} = \int_0^\infty a_1 J_1(a_1 x)\ \frac{g_1(x)}{D(x)}\ dx$$

$$2\sigma_{r_2} = (1-K)\int_0^\infty a_1 J_1(a_1 x)\ \frac{g_2(x)}{D(x)}\ dx$$

(2) Second interface

$$\sigma_{z_2} = (1-K)(1-N)\int_0^\infty a_1 J_1(a_1 x)\ \frac{F_1(x)}{D(x)}\ dx$$

$$2\sigma_{r_2} = -(1-K)\int_0^\infty a_1 J_1(a_1 x)\ \frac{G_1(x)}{D(x)}\ dx$$

$$2\sigma_{r_3} = -(1-K)(1-N)\int_0^\infty a_1 J_1(a_1 x)\,\frac{G_2(x)}{D(x)}\,dx$$

The symbols and functions in these expressions are defined as follows:

$$a_1 = a/h_2,\ H = h_1/h_2,\ k_1 = E_1/E_2,\ \text{and } k_2 = E_2/E_3,$$

$$K = \frac{k_1-1}{k_1+1},\quad N = \frac{k_2-1}{k_2+1}$$

$$f_1(x) = (1+Hx)\left\{e^{-Hx} - KN^2 e^{-(4+H)x}\right\} - (1-Hx)\left\{Ke^{-3Hx} - N^2 e^{-(3H+4)x}\right\}$$

$$-Np_1(x)e^{-(3H+2)x} - Np_2(x)e^{-(H+2)x}$$

$$g_1(x) = \frac{4}{1+k_1}\ (1-Hx)\left\{Ke^{-3Hx} - N^2 e^{-(3H+4)x}\right\} - \frac{4}{1+k_1}\ (1+Hx)\left\{e^{-Hx}\right.$$

$$\left.-KN^2 e^{-(H+4)x}\right\} + \frac{6k_1 Hx}{1+k_1}\left\{e^{-Hx} + KN^2 e^{-(H+4)x} - Ke^{-3Hx} - N^2 e^{-(3H+4)x}\right\}$$

$$-Np_3(x)e^{-(3H+2)x} - Np_4(x)e^{-(H+2)x}$$

$$g_2(x) = K(2-5Hx)e^{-3Hx} - (2-Hx)e^{-Hx} - N^2(2+Hx)e^{-(3H+4)x}$$

$$+KN^2(2+5Hx)e^{-(H+4)x} - Np_5(x)e^{-(3H+2)x} - Np_6(x)e^{-(H+2)x}$$

$$F_1(x) = -(1+x+Hx)e^{-(H+1)x} - KN(1-x+Hx-2Hx^2)e^{-(H+3)x}$$

$$+K(1+x-Hx-2Hx^2)e^{-(3H+1)x} + N(1-x-Hx)e^{-(3H+3)x}$$

$$G_1(x) = Kq_1(x)e^{-(3H+1)x} - q_2(x)e^{-(H+1)x} + Nq_3(x)e^{-(3H+3)x} - KNq_4(x)e^{-(H+3)}$$

$$G_2(x) = K(-2+x+5Hx-2Hx^2)e^{-(3H+1)x} + (2-x-Hx)e^{-(H+1)x}$$

$$- N(2-5x-5Hx)e^{-(3H+3)x} + KN(2-5x-Hx-10Hx^2)e^{-(H+3)x}$$

$$D(x) = 1+2KN(1+2x^2)e^{-2x} + K^2N^2e^{-4x} + K^2e^{-4Hx} + 2KN(1+2x^2)e^{-(4H+2)x}$$

$$+ N^2e^{-(4H+4)x} - 2K(1+2H^2x^2)e^{-2Hx} - K^2Np_7(x)e^{-(2H+2)x} - Np_8(x)e^{-(2H+2}$$

$$- 2KN^2(1+2H^2x^2)e^{-(2H+4)x}$$

and

$$p_1(x) = p_2(-x) = -K(1+2x-Hx+2x^2-2Hx^2-4Hx^3) + (1-2x-Hx+2x^2+2Hx^2)$$

$$p_3(x) = p_4(-x) = K(4+2Hx+8x^2+4Hx^3) - (2-4x-5Hx-2x^2-2Hx^2)$$

$$- K^2(2+4x-5Hx+10x^2+2Hx^2-20Hx^3)$$

$$p_5(x) = p_6(-x) = K(2+4x+Hx-2x^2-10Hx^2+4Hx^3) - (2-4x-5Hx-2x^2-2Hx^2)$$

$$p_7(x) = 2+4x^2-8Hx^2+4H^2x^2+16H^2x^4$$

$$p_8(x) = 2+4x^2+8Hx^2+4H^2x^2$$

$$q_1(x) = N(2+5x+Hx-10Hx^2) - (2-x-5Hx+2Hx^2)$$

$$q_2(x) = N(2+5x+5Hx) - (2-x-Hx)$$

$$q_3(x) = N(2+x+Hx) - (2-5x-5Hx)$$

$$q_4(x) = N(2+x+5Hx+2Hx^2) - (2-5x-Hx-10Hx^2)$$

The expression for $g_1(x)$ differs from that given by Acum and Fox in the fourth term in the third bracket. This was discovered when an unaccountable discrepancy was noted for values of $\sigma_{z_1} = \sigma_{r_1}$. An error was suspected when a certain lack of symmetry in the expression for $g_1(x)$ was noted. Inspection showed that the coefficient of $\exp\left[-(3H+4)x\right]$ should be N^2 on both occasions, whereas the paper of Acum and Fox shows N instead of N^2 in the third bracket. When this change was made the disagreement disappeared. The corrected expression was verified later when it was derived from first principles.

As a further check some results were obtained for comparison with those of Acum and Fox. These are presented in Appendix C (figures in brackets being taken from Acum and Fox's paper).

Appendix C

H = 0.25 k_1 = 5.0 k_2 = 5.0

a_1	σ_{z_1}	$\sigma_{z_1}-\sigma_{r_1}$	$\sigma_{z_1}-\sigma_{r_2}$	σ_{z_2}	$\sigma_{z_2}-\sigma_{r_2}$	$\sigma_{z_2}-\sigma_{r_3}$
0.5	0.74131	1.39458	0.37892	0.08783	0.38000	0.07600
	(0.7410)	(1.8900)	(0.3790)	(0.0879)	(0.3800)	(0.0761)
1.0	0.94443	1.25311	0.25062	0.26496	1.04512	0.20902
	(0.9470)	(1.2700)	(0.2540)	(0.2650)	(1.0400)	(0.2090)

k_1 = 5.0 k_2 = 100.0

0.5	0.72401	1.69907	0.33931	0.01171	0.70741	0.00707
	(0.7240)	(1.7000)	(0.3400)	(0.0117)	(0.7070)	(0.00707)
1.0	0.89239	0.49183	0.09836	0.04125	2.23183	0.02232
	(0.8970)	(0.5030)	(0.1020)	(0.0413)	(2.2300)	(0.0223)

k_1 = 50.0 k_2 = 5.0

0.5	0.30774	7.47254	0.14915	0.05798	0.23339	0.04768
	(0.3080)	(7.4700)	(0.1500)	(0.0580)	(0.2380)	(0.0477)
1.0	0.64196	12.73759	0.25475	0.19381	0.75223	0.15045
	(0.6420)	(12.7300)	(0.2550)	(0.1940)	(0.7520)	(0.1500)

k_1 = 50.0 k_2 = 100.0

0.5	0.23529	8.73121	0.17462	0.00791	0.46746	0.00467
	(0.2850)	(8.7200)	(0.1740)	(0.00791)	(0.4660)	(0.00466)
1.0	0.56937	17.17838	0.34958	0.02924	1.61943	0.01619
	(0.5700)	(17.1500)	(0.3490)	(0.0292)	(1.6100)	(0.0161)

Continued

H = 2.0 k_1 = 5.0 k_2 = 5.0

a_1	σ_{z_1}	$\sigma_{z_1}-\sigma_{r_1}$	$\sigma_{z_1}-\sigma_{r_2}$	σ_{z_2}	$\sigma_{z_2}-\sigma_{r_2}$	$\sigma_{z_1}-\sigma_{r_3}$
0.5	0.02848	0.21464	0.04293	0.00955	0.04100	0.00820
	(0.0285)	(0.2150)	(0.0430)	(0.00950)	(0.0409)	(0.00817)
1.0	0.09503	0.72664	0.14533	0.03649	0.15324	0.03065
	(0.0951)	(0.7270)	(0.1450)	(0.0364)	(0.1530)	(0.0306)
						k_1 = 50.0 k_2 = 5.0
0.5	0.00524	0.38265	0.00765	0.00269	0.00856	0.00171
	(0.00522)	(0.3820)	(0.00765)	(0.00268)	(0.00853)	(0.00170)
1.0	0.01867	1.36457	0.02729	0.01054	0.03237	0.00657
	(0.0187)	(1.3600)	(0.0273)	(0.0105)	(0.0330)	(0.0066)
						k_1 = 50.0 k_2 = 100.0
0.5	0.00280	0.51248	0.01025	0.00039	0.01430	0.00014
	(0.00281)	(0.5230)	(0.0105)	(0.00041)	(0.0147)	(0.00015)
1.0	0.00914	1.88310	0.03766	0.00156	0.05566	0.00056
	(0.00921)	(1.9300)	(0.0385)	(0.00163)	(0.0575)	(0.00058)
						k_1 = 10.0 k_2 = 5.0
0.5	0.01752	0.27077	0.02706	0.00671	0.02701	0.00540
	(0.0176)	(0.2720)	(0.0272)	(0.00670)	(0.0270)	(0.00540)
1.0	0.06004	0.93871	0.09388	0.02588	0.10202	0.02040
	(0.0600)	(0.9390)	(0.0938)	(0.0259)	(0.1020)	(0.0204)

Stress and Strain Factors for Three-Layer Elastic Systems

K. R. PEATTIE, Research Engineer, Thornton Research Centre, on temporary assignment at the Research Laboratory, Shell Oil Company, Wood River, Illinois.

Tables of stress factors for systems of three elastic layers under load have been published by A. Jones of the Thornton Research Centre of "Shell" Research Ltd. in connection with the development of a fundamental method of road design. For convenience in the analysis and design of road structures, it is desirable to present these factors graphically. Some stress and strain factors not directly tabulated in Jones' report have been derived from the data therein. A suitable graphical method for the presentation of the factors is described. A series of graphs covering four factors has been prepared.

•MOST METHODS of road design are empirical. They cannot be extended to cover new types of loading or materials of construction. Neither can they be used for the analysis of the behavior of roads.

A fundamental method for the design of flexible roads is being developed by Thornton. The basis of this method is to determine the thicknesses of the various layers so that the stresses and strains developed by moving traffic are within the permissible limits for the materials. It is therefore necessary to be able to calculate the values of these stresses and strains.

A real road structure may be represented by a system of elastic layers lying on a semi-infinite elastic mass. From a review of methods available for calculating stresses in such systems, it was concluded that the stresses should be obtained from rigorous solutions of the elastic equations for layered systems. Suitable solutions for a wide range of the parameters involved have been published by A. Jones of the Thornton Research Centre.

The stress factors are tabulated at wide intervals of the four parameters involved. In the analysis and design of road structures it is necessary to interpolate between the tabulated values. A convenient graphical method of doing this is described.

STRESS AND STRAIN FACTORS

Figure 1 shows a three-layer road structure and the stresses for which factors have been calculated. These have been confined to points at the interfaces on the vertical centerline through the loaded area because they have their maximum values under these conditions if the load is uniformly distributed.

The tables prepared by Jones (1) list the stress factors given in Table 1. The stresses are obtained by multiplying the contact stress by the stress factor.

These were the six stress factors given by Acum and Fox (2) whose tables were considerably extended by Jones (1). The difference between the vertical and horizontal stresses was tabulated for convenience in obtaining shear stresses. Because in the design and analysis of flexible pavements the stresses and strains existing at the bases of the upper two layers can be important, it would be convenient to have the stress factors, RR1 and RR'2, and the strain factors, $\frac{1}{2}$ (RR1-ZZ1) and $\frac{1}{2}$ (RR'2 - ZZ2), tabulated directly. They have been obtained from data in the Jones tables by computations carried out on the IBM 650 system computer at Wood River.

The horizontal strain is obtained from the strain factor by multiplying the factor by the contact stress and dividing by the elastic modulus of the layer.

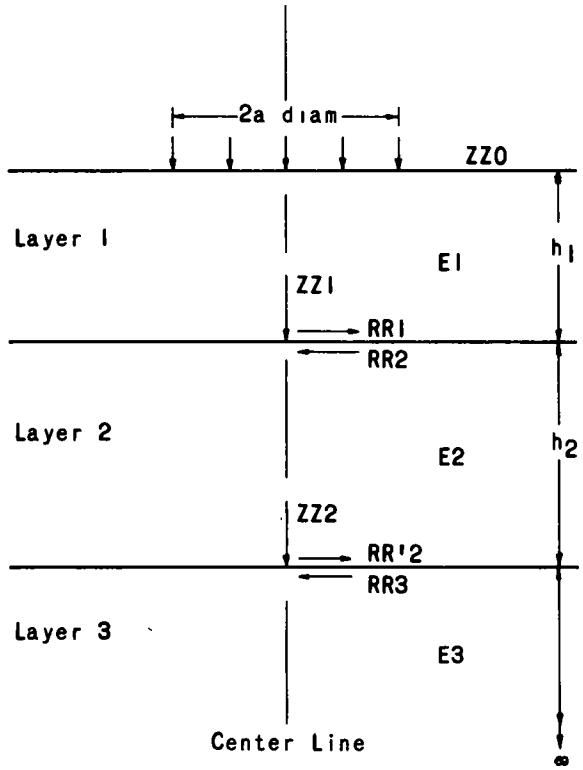

Legend:
- ZZ0 = Contact stress
- ZZ1 = Vertical stress at first interface
- ZZ2 = Vertical stress at second interface
- RR1 = Horizontal stress at base of top layer
- RR2 = Horizontal stress at top of middle layer
- RR'2= Horizontal stress at base of middle layer
- RR3 = Horizontal stress at top of bottom layer

Figure 1. Three-layer road structure.

TABLE 1
STRESS FACTORS TABULATED IN THORNTON REPORT

Stress	First Interface	Second Interface
Vertical	ZZ1	ZZ2
(Vertical horizontal)	(ZZ1 - RR1)	(ZZ2 - RR'2)
	(ZZ1 - RR2)	(ZZ2 - RR3)

GRAPHICAL PRESENTATION

The stress and strain factors in the tables by Jones (and in subsequent tables at Wood River) are listed in terms of the following parameters: $A = a/h_2$; $H = h_1/h_2$; $K_1 = E_1/E_2$; and $K_2 = E_2/E_3$; in which a is the radius of circular contact area; h_1 and h_2 are thicknesses of top and middle layers, respectively; and E_1, E_2, and E_3 are elastic moduli of top, middle, and bottom layers, respectively.

The stress and strain factors are tabulated for the following values of these parameters:

$A = 0.1,\ 0.2,\ 0.4,\ 0.8,\ 1.6,\ 3.2$
$H = 0.125,\ 0.25,\ 0.50,\ 1.0,\ 2.0,\ 4.0,\ 8.0$
$K_1 = 0.2,\ 2.0,\ 20.0,\ 200.0$
$K_2 = 0.2,\ 2.0,\ 20.0,\ 200.0$

These ranges were chosen to cover the conditions most likely to occur in flexible pavements. The individual values were selected to be convenient for interpolation. The data have now to be presented in a graphical form suitable for use in the analysis and design of flexible pavements.

There are four independent variables and one dependent variable involved. The dependent variable and one pair of independent variables can be represented on one "grid" figure. The parameters A and H are related to the geometry of the pavement and the load system. The parameters K_1 and K_2 are related to the elastic properties of the pavement. The same geometric arrangement may have to be analyzed for combinations of materials of different properties. It would therefore be convenient to construct

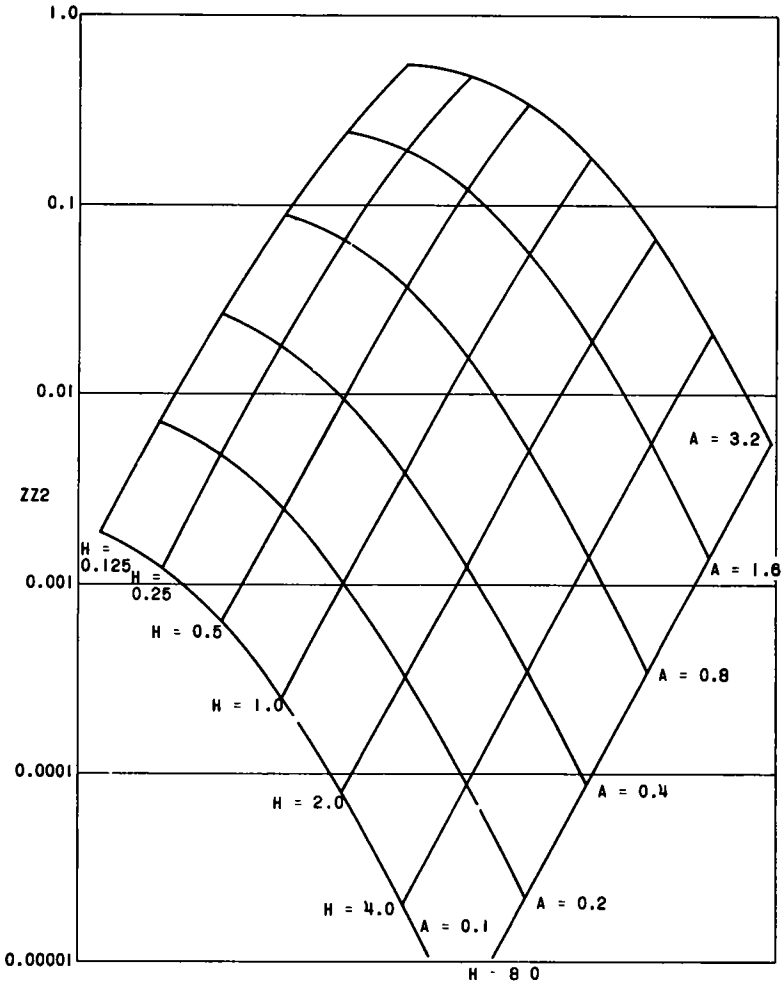

Figure 2. Vertical stress factor ZZ2 for $K_1 = K_2 = 20$.

a series of grids, each one of which covered the full range of A- and H-values for one pair of values of K1 and K2. The full range of any one stress or strain function can be covered on 16 grids.

The graphical representation of three or more variables is discussed by McIntosh (3) and the method is described in detail in Appendix B of this report. A specimen grid giving the vertical stress factor ZZ2, for $K_1 = K_2 = 20$, is shown in Figure 2.

The production of the grids for ZZ1 and ZZ2 is straightforward. At high values of A and low values of H the grid for ZZ1 becomes compressed but that is unimportant as it is in a range of very thin pavements where ZZ1 is approximately equal to unity.

The production of grids for the horizontal stress and strain factors is complicated by two features. First, the factors change sign over the range of the tables. Because only the regions of tensile stress and strain are of interest in the analysis of flexible pavements, the compressive values are disregarded in plotting. Second, when plotting

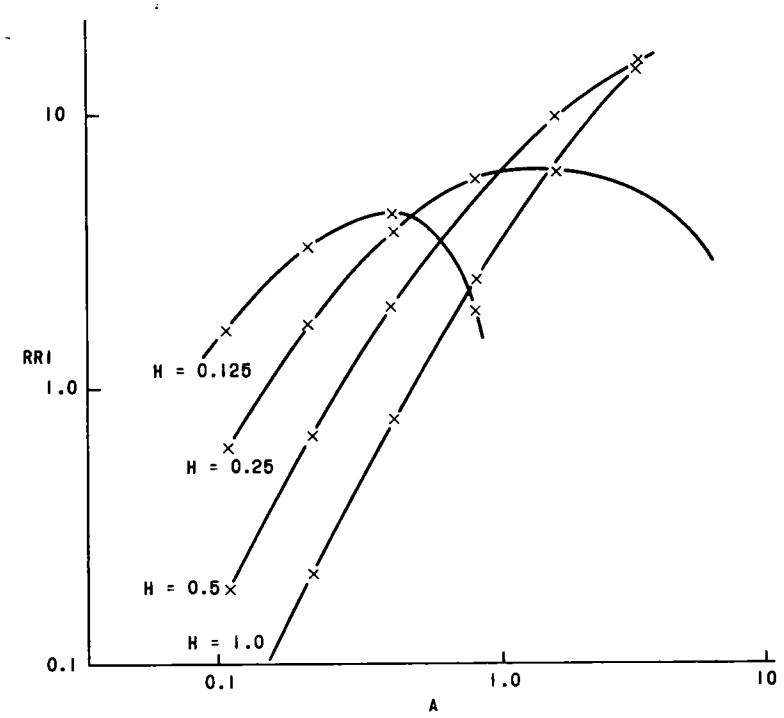

Figure 3. Horizontal stress factor RRI vs A for $K_1 = K_2 = 20$. Pavements corresponding to pairs of values of A at one value of H are compared in Table 2.

TABLE 2
VALUES TAKEN FROM FIGURE 3 FOR RRI = 3 (a = 6 IN.)

H	A	h_1 (in.)	h_2 (in.)	Total Thickness (in.)
0.125	0.17	4.4	35.3	39.7
	0.65	1.2	9.2	10.4
0.25	0.32	4.7	18.8	23.5
	5.8	0.26	1.03	1.29
0.5	0.54	5.5	11.1	16.6

the factors against A, for a given value of H, they are sometimes seen to pass through maxima as A increases. This occurs at high values of A and low values of H.

Graphs of the radial stress factor, RR1, as a function of A are shown in Figure 3. For H = 0.125 and 0.25 two values of A correspond to each value of RR1. A similar situation has been shown to exist in a two-layer structure by van der Poel (4). In practice, the pavements denoted by the larger of each pair of values of A are inadmissible because they are so thin that the soil would be overstressed. In plotting grids of the horizontal stress and strain factors the lines are stopped when peak values are reached. This simplifies interpolation, but there must be no extrapolation.

The pavements corresponding to the values of A of 0.65 and 5.8 are very thin and are unlikely to be able to protect the soil.

A typical grid showing the values of the horizontal stress factor, RR1, for $K_1 = K_2 = 20$ is given in Figure 4. A series of grids has been plotted for the vertical stress factors ZZ1 and ZZ2 and the horizontal stress and strain factors RR1 and ½ (RR1 - ZZ1). The former were chosen because of their importance in granular bases and subgrades; the latter because of their importance in bituminous carpets.

The full series of grids, which is given in Appendix A, is composed of the following figures: Figures 8 to 23, vertical compressive stress factor ZZ1; Figures 24 to 39, vertical compressive stress factor ZZ2; Figures 40 to 51, horizontal tensile stress factor RR1; and Figures 52 to 67, horizontal tensile strain factor ½ (RR1 - ZZ1).

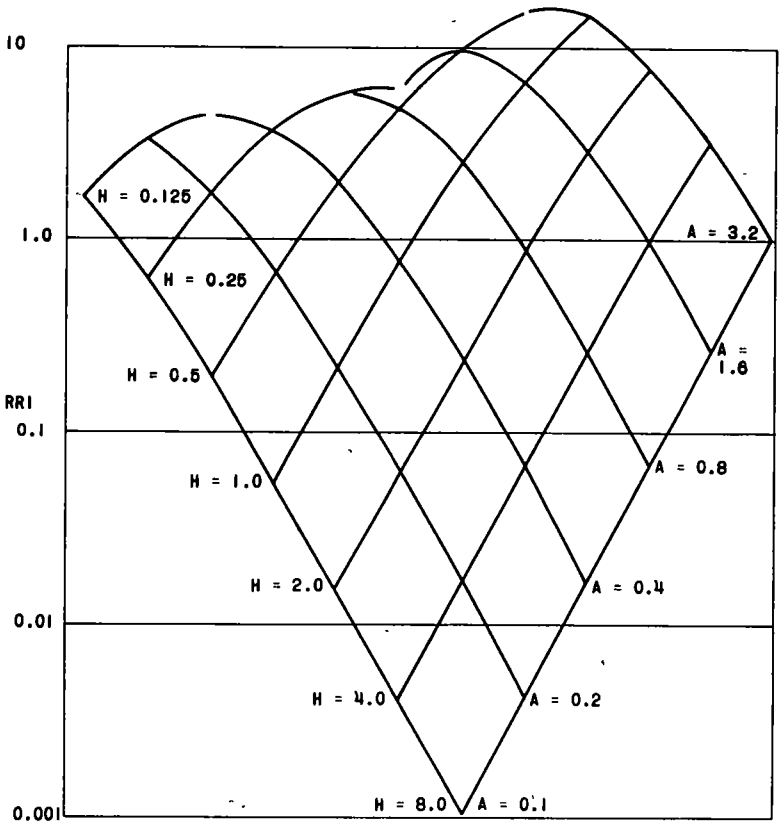

Figure 4. Horizontal stress factor RR1 for $K_1 = K_2 = 20.0$.

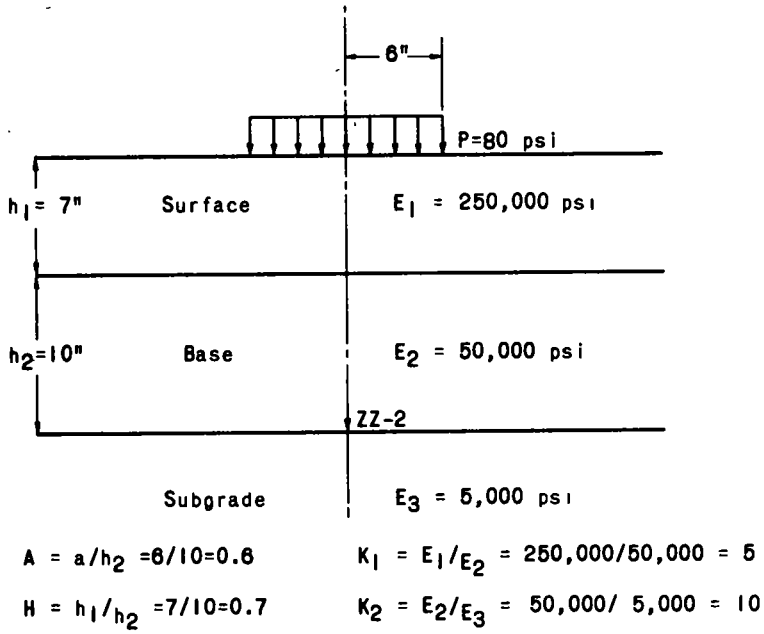

Figure 5. Hypothetical pavement.

TABLE 3
VERTICAL STRESS ON SUBGRADE FOR 9,000-LB WHEEL LOAD
(A = 0.6, H = 0.7)

	K_1 = 0.2		K_1 = 2.0		K_1 = 20.0		K_1 = 200.0	
K_2	Stress Factor ZZ-2	Stress[a] (psi)	Stress Factor ZZ-2	Stress[a] (psi)	Stress Factor ZZ-2	Stress[a] (psi)	Stress Factor ZZ-2	Stress[a] (psi)
0.2	0.19	15.2	0.21	16.8	0.13	10.4	0.05	4.0
2.0	0.13	10.4	0.11	8.8	0.05	4.0	0.017	1.36
20.0	0.045	3.6	0.026	2.08	0.013	1.04	0.0045	0.36
200.0	0.012	0.96	0.006	0.48	0.0028	0.22	0.0010	0.08

[a]For applied unit load of 80 psi.

EXAMPLE OF USE OF GRAPHS

The following numerical example demonstrates the use of the graphs. Considering a hypothetical pavement with properties and dimensions as shown in Figure 5, it is required to determine the vertical compressive stress produced on the subgrade by a uniform load of 80 psi at the surface. This load acting on an area of 6-in. radius is equal to a total load of 9,000 lb. It is similar to the load imposed by a truck wheel.

First, it is necessary to evaluate the parameters A, H, K_1, and K_2. These values shown at the bottom of Figure E are used to enter the graphs.

Next, a table like Table 3 is prepared, and stress factors (ZZ-2) are listed for different combinations of K_1 and K_2. These are the stress factors for a pavement of the given dimensions, but they represent different modular ratios between the layers. Each factor is obtained by interpolation on a separate graph. Thus, the factor of 0.19 for K_1 = 0.2 and K_2 = 0.2 is read from Figure 24 for values of the dimensional parameters A and H equal to 0.6 and 0.7. Factors for other combinations of K_1 and K_2 are read from Figures 25 through 39. Numerical stresses in separate columns of Table 3 are obtained by multiplying stress factors by the applied unit load of 80 psi.

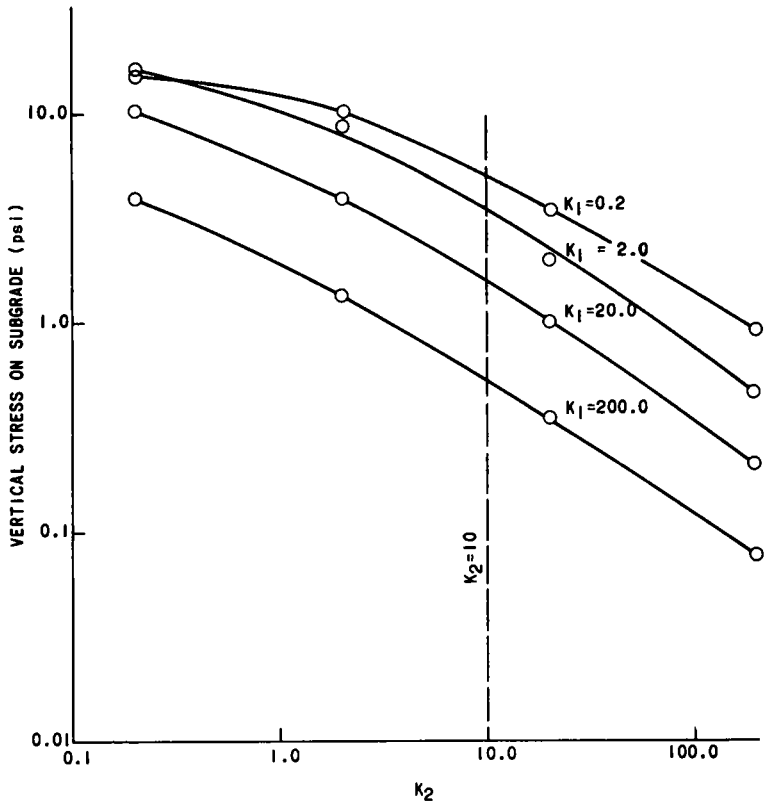

Figure 6. Relation of subgrade stress to modular ratio K_2.

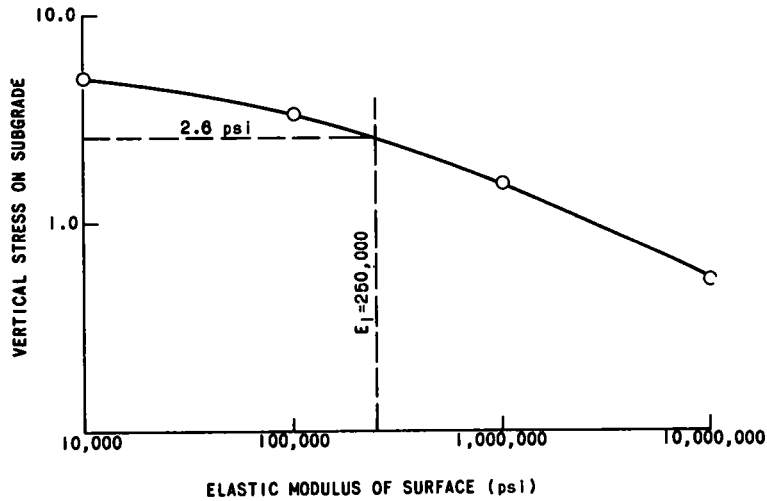

Figure 7. Relation of subgrade stress to elastic modulus of surface.

In Figure 6, subgrade stresses are plotted against corresponding values of K_1 and K_2. The figure demonstrates the influence of modular ratios on subgrade stress. For a constant subgrade modulus, an increase in base course modulus (increase in K_2) reduces subgrade stress. An increase in surface modulus (increase in K_1) also reduces stress.

Stresses for the pavement in the example are taken from Figure 6 at a value of K_2 equal to 10. These, in turn, are replotted in Figure 7. Here, subgrade stresses are shown as a function of the surface modulus $E_1(E_1 = K_1 \times E_2)$. For the designated surface modulus of 250, 000 psi, the vertical stress on the subgrade under an 80-psi load is 2.6 psi.

A graph like Figure 7 is frequently useful because it demonstrates how subgrade stresses are influenced by changes in the surface modulus.

The foregoing example illustrates the use of the graphs to calculate the theoretical stress on the subgrade. The graphs can be used in the same manner to calculate other values. These include the tensile stress or strain, and the vertical compressive stress at the bottom of the surface layer. Thus, stresses can be investigated at several critical points in a pavement structure.

CONCLUSIONS

In the design and analysis of flexible pavements it would be convenient to have the horizontal stress and strain factors directly tabulated. These factors have been calculated from the original data published by A. Jones of the Thornton Research Centre.

A suitable graphical method for presenting the stress and strain factors has been selected. A series of these graphs covering the factors commonly used in the analysis and design of flexible pavements has been produced.

REFERENCES

1. Jones. A., "Tables of Stresses in Three-Layer Elastic Systems." presented to Annual Meeting of the Highway Research Board 1962.
2. Acum, W. E. A., and Fox, L., Geotechnique, 2: 293-300 (1951).
3. McIntosh, J. D., Mag. Concrete Research, C.A.C.A. No. 3, pp. 145-148 (Dec. 1949).
4. van der Poel, C., "Building Materials." Ed. by M. Reiner, N. Holland Publishing Company, Amsterdam, Ch. 9, Fig. 2 (1956).

Appendix A

GRAPHICAL REPRESENTATION OF STRESS AND STRAIN FACTORS

The following factors are presented graphically:

ZZ1	=	Vertical compressive stress at first interface—Figures 8-23
ZZ2	=	Vertical compressive stress at second interface—Figures 24-39
RR1	=	Horizontal tensile stress at base of top layer—Figures 40-51
½ (RR1-ZZ1)	=	Horizontal tensile strain at base of top layer—Figures 52-67

The factors for all combinations of A and H appear on one grid. The grids are arranged in groups of four in ascending order of K_1. Within a group each grid corresponds to one value of K_2.

There must be no extrapolation on any of the grids.

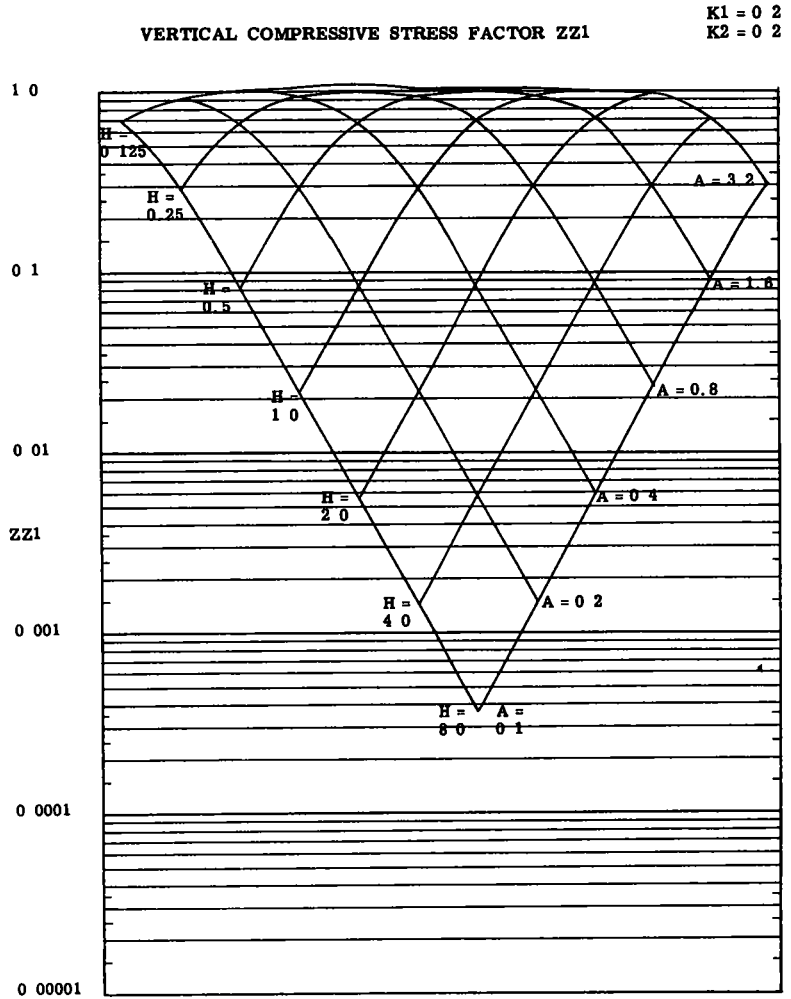

Figure 8.

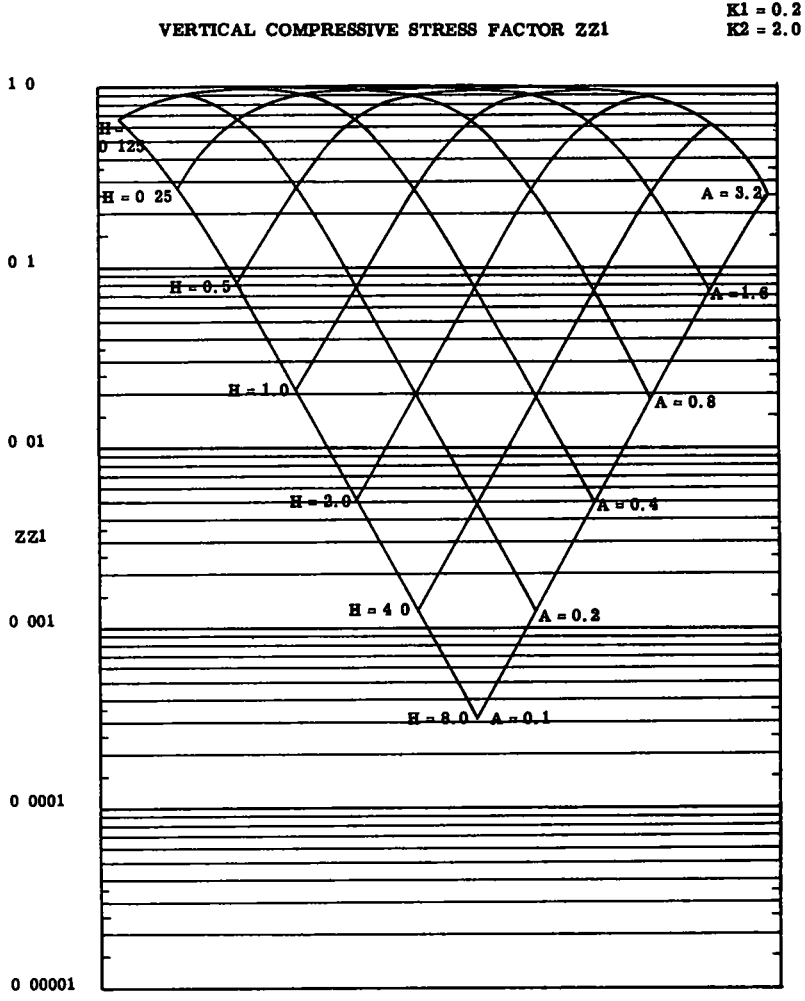

Figure 9.

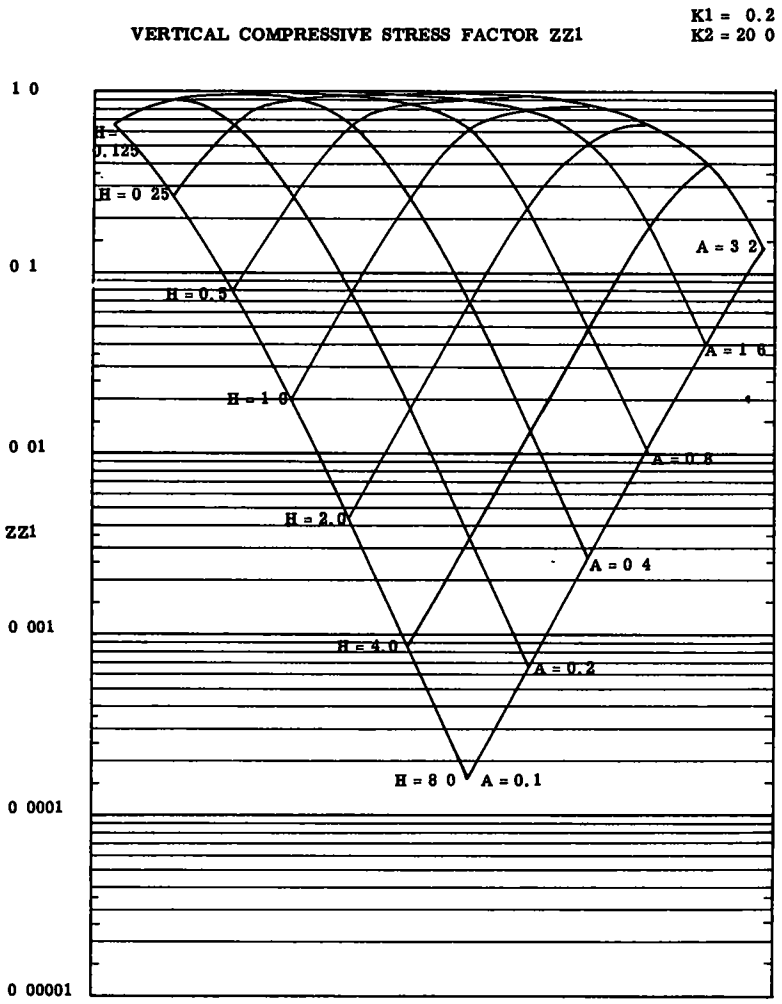

Figure 10.

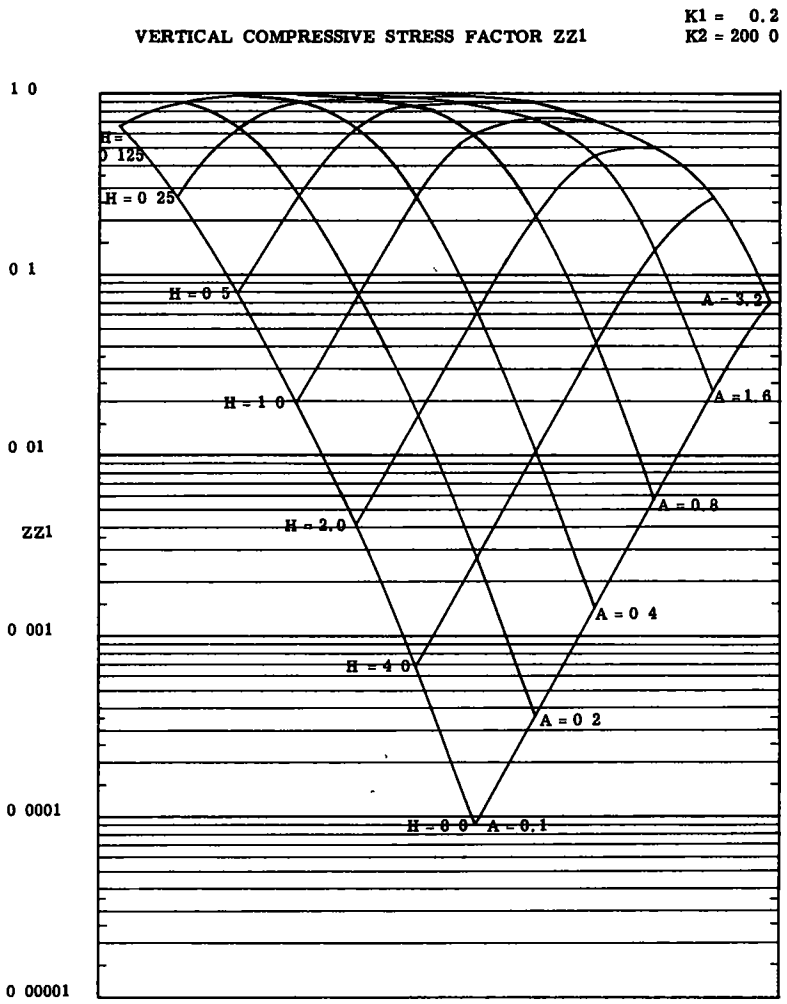

Figure 11.

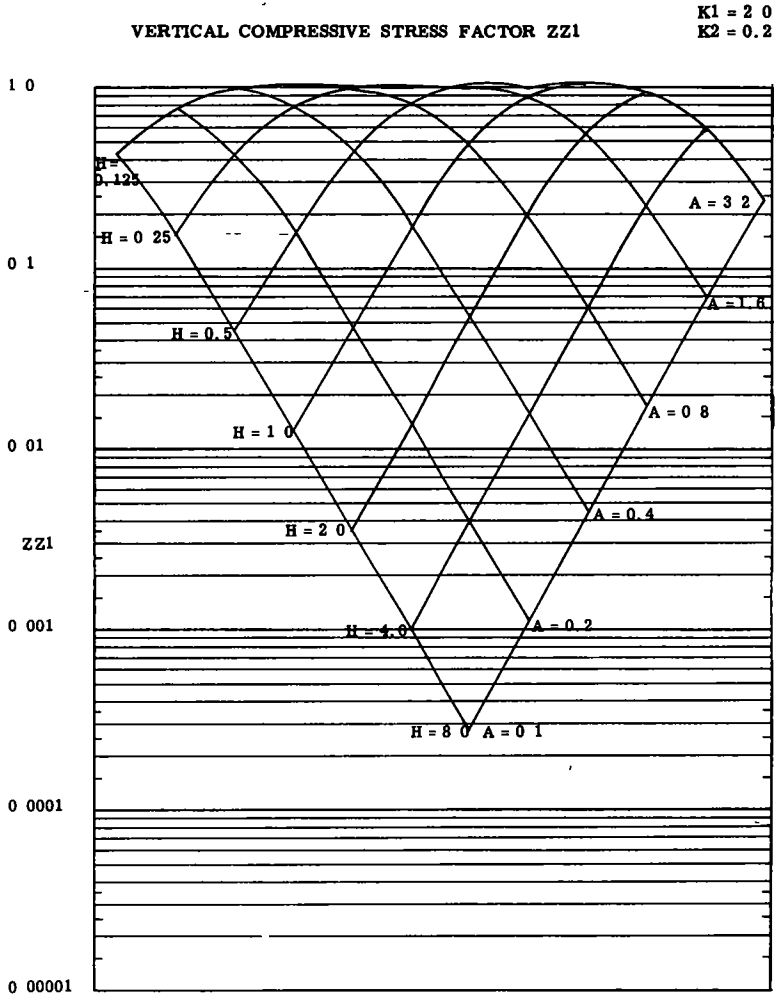

Figure 12.

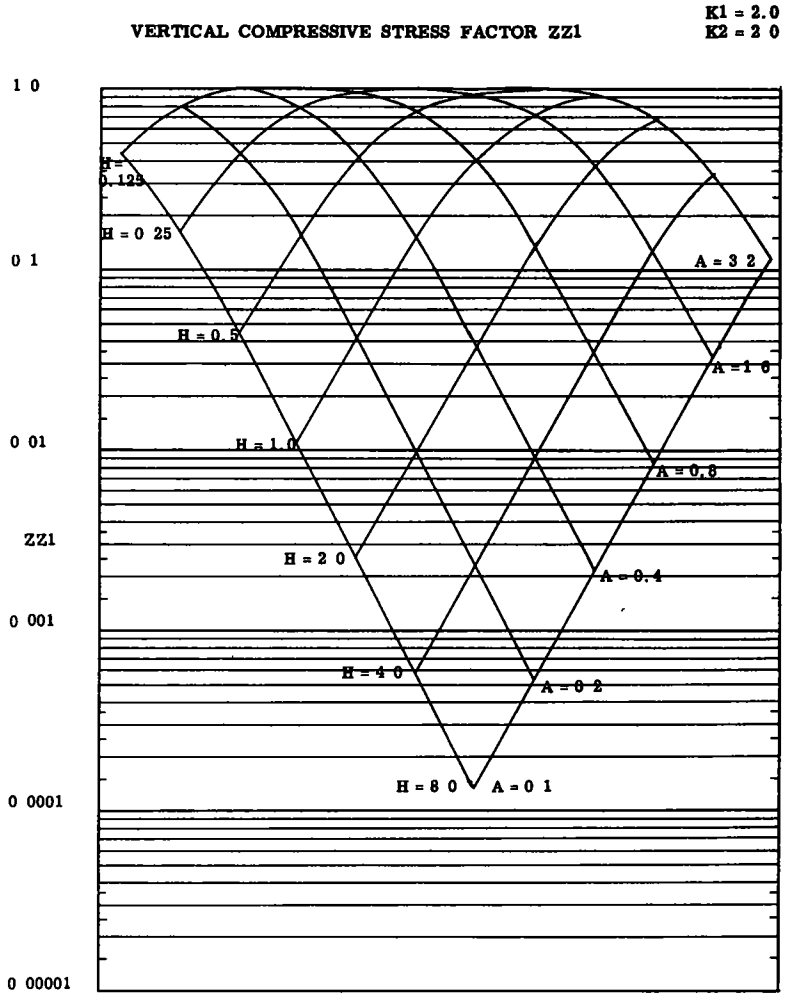

Figure 13.

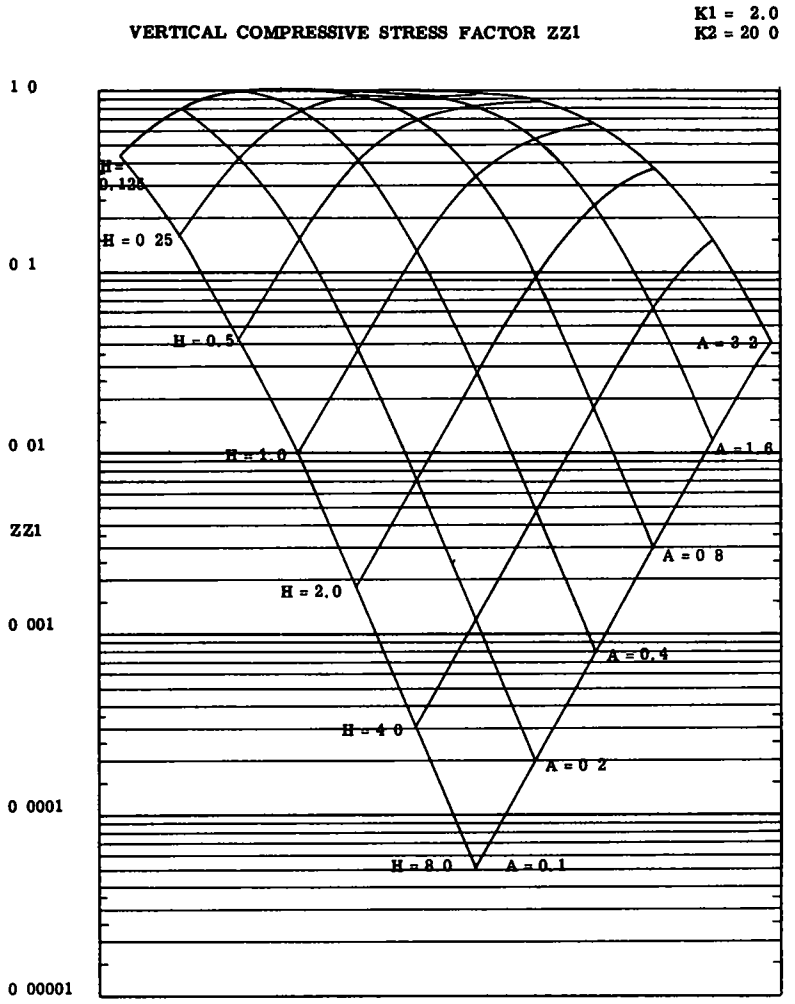

Figure 14.

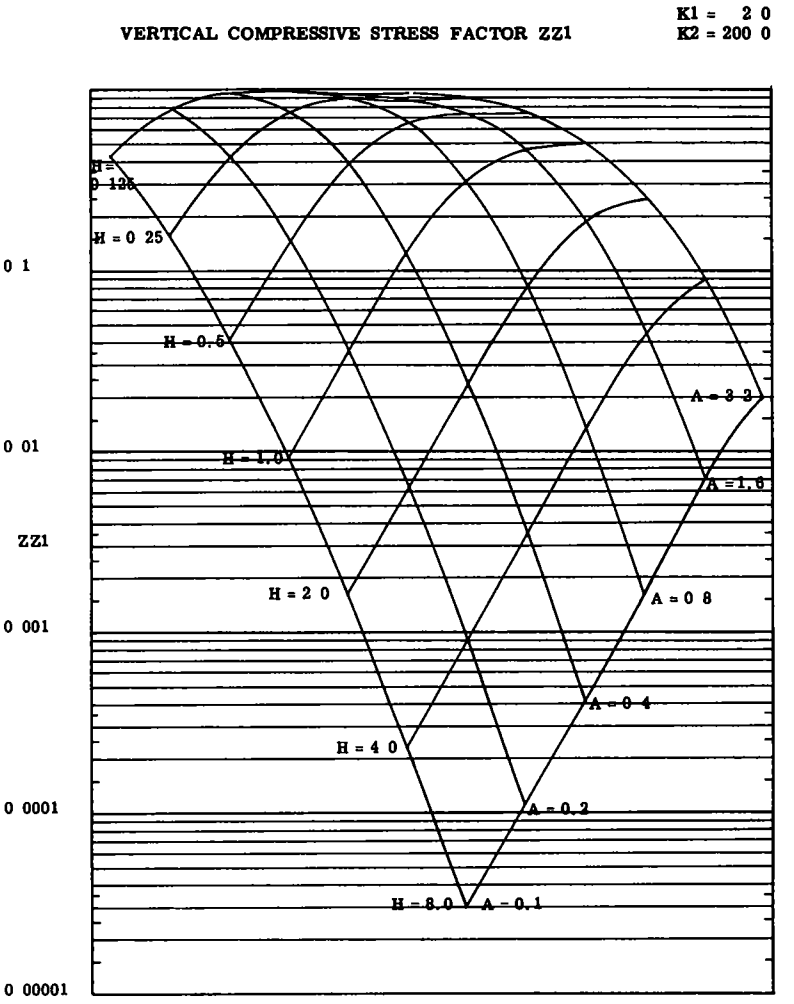

Figure 15.

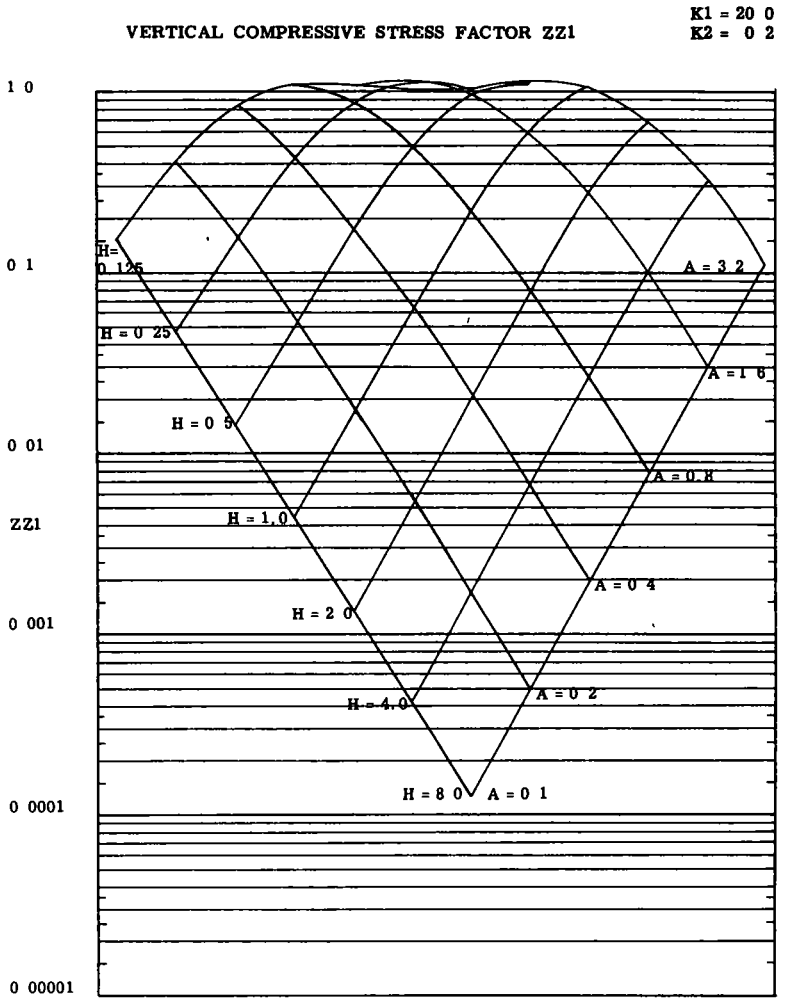

Figure 16.

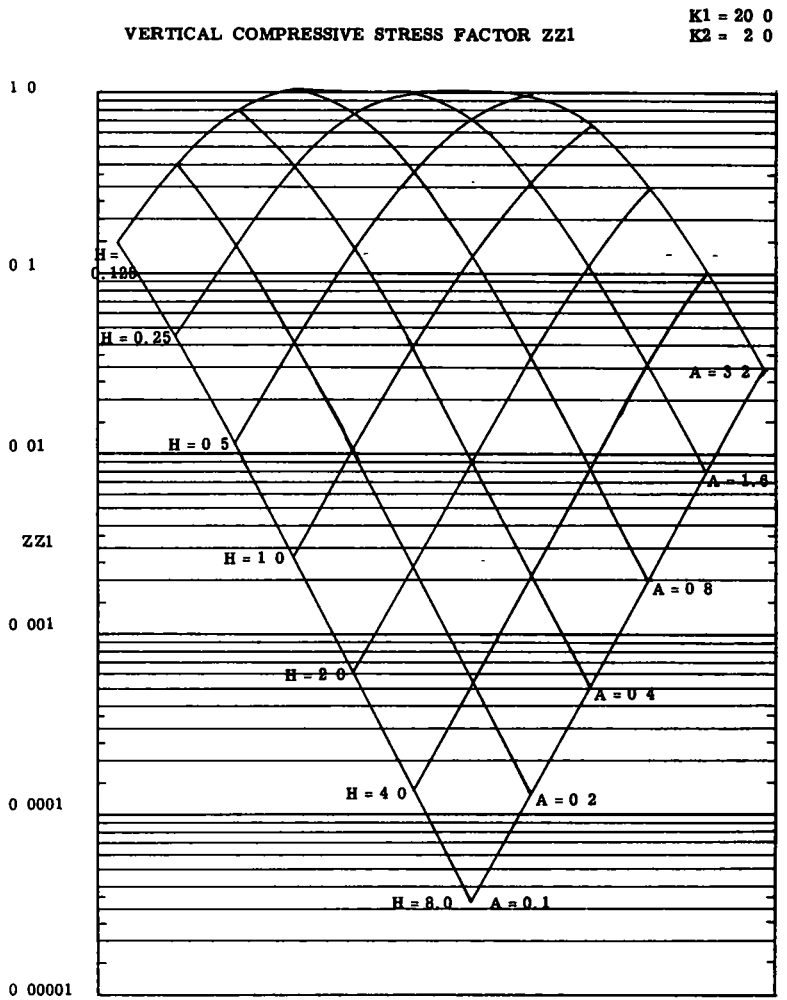

Figure 17.

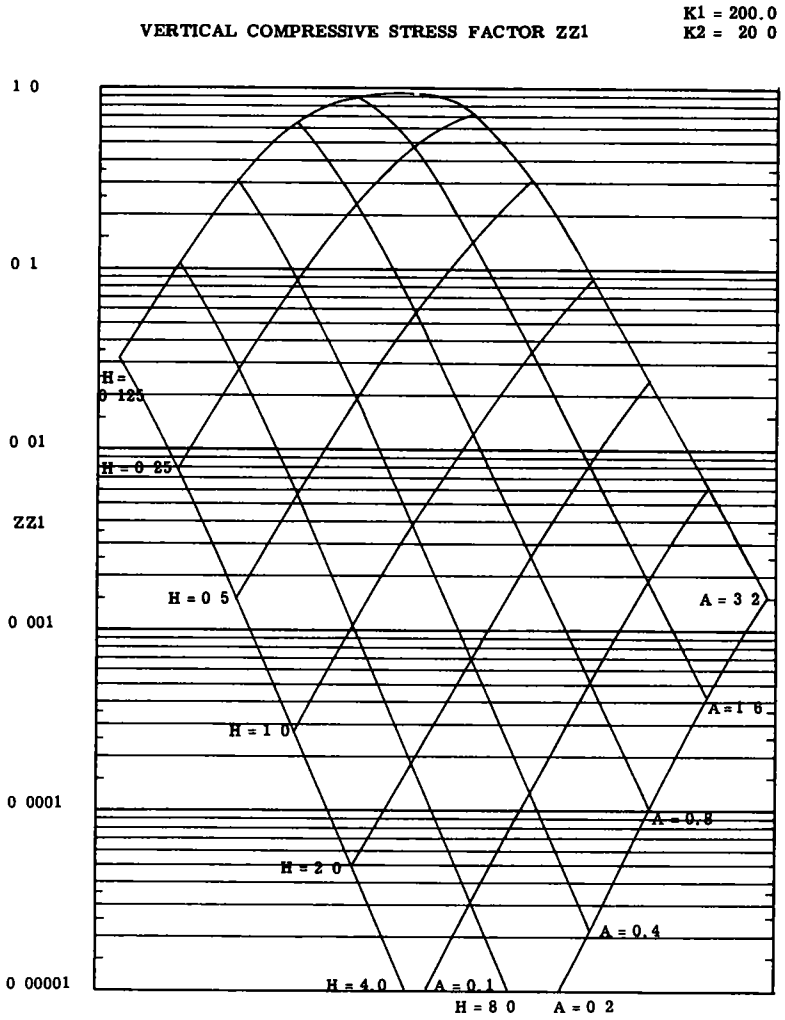

Figure 22.

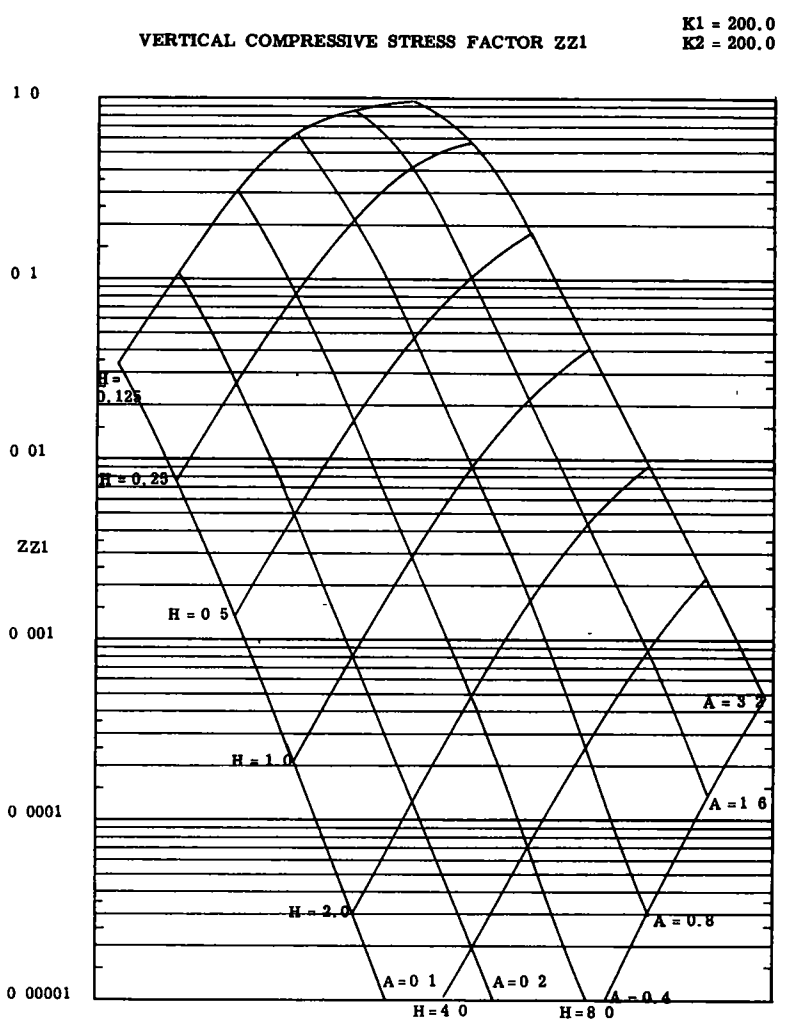

Figure 23.

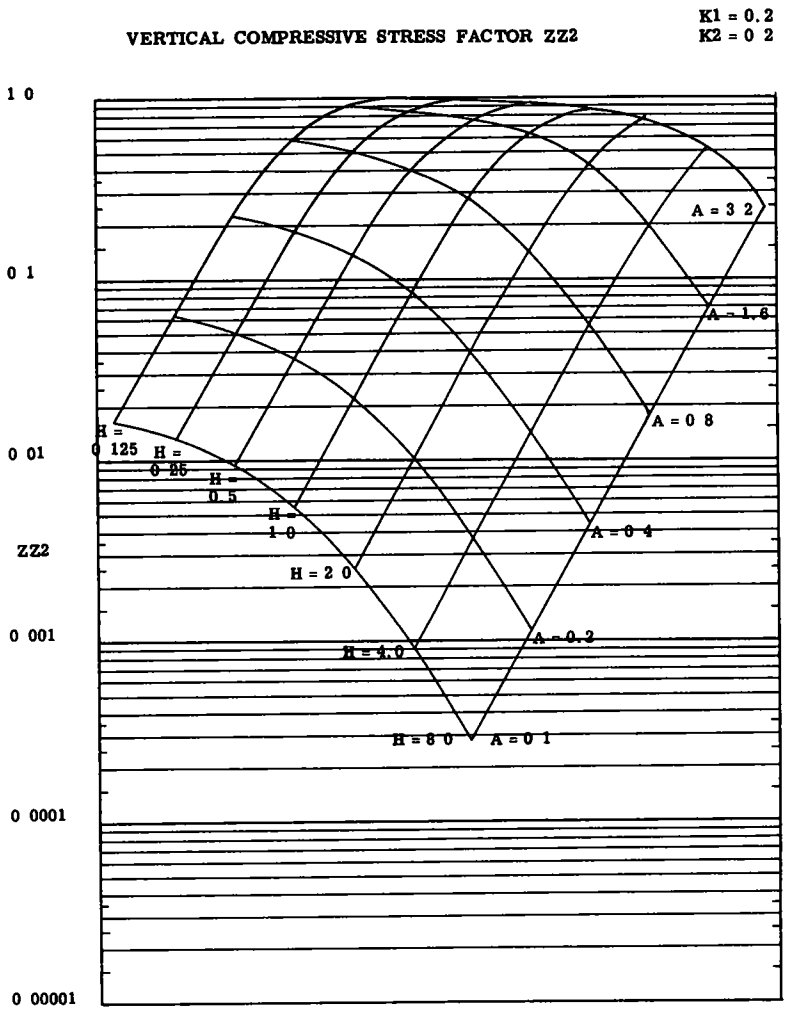

Figure 24.

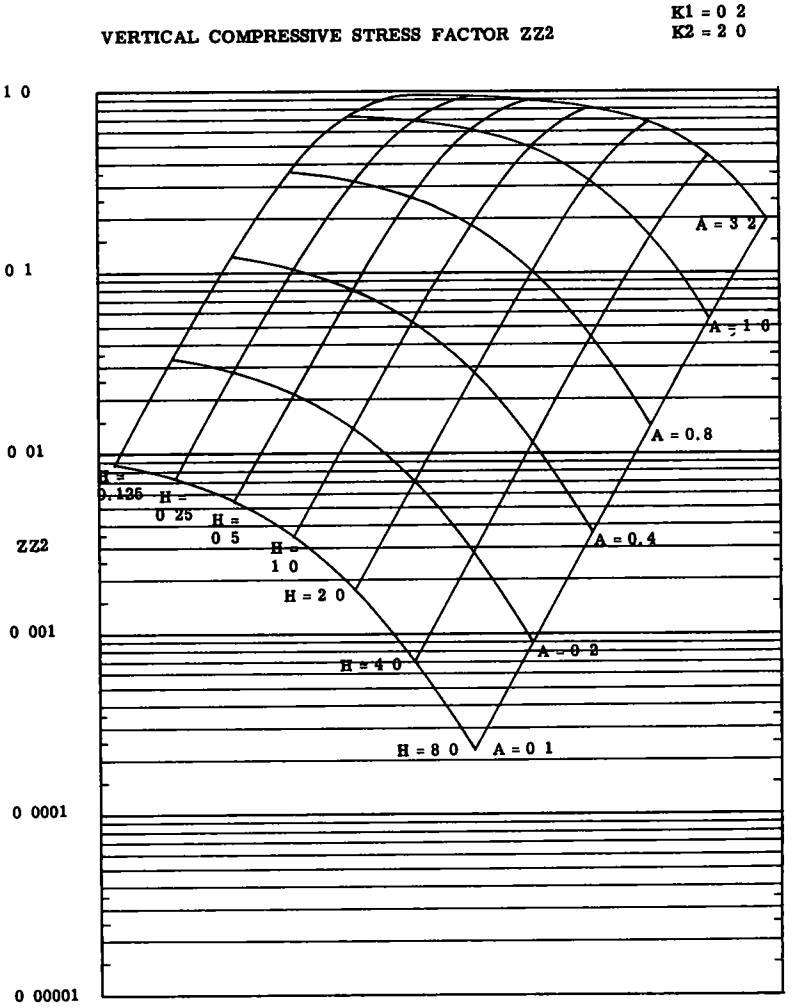

Figure 25.

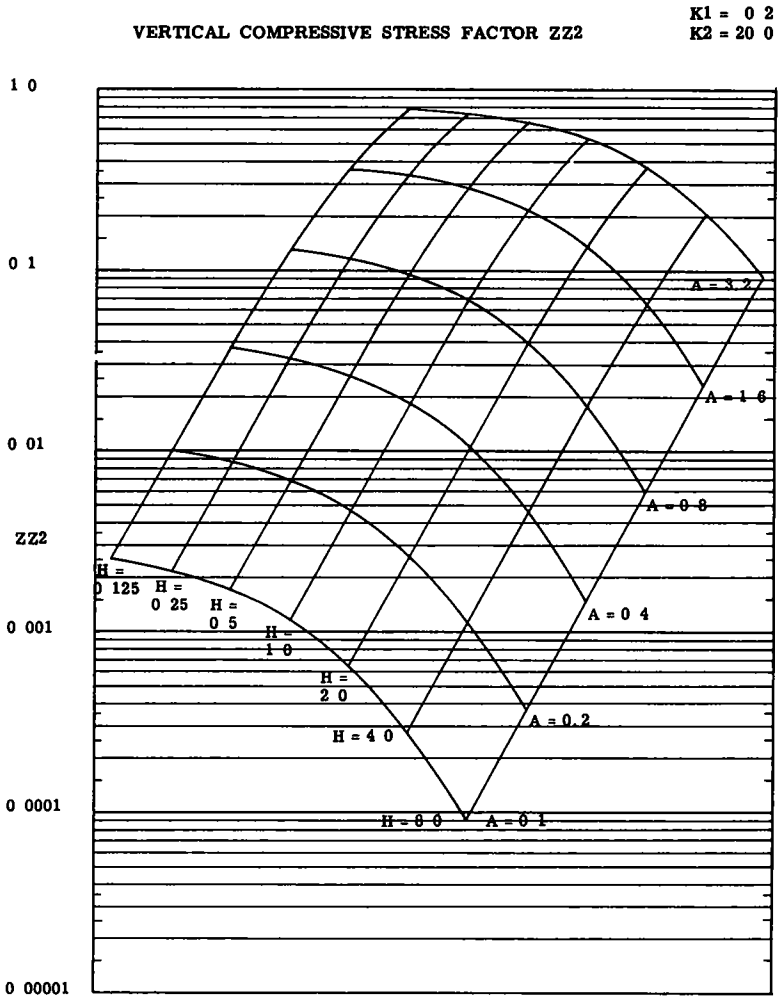

Figure 26.

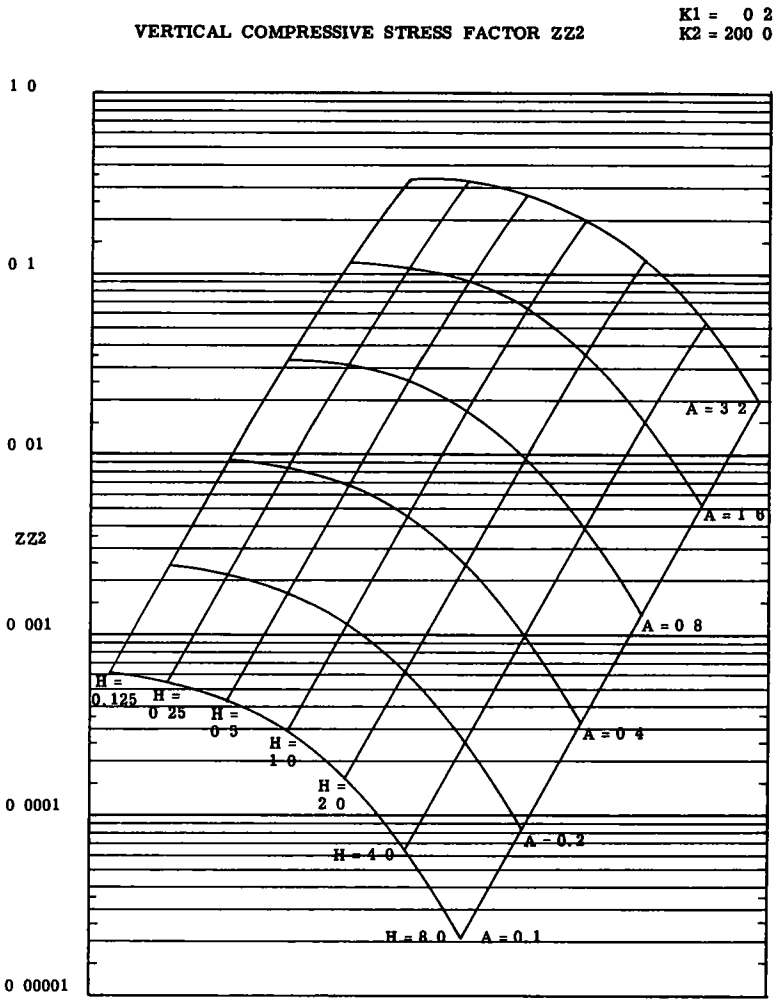

Figure 27.

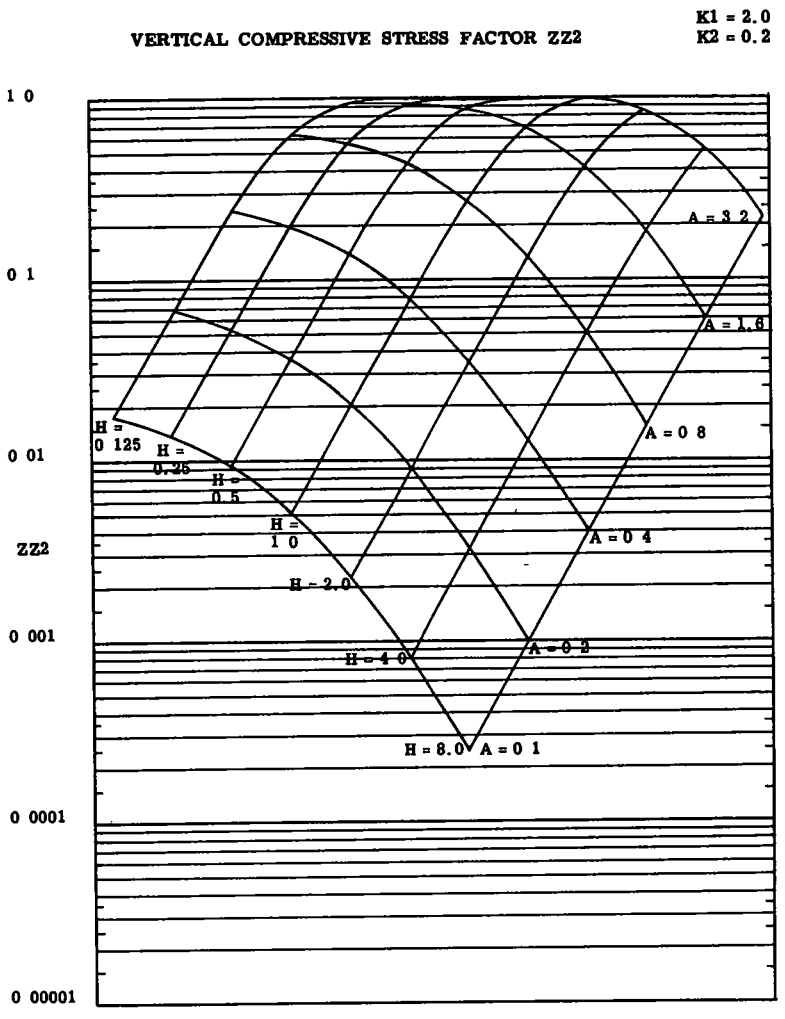

Figure 28.

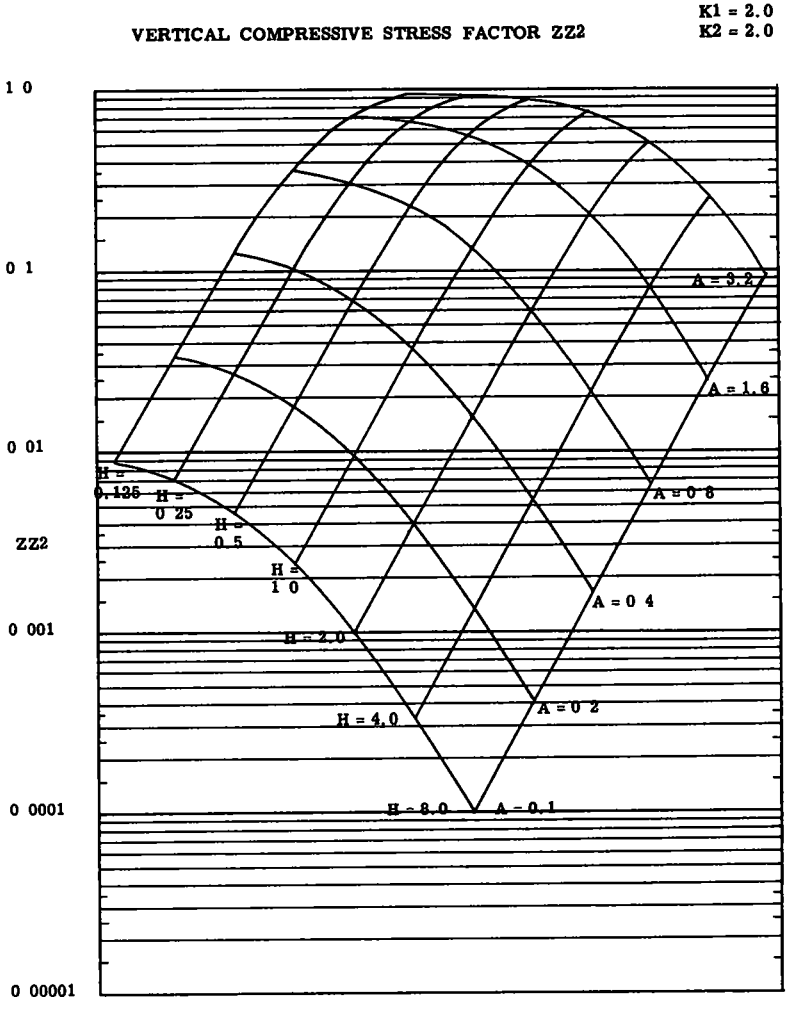

Figure 29.

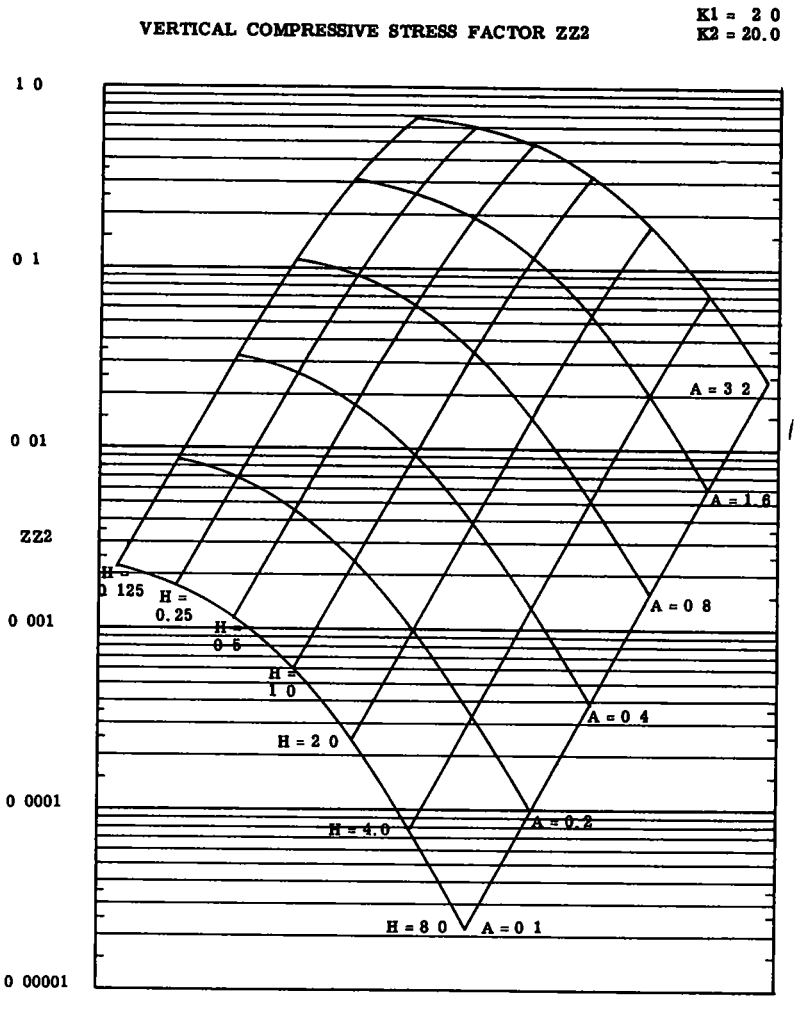

Figure 30.

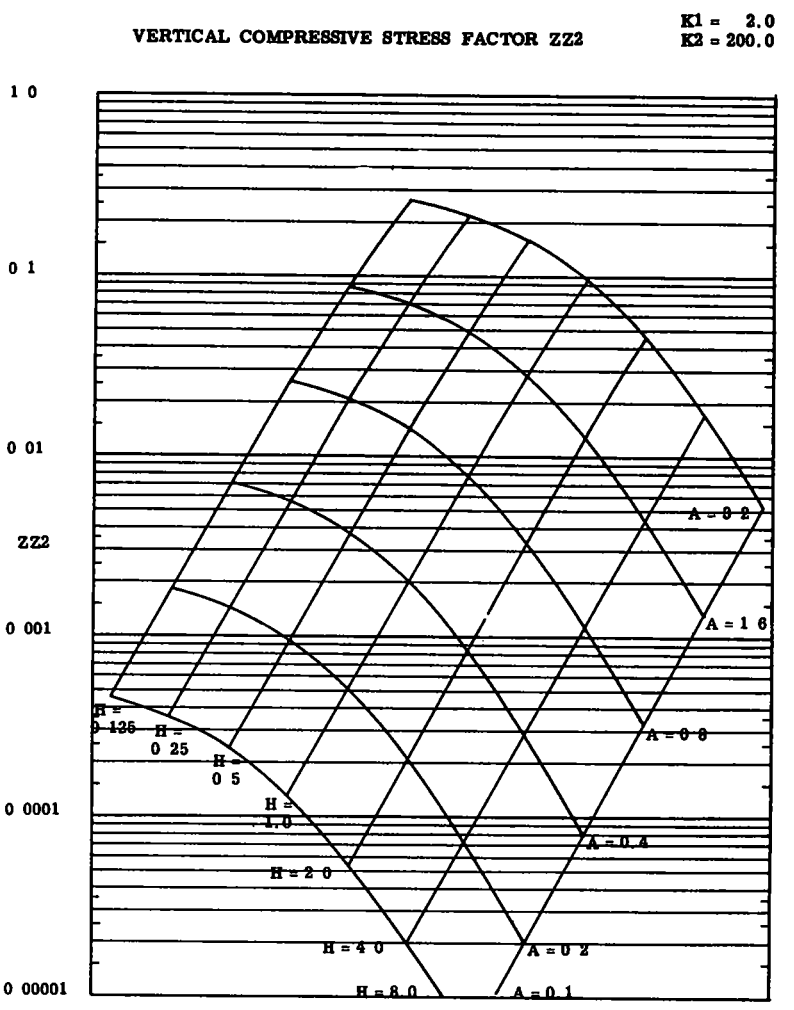

Figure 31.

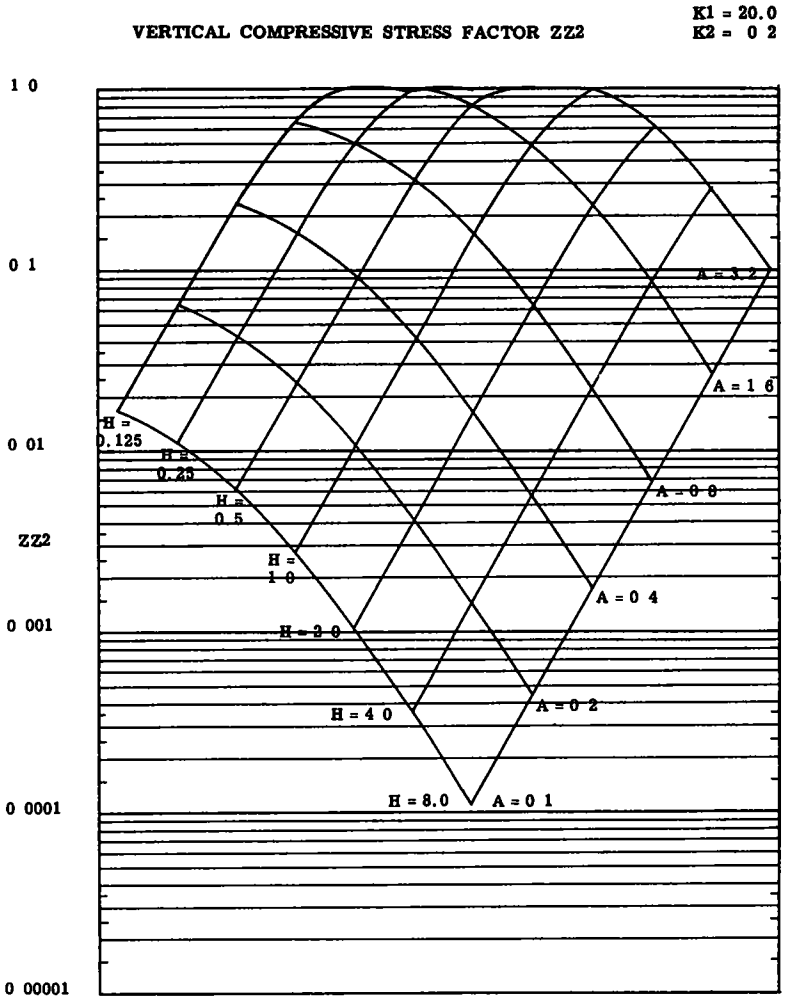

Figure 32.

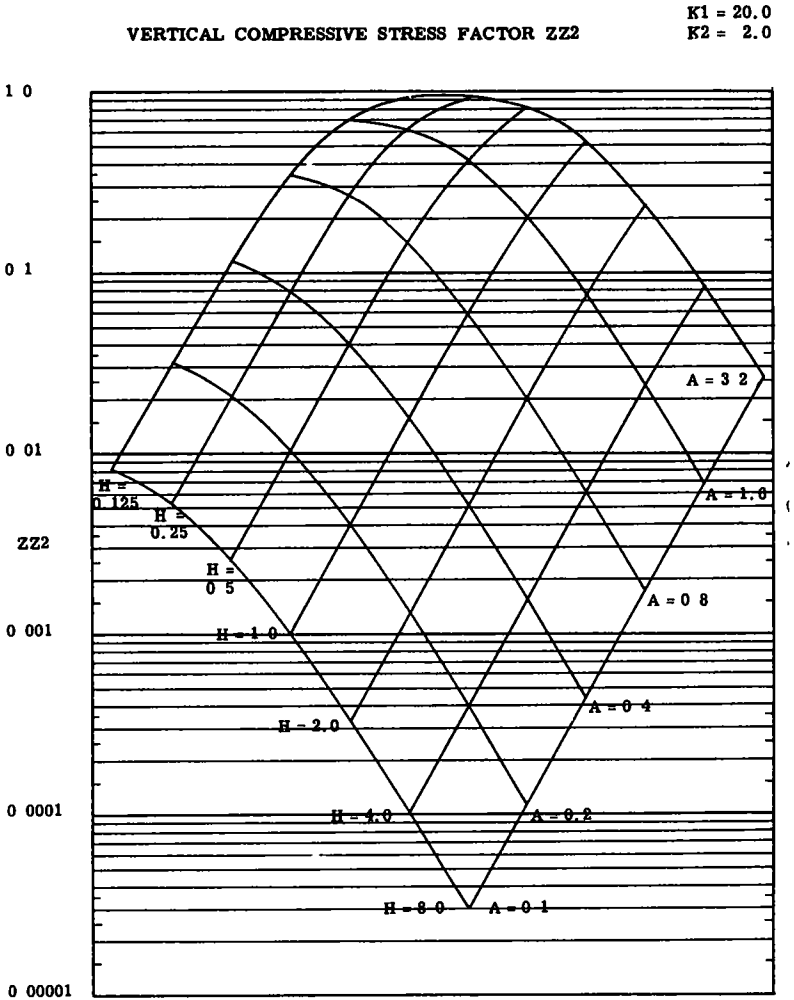

Figure 33.

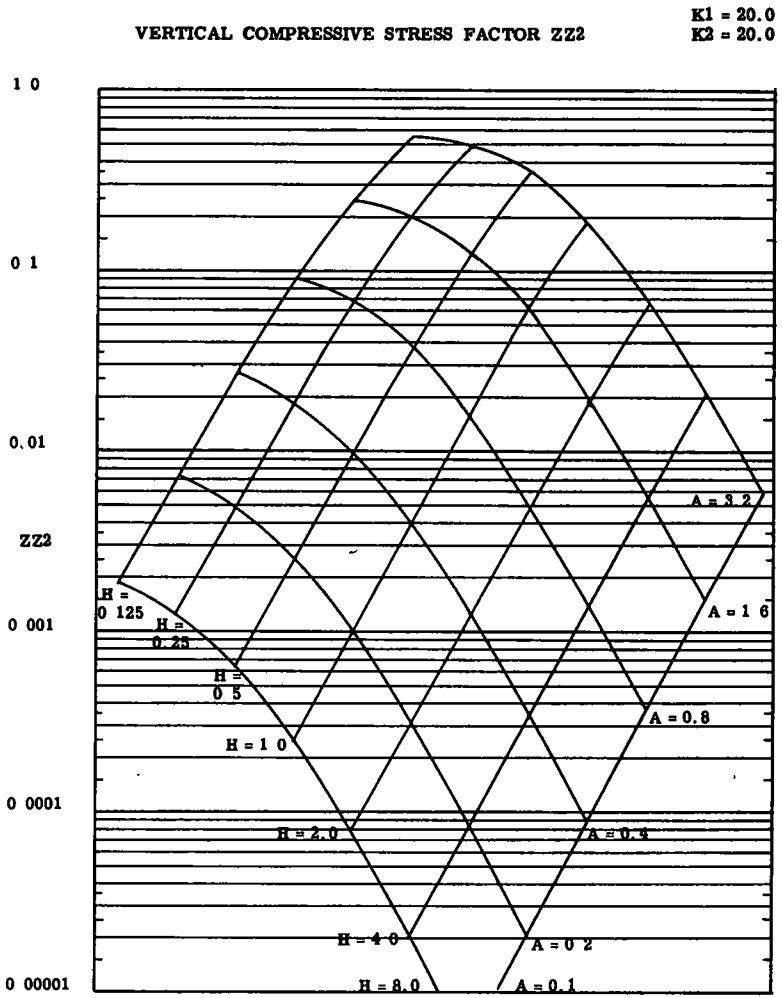

Figure 34.

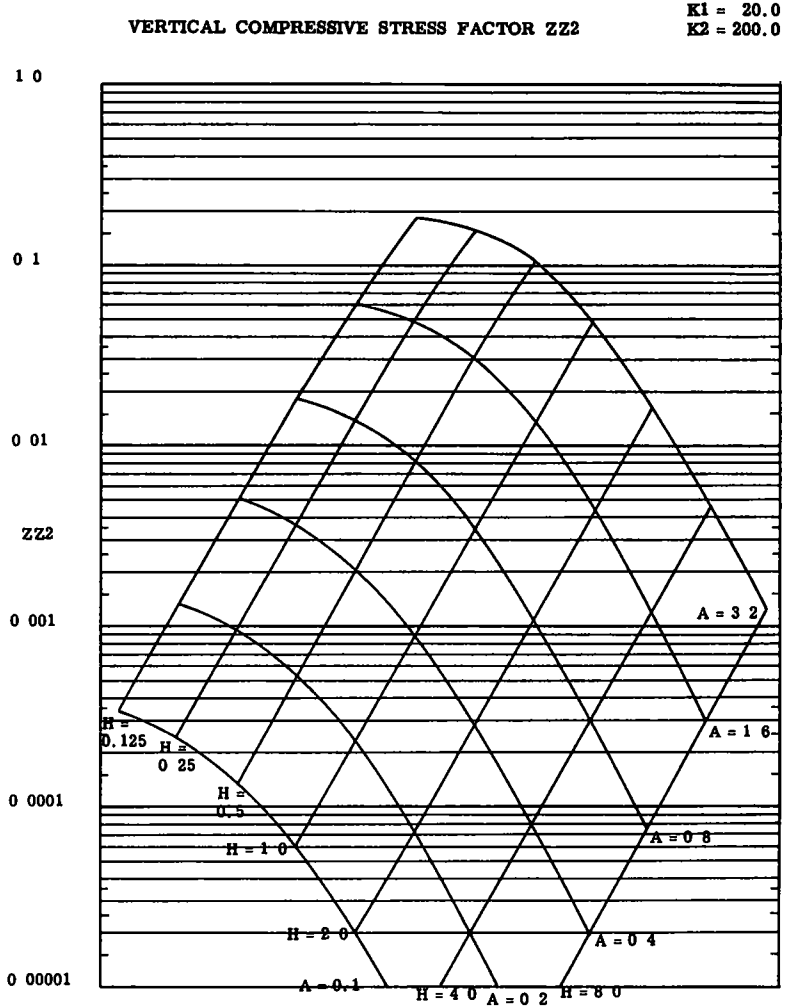

Figure 35.

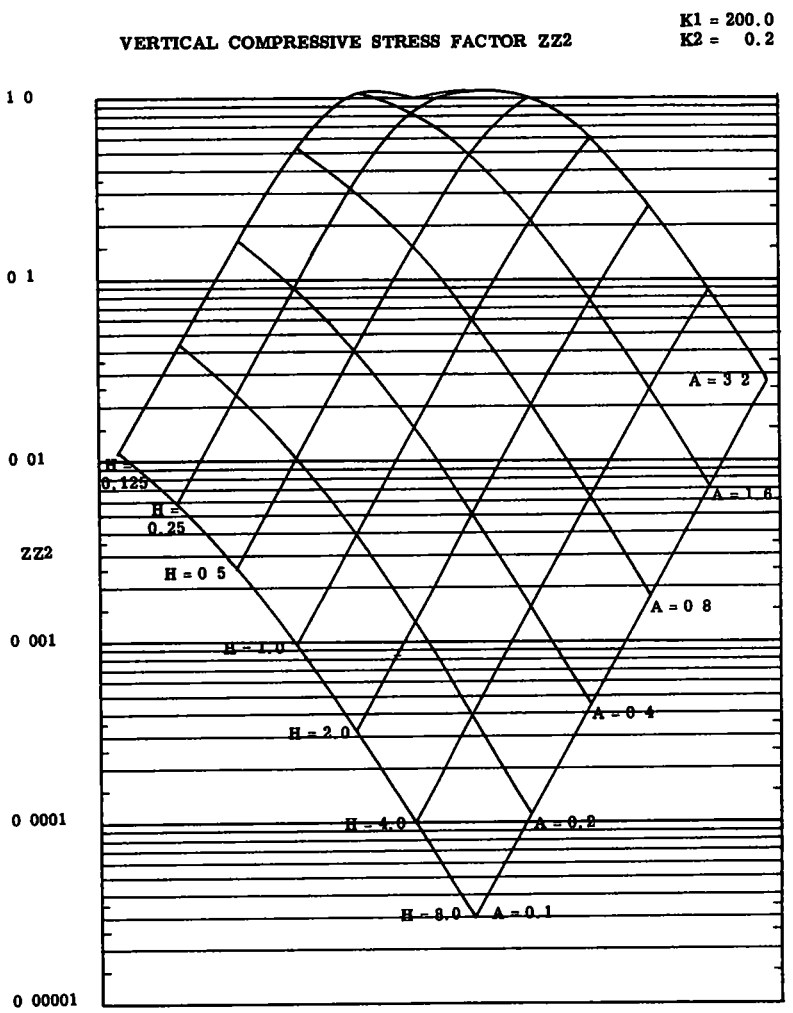

Figure 36.

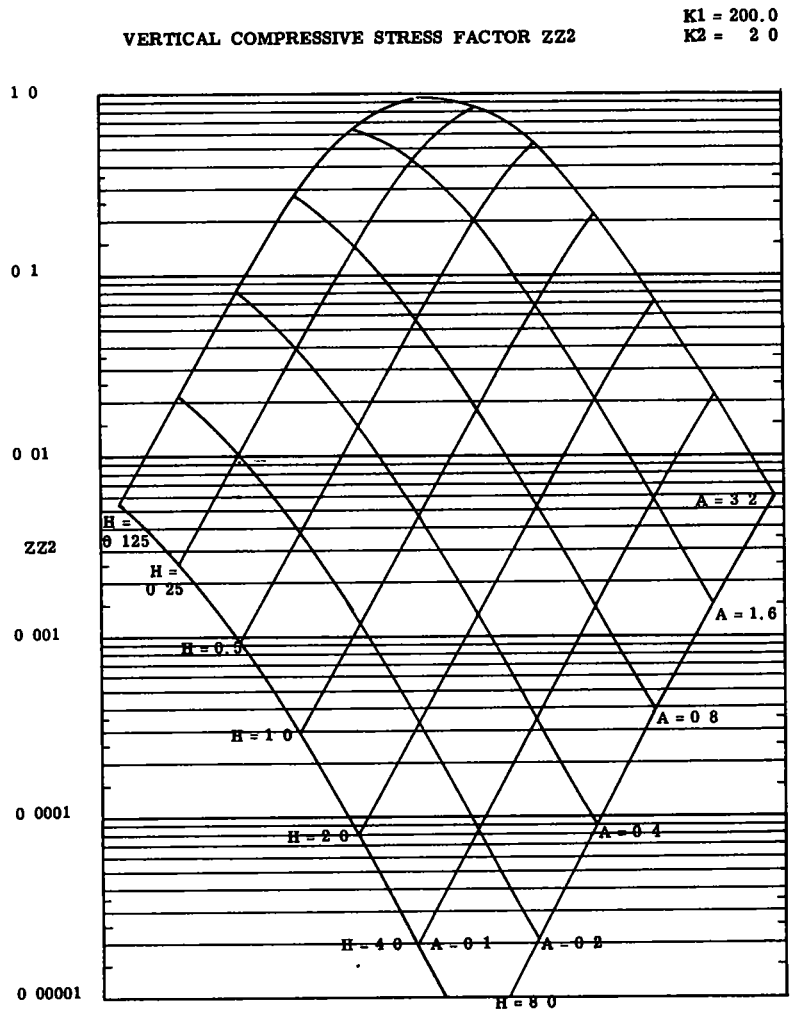

Figure 37.

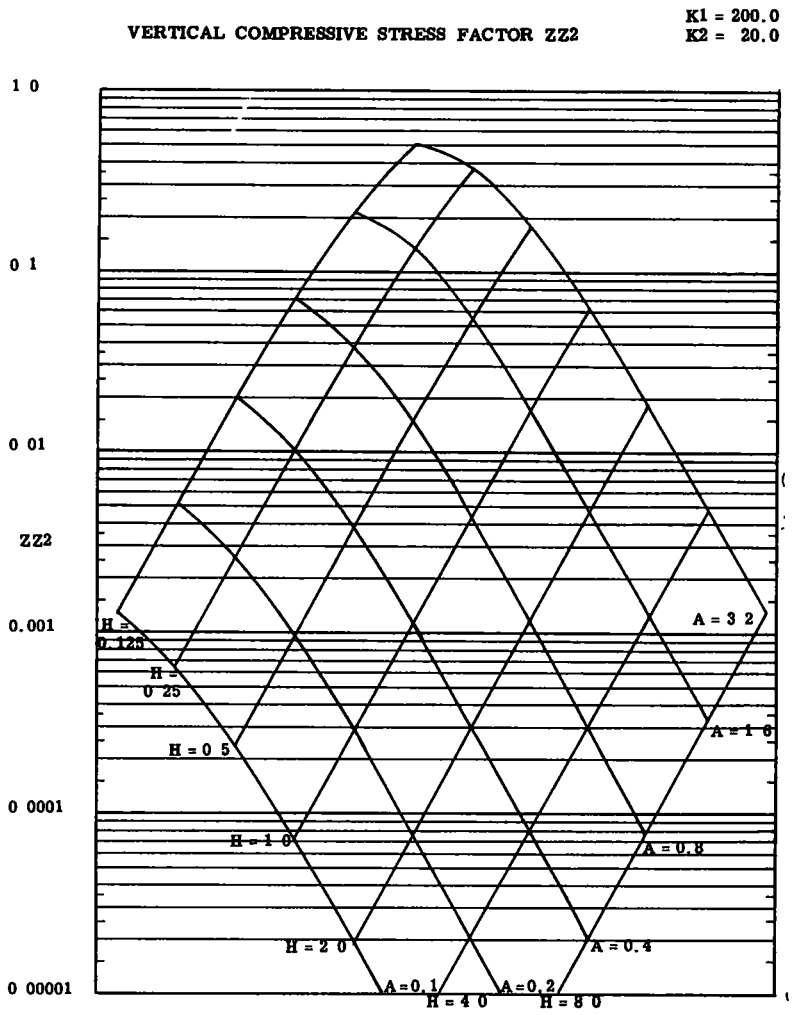

Figure 38.

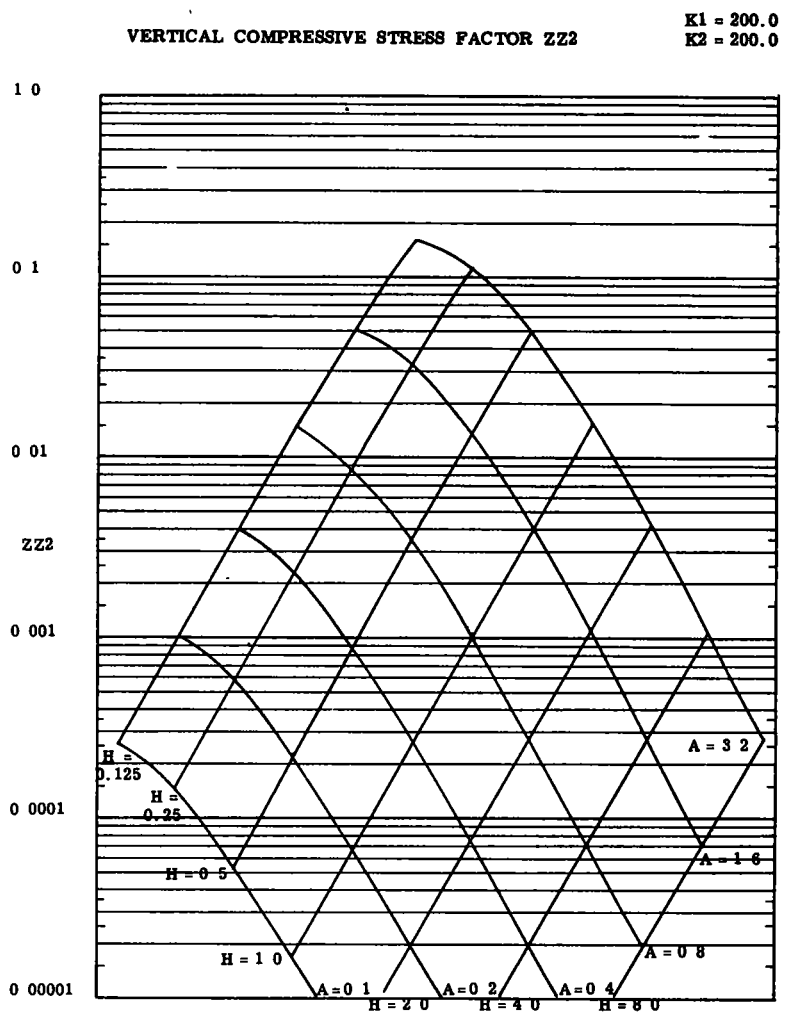

Figure 39.

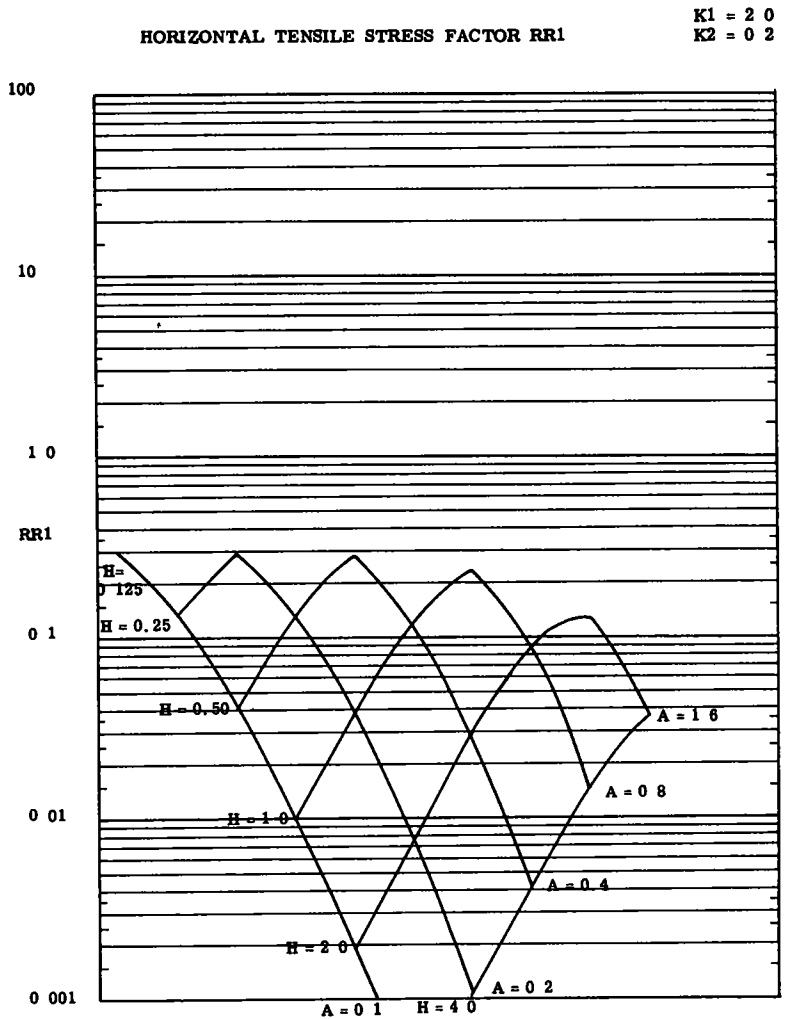

Figure 40.

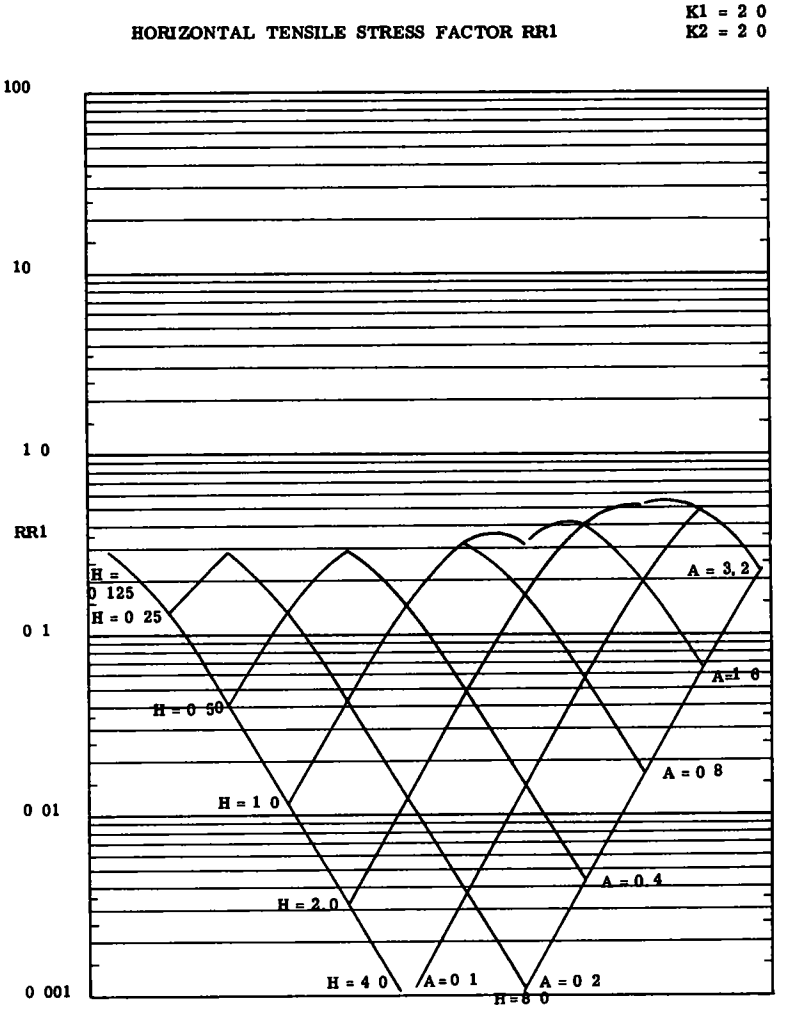

Figure 41.

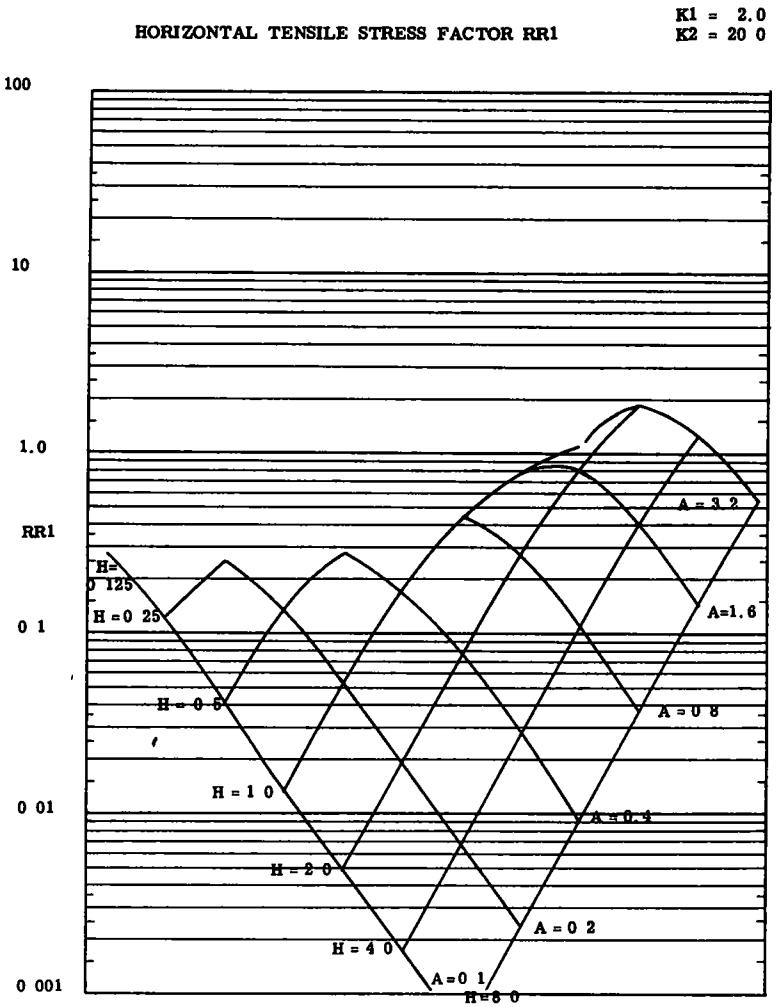

Figure 42.

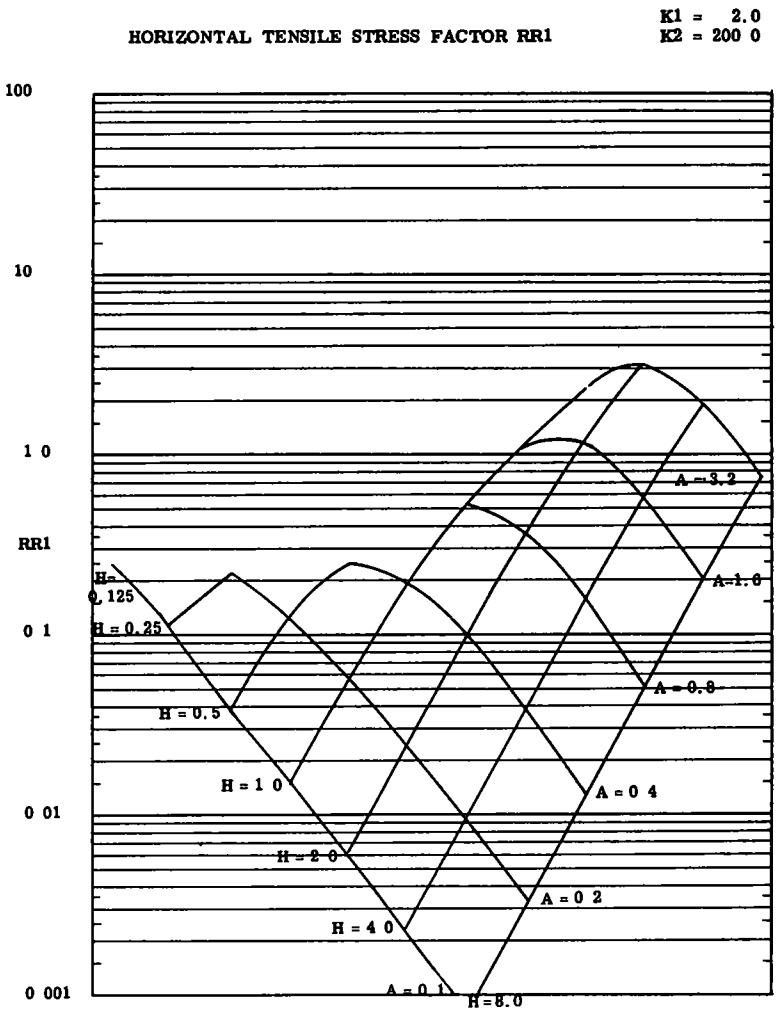

Figure 43.

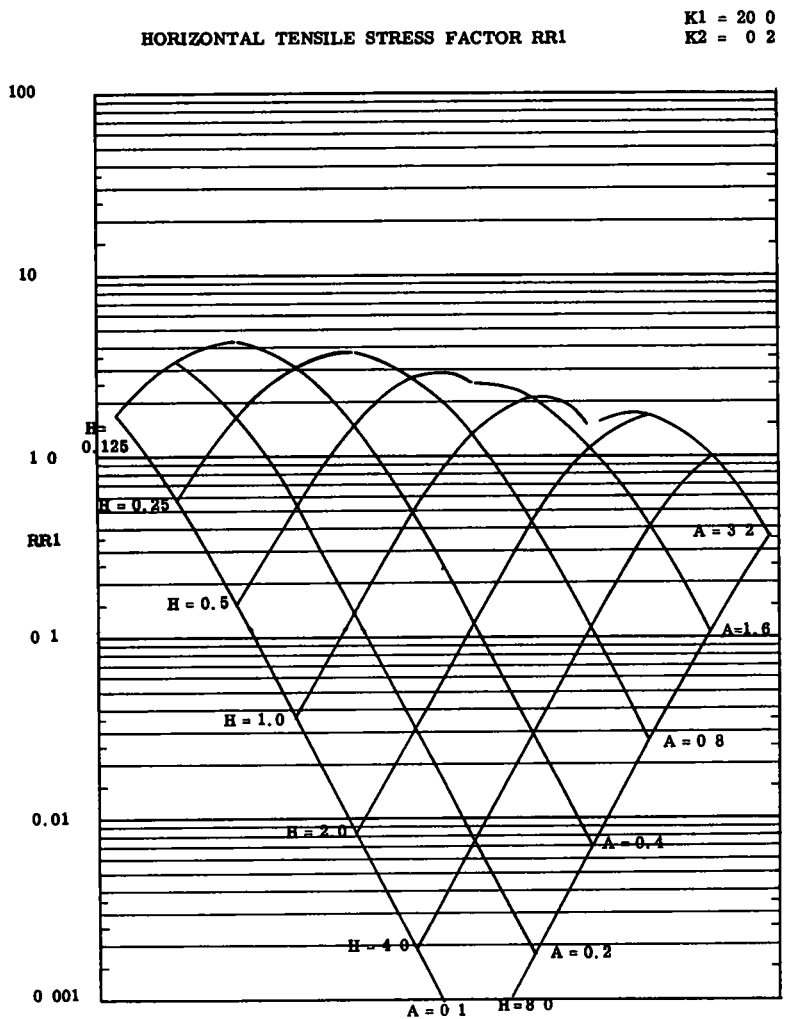

Figure 44.

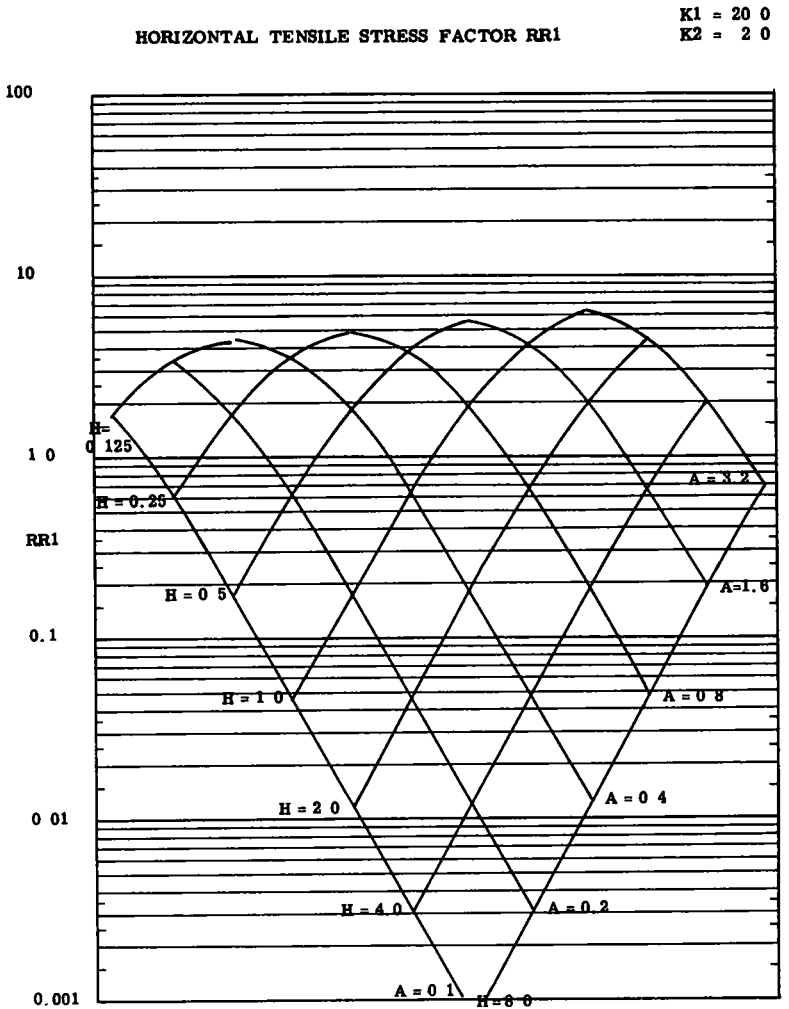

Figure 45.

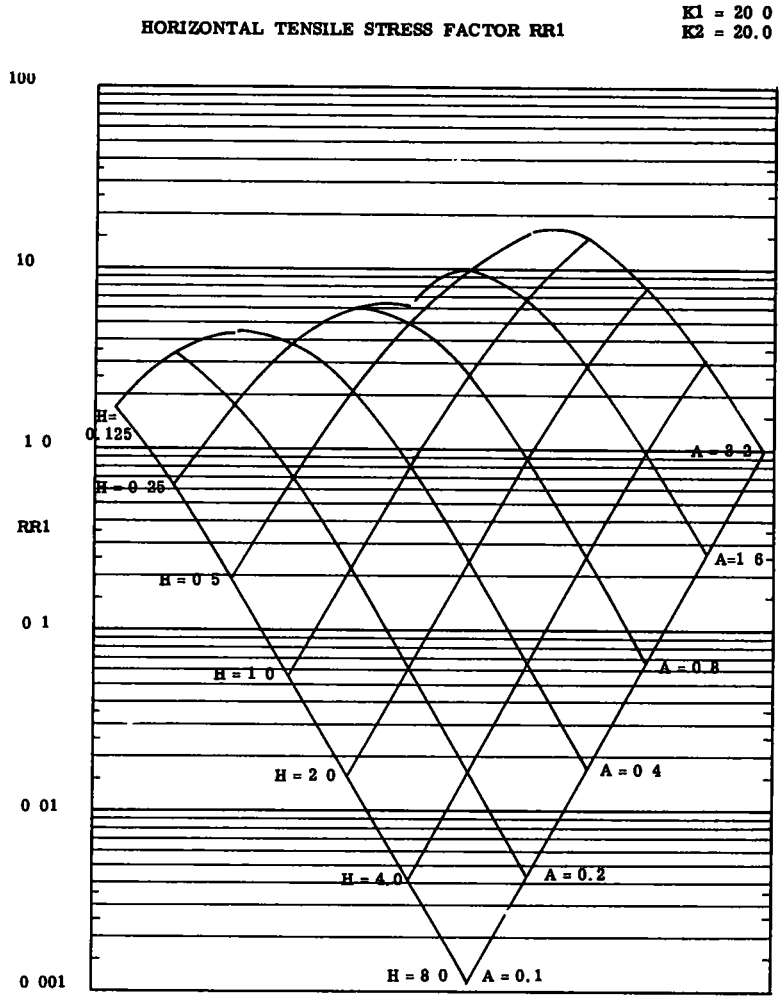

Figure 46.

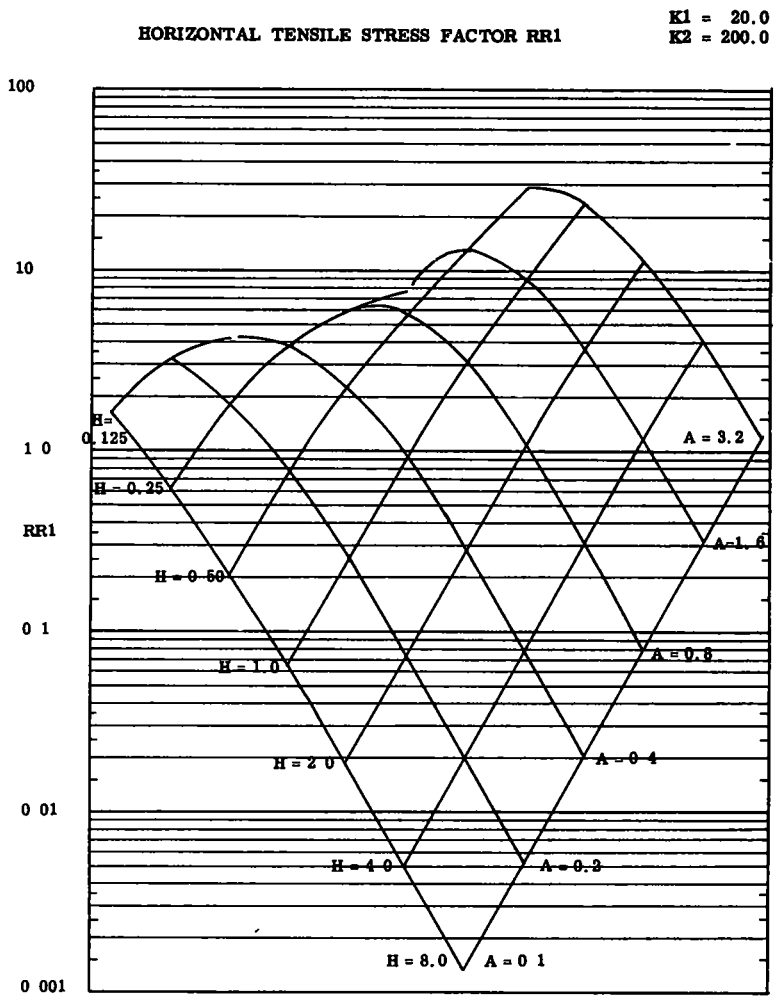

Figure 47.

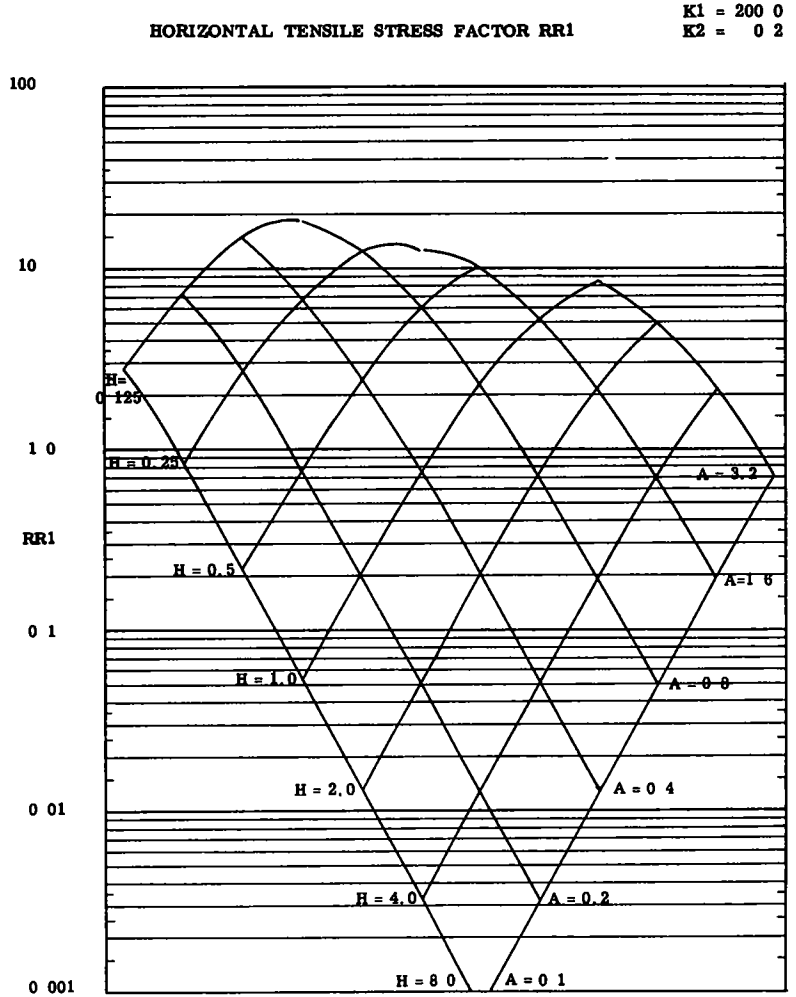

Figure 48.

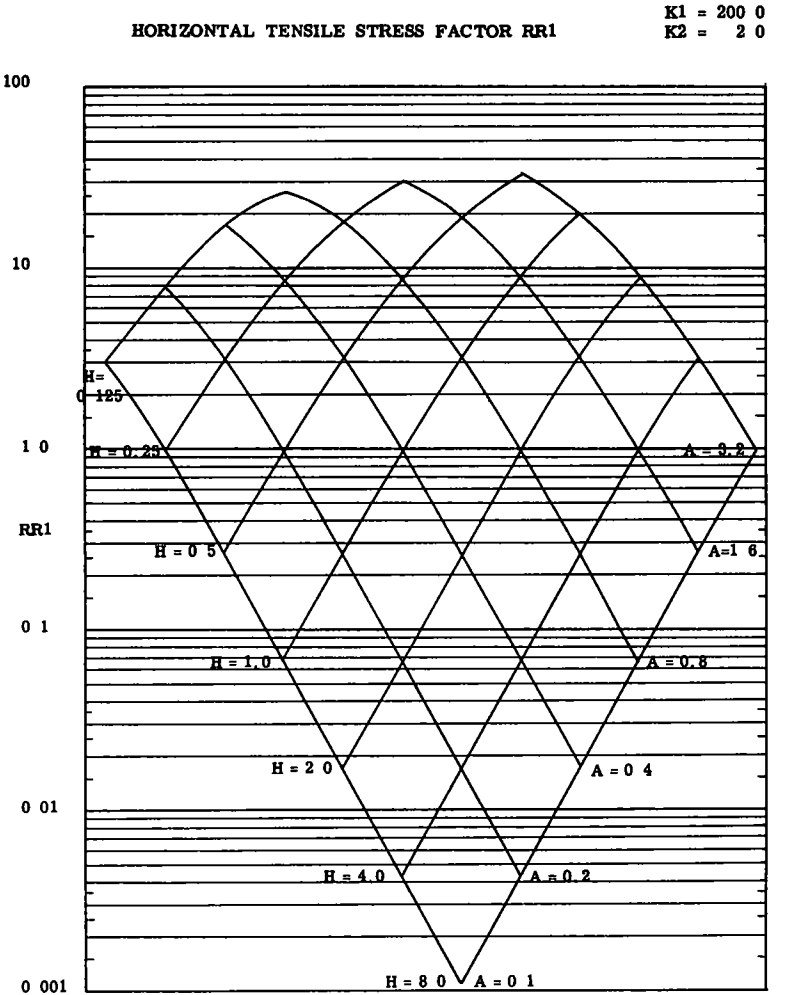

Figure 49.

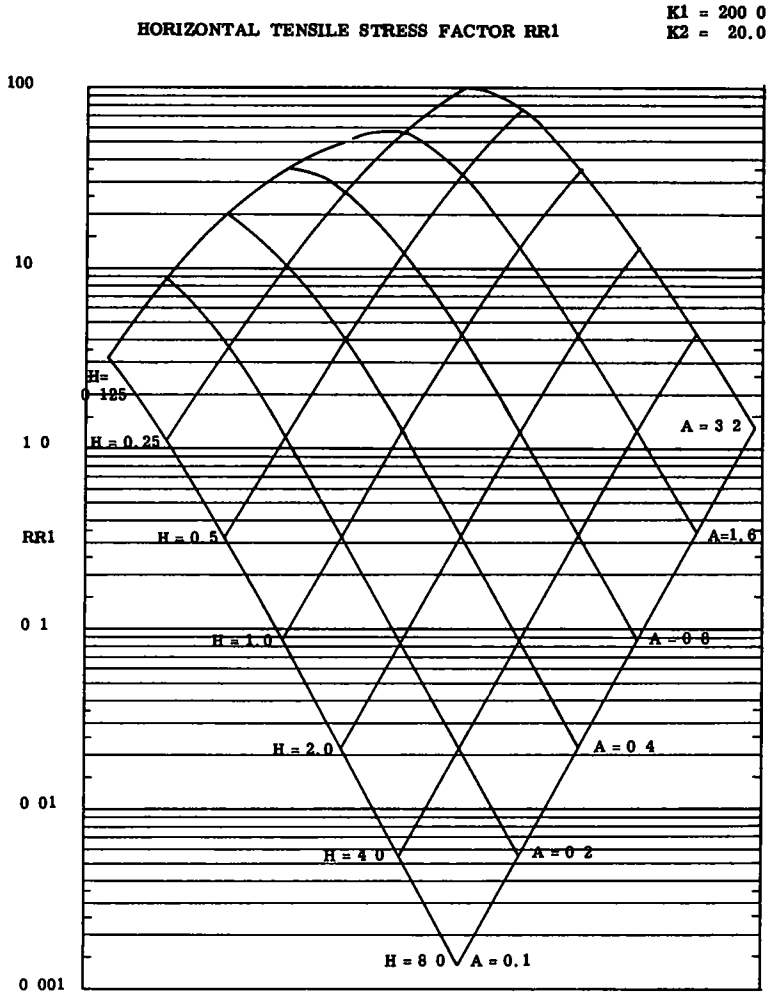

Figure 50.

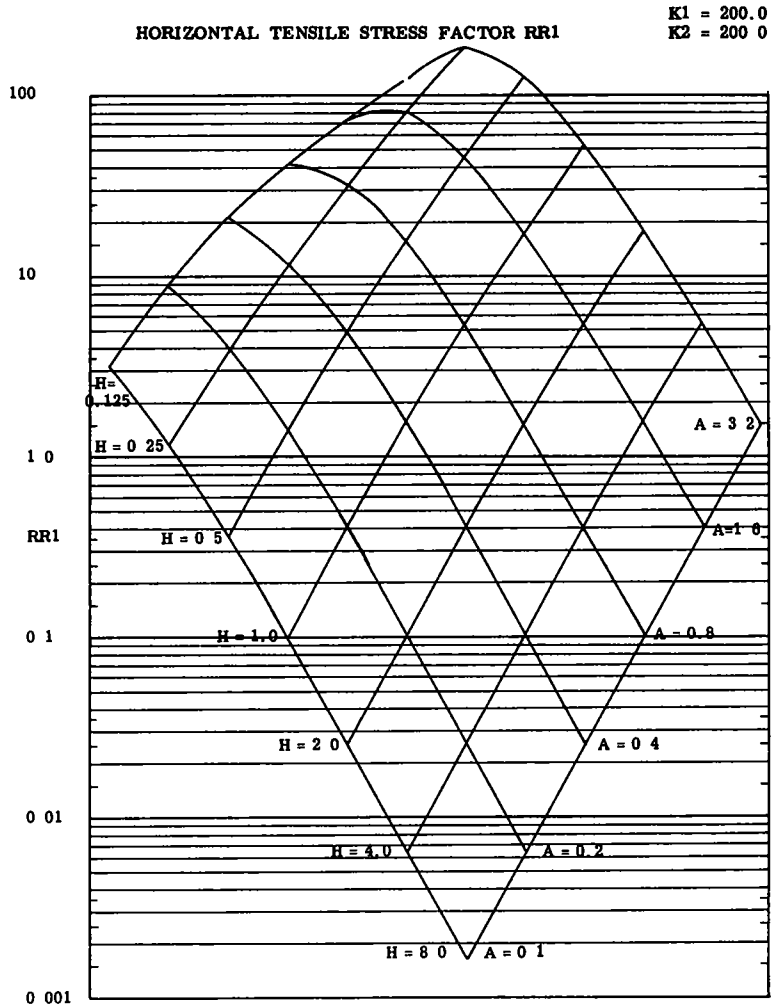

Figure 51.

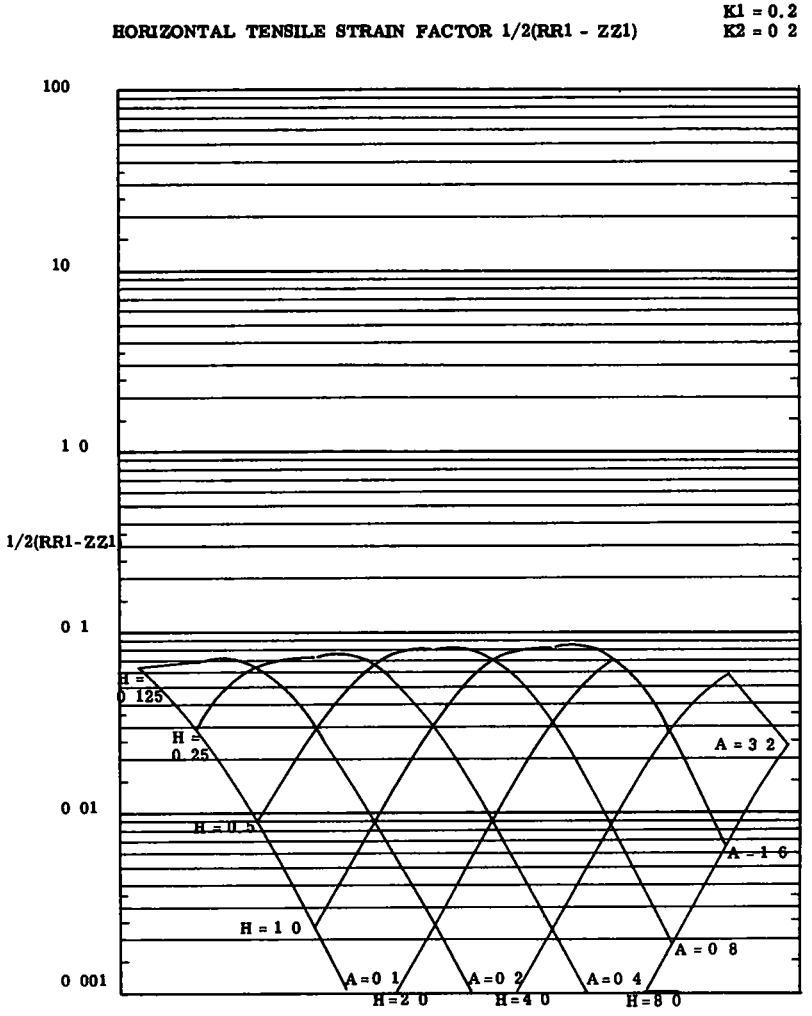

Figure 52.

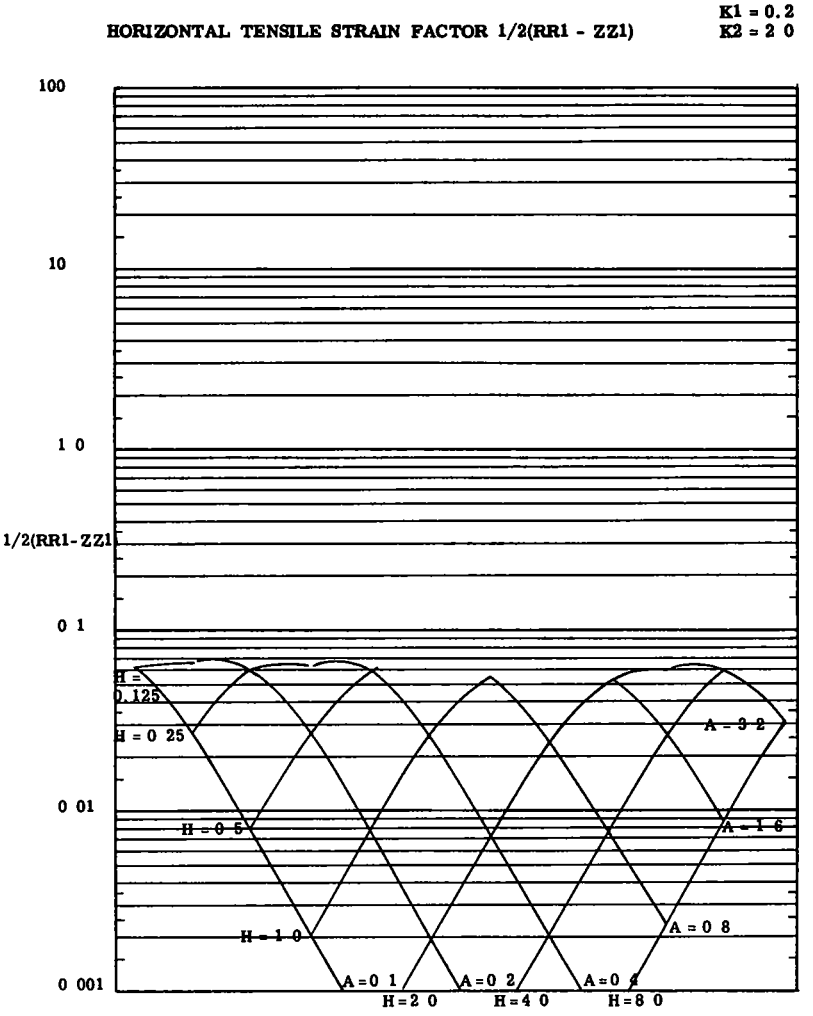

Figure 53.

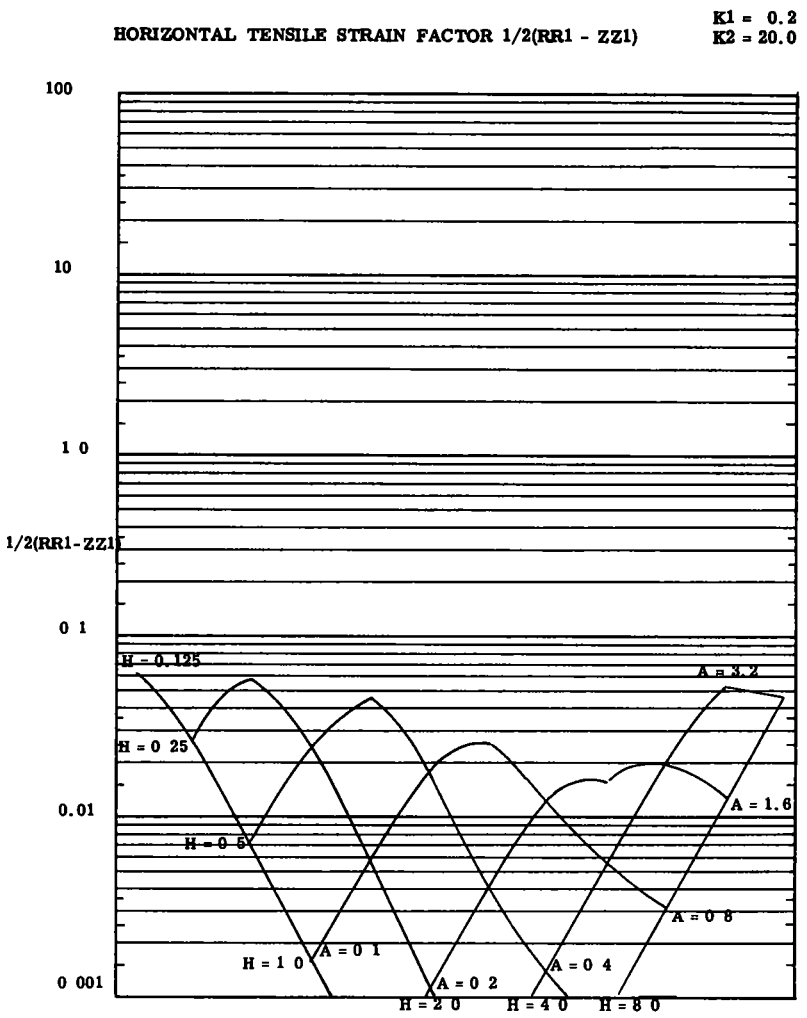

Figure 54.

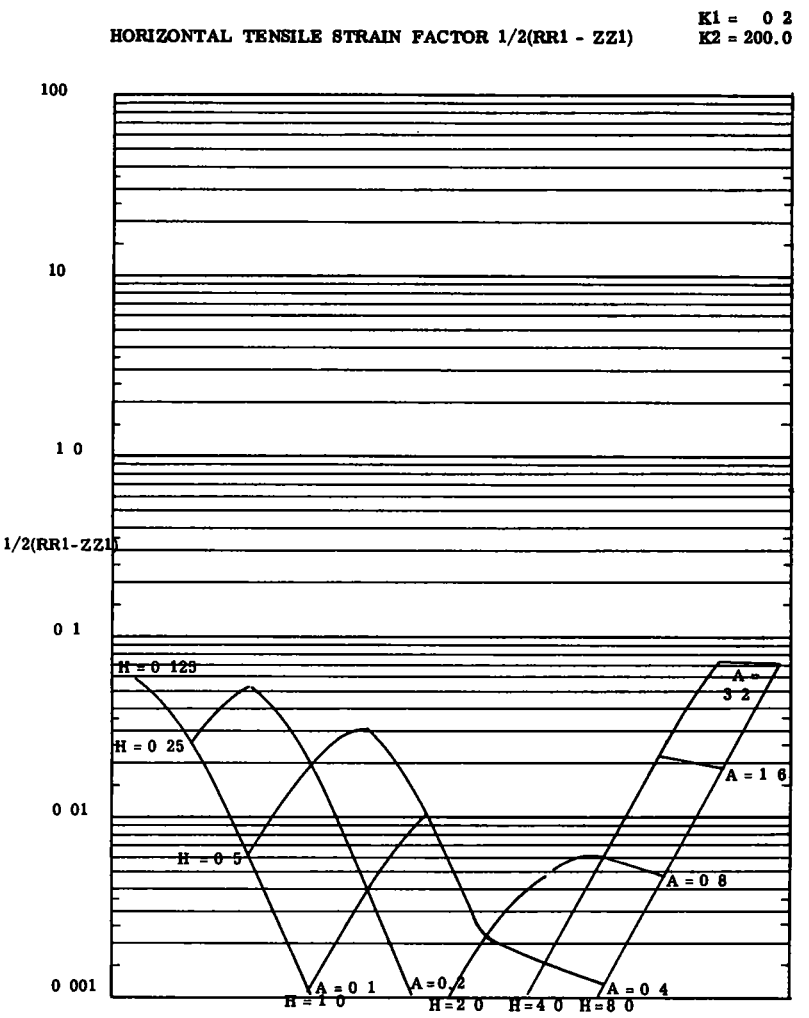

Figure 55.

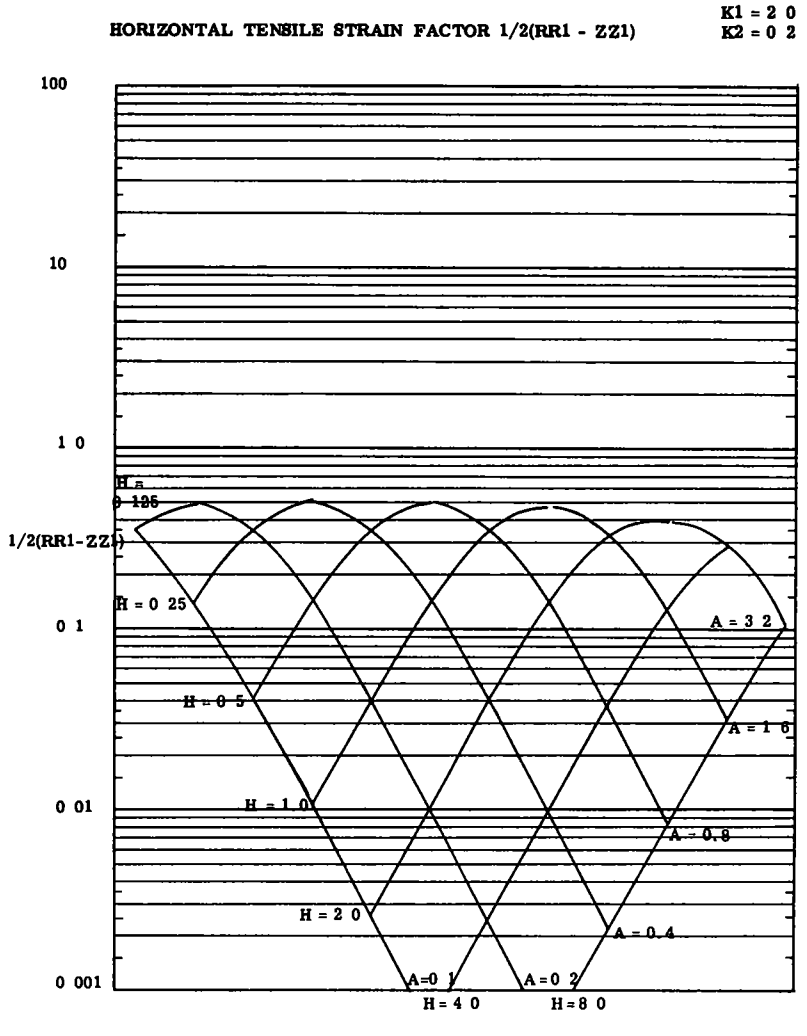

Figure 56.

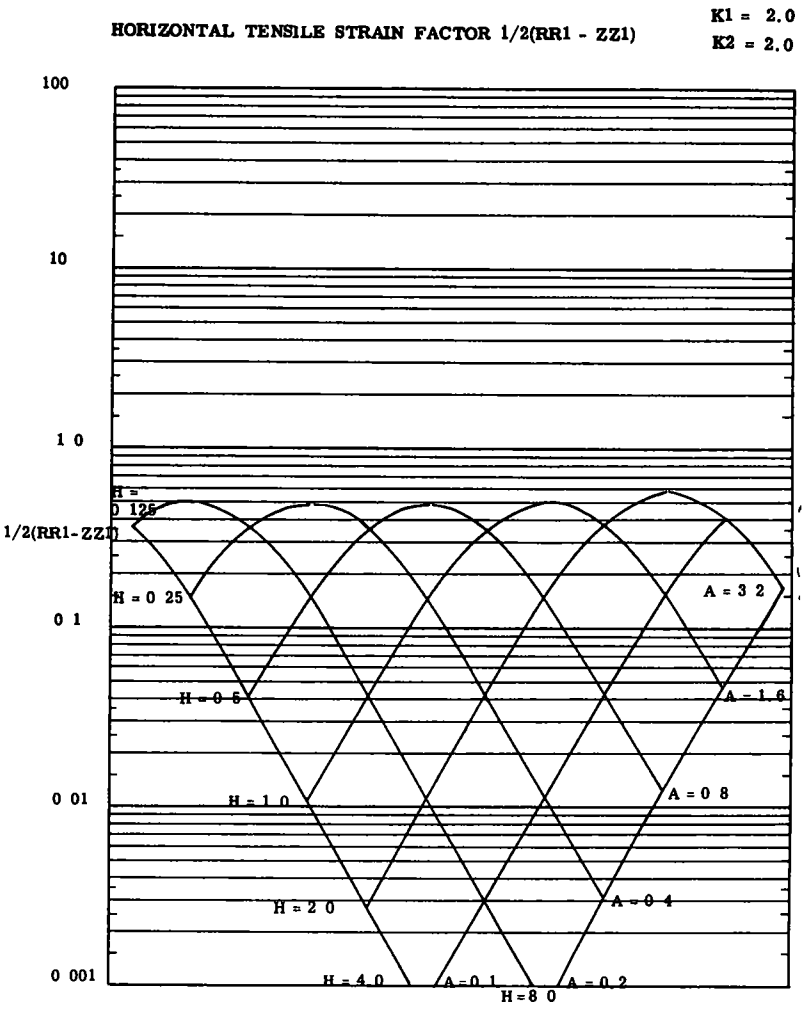

Figure 57.

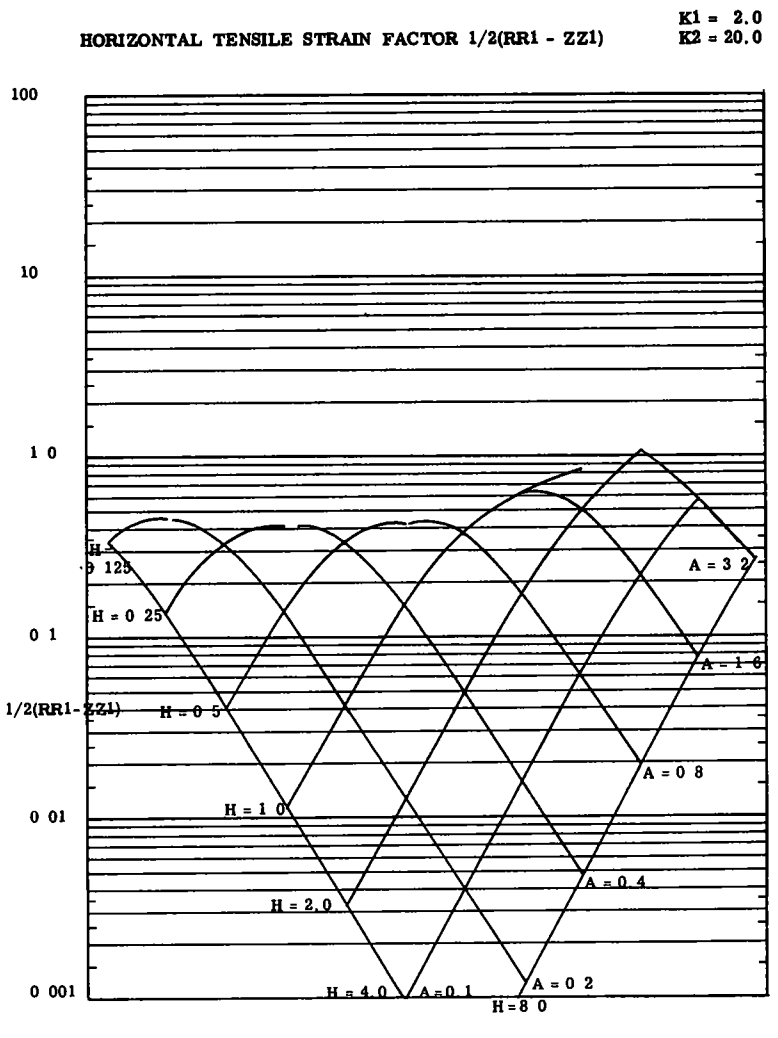

Figure 58.

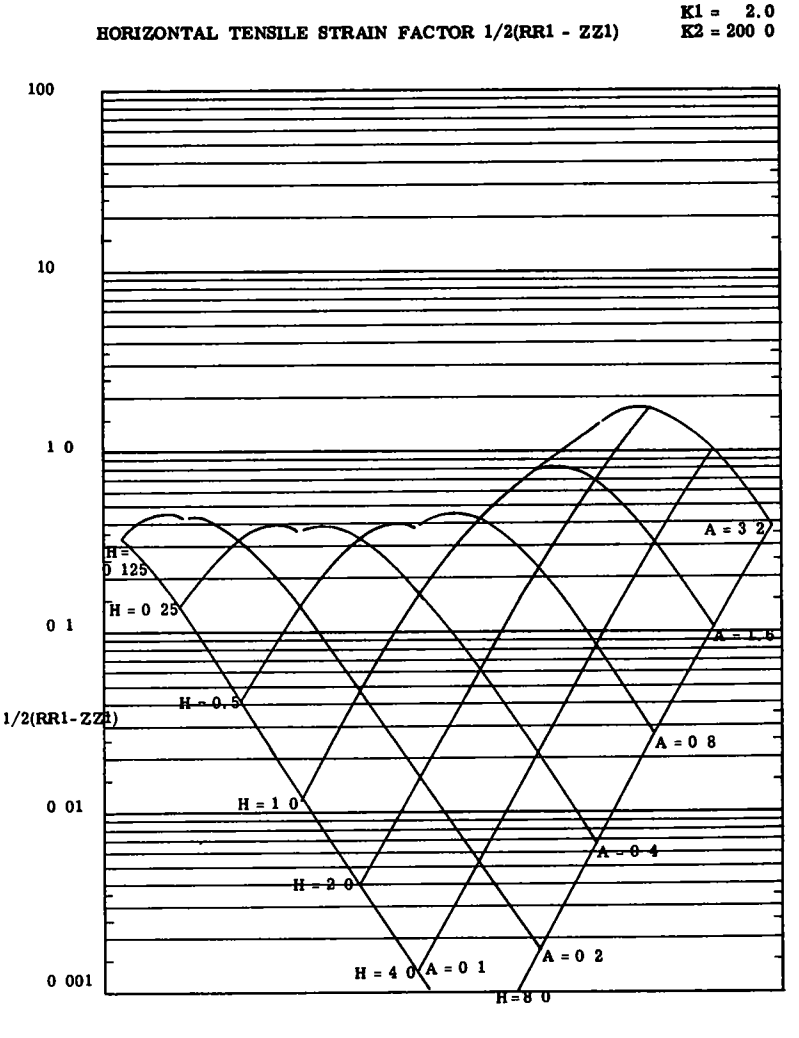

Figure 59.

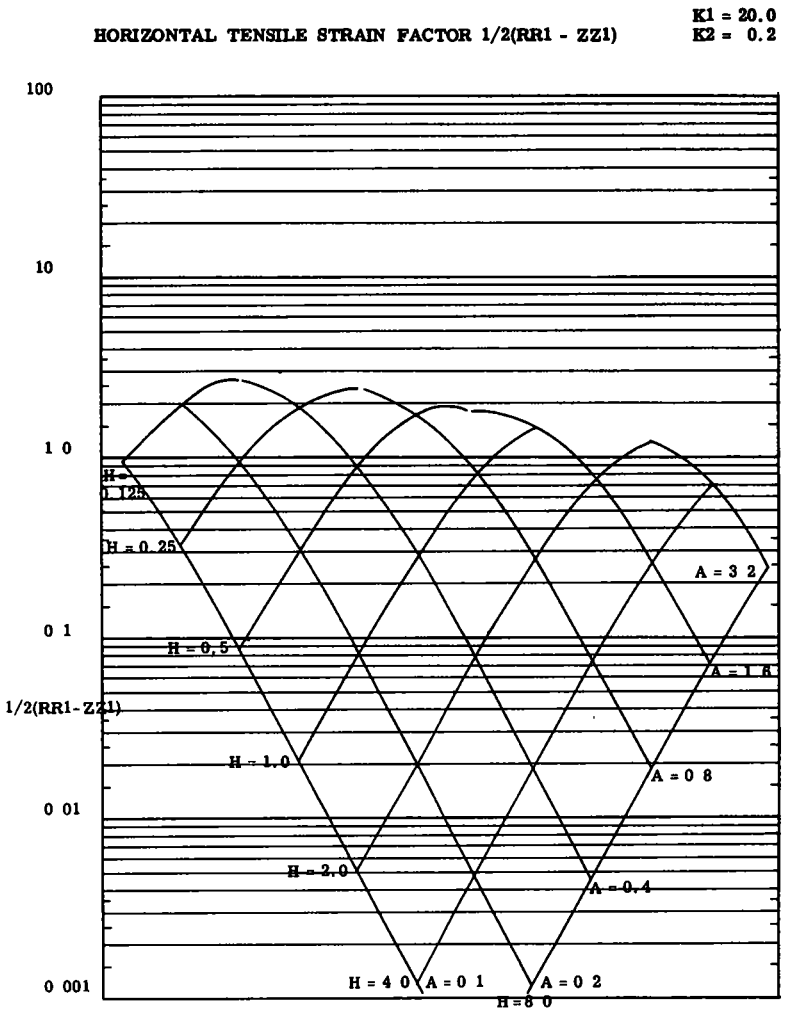

Figure 60.

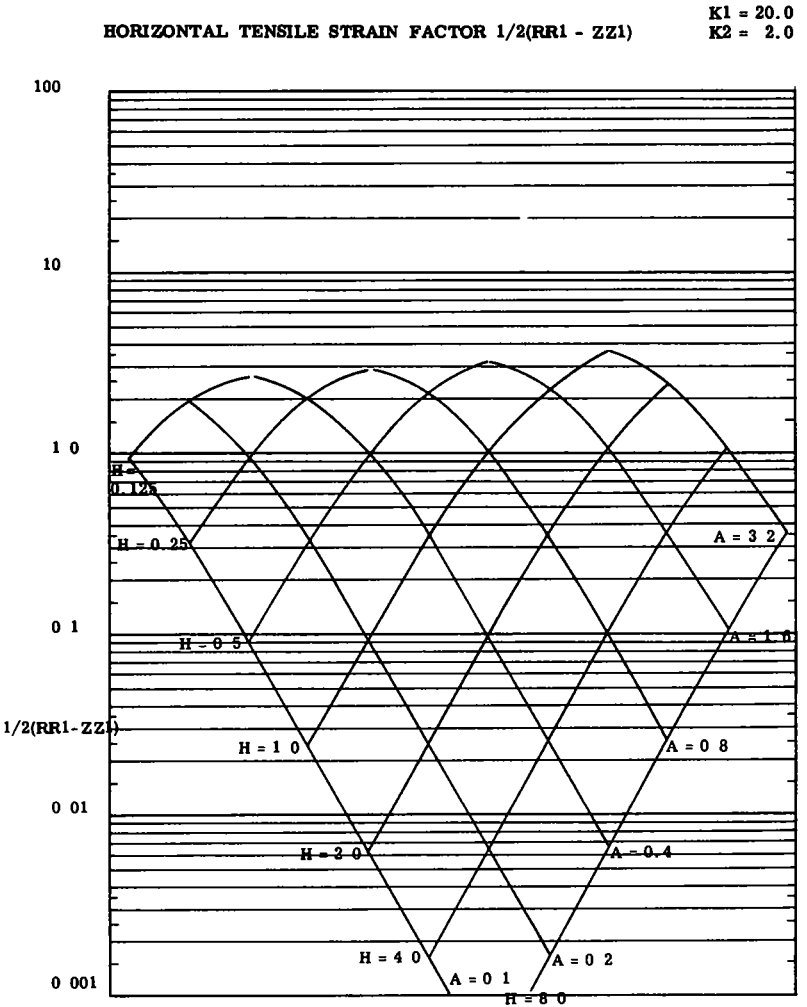

Figure 61.

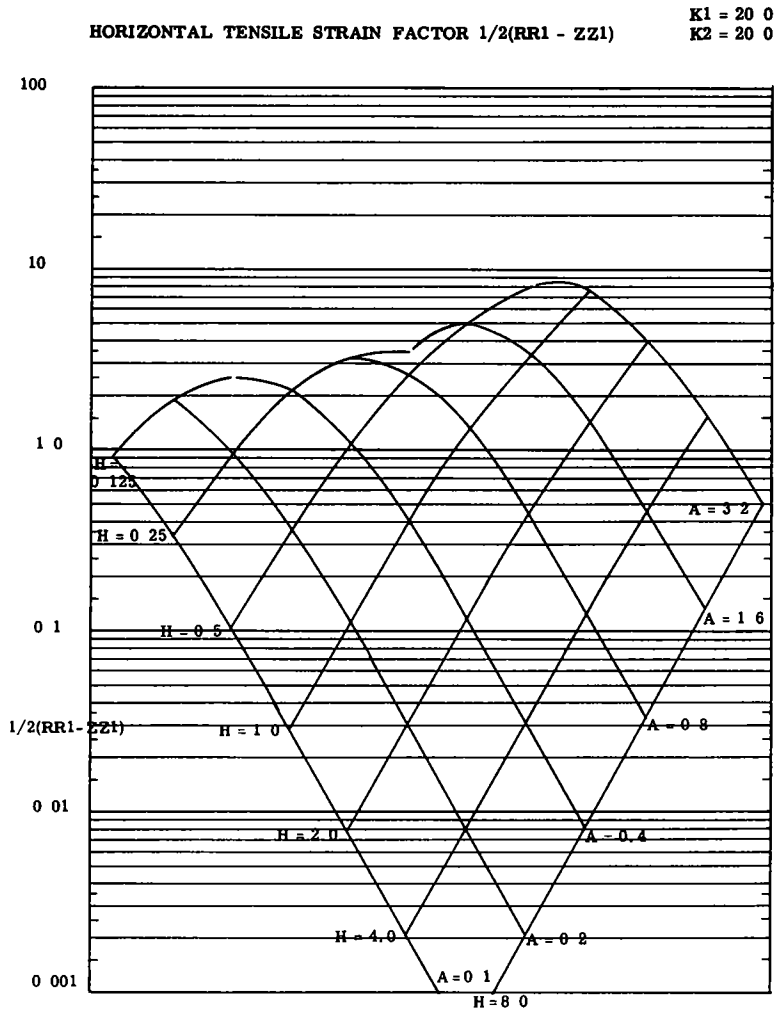

Figure 62.

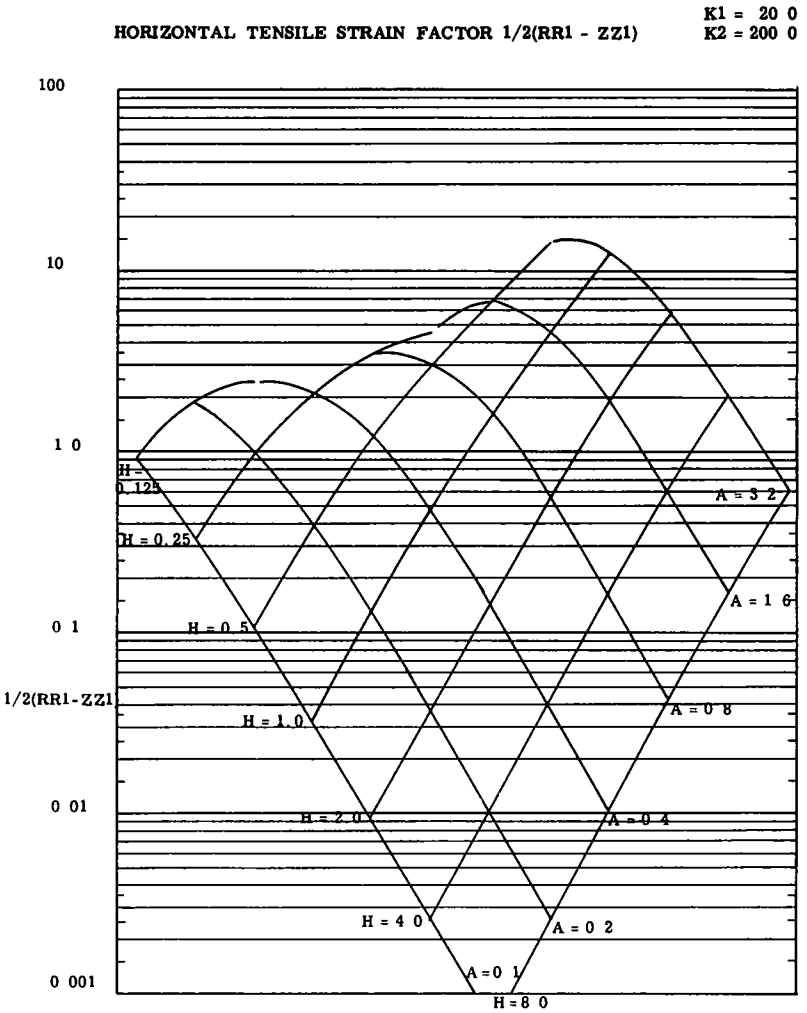

Figure 63.

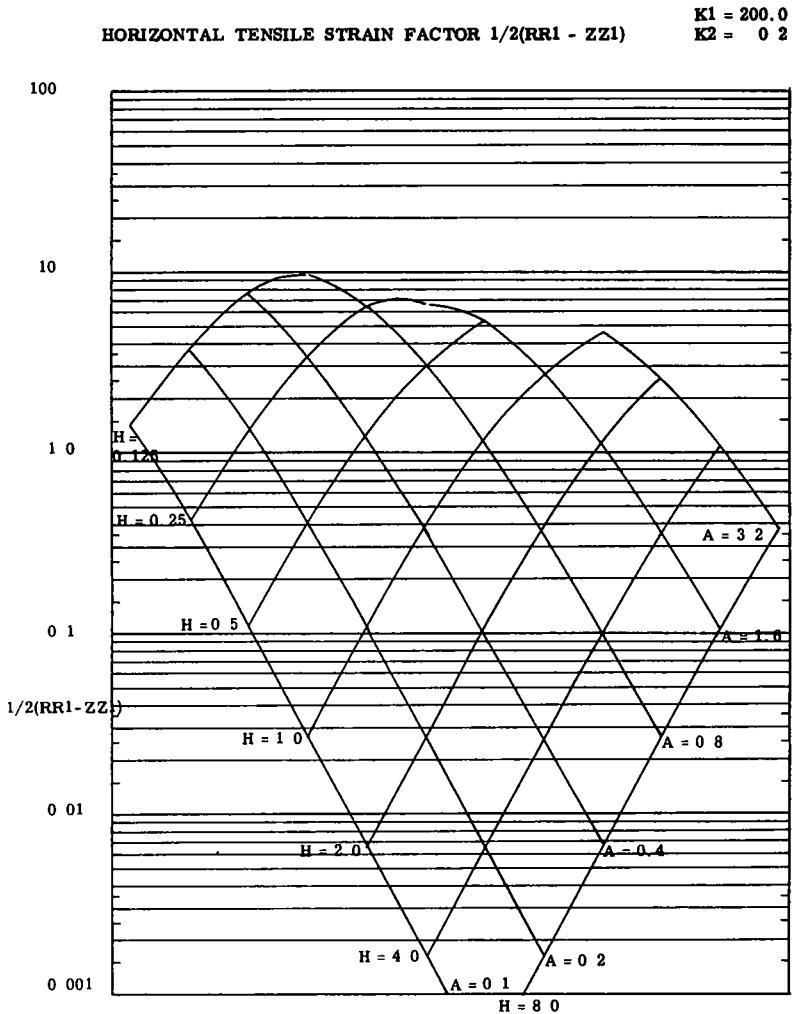

Figure 64.

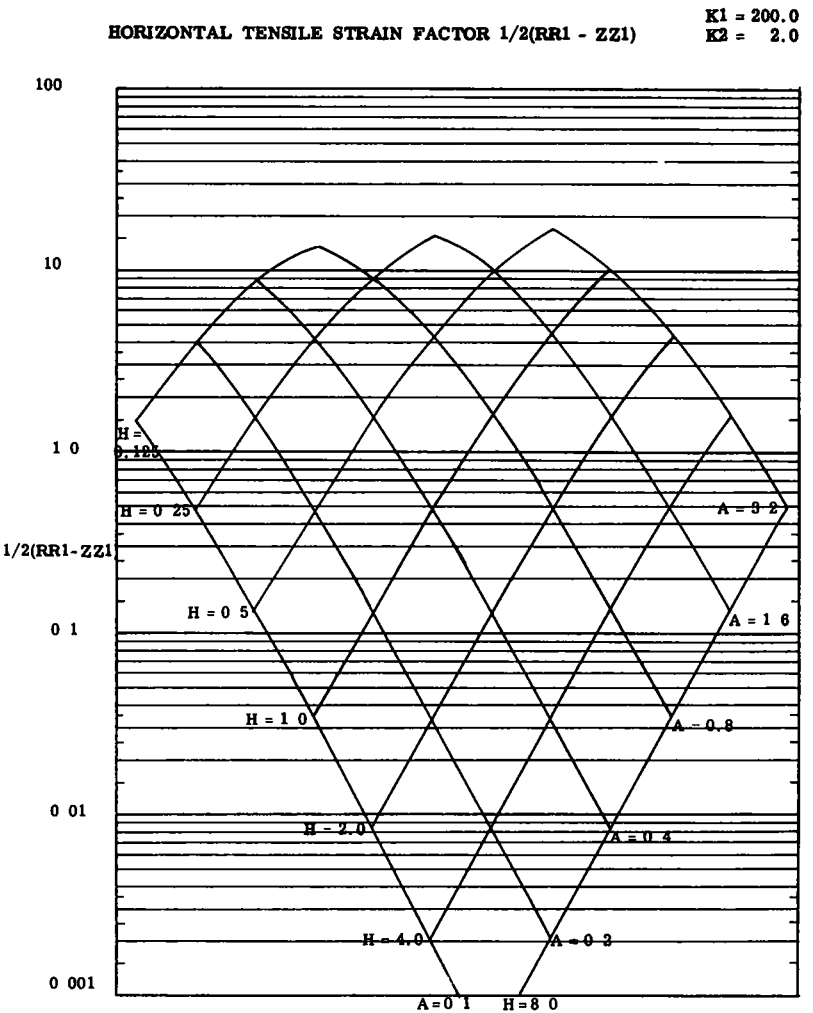

Figure 65.

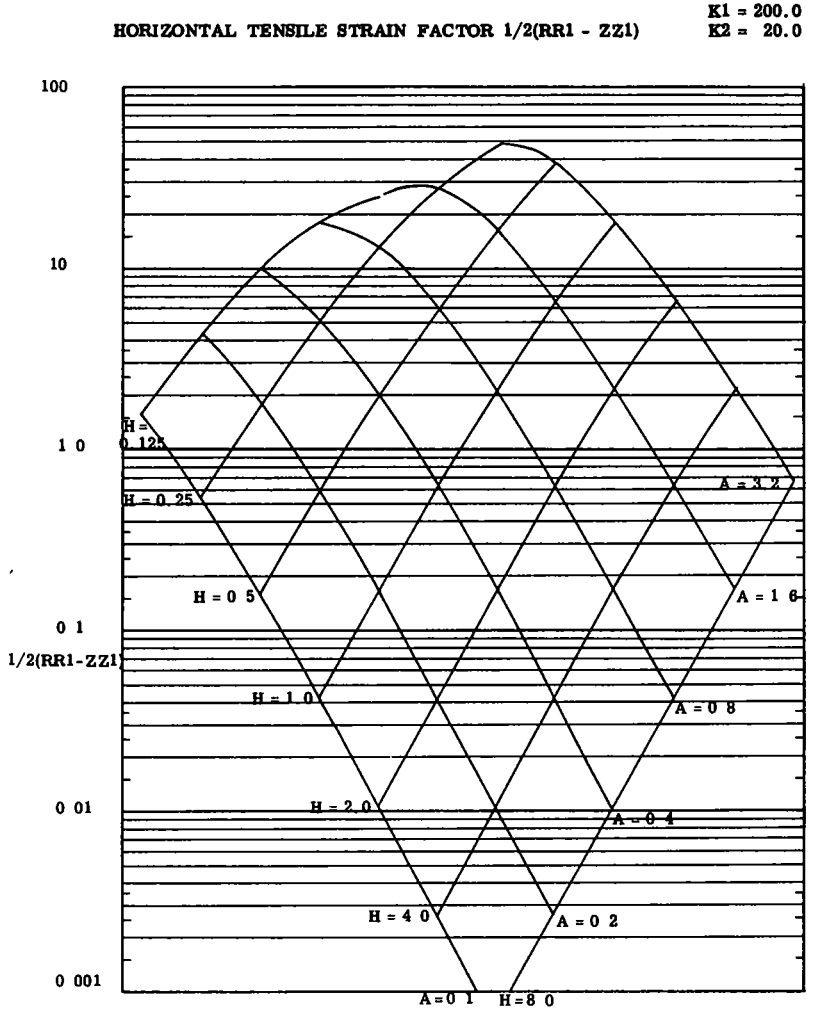

Figure 66.

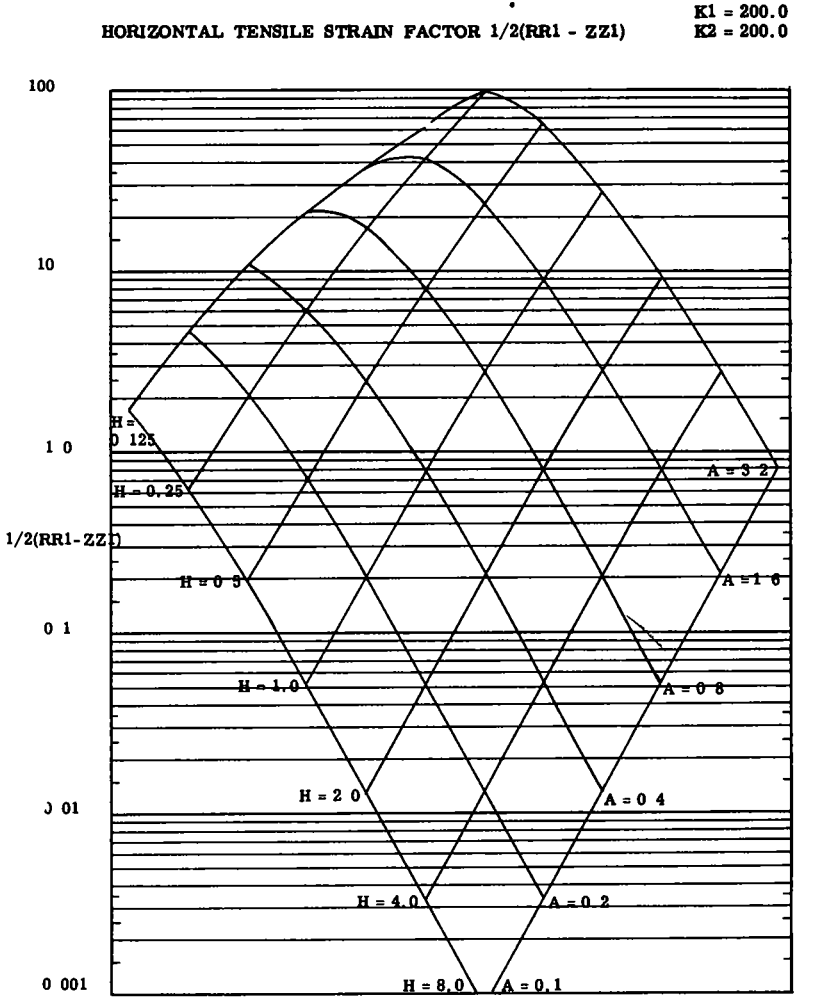

Figure 67.

Appendix B

PLOTTING OF THREE VARIABLES BY THE GRID METHOD

In the grid method of plotting (3), the dependent variable is plotted vertically in the conventional manner. The independent variables are plotted horizontally on a composite scale.

The dependent variable is plotted against one independent variable for one value of the other independent variable as shown by the solid line in Figure 68. The whole scale is then displaced horizontally and the second (dotted) line is plotted. A third displacement of the horizontal scale for A enables the (chain dotted) line for the next value of H to be plotted. Once all the plots of the stress factor against A have been drawn, the points of equal A-values are connected together to complete the grid.

The amount of displacement should be selected to give a good intersection of the grid lines; i.e., so that the lines intersect nearly at right angles. In the present series of graphs it has been found convenient to place the "0.1" point of each A-scale at a distance from the left-hand axis proportional to the logarithm of the relevant value of H.

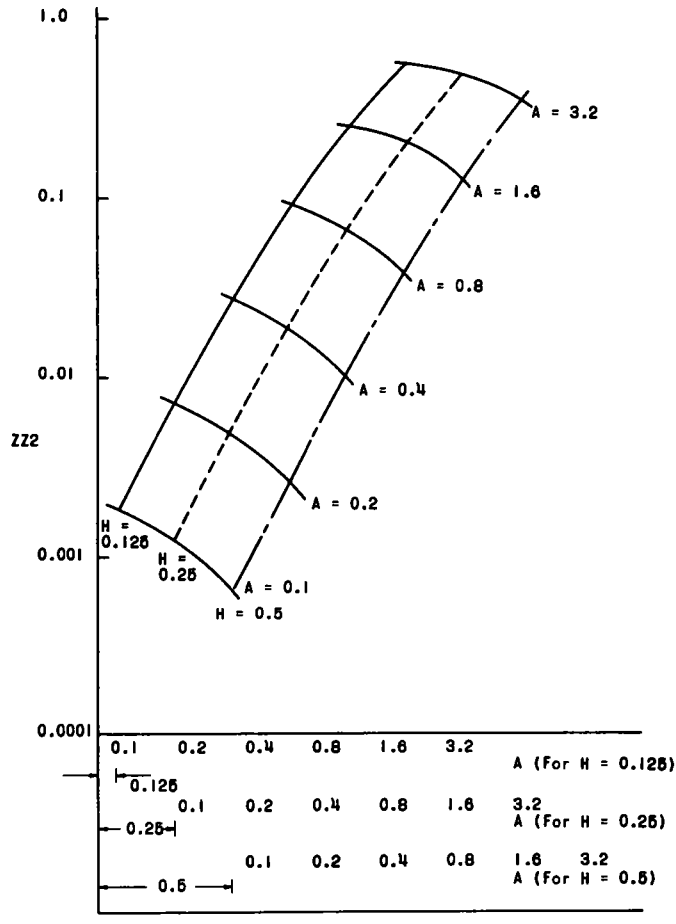

Figure 68. Construction of grid for vertical stress factor ZZ2.

THE NATIONAL ACADEMY OF SCIENCES—NATIONAL RESEARCH COUNCIL is a private, nonprofit organization of scientists, dedicated to the furtherance of science and to its use for the general welfare. The ACADEMY itself was established in 1863 under a congressional charter signed by President Lincoln. Empowered to provide for all activities appropriate to academies of science, it was also required by its charter to act as an adviser to the federal government in scientific matters. This provision accounts for the close ties that have always existed between the ACADEMY and the government, although the ACADEMY is not a governmental agency.

The NATIONAL RESEARCH COUNCIL was established by the ACADEMY in 1916, at the request of President Wilson, to enable scientists generally to associate their efforts with those of the limited membership of the ACADEMY in service to the nation, to society, and to science at home and abroad. Members of the NATIONAL RESEARCH COUNCIL receive their appointments from the president of the ACADEMY. They include representatives nominated by the major scientific and technical societies, representatives of the federal government, and a number of members at large. In addition, several thousand scientists and engineers take part in the activities of the research council through membership on its various boards and committees.

Receiving funds from both public and private sources, by contribution, grant, or contract, the ACADEMY and its RESEARCH COUNCIL thus work to stimulate research and its applications, to survey the broad possibilities of science, to promote effective utilization of the scientific and technical resources of the country, to serve the government, and to further the general interests of science.

The HIGHWAY RESEARCH BOARD was organized November 11, 1920, as an agency of the Division of Engineering and Industrial Research, one of the eight functional divisions of the NATIONAL RESEARCH COUNCIL. The BOARD is a cooperative organization of the highway technologists of America operating under the auspices of the ACADEMY–COUNCIL and with the support of the several highway departments, the Bureau of Public Roads, and many other organizations interested in the development of highway transportation. The purposes of the BOARD are to encourage research and to provide a national clearinghouse and correlation service for research activities and information on highway administration and technology.